GALAXY EVOLUTION: EMERGING INSIGHTS AND FUTURE CHALLLENGES

COVER ILLUSTRATION:

Conference Poster

Credit: Irina Marinova, Amanda Heiderman

ASTRONOMICAL SOCIETY OF THE PACIFIC CONFERENCE SERIES

A SERIES OF BOOKS ON RECENT DEVELOPMENTS IN ASTRONOMY AND ASTROPHYSICS

VOLUME **VOLUME**

PO Box 4666, Room N221 - ESC, Brigham Young University, Provo, Utah 84602-4666
Phone: 801-422-2111 Fax: 801-422-0553
E-mail: aspcs@byu.edu E-book site: http://www.aspbooks.org

Beginning 2004, ASP-CS Volumes may be found as e-books with color images at:
http://www.aspbooks.org

A listing of all IAU Volumes published
and the ASP Conference Series published during the past one year
may be found at teh back of this volume.

For all ASP-CS Volumes published see: http://www.astrosociety.org/pubs.html

ASTRONOMICAL SOCIETY OF THE PACIFIC
CONFERENCE SERIES

VOLUME **VOLUME**

GALAXY EVOLUTION: EMERGING INSIGHTS AND FUTURE CHALLLENGES

Proceedings of a workshop held at
The University of Texas, Austin, USA
11–14 November 2008

Edited by

S. Jogee
Department of Astronomy, University of Texas at Austin, 1 University Station C1400, Austin, TX 78712-0259, USA

I. Marinova
Department of Astronomy, University of Texas at Austin, 1 University Station C1400, Austin, TX 78712-0259, USA

L. Hao
Department of Astronomy, University of Texas at Austin, 1 University Station C1400, Austin, TX 78712-0259, USA

G. A Blanc
Department of Astronomy, University of Texas at Austin, 1 University Station C1400, Austin, TX 78712-0259, USA

SAN FRANCISCO

ASTRONOMICAL SOCIETY OF THE PACIFIC
390 Ashton Avenue
San Francisco, California, 94112-1722, USA

Phone: 415-337-1100
Fax: 415-337-5205
E-mail: service@astrosociety.org
Web site: www.astrosociety.org
E-books: www.aspbooks.org

ASP Conference Series – First Edition

ISBN: **ISBN**

Library of Congress (LOC) Cataloging in Publication (CIP) Data:
Main entry under title
Library of Congress Control Number (LCCN): **LCCN number**

Printed in the United States of America by Sheridan Books, Ann Arbor, Michigan

Contents

Preface x

Acknowledgments xi

Organizing Committees xii

Participants xiii

Conference Photograph xxiii

Part 1. Assembly of Disks, Bulges, and Ellipticals

Galactic Disk Formation and the Angular Momentum Problem 3
A. Burkert

Disk Galaxies at $z = 2$ in OWLS 10
J. F. Navarro, L. V. Sales, and the OWLS team

Forming Bulgeless Dwarf Galaxies 18
F. Governato

Bulge Formation by the Coalescence of Giant Clumps in Primordial Disk Galaxies 24
B. G. Elmegreen

Secular Evolution and the Assembly of Bulges 31
F. Combes

Dark Matter Substructure, Filaments, and Assembling Disks 39
I. Shlosman

Nuclear Star Clusters in Spheroidal and Late-Type Disk Galaxies 46
M. Milosavljević and M. Agarwal

Kinematics of LSB & Dwarfs: Implications for LCDM models 53
G. Rhee

Star-Forming Galaxies at $z \sim 2$: An Emerging Picture of Galaxy Dynamics and Assembly 60
K. L. Shapiro, R. Genzel, N. Bouché, P. Buschkamp, G. Cresci, R. Davies, F. Eisenhauer, N. Förster Schreiber, S. Genel, E. Hicks, D. Lutz, and L. Tacconi

The Elaboration of Spiral Galaxies: Morpho-Kinematics Analyses of their Progenitors with IMAGES 66
F. Hammer, on behalf of the IMAGES collaboration

Properties and Origin of Bulges in High Mass Spirals 74
T. Weinzirl, S. Jogee, S. Khochfar, A. Burkert, and J. Kormendy

Galaxy bulges from $z = 0$ to $z = 1$ 79
M. Balcells

The Elliptical–Spheroidal and Elliptical–Elliptical Galaxy Dichotomies . . 87
J. Kormendy

Stellar Populations and Mass-to-Light Ratios Throughout the Fundamental Plane 96
G. J. Graves

Mapping the Galaxy with Photometric Surveys: Insights from SDSS and Future Prospects 103
Mario Jurić and Željko Ivezić

The Star Formation Histories of the M31 and M33 Spheroids 110
T. M. Brown

M31's Giant Southern Stream: Constraints on the Progenitor's Mass, Phase, and Rotation 118
M. Fardal, P. Guhathakurta, K. Gilbert, A. Babul, C. Dodge, M. Weinberg, and Y. Lu

GALEX Observations of Disk and Bulge-Dominated Galaxies 123
D. Schiminovich and the GALEX Science Team

Galactic Bulges: the SAURON perspective 131
J. Falcón-Barroso, R. F. Peletier, R. Bacon, M. Cappellari, R. L. Davies, P. Tim de Zeeuw, E. Emsellem, D. Krajnović, H. Kuntschner, R. M. McDermid, M. Sarzi, R. C. E. van den Bosch, and G. van de Ven

The Properties of Local Barred Disks in the Field and Dense Environments: Implications for Galaxy Evolution 138
Marinova, I., S. Jogee, F. D. Barazza, A. Heiderman, M. E. Gray, M. Barden, C. Wolf, C. Y. Peng, D. Bacon, M. Balogh, E. F. Bell, A. Böhm, J. A. R. Caldwell, B. Häußler, C. Heymans, K. Jahnke, E. van Kampen, K. Lane, D. H. McIntosh, K. Meisenheimer, S. F. Sánchez, R. Somerville, A. Taylor, L. Wisotzki, and X. Zheng

Bars in Field and Cluster Galaxies at Intermediate Redshifts 145
F. D. Barazza, P. Jablonka, and the EDisCS collaboration

Detection of a Distinct Pseudobulge Hidden Inside the "Box-Shaped Bulge" of NGC 4565 150
J. C. Barentine and J. Kormendy

Simulations of Long-Lived Double-Barred Galaxies 154
J. Shen and V. P. Debattista

Beyond the *Best-Fit* Parameter: New Insight on Galaxy Structure Decomposition from GALPHAT 159
I. Yoon, M. D. Weinberg, and N. S. Katz

Analytical Galactic Models with Mild Cusps 164
T. Rindler-Daller

A Shared Tully-Fisher Relation for Spirals and S0 Galaxies 168
M. J. Williams, M. Bureau, and M. Cappellari

The Morphological Type Dependence of K-band Luminosity Functions . . 172
N. Devereux, P. Hriljac, S. P. Willner, M. L. N. Ashby, and C. N. A. Willmer

Dynamical Models of the Dark Halo of Elliptical Galaxy NGC 6702 . . . 176
A. Forestell and K. Gebhardt

Stellar Velocity Profiles and Line-Strengths out to Four Effective Radii in the Early-Type Galaxy NGC 3379 180
A. Weijmans, M. Cappellari, P. T. de Zeeuw, E. Emsellem, J. Falcón-Barroso, H. Kuntschner, R. M. McDermid, R. C. E. van den Bosch, and G. van de Ven

Part 2. History and Impact of Galaxy Mergers

Merger History of Galaxies and Disk+Bulge Formation 187
S. Khochfar

Galaxy Mergers and Secular Evolution over the Last 10 Gy 194
S. Jogee

Major Merger Statistics up to $z \sim 1$ 203
C. López-Sanjuan, M. Balcells, P. G. Pérez-González, G. Barro, C. E. García-Dabó, J. Gallego, and J. Zamorano

Are Mergers so Good at Triggering Starbursts? 208
A. R. Robaina, E. F. Bell, R. E. Skelton, D. H. McIntosh, R. Somerville, and STAGES collaboration

The Millennium Simulation Compared to Observations of $z \approx 2$ Galaxies 214
S. Genel

How Do Disks Survive Mergers? 220
P. F. Hopkins

The Impact of Minor Galaxy Mergers 227
T. J. Cox

Invisible Major Mergers: Why the Definition of a Galaxy "Merger Ratio" Matters 235
K. R. Stewart

Galactic Disk Transformation via Massive Satellite Accretion Events . . . 240
C. W. Purcell, S. Kazantzidis, and J. S. Bullock

The Impact of Mergers on the Survival and Abundance of Disk-Dominated Galaxies 245
J. Koda, M. Milosavljević, and P. R. Shapiro

Galaxy Mergers in the A901/902 Supercluster with STAGES 249
A. Heiderman, S. Jogee, I. Marinova, E. van Kampen, M. Barden, C. Y. Peng, C. Heymans, M. E Gray, E. F. Bell, D. Bacon, M. Balogh, F. D. Barazza, A. Böhm, J. A. R Caldwell, B. Häußler, K. Jahnke, K. Lane, D. H McIntosh, K. Meisenheimer, S. F. Sánchez, R. Somerville, A. Taylor, L. Wisotzki, C. Wolf, and X. Zheng

Numerical Simulations of Hot Halo Gas in Galaxy Mergers 254
M. Sinha and K. Holley-Bockelmann

The Effect of Dry Mergers on the Color-Magnitude Relation 258
R. E. Skelton, E. F. Bell, and R. S. Somerville

A Dynamical Miss: A Study of the Discrepancy Between Optical and Infrared Kinematics in Mergers 264
B. Rothberg

Part 3. Star Formation

CDM Substructure Problem and Star Formation in Dwarf Halos 271
A. Kravtsov

Fossil Signatures of the Reionization Epoch in the Galactic Halo 278
P. Madau

Star Formation Histories and Stellar Mass Growth out to $z > 1$ 286
K. G. Noeske

The Molecular Gas Content of Massive Spirals at $z = 1.5$ 294
E. Daddi

A Steep Faint-End Slope of the UV Luminosity Function at $z \sim 2 - 3$: Implications for the Missing Stellar Mass Problem 301
N. A. Reddy

Submillimeter Galaxies 308
A. W. Blain

Galaxy Star Formation in Different Environments 315
R. E. González and N. D. Padilla

The Chemical Evolution of Intermediate Mass Galaxies over the Last 8 Gyrs 319
Rodrigues M., Hammer F., Flores M., and Puech M.

The First Galaxies: Signatures of the Initial Starburst 323
J. L. Johnson, T. H. Greif, V. Bromm, R. S. Klessen, and J. Ippolito

The First Stars: Disk Formation and Fragmentation 327
A. Stacy, T. H. Greif, and V. Bromm

Part 4. AGN and Stellar Feedback

Missing Halo Baryons and Galactic Outflows 333
R. Davé
The Impact of Feedback on Disk Galaxy Scaling Relations 341
A. A. Dutton and F. C. van den Bosch
Gravitational Heating, Clumps, Overheating 349
Y. Birnboim
Empirical Evidence for Quasar Feedback 356
C. Tremonti, A. M. Diamond-Stanic, and J. Moustakas
Broad Absorption Line Quasars and Galaxy Evolution 363
B. J. Wills
Identifying the Obscured Black-Hole Growth Phase of Distant Massive Galaxies 368
D. M. Alexander
An Improved Black Hole Mass–Bulge Luminosity Relationship for AGNs 375
C. M. Gaskell and J. Kormendy
The Black Hole – Bulge Relationship for AGN at High Redshift 379
G. A. Shields and S. Salviander
Spectral Principal Component Analysis of SDSS Quasars: Beyond Eigenvector 1 385
R. R. Ludwig and B. Wills
Bars in Starbursts and AGNs – A Quantitative Reexamination 389
L. Hao, S. Jogee, F. Barazza, I. Marinova, and J. Shen
Stellar Feedback: A Multiphase Interstellar Medium and Galactic Outflows 396
D. Ceverino
The Environmental Impact of Galaxy Evolution 401
J. Rasmussen and T. Ponman
Author Index 407

Preface

The international conference, "Galaxy Evolution: Emerging Insights and Future Challenges", was held on on November 11 to 14 2008, on the campus of the University of Texas at Austin. The meeting was the first one to be sponsored by the McDonald Observatory and Department of Astronomy Board of Visitors Excellence Funds, whose generous support we gratefully acknowledge. We were honored to welcome 134 participants from 33 institutions and 11 countries.

The conference brought together leading observers and theorists in order to evaluate long-standing challenges facing hierarchical Λ cold dark matter (ΛCDM) cosmogonies, explore recent progress in charting the merger, star formation, and assembly history of galaxies, and brainstorm on outstanding challenges .

The defining signature of the meeting was the generous discussion time after each oral presentation and the vigorous debates on several central themes. What is the current status of long-standing challenges for ΛCDM models of galaxy evolution, such as the angular momentum problem, the problem of bulgeless galaxies, the sub-structure problem, and the cusp-core controversy? What are the implications of the surprising new insights emerging on the assembly of disks, bulges, and ellipticals over the last 12 Gyr? What are the relative roles of major mergers, minor mergers, smooth accretion, and secular processes in the assembly of massive galaxies? What is the impact of feedback from star formation and active galactic nuclei on galaxy evolution ? What constraints are needed from observers by theorists and vice-versa in order to tackle the next cosmic frontiers?

These proceedings, we hope, will mirror the conference in providing new insights, challenging long-standing paradigms and fostering much further work.

Shardha Jogee, SOC Chair and Editor

Irina Marinova, Editor

Lei Hao, Editor

Guillermo A. Blanc, Editor

Acknowledgments

I am grateful to McDonald Observatory and the Department of Astronomy at the University of Texas at Austin for generously funding this international conference. The meeting was supported with excellence funds from contributions made by the membership of the University of Texas at Austin McDonald Observatory and Department of Astronomy Board of Visitors (John Heasley, chair; David Chappell, vice-chair; Steve Bickerstaff, secretary)

I thank the department chair, Neal Evans, for his unwavering support of the meeting even at times of of tight budgetary constraints, and for his active interest in the scientific program.

I extend my appreciation to fellow members of the scientific organizing committee (SOC) for their input and numerous suggestions, which culminated in a stimulating and thought-provoking program.

Numerous participants commented on the excellent and high level organization and I would like to credit this to the tireless efforts of our excellent local organizing committee (LOC) and graduate students. I would particularly like to thank Monica Kidd, Debbie Winegarten, Jim Umbarger, Irina Marinova, Lei Hao, Guillermo Blanc, and Lara Eakins on the LOC for their outstanding efforts. I also want to express a special thanks to the graduate students who flawlessly coordinated the shuttle rides, namely Guillermo Blanc, Jeremy Murphy, Chalence Safranek, Irina Marinova, Meghan Agarwal, Tim Weinzirl, Randi Worhatch , Joshua Adams, John Barentine and JJ Hermes.

Shardha Jogee

Organizing Committees

Scientific Organizing Committee (SOC)

- Andreas Burkert *(University Observatory Munich, Germany)*
- Francoise Combes *(Observatoire de Paris, France)*
- Avishai Dekel *(Hebrew University, Israel)*
- Mark Dickinson *(National Optical Astronomy Observatory, USA)*
- Shardha Jogee [Chair] *(University of Texas at Austin, USA)*
- Robert Kennicutt *(Cambridge University, England)*
- John Kormendy *(University of Texas at Austin, USA)*
- Julio Navarro *(University of Victoria, Canada)*
- Hans-Walter Rix *(Max-Planck-Institut für Astronomie, Germany)*
- Isaac Shlosman *(University of Colorado, USA)*
- Rachel Somerville *(Space Telescope Science Institute, USA)*

Local Organizing Committee (LOC)

- Debbie Winegarten
- Monica Kidd
- Jim Umbarger
- Lara Eakins
- Joel Barna
- Gordon Orris
- Shardha Jogee
- Neal Evans
- Irina Marinova
- Lei Hao
- Amanda Heiderman
- Tim Weinzirl
- Guillermo Blanc
- Jeremy Murphy

Participants

J. Adams, University of Texas at Austin, Department of Astronomy, 1 University Station C1400, Austin, TX 78712-0259, USA ⟨ jjadams@astro.as.utexas.edu ⟩

M. Agarwal, University of Texas at Austin, Department of Astronomy, 1 University Station C1400, Austin, TX 78712-0259, USA ⟨ mepa@physics.as.utexas.edu ⟩

D. Alexander, Durham University, Department of Physics, Durham, DH1 3LE, United Kingdom ⟨ d.m.alexander@durham.ac.uk ⟩

A. Al Muhammad, University of Texas at Austin, Department of Astronomy, 1 University Station C1400, Austin, TX 78712-0259, USA ⟨ anwar@physics.utexas.edu ⟩

S. Anderson, University of Texas at Austin, Department of Astronomy, 1 University Station C1400, Austin, TX 78712-0259, USA ⟨ seth.anderson@mail.utexas.edu ⟩

S. Arabi-Katbi, University of Texas at Austin, Department of Astronomy, 1 University Station C1400, Austin, TX 78712-0259, USA ⟨ s.arabikatbi@mail.utexas.edu ⟩

M. Balcells, Instituto de Astrofisica de Canarias, 38200 La Laguna, Tenerife, Spain ⟨ balcells@iac.es ⟩

F. Barazza,, Observatoire de Sauverny, Laboratoire d'Astrophysique, EPFL, Observatoire de Sauverny, CH-1290 Versoix, Switzerland ⟨ fabio.barazza@epfl.ch ⟩

J. Barentine, University of Texas at Austin, Department of Astronomy, 1 University Station C1400, Austin, TX 78712-0259, USA ⟨ jcb@astro.as.utexas.edu ⟩

J. Barna, University of Texas at Austin, Department of Astronomy, 1 University Station C1400, Austin, TX 78712-0259, USA ⟨ jwbarna@astro.as.utexas.edu ⟩

R. Bello, University of Texas at Austin, Department of Astronomy, 1 University Station C1400, Austin, TX 78712-0259, USA ⟨ topexbell@yahoo.com ⟩

G. Benedict, University of Texas at Austin, Department of Astronomy, 1 University Station C1400, Austin, TX 78712-0259, USA ⟨ fritz@astro.as.utexas.edu ⟩

T. Bennett, University of Texas at Austin, Department of Astronomy, 1 University Station C1400, Austin, TX 78712-0259, USA ⟨tapioooka89@yahoo.com⟩

Y. Birnboim, Harvard Smithsonian Center for Astrophysics, 60 Garden Street, Cambridge, MA 02138, USA ⟨ybirnboim@cfa.harvard.edu⟩

A. Blain, California Institute of Technolgy, Astronomy Department, Mail Stop 105-24, Pasadena, CA91125, USA ⟨awb@astro.caltech.edu⟩

G. A. Blanc, University of Texas at Austin, Department of Astronomy, 1 University Station C1400, Austin, TX 78712-0259, USA ⟨gblancm@astro.as.utexas.edu⟩

J. Bowen, University of Texas at Austin, Department of Astronomy, 1 University Station C1400, Austin, TX 78712-0259, USA ⟨bowen.pi@gmail.com⟩

V. Bromm, University of Texas at Austin, Department of Astronomy, 1 University Station C1400, Austin, TX 78712-0259, USA ⟨vbromm@astro.as.utexas.edu⟩

T. Brown, Space Telescope Science Institute, 3700 San Martin Drive, Baltimore, MD 21218, USA ⟨tbrown@stsci.edu⟩

A. Burkert, University Observatory Munich, Scheinerstrasse 1, D-81679 Munich, Germany ⟨burkert@usm.lmu.de⟩

J. Byun, University of Texas at Austin, Department of Astronomy, 1 University Station C1400, Austin, TX 78712-0259, USA ⟨byun.joyce@gmail.com⟩

D. Ceverino, The Hebrew University, Racah Institute of Physics, Jerusalem 91904, Israel ⟨ceverino@nmsu.edu⟩

J. Chen , University of Texas at Austin, Department of Astronomy, 1 University Station C1400, Austin, TX 78712-0259, USA ⟨jhchen@astro.as.utexas.edu⟩

F. Combes, Observatoire de Paris, LERMA, 61 Av. de l'Observatoire, F-75014, Paris, France ⟨francoise.combes@obspm.fr⟩

M. Cornell, University of Texas at Austin, Department of Astronomy, 1 University Station C1400, Austin, TX 78712-0259, USA ⟨cornell@puck.as.utexas.edu⟩

T. Cox, Harvard-Smithsonian Center for Astrophysics, 60 Garden St., MS-51, Cambridge, MA 02138, USA ⟨tcox@cfa.harvard.edu⟩

E. Daddi, CEA, Laboratoire AIM - CNRS - Université Paris Diderot, Irfu/SAp, Orme des Merisiers, F-91191 Gif-sur-Yvette, France ⟨edaddi@cea.fr⟩

R. Davé, University of Arizona, Astronomy Department, Tucson, AZ 85721, USA ⟨rad@as.arizona.edu⟩

P. A. Dekel, The Hebrew University of Jerusalem, Racah Institute of Physics, Safra Campus, Jerusalem 91904, Israel ⟨dekel@phys.huji.ac.il⟩

N. Devereux, Embry-Riddle Aeronautical University, Department of Physics, Prescott, AZ 86301, USA ⟨ devereux@erau.edu ⟩

M. Dunham, University of Texas at Austin, Department of Astronomy, 1 University Station C1400, Austin, TX 78712-0259, USA ⟨ mdunham@astro.as.utexas.edu ⟩

A. Dutton, University of California, UCO/Lick Observatory, Santa Cruz, CA 95060, USA ⟨ dutton@ucolick.org ⟩

L. Eakins, University of Texas at Austin, Department of Astronomy, 1 University Station C1400, Austin, TX 78712-0259, USA ⟨ lara@astro.as.utexas.edu ⟩

B. Elmegreen, IBM Research Division, T.J. Watson Research Center, P.O. Box 218, Yorktown Heights, NY 10598, USA ⟨ bge@watson.ibm.com ⟩

N. Evans, University of Texas at Austin, Department of Astronomy, 1 University Station C1400, Austin, TX 78712-0259, USA ⟨ nje@astro.as.utexas.edu ⟩

R. Falcon, University of Texas at Austin, Department of Astronomy, 1 University Station C1400, Austin, TX 78712-0259, USA ⟨ cylver@astro.as.utexas.edu ⟩

J. Falcón-Barroso, European Space and Technology Centre, Keplerlaan 1, 2200 AG, European Space and Technology Centre, Noordwijk, The Netherlands ⟨ jfalcon@rssd.esa.int ⟩

M. Fardal, University of Massachusetts, Department of Astronomy, Amherst, MA 01003, USA ⟨ fardal@astro.umass.edu ⟩

D. Fisher, University of Texas at Austin, Department of Astronomy, 1 University Station C1400, Austin, TX 78712-0259, USA ⟨ dbfisher@astro.as.utexas.edu ⟩

A. Forestell, University of Texas at Austin, Department of Astronomy, 1 University Station C1400, Austin, TX 78712-0259, USA ⟨ amydove@astro.as.utexas.edu ⟩

K. Foyle,, Max-Planck-Institut für Astronomie, MPIA, Königstuhl 17, D-69117 Heidelberg, Germany ⟨ foyle@mpia.de ⟩

M. Frei, University of Texas at Austin, Department of Astronomy, 1 University Station C1400, Austin, TX 78712-0259, USA ⟨ mafrei@physics.utexas.edu ⟩

M. Gaskell, University of Texas at Austin, Department of Astronomy, 1 University Station C1400, Austin, TX 78712-0259, USA ⟨ gaskell@astro.as.utexas.edu ⟩

K. Gebhardt, University of Texas at Austin, Department of Astronomy, 1 University Station C1400, Austin, TX 78712-0259, USA ⟨ gebhardt@astro.as.utexas.edu ⟩

S. Genel,, Max Planck Institut für extraterrestrische Physik, Giessenbachstrasse, D-85748 Garching, Germany ⟨ shy@mpe.mpg.de ⟩

J. Gomez, University of Texas at Austin, Department of Astronomy, 1 University Station C1400, Austin, TX 78712-0259, USA ⟨josegmz@mail.utexas.edu⟩

R. Gonzalez, Pontificia Universidad Catolica de Chile, Departamento de Astronomia y Astrofsica, Santiago, Chile ⟨regonzar@astro.puc.cl⟩

F. Governato, University of Washington, Astronomy Department, Box 351580, Seattle, WA 98195-1580, USA ⟨fabio.governato@gmail.com⟩

G. Graves, UCO/Lick Observatory, Department of Astronomy and Astrophysics, University of California, Santa Cruz, CA 95064, USA ⟨graves@ucolick.org⟩

J. Green, University of Texas at Austin, Department of Astronomy, 1 University Station C1400, Austin, TX 78712-0259, USA ⟨joel@astro.as.utexas.edu⟩

R. Griffin, University of Texas at Austin, Department of Astronomy, 1 University Station C1400, Austin, TX 78712-0259, USA ⟨richardgriff@gmail.com⟩

A. Guess, University of Texas at Austin, Department of Astronomy, 1 University Station C1400, Austin, TX 78712-0259, USA ⟨a_guess@mail.utexas.edu⟩

E. Hamill, University of Texas at Austin, Department of Astronomy, 1 University Station C1400, Austin, TX 78712-0259, USA ⟨ericbhamill@mail.utexas.edu⟩

F. Hammer, Observatoire de Paris & CNRS, GEPI, Observatoire de Paris, 5 place Jules Janssen, 92195 Meudon, France ⟨francois.hammer@obspm.fr⟩

L. Hao, University of Texas at Austin, Department of Astronomy, 1 University Station C1400, Austin, TX 78712-0259, USA ⟨haol@astro.as.utexas.edu⟩

A. Heiderman, University of Texas at Austin, Department of Astronomy, 1 University Station C1400, Austin, TX 78712-0259, USA ⟨alh@astro.as.utexas.edu⟩

E. Hernandez, University of Texas at Austin, Department of Astronomy, 1 University Station C1400, Austin, TX 78712-0259, USA ⟨pescadolocoo@hotmail.com⟩

G. Hill, University of Texas at Austin, Department of Astronomy, 1 University Station C1400, Austin, TX 78712-0259, USA ⟨hill@astro.as.utexas.edu⟩

M. Hill, University of Texas at Austin, Department of Astronomy, 1 University Station C1400, Austin, TX 78712-0259, USA ⟨mileshill@mail.utexas.edu⟩

P. Hopkins, University of California Berkeley, Department of Astronomy, Berkeley, CA 94720, USA ⟨phopkins@astro.berkeley.edu⟩

G. Huggins, University of Texas at Austin, Department of Astronomy, 1 University Station C1400, Austin, TX 78712-0259, USA ⟨TheSeventies@msn.com⟩

D. Jackson, University of Texas at Austin, Department of Astronomy, 1 University Station C1400, Austin, TX 78712-0259, USA ⟨donna@astro.as.utexas.edu⟩

D. Jaffe, University of Texas at Austin, Department of Astronomy, 1 University Station C1400, Austin, TX 78712-0259, USA ⟨dtj@astro.as.utexas.edu⟩

J. Jardel, University of Texas at Austin, Department of Astronomy, 1 University Station C1400, Austin, TX 78712-0259, USA ⟨jardel@astro.as.utexas.edu⟩

S. Jogee, University of Texas at Austin, Department of Astronomy, 1 University Station C1400, Austin, TX 78712-0259, USA ⟨sj@astro.as.utexas.edu⟩

J. Johnson, University of Texas at Austin, Department of Astronomy, 1 University Station C1400, Austin, TX 78712-0259, USA ⟨jljohnson@astro.as.utexas.edu⟩

M. Juric, Institute for Advanced Study,, 1 Einstein Drive, Princeton, NJ 08540, USA ⟨mjuric@ias.edu⟩

S. Kannappan, University of North Carolina at Chapel Hill, Department of Physics and Astronomy, 290 Phillips Hall, CB3255, Chapel Hill, NC 27599, USA ⟨sheila@physics.unc.edu⟩

S. Khochfar,, Max Planck Institut für extraterrestrische Physik, Giessenbachstrasse, D-85748 Garching, Germany ⟨sadeghk@mpe.mpg.de⟩

M. Kidd, University of Texas at Austin, Department of Astronomy, 1 University Station C1400, Austin, TX 78712-0259, USA ⟨monicak@astro.as.utexas.edu⟩

H. Jeong Kim, University of Texas at Austin, Department of Astronomy, 1 University Station C1400, Austin, TX 78712-0259, USA ⟨hyojeong@astro.as.utexas.edu⟩

J. Koda, University of Texas at Austin, Department of Astronomy, 1 University Station C1400, Austin, TX 78712-0259, USA ⟨junkoda@physics.utexas.edu⟩

J. Kormendy, University of Texas at Austin, Department of Astronomy, 1 University Station C1400, Austin, TX 78712-0259, USA ⟨kormendy@astro.as.utexas.edu⟩

A. Kravtsov, University of Chicago, Department of Astronomy and Astrophysics, 5640 S. Ellis Ave., Chicago, IL 60637, USA ⟨andrey@oddjob.uchicago.edu⟩

D. Kuehner, University of Texas at Austin, Department of Astronomy, 1 University Station C1400, Austin, TX 78712-0259, USA ⟨astrophizz@gmail.com⟩

C. Lawson, University of Texas at Austin, Department of Astronomy, 1 University Station C1400, Austin, TX 78712-0259, USA ⟨chelsea.lawson@yahoo.com⟩

A. Liao, University of Texas at Austin, Department of Astronomy, 1 University Station C1400, Austin, TX 78712-0259, USA ⟨ galactic.senate@gmail.com ⟩

C. Lindner, University of Texas at Austin, Department of Astronomy, 1 University Station C1400, Austin, TX 78712-0259, USA ⟨ lindner@astro.as.utexas.edu ⟩

C. López-Sanjuan,, Instituto de Astrofísica de Canarias, Calle Vía Láctea s/n, E-38205 La Laguna, Tenerife, Spain ⟨ clsj@iac.es ⟩

P. Madau, University of California Santa Cruz, University of California Santa Cruz, Santa Cruz, CA, USA ⟨ pmadau@ucolick.org ⟩

R. R. Ludwig, University of Texas at Austin, Department of Astronomy, 1 University Station C1400, Austin, TX 78712-0259, USA ⟨ randi@astro.as.utexas.edu ⟩

J. Malone, University of Texas at Austin, Department of Astronomy, 1 University Station C1400, Austin, TX 78712-0259, USA ⟨ jake.mal@gmail.com ⟩

F. Mancilla, University of Texas at Austin, Department of Astronomy, 1 University Station C1400, Austin, TX 78712-0259, USA ⟨ allicnam08@yahoo.com ⟩

Y. Mao, University of Texas at Austin, Department of Astronomy, 1 University Station C1400, Austin, TX 78712-0259, USA ⟨ ymao@astro.as.utexas.edu ⟩

I. Marinova, University of Texas at Austin, Department of Astronomy, 1 University Station C1400, Austin, TX 78712-0259, USA ⟨ marinova@astro.as.utexas.edu ⟩

J. Martinez, University of Texas at Austin, Department of Astronomy, 1 University Station C1400, Austin, TX 78712-0259, USA ⟨ jesusmtz_101@yahoo.com ⟩

R. Matzner, University of Texas at Austin, Department of Astronomy, 1 University Station C1400, Austin, TX 78712-0259, USA ⟨ matzner2@physics.utexas.edu ⟩

E. Mata, University of Texas at Austin, Department of Astronomy, 1 University Station C1400, Austin, TX 78712-0259, USA ⟨ liz_longhorns@yahoo.com ⟩

B. May, University of Texas at Austin, Department of Astronomy, 1 University Station C1400, Austin, TX 78712-0259, USA ⟨ branyon@gmail.com ⟩

S. Meidt, University of New Mexico, 800 Yale Blvd, NE, Albuquerque, NM 87131, USA ⟨ shmeidt@unm.edu ⟩

M. Merello, University of Texas at Austin, Department of Astronomy, 1 University Station C1400, Austin, TX 78712-0259, USA ⟨ manuel@astro.as.utexas.edu ⟩

G. Miller, University of Texas at Austin, Department of Astronomy, 1 University Station C1400, Austin, TX 78712-0259, USA ⟨georgemil@alltel.net⟩

M. Milosavljevic, University of Texas at Austin, Department of Astronomy, 1 University Station C1400, Austin, TX 78712-0259, USA ⟨milos@astro.as.utexas.edu⟩

E. Mok, University of Texas at Austin, Department of Astronomy, 1 University Station C1400, Austin, TX 78712-0259, USA ⟨erazdude@yahoo.com⟩

R. Morbia, University of Texas at Austin, Department of Astronomy, 1 University Station C1400, Austin, TX 78712-0259, USA ⟨rpm2011@gmail.com⟩

J. Murphy, University of Texas at Austin, Department of Astronomy, 1 University Station C1400, Austin, TX 78712-0259, USA ⟨murphy@astro.as.utexas.edu⟩

J. Navarro, University of Victoria, Department of Physics and Astronomy, Victoria, BC V8P 5C2, Canada ⟨jfn@uvic.ca⟩

K. Noeske, Harvard-Smithsonian Center for Astrophysics, 60 Garden Street, MS 65, Cambridge, MA 02138, USA ⟨knoeske@cfa.harvard.edu⟩

M. Nordhaus, University of Texas at Austin, Department of Astronomy, 1 University Station C1400, Austin, TX 78712-0259, USA ⟨nordhaus@astro.as.utexas.edu⟩

G. Orris, University of Texas at Austin, Department of Astronomy, 1 University Station C1400, Austin, TX 78712-0259, USA ⟨argus@astro.as.utexas.edu⟩

O. Pena, University of Texas at Austin, Department of Astronomy, 1 University Station C1400, Austin, TX 78712-0259, USA ⟨pena_adrian@mail.utexas.edu⟩

J. Pounds, University of Texas at Austin, Department of Astronomy, 1 University Station C1400, Austin, TX 78712-0259, USA ⟨brav0babemagnet@aol.com⟩

C. Purcell, The University of California, Department of Physics and Astronomy, Center for Cosmology, Irvine, CA 92697, USA ⟨cpurcell@uci.edu⟩

E. Ramirez, University of Texas at Austin, Department of Astronomy, 1 University Station C1400, Austin, TX 78712-0259, USA ⟨erika_ramirez2869@yahoo.com⟩

J. Rasmussen, Carnegie Observatories, 813 Santa Barbara Street, Pasadena, CA 91101, USA ⟨jr@ociw.edu⟩

N. Reddy, National Optical Astronomy Observatory, 950 N. Cherry Ave., Tucson, AZ 85719, USA ⟨nar@noao.edu⟩

C. Rendon, University of Texas at Austin, Department of Astronomy, 1 University Station C1400, Austin, TX 78712-0259, USA ⟨crendon8@yahoo.com⟩

G. Rhee, University of Nevada Las Vegas, Department of Physics and Astronomy, Las Vegas, NV, USA ⟨grhee@physics.unlv.edu⟩

T. Rindler-Daller,, Institut für Theoretische Physik, Universität zu Köln, Zülpicher Strasse 77, 50937 Cologne, Germany ⟨trd@thp.uni-koeln.de⟩

A. Robaina,, Max-Planck-Institut für Astronomie, Königstuhl 17, D-69117 Heidelberg, Germany ⟨arobaina@mpia.de⟩

M. Rodrigues,, GEPI, Observatoire de Paris, CNRS, Université Paris Diderot, 5 Place Jules Janssen, 92190 Meudon, France ⟨myriam.rodrigues@obspm.fr⟩

B. Rothberg, Naval Research Laboratory, 4555 Overlook Ave SW, Code 7211, Washington D.C. 20375, USA ⟨barry.rothberg@nrl.navy.mil⟩

C. Safranek-Shrader, University of Texas at Austin, Department of Astronomy, 1 University Station C1400, Austin, TX 78712-0259, USA ⟨ctss@astro.as.utexas.edu⟩

S. Salviander, University of Texas at Austin, Department of Astronomy, 1 University Station C1400, Austin, TX 78712-0259, USA ⟨triples@astro.as.utexas.edu⟩

J. Scalo, University of Texas at Austin, Department of Astronomy, 1 University Station C1400, Austin, TX 78712-0259, USA ⟨scalo@astro.as.utexas.edu⟩

M. Scarine, University of Texas at Austin, Department of Astronomy, 1 University Station C1400, Austin, TX 78712-0259, USA ⟨mikeintx@mail.utexas.edu⟩

D. Schiminovich, Columbia University, 550 W. 120 St. MC 5246, NY 10027, USA ⟨ds@astro.columbia.edu⟩

A. Shabi, University of Texas at Austin, Department of Astronomy, 1 University Station C1400, Austin, TX 78712-0259, USA ⟨aeranx@yahoo.com⟩

K. Shapiro, University of California at Berkeley, Department of Astronomy, Berkeley, CA 94720, USA ⟨shapiro@astro.berkeley.edu⟩

P. Shapiro, University of Texas at Austin, Department of Astronomy, 1 University Station C1400, Austin, TX 78712-0259, USA ⟨shapiro@astro.as.utexas.edu⟩

J. Shen, University of Texas at Austin, Department of Astronomy, 1 University Station C1400, Austin, TX 78712-0259, USA ⟨shen@astro.as.utexas.edu⟩

G. Shields, University of Texas at Austin, Department of Astronomy, 1 University Station C1400, Austin, TX 78712-0259, USA ⟨shields@astro.as.utexas.edu⟩

I. Shlosman, University of Colorado, JILA, Boulder, CO 80309, USA ⟨shlosman@pa.uky.edu⟩

M. Sinha, Vanderbilt University, Department of Physics and Astronomy, 6301 Stevenson Center, Nashville, TN 37235, USA ⟨manodeep.sinha@vanderbilt.edu⟩

R. Skelton,, Max-Planck-Institut für Astronomie, Königstuhl 17, D-69117 Heidelberg, Germany ⟨skelton@mpia.de⟩

J. Smith, University of Texas at Austin, Department of Astronomy, 1 University Station C1400, Austin, TX 78712-0259, USA ⟨jamiesmith2008@gmail.com⟩

J. Sosa, University of Texas at Austin, Department of Astronomy, 1 University Station C1400, Austin, TX 78712-0259, USA ⟨jacquelynnsosa@mail.utexas.edu⟩

A. Stacy, University of Texas at Austin, Department of Astronomy, 1 University Station C1400, Austin, TX 78712-0259, USA ⟨minerva@astro.as.utexas.edu⟩

K. Stewart, The University of California at Irvine, Department of Physics and Astronomy, Center for Cosmology, Irvine, CA 92697, USA ⟨StewartK@uci.edu⟩

C. Tremonti, Max Planck Institut fur Astronomie, Konigstuhl 17, D-69117 Heidelberg, Germany ⟨tremonti@mpia-hd.mpg.de⟩

J. Umbarger, University of Texas at Austin, Department of Astronomy, 1 University Station C1400, Austin, TX 78712-0259, USA ⟨jimum@astro.as.utexas.edu⟩

R. van den Bosch,, Department of Astronomy, The University of Texas at Austin, Austin, TX 78712, USA ⟨bosch@astro.as.utexas.edu⟩

A. Weijmans,, Leiden University, Sterrewacht Leiden, Leiden University, Postbus 9513, 2300 RA Leiden, Netherlands ⟨weijmans@strw.leidenuniv.nl⟩

T. Weinzirl, University of Texas at Austin, Department of Astronomy, 1 University Station C1400, Austin, TX 78712-0259, USA ⟨imw@astro.as.utexas.edu⟩

M. Williams, University of Oxford, Department of Astrophysics, Denis Wilkinson Building, Oxford, Oxfordshire OX1 3RH, United Kingdom ⟨williams@astro.ox.ac.uk⟩

B. Wills, University of Texas at Austin, Department of Astronomy, 1 University Station C1400, Austin, TX 78712-0259, USA ⟨bev@astro.as.utexas.edu⟩

D. Winegarten, University of Texas at Austin, Department of Astronomy, 1 University Station C1400, Austin, TX 78712-0259, USA ⟨winegarten@astro.as.utexas.edu⟩

D. Winget, University of Texas at Austin, Department of Astronomy, 1 University Station C1400, Austin, TX 78712-0259, USA ⟨dew@astro.as.utexas.edu⟩

M. J. Wolf, University of Wisconsin-Madison, Department of Astronomy, 475 N. Charter Street, Madison, WI 53706, USA ⟨mwolf@astro.wisc.edu⟩

P. Yoachim, University of Texas at Austin, Department of Astronomy, 1 University Station C1400, Austin, TX 78712-0259, USA ⟨yoachim@astro.as.utexas.edu⟩

I. Yoon, University of Massachusetts, Department of Astronomy, Amherst, MA, USA ⟨ iyoon@astro.umass.edu ⟩

Part I

Assembly of Disks, Bulges, and Ellipticals

GALAXY EVOLUTION: EMERGING INSIGHTS AND FUTURE CHALLLENGES
ASP Conference Series, Vol.
@jourvol, © 2009
S. Jogee, I. Marinova, L. Hao, and G. A Blanc

Galactic Disk Formation and the Angular Momentum Problem

Andreas Burkert
University Observatory Munich, Scheinerstr. 1, D-81679 Munich, Germany

Abstract. Galactic disk formation requires knowledge about the initial conditions under which disk galaxies form, the boundary conditions that affect their secular evolution and the micro-physical processes that drive the multi-phase interstellar medium and regulate their star formation history. Most of these ingredients are still poorly understood. Recent high-resolution observations of young high-redshift disk galaxies provide insight into early phases of galactic disk formation and evolution. Combined with low-redshift disk data these observations should eventually allow us to reconstruct the origin of and evolution of the late-type galaxies. I will summarize some of the major problems that need to be addressed for a more consistent picture of galactic disk formation and evolution.

1. Initial and Boundary Conditions: The Cosmological Angular Momentum Problem

Galaxy formation to some extent is an initial condition problem. Whether a galactic disk can form at all depends on the amount of angular momentum present in the infalling gas. The disk structure is determined by the gravitational potential of the baryonic and dark component of the galaxy and the specific angular momentum distribution of the fraction of infalling gas that can cool and dissipate its potential and kinetic energy while settling into centrifugal equilibrium in the equatorial plane. Once a massive disk has formed and on timescales longer than the infall timescale secular disk evolution will become important, resulting in angular momentum redistribution of gas and stars in the disk by viscous effects and gravitational torques, coupled with star formation and selective gas loss in galactic winds (Kormendy & Kennicutt 2004).

The origin of angular momentum is generally believed to be cosmological. Before and during the early phase of protogalactic collapse, gas and dark matter are well mixed and therefore acquire a similar specific angular momentum distribution (Peebles 1969; Fall & Efstathiou 1980; White 1984). If angular momentum would be conserved during gas infall, the resulting disk size should be directly related to the specific angular momentum λ' of the surrounding dark halo where (Bullock et al. 2001)

$$\lambda' = \frac{J}{\sqrt{2} M_{\rm vir} V_{\rm vir} R_{\rm vir}} \qquad (1)$$

with $R_{\rm vir}$ and $V_{\rm vir}^2 = GM_{\rm vir}/R_{\rm vir}$ the virial radius and virial velocity of the halo, respectively, and $M_{\rm vir}$ its virial mass. Adopting a flat rotation curve, the disk scale length is (Mo et al. 1998; Burkert & D'Onghia 04)

$$R_{\rm d} \approx 8 \left(\frac{\lambda'}{0.035}\right) \left(\frac{H_0}{H}\right) \left(\frac{v_{\rm max}}{200 \text{ km s}^{-1}}\right) \text{kpc} \tag{2}$$

where $v_{\rm max}$ is the maximum rotational velocity in the disk and H is the Hubble parameter that depends on cosmological redshift z as

$$H = H_0 \left[\Omega_\Lambda + \Omega_M (1+z)^3\right]^{1/2}. \tag{3}$$

Typical values for a standard ΛCDM cosmology are $H_0 = 73$ km s^{-1} Mpc^{-1}, $\Omega_M = 0.238$ and $\Omega_\Lambda = 0.762$.

The upper panel of Figure 1 shows the correlation between the disk scale length $R_{\rm disk}$ and the maximum rotational velocity $v_{\rm max}$ for massive spiral galaxies (Courteau 1997) There is a linear relationship which can be fitted well by $\lambda' = 0.025$ which is somewhat smaller than the theoretically predicted value of $\lambda' = 0.035$, indicating that the gas could on average have lost some amount of angular momentum during the infall phase.

This result is promising. The situation is however more confusing if we look at the recent high-resolution observations of $z = 2$ star forming disk galaxies (Förster-Schreiber et al. 2006, 2009; Genzel et al. 2006, 2008; Cresci et al. 2009, Burkert et al. 2009). In contrast to their low-redshift counterparts, the high-z galaxies are characterized by high gas velocity dispersions of $\sigma \approx 40 - 80$ km s^{-1} In addition, the sample segregates strongly into two distinct classes at a critical value of $v_{\rm max}/\sigma \approx 3$. One can empirically define dispersion-dominated galaxies as objects with $v_{\rm max}/\sigma \leq 3$ while rotation-dominated galaxies are defined by $v_{\rm max}/\sigma > 3$. The lower panel of Figure 1 shows the half-light radii $r_{1/2}$ of the SINS high-redshift galaxies versus their maximum rotational velocity $v_{\rm max}$. Most of the dispersion-dominated galaxies (open triangles in Figure 1) have radii of order 1-2 kpc and rotational velocities of order 100 km s^{-1} while the radii and rotational velocities of the rotation dominated galaxies (filled triangles) are on average a factor of 2-3 larger. The correlation between scale length and velocity of this sample is however very similar to the low-redshift galaxies. According to equation (1), this requires a factor 3-4 larger spin parameter (dashed curves in the lower panel of Figure 1) for high-redshift disks as a result of the fact that at $z = 2$ the dark halo virial radii are a factor 3-4 smaller. Burkert et al. (2009) argue that this could be explained by turbulent pressure effects in the disk and a less centrally concentrated dark halo component that did not experience adiabatic contraction during disk formation.

Simulations of galactic disk formation suffer often from catastrophic angular momentum loss which leads to disks with unreasonably small scale lengths and surface densities that are too large. The origin might be strong clumping of the infalling gas, which loses angular momentum by dynamical friction within the surrounding dark matter halo (Navarro & Benz 1991, Navarro & Steinmetz 2000), low numerical resolution (Governato et al. 2004, 2007), substantial and major mergers (d'Onghia et al. 2006) and artificial secular angular momentum transfer from the cold disk to its hot surrounding (Okamoto et al. 2003). It has

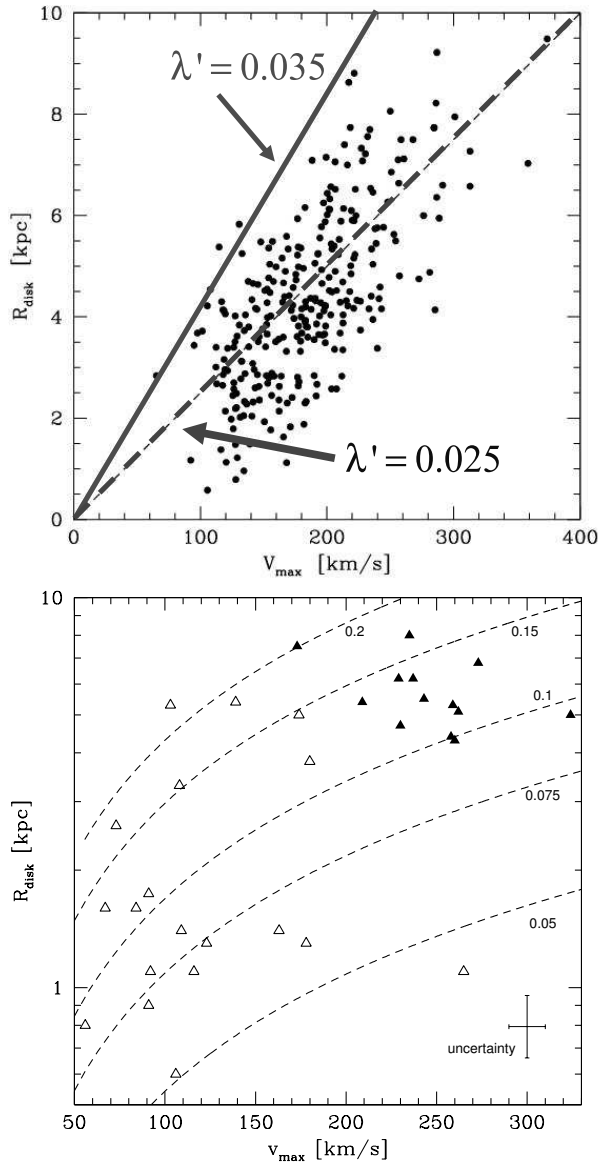

Figure 1. The upper panel shows the observed scale lengths versus the maximum rotational velocities of galactic disks for the Courteau (1997) sample. The solid line shows the theoretically predicted correlation for $\lambda' = 0.035$. The dashed curve corresponds to $\lambda' = 0.025$. The lower panel shows the disk scale length versus the maximum velocity of the SINS high-redshift disk sample. Open and filled triangles correspond to dispersion-dominated and rotation-dominated galaxies, respectively. Note that here the vertical axis is plotted logarithmically for better resolution of the dispersion-dominated galaxies. Dashed curves show the Mo, Mao & White models with spin parameters as indicated by the labels.

been argued that this problem might be solved by including star formation and energetic feedback (e.g. Sommer-Larsen et al. 2003, Abadi et al. 2003, Springel & Hernquist 2003, Robertson et al. 2004, Oppenheimer & Dave 2006, Dubois & Teyssier 2008). No reasonable, universally applicable feedback prescription has however yet been found that would lead to the formation of large-sized, late-type disks, not only for special cases, but in general.

Recently Zavala et al. (2008) showed that the specific angular momentum distribution of the disk forming material follows closely the angular momentum evolution of the dark matter halo. The dark matter angular momentum grows at early times as a result of large-scale tidal torques, consistent with the prediction of linear theory and remains constant after the epoch of maximum expansion. During this late phase angular momentum is redistributed within the dark halo with the inner dark halo regions losing up to 90% of their specific angular momentum to the outer parts which is probably related to minor mergers with mass ratios less than 10:1. It is then likely that any gas residing in the inner regions during such an angular momentum redistribution will also lose most of its angular momentum, independent of whether the gas resides already in a protodisk, is still confined to dark matter substructures or is in an extended, diffuse distribution. Zavala et al. (2008) (see also Okamoto et al., 2005 and Scannapieco et al., 2008) show that efficient heating of the gas component can prevent angular momentum loss, probably because most of the gaseous component resides in the outer parts of the dark halo during its angular momentum redistribution phase. The gas would then actually gain angular momentum rather than lose it and could later on settle smoothly into an extended galactic disk in an ELS-like (Eggen, Lynden-Bell & Sandage 1962) accretion phase.

Little is known about the energetic processes that could lead to such an evolution. Obviously, star formation must be delayed during the protogalactic collapse phase in order for the gas to have enough time to settle into the plane before condensing into stars. However star formation is also required in order to heat the gas, preventing it from collapsing prior to the angular momentum redistribution phase. Scannapieco et al. (2008) show that their supernova feedback prescription is able to regulate star formation while at the same time pressurizing the gas. Their models are however still not efficient enough in order to produce disk-dominated, late-type galaxies. Large galactic disks are formed. The systems are however dominated by a central, massive, low-angular momentum stellar bulge component. This is in contradiction with observations which indicate a large fraction of massive disk galaxies with bulge-to disk ratios smaller than 50% (Weinzirl et al. 2009) that cannot be produced currently by numerical simulations of cosmological disk formation.

2. Energetic Feedback and Star Formation

As argued in the last section star formation and energetic feedback plays a dominant role in understanding the origin and evolution of galactic disks and in determining the morphological type of disk galaxies. Scannapieco et al. (2008) for example demonstrate that the same initial conditions could produce either an elliptical or a disk galaxy, depending on the adopted efficiency of gas heating during the protogalactic collapse phase. A consistent model of the structure and

evolution of the multi-phase, turbulent interstellar medium and its condensation into stars is still missing. This situation is however improving rapidly due to more sophisticated numerical methods and fast computational platforms that allow us to run high-resolution models, incorporating a large number of possibly relevant physical processes (Wada & Norman 2002, Krumholz & McKee 2005, Tasker & Bryan 2008, Robertson & Kravtsov 2008).

Cosmological simulations often adopted simplified observationally motivated descriptions of star formation that are based on the empirical Kennicutt relations (Kennicutt 1998, 2007) that come in two different version. The first relation (K1) represents a correlation between the star formation rate per surface area $\Sigma_{\rm SFR}$ and the gas surface density $\Sigma_{\rm g}$, averaged over the whole galaxy

$$\Sigma_{\rm SFR}^{(K1)} = 2.5 \times 10^{-4} \left(\frac{\Sigma_{\rm g}}{M_\odot/{\rm pc}^2} \right)^{1.4} \frac{M_\odot}{{\rm kpc}^2 \ {\rm yr}} \tag{4}$$

The second relation (K2) includes a dependence on the typical orbital period $\tau_{\rm orb}$ of the disk

$$\Sigma_{\rm SFR}^{(K2)} = 0.017 \left(\frac{\Sigma_{\rm g}}{M_\odot/{\rm pc}^2} \right) \left(\frac{10^8 yrs}{\tau_{\rm orb}} \right) \frac{M_\odot}{{\rm kpc}^2 \ {\rm yr}}. \tag{5}$$

These relationships have been derived from observations as an average over the whole disk. They are however often also used as theoretical prescriptions for the local star formation rate which appears observationally justified if the total gas surface densitiy $\Sigma_{\rm g}$ is replaced by the local surface density of molecular gas. The origin of both relationships is not well understood yet. One can combine K1 and K2 and derive a relationship between the average gas density in galactic disks and their orbital period

$$\Sigma_{\rm g} \sim \tau_{\rm orb}^{-2.5} \sim \left(\frac{v_{\rm rot}}{R_{\rm disk}} \right)^{2.5} \tag{6}$$

where $v_{\rm rot}$ and $R_{\rm disk}$ are the rotational velocity and the size of the galactic disk, respectively. This result is puzzling as it is not clear why the kinematical properties of galactic disks should correlate with their gas surface densities especially in galaxies of Milky Way type or earlier where the gas fraction is small compared to the mass in stars (see e.g. Robertson & Kravtsov 2008).

3. Secular Evolution and Turbulence in Galactic Disks

Dark halos have a universal angular momentum distribution that should also be characteristic for the infalling gas component (Bullock et al 2001). Van den Bosch et al. (2001) lateron showed that this angular momentum distribution is not consistent with the observed distribution of exponential galactic disks. One possibility is angular momentum redistribution during filamentary cold gas infall (Dekel et al. 2009). Another suggestion is viscous disk evolution. The viscosity is likely driven by interstellar turbulence which is a result of stellar energetic feedback processes or global disk instabilities (magneto-rotational instability or gravitational instability). Viscous effects will however increases the

angular momentum problem substantially as viscosity in general removes angular momentum from the dominante mass component in the disk and transfers it to the outermost parts of the disk.

Slyz et al. (2002) studied the viscous formation of exponential stellar disks from gas disks with various different surface density distributions. Their numerical simulations show that exponential disks form if the star formation timescale is of order the viscous timescale. Genzel et al. (2008) derive a timescale for turbulent viscosity in galactic disks of (see also Dekel et al. 2009)

$$\tau_{\rm visc} = \frac{1}{\alpha}\left(\frac{v_{\rm rot}}{\sigma}\right)^2 \tau_{\rm orb} \tag{7}$$

where α is of order unity. $\tau_{\rm visc} \approx 10^{10}$ yrs for disks like the Milky Way with $\sigma \approx$ 10-20 km s^{-1} and self-regulated low star formation rates. $z \sim 2$ star forming disk galaxies on the other hand are characterized by large random gas motions of order 40 km s^{-1} to 80 km s^{-1} and viscous timescales of less than 10^9yrs (Genzel et al., 2006, 2008, Förster-Schreiber et al. 2006). Inte restingly, for these objects, the star formation timescales are again similar to the viscous timescale, leading to star formation rates of 100 $M_\odot$ yr^{-1} and confirming that galactic disk gas turbulence, star formation and secular evolution are intimately coupled.

Burkert et al. (2009) find a good correlation between the observed irregular gas motion in high-redshift disk galaxies and the theoretically expected gas velocity dispersion, adopting a Toomre Q parameter of unity. This is expected if the main driver of clumpiness and turbulence is gravitational disk instability. A disk that is kinematically too cold with small velocity dispersions is highly gravitationally unstable. Gravitational instabilites generate density and velocity irregularities that drive turbulence and heat the system kinematically. The gas velocity dispersion increases till it approaches the stability limit characterised by Q=1 where kinetic driving by gravitational instabilities saturates. A disk with even higher velocity dispersions would be stable, turbulent energy would dissipate efficiently and the velocity dispersion would decrease again until it crosses the critical velocity dispersion limit at Q=1 where gravitational instabilities become efficient again in driving turbulent motions. More simulations are required to investigate this process in greater details.

4. Summary

Many complex non-linear processes affect galactic disk formation and evolution. We are still in an early stage of understanding these processes. One of the most interesting questions is how the observations of high-redshift disk galaxies can be combined with galaxies in the local universe. The high-z disks generate stellar systems with high velocity dispersions that resemble more rotating early-type or S0 galaxies than Milky-Way type objects. Where are then the progenitors of present-day disks? In addition, why did their progenitors evolve differently with respect to the observed high-z galaxies? How do bulge-less disk galaxies form? Given the recent progress both in observations and theoretical modelling the time seems ripe to solve these questions.

Acknowledgments. I would like to thank Shardha Jogee for inviting me to this interesting conference, her great hospitality and for financial support.

References

Abadi, M.G., Navarro, J.F., Steinmetz, M. & Eke, V.R. 2003, ApJ, 591, 499
Bournaud, F., Elmegreen, B.G. & Elmegreen, D.M. 2007, ApJ, 670, 237
Bullock, J.S., Dekel, A., Kolatt, T.S., Kravtsov, A.V., Klypin, A.A., Porciani, C. & Primack, J.R. 2001, ApJ, 555, 240
Burkert,A. & d'Onghia, E. 2004, in Penetrating Bars through Masks of Cosmic Dust: The Hubble Tuning Fork Strikes a New Note, eds. D.L. Block, I. Puerari, K.C. Freeman, R. Groess and E.K. Block, ASSL 319, 341
Burkert,A. et al. 2009, arXiv:0907.4777
Cresci, G. et al. 2009, ApJ, in press.
Courteau, S. 1997, AJ, 114, 2402
Dekel, A., et al. 2009, Nat, 457, 451
Dekel, A., Sari, R. & Ceverino,D. 2009, arXiv:0901.2458
Dubois, Y., Teyssier, R. 2008, AA, 477, 79
D'Onghia, E., Burkert, A., Murante, G. & Khochfar, S. 2006, MNRAS, 372, 1525
Eggen, O.J., Lynden-Bell, D. & Sandage, A.R. 1962, ApJ, 136, 748
Fall, S.M. & Efsthatiou, G. 1980, MNRAS, 193, 189
Förster Schreiber, N. M., et al. 2006, ApJ, 645, 1062
Förster-Schreiber, N.M. et al. 2009, ApJ, in press
Genzel, R. et al. 2006, Nature, 442, 786
Genzel,R. et al. 2008, Apj, 687, 59
Governato, F. et al. 2004, ApJ, 607, 688
Governato, F. et al. 2007, MNRAS, 374, 1479
Kennicutt, R.C. 1998, ApJ, 498, 541
Kennicutt, R.C. et al. 2007, ApJ, 671, 333
Kormendy, J., & Kennicutt, R. C., Jr. 2004, ARA&A, 42, 603
Krumholz, M.R. & McKee, C.F. 2005, ApJ, 630, 250
Mo, H.J., Mao, S. & White, S.D.M. 1998, MNRAS, 295, 319
Navarro, J. & Benz, W. 1991, ApJ, 380, 320
Navarro, J. & Steinmetz, M. 2000, ApJ, 538, 477
Okamoto, T., Jenkins, A., Eke, V.R., Quilis, V. & Frenk, C.S. 2003, MNRAS, 345, 429
Okamoto, T., Eke, V.R., Frenk, C.S. & Jenkins, A. 2005, MNRAS, 363, 1299
Oppenheimer, B.D. & Dave, R. 2006, MNRAS, 373, 1265
Peebles, P.J.E. 1969, ApJ, 155, 393
Robertson, B., Yoshida, N., Springel, V. & Hernquist, L. 2004, ApJ, 606, 32
Robertson, B. & Kravtsov, A.V. 2008, ApJ, 680, 1083
Scannapieco, C., Tissera, P.B., White, S.D.M. & Springel, V. 2008, MNRAS, 389, 1137
Slyz, A.D., Devriendt, J.E.G., Silk, J. & Burkert,A. 2002, MNRAS, 333, 894
Sommer-Larsen, J., Götz, M., & Portinari, L. 2003, ApJ, 596, 47
Springel, V. & Hernquist, L. 2003, MNRAS, 339, 289
Tasker, E.J. & Bryan, G.L. 2008, ApJ, 673, 810
Van den Bosch, F.C., Burkert, A. & Swaters, R.A. 2001, MNRAS, 326, 1205
Wada, K., & Norman, C.A. 2007, ApJ, 660, 276
Weinzirl, T., Jogee, S., Khochfar, S., Burkert, A., & Kormendy, J. 2009, ApJ, 696, 411
White, S.D.M. 1984, MNRAS, 286, 38
Zavala, J., Okamoto, T., & Frenk, C.S. 2008, MNRAS, 387, 839

GALAXY EVOLUTION: EMERGING INSIGHTS AND FUTURE CHALLLENGES
ASP Conference Series, Vol.
@jourvol, © 2009
S. Jogee, I. Marinova, L. Hao, and G. A Blanc

Disk Galaxies at z=2 in OWLS

Julio F. Navarro[1], Laura V. Sales[2] & the OWLS team

[1] *Department of Physics and Astronomy, University of Victoria, Victoria, BC V8P 5C2, Canada*
[2] *Kapteyn Astronomical Institute, P.O. Box 800, Groningen, The Netherlands*

Abstract. We use the OWLS (OverWhelmingly Large Simulations) set of cosmological Nbody/gasdynamical simulations to study the properties of simulated galaxies at $z = 2$. We focus on the effect of feedback from evolving stars on the baryonic mass and angular momentum content of galaxies that assemble at the center of 10^{11}-$10^{12}\,h^{-1}M_\odot$ halos. Our main finding is that the mass and angular momentum of such galaxies are strongly coupled, in a way that is approximately independent of feedback: varying the feedback strength leads, in a given halo, to large variations in galaxy mass but leaves the galaxy mass-angular momentum correlation largely unaltered. In particular, the ratio between the angular momentum of a galaxy and that of its surrounding halo ($j_d = J_{\rm gal}/J_{\rm vir}$) correlates closely with the galaxy mass (expressed in units of the virial mass of the halo; $m_d = M_{\rm gal}/M_{\rm vir}$). This correlation differs substantially from the $m_d = j_d$ assumption commonly adopted in semianalytic models of galaxy formation. We use these results to infer the sizes of disk galaxies at $z = 2$ expected in the LCDM scenario and to interpret recent observations of extended disks at $z \sim 2$ by the SINS collaboration.

1. Introduction

It is widely thought that the properties of disk galaxies formed hierarchically (as expected in the prevailing LCDM paradigm) are largely determined by the properties of the dark matter halos in which they form. In this scenario, the scaling laws linking various disk galaxy properties, such as their mass, size, and rotation speed, simply reflect analogous correlations between the mass, spin, and potential depth of their surrounding halos (see, e.g., Navarro & Steinmetz 2000). Since the correlations linking various halo properties have been studied extensively through N-body simulations, the presumed association between disk and halo scaling laws enables a host of predictions for the properties of disk galaxies and their evolution with redshift. The general analytical framework has been developed in some detail by Mo, Mao & White (1998, hereafter MMW98), who showed that a number of properties of the present-day disk population may be reproduced with well-motivated choices for the small number of free parameters in the model.

One important prediction of this modeling is that, at fixed rotation speed, disk galaxies should become smaller with increasing redshift. This prediction has come recently under scrutiny given the results of the SINS collaboration, who report the discovery of a population of extended disk galaxies at $z = 2$

(Genzel et al. 2006, Förster Schreiber et al. 2006). In some cases, these galaxies have rotation speeds comparable to L_* disks today and are as extended as their $z = 0$ counterparts. This in apparent contradiction with the predictions of the MMW98 modeling, unless these galaxies are embedded in halos with unusually high angular momentum (Bouché et al. 2007).

The interpretation of this disagreement is unclear, however, because N-body/gasdynamical simulations of galaxy formation have shown that a number of the assumptions made in the MMW98 model are not readily verified in the simulations. In particular, the mass and angular momentum of galaxies assembled hierarchically are not simple functions of the mass and spin of their surrounding halos (Navarro & Steinmetz 1997, 2000). The time of collapse; the importance of mergers; the feedback from evolving stars; all of these effects can alter dramatically the simple correspondence between galaxies and host halos envisioned in semianalytic models (Okamoto et al. 2005; Robertson et al. 2006; Governato et al 2007). As a result, it is unclear whether the extended disks observed by the SINS collaboration present a challenge for the LCDM paradigm or whether they may be accommodated by reasonable tuning of the model free parameters.

We address these issues here using simulated galaxies selected from the OverWhelmingly Large Simulations (OWLS) project. We use these simulations to examine the relation between mass and angular momentum (and its dependence on feedback) in $z = 2$ galaxies assembled in the LCDM scenario. We use these results to validate the MMW98 model and to compare with the results from the SINS collaboration.

2. The numerical simulations

The OverWhelmingly Large Simulation (OWLS) project is a collection of roughly 50 Nbody/gasdynamical cosmological simulations of representative volumes in an LCDM universe. The various OWLS runs explore systematically the effect on the simulated galaxy population of varying numerical resolution, star formation laws, cooling function, sub-grid physics, and feedback recipes.

We select for this study four different OWLS runs that differ from each other only in the way feedback from evolving stars is implemented. Each run follows the evolution of 512^3 dark mater and 512^3 gas particles in a $25\,h^{-1}$Mpc box. The mass per particle in these runs is $\sim 6\times10^6\,h^{-1}M_\odot$ for the dark matter and six times lower for the baryons. Gas is allowed to cool radiatively, and to turn into stars in a manner consistent with an empirically calibrated Schmidt-Kennicutt law. Feedback energy from evolving stars is incorporated assuming that a fixed fraction of the available energy is channelled into bulk motions of the gas particles in order to mimic feedback-driven "winds" outflowing from regions of active star formation. The main differences between runs are the choices made for the wind velocity (V_w) and mass loading (μ) factor. The parameter μ specifies the number of gas particles among which the feedback kinetic energy is split, whereas V_w characterizes the outflow velocity of the wind particles.

As expected, the effects of feedback (in terms of how effectively it regulates star formation and/or removes gas from galaxies) decrease with increasing μ and decreasing V_w, respectively. We refer to each of the 4 runs, in order of

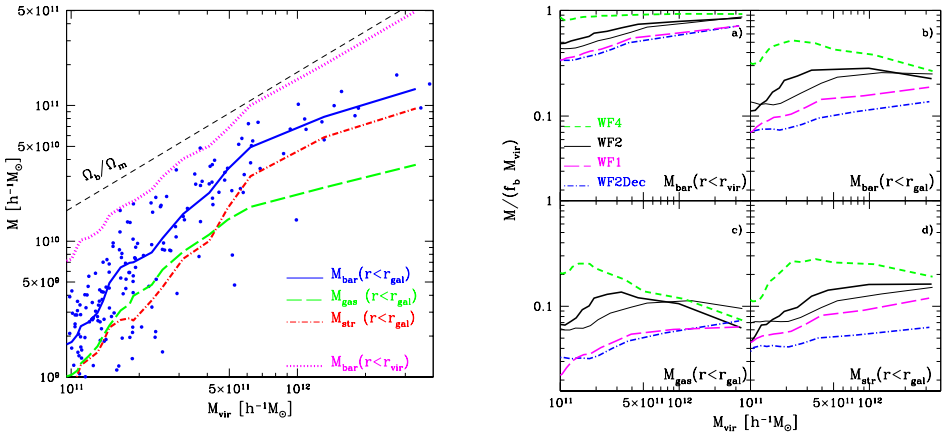

Figure 1. *Left:* Galaxy mass as a function of halo virial mass for galaxies in the WF2 run. The various curves are described in the text, and trace medians in equal-number bins of virial mass. Dot-dashed, dashed, and solid lines correspond to stars, gas and all baryons (=gas+stars), respectively. Individual values are shown for the gas+stars case, in order to illustrate the halo-to-halo scatter. *Right:* Galaxy mass in units of the total baryon mass of the halo. Different curves in each panel correspond to runs with different feedback strengths. Clockwise from the top left, each panel shows (a) the baryonic mass within the virial radius; (b) the baryonic mass in the central galaxy (i.e., within $r_{\rm gal}$); (c) the stellar mass within $r_{\rm gal}$, and (d) the gaseous mass within $r_{\rm gal}$. The thin solid line correspond to a run with the same parameters as WF2 but with 8 times fewer particles, a good indicator of numerical convergence.

increasing overall feedback strength, as: WF4 ($\mu = 4$ particles and $V_w = 424$ km/s), WF2 ($\mu = 2$ and $V_w = 600$ km/s), WF1 ($\mu = 1$ and $V_w = 848$ km/s) and WF2Dec. The latter is equivalent to WF2 but "wind" particles are temporarily decoupled from the hydrodynamical equations (see Dalla Vecchia & Schaye 2008 for details).

Our simulated galaxy sample consists of all galaxies assembled (at $z = 2$) at the centers of dark halos in the mass range $\rm M_{vir} = 10^{11}$ to $3\times10^{12}\,h^{-1}M_\odot$. These halos contain between $50,000$ and $500,000$ particles within the virial radius (defined as the radius where the mean inner density is $\Delta = 178$ times the critical density of the universe at $z = 2$). The gravitational softening is $0.5\,h^{-1}$kpc (physical). With these definitions, the simulated galaxy sample in each run contains roughly ~ 170 objects.

3. Results

3.1. Mass and angular momentum content

The left panel of Figure 2 shows, as a function of halo virial mass, the baryonic mass in various components for galaxies identified in the WF2 run. The (top) dashed straight line indicates the baryon mass associated with each halo through the universal baryon fraction $f_b = \Omega_b/\Omega_{\rm M}$. The bottom four curves show the baryon mass in different regions of the halo. The dotted line corresponds to all

baryons within $r_{\rm vir}$. This shows that halos at the high-mass end of the considered range are able to retain all baryons but that those at the low mass end have experienced a net loss of about $\sim 50\%$ of their baryons. This illustrates the decreasing efficiency of feedback-driven winds in the deeper potential wells of more massive halos.

The effect is even more pronounced when considering the total amount of baryons locked in the central galaxy (i.e., those within $r_{\rm gal} = 0.1\, r_{\rm vir}$ from the halo centre). The dots in the left panel of Figure 2 show that the total baryon mass of the central galaxy is not simply proportional to the halo mass. The relation has substantial scatter and it varies systematically as a function of $M_{\rm vir}$. (All curves in this plot trace the median in equal-number bins of virial mass.) At low $M_{\rm vir}$ central galaxies collect on average only about 10% of the baryon mass associated with the halo through the universal baryon fraction. This fraction rises to almost 50% for $6 \times 10^{11} h^{-1} M_\odot$ halos, but appears to decline in more massive halos.

The decline at the high-mass end is likely a result of the longer cooling times characteristic of massive halos, which hinder the assembly of massive central galaxies. The bottom two curves indicate how the baryon mass of central galaxies splits into gas (dashed) and stars (dot-dashed). Gas and stars contribute about equally at low masses, but central galaxies in high-mass halos are predominantly stellar. This is presumably a result of the inability of feedback to delay or prevent the efficient conversion of gas into stars in halos with a deep potential well. The effect on these trends of different feedback prescriptions may be seen on the right panel of Figure 2. Clearly, variations in feedback strength have a large effect on the mass (and gas fraction) of central galaxies. In low mass halos (e.g., $M_{\rm vir} \sim 2 \times 10^{11} h^{-1} M_\odot$) WF4 and WF2Dec galaxies differ by more than a factor of 5, illustrating the wide range of feedback strength surveyed in the OWLS simulations.

The left panel of Figure 2 shows the *specific* angular momentum as a function of halo mass for various components in the WF2 galaxy sample. The dark matter angular momentum scales roughly as $j_{\rm drk} \propto M^{2/3}$; the expected scaling for systems with similar dimensionless spin parameter λ. This scaling is followed closely by all baryons within the virial radius (dotted line), a result that illustrates the fact that both baryons and dark matter were torqued and spun by the same amount during the early expansion phase of each system (see, e.g., Navarro et al 2004).

By comparison, the baryons in the central galaxies have much lower specific angular momentum; a factor of ~ 3 lower on average (solid curve and dots in the left panel of Figure 2). It is also clear from this figure that the gas (dashed curve) has typically higher angular momentum than the stars (dot-dashed). This reflects the higher efficiency of transformation of gas into stars in the central (denser) regions of a galaxy and implies that gaseous disks will be, on average, larger than stellar ones. As we discuss below, it is important to take this effect into account when comparing theoretical predictions with observations.

These trends are common to all our feedback implementations, as may be verified by inspecting the right panel of Figure 2. Note, however, that feedback-driven winds tend to remove predominantly low-angular momentum baryons. Indeed, compare, at given halo mass, the central galaxy masses (top-right panel of Figure 2) and spins (top right panel of Figure 2) of models WF4 and WF2Dec,

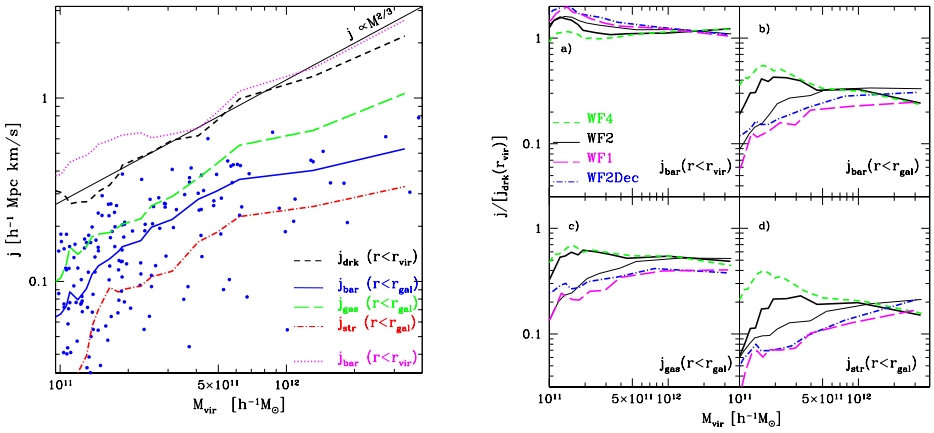

Figure 2. *Left:* Specific angular momentum (j) as a function of halo virial mass in the WF2 galaxy sample. Line types are as in Figure 2. The dashed black curve shows that the specific angular momentum of the dark halo scales roughly as $M^{2/3}$, as expected for systems with constant dimensionless spin parameter λ. The bottom curves show the specific angular momentum of stars (red dot-dashed), gas (green long-dashed) and all baryons (blue solid) within $r_{\rm gal}$. The mean angular momentum of all baryons within the virial radius ($j_{\rm bar}(r < r_{\rm vir})$) is shown in magenta dotted line. *Right:* Specific angular momentum of various components expressed in units of the halo's, as a function of halo virial mass. Different lines in each panel correspond to various feedback prescriptions, as described in the caption to Figure 2.

our two extreme feedback runs. For example, in high-mass halos the baryonic mass of the central galaxy varies by a factor of 2-3 but its specific angular momentum remains largely unchanged. This implies that it is low-angular momentum baryons that are most efficiently removed by feedback-driven winds (see also Dutton & van den Bosch 2008).

This non-linear interplay between mass and spin of the baryons that are assembled into central galaxies is explored in Figure 3, where we show the galaxy's mass ($m_d = {\rm M_{gal}/M_{vir}}$) and angular momentum ($j_d = J_{\rm gal}/J_{\rm vir}$), each expressed in units of the corresponding halo values. Semianalytic models of galaxy formation typically assume that the specific angular momentum of the central galaxy is similar to that of its host halo' i.e., that $m_d = j_d$. In the MMW98 formalism, these parameters enable prediction of the exponential scalelength of a disk galaxy once the virial radius ($r_{\rm vir}$) and spin parameter (λ) of a halo are specified,

$$R_d = (2f_c)^{-1/2}(j_d/m_d)\,\lambda\, r_{\rm vir}\, f_R(j_d, m_d, c, \lambda), \qquad (1)$$

and where f_R and f_c are factors that account for the concentration and "contraction" of the dark halo.

The m_d-j_d relation in our simulations is shown in Figure 3, where each panel corresponds to a different feedback implementation. A few things are worth noting in this figure. (i) Simulated galaxies deviate strongly from the $m_d = j_d$ line, which assumes that galaxies and halos have the same specific angular momentum (i.e., $j_{\rm gal} = j_{\rm drk}$). (ii) The scatter in the relation is large, and in every

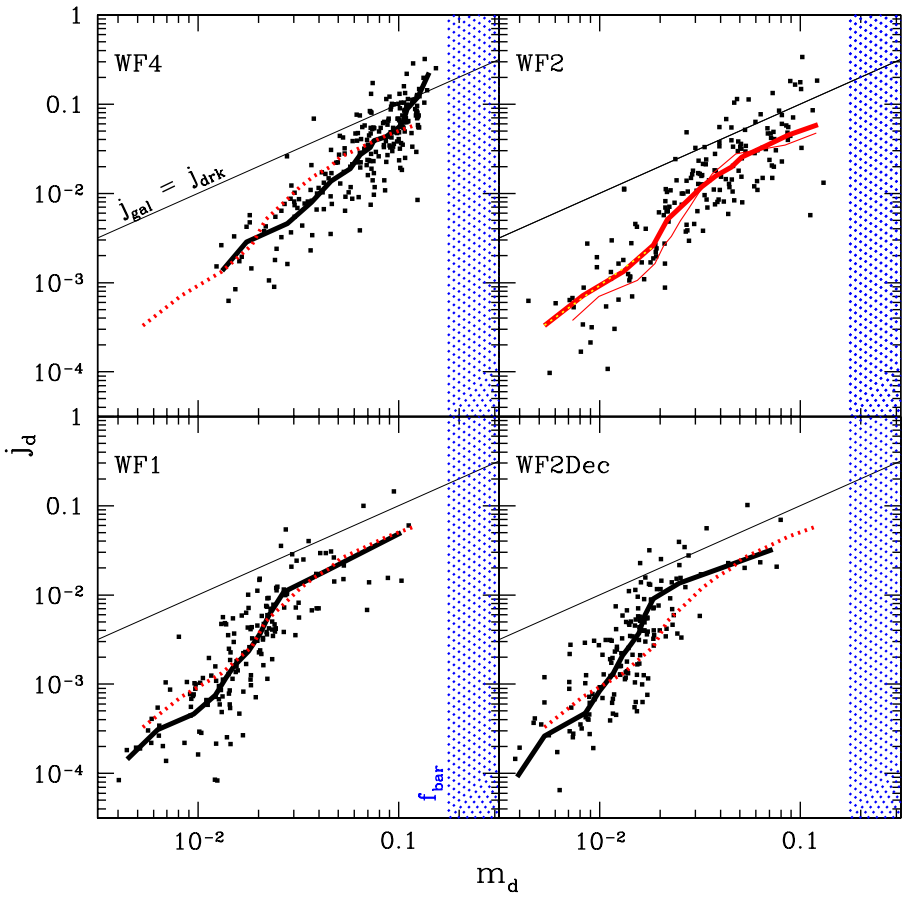

Figure 3. Baryonic mass $m_d = M_{\rm gal}/M_{\rm vir}$ and angular momentum $j_d = J_{\rm gal}/J_{\rm vir}$ of central galaxies, in units of the halo virial mass and angular momentum. Each panel corresponds to a different feedback prescription. Thick lines in each panel show the median j_d in equal-number m_d bins for each run. (The thin line in the WF2 panel corresponds to a similar simulation with 8 times fewer particles.) The red dotted line, corresponding to WF2, is repeated all panels, and highlights our result that the m_d-j_d relation is approximately independent of feedback strength.

panel there are cases where $j_{\rm gal} > j_{\rm drk}$. These are galaxies where feedback has been able to push out a substantial fraction of low-angular momentum baryons. As a result, those that remain attached to the central galaxy have specific angular momentum higher than the system as a whole. (iii) Feedback strength largely determines the average m_d of central galaxies. As discussed above, WF4 galaxy masses are on average 3 to 5 times larger than WF2Dec galaxies. This may be seen as a horizontal shift of points between the corresponding panels. (iv) The m_d-j_d relation is approximately independent of feedback. This is illustrated by the dotted curve, which is repeated in each panel, and which reproduces

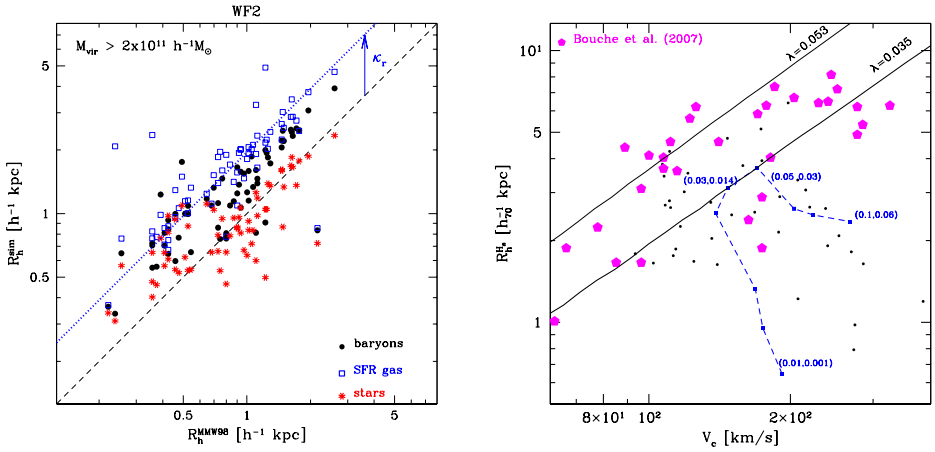

Figure 4. *Left:* Cylindrical half-mass radii predicted by the MMW98 formalism (x-axis) versus projected half-mass radius of simulated galaxies. Stars are shown by red asterisks, star-forming gas by empty blue squares, and all baryons by solid black dots. *Right:* The size-velocity plane of $z = 2$ SINS galaxies (magenta dots), together with the prediction of MMW98 for disks in a halo with $V_{\rm vir} = 150$ km/s, average concentration, and spin parameter $\lambda = 0.035$. The disk parameters m_d and j_d are assumed to follow the median m_d-j_d relation found in the simulations. The solid black curves outline the size-velocity relation expected for disks with $(m_d, j_d) = (0.05, 0.03)$ in halos with $\lambda = 0.035$ and 0.053, respectively. Black dots correspond to a subset of our simulated galaxies with m_d-j_d values close to the values that maximize disk size: $m_d = 0.05$ and $j_d = 0.03$. These show that extended disks are indeed present at $z = 2$ in our simulations.

the median j_d as a function of m_d in the WF2 run. This curve approximates reasonably well the j_d-m_d relation in *all* panels. In other words, for the feedback implementation adopted in our simulations the fraction of baryons that collects into the central galaxy is the primary factor determining the angular momentum content this galaxy retains.

3.2. Implications for disk galaxy sizes

We may also use our simulations to check the validity of the MMW98 formula for predicting galaxy sizes. This is shown in the left panel of Figure 2, where we plot the predicted (cylindrical) half mass radius ($R_h^{\rm MMW98}$) versus the projected half-mass radius of stars (red asterisks), star forming gas (empty blue squares) and baryons (black circles), for galaxies identified in the WF2 simulation.

The agreement is quite good for the stellar component, which is quite striking given the number of simplifying assumptions that go into the prediction and that are not matched in detail by the simulations. For example, the MMW98 prediction assumes that all baryons are in a centrifugally-supported exponential disk; simulated galaxies, on the other hand, exhibit a very wide range of disk-to-spheroid ratio. Interestingly, when scaled by a constant factor $\kappa_r \sim 2$ the MMW98 formula also predicts rather accurately the size of the star-forming *gaseous* disks (see upper dotted curve in the left panel of Figure 2).

We can combine this result with the m_d-j_d relation discussed above to compute the expected size of (gaseous) disks at $z = 2$. As shown in the right panel of Figure 2, the disk size and rotation speed depend sensitively on j_d and m_d. The jagged curve in this panel shows how the size of gaseous disks formed in a halo of fixed virial velocity $V_{\rm vir} = 150$ km/s changes as j_d and m_d are varied. The halo is assumed to have average concentration for its mass, and average spin, $\lambda = 0.035$. The jagged curve maps, in the disk size-rotation speed plane, variations in (m_d,j_d) chosen to lie along the average relation shown in Figure 3, from (0.01,0.001) to (0.1,0.06). The disk radius depends critically on the value of j_d and m_d: *disk sizes vary by a factor of* ~ 8*, even though the halo mass, concentration, and spin are fixed.* Clearly, predicting the size of disks is a rather uncertain endeavour unless one is able to constrain the values of the parameters j_d and m_d to within a very narrow range.

One further point to note is that disk radii are maximized for a particular combination of (m_d,j_d): $m_d = 0.05$ and $j_d = 0.03$ for the example in Figure 2. For such combination, gaseous disk half-mass radii in a $V_{\rm vir} = 150$ km/s halo would be of order $\sim 4\,h_{70}^{-1}$ kpc, comparable to the size of disks in the SINS sample. (SINS data are shown by large pentagons in the right-hand panel of Figure 2.) Larger disks may also exist, for example, in halos with higher-than-average λ or in systems where galaxies have retained an unusually high fraction of its angular momentum (i.e., those that scatter *above* the mean m_d-j_d relation in Figure 3). Taking, as an example, the WF2 run, we find, at $z = 2$, about 5×10^{-3} gaseous disks exceeding $\sim 2\,h_{70}^{-1}$ kpc (physical) in size per cubic h^{-1} Mpc (comoving). These numbers are in rough agreement with the findings of the SINS collaboration (Bouché et al 2007). We hasten to add that these are not "typical" galaxies at that redshift, but rather some of the largest ones present then. The selection of SINS galaxies favors large disks in order to enhance the probability of obtaining a resolved velocity map, and therefore they cannot be considered "average" at that redshift either. The presence of a (reasonable!) number of extended disks at $z = 2$ might thus not require unusually high halo spins nor present an insurmountable challenge to the LCDM structure formation paradigm.

References

Bouché N., et al. 2007, ApJ, 671, 303
Dalla Vecchia C., Schaye J., 2008, MNRAS, 387, 1431
Dutton A. A., van den Bosch F. C., 2008, ArXiv e-prints
Förster Schreiber N., et al. 2006, ApJ, 645, 1062
Genzel, R., et al. 2006, Nat, 442, 786
Governato, F., et al 2007, MNRAS, 374, 1479
Mo H. J., Mao S., White S. D. M., 1998, MNRAS, 295, 319
Navarro, J. F., & Steinmetz, M. 1997, ApJ, 478, 13
Navarro J. F., Steinmetz M., 2000, ApJ, 538, 477
Navarro, J. F., Abadi, M. G., & Steinmetz, M. 2004, ApJ, 613, L41
Okamoto T., Eke V. R., Frenk C. S., Jenkins A., 2005, MNRAS, 363, 1299
Robertson B., et al 2006, ApJ, 645, 986

GALAXY EVOLUTION: EMERGING INSIGHTS AND FUTURE CHALLLENGES
ASP Conference Series, Vol.
@jourvol, © 2009
S. Jogee, I. Marinova, L. Hao, and G. A Blanc

Forming Bulgeless Dwarf Galaxies

Fabio Governato

Astronomy Dept., University of Washington, Seattle, WA 98195, US

Abstract. We present hydrodynamical simulations in a ΛCDM framework[1] with resolution sufficient to resolve the inhomogeneous structure of the interstellar medium. Feedback from star formation is then able to unbind gas, creating strong gas outflows. These simulations form analogues of present day dwarf galaxies (V_{peak} <60 km s^{-1}) that are simultaneously "bulgeless" and have a cored DM distribution, demonstrating for the first time that the formation of a central dense stellar and DM component is not inevitable in hierarchical models, and reconciling observations of dwarf galaxies with the CDM model.

1. Introduction

In the ΛCDM paradigm galaxy disks form as the gas cools and collapses inside spinning halos of collisionless DM, reaching centrifugal equilibrium[2]. Stars then form as the gas cools and fragments further. Repeated mergers between halos are frequent and computer simulations have shown that the rapidly changing potential should lead to low angular momentum gas inflows at the center of galaxies that then rapidly turn into stars[3]. If the stellar component of galaxies inherits the angular momentum distribution of their DM halos then the simultaneous formation of a centrally concentrated stellar bulge and central cuspy DM profile is inevitable independently of galaxy mass, creating the so called "angular momentum problem"[4,5] for CDM models. In stark contrast the vast majority of dwarf galaxies show light profiles with no stellar bulges, and the observed rotation curves of small galaxies often rise almost linearly in the central kpc, consistent with a centrally cored DM distribution[6]. Numerical simulations in a CDM context have so far failed to form disk dominated systems that resemble present day small galaxies.

2. Simulations

Here we report results from novel cosmological simulations of dwarf galaxy formation in a ΛCDM cosmology. Hydrodynamical processes are included, together with a physically motivated treatment of star formation, cooling[7], heating from the cosmic UV field and SN driven gas heating. Simulations using the same implementation of star formation and feedback reproduce some of the global scaling properties of observed galaxies across a range of masses and redshifts[8,9]. In the simulations described in this is work dense gas clumps as small as 10^5 $M_\odot$ are resolved, hence SF is allowed only in cold gas regions with a local density higher than 100 amu cm^{-3}, similar to real SF regions.

Here we analyze a single dwarf galaxy (DG1), but we obtained equivalent results with galaxies of similar mass and different assembly histories or halo spin (a galaxy of similar mass is analyzed in the supplemental material). DG1 has a rich merger history: three proto-galaxies of similar mass merge at $z \sim 3$, a large satellite is accreted at $z \sim 1.2$ that has a mass 1/3 that of the central galaxy (a "major" merger). Several other satellites are accreted, including one at low redshift. Nevertheless, the majority of the gas is accreted smoothly from the intergalactic medium as the halo grows, particularly along cosmic filaments at early times, rather than from mergers. Star formation is bursty, as observed in nearby dwarfs, peaking at 0.25 $M_\odot$ yr^{-1} during interactions at $z \sim 2$.

Energy feedback from supernovae plays a fundamental role in the outcome of this simulation; as the potential is shallow, individual bursts of star formation generate strong gas outflows from the proto galaxy (Figure 1, top left). SF is localized in the dense regions across the disk, with SN feedback creating holes in the HI distribution due to bubbles of hot gas expanding perpendicular to the disk plane. The disk component assembles shortly after that (Figure 1, top). At $z = 0$ the HI disk surrounds a thin exponential stellar disk and the cold gas extends out to six stellar disk scale lengths. The galaxy shows no sign of a stellar spheroid (Figure 1, bottom right). The star formation rate declines after $z = 1$, and by the present time it is around 0.01 $M_\odot$ yr^{-1}, in agreement with galaxies of similar magnitude. Once at $z = 0$ simulations are analyzed in a manner which closely mimics observations, allowing a direct comparison with real data.

3. Results and Discussion

Mock images[10] in SDSS photometric bands (Figure 1, lower panels) were created showing that in redder bands the optical disk is relatively featureless, although localized star forming regions are visually associated with short lived spiral arms and holes in the HI distribution. The radial light distribution in all optical and near-IR bands has an almost perfect exponential profile as observed in dwarf galaxies. The striking feature of this galaxy is the complete absence of a stellar spheroid even when observed edge-on (Figure 1). A fit to the light distribution gives a bulge to disk (B/D) ratio of 0.04 and a disk scale length of about 1 kpc in all optical bands. This galaxy would thus be classified as "bulgeless" by observers, i.e. lacking of a visible central stellar spheroid. The formation of pure disk galaxies at the end of a prolonged merger phase is then a success of this set of simulations, even more as their structural parameters are quite typical of small, star forming galaxies.

Its rotation curve was obtained measuring the rotational motion of cold ($T < 10^4$ K) gas as a function of radius using the "tilted ring analysis" which reproduces the effects of observational biases such as disk distortions and warping, bars and pressure support from non circular motions[11]. DG1 shows a rotation curve which rises almost linearly out to one stellar disk scale length, and is still rising at 4 scale lengths ($\sim$ 4 kpc). The shape of this curve is reminiscent of the rotation curves of real dwarf galaxies. This is a great success as simulated galaxies have persistently produced rotation curves which rise rapidly in the inner regions, peak inside one scale length before falling off, symptomatic of their steep central mass distributions. Finally, the DM density profile of DG1

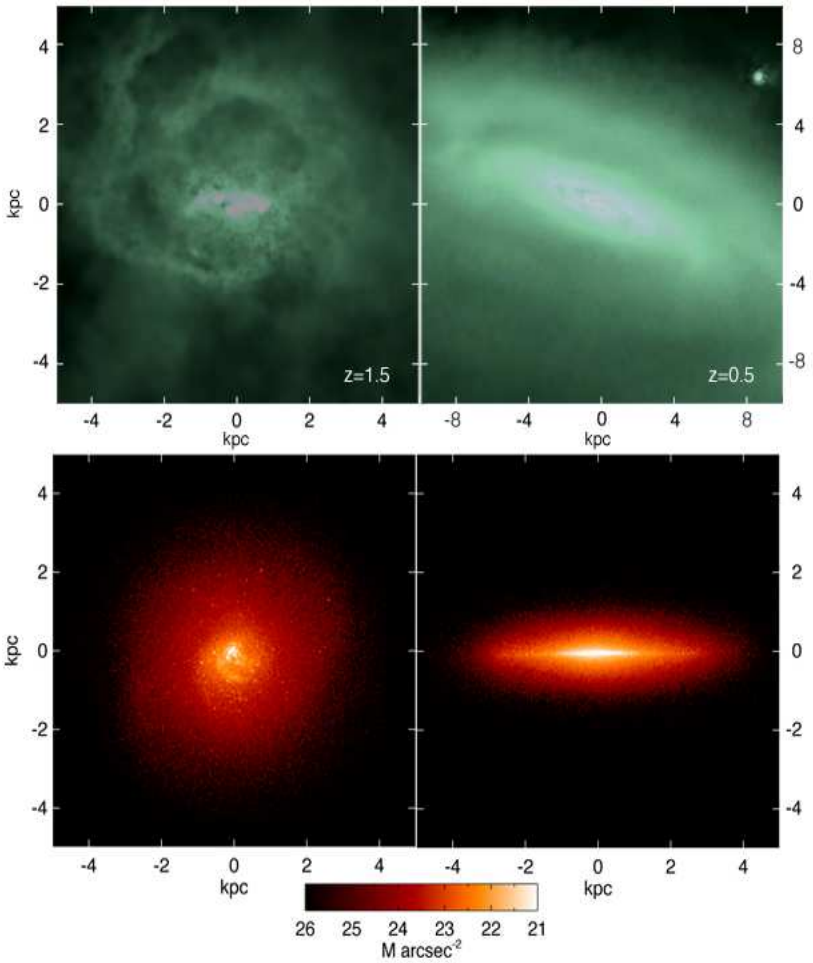

Figure 1. Top Left: Color-coded density map of the gas distribution at $z = 1.5$, showing the gas outflows and super shells. Top Right: The gas distribution at $z = 0.5$ when the disk has fully formed (note the larger scale). At $z = 0$ the total mass of the system is $3 \times 10^{10} M_{\odot}$ within the virial radius and the resulting disk is dominated by cold gas, rather than by the stellar component, with $M_{\rm gas}/(M_{\rm gas} + M_{\rm star}) = 0.7$ and a $M_{\rm HI}/L_{\rm B}$ ratio of 1.2. Bottom Left: The face on light distribution at $z = 0$ in the SDSS i band. Bottom Right: The galaxy seen edge on in the same band. The effect of dust absorption is included in both panels. The total magnitude of the galaxy in the i SDSS band is -16.7 giving an i band M/L ratio of 20. The galaxy $g - r$ color is 0.52, typical of star forming dwarf galaxies[29]. The rotation velocity is $\sim$ 55 km s^{-1}, as measured using the $W_{20}/2$ line width of the HI distribution. Using the "zoom in" technique, this simulation resolves the internal structure of galaxy DG1 with several million resolution elements, achieves a mass resolution of 10^3 $M_{\odot}$ for each star particle and a force resolution of 75 pc.

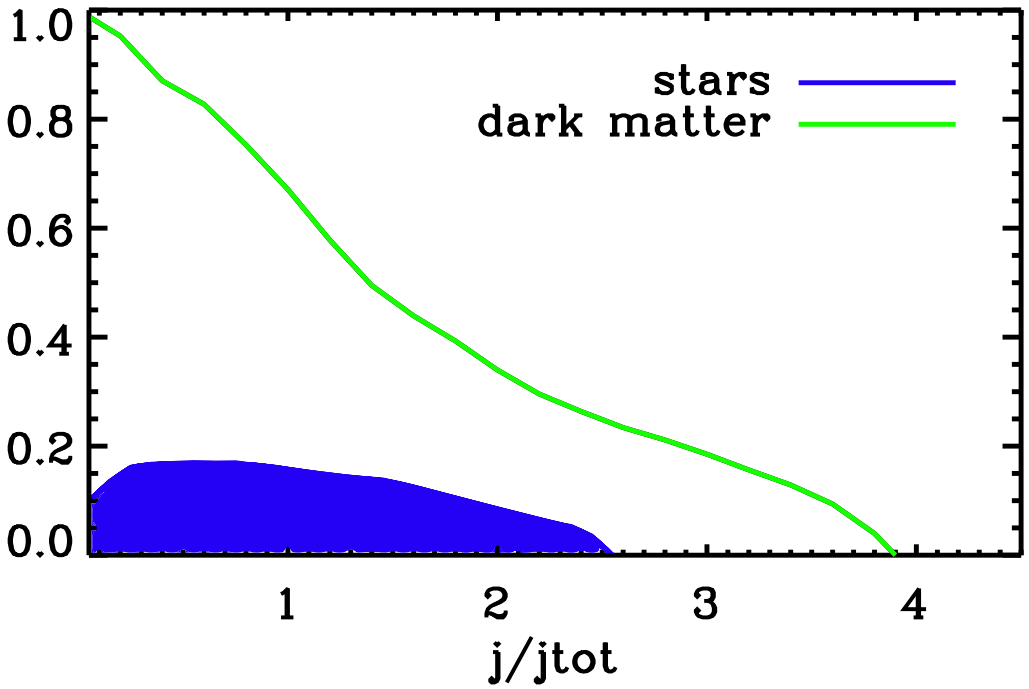

Figure 2. The (shaded blue) angular momentum histogram distribution of disk stars and DM particles (area below the continuous green line) vs the average for the whole DM halo ($jtot = 1$). The angular momentum distribution of star particles has a narrower distribution, a higher average and comparatively less low angular momentum material than the DM, due to centrally concentrated outflows preferentially removing low angular momentum baryons. The radial stellar distribution is similar to that measured from normal dwarf galaxies.

shows a core of roughly 1 kpc in size, comparable to the estimate for some dwarf galaxies[12]. Accordingly, the central DM density averaged over the same radius is $10^{7.5}$ $M_{\odot}$ kpc^{-3}, about 50 times lower than in a control run where the gas is not allowed to cool or form stars, and where the slope of the inner DM profile is instead cuspy, as in typical DM only simulations[13].

In these galaxies the gas being ejected has a much lower angular momentum per unit mass than the average gas being accreted (a factor of ten at $z > 1$). Outflows correlate with spatially resolved and centrally concentrated SF outbursts, the strongest happening during and after mergers and strong interactions. Outflows selectively remove low angular momentum gas before it is transformed into stars, effectively quenching the processes that would lead to a concentrated distribution of stars and the formation of bulges[14] (Figure 2).

Simultaneously solving the long standing problem of the joint distribution of baryons and dark matter at the center of small mass galaxies shows how the creation of DM cores is naturally related to the suppression of bulge formation. The results presented here explain naturally why many low-mass, bulgeless disk galaxies also are well described by cored potentials and predicts that these two properties should be correlated in observed samples of nearby small galaxies. Gas outflows generated by powerful SN explosions then provide a unique mechanism to explain the properties of small disk galaxies within the Cold Dark Matter model.

Acknowledgments. I thank L. Mayer, C. Brook, A.Brooks, P.Jonsson, P.Madau, Tom Quinn and the other co-authors in this project. We acknowledge stimulating discussions with A. Kravtsov and I. Trujillo. We thanks the THINGS team for sharing some of their data with us. FG acknowledges support from HST GO-1125, NSF ITR grant PHY-0205413 (also supporting TQ), NSF grant AST-0607819 and NASA ATP NNX08AG84G. CBB acknowledges the support of the UK's Science & Technology Facilities Council (ST/F002432/1). PJ was supported by programs HST-AR-10678 and 10958 and by Spitzer Theory Grant 30183 from the Jet Propulsion Laboratory. We thank the computer resources and technical support by TERAGRID, ARSC, NAS and the UW computing center, where the simulations were run.

References

1) Spergel, D. N. et al. 2003, ApJS, 148, 175
2) Fall, S. M. & Efstathiou, G. 1980, MNRAS, 193, 189
3) Barnes, J. E. & Hernquist, L. 1996, ApJ, 471, 115
4) van den Bosch, F. C., Burkert, A., & Swaters, R. A. 2001, MNRAS, 326, 1205
5) Dutton, A. A. 2009, MNRAS, 396, 121
6) de Blok, W. J. G., Walter, F., Brinks, E., Trachternach, C., Oh, S.-H., & Kennicutt, R. C. 2008, AJ, 136, 2648
7) Mashchenko, S., Wadsley, J., & Couchman, H., M. P 2008, Science, 319, 174
8) Brooks, A., Governato, F., Booth, C. M., Willman, B., Gardner, J. P., Wadsley, J., Stinson, G., & Quinn, T. 2007, ApJ, 655, L17
9) Pontzen, A., Governato, F., Pettini, M., Booth, C. M., Stinson, G., Wadsley, J., Brooks, A., & Quinn, T. 2008, MNRAS, 390, 1349
10) Jonsson, P. 2006, MNRAS, 372, 2
11) Valenzuela, O., Rhee, G., Klypin, A., Governato, F., Stinson, G., Quinn, T., & Wadsley, J. 2007, ApJ, 657, 773

12) Gentile, G., Salucci, P., Klein, U., Vergani, D., & Kalberla, P. 2004, MNRAS 351, 903
13) Diemand, J., Kuhlen, M., & Madau, P. 2007, ApJ, 667, 859
14) Binney, J., Gerhard, O. & Silk J. 2001, MNRAS, 321, 471

GALAXY EVOLUTION: EMERGING INSIGHTS AND FUTURE CHALLLENGES
ASP Conference Series, Vol.
@jourvol, © 2009
S. Jogee, I. Marinova, L. Hao, and G. A Blanc

Bulge Formation by the Coalescence of Giant Clumps in Primordial Disk Galaxies

Bruce G. Elmegreen

IBM Research Division, Yorktown Heights, NY 10598, USA, bge@us.ibm.com

Abstract. The observations and evolution of clumpy, high-redshift galaxies are reviewed. Models suggest that the clumps form by gravitational instabilities in a gas-rich disk, interact with each other gravitationally, and then merge in the center where they form a bulge. The model requires smooth gas accretion during galaxy growth.

1. Introduction: Secular Evolution of Classical Bulges

There is growing evidence for secular bulge evolution, even for classical bulges. The classical bulge fraction (i.e., with high Sersic index, n) decreases out to $z \sim 1$ (Sargent et al. 2007); bulge and disk colors correlate with each other, suggesting that classical bulges and disks coevolve (Balcells & Dominguez-Palmero 2008); the Milky Way old thick disk and bulge have similar metallicities, suggesting co-evolution (Meléndez et al. 2008); the central disk mass concentration (which is essentially the bulge to disk ratio) increases over time at $z \sim 2$ (Genzel et al. 2008); and young disks have clumpy structure and young bulges are similar to disk clumps (Elmegreen et al. 2008). In addition, simulations suggest that disks with high gas fractions and high turbulent speeds form massive clumps that move to the center and make a "classical" bulge (Noguchi 1999; Immeli et al. 2004; Bournaud, Elmegreen, Elmegreen 2007, Elmegreen, Bournaud, & Elmegreen 2008ab). At the same time, ΛCDM cosmological simulations have not reproduced the observed small value of $M(\text{bulge})/M(\text{disk})$ (e.g., Graham & Worley 2008), suggesting there were few major mergers during disk formation (Weinzirl et al. 2009).

2. Chain Galaxies and Clump Clusters

We have been observing the properties of star-forming clumps in galaxies in the Hubble Space Telescope Ultra Deep Field (UDF), and in the GEMS and GOODS fields. The UDF shows clumpy, star-bursting galaxies out to $z \sim 6$, where the Lyman α Hydrogen line begins to shift out of the reddest band in the Advanced Camera for Surveys. A catalog of galaxy types is in Elmegreen et al. (2005a). Of greatest interest are the extremely clumpy galaxies, the chains and the clump-clusters (Fig. 1), which comprise 31% of all 1003 UDF galaxies larger than 10 pixels in diameter. In comparison, spirals comprise another 31%, ellipticals 13%, and likely interacting galaxies, the double-clump and tadpoles, 25%. The clumpy types are somewhat uniformly distributed over redshift out to

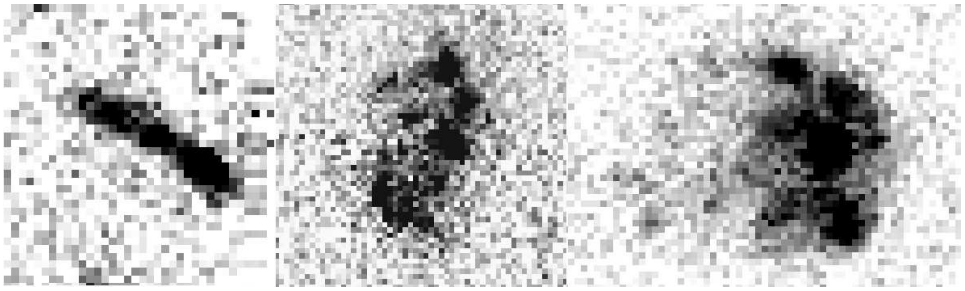

Figure 1. Chain (left) and clump cluster galaxies from the background field of the Tadpole galaxy, which was one of the first deep images taken with the HST ACS camera (From Elmegreen, Elmegreen & Hirst (2004).

$z \sim 5$, while the spirals and ellipticals concentrate within $z \sim 1.5$ because of their intrinsically red colors (Elmegreen et al. 2007). These fractions emphasize the importance of the clumpy phase of galaxy evolution. Their co-moving density (chains + clump clusters) is about 10^{-3} Mpc^{-3} for $z > 2$, with an increase to $\sim 3 \times 10^{-3}$ Mpc^{-3} for $z < 1$ (Elmegreen et al. 2007). In comparison, the co-moving densities of spirals and ellipticals in the UDF are $\sim 4 \times 10^{-3}$ and $\sim 1 \times 10^{-3}$ Mpc^{-3}, respectively. It is conceivable, considering the short life of the clumpy phase, that all spiral galaxies go through this phase before they settle down to a smooth disk with a bulge in the center.

We believe there is a link between chain galaxies, which are linear alignments of clumps, and clump clusters, which are round or irregular conglomerates of clumps. The galaxy and clump properties are the same in these two types (Elmegreen, Elmegreen, & Hirst 2004), and their combined distribution on a histogram of the ratio of axes (width/length) is nearly flat with a drop off below ~ 0.2 and above ~ 0.8 (Elmegreen & Elmegreen 2005). A disk viewed in random projection has a flat distribution on such a plot, with a fall-off at low ratio from the relative disk thickness. There should be no fall-off at high ratio for a uniform disk, but for a clumpy disk, there is always some irregularity at the edge because of the discrete clump positions. This irregularity fits the clumpy galaxy distribution for the observed number of 5-10 clumps per galaxy (Elmegreen & Elmegreen 2005). This result implies that chain galaxies are edge-on clump clusters.

The clump positions in a chain galaxy are also consistent with their being edge-on projections of clump positions in disk galaxies. The clumps are not uniformly spaced, for example, as might be the case for condensations in a filament. Figure 2 shows relative clump positions in all of the UDF chains, measured relative to the end clumps. The curve is a model for clumps that are distributed randomly in azimuth around a disk, and exponentially in radius on average with two scale lengths (as observed for clump clusters – Elmegreen et al. 2005b). The similarity between the curve and the histogram suggests again that chain galaxies are edge-on clump clusters.

It is important to establish this projection link between chain galaxies and clump clusters because the chain galaxies have their clumps highly confined to the mean line connecting them. They deviate in position from this mean line by an average distance of only ~ 100 pc. This is much smaller than the average

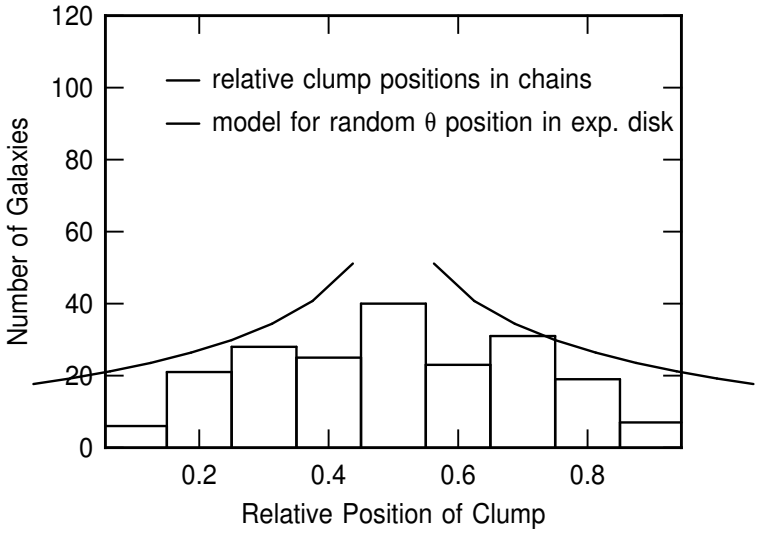

Figure 2. Average clump distribution along the length of a chain galaxy is plotted as a histogram. The curves show a model distribution for an edge-on disk with an exponential radial profile having two scale lengths for the average clump position and a random angular distribution around the center.

thickness of the galaxies themselves, which is $z_0 \sim 900$ pc for scale height z_0 in the functional fit $\mathrm{sech}z/z_0$. We infer from this that the clumps in both chains and clump clusters are confined to a disk midplane, and therefore that they formed there. The alternative possibility, that the clumps entered the galaxy from outside (as in a hierarchical build up scenario) seems untenable with their observed midplane positions. For in-situ formation, the clumps are most likely giant star-forming regions that formed in a gas disk. This makes them similar to star complexes in modern galaxies, although the high redshift clumps are more massive by a factor of ~ 100 than today's complexes (Elmegreen et al. 2009).

3. Bulges in Clumpy Galaxies

The clumpy large galaxies in the UDF (diameters > 10 pixels) were examined on both ACS images in optical bands and NICMOS images in near-IR bands. In 30% of the chains and 50% of the clump clusters, bulges or bulge-like objects can be seen in the NICMOS images even if they are not present or easily recognized in the ACS images. In the other cases, there are no obvious bulges, although there is usually some NICMOS emission associated with either the brightest clumps or the underlying disk.

ACS + NICMOS measurements of bulges-like objects were made in 47 clump clusters and 27 chains. Bulges were also measured in 131 spiral galaxies. ACS measurements of clumps were made in 184 clump clusters, 112 chains, and 118 spirals, yielding 898, 406, and 845 clumps respectively. We fit the clump SEDs to Bruzual & Charlot (2003) models with free parameters for clump age, star formation exponential decay time, and extinction. We included Madau (1995) intergalactic hydrogen absorption, as well as Calzetti et al. (2000) and

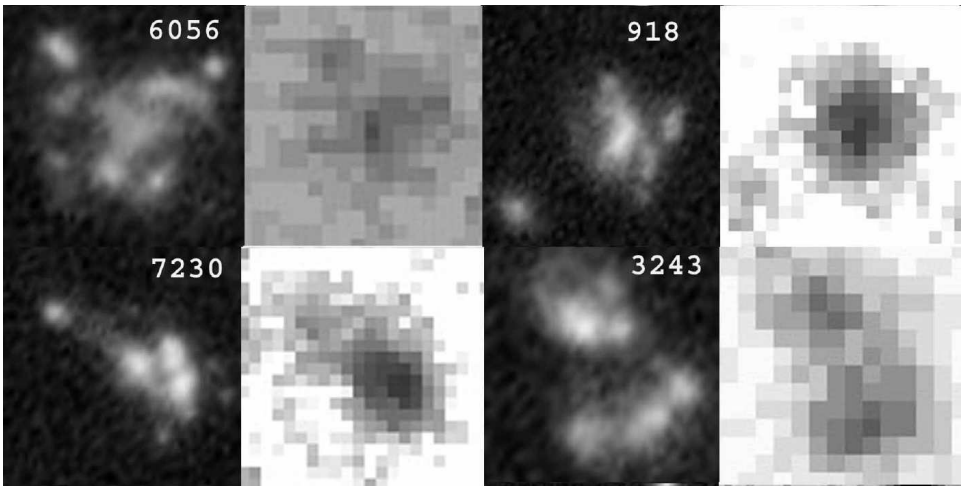

Figure 3. Four clump cluster galaxies are shown, each with an ACS image on the left (a grayscale version of the Skywalker color image, containing all of the ACS passbands) and a NICMOS version on the right, with 3× lower resolution. The top two galaxies have NICMOS concentrations in the center that could be bulges, while the bottom two galaxies have diffuse NICMOS emission only from the star forming regions, which are not centralized.

Leitherer et al. (2002) extinction. The metallicity was assumed to be 0.4 solar because of measurements like this in one case (Bournaud et al. 2008). The metallicity dependence for mass and age are small anyway. Then we get the clump mass from its brightness, star formation history, and extinction. A complete discussion is in Elmegreen et al. (2009).

Figure 3 shows two clumpy galaxies with bulges (top) and two without bulges (bottom). UDF numbers are indicated. Each galaxy is represented by two panels, the left showing a grayscale version of the color image from Skywalker[1], at the full ACS resolution, and the right showing the NICMOS image at 3× worse resolution. There are dense central objects in the NICMOS images for the top two galaxies, and only diffuse IR emission following the star formation in the bottom two galaxies.

The measurements in this survey indicated that the bulges in clumpy galaxies are a lot like the clumps in both age and mass, whereas in spiral galaxies, the bulges are significantly more massive than the clumps, and also much older. Thus the bulges look recently formed in the clumpy cases, and similar enough to the clumps to lead us to think that they formed from the clumps. The relative youth of the bulges in clumpy galaxies is consistent with bulge morphology because often the bulge-like objects are slightly off center and irregular for the clumpy cases, and the surrounding disks are not generally exponential along any radial cut. Spiral galaxies have more regular radial profiles and more centralized clumps.

[1]http://www.aip.de/groups/galaxies/sw/udf/index.php

4. Star Formation in Clumpy Galaxies

The regular spacing of clumps in tidal arms, their midplane positions in chains, the similarity between their sizes and the disk thicknesses in chains, and their universally high masses all point to clump formation by gaseous gravitational instabilities. The clumps contain a stellar mass $M \sim 10^7 - 10^8\ M_\odot$, and may contain gas too for the youngest cases, perhaps even $10^8 - 10^9\ M_\odot$ of gas. The clump size is typically 3× the local star complex size (2000 pc compared to 600 pc – Efremov 1995), and the clump mass is typically 100× the local star-complex mass (which is $10^4 - 10^5\ M_\odot$).

We can use these size and mass scalings to determine the implications for the interstellar medium. The cloud size for gravitational instabilities is $L_{\rm Jeans} \sim \sigma^2/G\Sigma$, and the cloud mass is $M_{\rm Jeans} \sim \sigma^4/G^2\Sigma$. The scale-up then implies at high redshift, $\sigma \sim 5\times$ the local σ, which means $\sigma \sim 40$ km s^{-1}. This is the dispersion observed for the ionized component of the gas in these galaxies (Forster Schreiber et al. 2006; Genzel et al. 2006; Weiner et al. 2006). Also at high redshift, $\Sigma \sim 10\times$ the local Σ, which means $\Sigma \sim 100\ M_\odot$ pc^{-2} in the gas (this corresponds to 1×10^{22} H cm^{-2} for the neutral ISM and has not been observed yet unless it causes the damped Lyman α absorption).

Evidently, clump clusters and chains are forming the inner disks and bulges of today's spiral galaxies. The process of star formation is the same as it is locally, but at higher velocity dispersion and gas column density, and most likely at higher gas fraction too, as the disk forms roundish clumps instead of swing amplified spirals. The roundness implies that the instability and energy dissipation is faster than a shear time.

5. Models of Bulge Formation by the Coalescence of Disk Clumps

These observations have led us to re-investigate an old model by Noguchi (1999) and Immeli (2004ab) in which a massively unstable disk fragments into a few giant clumps that interact and migrate to the center to make a bulge. We chose parameters typical of the clumpy galaxies we see (e.g., mass, size) and assumed a high gas fraction (50% in typical cases) and a high initial velocity dispersion. The initial disk was uniform in density profile out to a sharp edge. It breaks into $M_{\rm Jeans}$ clumps quickly, within a fraction of a rotation, and the clumps form stars, interact gravitational with each other and with the rest of the galaxy, and migrate to the center where they coalesce. The result is a bulge surrounded by a double-exponential disk.

Figure 4 shows the basic model in 6 timesteps for a standard case. The clumps form quickly, interact with each other, and migrate to the center to make a bulge. Many different cases with about the same result were discussed in Bournaud, et al. (2007). The bulge that forms is slowly rotating and has a Sersic $n = 4$ profile like a classical bulge (Elmegreen et al. 2008b). If we put point particle tracers in the center of each clump, representing intermediate mass black holes formed by main sequence star coalescence in the dense cluster cores (e.g., Ebisuzaki et al. 2001), then these black holes migrate to the center with the clumps, and there they can merge into a supermassive black hole. The

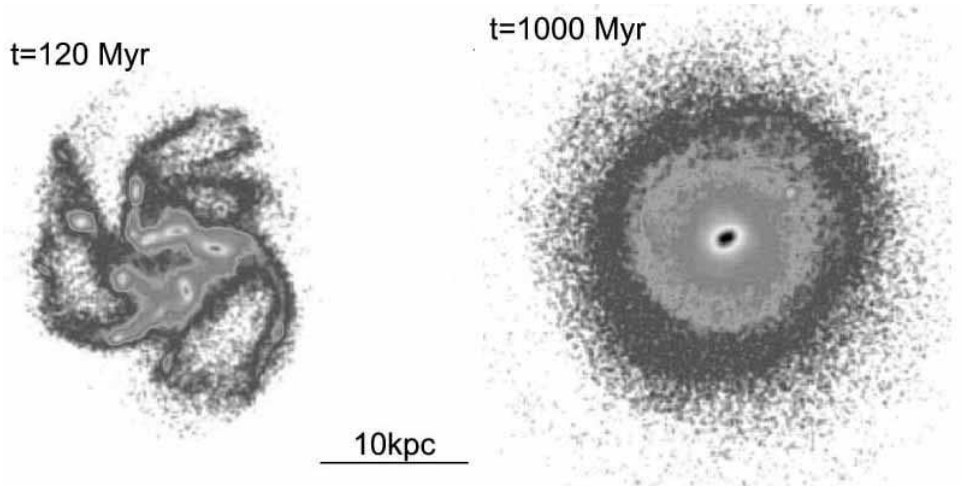

Figure 4. Model showing the early and late stages of a typical simulation of a clump cluster galaxy, from BEE07. Characteristic of the model is the high initial gas fraction in the disk (50%) and a high gas turbulent speed. The initial disk is uniform with a sharp edge and half the size of the final disk. Clumps form quickly with the Jeans mass, interact, and move to the center to make a bulge. The final disk has a double-exponential radial profile, with the outer part coming from clump debris.

correlation between black hole mass and bulge velocity dispersion is reproduced in this fashion, to within a factor of ~ 3 (Elmegreen et al. 2008a).

There are several interesting results about clumps and their coalescence. First, feedback does not destroy the clumps because they are too tightly bound. The high velocity dispersion of the average ISM makes the clumps have a high dispersion too, and this makes them hard to break apart by supernovae. Second, the swirling clumps in the center mix the dark matter there just before they coalesce, and this can decrease the density in any dark matter cusp by about a factor of 3. Third, an existing bulge can tidally destroy the smaller disk clumps and prevent them from accreting in the center. In this way, the bulge formation process might be self-limiting.

6. Conclusions

There is a new galaxy morphology at $z > 1$: disks with massive clumps. The clumps appear to form in these disks by gravitational instabilities. This conclusion follows from the similarity between the clump sizes and the disk thicknesses, from the midplane positions, and from the boundedness (relatively long lives) of the clumps. Clump masses range from 10^7 to 10^8, and up to 10^9 $M_\odot$ in some cases. The large mass is most likely the result of a large turbulent speed of 25 to 50 km s^{-1}, and a large gas mass column density of ~ 100 $M_\odot$ pc^{-2}. Dispersal and merging of the clumps builds an exponential disk and a bulge.

Clumpy disks are observed to at least $z \sim 5$ where they appear to dominate spiral galaxies. This distribution suggests that spirals evolve from relatively isolated clumpy disks and at least some of the classical bulges in those spirals

form by internal processes. The model requires rapid gas assembly, however, not hierarchical merging of pre-existing star-rich galaxies as in some hierarchical build-up models.

There may be a way for the model to explain the Hubble type too: late Hubble types could have a low gas velocity dispersion, in which case the clumps would be relatively low-mass, they would not interact much, and they would be easily destroyed by feedback. The clumps would not form a bulge in that case. Early Hubble types could have a high gas dispersion, and this would make their clumps massive, strongly interacting, somewhat impervious to star formation feedback, and quickly brought to the center where they would merge to make a bulge.

Acknowledgments. Most of this research was done in collaboration with Debra Meloy Elmegreen, Frederic Bournaud, and numerous undergraduate students at Vassar College.

References

Balcells, M., & Dominguez-Palmero, L. 2008, IAU Symposium 245, p. 439 astroph/0710.0494
Bournaud, F., Elmegreen, B.G., & Elmegreen, D.M. 2007, ApJ, 670, 237
Bournaud, F., Daddi, E., Elmegreen, B.G., Elmegreen, D.M., Nesvadba, N., Vanzella, E., de Matteo, P., Le Tiran, L., Lehnert, M., & Elbaz, D. 2008, A&A, 486, 741
Bruzual, G. & Charlot, S. 2003, MNRAS, 344, 1000
Calzetti, D., Armus, L., Bohlin, R., Kinney, A., Koornneef, J., & Storchi-Bergmann, T. 2000, ApJ, 533, 682
Ebisuzaki, T. et al. 2001, ApJ, 562, L19
Efremov, Y.N. 1995, AJ, 110, 2757
Elmegreen, D.M., Elmegreen, B.G., & Hirst, A.C. 2004, ApJ, 604, L21
Elmegreen, B.G., & Elmegreen, D.M. 2005, ApJ, 627, 632
Elmegreen, D.M., Elmegreen, B.G., Rubin, D.S., & Schaffer, M.A. 2005a, ApJ, 631, 85
Elmegreen, B.G., Elmegreen, D.M., Vollbach, D.R., Foster, E.R., & Ferguson, T.E., 2005b, ApJ, 634, 101
Elmegreen, D.M., Elmegreen, B.G., Ravindranath, S., & Coe, D.A., 2007, ApJ, 658, 763
Elmegreen, B.G., Bournaud, F., & Elmegreen, D.M. 2008a, ApJ, 684, 829
Elmegreen, B.G., Bournaud, F., & Elmegreen, D.M. 2008b, ApJ, 688, 67
Elmegreen, B.G., Elmegreen, D.M., Fernandez, M.X., Lemonias, J.J. 2009, ApJ, in press, arXiv0810.5404
Förster Schreiber, N. M., et al. 2006, ApJ, 645, 1062
Genzel, R. et al. 2006, Nat, 442, 786
Genzel, R., Burkert, A., Bouché, N., et al. 2008, ApJ, 687, 59
Graham, A.W., & Worley, C. C. 2008, MNRAS, 388, 1708
Immeli, A., Samland, M., Westera, P., & Gerhard, O. 2004a, ApJ, 611, 20
Immeli, A., Samland, M., Gerhard, O., & Westera, P. 2004b, A&A, 413, 547
Leitherer, C., Li, I.-H., Calzetti, D., Heckman, T.M. 2002, ApJS, 140, 303
Madau, P. 1995, ApJ, 441, 18
Meléndez, J., Asplund, M., Alves-Brito, A., et al. 2008, A&A, 484, L21
Noguchi, M. 1999, ApJ, 514, 77
Sargent, M.T. et al. 2007, ApJS, 172, 434
Weiner, B. J., et al. 2006, ApJ, 653, 1027
Weinzirl, T., Jogee, S., Khochfar, S., Burkert, A. & Kormendy, J. 2009, ApJ, 696, 41

GALAXY EVOLUTION: EMERGING INSIGHTS AND FUTURE CHALLLENGES
ASP Conference Series, Vol.
@jourvol, © 2009
S. Jogee, I. Marinova, L. Hao, and G. A Blanc

Secular Evolution and the Assembly of Bulges

F. Combes
Observatoire de Paris, LERMA, 61 Av. de l'Observatoire, F-75014, Paris

Abstract. Bulges are of different types, morphologies and kinematics, from pseudo-bulges, close to disk properties (Sersic index, rotation fraction, flatenning), to classical de Vaucouleurs bulges, close to elliptical galaxies. Secular evolution and bar development can give rise to pseudo-bulges. To ensure prolonged secular evolution, gas flows are required along the galaxy life-time. There is growing evidence for cold gas accretion around spiral galaxies. This can explain the bar cycle of destruction and reformation, together with pseudo-bulge formation. However, bulges can also be formed through major mergers, minor mergers, and massive clumps early in the galaxy evolution. Bulge formation is so efficient that it is difficult to explain the presence of bulgeless galaxies today.

1. Secular evolution and bulges, gas flows

There are excellent recent reviews on secular evolution (Kormendy & Kennicutt 2004, Jogee 2006), and in particular the formation of bulges has been debated in detail last year in Oxford, with the IAU Symposium 245 on "Formation and Evolution of Bulges". Only more recent work will then be reviewed here.

A clear distinction is now well established between classical bulges and pseudo-bulges, from the luminosity distribution (Sersic index, flattening, color) and the kinematics. On the color-magnitude diagram, the pseudo-bulges, similar in properties to disks, are clearly on the blue cloud, while the classical bulges sit on the red sequence (Drory & Fisher 2007). There is a clear bimodality in Sersic index, with the pseudo-bulge peak at $n = 1 - 2$, and the classical bulge peak at $n = 4$ (Fisher & Drory 2008).

Gaseous haloes around galaxies

The secular evolution is fueled by external gas accretion, and there is now growing evidence of gas infalling on nearby spiral galaxies, although this gas is quite diffuse. One of the best example is the edge-on galaxy NGC891 (Fraternali et al. 2007). HI gas is observed up to 20 kpc above the plane, with its rotation decreasing with the altitude. Part of this gas could come from galactic fountain, but not all, since the angular momentum should then be conserved. Moreover, modelisation of the fountain effect predicts gas outflow (cf the non edge-on galaxy NGC 2403), while mostly inflow is observed, like for high velocity clouds in the Milky Way. Gaseous haloes require accretion of external gas (Fraternali & Binney 2006).

A recent review by Sancisi et al. (2008) gathers many examples of extra-planar gas. Part of it is due to dwarf companions or tidal streams, but evidence is mounting for extragalactic inflow of gas due to cosmic accretion. This external

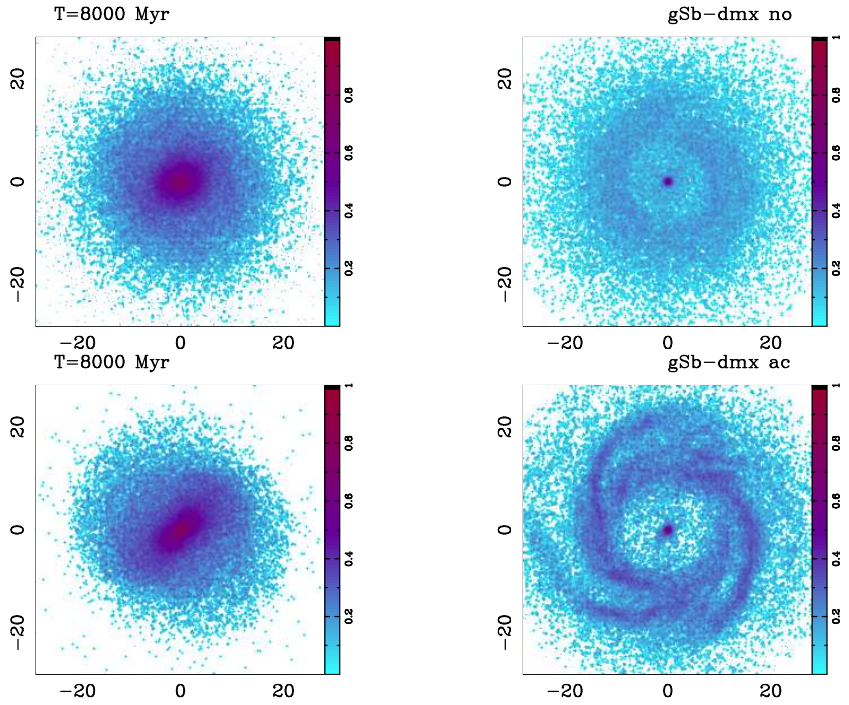

Figure 1. Comparison between two Sb galaxy models, without gas accretion (**top**) and with accretion (**bottom**). The Sb model is the maximum disk model (Combes 2008), the gas accretion rate is 5 $M_\odot$/yr, and the snapshot corresponds to T=8 Gyr. Note that a bar is maintained only in the case of gas accretion.

gas inflow produces lopsideness and fuels star formation. When the angular momentum of the accreted gas is close to perpendicular to that of the galaxy, polar rings can form. The simulation of this phenomenon by Brooks et al. (2008) reveals how successively star formation is occuring in the inner equatorial disk, then in the outer polar disk. After 1.5 Gyr, the interaction between the two disks destroys the polar ring. The velocity curve is about the same in both equatorial and polar planes.

Relative role of gas accretion and mergers

In the standard hierarchical scenario, galaxies are thought to assemble their mass essentially through mergers. However, the gas accretion from cosmic filaments has been under-estimated. Analysis of a cosmological simulation with gas and star formation shows that most of the starbursts are due to smooth flows (Dekel et al. 2009). Corresponding inflow rates are sufficient to assemble galaxy mass (10-100 $M_\odot$ yr^{-1}).

2. Bar destruction, re-formation, role of gas

It is now well established that bar redistribution of mass and the vertical resonance can buiid secularly pseudo-bulges (e.g. Combes et al. 1990). However, in

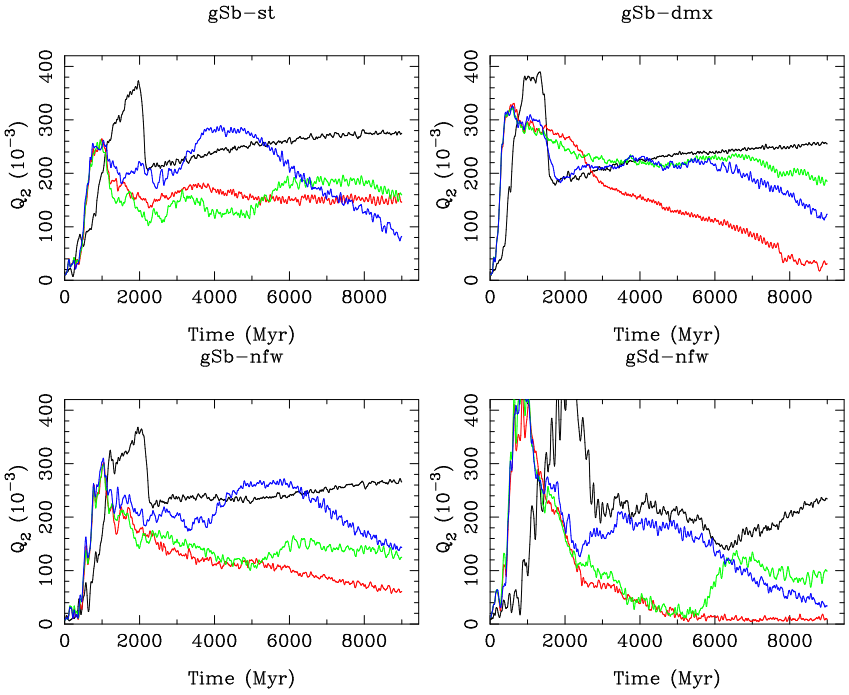

Figure 2. Evolution of bar strength, measured as the ratio Q_2 of the maximal $m = 2$ tangential force to the radial force, measured at a radius of 3.3kpc. The black curve corresponds to the purely stellar run, the red curve, to the spiral galaxy with initial gas, subject to star formation, but not replenished. These two curves are respectively the top and the bottom curves. The other curves corresponds to the models with gas accretion, 5 $M_\odot$/yr for the green one, and 5 $M_\odot$/yr for the blue one. There are 3 galaxy models corresponding to an Sb galaxy, with different mass ratios between disk and halo, and an Sd galaxy, with an NFW dark profile.

a gaseous disk, not dominated by dark matter, the bar can quickly weaken and even be destroyed (cf Figure 1). With only 2% of the mass, gas infall is enough to transform a bar in a lens (Friedli 1994, Berentzen et al. 1998, Bournaud & Combes 2002, Bournaud et al. 2005). To pursue bulge formation, and explain the large frequency of bars, external gas accretion has to be invoked, in a self-regulated cycle: in a first phase, a bar forms through gravitational instability in a cold disk. The bar produces gas inflow, which itself weakens or destroys the bar, through angular momentum transfer to the bar. Then external gas accretion can replenish the disk, to turn back to the first phase.

Figure 2 illustrates such cycles, for different galaxy models, giant disks with different dark matter fractions, and different dark matter concentrations (Combes 2008). Although gas is provided at a constant inflow rate in the outer parts of the disks, it enters the galaxy disk by intermittence, and produces starbursts. Indeed, while the bar is strong, positive torques between corotation and OLR confine the gas outside OLR. Only when the bar weakens, the gas can replenish the disk, to make it unstable again to bar formation. Through these cycles, the pseudo-bulge can form, as shown in Figure 3.

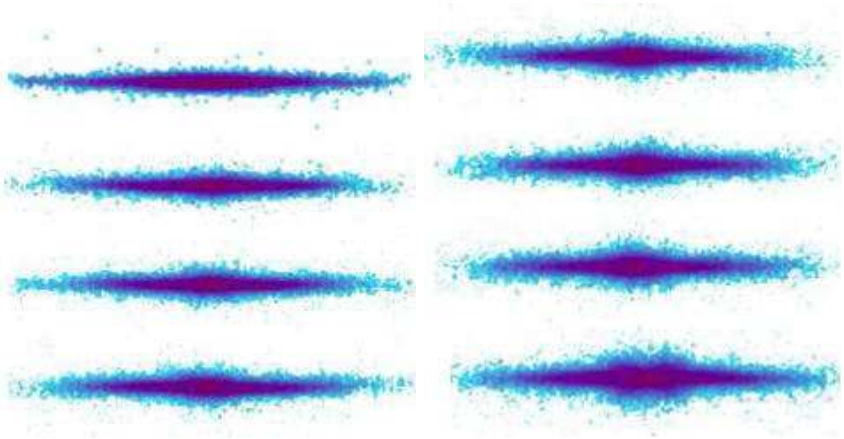

Figure 3. Formation of a peanut bulge, during bar formation, destruction, and reformation, for the standard Sb model. Time is running from top left to bottom left, then from top right to bottom right.

Formation in a cosmological context

In cosmological simulations, it is possible to take into account cosmic gas accretion more realistically. When spatial resolution is sufficient, it is possible to see bars form, destroy and reform (Heller et al. 2007).

There is clearly in all these processes the influence of the adopted gas physics: bar formation is more easy with isothermal gas, while adiabatic gas heats and prevents disk instability. Star formation and feedback are then important keys to regulate the dynamics.

Angular momentum transfer with dark matter haloes In presence of a massive dark halo, the angular momentum transfer is essentially towards the dark component, which helps to reform the bar. However, the bar destroys more quickly in presence of gas (Berentzen et al. 2007). The weakening of the bar is then interpreted as due to the central mass concentration provided by the gas. It cannot be due to the vertical resonance, which is also weakened or suppressed in presence of large quantities of gas.

3. Bar and bulge statistics and high z evolution

The frequency of bars has been quantified on many samples, and in particular in the near infrared, where bars are easier to define (e.g. the OSU NIR sample, Eskrige et al. 2002). In all samples, the main result is the paucity of weak bars (Marinova & Jogee 2007). Whatever the tool to measure bar strength, the number of strong bars is high at $z = 0$ (Whyte et al. 2002, Block et al. 2002, Buta et al. 2004).

Bar frequency with redshift

If at $z = 0$ about 2/3 of galaxies are barred, with at least 30% strongly barred, the strong bars (ellipticity higher than 0.4) in the optical remain about 30% at redshift between 0.2 and 1 (Jogee et al. 2004). At high z, however,

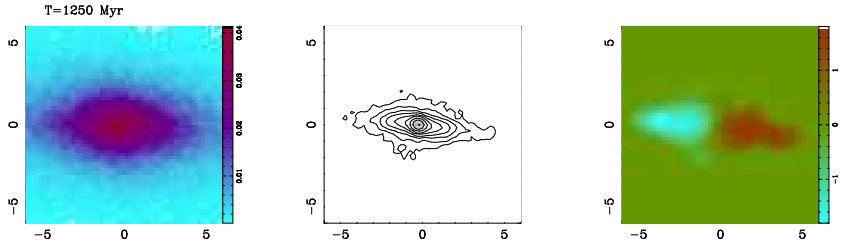

Figure 4. Result of the major merger of two equal-mass spiral galaxies, after 1250 Myr. Left is the stellar density, middle the gas density contours, and right the gas velocity field, where the wedge indicate the amplitude of the projected velocity in units of 100km/s. Not all mergers end up in an elliptical galaxy, but a significant pseudo-bulge is formed (Crocker et al. 2008).

results are more uncertain, because of the K-correction, and the lack of spatial resolution, preventing to detect small bars. From a recent study of the COSMOS field, the bar fraction is found to decrease at high z (Sheth et al. 2008). This is easy to interprete in terms of gas fraction: galaxy disks are more gas rich at high redshifts, and the gas inflow is destroying bars. The time spent in a barred phase is then expected to be smaller for galaxies at $z \sim 1$.

B/T and n statistics

The bulge-to-total luminosity ratio (B/T) and the Sersic index n have been studied by several groups in near-infrared samples. A clear decrease of B/T and n has been found with the Hubble type, whatever the barred or unbarred character (Laurikainen et al. 2007). In the OSU sample of 146 bright spirals in H-band, where 2/3 of galaxies are barred, 60% have $n < 2$, and $B/T < 0.2$, barred or not (Weinzirl, Jogee, Khochfar et al. 2009). There is in addition a clear correlation between B/T and n.

This large observed fraction of low bulge galaxies is a constraint for models. In ΛCDM, a $B/T < 0.2$ galaxy requires no merger since 10 Gyr (or last merger before $z > 2$). The predicted fraction of these low-bulge bright spiral is 15 times lower than observed (Weinzirl et al. 2009). Most of these low-bulge bright spirals must be explained either by rare minor mergers or secular evolution, without mergers. With semi-analytical criteria, Koda et al. (2007) propose a solution in terms of the tail of the distribution.

Frequency of bulge-less galaxies

Locally, about 2/3 or the bright spirals are bulgeless, or with a low-bulge (Kormendy & Fisher 2008, Weinzirl et al. 2009). Some of the remaining have both a classical bulge and a pseudo-bulge, plus nuclear clusters (Böker et al. 2002).

From the observed frequency of edge-on superthin galaxies, Kautsch et al. (2006) estimate that 1/3 of galaxies are completely bulgeless. In the SDSS sample, 20% of bright spirals are bulgeless until $z = 0.03$ (Barazza et al. 2008). Disk-dominated galaxies are more barred than bulge-dominated ones. How can this be reconciled with the hierarchical scenario?

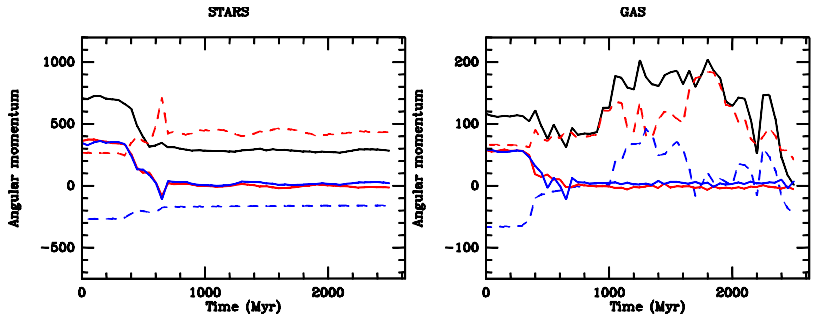

Figure 5. Angular momentum evolution of the stars (left) and gas (right) in the major merger simulation of Fig 4. The red curves correspond to the prograde galaxy, and the blue curves to the retrograde. The solid lines indicate the orbital angular momentum, while the dash lines indicate the internal spins. The scale is in units of 2.3 10^{11} $M_\odot$ kpc km/s (Crocker et al. 2008).

4. Mergers and bulge formation scenarios

We can first remark that major mergers do not always lead to spheroids, or classical bulges, but sometimes also to pseudo-bulges. An extreme example is shown in Figure 4, the result of an equal mass merger, to reproduce the NGC 4550 system. This simulation is run with one disk prograde with respect to the relative orbit, and one disk retrograde, which leads to counter-rotation (e.g. Di Matteo et al. 2007). In this system, the gas eventually settles in the prograde sense, in corotation with the prograde stellar disk, which is also the most perturbed in the interaction, thus ends up as a thicker disk. The angular momentum exchange between stars, gas and the orbit can be seen in Figure 5 (Crocker et al. 2008). This major merger forms a bulge with low $n \sim 1-2$. This must also be the case for similar encounter geometries, i.e. for almost aligned or anti-aligned spins.

Scenarios of bulge formation

Although four different processes have been identified to form bulges, major mergers, minor mergers, bars and clumpy young galaxies, it is usually not easy to separate them in each galaxy, since they can occur successively.

In major mergers, the tidal trigger first forms strong bars in the partner galaxies, which drive the gas inward; this forms first a pseudobulge in each galaxy. Then the merger of the two galaxies could provide a classical bulge, according to the encounter geometry, which will co-exist with the pseudo ones.

Alternatively, after a classical bulge has formed in a system, subsequent gas accretion could re-form a disk and a bar, which drives the gas towards the center, and form a pseudobulge.

It is likely that most galaxy disks begin gas-rich, without central concentration, without bulge, and therefore are highly unstable to form clumpy galaxies at high z. Simulations show that there is rapid formation of an exponential disk and a bulge, through dynamical friction (Noguchi 1999, Bournaud et al. 2007b). The evolution is slightly quicker than with spirals and bars. The rapid bulge formation is again a problem for the bulgeless galaxies today.

Clues from high z galaxies

Spheroids appear in place quite early (Conselice 2007). There is a deficit of disk galaxies at $z = 1$. Could it be a bias of the observations with limited sensitivity? Or disky galaxies have formed only recently, and in poor environment? Big disks in rotation are however observed (Genzel et al. 2008, Neichel et al. 2008).

Massive bulges ($B/T > 0.2$) and ellipticals have the same early formation, as shown by the GOODS study of 0.1 <z <1.2 galaxies (MacArthur et al. 2008). Their star formation history (SFH) is compatible with a single early burst. There is however a degeneracy, the same SFH can be obtained, if the mass is assembled more recently from dry mergers.

Multiple minor mergers

The bulges formed by minor mergers are often the same as for major mergers, since they are more numerous. The issue is not the mass ratio of individual mergers, but the total mass accreted. As soon as a given spiral galaxy has accreted 30-40% of its initial mass, either in one event, or a series of small minor mergers, then the final result is likely to be an elliptical galaxy. Bournaud et al. (2007a) have shown through simulations that 50 mergers of 50:1 mass ratio can easily form an elliptical, and this is certainly more frequent than a 1:1 merger.

5. Conclusion

Secular evolution and bars play a major role in pseudo-bulge formation, and this explains their presence in the blue sequence of galaxies. Since gas inflow weakens or destroy the bar, a galaxy can have several bar episodes, and each accumulates mass in the pseudo-bulge. Cold gas accretion, from cosmic filaments, can replenish galaxy disks, and reform bars. It is expected that bars were destroyed more frequently at high z, since galaxy disks contained more gas. This is in line with the observation of decreasing bar fraction at high z.

There are several scenarios for bulge formation, classical bulges through major mergers, but also a succession of minor mergers, clumps in young galaxies, coalescing in the center, due to dynamical friction, bars.. In most galaxies, there is coexistence of many processes and it is not easy to reconstruct the dynamical history of the bulge assembly. In any case, it is quite easy to form a bulge, in any galaxy environment, and it is a surprise to observe a large fraction of bulgeless galaxies. It is a challenge both for the hierarchical scenario, but also for the secular evolution. It is difficult in particular to find high-z precursors of these bulgeless galaxies. Have those disks formed recently?

Acknowledgments. Many thanks to Shardha Jogee and the organising committee to invite me at this stimulating conference.

References

Barazza F. D., Jogee, S., & Marinova, I. 2008, ApJ, 675, 1194
Berentzen I., Heller, C. H., Shlosman, I., & Fricke, K. J. 1998, MNRAS, 300, 49
Berentzen I., Shlosman, I., Martinez-Valpuesta, I., & Heller, C. 2007, ApJ, 666, 189
Block, D. L., Bournaud, F., Combes, F., Puerari, I., & Buta, R. 2002, A&A, 394, L35

Boeker T., Laine, S., van der Marel, R. P. et al. 2002, AJ, 123, 1389
Bournaud F. & Combes F. 2002, A&A, 392, 83
Bournaud F., Combes F., & Semelin B. 2005, MNRAS, 364, L18
Bournaud F., Jog C., & Combes F. 2007a, A&A, 476, 1179
Bournaud F., Elmegreen, B. G., & Elmegreen, D. M. 2007b, ApJ, 670, 237
Brooks A. M., Governato, F., Quinn, T., Brook, C. B., & Wadsley, J. 2008, arXiv0812.0007
Buta, R., Laurikainen, E., & Salo, H. 2004, AJ, 127, 279
Combes F., Debbasch F., Friedli D., & Pfenniger D. 1990, A&A, 233, 82
Combes F. 2008, in Pattern Speeds along the Hubble Sequence, ed. E. Corsini & V. Debattista, arXiv:0811.0153
Conselice C. J. 2008 IAUS, 245, 429
Crocker, A. F., Jeong, H., Komugi, S., Combes, F., Bureau, M., Young, L. M., & Yi, S. 2008, arXiv0812.0178
Dekel, A., Birnboim, Y., Engel, G. et al. 2009, Nat, 457, 451
Di Matteo P., Combes F., Melchior A-L., & Semelin B. 2007, A&A, 468, 61
Drory N. & Fisher D. B. 2007, ApJ, 664, 64
Eskridge, P. B., Frogel, J. A., & Pogge, R. W. et al. 2002, ApJS, 143, 73
Fisher D. B. & Drory N. 2008, AJ, 136, 773
Fraternali F. & Binney J. J. 2006, MNRAS, 366, 449
Fraternali F., Binney J. J., Oosterloo T., & Sancisi R. 2007, NewAR, 51, 95
Friedli, D. 1994, in Mass-Transfer Induced Activity in Galaxies, ed. I. Shlosman (Cambridge: Cambridge University Press), 268
Genzel R., Burkert, A., Bouché, N. et al. 2008, ApJ, 687, 59
Heller C. H., Shlosman, I., & Athanassoula, E. 2007, ApJ, 657, L65
Jogee S., Barazza, F. D., Rix, H.-W. et al. 2004, ApJ, 615, L105
Jogee S. 2006, in Lecture Notes in Physics, Vol. 693, Physics of Active Galactic Nuclei at all Scales, ed. D. Alloin, R. Johnson & P. Lira (Berlin and Heidelberg: Springer), 143
Kautsch S. J., Grebel, E. K., Barazza, F. D., & Gallagher, J. S. 2006, A&A, 451, 1171
Koda, J., Milosavljevic, M., & Shapiro, P. R. 2007, ApJ, 696, 254
Kormendy J. & Kennicutt R. C. 2004, ARAA, 42, 603
Kormendy J. & Fisher D. B. 2008, ASPC, 396, 297
Laurikainen E., Salo, H., Buta, R., & Knapen, J. H. 2007, MNRAS, 381, 401
MacArthur L. A., Ellis, R. S., Treu, T., et al. 2008, ApJ, 680, 70
Marinova I. & Jogee S. 2007, ApJ, 659, 1176
Neichel B., Hammer, F., Puech, M. et al. 2008, A&A 484, 159
Noguchi M. 1999, ApJ, 514, 77
Sancisi R., Fraternali, F., Oosterloo, T., & van der Hulst, T. 2008, A&ARv, 15, 18
Sheth K., Elmegreen, D. M., Elmegreen, B. G. et al. 2008, ApJ, 675, 1141
Whyte, L. F., Abraham, R. G., Merrifield, M. R. et al. 2002, MNRAS, 336, 1281
Weinzirl, T., Jogee, S., Khochfar, S., Burkert, A. & Kormendy, J. 2009, ApJ, 696, 41

GALAXY EVOLUTION: EMERGING INSIGHTS AND FUTURE CHALLLENGES
ASP Conference Series, Vol.
@jourvol, © 2009
S. Jogee, I. Marinova, L. Hao, and G. A Blanc

Dark Matter Substructure, Filaments and Assembling Disks

Isaac Shlosman

JILA, University of Colorado, Boulder, CO 80309, USA

Abstract. We review some general properties of assembling galactic dark matter (DM) halos which have a direct effect on the baryon dynamics. Specifically, we focus on the mutual dynamical feedback between baryons and DM which influence disk formation and evolution, by comparing models with and without baryons evolved from identical initial conditions. Baryons are found to be capable of modifying the DM density profiles of inner halos, leading to isothermal profiles rather than the NFW cusps. Those can be leveled off by the subsequent dynamical friction of the subhalos at lower z. Furthermore, subhalos appear efficient in triggering galactic bars and ablating cold gas from the disks, and therefore quenching of star formation there.

1. Adding Baryons to Forming Galaxies

Formation of luminous parts of galaxies is inherently connected with baryon dynamics in the background of the dark matter (DM). While only one sixth of the matter is baryonic in the WMAP3 Universe (e.g., Spergel et al. 2007), it apparently dominates the inner regions of galaxies because of the ability to dissipate energy. The associated efficiency in getting rid of the angular momentum leads to de facto separation between baryons and DM. The relevant galactic dynamics probably transcends the simple adiabatic contraction (e.g., Blumenthal et al. 1986) and the actual evolution appears to be more complex. To more fully understand the role of baryons in galaxy evolution, we focus on two issues: (1) how do baryons affect the background DM in galaxies, and (2) how does the distribution of DM on scales larger and smaller than galactic halos influences the accumulation and dynamics of baryons in the central regions, where disks form and grow. In the following, we make a broad use of representative models of pure DM (PDM models) and baryon+DM (BDM models), which have been evolved from identical initial conditions (Romano-Diaz et al. 2009a). The general properties of DM halos which have been established so far lead to important consequences for baryon evolution in the galactic centers. Those in turn exert feedback on the DM, which affects shapes, density profiles, angular momentum and substructure. We limit out discussion to those properties which have a direct impact on disk evolution.

Filaments and accretion through filaments emerge as the dominant mode of galaxy growth (e.g., Dekel et al. 2008). It is important that the cosmological filaments which dominate the large-scale DM structure initially extend to the very small scales of a few kpc where the seed galactic disks form at intermediate z (Shlosman 2009). The characteristic "cat's cradle" displays how the inflowing baryons smoothly join the disk, experiencing little 'shocking' (Fig. 3 in Heller

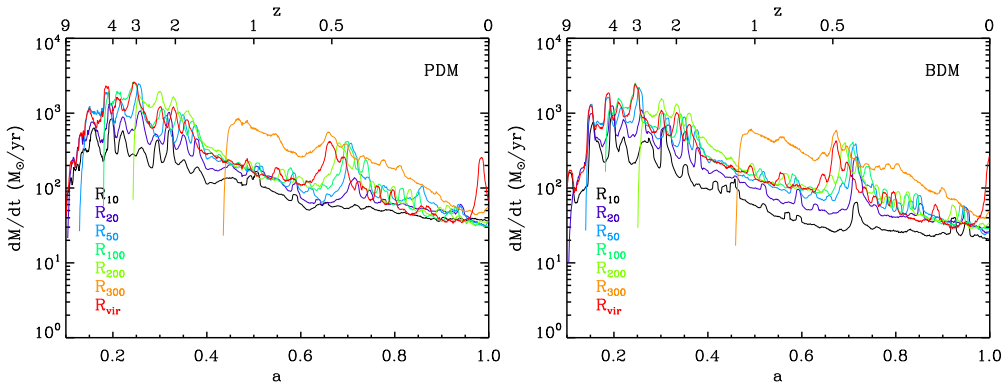

Figure 1. DM influx rates along the filaments in the pure DM (left) and baryons+DM (right) models, with identical initial conditions. The color-coded curves correspond to the fixed radii of 10 kpc – 300 kpc and the DM virial radii, as a function of z and the cosmological expansion parameter a (Romano-Diaz et al. 2009b).

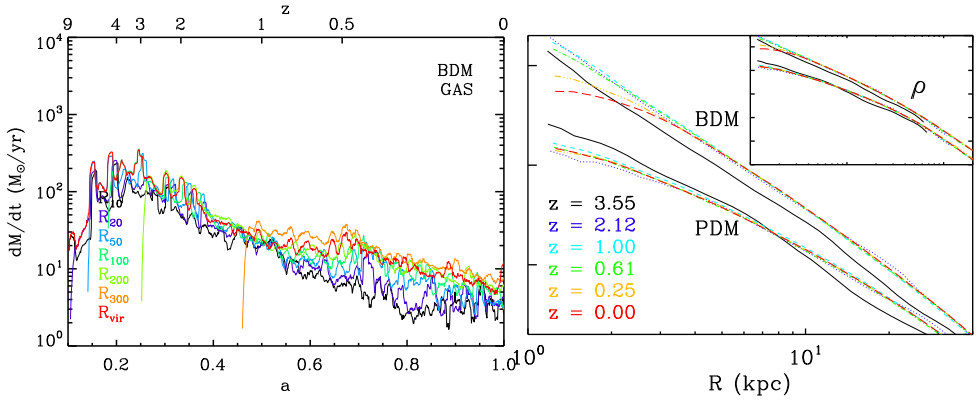

Figure 2. *Left:* As in Fig. 1 but for the gas inflow along the filaments (Romano-Diaz et al. 2009b). *Right:* Evolution of DM density profiles $\rho(R)$ within the inner 20 kpc in the PDM and BDM models. The insert shows ρ within 200 kpc. The curves are displaced vertically for clarity (Romano-Diaz et al. 2008a).

et al. 2007). At small radii, the clumpy gas influx appears tangent to the protodisk, in apparent repeling action of the angular momentum. The inflow along the DM filaments prevents the gas from being virialized before it joints the disk. Furthermore, it assures that the gas will lose some fraction of its angular momentum to a filament. The typical DM accretion rates along the filaments decay with time and show a mild difference between the PDM and BDM models (Fig. 1a,b). This difference amounts to a somewhat supressed influx rate in the inner 10 kpc—20 kpc after $z \sim 1$ and is related to the action of baryons as we discuss below. The typical gas accretion rate along the filaments fits comfortably to the overall picture of galaxy growth. Fig. 2a exhibits inflow

which is sufficient for a massive disk formation in the long run and can support the currently observed star formation rates in a Milky Way-type galaxies.

2. DM and Baryon Settling in Pure DM and DM+Baryons Models

The DM halo buildup, in the absence of baryons, is known to lead to a universal density profile with a characteristic scale R_s corresponding to the logarithmic slope of –2 (e.g., Navarro et al. 1997, NFW). Within this radius, the density is cuspy, its slope tends to –1 when $R \to 0$. The reason for this universality is currently debated but it is important that baryons can substantially modify this density profile (El-Zant et al. 2001; 2004; Tonini et al. 2006), bridging the gap with observations. Those hint at a central flat density core rather than a cusp (e.g., de Blok 2007; Kuzio de Naray et al. 2008). Romano-Diaz et al. (2008b) find that the NFW cusp formation is by-passed in favor of an isothermal DM cusp, in BDM models (Fig 2b). The isothermal cusp in turn can be leveled off by the action of penetrating minor mergers after $z \sim 1$. To avoid the ambiguity in the definition of R_s in the BDM models, we invoke the radius of a maximal circular velocity, $R_{\rm vmax}$, in the halo instead. The fraction $\gamma \equiv R_s/R_{\rm vmax} \sim 0.46$ is universal for the NFW fit. For all models we define $\tilde{R}_s \equiv \gamma R_{\rm vmax}$.

While formation of isothermal cusps is related to the adiabatic contraction and involves a certain degree of dissipation by baryons, their demise can be associated with clumpy accretion of DM subhalos glued by baryons. It happens well beyond the epoch of major mergers, after $z \sim 1$. Romano-Diaz et al. (2008a,b) have shown that the late stages of inflow along the filaments involve subhalos which cluster there, and enter the prime halo before they merge among themselves. Due to higher binding energy, the subhalos in the BDM models can penetrate the inner halo. Within the virial radius of the prime halo, the mass function of subhalos evolves strongly, especially when baryons are present (Romano-Diaz et al., in preparation). The mass ratio of the most massive subhalo to the prime halo decreases with time, but is $\sim 8 \times 10^{-4}$ even at $z = 0$, higher than the minimum required by El-Zant et al. (2001) for the dynamical friction to be efficient over orbital times. The influx of subhalos is well correlated with the 'smooth' DM streaming out of the center and 'cooling' down.

Cold, rotationally supported baryons are expected to accumulate within $\tilde{R}_s$, subject to expulsion by stellar or AGN feedback. Some baryons will be trapped in the filaments and in shells outside the virial radius, $R_{\rm vir}$. These shells form when incoming subhalos are tidally disrupted but avoid capture by the gravitational well. Hence, it is not clear at present to what extent the baryonic content of a galaxy corresponds to the universal fraction of baryons. For a MW-type galaxy, Romano-Diaz et al. (2009a) find that major mergers tend to increase the baryon fraction, while minor mergers decrease it — the net effect appears to be negligible. This result is based on a fine-tuning of the stellar feedback parameter, based on a large number of disk models (Heller et al. 2007).

What is the source of the inner halos' DM, say within $\tilde{R}_s$, and when do the inner halos form? Does the DM accumulation within $\tilde{R}_{\rm s}$ end with the major mergers epoch (e.g., Wechsler et al. 2002). Comparison between the PDM and BDM models reveals that only about 15% and 33% of the DM mass found within this radius at $z = 0$ is contributed by the subhalos, for PDM and BDM

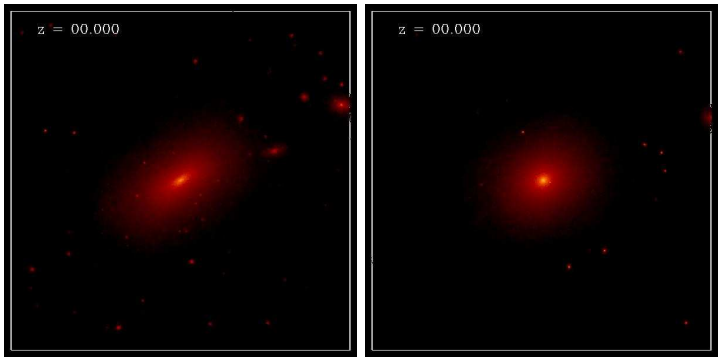

Figure 3. Example of DM halos at $z = 0$ without (left frame) and with (right frame) baryons. The frames are about 1 Mpc on the side. The halos have been evolved from identical initial conditions (Romano-Diaz et al. 2009a).

respectively. The rest comes from the 'smooth' accretion. Here we, rather arbitrary, limit the 'clumpy' (i.e., subhalo) accretion to the clump-to-prime halo mass ratios in excess of 10^{-4} of the prime halo virial mass at $z = 0$. This includes about 4% and 20% (PDM and BDM) coming from the major mergers, i.e., the mass ratios of $\gtrsim 1:3$, and 11% and 13% (PDM and BDM) from the minor mergers. Overall merger contribution to the central mass falls slowly with the decreasing merger mass ratio. Second, while the DM density profile is established early (except in the central few kpc), most of the DM is not confined to within the characteristic radii, $\tilde{R}_{\rm s}$ and $R_{\rm vmax}$ — only 13% and 20% of DM found within these radii, respectively, are bound there. The majority makes much larger radial excursions. Hence the buildup of the inner halos continues to $z = 0$. The flow of the unbound DM contributes about 80% of the DM within $\tilde{R}_{\rm s}$ after the merger epoch, but the net influx of this material is zero, and this region appears to be rather in a steady state. Most of the DM particles within $\tilde{R}_{\rm s}$ reside there for a short crossing time only. One hopes that these numbers are representative and reflect the basics of the DM halo assembly.

Equally important for the disk evolution appears to be the highly anisotropic flux of DM and baryons toward the center. The background potential of the DM is strongly triaxial at the peak of the inflow. The shapes of DM halos respond to the presence of baryons by reducing their triaxiality (e.g., Kazantzidis et al. 2004; Berentzen & Shlosman 2006) and a number of factors are involved (Fig. 3). Both, the clumpiness of baryons, their central concentration and out-of-phase response to the DM driving lead to a decrease in the halo flatness and to a loss of its equatorial ellipticity, when the disks form (e.g., Shlosman 2008). Moreover, the halo figure tumbling appears insignificant both with and without baryons, irrespective of whether it is located in the field (i.e., isolated) or in a denser environment of a filament, based on ~ 900 snapshots (Heller et al. 2007; Romano-Diaz et al. 2009a), which agrees well with Bailin & Steinmetz (2004) estimates. The angular momentum acquired by halos is channeled into the internal streaming rather than figure rotation. Such an exceedingly slow tumbling of DM halos has important dynamical consequences for growing disks by moving the halo's outer inner Lindblad resonance to very large radii, beyond $R_{\rm vir}$.

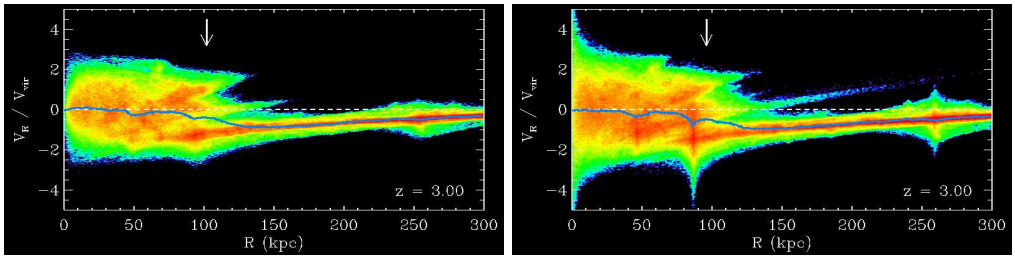

Figure 4. Evolution of the DM halo in the PDM (left) and BDM (right) models shown in the $R - v_{\rm R}$ plane at $z = 3$, i.e., during the major merger epoch and the appearance of fingers. The colors correspond to the DM particle density on the $R - v_{\rm R}$ surface. The vertical arrows show $R_{\rm vir}$, the dashed white line – $v_{\rm R} = 0$, and the blue line — the average $v_{\rm R}$ at each R. Accretion along the large-scale filament is seen as a stream at $v_{\rm R} < 0$ (Romano-Diaz et al. 2009a).

3. DM Halo Relaxation Beyond Virialization

While the DM halos are being virialized, this process is clearly incomplete because a cosmological halo is an open system. In addition, when the density profile is established early, oscillations of the central potential decay fast, except during major mergers. This limits the efficiency of the violent relaxation process (Lynden-Bell 1967). However, the ongoing accretion of a clumpy material can steer the halo, especially its outer region where they are favored because of the material influx along the large-scale filaments. It is informative, therefore, to look at the fate of the incoming subhalos and compare the PDM and BDM models. For this purpose we use the $R - v_{\rm R}$ phase diagrams which allow to quantify the substructure contributions, where R is the spherical radius (Fig. 4).

We define three types of subhalo relics, which partially represent various stages of their dissolution. The (bound) subhalos can be easily seen because of their vertical spikes (subhalo internal velocities) in Fig. 4. Those that are in the process of tidal disruption are accompanied by inclined spikes ('fingers,' partially bound). Lastly, the tidally disrupted subhalos persist as streamers for a long time, those represent $R - v_{\rm R}$ correlations (unbound). The cold filament-driven influx appears de-focused after passing the pericenter of its motion. As its constituents move out, their slowdown in tandem with the tidal disruption lead to the formation of shells that persist for a long time. Shells that form later in time have larger outflow velocities and can cross shells that formed earlier. For the survival of these shells it is important that they form after subhalos pass the pericenters of their orbits.

Both the spikes and fingers appear longer by ~ 2 in the presence of baryons. The streamers survive for a long time, and those that form after $z \sim 1$ survive till present. Hence, the prime halo goes through inefficient relaxation beyond its virialization. The ability of subhalos in the presence of baryons to penetrate deeper into the prime halo and survive for a long time has also impications for the disk evolution in the BDM models. The residual currents in the halo continue to mix the halo environment even in the absence of large-amplitude variability in the central potential.

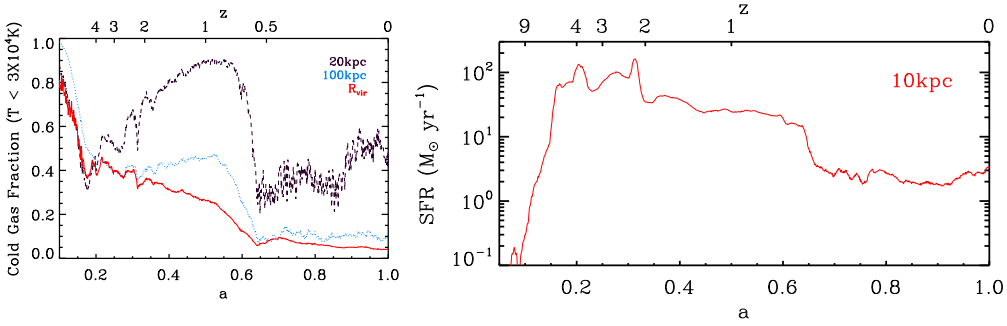

Figure 5. *Left:* Fraction of the cold, $T \lesssim 3 \times 10^4$ K gas (of the total gas) within the inner 20 kpc (disk), 100 kpc and $R_{\rm vir}$ of assembling DM halo. The sharp decrease in the gas mass at $z \sim 0.5 - 0.6$ is related to the beginning of the subhalo influx along the large-scale filament and subsequent ablation from the disk; *Right:* Star formation rates shown within the inner 10 kpc of the disk (Romano-Diaz et al. 2008a; 2009a).

4. Disk-Substructure Interactions

Evidence points to a variety of processes that affect the disk assembly in a DM halo. Major mergers act to destroy the forming disk, but if the system has a substantial reservoir of cold gas and/or large-scale filaments continue to supply such gas, the disk can be rebuilt at lower z. From general arguments, the gravitational potential of the inner halo is not axisymmetric, and can include the penetrating filaments, at least at high z. Under these conditions, the initially gas-dominated disk will be strongly non-axisymmetric and turbulent. Bar formation is favored and the properties of such gas/stellar bars differ from those studied in the galactic dynamics. Because of the low central density concentration, the first generation of bars will tumble with very low speeds (e.g., Heller et al. 2007; Romano-Diaz et al. 2008b). This property is crucial to avoid the developing chaos (Shlosman 2009) which is expected to dissolve the bars formed in non-axisymmetric potentials because of the destructive interactions between stellar and DM quadrupoles (El-Zant & Shlosman 2002). A rapid growth of the disk brings along the bar growth as well, together with the pattern speed-up. Moreover, the disk material, especially the gas but also the stars, is aware of the large-scale orientation of the DM potential. One should expect a nonlinear response of the disk shape to this perturbations. Numerical simulations show that this leads to large distortions in the outer disk, including prominent spiral arms, which are followed by a nearly axisymmetric stage (Heller et al. 2007). Various waves are excited in the disk and the beat phenomenon is frequently observed. Due to the presence of the gas, nested bar cascade is plausible and will lead to a rapid angular momentum loss from the central regions, leading to the formation of a single massive object (Begelman et al. 2006).

The DM substructure can have a profound effect on the prevailing morphology in the disk (Gauthier et al. 2006; Romano-Diaz et al. 2008b). Here, we mention two effects only: triggering of galactic bars and cold gas ablation from the disk. The former constitutes a finite perturbation and allows to circumvent various problems associated with the linear stage of the bar instability. Trigger-

ing bars with galaxy perturbations has been known for some time (e.g., Byrd et al. 1986; Noguchi 1987), but subhalos can make it even more efficient and, paradoxically, less dependent on the environment.

A potentially new effect is the ablation of the cold disk gas by subhalos, as shown in Fig, 5a. It is clearly related to the penetrating encounters with the subhalos. In addition to heating up the cold gas, the hot gas component is driven out, in conjunction with the inner DM, as discussed in §1. The immediate corollary of this process is a sharp, factor of 10 decrease in the star formation rate associated with the disk (Fig. 5b). This can be a general stage in the evolution galaxies, when the star formation is quenched by interactions with the DM substructure.

Acknowledgments. I thank the organizer, Shardha Jogee, for an interesting and stimulating conference, and Emilio Romano-Diaz, Clayton Heller and Yehuda Hoffman for collaboration on various topics discussed here. Support from NASA and NSF grants is gratefully acknowledged.

References

Bailin, J. & Steinmetz, M. 2004, ApJ, 616, 27
Begelman, M.C., Volonteri, M. & Rees, M.J. 2006, MNRAS, 370, 289
Berentzen, I. & Shlosman, I. 2006, ApJ, 648, 807
Blumenthal, G.R., Faber, S.M., Flores, R. & Primack, J.R. 1986, ApJ, 301, 27
Byrd, G.G., Valtonen, M.J., Valtaoja, L. & Sundelius, B. 1986, A&A, 166, 75
de Blok, W.J.G. 2007, in Island Universe, ed. R.S. de Jong (Dordrecht: Springer), 89
Dekel, A., Birnboim, Y., Engel, G. et al. 2009, Nat, 457, 451
El-Zant, A., Shlosman, I. & Hoffman, Y. 2001, ApJ, 560, 636
El-Zant, A. & Shlosman, I. 2002, ApJ, 577, 626
El-Zant, A., Hoffman, Y., Primack, J., Combes, F. & Shlosman, I. 2004, ApJ, 607, L75
Gauthier, J.-R., Dubinski, J. & Widrow, L.M. 2006, ApJ, 653, 1180
Heller, C.H., Shlosman, I. & Athanassoula, E. 2007, ApJ, 671, 226
Kazantzidis, S. et al. 2004, ApJ, 611, L73
Kuzio de Naray, R., McGaugh, S.S. & de Blok, W.J.G. 2008, ApJ, 676, 920
Lynden-Bell, D. 1967, MNRAS, 136, 101
Navarro, J.F., Frenk, C.S. & White, S.D.M. 1997, ApJ, 490, 493 (NFW)
Noguchi,M. 1987, MNRAS, 228, 635
Romano-Diaz, E., Shlosman, I., Hoffman, Y. & Heller, C.H. 2008a, ApJ, 685, L105
Romano-Diaz, E., Shlosman, I., Heller, C.H. & Hoffman, Y. 2008b, ApJ, 687, L13
Romano-Díaz, E., Shlosman, I., Heller, C., & Hoffman, Y. 2009a, ApJ, 702, 1250
Romano-Diaz, E., Shlosman, I., Heller, C.H. & Hoffman, Y. 2009b, ApJ, submitted
Shlosman, I. 2008, in ASP Conference Series Vol. 390, Pathways Through an Eclectic Universe, ed. J. H. Knapen, T. J. Mahoney & A. Vazdekis (San Francisco: ASP), 440
Shlosman, I. 2009, in Mem. Soc. Astron. Ital., Pattern Speeds Along the Hubble Sequence, ed. E. M. Corsini et al., arXiv:0812.0808
Spergel et al. 2007, ApJS, 170, 377
Tonini, C., Lapi, A. & Salucci, P. 2006, ApJ, 649, 591
Wechsler, R.H., Bullock, J.S., Primack, J.R., Kravtsov, A.V. & Dekel, A. 2002, ApJ, 568, 52

GALAXY EVOLUTION: EMERGING INSIGHTS AND FUTURE CHALLLENGES
ASP Conference Series, Vol.
@jourvol, © 2009
S. Jogee, I. Marinova, L. Hao, and G. A Blanc

Nuclear Star Clusters in Spheroidal and Late-Type Disk Galaxies

Miloš Milosavljević

Department of Astronomy, The University of Texas at Austin, 1 University Station C1400, Austin, TX 78712

Meghann Agarwal

Department of Physics, The University of Texas at Austin, 1 University Station C1600, Austin, TX 78712

Abstract.
Photometrically distinct nuclear star clusters (NSCs) are common in late-type disk galaxies and in spheroidal galaxies. The formation of NSCs is inevitable in the context of normal star formation, in which a majority of stars form in clusters. A young, mass-losing cluster embedded in a galactic disk or in a starburst region remains gravitationally bound over a period determined by its initial mass and the galactic tidal field. The cluster migrates radially, toward the center of the galaxy, and becomes integrated in the NSC if it reaches the center. The rate at which the NSC grows by accreting young clusters can be estimated from empirical cluster formation rates and dissociation times. It seems that the NSCs in late-type disks and in spheroidals could have assembled from migrating clusters. In spheroidals, the resulting photometrically-distinct stellar nucleus can contain a small fraction (e.g., $0.1\% - 1\%$) of the stellar mass of galaxy, depending on the galactic and dark matter halo structural parameters and the ICMF, which is consistent with the empirical ratios obtained by Ferrarese et al. (2006b) and Wehner & Harris (2006). In this picture, NSC assembly is collisionless and non-dissipative, and thus, no relation is expected to the processes that facilitate central black hole assembly in more massive galaxies. In disks, this scenario predicts a relation between the central stellar light in excess of the inward-extrapolated exponential law of the outer disk and the NSC mass.

1. Introduction

Photometrically distinct nuclear star clusters (NSCs) are ubiquitous in dynamically primitive galaxies, which are the galaxies that lack structural signatures of major mergers. Imaging with the *Hubble Space Telescope* has revealed that 75% of late-type (Sc–Sd) disk galaxies contain compact, luminous star clusters at their centers with masses between $8 \times 10^5 M_\odot$ and $6 \times 10^7 M_\odot$ and with uniform structural properties (e.g., Böker et al. 2004; Walcher et al. 2005). Similarly, an HST survey of the spheroidal nuclei in the Virgo cluster (Ferrarese et al. 2006a; Côté et al. 2006) has revealed stellar nuclei that contain $\sim 0.2\%$ of the galaxy mass (Ferrarese et al. 2006b; Wehner & Harris 2006). It seems that photometrically distinct NSCs are common in galaxies that have not experienced major mergers in the epoch following the initial burst of star formation, but are still evolved enough to have a well-defined dynamical center. Here we discuss the

formation of NSCs in such galaxies in the context of normal star formation in which most stars form in clusters.

A successful theory of NSC formation should explain the observed uniformity of their properties, and should relate their evolution to that of the inner regions of their host galaxies. NSCs can grow from the local ISM if the galactic gas accretes inward and accumulates at the center (e.g., Seth et al. 2006). In gas disks, sufficient gas accretion to form NSCs may be driven by magnetic stresses in the gas that are amplified by the magnetorotational instability (Milosavljević 2004), which is generic in differentially rotating galactic disks (e.g., Kim et al. 2003), or by stellar and gaseous bar torques (e.g., Kormendy & Kennicutt 2004; Schinnerer et al. 2007, and references therein). NSCs in late-type disks typically contain young stellar components, and their star formation seems to be intermittent (Rossa et al. 2006; Walcher et al. 2006). This may argue in favor of the gas accretion scenario in late-type disks. However, a substantial fraction of the NSC mass could have first assembled in off-center stellar associations (clusters) that have migrated into the galactic center and have merged with the NSC as intact entities (Capuzzo-Dolcetta & Miocchi 2008a,b), consistent with the observation that nuclear cluster phase space densities are on average smaller than those of globular clusters (Walcher et al. 2005). Since phase space density increases in collisionless mergers, the observed NSC phase space densities allow the scenario in which NSCs assemble from migrating globular cluster-like precursors (see, e.g., simulations by Capuzzo-Dolcetta & Miocchi 2008a,b). The NSCs thus assembled would inherit the orbital angular momentum of the migrating disk clusters and should be rotating (see, e.g., Seth et al. 2008).

Here we study the influx of migrating young embedded clusters in a star-forming galaxy. A new star that has formed in one of the young clusters remains inside the cluster for a period of time. Stellar mass loss, dynamical evaporation, and external perturbations lead to progressive tidal mass loss, and the star eventually becomes unbound. Now orphaned by its dissolving cluster, the star joins the unclustered stellar component of the galaxy. Since even in very late type disks circular test particle orbits rotate differentially throughout, cluster dissolution is inevitable except if the cluster forms at, or migrates into, the galactic center. Clusters with off-center birthplaces can avoid dissociation if they migrate to the dynamical center quickly enough.

2. Young Cluster Formation, Migration, and Dissociation

The initial cluster mass function (ICMF) contains about equal mass on all cluster mass scales, i.e., $dn/dM \propto M^{-\alpha}$ with $\alpha \sim 1.75 - 2$ for $M_{\rm min} < M < M_{\rm max}$, where M denotes cluster mass and $M_{\rm min}$ and $M_{\rm max}$ are galaxy-dependent cutoffs. Frequently, an ICMF with an exponential cutoff $dn/dM \propto M^{-\alpha}e^{-M/M_\star}$ is found to be a good fit. In spirals and irregulars $M_\star \sim 2\times10^5 - 10^{7.5}$ (see, e.g., Zhang & Fall 1999; Bik et al. 2003; de Grijs et al. 2003; Dowell et al. 2008; Larsen 2009; Gieles 2009) with typical values $M_\star \sim 2\times10^5 M_\odot$ (Gieles 2009; Larsen 2009) and $M_{\rm max} \sim 10^6\ M_\odot$ in, e.g., NGC 6946, M51, and the Antennae (Gieles et al. 2006b,c). The mass truncation scale $M_\star$ is larger in denser starburst environments. We adopt $\alpha = 2$ and $M_{\rm min} = 100\ M_\odot$ in what follows.

A young cluster migrates on a time scale $t_{\rm mig} = (dJ/d\ln R)/T_{\rm df}$, where $J = MR^2\Omega$ is the angular momentum of the cluster and $T_{\rm df}$ is the dynamical friction torque. All galactic mass components (dark matter, gas disk, stars) respond dynamically to the cluster but the mechanism of torque coupling varies. N-body simulations have shown that the torque from a nonrotating spheroidal collisionless halo scales just like in Chandrasekhar's formula, in which the torque is proportional to the Coulomb logarithm $\ln(\Lambda)$. Because the kinematic structure of actual halos differs from the premises of Chandrasekhar's derivation, N-body simulations are necessary to obtain the correct normalization of the torque amplitude. The numerically evaluated torques (e.g., Velazquez & White 1999; Peñarrubia et al. 2002, 2004; Spinnato et al. 2003) can be modeled with Chandrasekhar's formula if the Coulomb logarithm is treated as an empirical free parameter and set to $\ln(\Lambda) \sim 2 - 7$.

In differentially rotating gas or stellar disks, the torque is provided by the flow in the corotation region and by angular momentum transfer at Lindblad resonances (e.g., Goldreich & Tremaine 1980; Quinn & Goodman 1986). Disk clusters with masses $M \lesssim 10^6 M_\odot$ have Roche tidal radii $r_{\rm t} \sim (GM/|d\Omega/d\ln R|)^{1/3}$ that are smaller than the thickness of the disk. In this regime, the disk torque is a generalization of the "Type I" torque acting on small planets in protoplanetary disks (e.g., Tanaka et al. 2002; D'Angelo et al. 2003; Baruteau & Masset 2008) to non-Keplerian disks and is proportional to $T_{\rm df,disk} \propto G^2M^2\Sigma/\sigma^2$, where Σ is the surface density of the gas or stellar disk, and σ is the gas sound speed or the stellar velocity dispersion in the disk.

The timescale on which a cluster dissolves in the galactic tidal field has been determined empirically by modeling the luminosity and age functions of clusters in nearby disk galaxies. Theoretical models tracking stellar and dynamical evolution of a cluster in a tidal field (e.g., Gieles et al. 2008; Gieles & Baumgardt 2008) have reproduced the observationally inferred variation of the dissociation time with cluster mass, $t_{\rm dis} = t_0(M/M_\odot)^\gamma$, where $\gamma \approx 0.62$ (Boutloukos & Lamers 2003). The normalization t_0 varies between galaxies, which is a consequence of the variation in the tidal field strength and of any cluster-scale density inhomogeneities of the galactic environment. Gieles et al. (2008) assessed the role of the tidal field by comparing cluster lifetimes in several galaxies with the angular frequency of galactic rotation at observed cluster radii, Ω, and found consistency with $t_{\rm dis} \propto \Omega^{-1}$. The tidal radius really depends on the degree of differential rotation and thus $t_0 \propto |d\Omega/d\ln R|^{-1}$. Lamers et al. (2005a) modeled the observed cluster population in M33 and find, at an arbitrary radius, $t_0 \approx f_{\rm dis}/\Omega(R)$ with $f_{\rm dis,M33} \approx 0.16$. The theoretical estimate in Lamers et al. (2005a) based on Baumgardt & Makino (2003) is more optimistic, $f_{\rm dis} \sim 0.3$. The clusters originating in M33's central disk could be denser and more resistant to tidal disruption than those in the sample of Lamers et al. (2005a). The above relations were obtained for clusters originating in a galactic disk. For the lack of an equivalent empirical result for spheroidal starbursts, we assume that these relations hold universally, and adopt the crude relation $t_0 = 0.2\,|d\Omega/d\ln R|^{-1}$. We proceed to discuss NSC assembly from embedded cluster migration in spheroidal and disk galaxies separately.

2.1. Spheroidal Galaxies

The surface density profiles of spheroidal galaxies are well described by a two component model $\Sigma(R) = \Sigma_{\rm Sersic}(R) + \Sigma_{\rm nucl}(R)$. The Sérsic law component $\Sigma_{\rm Sersic}(R) \propto e^{-(R/R_0)^{1/n}}$, where n is the Sérsic index and R_0 is a scale radius, contains most of the light, and the compact nuclear component $\Sigma_{\rm nucl}(R)$ contains a small fraction of the light. In spheroidals the Sérsic index varies, $n \sim 1-2$ (Ferrarese et al. 2006a; Kormendy et al. 2009). We consider an initial galaxy with a spherically-averaged stellar density profile that lacks a nucleus. Then, the stellar density profile $\rho_\star(r)$ can be obtained via deprojection. The total density profile includes a dark matter component $\rho(r) = \rho_\star(r) + \rho_{\rm DM}(r)$. Spheroidals are often dark matter dominated, $\rho_{\rm DM}(r) \gtrsim \rho_\star(r)$. Let $d^2n/dMdr$ be the number of clusters per unit initial cluster mass per unit radius in the galaxy such that $\int_0^\infty d^2n/dMdr\,dr$ equals the cluster initial mass function, while $\int d^2n/dMdrMdM = 4\pi r^2\rho_\star$. For a specific choice of $M_{\rm max}$, we distribute clusters randomly according to the distribution $d^2n/dMdr$. We then proceed to model cluster migration and dissolution by following the cluster orbital decay $dr/dt = -\beta_{\rm mig} r/t_{\rm mig}$ and mass loss $dM/dt = -\beta_{\rm dis} M/t_{\rm dis}$, where $\beta_{\rm mig} \geq 1$ and $\beta_{\rm dis} \geq 1$ are factors that model the influence of a cluster's orbital eccentricity on the migration and mass loss rate. We keep track of the tidally stripped mass of the kth cluster $\Delta\rho_{\star,k} = (4\pi r^2)^{-1}(dM_k/dt)/(dr_k/dt)$ and include it in the final density profile. The migrating cluster mass that reaches the center, $r \lesssim 5$ pc, is added to the central cluster.

In Figure 1, we show the projected surface density profile for stars ($M_{\rm gal} = 10^{10}\ M_\odot$, $R_0 = 500$ pc, $n = 1.5$), dark matter ($M_{\rm halo} = 10^{11}\ M_\odot$), and the NSC, where for the latter we have arbitrarily adopted the Sérsic profile $\Sigma(R) \propto e^{-(R/R_{\rm NSC})^{1/n_{\rm NSC}}}$ with index $n_{\rm NSC} = 2$ and scale radius $R_{\rm NSC} = 0.5$ pc, assuming $M_{\rm max} = 2\times10^5 M_\odot$ and $\ln\Lambda = 5$. The resulting NSC contains 1.5% of the stellar mass of the galaxy; smaller or larger NSC masses can be obtained with different values of these two parameters. This illustrates that the assembly of NSCs can be collisionless and nondissipative, thus no relation should exist to the formation of the central massive black holes in the spheroidals' higher-luminosity cousins, the ellipticals, which must involve a dissipative, gas dynamical process.

2.2. Disk Galaxies

One of the best-studied disk galaxy NSCs is that in the center of M33. Its mass, photometric FWHM radius, and stellar velocity dispersion are $M_{\rm nuc} \sim (0.5-2)\times10^6 M_\odot$, $r_{\rm h} \sim 2$ pc, and $\sigma_{\star,{\rm nuc}} = 21$ km s^{-1}, respectively (Gallagher et al. 1982; Kormendy & McClure 1993; Gordon et al. 1999). The cluster contains relatively young stellar components (van den Bergh 1976; Gallagher et al. 1982; Davidge 2000; Stephens & Frogel 2002; Long et al. 2002). The mass and the phase space density [$\sim \frac{1}{2}M(\frac{4}{3}\pi r_{\rm h}^3{\sigma_{\star,{\rm nuc}}}^3)^{-1}$] of the NSC in M33 are consistent with, and at the lower and upper ends, respectively, of the masses and phase space densities of NSCs in other bulgeless disk galaxies in the sample of Böker et al. (2002). The star formation rate density in the central 0.5 kpc of M33 is $\dot\Sigma_\star = (30-40)M_\odot$ pc^{-2} Gyr^{-1} (Heyer et al. 2004). The average stellar density in the central 0.5 kpc is $\Sigma_\star \approx (400-500)M_\odot$ pc^{-2} (Corbelli 2003); there, the projected stellar density exhibits an excess over of the exponential profile extrapolated

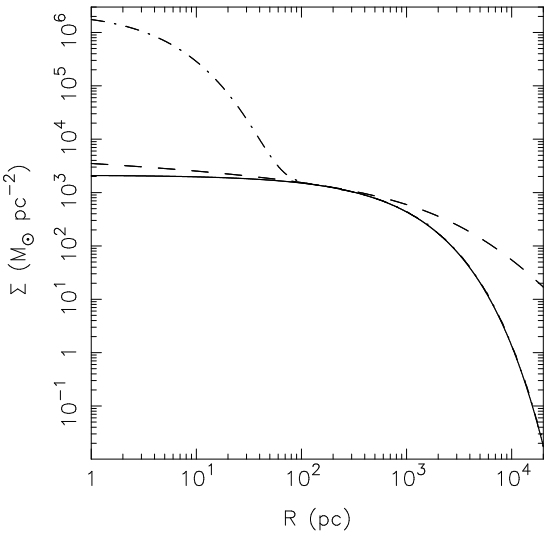

Figure 1. Projected surface density profiles of stars (solid line) and dark matter (dashed line) in the initial galaxy, and that resulting from migration of stellar clusters from off-center locations (dashed-dotted line) for a maximum young cluster mass $M_{\rm max} = 2 \times 10^5 M_\odot$ and Coulomb logarithm $\ln \Lambda = 5$.

from the outer disk (Regan & Vogel 1994). The estimated dark matter density is $R\rho_{\rm dm} \sim 100\ M_\odot\ {\rm pc}^{-2}$ (Corbelli 2003). The central total gas density, however, is $\Sigma_{\rm gas} \lesssim 15 M_\odot\ {\rm pc}^{-2}$ (Corbelli & Walterbos 2007), implying that the stars dominate dynamical mass in the center of M33 and perhaps out to $R = 4$ kpc (Corbelli 2003). The stellar rotation increases linearly near the center and is much below that of the gas (Corbelli & Walterbos 2007).

Since the stellar velocity dispersion is $\sigma_\star \sim 30\ {\rm km\ s}^{-1}$ (Corbelli & Walterbos 2007), the central stellar distribution is quasi-spheroidal and dynamically hot. The migration time scale due to quasi-isotropic perturbers is $t_{\rm mig} = (d \ln R/dt)^{-1} \sim f_{\rm df} \Omega^{-1} M_\star(R)/M$, where $M_\star(R) \sim RV^2/G$ is the total mass contained within R, and $f_{\rm df}$ is a factor parameterizing the details of the stellar dynamical response to the cluster; e.g., McMillan & Portegies Zwart (2003) adopt $f_{\rm df} \sim 0.3$ for clusters orbiting near the Galactic center. Noguchi (1999) simulated disk satellite orbital decay and found $t_{\rm mig} \sim 0.5 (M/M_\star)^{-1/2} \Omega^{-1}$ when the disk provides most of the dynamical mass, which is shorter than our estimate when $M \ll M_\star$. The present flattening of the gas rotation curve in M33 could be due to an accumulation of material in the central few hundred parsecs by star cluster and gas accretion in the inner disk, in which case the central circular velocity prior to NSC formation would have been lower.

In general, the differential cluster mass formation rate $d\dot\Sigma_{\rm cluster}/dM$ in late-type disk galaxies, integrated over cluster mass, should reproduce the total star formation rate $\dot\Sigma_\star$. The cluster mass dependence in such galaxies is given by the empirical ICMF, $dn/dM \propto M^{-2}$. Typical maximum young cluster masses $M_{\rm max}$ found in disks are only somewhat smaller than the Jeans stellar mass of the disk $M_{\star,{\rm J}} \sim f_{\rm eff} c_{\rm s}^4/G^2\Sigma \sim 5 \times 10^6 M_\odot (f_{\rm eff}/0.1)(c_{\rm s}/10\ {\rm km\ s}^{-1})^4 (\Sigma/10 M_\odot\ {\rm pc}^{-2})^{-1}$,

where the star formation efficiency $f_{\rm eff}$ is the fraction of the gas mass in a collapsing Jeans patch that transforms into stars, $c_{\rm s}$ is the gas velocity dispersion, and Σ is the gas surface density. Only the clusters that form within a few hundred parsecs of the center of the galaxy live long enough to have chance of migrating into the center. More massive clusters can migrate from larger radii. Most of the mass reaching the center of the galaxy to be integrated in the NSC arrives in the most massive embedded clusters that have initial masses comparable to the ICMF truncation scale $M_{\rm max}$ or $M_{\star}$. A cluster's migration and mass loss history are most sensitive to the tidal field strength $d\Omega(R)/dR$ at the innermost radius that the cluster reaches before dissociating, or to the strength just before reaching the center of the galaxy. The tidal field itself evolves as cluster migration transports mass in the galactic disk. For example, if the star formation rate profile is exponential, $\dot{\Sigma}_{\star} \propto e^{-R/R_{\rm s}}$, where $R_{\rm s}$ is a scale radius, tidal stripping during cluster migration modifies the exponential profile in the inner disk into a power law profile, possibly in excess of the inward-extrapolated exponential profile. The resulting central light excess (CLE)—a precursor of the pseudobulge phenomenon—has been detected in some but not all late type disks (Böker et al. 2003). If the observed CLE is indeed produced by cluster migration, the excess stellar surface density should be tightly related to the mass of the NSC. For example, in the special case in which the tidal field strength $d\Omega/dR$ is approximately independent of radius, we expect that the CLE be proportional to the square root of the NSC mass.

The mass of the NSC that assembles from stars clusters forming and migrating in the central disk of a galaxy is sensitive to the maximum mass of star clusters that form in the disk, and also depends on the amplitude of dynamical torques that drive cluster migration. For $M_{\rm max} \sim 5 \times 10^5 M_{\odot}$ and $f_{\rm df} \sim 1$, the NSC mass is $M_{\rm nuc} \sim 2 \times 10^7 M_{\odot}$, larger than the photometric mass of the NSC in M33, and compatible with NSC masses in other late type disks which range from 8×10^5 to $6 \times 10^7 M_{\odot}$ (Walcher et al. 2005). The NSC mass may be smaller if processes other than tidal stripping affect disk cluster dissociation. Our preliminary estimates of the accumulated NSC mass can be improved with improved measurements of ICMF truncation, and with numerical simulations calibrating the force of dynamical friction in stellar and gas disks.

References

Baruteau, C., & Masset, F. 2008, ApJ, 678, 483
Baumgardt, H., & Makino, J. 2003, MNRAS, 340, 227
Bik, A., Lamers, H. J. G. L. M., Bastian, N., Panagia, N., & Romaniello, M. 2003, A&A, 397, 473
Böker, T., Laine, S., van der Marel, R. P., Sarzi, M., Rix, H.-W., Ho, L. C., & Shields, J. C. 2002, AJ, 123, 1389
Böker, T., Stanek, R., & van der Marel, R. P. 2003, AJ, 125, 1073
Böker, T., Sarzi, M., McLaughlin, D. E., van der Marel, R. P., Rix, H.-W., Ho, L. C., & Shields, J. C. 2004, AJ, 127, 105
Boutloukos, S. G., & Lamers, H. J. G. L. M. 2003, MNRAS, 338, 717
Capuzzo-Dolcetta, R., & Miocchi, P. 2008a, MNRAS, 388, L69
Capuzzo-Dolcetta, R., & Miocchi, P. 2008b, ApJ, 681, 1136
Corbelli, E. 2003, MNRAS, 342, 199
Corbelli, E., & Walterbos, R. A. M. 2007, ApJ, 669, 315

Côté, P., et al. 2006, ApJS, 165, 57
Davidge, T. J. 2000, AJ, 119, 748
D'Angelo, G., Kley, W., & Henning, T. 2003, ApJ, 586, 540
Dowell, J. D., Buckalew, B. A., & Tan, J. C. 2008, AJ, 135, 823
de Grijs, R., Anders, P., Bastian, N., Lynds, R., Lamers, H. J. G. L. M., & O'Neil, E. J. 2003, MNRAS, 343, 1285
Ferrarese, L., et al. 2006a, ApJS, 164, 334
Ferrarese, L., et al. 2006b, ApJ, 644, L21
Gallagher, J. S., Goad, J. W., & Mould, J. 1982, ApJ, 263, 101
Gieles, M., Larsen, S. S., Scheepmaker, R. A., Bastian, N., Haas, M. R., & Lamers, H. J. G. L. M. 2006b A&A, 446, L9
Gieles, M., Larsen, S. S., Bastian, N., & Stein, I. T. 2006c, A&A, 450, 129
Gieles, M., Lamers, H. J. G. L. M., & Baumgardt, H. 2008, IAU Symposium, 246, 171
Gieles, M., & Baumgardt, H. 2008, MNRAS, 389, L28
Gieles, M. 2009, MNRAS, 277
Goldreich, P., & Tremaine, S. 1980, ApJ, 241, 425
Gordon, K. D., Hanson, M. M., Clayton, G. C., Rieke, G. H., & Misselt, K. A. 1999, ApJ, 519, 165
Heyer, M. H., Corbelli, E., Schneider, S. E., & Young, J. S. 2004, ApJ, 602, 723
Kim, W.-T., Ostriker, E. C., & Stone, J. M. 2003, ApJ, 599, 1157
Kormendy, J., & McClure, R. D. 1993, AJ, 105, 1793
Kormendy, J., & Kennicutt, R. C., Jr. 2004, ARA&A, 42, 603
Kormendy, J., Fisher, D. B., Cornell, M. E., & Bender, R. 2009, ApJS, 182, 216
Lamers, H. J. G. L. M., Gieles, M., & Portegies Zwart, S. F. 2005a, A&A, 429, 173
Lamers, H. J. G. L. M., Gieles, M., Bastian, N., Baumgardt, H., Kharchenko, N. V., & Portegies Zwart, S. 2005b, A&A, 441, 117
Larsen, S. S. 2009, A&A, 494, 539
Long, K. S., Charles, P. A., & Dubus, G. 2002, ApJ, 569, 204
McMillan, S. L. W., & Portegies Zwart, S. F. 2003, ApJ, 596, 314
Milosavljević, M. 2004, ApJ, 605, L13
Noguchi, M. 1999, ApJ, 514, 77
Peñarrubia, J., Kroupa, P., & Boily, C. M. 2002, MNRAS, 333, 779
Peñarrubia, J., Just, A., & Kroupa, P. 2004, MNRAS, 349, 747
Quinn, P. J., & Goodman, J. 1986, ApJ, 309, 472
Regan, M. W., & Vogel, S. N. 1994, ApJ, 434, 536
Rossa, J., van der Marel, R. P., Böker, T., Gerssen, J., Ho, L. C., Rix, H.-W., Shields, J. C., & Walcher, C.-J. 2006, AJ, 132, 1074
Schinnerer, E., Böker, T., Emsellem, E., & Downes, D. 2007, A&A, 462, L27
Seth, A. C., Dalcanton, J. J., Hodge, P. W., & Debattista, V. P. 2006, AJ, 132, 2539
Seth, A. C., Blum, R. D., Bastian, N., Caldwell, N., & Debattista, V. P. 2008, ApJ, 687, 997
Spinnato, P. F., Fellhauer, M., & Portegies Zwart, S. F. 2003, MNRAS, 344, 22
Stephens, A. W., & Frogel, J. A. 2002, AJ, 124, 2023
Tanaka, H., Takeuchi, T., & Ward, W. R. 2002, ApJ, 565, 1257
van den Bergh, S. 1976, ApJ, 203, 764
Velazquez, H., & White, S. D. M. 1999, MNRAS, 304, 254
Walcher, C. J., et al. 2005, ApJ, 618, 237
Walcher, C. J., Böker, T., Charlot, S., Ho, L. C., Rix, H.-W., Rossa, J., Shields, J. C., & van der Marel, R. P. 2006, ApJ, 649, 692
Wehner, E. H., & Harris, W. E. 2006, ApJ, 644, L17
Zhang, Q., & Fall, S. M. 1999, ApJ, 527, L81

GALAXY EVOLUTION: EMERGING INSIGHTS AND FUTURE CHALLLENGES
ASP Conference Series, Vol.
@jourvol, © 2009
S. Jogee, I. Marinova, L. Hao, and G. A Blanc

Kinematics of LSB & Dwarfs: Implications for LCDM Models

George Rhee

Department of Physics and Astronomy, University of Nevada, Las Vegas

Abstract. I briefly set the stage regarding the confrontation of LCDM models with observations of galaxy rotation curves. I then review some recent theoretical developments regarding the predictions of LCDM models. I then discuss the results of observational studies of dwarf and LSB galaxies at both optical and radio wavelengths. I finally present some preliminary results of a case study of the galaxy NGC 6822 which suggest that non-circular motions in this galaxy are more significant than was previously thought to be the case.

1. Introduction

Cosmological models based on the inflationary paradigm, cold dark matter and dark energy (ΛCDM) are very successful in explaining the large-scale structure of the universe (Spergel et al. 2003). It has been widely argued that ΛCDM models face a number of challenges on galactic scales. One of the most persistent problems is the apparent incompatibility of galaxy kinematics with the predicted structure of dark matter halos.

The problem arises because cosmological n-body simulations predict halos with a central cusp (Navarro et al. 1997, NFW). Galaxy kinematics seem to suggest that actual galaxy halos do not have a central cusp in density. Low surface brightness galaxies and dwarf galaxies, considered to be dark matter dominated at all radii, have been used to measure the properties of dark matter halos. Observational data for these galaxies seem to favor dark matter halos that have a core.

The solution to this problem lies in understanding the uncertainties in the measurements. Workers in the field do not agree on a standard procedure for deriving the dark matter density from the spectra of the gas or stars in a galaxy. In general it is found that in some cases cuspy dark matter profiles provide acceptable fits while in other cases cusps are ruled out.

It is essential to carefully model and understand the systematic errors in order to firmly establish whether there is a conflict with cosmological predictions. Recent analyses of high resolution hydrodynamical simulations of dwarf galaxies illustrate this point. Valenzuela et al. (2007) show that the cold gas can rotate slower than the circular velocity due to the combined effects of stellar feedback and a weak bar. It was also found that the gas rotation and the stellar rotation are quite comparable in the central regions.

2. Theoretical Developments

Navarro et al. (2008) have followed the formation of six different galaxy-sized halos simulated several times at varying numerical resolution. The highest resolution represents a single dark matter halo using 4.4 billion particles, of which 1.1 billion end up within the virial radius. A cusp is present on scales between 0.2 and 1 kpc with a slope steeper than -1. This is a reliable prediction of the halo structure when baryonic effects are neglected. The question then arises as to the amplitude and direction of the effects of baryons; do they steepen the cusp or make it shallower?

Some argue that the inclusion of baryons will produce models which have a core. For example, Weinberg and Katz (2002) have argued that a disk bar can produce cores in cuspy cold dark matter profiles within five bar orbital times. A 10 kpc primordial bar in a Milky Way sized galaxy would remove the cusp out to $\sim$2.5 kpc in $\sim$ 1.5 Gyr. Weinberg and Katz claim that if a strong bar forms in the gas rich disk of a dwarf galaxy, much of the gas will be driven towards the center. This dense cold gas would then be expected to undergo a strong starburst and would be expelled as a supernova driven wind. The remaining galaxy would have low surface brightness and possess a core in its dark matter distribution.

El-Zant and Shlosman (2001) have suggested that the central dark matter distribution can be substantially altered if the gas in the system is concentrated in clumped. The clumps must have a mass $\geq$ 0.01% of the total mass of the system if the central dark matter distribution is to be substantially altered. Dynamical friction dissipates the clumps orbital energy and deposits it in the dark matter. Depending on the initial conditions, the total density distribution may become more or less concentrated. Romano-Diaz et al. (2008) have investigated this further and find that the cusp is effectively erased on scales less than 2 kpc by redshift zero.

Mashchenko et al. (2006) also argue that random bulk motions of gas in small primordial galaxies will result in a flattening of the dark matter cusp on relatively short timescales (10^8) years. These gas bulk motions are driven by supernova explosions that result from ongoing star formation.

We conclude that the efficiency of various competing mechanisms to erase or enhance the cusp is still an open question. However, the prediction of cusp formation (on the relevant galactic scales) in pure N-body simulations remains robust.

3. Recent Observational Studies

Kuzio de Naray et al. (2008) derive rotation curves for a sample of low surface brightness galaxies. The high resolution optical velocity fields are obtained using DensePak integral field spectroscopy. They find that to reconcile their data with ΛCDM, *non-circular motions of amplitude* $\sim 20\ km\ s^{-1}$ are needed. They argue that non-circular motions of this magnitude are not supported by the data, indeed they argue non-circular motions are negligible (typically $\sim$ 2 km s^{-1}). This would mean that Hα emitting gas is a good tracer of the potential. However, a comparison with the data of de Blok and Bosma (2002) suggests the scatter

in estimates of the rotation velocity can be as large as 20 km s^{-1}. At small radii (see eg UGC 128) the difference between HI and Hα estimates can be as large as 20 km s^{-1}. It thus seems that the errors in the rotation curves have been underestimated.

Recent data suggest that non-circular motions in the Hα gas are in fact much larger than 2 km s^{-1}. Pizzella et al. (2008) present ESO/VLT photometry and long slit spectroscopy of a sample of six galaxies with a low surface brightness disc and a bulge. The stellar kinematics turn out to be more regular and symmetric than the ionized gas kinematics. The ionized gas often shows the presence of non-circular motions. Pizzella et al. conclude that the ionized gas is not a reliable tracer of circular velocity particularly in the central regions of low surface brightness galaxies.

When one plots radial velocity along the galaxy minor axis, the gas velocities have larger amplitude than the stellar velocities. Of course any object on a circular orbit should have zero observed radial velocity when it passes the minor axis. In practise the measured gas velocities range from zero to $\pm$20 km s^{-1} and can be as large as 50 km s^{-1} in the case of ESO-LV 2060140. Pizzella et al. (2008) also present maps of the residuals after subtracting the best fit circular velocity field for three ESO-LV galaxies. The scatter is of order 20 km s^{-1} and the residuals are not randomly distributed in space underlining the complexity of the velocity fields.

Some workers clearly measure significant non-circular motions in LSB galaxies. If one is to derive reliable measures of the dark matter content in these galaxies these motions must be taken into account.

HI 21cm observations have been crucial to the study of rotation curves of spiral galaxies. A recent survey that is relevant for the study of the core-cusp problem is the HI Nearby Galaxy Survey (known by its acronym THINGS). The data are of high quality (7" angular resolution and 5 km s^{-1} velocity resolution). A sample of 34 objects at distances great than 3 Mpc and less than 15 Mpc covering a wide range of star formation rates, total masses was observed. These data complement the SINGS (Spitzer Infrared Nearby Galaxies Survey). The high spatial and velocity resolution of THINGS observations makes these the highest quality HI rotation curves available to date for a large sample of nearby galaxies.

A series of three papers have examined the core-cusp problem using the THINGS database (Oh et al., 2008, de Blok et al., 2008, Trachternach et al., 2008). de Blok et al. (2008) present rotation curves of 19 galaxies from the database (essentially galaxies with HI inclinations greater than 40°). They do not find any declining rotation curves. The disk masses derived from rotation curves are in good agreement with photometric disk masses derived from 3.6 μm images in combination with stellar synthesis arguments. They find that for massive galaxies the core and cusp models give equally good fits to the rotation curves. They find that for low-mass galaxies a core dominated halo is preferred over a cuspy halo.

de Blok et al. compare four different methods for estimating the velocity at a given pixel on the sky. The first is the standard first moment or intensity weighted method. The second method selects the velocity where the HI profile peaks as the rotation velocity. The third is to fit single gaussians to velocity profiles. The fourth is to fit multiple gaussian profiles, or in practise fit a single

gaussian function to the profile, subtract it and subsequently make a second gaussian fit to the residual profile (Oh et al. 2008). The fourth method includes an asymmetry term in the fitting function. de Blok et al. use a Gauss-Hermite polynomial that includes an h_3 (skewness) term (van der Marel and Franx, 1993). Oh et al. (2008) derive high resolution rotation curves of IC 2574 and NGC 2366 based on THINGS VLA bulk velocity fields.

Trachternach et al. (2008) present harmonic decompositions of the velocity fields of 19 THINGS galaxies in order to quantify the magnitude of the non-circular motions in these galaxies. The velocity is expanded as:

$$v_{los}(r) = v_{sys}(r) + \sum_{m=1}^{N} c_m(r)\cos m\theta + s_m(r)\sin m\theta$$

In practice, the decompositions are carried out up to third order. This method results in estimates for non-circular motions of order 7 km s^{-1}. However when one examines the maps of residuals of the model fit to the data (de Blok et al) the residuals are seem to be larger than this in the central parts for a number of cases. For example, the residuals for the galaxy NGC 3198 range from -30 km s^{-1} to 30 km s^{-1} in the central parts while the harmonic coefficients are quoted as being of order 2-3 km s^{-1}. This suggests that the decompositions are not measuring all of the non-circular motions in these galaxies but only the component that varies with a systematic pattern.

Since spiral galaxies are used for rotation curve studies and most spirals have bars, the effects of bars should be included in the models. Spekkens and Sellwood (2007) have proposed a procedure to fit non-axisymmetric flow patterns to 2-D velocity maps. The method applies to flows caused by bar-like or oval distortions to the total potential that may arise either from a non-axially symmetric halo, or a bar in the luminous disk. They applied the method to the nearby low-mass spiral NGC 2976 and find a good fit to a bar like model. Note that there is visual evidence of a candidate bar from the Two Micron All Sky Survey with a position angle consistent with that derived from the kinematic data. All these issues can be best demonstrated by a case study.

4. A Case Study; NGC 6822

We (Valenzuela et al. 2007, Rhee et al. 2009) have chosen to study this galaxy because in its case the discrepancy with cosmological predictions is so large that is seems impossible to explain the observed kinematics with a cosmologically motivated halo. NGC 6822 is a local group member that has been the subject of high resolution studies. It is the third nearest dwarf irregular after the LMC and the SMC. Although the galaxy is classified as barred this fact has been neglected in previous dynamical analyses. The stellar distribution shows a short but rather strong bar. The distribution of starlight in the the central ~ 1.5 kpc is misaligned with HI at large radii. Hodge (1977) and Cioni and Habing (2005) give the position angle of the bar as 10°, while the position angle of the HI disk is 125° (Weldrake et al. 2003). Weldrake et al. find that a model of NGC 6822 with a realistic dark matter halo gives a very bad fit: $\chi^2 = 1200$.

We have fit N-body models to the rotation curve of NGC 6822. The simulations were made with the parallel adaptive refinement tree code (Kravtsov et

al. 1997). Initially the models have two components, an exponential disk and a dark matter halo with an NFW density profile. We evolved the models for many disk rotation periods and they developed bars. We then scaled the models linearly in velocity and spatial coordinates to get the best fit to the NGC 6822 rotation curve, and the observed position angle and inclination as a function of radius. These observables were measured for the model by fitting a tilted ring model to the nbody 'data'.

After fitting the model to the data we can derive parameters for the best fit dark matter halo. The halo has a virial mass of $3.4 \times 10^{10}_{\odot}$. The model has a disk mass of 10^9 $M_{\odot}$. The halo has a concentration $C_{vir} = 22$ consistent (to within 1σ) with the concentration of halos measured in cosmological simulations Eke et al. (2001).

Valenzuela et al. (2007) show that it is indeed possible to reconcile the rotation of curves of local group dwarf galaxies with cuspy dark matter halos if one takes into account the effects of non circular motions induced by a bar, projection effects and gas pressure support. These effects combined lead to a large underestimation of the circular velocity in the central $\sim$ 1 kpc region creating the illusion of a constant density core.

The data are thus consistent with the presence of a cuspy or cored dark matter halo depending on one's assumption for the amplitude of non-circular motions and projection effects. We now turn to the HI data of NGC 6822 to determine the amplitude of non-circular motions in the cold gas used to determine the rotation curve.

5. Non-Circular Motions in the HI data of NGC 6822

Weldrake et al. (2003) present a high resolution rotation curve of NGC 6822. The best curves have an angular resolution of 8 arcsec or 20 pc. The data were obtained with the Australia Telescope Compact Array and reduced using the MIRIAD data reduction package. The reduced data have a velocity resolution of 1. km s^{-1}. W. de Blok has very kindly made the data available to us. We have used a data cube which has a beam size of 42.4×12 arcseconds and a pixel size of 4×4 arcseconds.

We have analyzed the data using the standard tilted ring analysis. We have paid particular attention to the residuals from the best fit tilted ring model. The radial velocity of the gas was measured in two ways. Firstly we determined the intensity weighted velocity at each location on the sky. Secondly we determined the maximum measurable velocity at each location on the sky. This is sometimes referred to as maximum envelope tracing. We define the maximum velocity to be the velocity measured at the point where the signal to noise is 3σ. The basis for doing this is that when viewing a disk inclined to the line of sight, the tangential velocity of the gas (i.e. the rotational velocity) is the largest measured velocity along the line of sight. The difference between these two methods is quite substantial as is seen in Figure 1. Figure 2 shows the residuals in the data after the maximum envelope tracing model has been subtracted. One can clearly see the presence of a bar. The residuals appear to form a structure with position angle $\sim 20^{\circ}$, close to the position angle of the optical bar. The

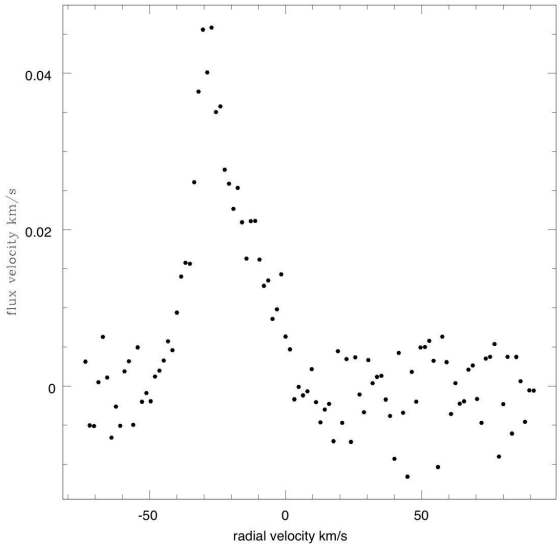

Figure 1. Spectrum of the HI gas along a line of sight in NGC 6822.The intensity weighted mean velocity is -24.3 km s^{-1} while the maximum envelope tracing velocity is -36.8 km s^{-1}

residuals are as large as 30 km s^{-1} in the region of the bar, but much lower along the major axis of the galaxy (of order 3 km s^{-1}).

The non-circular motions are also clearly visible in the central parts of the galaxy if one uses the intensity weighted velocities to estimate rotation.

The rms deviations from the tilted ring fit are of order 12 km s^{-1}. The deviations are clearly non-gaussian, so just measuring the rms does not tell the whole story. It is clear from these residual maps that there are systematic gas motions in this galaxy that are associated with a bar. This supports our contention that the bar cannot be ignored in the analysis of these data if one wishes to obtain a reliable rotation curve for the central parts of this galaxy.

6. Conclusion

The disagreement over the shape of the dark matter potential stems from a disagreement on how to extract rotation curves and non-circular motions from the data. Estimates of amplitude of non-circular motions in dwarf and LSB galaxies disagree by an order of magnitude. What is needed to reach consensus is for authors to independently examine the same datasets and reach agreement on the methods to be used for determining the rotation curves, non-circular motions and finally dark matter halo profiles.

Acknowledgments. I thank my collaborators Anatoly Klypin, Octavio Valenzuela and Fabio Governato for stimulating conversations. This work was supported by a grant from the NSF (AST-0709055).

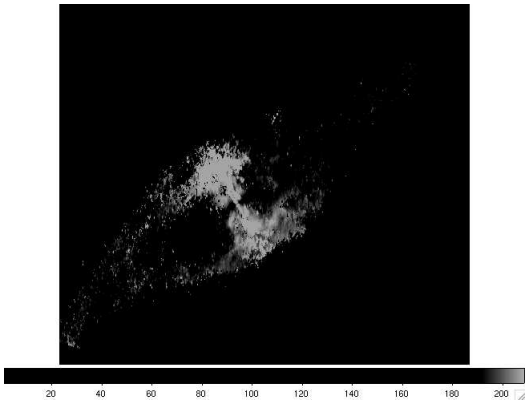

Figure 2. Velocity residuals after the rotational velocity has been subtracted from the data. The rotational velocity was computed using the maximum envelope tracing method.

References

de Blok, W. J. G. & Bosma, A. 2002, A&A, 385, 816
de Blok, W. J. G., Walter, F., Brinks, E., Trachternach, C., Oh, S.-H., & Kennicutt, R. C. 2008, AJ, 136, 2648
El-Zant, A. 2001, ApJ, 560, 636
Eke, V. et al. 2001, ApJ, 554, 114
Kuzio de Naray, R. et al. 2008, ApJ, 676, 920
Mashchenko, S. et al. 2006, Nature, 442, 539
Navarro, J. et al. 1997, ApJ, 490, 493
Navarro, J. et al. 2008, arXiv:0810.1522
Oh, S.-H., de Blok, W. J. G., Walter, F., Brinks, E., & Kennicutt, R. C. 2008, AJ, 136, 2761
Pizzella, A., Corsini, E. M., Sarzi, M., Magorrian, J., Méndez-Abreu, J., Coccato, L., Morelli, L., & Bertola, F. 2008, MNRAS, 387, 1099
Pizzella, A., Tamburro, D., Corsini, E. M., & Bertola, F. 2008, A&A, 482, 53
Romano-Diaz, E. et al. 2008, ApJ, 685, L105
Spekkens, K. & Sellwood, J. 2008, ApJ, 664, 204
Spergel, D. et al. 2003, ApJS, 148, 175
Valenzuela, O. et al. 2007, ApJ, 657, 773
Weldrake D. T. F. et al. 2003, MNRAS, 340, 12

GALAXY EVOLUTION: EMERGING INSIGHTS AND FUTURE CHALLLENGES
ASP Conference Series, Vol.
@jourvol, © 2009
S. Jogee, I. Marinova, L. Hao, and G. A Blanc

Star-Forming Galaxies at $z \sim 2$: An Emerging Picture of Galaxy Dynamics and Assembly

Kristen L. Shapiro,[1] Reinhard Genzel,[1,2] Nicolas Bouché,[2] Peter Buschkamp,[2] Giovanni Cresci,[2] Ric Davies,[2] Frank Eisenhauer,[2] Natascha Förster Schreiber,[2] Shy Genel,[2] Erin Hicks,[2], Dieter Lutz,[2] and Linda Tacconi[2]

Abstract. In these proceedings, we summarize recent results from our "SINS" *VLT*/SINFONI integral-field survey, focusing on the 52 detected UV/optically-selected star-forming galaxies at $z \sim 2$. Our Hα emission-line imaging and kinematic data of these systems illustrates that a substantial fraction ($\geq 1/3$) of these galaxies are large, rotating disks and that these disks are clumpy, thick, and forming stars rapidly. We compare these systems to local disk scaling relations and find that the backbones of these relations are already in place at $z \sim 2$. Detailed analysis of the large disks in our sample provides strong evidence that this population cannot result from a merger-dominated formation history and instead must be assembled by the smooth but rapid inflow of gas along filaments. These systems will then secularly evolve from clump-dominated disks to bulge-dominated disks on short timescales, a phenomenon that is observed in our SINS observations and is consistent with predictions from numerical simulations. These results provide new and exciting insights into the formation of bulge-dominated galaxies in the local Universe.

1. Introduction: The SINS Survey

The $z \sim 2$ Universe is now known to represent a critical epoch in matter assembly; during this era, both the cosmic star formation rate and the luminous quasar space density are at their peaks (e.g., Fan et al. 2001; Chapman et al. 2005). The assembly of galaxies is correspondingly rapid, with the total stellar mass density in galaxies increasing from $\sim 15\%$ to $50 - 75\%$ it current value between $z \sim 3$ and $z \sim 1$ (e.g., Dickinson et al. 2003; Rudnick et al. 2003, 2006). Observations of the dynamical and baryonic processes driving this evolution are therefore central to our understanding of galaxy formation.

To this end, we have conducted the SINS survey (Spectroscopic Imaging in the Near-infrared with SINFONI). The near-infrared integral-field capabilities of SINFONI allow us to probe the two dimensional distribution and kinematics of redshifted Hα and other key diagnostic emission lines. Our selection techniques and large sample size (52 detected UV/optically-selected galaxies, of 62 observed) enable us to probe a representative subset of the population of star-forming galaxies at $z \sim 2$, with an observationally-imposed slight bias towards

[1]Department of Astronomy, University of California at Berkeley, Berkeley, CA 94720, USA

[2]Max-Planck-Institut für extraterrestrische Physik, Giessenbachstr.1, D-85748 Garching, Germany

more massive and more rapidly star-forming galaxies ($\langle M_* \rangle \sim 3 \times 10^{10}\ M_\odot$, $\langle \mathrm{SFR} \rangle \sim 50\ M_\odot\ \mathrm{yr}^{-1}$; Förster Schreiber et al. in preparation). With SINFONI, we study this population with typical spatial resolution of $0.5 - 0.6''$ ($\sim 4 - 5$ kpc) and spectral resolution of 70 km s^{-1}. A subset of this sample has additionally been observed with adaptive optics and resolved at $0.15 - 0.3''$ ($\sim 1 - 2$ kpc).

The SINS data reveal a diversity in kinematics and morphologies of these systems, as seen in Hα emission (Förster Schreiber et al. 2006; Genzel et al. 2006; Bouché et al. 2007; see also related work by Law et al. 2007; Wright et al. 2008). The population at this redshift includes large rotating disks, compact dispersion-dominated systems, and several interacting or merging galaxies, each accounting for roughly 1/3 of the total population (Förster Schreiber et al. in preparation). Of these, the large rotating disks, discovered and probed for the first time with our SINS observations, have revealed much about the nature and evolution of high-redshift galaxies.

In these proceedings, we summarize the properties of the large rotating disk population at $z \sim 2$ and review the implications of this population for galaxy assembly. These proceedings are organized as follows: In §2., we present the main properties of the large rotating disk population revealed in our SINFONI integral-field spectroscopic data (originally presented in Förster Schreiber et al. 2006; Genzel et al. 2006; Bouché et al. 2007; Shapiro et al. 2008). In §3., we examine the fueling mechanisms for the high star formation rates in these systems and find that the smooth but rapid accretion of cold gas is the only mechanism consistent with the observations (see also Genzel et al. 2006; Shapiro et al. 2008). In §4., we show that detailed dynamical modeling of these galaxies reveals an evolutionary sequence through which young classical bulges are secularly formed (originally presented in Genzel et al. 2008). Finally, in §5., we conclude.

2. Properties of $z \sim 2$ Star-Forming Disks

2.1. Characteristics of the Population

Perhaps the most surprising result of the SINS survey was the discovery of a significant population of large ($r_{1/2} \sim 5 - 10$ kpc) rotation-dominated objects. The shape and amplitudes of the rotation curves in these galaxies are consistent with those measured in ionized gas in local spiral galaxies (Bouché et al. 2007). Fourier decomposition (kinemetry) of the velocity and velocity dispersion maps of these galaxies and comparison with local systems establishes quantitatively that these galaxies have "spider diagrams" consistent with those observed in local disk galaxies (Shapiro et al. 2008).

However, though dynamically similar to local spiral galaxies, high-redshift disks have many characteristics unparalleled in the $z = 0$ Universe. The spatial distribution of Hα emission reveals a marked "clumpiness" of the star formation activity into regions of FWHM size $= 1 - 3$ kpc (e.g., Genzel et al. 2008). Broad-band *Hubble Space Telescope* imaging of these systems illustrates that these features are also prominent in the stellar distribution (Elmegreen & Elmegreen 2006; Förster Schreiber et al. in preparation). Dynamical and spectral energy distribution fitting converge on masses of these super-star-forming clumps of $10^8 - 10^9\ M_\odot$ (Genzel et al. 2006; Elmegreen et al. 2008), a few percent of the

total galaxy stellar mass (typically 5×10^{10} $M_{\odot}$). The typical $z \sim 2$ disk galaxy contains $8-10$ such clumps (Genzel et al. 2006; Elmegreen et al. 2008).

Observations of both face-on and edge-on systems suggests that these clumps are roughly spherical, implying a large scale-height in the disks ($h_z \sim 1$ kpc, versus $r_{1/2} \sim 5-10$ kpc; e.g., Förster Schreiber et al. 2006; Elmegreen & Elmegreen 2006; Genzel et al. 2008). This is confirmed in the large velocity dispersions observed with SINFONI; detailed dynamical modeling accounting for projection and observational effects indicates the typical random motions are large, $v/\sigma \sim 1-7$ (Genzel et al. 2008; Cresci et al. submitted). High-redshift disks are therefore much thicker than their low redshift counterparts ($v/\sigma \sim 10-20$), and the implications of this difference are examined in §4. below.

Finally, high-redshift disks also exhibit much larger star formation rates ($\sim 30-200$ $M_{\odot}$ yr^{-1}) than local disk galaxies, indicative of the high gas fractions in these systems (Förster Schreiber et al. 2006; Genzel et al. 2006, 2008). In the local Universe, such high SFR are nearly always associated with a recent major merger; however, at high redshift, kinemetry analysis has shown these galaxies to have kinematic properties inconsistent with recent major interactions (Shapiro et al. 2008). Moreover, modeling of the spectral energy distributions of these galaxies indicates that the current SFR has been roughly constant over at least 0.5 Gyr in these systems (Genzel et al. 2006; Daddi et al. 2007; Förster Schreiber et al. in preparation). Such long-lasting high SFR and gas fraction suggests that the fueling of high SFR at high redshift occurs very differently than that at low redshift (see discussion in §3.).

2.2. The Appearance of Local Scaling Relations

The above evidence suggests that high-redshift disks, given their clumpiness and thickness, cannot passively evolve into their low-redshift late-type disk counterparts (see §4.). Nevertheless, their rotation curves obey the same radius-velocity relation as observed at $z = 0$ (Bouché et al. 2007). It is therefore of interest to examine scaling relations at $z \sim 2$, in order to probe the fundamental physics governing these relations.

Despite $z \sim 2$ systems having similar rotation velocities to local disk galaxies, detailed dynamical modeling of these systems coupled with spectral energy distribution analysis reveals that high-redshift disks are significantly offset from the local Tully-Fisher ($M_* - v$) relation (Cresci et al. submitted). This may reflect the high gas fractions in these $z \sim 2$ disks relative to local disks, or it may reflect a fundamental evolution of this relation with time.

In contrast, the high gas fractions and gas surface densities present at $z \sim 2$ drive star formation with an efficiency consistent with a universal Schmidt-Kennicutt scaling relation at high and low redshifts (Bouché et al. 2007). The presence of super-star-forming clumps in $z \sim 2$ disks thus does not seem to fundamentally alter the physics of star formation within these galaxies.

In cosmological models, this rapid star formation is often associated with rapid accretion onto a growing supermassive black hole (SMBH), a process that should be apparent via broad emission lines in our SINS galaxies. Indeed, stacking of our SINFONI spectra for all objects reveals a broad component underneath the Hα-[NII] complex (Shapiro et al. in preparation). If this feature is interpreted as evidence of active galactic nuclei in the SINS galaxies, SMBH masses can be

inferred from the luminosity and FWHM of the broad line. These SMBH masses are offset from local relations by an order of magnitude, in that the SMBH are under-massive for their host galaxies, implying a delayed assembly of black holes in $z \sim 2$ disk galaxies (Shapiro et al. in preparation).

It seems, then, that some processes (star formation and the physics governing the radius-velocity relation of galaxy disks) are independent of redshift, while those involving the gradual growth of stellar and SMBH mass are not preserved out to $z \sim 2$.

3. Creating Clumpy Disks: Cold Flows vs. Major Mergers

3.1. Differences from Major Merger Remnants

Given the lack of low-redshift analog for the clumpy, thick, rapidly star-forming disks seen at $z \sim 2$, the formation of these high-redshift objects begs explanation. The traditional paradigm through which systems with high SFR were explained was via gas-rich major mergers. Indeed, it has been known for some time that a merger with a sufficiently large gas fraction can result in very high SFR and in a gas-rich remnant disk (e.g., Barnes & Hernquist 1996).

However, this almost certainly is not the explanation for the high-redshift disks seen in our SINS sample. As described above, the SINS high-redshift disks show no kinematic evidence of recent disturbances and have likely experienced constant SFR over at least 0.5 Gyr, unlike the bursty star formation histories associated with galaxy interactions.

Several other key features in the data argue against a major merger origin for these systems. Most critically is the lack of central mass concentrations in some systems. While a major merger always creates a central concentration of mass, a significant fraction of high-redshift disks exhibit mass concentrations that peak in rings located $2 - 8$ kpc away from the galaxy center (Genzel et al. 2008), a configuration that cannot readily be created in a major merger.

Another relevant characteristic of the high-redshift disks is the observed clumpiness; the ~ 10 clumps in a galaxy, each with a few percent of the galaxy's mass, together make up a dynamically important component in these systems. With this significant fragmentation, high-redshift disks do not resemble the smooth and idealized remnants of simulated gas-rich major mergers; it is not obvious that such a merger could simultaneously produce gas-rich and fragmented disks, as are observed. In contrast, these mergers probably correspond to the sub-mm population detected at $z \sim 2$, whose compact and bursty star formation history almost certainly results from a major merger of two gas-rich systems (Tacconi et al. 2008).

3.2. Evidence for a Smooth Accretion Mechanism

Consequently, an alternative mechanism must fuel the constant high SFR seen in high-redshift disks. A natural explanation can be found in the "cold" (with respect to the virial temperature) gas flows entering these (high-σ peak) haloes along filaments. Such accretion has been shown to penetrate through to the center of the halo, replenishing the gas reservoir within the galaxy in a smooth (average merger ratio > 10:1) manner (e.g., Dekel & Birnboim 2006). This picture is in keeping with the SINS observations of kinematically undisturbed

disks forming stars at constant and very high rates (Genzel et al. 2006; Shapiro et al. 2008).

Statistical studies of high-redshift populations are also converging on this picture with independent arguments. The detection of a tight SFR-M_* relation from $z \sim 0 - 2$ implies that the primary driver for star formation cannot be a bursty mechanism such as a series of major mergers and instead must be a smooth mass-dependent process (Noeske et al. 2007; Daddi et al. 2007). Additionally, analysis of the accretion histories of dark matter haloes in the Millennium simulation indicates that only a small fraction of galaxies with the masses and star formation rates of the SINS high-redshift disks would be expected to have undergone a recent major (< 3:1) merger (Genel et al. 2008).

4. Evolution of Clumpy Disks and the Formation of Bulges

In addition to revealing the importance of the cold flow accretion mechanism in galaxy formation at high redshift, the SINS galaxies have also provided detailed insight into the modes of galaxy and bulge growth in the high gas fraction, high turbulence regime. In particular, the observed clumpiness can be understood simply as the characteristic Jeans length in these systems (Genzel et al. 2008). The expectation for a gas-rich disk to fragment in this manner has also been borne out in hydrodynamical simulations of this process, which generate systems remarkably similar to the observations (e.g., Immeli et al. 2004; Bournaud et al. 2007).

Once present, the dynamical timescale of these clumps in such highly turbulent, gas-rich disks implies that they should migrate to the center of the disk within ~ 1 Gyr (Genzel et al. 2008). The coalescence of several such clumps would then be expected to produce a young classical bulge, despite its secular origins (Elmegreen et al. 2008). Indeed, such features are observed in some of the SINS galaxies (Genzel et al. 2008; Förster Schreiber et al. in preparation). Moreover, the mass of the central concentration correlates well with the metallicity and therefore chemical age of the galaxy; older galaxies in which clumps would have had more time to migrate and merge are observed to contain the expected massive bulges (Genzel et al. 2008).

These bulges can then stabilize the remaining disk against the formation of future super-star-forming clumps (Dekel et al. 2009), such that the remaining disk, supplemented by subsequent gas accretion, exhibits a smooth exponential surface brightness profile (Bournaud et al. 2007). In this manner, the high-redshift disks can evolve into local bulge-dominated systems (e.g., elliptical, lenticular, and Sa galaxies). This scenario is in keeping with the similar number densities of the high-redshift disks and their probable descendants and with predictions based on cosmological simulations (e.g., Conroy et al. 2008; Genel et al. 2008).

5. Conclusions

From the SINS survey, and from complementary observational and theoretical campaigns, a new understanding of the formation and evolution of massive galaxies has emerged. In particular, a substantial fraction of these systems are

now known to undergo a disk-like stage, in which the galaxy consists of a large, rotating, thick, clumpy disk. Moreover, these disks are observed to form stars rapidly and to do so at a continuous rate for up to and exceeding one Gyr.

In contrast to local objects with high SFR, these galaxies are inconsistent with a major merger origin; evidence against a recent major merger is apparent in both their star formation histories and their internal dynamics. Instead, the high SFR in $z \sim 2$ star-forming disks is likely driven by the smooth but rapid inflow of gas along filaments in the cosmic web.

The gas-rich disks that result from this process are globally unstable and are observed to collapse into kpc-scale clumps, in keeping with theoretical expectations. With time, these clumps migrate to the center of the potential and combine to form a nascent bulge, a process that is directly observed in the SINS data. At $z = 0$, the eventual product of this system will be a bulge-dominated galaxy, whose central mass concentration was generated without a major merger.

Acknowledgments. The SINS project would not have been possible without the helpful and enthusiastic support of the ESO staff, particularly at Paranal Observatory, over the many observing runs and several years during which these observations were carried out. We also thank the SINFONI and PARSEC teams for their hard work on the instrument and the laser, which allowed our program to be so successful.

References

Barnes, J. E., & Hernquist, L. 1996, ApJ, 471, 115
Bouché, N., et al. 2007, ApJ, 671, 303
Bournaud, F., Elmegreen, B. G., & Elmegreen, D. M. 2007, ApJ, 670, 237
Chapman, S. C., Blain, A. W., Smail, I., & Ivison, R. J. 2005, ApJ, 622, 772
Conroy, C., Shapley, A. E., Tinker, J. L., Santos, M. R., & Lemson, G. 2008, ApJ, 679, 1192
Daddi, E., et al. 2007, ApJ, 670, 156
Dekel, A., Sari, R., & Ceverino, D. 2009, arXiv:0901.2458
Dekel, A., & Birnboim, Y. 2006, MNRAS, 368, 2
Dickinson, M., Papovich, C., Ferguson, H. C., & Budavári, T. 2003, ApJ, 587, 25
Elmegreen, B. G., & Elmegreen, D. M. 2006, ApJ, 650, 644
Elmegreen, B. G., Bournaud, F., & Elmegreen, D. M. 2008, ApJ, 688, 67
Elmegreen, B. G., Elmegreen, D. M., Fernandez, M. X., & Lemonias, J. J. 2009, ApJ, 692, 12
Fan, X., et al. 2001, AJ, 121, 54
Förster Schreiber, N. M., et al. 2006, ApJ, 645, 1062
Genel, S., et al. 2008, ApJ, 688, 789
Genzel, R., et al. 2008, ApJ, 687, 59
Genzel, R., et al. 2006, Nat, 442, 786
Immeli, A., Samland, M., Gerhard, O., & Westera, P. 2004, A&A, 413, 547
Law, D. R., Steidel, C. C., Erb, D. K., Larkin, J. E., Pettini, M., Shapley, A. E., & Wright, S. A. 2007, ApJ, 669, 929
Noeske, K. G., et al. 2007, ApJ, 660, L43
Rudnick, G., et al. 2006, ApJ, 650, 624
Rudnick, G., et al. 2003, ApJ, 599, 847
Shapiro, K. L., et al. 2008, ApJ, 682, 231
Tacconi, L. J., et al. 2008, ApJ, 680, 246
Wright, S. A., Larkin, J. E., Law, D. R., Steidel, C. C., Shapley, A. E., & Erb, D. K. 2009, ApJ, 699, 421

GALAXY EVOLUTION: EMERGING INSIGHTS AND FUTURE CHALLLENGES
ASP Conference Series, Vol.
@jourvol, © 2009
S. Jogee, I. Marinova, L. Hao, and G. A Blanc

The Elaboration of Spiral Galaxies: Morpho-Kinematics Analyses of their Progenitors with IMAGES

F. Hammer, on behalf of the IMAGES collaboration

GEPI, Observatoire de Paris & CNRS

Abstract. The IMAGES (Intermediate MAss Galaxy Evolution Sequence) project aims at measuring the velocity fields of a representative sample of 100 massive galaxies at $z = 0.4 - 0.75$, selected in the CDFS, the CFRS and the HDFS fields. It uses the world-unique mode of multiple integral field units of FLAMES/ GIRAFFE at VLT. The resolved-kinematics data allow us to sample the large scale motions at $\sim$ few kpc scale for each galaxy. They have been combined with the deepest HST/ACS, Spitzer (MIPS and IRAC) and VLT/FORS2 ever achieved observations. Most intermediate redshift galaxies show anomalous velocity fields: 6 Gyrs ago, half of the present day spirals were out of equilibrium and had peculiar morphologies.
The wealth of the data in these fields allow us to modelize the physical processes in each galaxy with an accuracy almost similar to what is done in the local Universe. These detailed analyses reveal the importance of merger processes, including their remnant phases. Together with the large evolution of spiral properties, this points out the importance of disk survival and strengthens the disk rebuilding scenario. This suggests that the hierarchical scenario may apply to the elaboration of disk galaxies as it does for ellipticals.

1. Introduction

Half of the present-day stellar mass density has been formed since $z = 1$, during the last 8 Gyr (Dickinson et al. 2003; Fontana et al. 2003). This result is particularly robust as it has been derived from two independent methods: the evolution of the cosmic stellar mass density and by integrating the universal star formation density including infra-red measurements (Flores et al. 1999). The two methods have their own weaknesses depending on the contribution of massive stars to the near-IR light (e.g. Maraston et al. 2006) or to the conversion of the mid-IR luminosity in star formation rate. However the good agreement between their predictions – at least below $z = 1$ – is rather compelling.

Hammer et al. (2005) and Bell et al. (2005) have shown that most of the stellar mass formation during the last 8 Gyrs is associated to luminous IR galaxies (LIRGs, SFR$>$ 19 $M_\odot\ yr^{-1}$) which may account from 50% to 100% of the star formation density in the $z = 0.5 - 1$ range. Most LIRGs have stellar masses ranging from 2 to 20$\times$ $10^{10} M_\odot$, those being responsible for the bulk of the star formation density reported by deep galaxy surveys (e.g. CFRS) and by studies of the past history of present-day galaxies (e.g. Heavens et al. 2004). Present-day intermediate mass galaxies are mostly spiral galaxies (70% of them from the SDSS, Nakamura et al. 2004). How galaxies, mostly spirals with masses similar to that of the Milky Way, have assembled half of their stars over the

past 8 Gyrs? To identify the main physical processes at the origin of the star formation, we are now embarked in a complete study of their progenitors, i.e. galaxies having emitted their light 4 to 7 Gyrs ago.

2. One hundred distant galaxies with spatially resolved kinematics from the IMAGES survey

We gathered a sample of 100 galaxies selected on the sole basis of their absolute magnitude in J band ($M_J(AB)$<-20.3 corresponding to $M_{\rm stellar} > 1.5\ 10^{10} M_\odot$) and their redshift ($0.4 < z < 0.9$). A considerable effort was made to ensure that our sample is representative of the intermediate mass galaxies at $z \sim 0.6$. First, observations of their kinematics with VLT/GIRAFFE require the presence of the [OII]λ3726,3729 doublet in their spectra. Flores et al. (2006) and Yang et al. (2008a) convincingly demonstrated that for all the targets with $W_0([OII]) >$ 15Å, sufficiently high S/N velocity fields may be retrieved after exposure times from 8 to 24 hours with VLT/GIRAFFE. However, this does not account for galaxies without or with faint emission lines that represent 40% of the galaxies at $z \sim 0.6$ (e.g. Hammer et al. 1997). These galaxies are quiescent galaxies mostly made of E/S0 and quiescent spirals (e.g. Zheng et al. 2005; Delgado et al. 2009, in preparation). In the following they will be considered as having relaxed kinematics, either supported by dispersion or by rotation. Second we have verified that our sample is representative of the galaxy luminosity function observed at $z \sim 0.6$ (see e.g. Ravikumar et al, 2007). In the latter study it was shown that the luminosity density in UV, near-IR and mid-IR of our sample is indeed representative of the median value observed in the same redshift range. Third, galaxies were selected in 4 different fields of view (Yang et al. 2008) to minimise possible cosmological variance effects.Thus our sample is mostly limited by the Poisson statistical variance related to the number of galaxies with resolved kinematics. Notice that it is by far the much larger existing sample of distant galaxies with spatially resolved kinematics, because GIRAFFE at VLT is still the unique multi-IFU spectrograph allowing the observation of 15 galaxies at the same time.

An important step is the methodology used in identifying the nature of the velocity fields of distant galaxies. Because of their distances, the GIRAFFE IFU cannot resolve rotation curves as it can be done for local galaxies. This had let Flores et al. (2006) to propose a robust method to classify their velocity fields by using the supplementary information of their dispersion maps. To illustrate this, let us consider a rotating disk. In its outskirts the dispersion map with 0.52 arcsec pixel ($\sim$ 3 kpc) is able to recover the random motions within the disk, while in the centre it samples the convolution of these motions with the large gradient of the rotational curve. This unavoidably results in a dispersion peak located at the mass centre, in the middle of the two extrema velocities. A diagnostic diagram thus tests the discrepancy of the dispersion peak both in location and intensity, through a comparison with expectations from the observed/modeled velocity field (see details in Flores et al. 2006; Yang

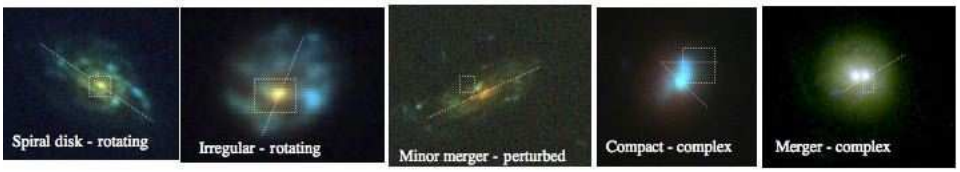

Figure 1. Images of $z \sim 0.6$ galaxies are combined b+v, i and z frames from HST/ACS. On each galaxy are superimposed the dynamical axis (dotted lines) and the dispersion peak (box with vertical size of 0.5 arcsecond). Morphological and kinematics classifications from Neichel et al. (2008) and Yang et al. (2008), respectively.

et al. 2008a)[1]. Notice also that the high spectral resolution of GIRAFFE ($R \sim 13000$) ensures a proper removal of sky lines, the large exposure time warrants a very high S/N (>3 for each pixel, average of 10) and and the presence of the [OII]λ3726,3729 doublet provides reproducible measurements of the kinematics.

Three kinds of velocity fields were retrieved by Flores et al. (2006), including rotating disks (rotation axis following the main optical axis and dispersion peak in the centre), perturbed rotations (rotation axis following the main optical axis but offset of the dispersion peak) and complex kinematics (kinematical axis not aligned with the optical axis, or chaotic velocity fields and dispersion maps). Examples can be found in Flores et al. (2006), Puech et al. (2006), Yang et al. (2008a) and Figure 1. It results that among the 63 velocity fields studied in Yang et al. (2008a), 32% are rotationally supported, 25% are perturbed rotation, 43% are complex. Notice that 9% are too compact for being resolved with GIRAFFE and in the following, they are assumed to follow the same distribution than the above. Accounting for the whole population of $z \sim 0.6$ galaxies, this reveals 33% of rotating disks, while 41% have anomalous kinematics, including 26% with complex velocities. GIRAFFE is only sensitive to large scale motions and not to small variations as those caused by bars or by ordinary warps. Thus galaxy kinematics evolve strongly since the last 6 Gyrs (Yang et al. 2008a). Galaxies with anomalous kinematics are responsible for all the observed dispersion of the Tully-Fisher relation at $z \sim 0.6$ (Flores et al. 2006; Puech et al. 2008a): it evidences how strong their kinematics are perturbed.

3. Half of the present-day spirals had peculiar morphologies and anomalous kinematics, 6 Gyr ago

The fields in which IMAGES galaxies have been studied all possess deep and high resolution imaging with two to four colours, mostly from deep exposures with HST/ACS. For a spiral galaxy, this ensures that we are able to identify galaxy morphological features within the optical radius up to z=0.5. Neichel et al. (2008) described a semi-automatic decision tree to classify the distant galaxy morphologies, based on the systematic use of the GALFIT software, of the calibrated and S/N weighted colour maps (Zheng et al. 2005) and finally visual inspections by three independent co-workers. We chose a very conser-

[1]This has been allowed by the absence of cross talks in the GIRAFFE design.

vative method to classify galaxy morphology, keeping in mind the well known morphologies of local galaxies that populate the Hubble sequence. For example, we did not try to evaluate the morphology of compact galaxies (classified as compact), all galaxies for which the GALFIT sofware failed were classified as peculiar or merger, and we further imposed that spiral galaxies, whenever they possess a bulge, it should have a redder colour than the disk.

Table 1. Morpho-kinematical classification of $z \sim 0.6$ galaxies from Neichel et al.; for comparison, the last column shows the fractions derived from the SDSS (Nakamura et al; 2004) for galaxies in the same mass range.

Type	$z \sim 0.6$ $W_0(OII)$ ≥15Å Neichel et al.	$z \sim 0.6$ $W_0(OII)$ <15Å Zheng et al. Delgado et al.	$z \sim 0.6$ all galaxies Neichel et al.	local galaxies Nakamura et al. Hammer et al.
E/S0	0%	57%	23%	27%
Rotating spiral	27%	43%	33%	70%
Peculiar/comp./merger	73%	0%	44%	∼ 3%
With anomalous kinematics	68%	0%	41%	

Applying this classification to emission line galaxies observed by GIRAFFE, we find only 29% of spiral galaxies. We have thus compared our morphological classification to that of their kinematics, and found a remarkable agreement (e.g. Neichel et al. 2008). Almost all (95%) but one galaxy with complex velocity fields have peculiar, compact or merger morphologies and most galaxies (80%) with rotational velocity fields have spiral morphologies. Such an excellent agreement brings a considerable support to our conservative classification scheme. It should not be very sensitive to star formation since all the GALFIT measurements were done in the observed z band (rest-frame V band at $z \sim 0.7$). In contrast, semi-automatic classification methods such as C-A or Gini-M20 are not predictive of their kinematics and strongly overestimate the number of spiral galaxies.

The combination of morphological and kinematical classifications results in a quite small fraction (16%) of rotational spiral disks with emission lines ($W_0(OII) \geq 15$Å). Table 1 summarises the statistics at $z \sim 0.6$ and compares them to local galaxies from SDSS (Nakamura et al.). We were conservative in doing such a comparison assuming that rotating spirals should have spiral morphologies and have a rotating velocity field. Similar statistics combining kinematics and morphology does not exist for local galaxies, although this is in progress (Puech et al. 2009, in preparation).

Table 1 evidences that E/S0 were mostly in place at $z \sim 0.6$, while half of rotating spirals were not. Six Gyrs ago, half of the local spirals had peculiar morphologies and anomalous kinematics. This result supersedes earlier results from Lilly et al. (1998) which were based on lower spatial resolution and S/N imagery, without kinematics. Most of the star formation is related to LIRGs that number density evolves also considerably (by factors 30 to 40, e.g. Elbaz and Cesarsky, 2003). Thus spiral galaxies are aggregating half of their stellar masses during violent star formation episodes (Hammer et al. 2005), and half of them are transformed from unstable kinematics and peculiar morphologies to regular, relaxed galaxies dominated by thin disks. This suggests that galaxy collisions and their reminiscence may play a major role during the elaboration of their disks. Another line of support for such a suggestion is provided by

Rodrigues et al. (2008, see also Rodrigues et al. this volume). The evolution of chemical abundance of the gaseous phases of galaxies shows a linear slope from z=0 to z=3, in strong contradiction with close box models that predict a much moderate evolution at z=0.4-0.8. Thus galaxies are not isolated systems and are exchanging gas, as expected during interactions.

4. The elaboration of disk galaxies and of the Hubble sequence: disk rebuilt after mergers?

There is a considerably growing set of evidences that the elaboration of disks is linked with galaxy mergers. The spiral rebuilding scenario was proposed by Hammer et al. (2005) to explain the observations of distant galaxies, including the simultaneous evolution of the global stellar mass, Luminosity-Metallicity relationship, pair statistics, IR light density, colors of spiral cores and number density of peculiar galaxies. This is supported by a similar evolution of their kinematics. Since Barnes et al. (2002), simulations have shown that under the condition of enough large gas content (generally $f_{gas} \geq 50\%$), major mergers may lead to the formation of a new disk (Robertson et al. 2006; Governato et al. 2007; Hopkins et al. 2008). Such high gas fractions are currently observed in the distant Universe at $z \sim 2$ (Erb et al. 2007) and even at $z \sim 1$ (Liang et al. 2006; Rodrigues et al. 2008).

Is the high fraction of anomalous kinematics consistent with a merger hypothesis? The most robust quantity derived to estimate the merger rate is the pair fraction of intermediate mass galaxies at $z \sim 0.6$, for which all studies find 5±1% (see e.g. Bell et al. 2006 and more recently, Lotz et al. 2008; Rawat et al. 2008). At first glance this appears to be contradictory with the higher fraction (26%) of galaxies with complex kinematics. However the latter are found in pairs or could be merger remnants, so they could be quite numerous. Galaxy simulations predict a relatively small time scale for pairs to merge(τ_{pair}=0.35-0.5 Gyrs for M* galaxies). There are 5 times more galaxies with complex kinematics than galaxies in pairs: this is consistent if the complex velocity fields are related to merging, either during the first interaction in the pair or during the remnant phase. Such a reminiscence phase duration would be: $\tau_{remnant}$= 3-5 × τ_{pair}. Such values ($\tau_{remnant}$= 1.2-2 Gyrs) are indeed predicted by simulations of gas rich mergers to rebuilt significant disks (e.g. Robertson et al. 2006; Governato et al. 2007; Hopkins et al. 2008).

Is the merger hypothesis consistent with the evolution of Tully Fisher relation and angular momentum? Puech et al. (2007a) have shown that galaxies with anomalous kinematics are outliers in the Tully Fisher and the j_{disk}-V_{rot} relations. They demonstrated that major mergers can easily explain such a deviation during which galaxies are experiencing a random walk evolution in such planes.

How this could be reconciled with the past history of the Milky Way? The Milky Way disk is well known to have not been impacted by significant collisions since z=3-4. However, many evidences show that other spirals in the same mass range (e.g. M31, M81) have had a much more tumultuous past history (Ibata et al. 2005; Brown et al. 2008 and in this volume, Davidge 2008). By comparing Milky Way properties to those of other spirals from the SDSS, Hammer et al.

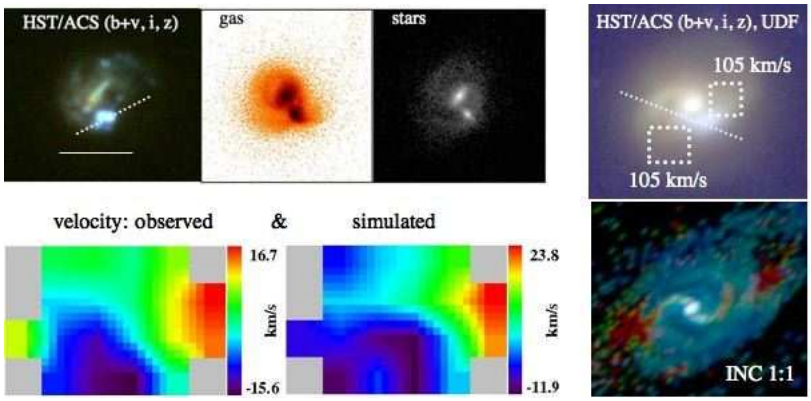

Figure 2. Morphologies and kinematics (same symbols than in Figure 1) for two distant galaxies. On the left, J033239.72-275154.7 at z=0.4158 (modelled with GADGET2 including velocity field in the bottom); on the right, J033245.11-274724.0 at z=0.43462 (bottom: modelled with ZONE from Barnes et al, 2002, with dispersions seen in red colors).

(2007) have shown that the Milky Way is rather exceptional, having a too small radius, angular momentum and stellar mass. Only 7±1% of local spirals are Milky Way-like, conversely to M31 which is a rather ordinary spiral. Milky Way could be even more exceptional: it is still the only known galaxy in its mass range with an essentially primordial halo.

5. Modelling z ∼ 0.6 galaxies with a similar accuracy than for local galaxies and concluding remarks

Whether galactic disks have been produced as a by product of the last major merger may considerable change the theory of galaxy formation by superseding the tidal torque theory. Hopkins et al. (2008) have demonstrated that most of the process in the disk rebuilding phase is fundamentally dynamical, while feedback mostly remove part of the gas at large radii and preserve the disk from fragmentation. A crucial test is to examine with sufficient details the real galaxies and derive their accurate properties.

At $z \sim 0.6$, the IMAGES galaxies sample an epoch of decreasing star formation, although significantly higher than at present epoch. To examine them we have a huge amount of details provided by the combination of their kinematics at ∼ 3kpc scales, their morphologies at ∼ 200 pc scales, their star formation rate (from Spitzer/MIPS photometry), and their stellar population properties (from their VLT/FORS2 spectra). For example Puech et al. (2007b) have been able to identify the impact of a 1:18 satellite infall in J033226.23-274222.8 at z= 0.66713 (see Figure 1, third panel), which is reponsible for only a small fraction of the star formation activity in this galaxy. The modelling of $z \sim 0.6$ galaxies may be done following the steps of former models of nearby systems. The giant and star-bursting bar as well as the complex kinematics of J033239.72-275154.7 (see Figure 2) has been modelled by Peirani et al. (2008) by a 1:3 merger, the resulting galaxy being an $S0_a$. Yang et al. (2009, submitted) has shown that for J033210.76-274234.6 (see Figure 1, fifth panel), the 1:6 satellite has impacted the

main galaxy with a very inclined orbit and near its core, letting the disk survive to the collision. Hammer et al. (2009) show that a compact LIRG (J033245.11-274724.0 at z=0.43462, see Figure 2) may have all its very peculiar properties (disk redder than the bulge, dynamical axis well offset from the optical main axis) reproduced by a 1:1 gaseous rich merger remnant leading to a Sc galaxy. Puech et al. (2008b, see arXiv0811.3893) has identified that for a significant part of J033241.88-274853.9, a gas rich galaxy at z=0.66702, the gas is ionised by shocks, revealed to large gas dispersions, which is predicted by a model of a 1:1 gas rich merger remnant.

More detailed analyses are in progress. Having been done for a representative mass selected sample of galaxies at $z \sim 0.6$, they will definitively probe whether the present-day Hubble sequence has been elaborated from the last major merger, from ellipticals to late type spirals. Comparison with state of the art simulations would be invaluable for understanding the detailed paths of angular momentum built-up, the influence of gas viscosity, the way the expelled material can be re-accreted during the post-merger stage and possibly the formation of bars, rings and other spiral disk features. A detailed examination of the physics of the galaxy formation is now within our range: we may revisit how the Hubble sequence has been elaborated as well as how disks have acquired their large angular momentum and thin disks.

Acknowledgments. I express my gratefulness to the organisers, the administrative persons and students for organising such an excellent meeting.

References

Barnes, J.E. 2002, MNRAS, 333, 481
Bell, E. F. et al. 2006, ApJ, 652, 270
Brown, T., et al. 2008, ApJ, 685, 121
Davidge, T. et al. 2008, PASP, 120, 1145
Dickinson, M. et al. 2003, ApJ, 587, 25
Elbaz, D. & Cesarsky, C. J. 2003, Science, 300, 270
Erb, D. K. et al. 2006, ApJ, 644, 813
Flores, H. et al. 2006, A&A, 455, 107
Fontana, A. et al. 2003, ApJ, 594, 9
Governato, F. et al. 2007, MNRAS, 374, 1479
Hammer, F. et al. 1997, ApJ, 481, 49
Hammer, F. et al. 2005, A&A, 430, 115
Hammer, F. et al. 2007, ApJ, 662, 322
Hammer, F. et al. 2009, A&A, 496, 381
Heavens, A. et al. 2004 Nature 428, 625
Hopkins, P. et al. 2008, ApJ, 688, 757
Ibata, R. et al. 2005, ApJ, 634, 287
Liang, Y. C., Hammer, F., & Flores, H. 2006, A&A, 447, 113
Lilly, S. et al. 1998, ApJ, 500, 75
Lotz, J. M. et al. 2008, ApJ, 672, 177
Maraston, C. et al. 2006, ApJ, 652, 85
Nakamura et al. 2004, AJ, 127, 2511
Neichel, B., et al. 2008, A&A, 484, 159
Peirani, S. et al. 2009, A&A, 496, 51
Puech, M. et al. 2006, A&A, 455, 119
Puech, M. et al. 2007, A&A, 484, 173
Puech, M. et al. 2007, A&A, 476, 21
Puech, M. et al. 2008, A&A, 484, 173

Puech, M. et al. 2009, A&A, 493, 899
Ravikumar, C. et al. 2008, A&A, 465, 1099
Rawat, A. et al. 2008, ApJ, 681, 1089
Robertson, B. et al. 2006, ApJ, 645, 986
Rodrigues, M. et al. 2008, A&A, 492, 371
Yang, Y. et al. 2007, A&A, 477, 789
Zheng, X. Z. et al. 2005, A&A, 435, 507

GALAXY EVOLUTION: EMERGING INSIGHTS AND FUTURE CHALLLENGES
ASP Conference Series, Vol.
@jourvol, © 2009
S. Jogee, I. Marinova, L. Hao, and G. A Blanc

Properties and Origin of Bulges in High Mass Spirals

Tim Weinzirl,[1] Shardha Jogee,[1] Sadegh Khochfar,[2,3] Andreas Burkert,[4] and John Kormendy[1]

Abstract. The distributions of bulge-to-total mass ratio (B/T) and bulge Sérsic index n are quantified to explore the fundamental question of how bulges form. We perform $2D$ bulge-disk and bulge-disk-bar decomposition on H-band images of bright ($M_B \leq -19.3$), high mass ($M_\star \geq 1.0 \times 10^{10} M_\odot$), moderately inclined ($i < 70°$) spirals. A large fraction of high mass spirals ($\sim 74\%$) have $n \leq 2$ bulges, and 66% have $B/T \leq 0.2$. Such low-B/T and low-index bulges exist in barred and unbarred galaxies across a wide range of Hubble types. We compare the results with predictions from a set ΛCDM-based galaxy formation models. The predicted fraction ($\sim 1.6\%$) of high mass spirals with a past major merger since $z \leq 4$ and a bulge with a present-day $B/T \leq 0.2$ is over 30 times smaller than observed. The majority of $B/T \leq 0.2$ bulges in high mass model galaxies exist in systems that have experienced only minor mergers, and no major mergers. Bulges built via major mergers seriously fail to account for the bulges present in most high mass spirals. Most bulges appear to be created by some combination of minor mergers, smooth accretion, and secular processes.

1. Introduction

Galactic bulges are valuable relics of galaxy formation. Elucidating the structure, kinematics, dynamics, and stellar content of bulges reveals clues about galaxy formation and assembly mechanisms. Major and minor mergers, secular processes (e.g. Genzel et al. 2008), and smooth accretion (e.g. Dekel et al. 2009) are all known to be relevant, yet the relative importance and timescales over which these mechanisms are effective remain contested.

Within the ΛCDM paradigm, galaxies having a past major merger when their mass was a large fraction of their present-day mass are expected to have a significant bulge-to-total mass ratio (B/T ; see Figure 23 of Weinzirl et al. 2009, hereafter WJKBK09) and high Sérsic index (Hopkins et al. 2009). Galaxies that experienced major mergers only in their distant past will not have a prominent classical bulge. Either a large or small fraction of present-day galaxies with low B/T may result depending on merger history. Quantifying the distribution of B/T and bulge Sérsic index for low and high-mass galaxies can constrain the merger and mass assembly history in ΛCDM-based models.

[1]Department of Astronomy, University of Texas at Austin, Austin, TX

[2]Sub-Department of Astrophysics, University of Oxford, Denys Wilkinson Bldg., Keble Road, OX1 3RH, Oxford, UK

[3]Max Planck Institut für extraterrestrische Physik, P.O Box 1312, D-85478 Garching, Germany

[4]Universitäts-Sternwarte München, Scheinerstr. 1, 81679 München, Germany

There is mounting evidence that bulgeless and low B/T galaxies are common locally. Böker et al. (2002) find Sd galaxies often possess no bulge. Based on analysis of several thousand late-type SDSS galaxies, Kautsch et al. (2006) and Barazza, Jogee, & Marinova (2008) find 15-20% of edge-on and moderately inclined disks out to $z \sim 0.03$ appear bulgeless. Of the 19 galaxies with distance < 8 Mpc and $V_c > 150$ km s^{-1}, 11 have pseudobulges instead of merger-built classical bulges (Kormendy & Fisher 2008); even the biggest disks can grow with no evidence of a merger-built bulge. However, there exist few, if any, rigorous comparisons with predictions in the literature. Therefore, as a first step, in WJKBK09 we perform a structural analysis to derive B/T and bulge indices for nearby, high stellar mass ($M_\star \geq 10^{10} M_\odot$) galaxies and compare with hierarchical galaxy formation models. We highlight here the main results from WJKBK09.

Sample selection and methodology are detailed in WJKBK09, but we include here a brief summary. The sample is derived from the Ohio State University Bright Spiral Galaxy Survey (OSUBSGS; Eskridge et al. 2002). These galaxies are a subset of RC3 and have $m_B \leq 12$, Hubble types S0/a to Sm, $D_{25} \leq 6'.5$, and $-80^\circ < \delta < +50^\circ$. Imaging is available in $BVRJHK$ filters for most galaxies. NIR images are better tracers of stellar mass than optical imaging. We use the H-band images as they provide the best compromise between data quality and insensitivity to age gradients and obscuration by dust and star formation. Our main sample is 143 bright galaxies with $M_B \leq -19.3$ and low-to-moderate inclination ($i < 70^\circ$). Photometric stellar masses for 126 objects are derived using the relation between stellar mass and rest-frame $B-V$ colors from Bell et al. (2003). Our sample is fairly complete for $M_\star \geq 1.0 \times 10^{10} M_\odot$.

In this analysis, we perform $2D$ bulge-disk and bulge-disk-bar decomposition with GALFIT (Peng et al. 2002), which uses a Levenberg-Marquardt algorithm to minimize χ^2 based on input guesses. We adopt an iterative technique that recycles output from each step as initial input guesses in the subsequent step. In Stage 1, a single Sérsic component is fit to the galaxy. In Stage 2, a Sérsic plus exponential disk model is applied. The Sérsic profile can represent either a bulge or a bar. The shape and position of the disk component are predetermined with ellipse fitting and held fixed. In Stage 3, a Sérsic bulge, exponential disk, and Sérsic bar model is fit; again, the disk is constrained as before. All three stages are applied to each galaxy. Either the bulge-disk or bulge-disk-bar model is selected as the best fit. Selection criteria that fold into the decision include χ^2, the residual images, and the model parameters. A model was only adopted as long all model parameters were physically well-behaved.

2. Results and Comparison With Models

Here we summarize the main results from WJKBK09. We also discuss our models of galaxy formation and how they compare with observations.

1. Distribution of B/T and Bulge Sérsic Index: In Figure 1, the relation between B/T and bulge index is shown on the left, and mean B/T and bulge index is plotted versus Hubble type on the right. For galaxies with $M_\star \geq 10^{10} M_\odot$, low-$B/T$ and low-index galaxies exist in barred and unbarred galaxies across a wide range of Hubble types: $\sim 66\%$ have $B/T \leq 0.2$, while $\sim 74\%$ have bulge index $n \leq 2$. These statistics agree

with other $1D$ (bulge-disk) and $2D$ (bulge-disk, bulge-disk-bar) decompositions (e.g. Graham & Worley 2008; Laurikainen et al. 2007).

2. Bar Fraction: An H-band bar fraction of $\sim$ 58% (83 of 143) is found based on choosing between bulge-disk and bulge-disk-bar models, in agreement with other studies using different methods on the same dataset (Laurikainen et al. 2004; Marinova & Jogee 2007). The bar fraction changes as a function of B/T and bulge index. In massive galaxies with $B/T \leq 0.2$ and $n \leq 2$, the bar fractions are $\sim 68\%$ and $\sim 63\%$, respectively, $\sim 1.5-2$ times greater than the bar fraction for $B/T > 0.2$ ($\sim$ 37%) and $n > 2$ ($\sim$ 41%). The high incidence of bars in disks with pseudobulges suggests secular processes like gas inflow driven by non-axisymmetric features may play a significant role in building such bulges. An alternative explanation is that low-B/T disks with no inner Lindblad resonances are more susceptible to bars induced by swing amplification in the presence of a feedback loop (Julian & Toomre 1966; Toomre 1981; Binney & Tremaine 1987).

3. Description of Theoretical Models: In WJKBK09, we compare our data with predictions from ΛCDM-based hierarchical models from Khochfar & Burkert (2005) and Khochfar & Silk (2006), as well as Hopkins et al. (2009). The DM merger trees are based on the extended Press-Schechter formalism, while the merger timescale of galaxies in merging DM halos is based on the dynamical friction timescale of satellite galaxies. Baryonic physics are handled with semi-analytic prescriptions for radiative cooling, star formation, and SN feedback. A major merger ($M_1/M_2 \geq 1/4$) converts a fraction of gas to stars, and all existing stars undergo violent relaxation to form a spheroid, thereby destroying any existing stellar disk. The B/T ratio after a major merger is always unity, but declines over time as the stellar disk is rebuilt from star formation fueled by cold gas accretion. If a galaxy is to have $B/T \leq 0.2$, then the last major merger must have occurred at $z > 2$ (see Figure 23 of WJKBK09). Bulge growth from minor mergers ($1/10 < M_1/M_2 < 1/4$) is modeled simply by adding the stellar content of the merging satellite to the bulge of the primary. Secular processes likely facilitate bulge growth through bar-driven gas inflow or bar buckling instabilities in non-interacting galaxies, but they are not presently implemented.

4. Comparing Data With Models: The cumulative distribution of B/T for $M_\star \geq 10^{10} M_\odot$ galaxies is plotted in Figure 2. A large percentage ($\sim 66\%$) of observed galaxies have $B/T \leq 0.2$. The distribution of present-day B/T predicted by the theoretical models depends on the model galaxy merger history. In the models, $\sim 13.5\%$ and $\sim 20\%$ of high mass spirals have undergone major mergers since $z \leq 2$ and $z \leq 4$, respectively (see Table 1). These predications agree within a factor of ~ 2 with empirical results from Jogee et al. (2009) out to $z \sim 0.8$ and the general trends at higher redshifts (e.g., Conselice et al. 2003). With the above merger history, $\sim 67\%$ of model galaxies having $B/T \leq 0.2$, in overall agreement with the observed B/T distribution. Table 1 yields a striking realization by distinguishing between galaxies with a major merger since $z \leq 4$ versus those having solely minor mergers. Only $\sim 1.6\%$ of galaxies with a major

merger since $z \leq 4$ have $B/T \leq 0.2$. The remaining model galaxies with $B/T \leq 0.2$ experience only minor mergers over $z \leq 4$. Therefore, it is unlikely that major mergers played a significant role in building low-B/T bulges. Rather, the dominant formation pathway is some combination of minor mergers, smooth accretion, and secular processes.

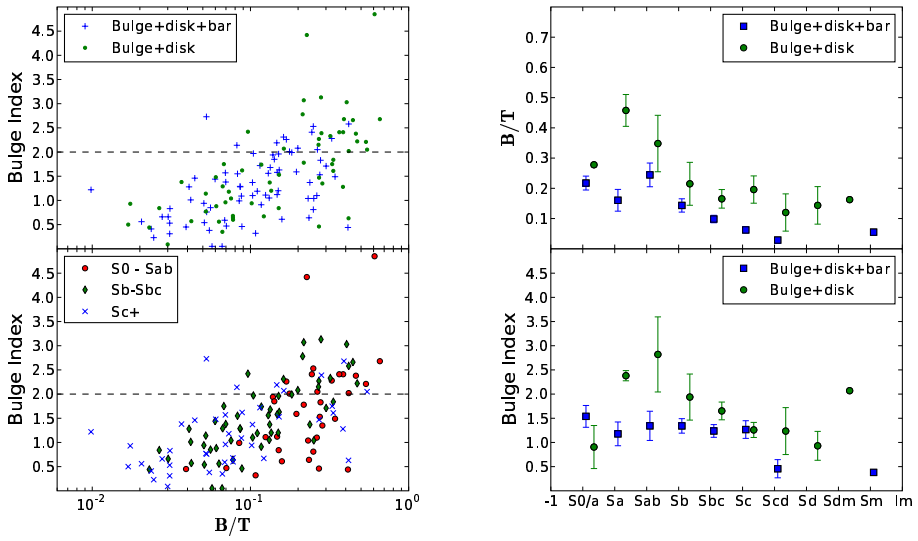

Figure 1. **Left:** The relation between B/T and bulge index for all 143 galaxies. The upper panel is coded by bar class; the legend indicates the type of best-fit model adopted. The lower panel is coded according to Hubble type. **Right:** Mean B/T and bulge index for the full sample are plotted against Hubble type. The error bars indicate the standard deviation of the population around the mean in each bin. (Figures adapted from WJKBK09.)

Table 1. B/T: Data versus Hierarchical Models of Galaxy Evolution

(1)	Data (2)	Model spirals with major mergers since redshift z_1 (3)	Model spirals with no major merger since redshift z_1 (4)	All model spirals (5)
		For $z_1 \leq 4$	For $z_1 \leq 4$	
Fraction of spirals with $B/T \leq 0.2$	66.4% ± 4.44%	1.6%	65.7%	67.3%
Fraction of spirals with $0.2 < B/T \leq 0.4$	25.7% ± 4.11%	5.5%	13.3%	18.8%
Fraction of spirals with $0.4 < B/T \leq 0.75$	8.0% ± 2.5%	12.6%	1.3%	13.9%
Fraction of spirals with $B/T \leq 0.75$	100%	19.8%	80.2%	100.0%

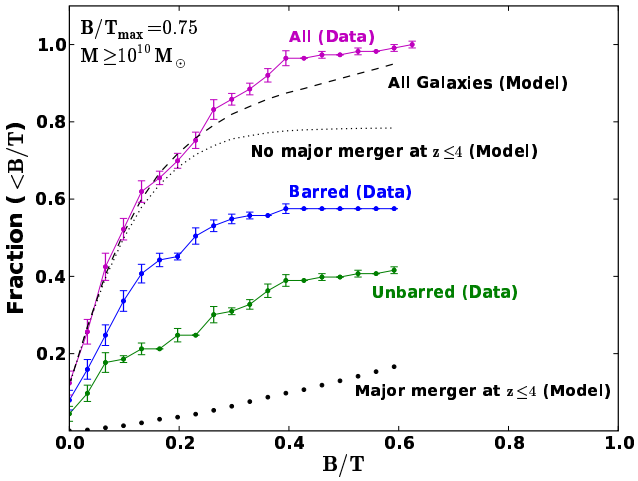

Figure 2. The cumulative fraction of high-mass ($M_\star \geq 1.0{\times}10^{10} M_\odot$) spirals as a function of present-day B/T is shown for data and hierarchical models. Spirals are defined as systems with $B/T \leq 0.75$. (Figures adapted from WJKBK09.)

References

Böker, T., Laine, S., van der Marel, R. P., Sarzi, M., Rix, H.-W., Ho, L. C., & Shields, J. C. 2002, AJ, 123, 1389

Barazza, F. D., Jogee, S., & Marinova, I. 2008, ApJ, 675, 1194

Bell, E. F., McIntosh, D. H., Katz, N., & Weinberg, M. D. 2003, ApJS, 149, 289

Binney, J., & Tremaine, S. 1987, Galactic Dynamics (Princeton: Princeton Univ. Press)

Conselice, C. J., Bershady, M. A., Dickinson, M., & Papovich, C. 2003, AJ, 126, 1183

Dekel, A., et al. 2009, Nat, 457, 451

Eskridge, P. B., et al. 2002, ApJS, 143, 73

Genzel, R., et al. 2008, ApJ, 687, 59

Graham, A. W., & Worley, C. C. 2008, MNRAS, 752

Hopkins, P. F., Cox, T. J., Dutta, S. N., Hernquist, L., Kormendy, J., & Lauer, T. R. 2009, ApJS, 181, 135

Jogee, S., et al. 2009, ApJ, 697, 1971

Julian, W. H., & Toomre, A. 1966, ApJ, 146, 810

Kautsch, S. J., Grebel, E. K., Barazza, F. D., & Gallagher, J. S., III 2006, A&A, 445, 765

Khochfar, S., & Burkert, A. 2005, MNRAS, 359, 1379

Khochfar, S., & Silk, J. 2006, MNRAS, 370, 902

Kormendy, J., & Fisher, D. B. 2008, in Formation and Evolution of Galaxy Disks, ed. J. G. Funes, S. J., & E. M. Corsini (San Francisco: ASP), 297

Laurikainen, E., Salo, H., & Buta, R. 2004, ApJ, 607, 103

Laurikainen, E., Salo, H., Buta, R., & Knapen, J. H. 2007, MNRAS, 381, 401

Marinova, I., & Jogee, S. 2007, ApJ, 659, 1176

Peng, C. Y., Ho, L. C., Impey, C. D., & Rix, H.-W. 2002, AJ, 124, 266

Toomre, A. 1981, in The Structure and Evolution of Normal Galaxies, ed. S. M. Fall & D. Lynden-Bell (New York: Cambridge University Press), 111

Weinzirl, T., Jogee, S., Khochfar, S., Burkert, A., & Kormendy, J. 2009, ApJ, 696, 411

GALAXY EVOLUTION: EMERGING INSIGHTS AND FUTURE CHALLLENGES
ASP Conference Series, Vol.
@jourvol, © 2009
S. Jogee, I. Marinova, L. Hao, and G. A Blanc

Galaxy bulges from $z = 0$ to $z = 1$

Marc Balcells

Instituto de Astrofísica de Canarias, 38200 La Laguna, Tenerife, Spain

Isaac Newton Group of Telescopes, Aptdo. 321, 38700 Santa Cruz de La Palma, Spain

Abstract. The last decade has seen an amazing transformation in our ideas about the central bulges of disk galaxies. We are probably only half-way through this change. In this talk I give an overview of three areas of my specific interest; all are presented as ingredients for further refining our concept of bulge. First, I discuss whether the inner few hundred parsec of disk galaxies do pertain to the bulge or to the disk. Second, I present results on colors of bulges and disks from the local Universe to $z \sim 1$: I will put emphasis on the fact that colors of bulges and inner disks are very similar. Third, I will use combined data on colors and central surface brightness to identify bulges growing inside disks at $z \sim 1.0$, and to conjecture that the descendants of these forming events may correspond to today's so-called pseudo-bulges.

1. Introduction

Our notions about the nature of the central bulges of disk galaxies have dramatically evolved in the past two decades. In the eighties, a hypothesis with long-lasting influence stated that bulges were elliptical galaxies that, for some reason, had grown a disk around them (Renzini 1999). Such was the wish to identify bulges with ellipticals that a driver behind bulge studies was to search for clues on the competing models for formation of *ellipticals*, i.e., monolithic collapse vs. mergers. Such was the *classical view* of bulges, which led to the term *classical bulges*, a class which would include those bulges that do conform to the classical view of being similar to ellipticals. (One often hears that 'classical bulges' is equivalent to 'merger-built'. I believe the originating meaning was 'similar to ellipticals'. Operationally, 'classical bulges' are often identified as high-surface brightness, high-Sérsic index components, and we will use this meaning of the term here.)

The bulge landscape has changed thanks to a number of developments, amply addressed in this conference. The first progress came from developments in the understanding of bar dynamics. Bars have a vertical instability that pumps disk material above the plane, thus allowing stars originally in the thin disk to form a *bulging* region (Combes & Sanders 1981; Pfenniger & Norman 1990). Bars may further be destroyed by central mass concentrations, leading to a bulge that is not prolate: the bar dynamics could lead the galaxy to ultimately grow a central axi-symmetric bulge.

A second attack on the classical model for bulges, initiated by Kormendy (1993), came from observational evidence that some components assumed to

be bulges share properties of disks, including: flattened shapes; rotation above the level expected from an isotropic oblate rotator; spiral arms; and, ongoing star formation. Such structures have been named pseudo-bulges (Kormendy & Kennicutt 2004). In astronomy, we tend to like it when things are turned upside-down; the exercise allows us to put the general robustness of our concepts to test. The bulge-pseudobulge problem is a case in point. Two poles characterize galactic components, namely rotationally-supported, thin disks and pressure-supported, fat spheroids; bulges had always been bundled in the second class, but disky evidences for bulges would question the classification: perhaps we have been fooled all along, and (many) bulges turn out to be disks?

Amply analyzed in the Kormendy & Kennicutt (2004) review, the so-called *pseudobulge* problem may be phrased as follows. *If the disks of all galaxies have exponential surface brightness profiles all the way in, then the excess central light in many galaxies, i.e. the bulges, show disk properties.* Kormendy (1993) introduced the term pseudo-bulge to name systems that masquerade as bulges, but are something else (disks). The term pseudo-bulge will be useful while we fail to distinguish true bulges from disguised disks. The attention received by pseudo-bulges today probably signals that progress is to be expected soon. It is indeed an exciting time to be working on bulges.

In this paper, I will use both the binomial *bulge, pseudo-bulge* and the more physical terms *disk, spheroid*. I provide an overview of recent work by myself and collaborators on bulges at low and high redshift. The issue of disk vs. spheroid will first be addressed by looking at standard bulge-disk decompositions of nearby bulges (§ 2.). Then, I will address colors of bulges and disks, at intermediate z as well as in the local Universe (§ 3.). I will finally address evidence for strong bulge-growth events inside disks at $z \sim 1$ (§ 4.).

2. Inner disks in disk galaxies

When disks are assumed to have exponential surface brightness profiles, the densest parts of the galaxy, at the center, belong in the bulge. Surface brightness profile fitting using a Sérsic and an exponential model (Allen et al. 2006; Balcells et al. 2007a) assigns the central dense parts to the bulge (the spheroid), while alternative approaches based on ellipticity have been implemented by Kent (1986) and Andredakis et al. (1995).

The Sérsic model is so successful at modeling bulges imaged at ground-based (GB) resolutions (Andredakis et al. 1995; Graham 2001; MacArthur et al. 2003), that we investigated whether it survives the test of describing surface brightness profiles at *HST* resolutions. Data consisted of NICMOS2 F160W images, complemented in the optical with WFPC2 F475W and F814W images, for a sample of 19 inclined early- to intermediate-type disk galaxies from (Peletier et al. 1999). Our method involved extraction of 1-D H-band surface brightness profiles through ellipse fitting, in both *HST* and GB images, and fitting the combined profiles with a Moffat-convolved Sérsic plus exponential model. Details and profiles are shown in Balcells et al. (2007a). The results show that only $\sim$10% of the galaxies allow for a pure Sérsic plus exponential model. For the remainder, we need to put additional light in the center. Unresolved nuclear sources were found in $\sim$60% of the cases, while extended nuclear sources

were found in another ∼60% of the cases. What makes these additional nuclear components interesting is the fact that every nucleus for which the surface brightness profile shows an extended excess wrt the Sérsic model, it additionally shows isophotal signatures of being a flattened system: a local rise in the ellipticity, and a positive a_4 diskiness coefficient.

We modeled this extra light using an exponential function; the central face-on brightness I_0 and scale lengths h scale as

$$I_0/L_{K,\odot} = 10^{-3.12\pm0.16}(h/10\,\mathrm{pc})^{-1.26\pm0.31}, \quad (1)$$

Typical sizes are a few hundred pc. Central surface brightness are typically 5 mag above those of the outer disks, and comparable to those of the Sérsic component. The implication is that the densest parts of many disk galaxies are flattened systems, more akin to disks than to spheroids. If we assign these systems to the galaxy's disk, then the spheroid becomes less centrally concentrated. This choice has several consequences. First, bulge Sérsic indices become significanly lower than the de Vaucouleurs $n = 4$ value (Balcells et al. 2003; Weinzirl et al. 2009). Second, the correlation between Sérsic index and spheroid luminosity, which Andredakis et al. (1995) found for bulges, gets diluted (Balcells et al. 2007b). And, third, formation of the spheroid now requires less dissipation than previously thought. Stronger dissipation is needed now to form the disk, which now contains an inner region with density far above the canonical Freeman (1970) value. As suggested by P. Hopkins at the conference, mergers of very gas rich precursors could lead to the formation of such nuclear disks (Hopkins et al. 2009). This situation points to another reversal of established concepts as mentioned in § 1., – (major) mergers as origins of galaxy disks.

3. Bulges at intermediate redshifts: colors

Bulge-disk relative age diagnostics would provide important clues on the formation mechanisms of both components. In the local Universe, bulge and disk colors strongly correlate with each other (Peletier & Balcells 1996; Cameron et al. 2009), leading to indistinguishable ages. By looking at bulges in more distant galaxies, we may hope to obtain more significant differences. To that end, we have undertaken a study of disk galaxies at intermediate redshifts.

Recent works on bulges at intermediate redshifts reach conflicting conclusions on whether we should think that 'bulges are already old at $z = 0.8$', or that '(many) bulges were still growing at $z \sim 0.8$'. Koo et al. (2005) worked with a magnitude-limited sample from the Groth strip, which encompasses both bulges inside disks as well as pure spheroids, as determined from 2D bulge-disk decomposition using GIM2D (Simard et al. 2002). He finds that 85% of bulges are very red (rest-frame $U - B > 0.25$), hence old. In contrast, Ellis et al. (2001) and Menanteau, Abraham & Ellis (2001), working on morphologically-selected early-types from the Hubble Deep Field North (HDFN) conclude, on the basis of color inhomogeneities, that 30% and perhaps as much as 50% of spheroids are forming stars.

Sample selection and methodology differences likely explain the differing conclusions of both works. Population ages, and star formation activity, likely

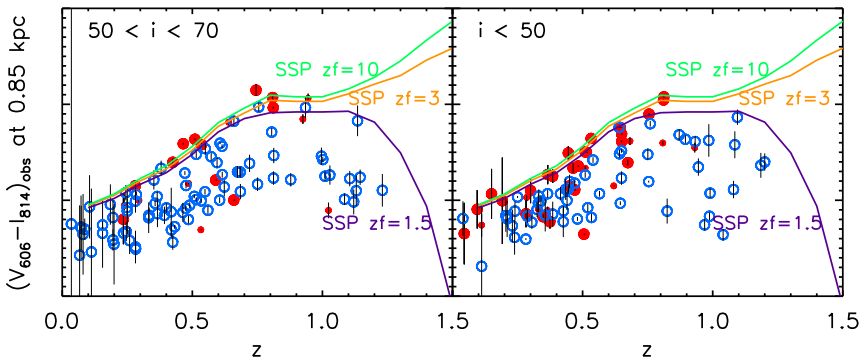

Figure 1. Observer-frame $V-I$ colors measured at 0.85 kpc from the galaxy centers, along the minor axis less affected by dust. (*Filled circles*) bulge sample. (*Open circles*) Non-bulge galaxies. (*a*) high-inclination sample. (*b*) Low-inclination sample. The solid lines are passive evolution tracks for the indicated formation redshifts.

depend not only on the morphological types but also on galaxy mass, as found by MacArthur et al. (2008).

Our approach was to work with bulges residing inside disks. With this choice, we stay close to the original concept of bulges - a central distinct region inside disk galaxies. Lumping bulges of disk galaxies together with pure spheroids would carry the implicit assumption that bulges and pure ellipticals share the same formation history, which is one of the hypotheses one wants to test in any study of bulges. We want to avoid doing this. Admittedly, our choice also has its limitations. To a large extent, we all study bulges at high z to learn on the formation history of *today's* bulges. Our approach excludes any naked bulges that might have grown a disk at epochs more recent than our observations.

In practice, we start with a diameter-limited sample (SExtractor radii above 1.4 arcsec), and define bulges as any central region with observed I-band surface brightness 1.0 mag/arcsec^2 above the inward extrapolation of the exponential fit to the outer disk. Galaxies without such central excess define the bulge-less comparison sample. High- and low-inclination subsamples, on the basis of axis ratios, are used to control contamination by pure ellipticals, which may be present in the low-inclination sample but not in the high-inclination sample. We would have preferred to select bulges on the basis of rounder inner isophotes in inclined samples. Unfortunately, even with *HST* data, we lack the spatial resolution to resolve but the largest bulges (1 kpc = 0.125 arcsec at $z = 1$, $\Omega_\Lambda = 0.7$, $\Omega_M = 0.3$, $h_{100} = 0.7$). The study was separately done with data from the Groth and the GOODS-N fields.

In Domínguez-Palmero et al. (2008) we present samples, color data, color profiles and color gradients for the Groth sample. The parent sample comprises 248 galaxies, of which 54 have bulges, 137 don't, and the rest are too disturbed to decide. All the data are available in electronic format trough CDS. Two main results arise from these data (Domínguez-Palmero & Balcells 2008). First,

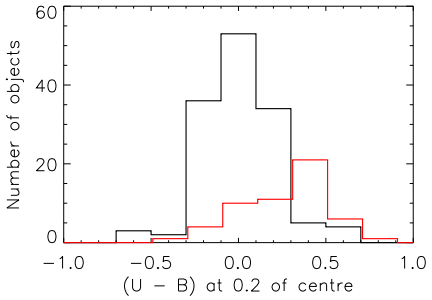

Figure 2. Histogram of $U - B$ colors, measured at 0.2" from the galaxy center, for galaxies with bulges (red) and without bulges (black).

60% of bulges have colors consistent with passive evolution of a population that does not form stars, the rest of bulges having bluer colors expected from star-forming populations (Fig. 1). Bulge-less galaxies show a range of colors, typically blue. Figure 2 shows histograms of rest-frame $U - B$ colors. This figure demonstrates that, when chosen solely on the basis of central surface brightness excess, the nuclear colors of disk galaxies show a clear bi-modality: red, passive colors are strongly linked to central surface brightness excess with respect to the surrounding disk.

The second lesson from our analysis in the Groth field is that colors of bulges strongly correlate with global and with disk colors. Redder bulges live in redder disks. To be sure, bulges tend to be slightly redder than their host disks. However, the color difference between nuclei (with or without bulge) and disks is independent of whether a bulge sits at the galaxy center or not. The vast majority of our galaxies show color profiles with negative gradients (bluer outward); on the mean, color gradients are of the same amplitude for the subsamples with and without bulges. That the color gradient is driven by the presence of the bulge is a deeply ingrained concept. However, plenty of independent evidence is available today to abandon this old idea, including detailed studies in the local Universe where spatial resolution is not a problem. Peletier & Balcells (1996) already pointed out that bulges ('round things') do not exist in color space. Indeed, color maps do not show features spatially corresponding to the high-surface brightness region of bulges. A similar conclusion was reached with the Millenium galaxy catalog by Cameron et al. (2009).

4. Growing bulges at $z \sim 1$

The 40% of bulges with blue colors found by Domínguez-Palmero & Balcells (2008) must be forming stars, hence they may trace processes of bulge growth. One can postulate two models for such bulges. In the rejuvenation hypothesis, a blue bulge is an old bulge that is now forming stars, due perhaps to a merger or an accretion of gas. Alternatively, a blue bulge may simply correspond to an central concentration of star formation activity in a galaxy without, or with a

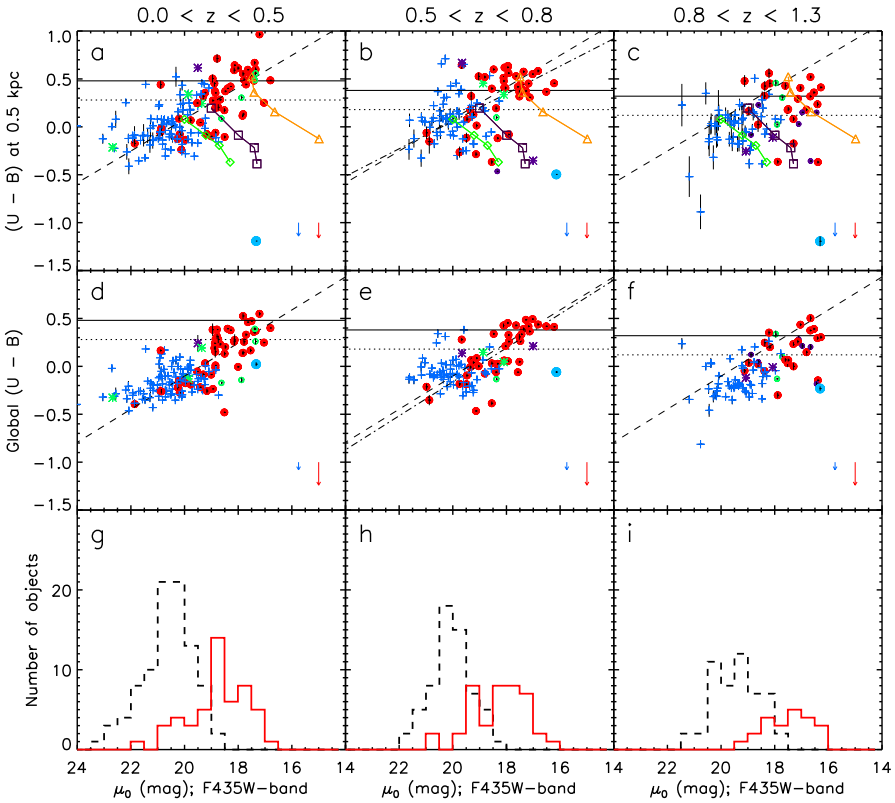

Figure 3. **a,b,c)** and **d,e,f)** galaxy nuclear and global rest-frame $(U-B)$, respectively, vs $F435W$-band μ_0. *Intermediate red filled circles*: normal bulge galaxies. *Small green open circles*: bulge galaxies hosting a LL AGN. *Small dark blue filled circles*: bulge galaxies harbouring a NL AGN. *Large blue filled circles*: bulge galaxies hosting a BL AGN. *Blue crosses*: normal non-bulge galaxies. *Green asterisks*: non-bulge galaxies harbouring a LL AGN. *Blue asterisks*: non-bulge galaxies hosting a NL AGN. *Horizontal solid and dotted lines*: mean color and blue boundary of the RS. *Dashed lines*: linear least-squares fits to the color-μ_0 distribution of bulge galaxies in the $z < 0.5$ bin. *Dot-dashed lines*: least-squares fits at $0.5 < z < 0.8$ bin. **g,h,i)** $F435W$-band μ_0 histograms for the three redshifts ranges. *Solid red lines*: normal bulge galaxies. *Dashed black lines*: normal non-bulge galaxies.

smaller, preexisting bulge. Distinguishing between the two models may be done studying the trends between color and surface brightness. The central surface brightness of a rejuvenated bulge should be higher than that of passive bulges, as the burst light is added to the brightness of the underlying old bulge.

We analyzed the correlation of central surface brightness μ_0 and color in our bulge sample in the GOODS-N field (Domínguez-Palmero & Balcells 2009). Sample selection and color analysis were done identically as with the Groth data described in Sect. 3. From a diameter-limited parent sample of 398 galaxies, we found 131 galaxies with bulges, 214 without, 20 pure ellipticals, and 53 distorted cases. As a proxy for central surface brightness we took the average I-band surface brightness within a radius of 0.5 kpc, whereas nuclear colors were measured at 0.85 kpc from the center, for galaxies with and without bulges.

The results are summarized in Figure 3. Up to $z = 0.8$ colors and central surface brightness strongly correlate with each other, in the sense that high-surface brightness bulges are redder while blue, star-forming galaxies show fainter surface brightness. Because mass-to-light ratios are higher for redder populations, the trends indicate that *redder bulges have higher surface density.* That bluer bulges have lower surface brightness argues against the rejuvenation hypothesis for such bulges. Note that galaxies without bulges show a very similar correlation between color and surface brightness. This indicates that *the color–μ_0 trend is not entirely driven by the presence of a bulge component.*

At redshifts above $z = 0.8$, the color-μ_0 breaks down. This is in part due to the fact that we progressively miss smaller and low-prominence bulges as we move to higher z. However, the main culprit is the appearance of galaxies with blue nuclei and high surface brightness (panel c in Fig. 3). These galaxies show strongly-inverted color profiles (positive nuclear color gradients), with blue nuclei. Half of those cases are narrow-line AGN on the basis of their X-ray emission (Treister et al. 2006) and optical spectroscopy. It is unlikely that these AGN dominate the broad-band colors, and thus, the blue nuclei likely trace strong episodes of star formation concentrated in the central kpc of the galaxies.

We investigated possible evolutionary links between these blue nuclei and local bulges. Evolutionary synthesis models from Bruzual & Charlot (2003) were used to track the evolution of color and surface brightness, adopting standard assumptions on the evolution of the star-formation rate, and requiring the models to end on three distinct points along the $z \sim 0$ color-magnitude trend (panels abc in Fig. 3. The main lesson we extract from this modeling, that does not pretend to provide unique evolutionary tracks, is that such tracks are diagonal in the μ_0–color plane. This reflects the simple fact that stellar populations lose surface brightness as they redden with age.

The models suggest that blue, high-μ_0 bulges at $z \sim 1$ do not evolve into the high surface brightness end of the μ_0–color distribution at $z \sim 0$ (into 'classical bulges'): the precursors of such classical bulges must have had much higher surface brightness (yellow tracks). Similarly, the values of μ_0 at $z > 0.8$ show that blue, high-μ_0 bulges at $z \sim 1$ do not descend from red, passive bulges at the same redshifts: they are not rejuvenated bulges. If they were, they would have higher surface brightness than their red counterparts. The models invite the conjecture that blue bulges at $z > 0.8$ may be precursors of intermediate color, intermediate-μ_0 bulges in the local Universe, the so-called pseudo bulges.

Acknowledgments. This work is based on archival data from the HST, obtained from the data archive at STScI, which is operated by AURA under NASA contract NAS5-26555. Support has been provided by the Spanish Programa Nacional de Astronomía y Astrofísica through project number AYA2006-12955 and through the Consolider-Ingenio 2010 Program grant CSD2006-00070: First Science with the GTC (http://www.iac.es/consolider-ingenio-gtc/).

References

Allen, P. D., Driver, S. P., Graham, A. W., Cameron, E., Liske, J., & de Propris, R. 2006, MNRAS, 371, 2
Andredakis, Y. C., Peletier, R. F., & Balcells, M. 1995, MNRAS, 275, 874
Balcells, M., Graham, A. W., Domínguez-Palmero, L., & Peletier, R. F. 2003, ApJ, 582, L79
Balcells, M., Graham, A. W., & Peletier, R. F. 2007, ApJ, 665, 1084
Balcells, M., Graham, A. W., & Peletier, R. F. 2007, ApJ, 665, 1104
Bruzual, G., & Charlot, S. 2003, MNRAS, 344, 1000
Cameron, E., Driver, S. P., Graham, A. W., & Liske, J. 2009, ApJ, 699, 105
Combes, F., & Sanders, R. H. 1981, A&A, 96, 164
Domínguez-Palmero, L., & Balcells, M. 2009, ApJ, 694, L69
Domínguez-Palmero, L., Balcells, M., Erwin, P., Prieto, M., Cristóbal-Hornillos, D., Eliche-Moral, M. C., & Guzmán, R. 2008, A&A, 488, 1167
Domínguez-Palmero, L., & Balcells, M. 2008, A&A, 489, 1003
Ellis, R. S., Abraham, R. G., & Dickinson, M. 2001, ApJ, 551, 111
Freeman, K. C. 1970, ApJ, 160, 811
Graham, A. W. 2001, AJ, 121, 820
Hopkins, P. F., Cox, T. J., Younger, J. D., & Hernquist, L. 2009, ApJ, 691, 1168
Kent, S. M. 1986, AJ, 91, 1301
Koo, D. C. et al. 2005, ApJ, 157, 175
Kormendy, J. 1993, Galactic Bulges, IAU Symposium, 153, 209
Kormendy, J., & Kennicutt, R. C., Jr. 2004, ARA&A, 42, 603
MacArthur, L. A., Courteau, S., & Holtzman, J. A. 2003, ApJ, 582, 689
MacArthur, L. A., Ellis, R. S., Treu, T., U, V., Bundy, K., & Moran, S. 2008, ApJ, 680, 70
Menanteau, F., Abraham, R. G. & Ellis, R. S. 2001, *MNRAS*, 322, 1
Peletier, R. F. & Balcells, M. 1996, AJ, 111, 2238
Peletier, R. F., Balcells, M., Davies, R. L., Andredakis, Y., Vazdekis, A., Burkert, A., & Prada, F. 1999, MNRAS, 310, 703
Pfenniger, D., & Norman, C. 1990, ApJ, 363, 391
Renzini A., in 'The formation of galactic bulges', 1999, Carollo M., Ferguson H.C., Wyse R.F.G., New York - Cambridge University Press
Simard, L. et al. 2002, ApJS, 142, 1
Treister, E., Urry, C. M., Van Duyne, J., Dickinson, M., Chary, R.-R., Alexander, D. M., Bauer, F., Natarajan, P., Lira, P., & Grogin, N. A. 2006, ApJ, 640, 603
Weinzirl, T., Jogee, S., Khochfar, S., Burkert, A., & Kormendy, J. 2009, ApJ, 696, 411

GALAXY EVOLUTION: EMERGING INSIGHTS AND FUTURE CHALLLENGES
ASP Conference Series, Vol.
@jourvol, © 2009
S. Jogee, I. Marinova, L. Hao, and G. A Blanc

The Elliptical–Spheroidal and Elliptical–Elliptical Galaxy Dichotomies

John Kormendy

Department of Astronomy, University of Texas at Austin, 1 University Station C1400, Austin, TX 78712-0259, USA

Abstract. This paper summarizes Kormendy et al. (2009, ApJS, 182, 216). We confirm that spheroidal galaxies have fundamental plane correlations that are almost perpendicular to those for bulges and ellipticals. Spheroidals are not dwarf ellipticals. They are structurally similar to late-type galaxies. We suggest that they are defunct ("red and dead") late-type galaxies transformed by a variety of gas removal processes. Minus spheroidals, ellipticals come in two varieties: giant, non-rotating, boxy galaxies with cuspy cores and smaller, rotating, disky galaxies that lack cores. We find a new feature of this "E–E dichotomy": Coreless ellipticals have extra light at the center with respect to an inward extrapolation of the outer Sérsic profile. We suggest that extra light is made in starbursts that swamp core scouring in wet mergers. In general, only giant, core ellipticals contain X-ray gas halos. We suggest that they formed in mergers that were kept dry by X-ray gas heated by active galactic nuclei.

1. High-Dynamic-Range Surface Photometry of E and Sph Galaxies

Figure 1 shows examples of photometry of all known ellipticals in the Virgo cluster from Kormendy et al. (2009; hereafter KFCB). The key to this paper is the accuracy and large dynamic range attained when data from many telescopes with different resolutions and field sizes are combined into composite profiles.

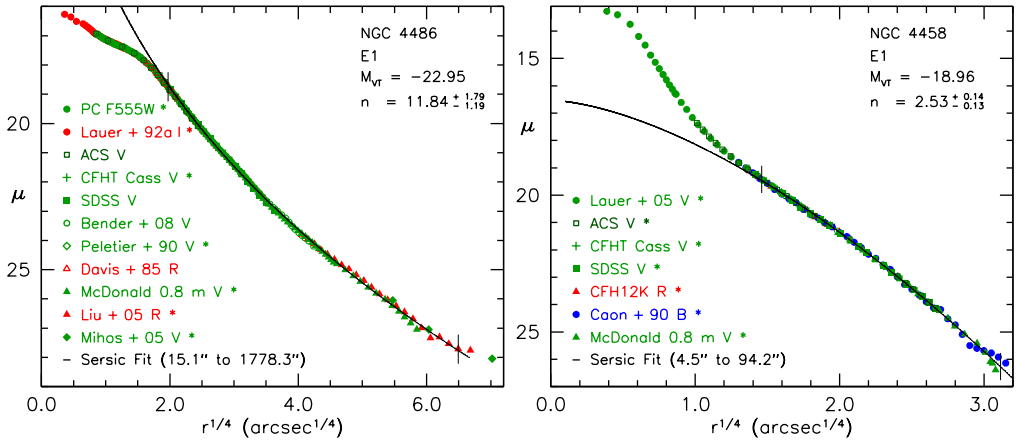

Figure 1. Major-axis brightness profiles of Virgo ellipticals from KFCB. Surface brightness μ is in V mag arcsec^{-2}. The curve is a Sérsic (1968) fit between the vertical dashes; the index n and total galaxy absolute magnitude M_{VT} are in the key. This figure illustrates the E–E dichotomy: NGC 4486 is a core galaxy with $n > 4$; NGC 4458 is an extra light galaxy with $n \lesssim 4$ (§ 3).

2. The E – Sph Dichotomy

Integrating the KFCB photometry leads to improved measurements of structural parameters. Figure 2 shows the resulting projections of the fundamental plane ("FP") (Djorgovski & Davis 1987; Faber et al. 1987; Djorgovski et al. 1988).

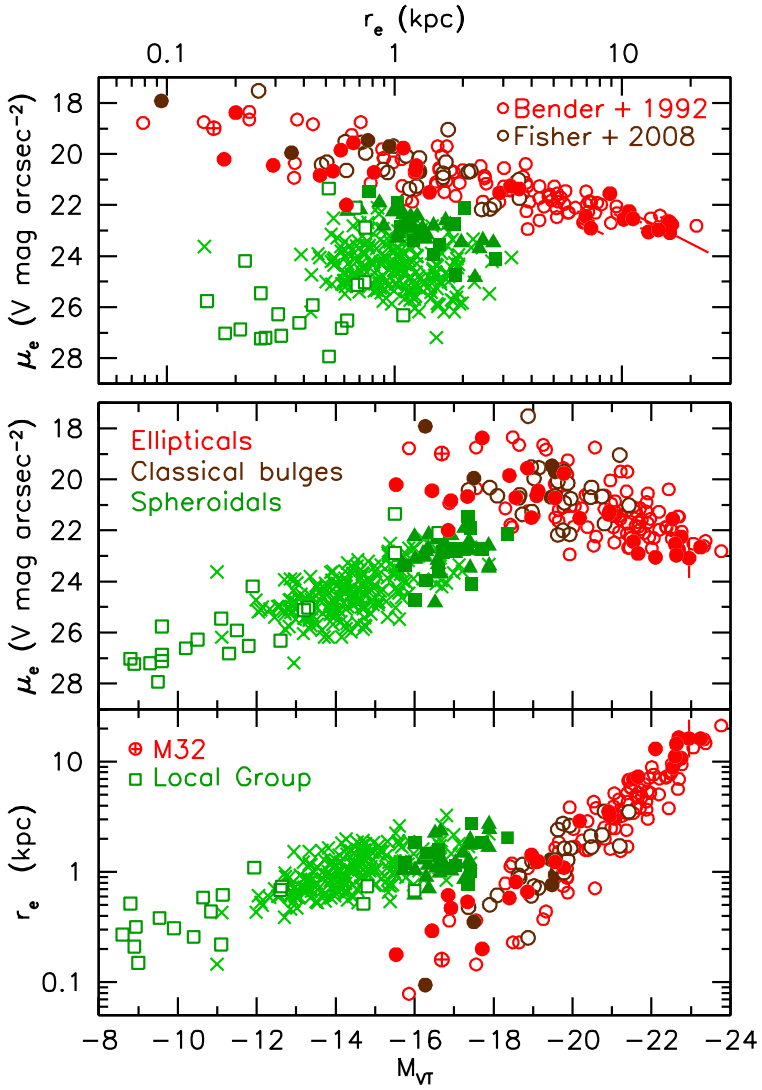

Figure 2. Global parameter correlations for ellipticals (red), classical bulges (brown), and spheroidals (green). Filled circles, filled squares, and M 32 are from KFCB. Green triangles show all spheroidals from Ferrarese et al. (2006) that are not in KFCB. Crosses show all spheroidals from Gavazzi et al. (2005) that are not in KFCB or in Ferrarese et al. (2006). The bottom panels show effective radius r_e and surface brightness μ_e at the effective radius versus galaxy absolute magnitude. The top panel shows μ_e vs. r_e (the Kormendy 1977 relation, which shows the FP almost edge-on). We confirm the E – Sph dichotomy found by Kormendy (1985, 1987). However, the separation between the E and Sph sequences is larger in near-central parameters, so KFCB use these to classify galaxies as elliptical or spheroidal.

KFCB and Figure 2 strongly confirm the reality of the E – Sph dichotomy. Ellipticals and spheroidals form almost-perpendicular parameter sequences. That E and Sph galaxies are physically different was presciently suggested by Wirth & Gallagher (1984) based on a very few objects. It was first demonstrated for substantial galaxy samples by Kormendy (1985, 1987).

The KFCB sample is augmented in Figure 2 with ellipticals from the FP study of Bender, Burstein, & Faber (1992). They, too, confirm the E – Sph dichotomy; their sample substantially strengthens our results. Bulges from Fisher & Drory (2008) are also included. We confirm that classical bulges are indistinguishable from ellipticals, as they should be if we understand correctly that they – like ellipticals – were formed in major mergers (Steinmetz & Navarro 2002). The same is not true of pseudobulges: some of these are much less dense than classical bulges (Carollo 1999; Fisher & Drory 2008; Kormendy & Fisher 2008). We believe they did not form via mergers (Kormendy & Kennicutt 2004).

The existence of an E – Sph dichotomy has been criticized by many authors, although it is often visible in their correlation diagrams. Early ambivalence is evident in Sandage, Binggeli, & Tammann (1985). They found continuous (but not monotonic) correlations involving r_e and μ_e, because their small Es were poorly resolved in ground-based seeing. This led them to believe that Es and "dEs" (as they called spheroidals) are continuous. On the other hand, they correctly noted that E and dE galaxies have different luminosity functions. In fact, "ellipticals" and "dwarf ellipticals" overlap in luminosity! The schizophrenic caption of their Figure 7 reads: "The luminosity functions for E and dE types suggesting that the two types, although part of a continuum of physical properties, form two families." Soon afterward, Binggeli & Cameron (1991) saw the dichotomy in global parameters. But Jerjen & Binggeli (1997) changed their minds: "The $[n - M_B]$ relation for Es and that for dEs smoothly and continuously merge into each other, giving the impression of one global relation for dwarf and giant ellipticals." This observation, similarly interpreted by Graham & Guzmán (2003), Gavazzi et al. (2005), and Ferrarese et al. (2006), is confirmed also by KFCB. But the observation that n is not sensitive to the difference between Es and Sphs does not mean that they are related. Another parameter that shows continuous E – Sph and even E – S – Im – Sph correlations is metallicity, because self-enrichment depends on potential well depth and not on structure. To decide whether various galaxies are related, we need to look at all correlations. Then Figure 2 shows that E and Sph galaxies are different.

Other criticisms followed. Graham & Guzmán (2003) and Gavazzi et al. (2005) argued that core Es deviate from a continuous correlation beween Sphs and low-luminosity Es because of the light that is missing in cores. This is unrealistic: only 0 – 2 % of the galaxy light is missing; such small amounts have no effect on measurements of global parameters. Moreover, the Sph sequence approaches the E sequence near its middle, not near its faint end. Similarly, it is unrealistic to argue (Binggeli 1994; Graham & Guzmán 2003; Gavazzi et al. 2005; Ferrarese et al. 2006) that "the striking dichotomy observed by Kormendy (1985) could partly be due to the lack, in Kormendy's sample, of galaxies in the -20 mag $< M_B < -18$ mag range, corresponding precisely to the transition region between the two families." Kormendy (1985, 1987) showed that the families strongly diverge in the magnitude range where they overlap. Also, KFCB and Figure 2 here suffer from no lack of galaxies at overlap magnitudes.

Finally, the Sph galaxies in KFCB are biased in favor of those that are most like ellipticals, because we did not know which galaxies were E and which were Sph – or whether these could be distinguished – until the photometry was completed.

Thus the E – Sph dichotomy is a robust result, visible in central parameters (KFCB Figure 34), in global parameters (KFCB Figures 37, 38, 41; Figure 2 here) and in the surface brightness profiles (KFCB Figures 35, 36, 39).

Figure 2 shows that lower-luminosity Es are monotonically higher in density, whereas lower-luminosity Sphs are monotonically lower in density. Ellipticals define a sequence of increasing dissipation in lower-mass mergers (Kormendy 1989). It is reproduced by merger simulations that include gas and star formation (Robertson et al. 2006; Hopkins et al. 2008, 2009c). In contrast, Kormendy (1985, 1987) showed that the parameter correlations of Sph galaxies are similar to those of dwarf spiral and irregular galaxies. The above papers and KFCB suggest that spheroidals are defunct late-type galaxies transformed by internal processes such as supernova-driven gas ejection (Dekel & Silk 1986) and environmental processes such as galaxy harassment (Moore et al. 1996, 1998) and ram-pressure gas stripping (Chung et al. 2007). Smaller Sph + S + Im galaxies form a sequence of decreasing baryon retention caused by the shallower gravitational potential wells of tinier galaxies (Dekel & Silk 1986).

3. The E – E Dichotomy

Minus spheroidals, ellipticals and classical bulges of disk galaxies (red and brown points in Figure 2) form a homogeneous collection of objects that are consistent with our paradigm of galaxy formation. We believe that both formed in galaxy mergers that are an inevitable consequence of the hierarchical clustering that makes all structure in the Universe (Toomre 1977; White & Rees 1978; Steinmetz & Navarro 2002). We see mergers in progress, often with gas dissipation and bursts of star formation (Schweizer 1990). Most spectacular are ultraluminous infrared galaxies (ULIRGs) (e. g., Joseph & Wright 1985; Sanders et al. 1988). Their remnants are quantitatively consistent with the properties of ellipticals. What do we still need to learn?

Research now focuses on the exact sequence of events that made ellipticals. One complication is that star formation and galaxy assembly via mergers can be very disconnected. Which galaxies are remnants of gas-free ("dry") mergers and which are remnants of gas-rich ("wet") mergers? Also, close correlations of bulges and ellipticals with their central black holes (BHs) imply that BHs and their hosts evolved together (Ho 2004). BH growth may inject so much energy into protogalactic gas that it becomes a dominant force in galaxy formation (Silk & Rees 1998; Hopkins et al. 2006). How do BHs affect galaxy formation? Third, much of the emphasis in understanding galaxy formation has shifted from explaining structure to explaining star formation histories in the context of the Sloan Digital Sky Survey observations of the color-magnitude diagram (e. g., Strateva et al. 2001) in which galaxies divide themselves into a "red sequence" of passively evolving objects and a "blue cloud" of galaxies that actively form stars. Ellipticals dominate the bright part of the red sequence. How did they evolve from fainter red-sequence and blue-cloud galaxies? What observed properties of ellipticals provide clues to an understanding of the above issues?

The most fundamental such properties consist of the observations that elliptical galaxies come in two distinct varieties. In the following list of properties, italics highlight new aspects of the dichotomy found in KFCB or known aspects for which the observational evidence is strengthened in KFCB.

Giant ellipticals ($M_V \lesssim -21.5 \pm 1$ for $H_0 = 72$ km s^{-1} Mpc^{-1}) generally
(1) have cores, i. e., central missing light with respect to the outer profile (Fig. 1);
(2) rotate slowly, so rotation is of little importance dynamically; hence
(3) are anisotropic and modestly triaxial;
(4) are less flattened (ellipticity ~ 0.15) than smaller ellipticals;
(5) have boxy-distorted isophotes;
(6) *have Sérsic function outer profiles with* $n > 4$ (Fig. 1);
(7) *mostly are made of very old stars that are enhanced in* α *elements* (Fig. 3).
(8) often contain strong radio sources, and
(9) *contain X-ray-emitting gas, more of it in more luminous galaxies* (Fig. 4).

Normal and dwarf ellipticals ($M_V \gtrsim -21.5$) generally
(1) are coreless – *have central extra light with respect to the outer profile* (Fig. 1);
(2) rotate rapidly, so rotation is dynamically important to their structure;
(3) are nearly isotropic and oblate spheroidal, albeit with small axial dispersions;
(4) are flatter than giant ellipticals (ellipticity ~ 0.3);
(5) have disky-distorted isophotes;
(6) *have Sérsic function outer profiles with* $n \lesssim 4$ (Fig. 1); Fig. 3:
(7) *are made of (still old but) younger stars with little* α*-element enhancement*;
(8) rarely contain strong radio sources, and
(9) *rarely contain X-ray-emitting gas* (Fig. 4).

These results are established in many papers (e. g., Davies et al. 1983; Bender 1988; Bender et al. 1989; Nieto et al. 1991; Kormendy et al. 1994; Lauer et al. 1995, 2005, 2007; Kormendy & Bender 1996; Tremblay & Merritt 1996; Gebhardt et al. 1996; Faber et al. 1997; Thomas et al. 2005; Emsellem et al. 2007; Cappellari et al. 2007). A few ellipticals are exceptions to $\geq$ one of (1) – (9).

How did the E – E dichotomy arise? The "smoking gun" for an explanation is a new aspect of the dichotomy found in KFCB and illustrated here in Figure 1. Coreless galaxies do not have featureless, central "power law profiles". Rather, all coreless galaxies in the KFCB sample show a new structural component, i. e., extra light near the center above the inward extrapolation of the outer Sérsic profile (e. g,, M 32: Kormendy 1999; NGC 4458: Fig. 1, right). Kormendy (1999) suggested that this extra light is the signature of starbursts produced in dissipative mergers as predicted by Mihos & Hernquist's (1994) simulations. Similar extra light components are seen in all coreless ellipticals in KFCB. Like Faber et al. (1997, 2007), KFCB suggest that the origin of the E – E dichotomy is that core Es formed in dry mergers whereas coreless Es formed in wet mergers. Simulations of dry and wet mergers now reproduce the structural properties of core and extra light ellipticals in beautiful detail (Hopkins et al. 2009a, b).

When did the E – E dichotomy arise? We cannot answer yet, but Figure 3 provides constraints. It shows observation (7) that core ellipticals mostly are made of old stars that essentially always are enhanced in α elements; in contrast, coreless ellipticals are made of younger stars with more nearly solar compositions. This means (Thomas et al. 2005) that the stars that now are in core Es formed in the first few billion years of the Universe and over a short period of $\lesssim 1$ Gyr,

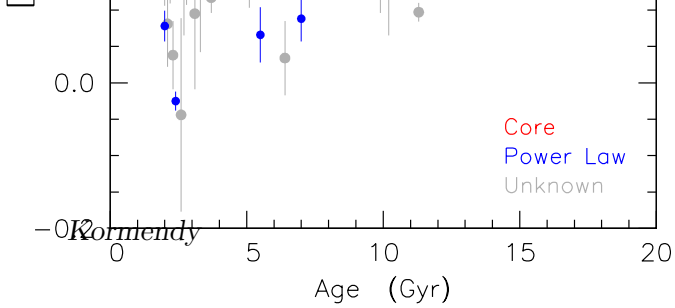

Figure 3. Alpha element overabundance (log solar units) versus relative age of the stellar population (data from Thomas et al. 2005). Red and blue points denote core and power law ellipticals. This figure is from KFCB.

so quickly that Type I supernovae did not have time to dilute with Fe the α-enriched gas recycled by Type II supernovae. However, this does not mean that core ellipticals were made at the same time as their stars. Mass assembly via dry mergers – as required to explain their structure – could have happened at any time after star formation stopped. Our problem is to explain how star formation was quenched so quickly and not allowed to recur. In contrast, coreless ellipticals have younger, less-α-enhanced stellar populations. They are consistent with a simple picture in which a series of wet mergers with accompanying starbursts formed their stellar populations and assembled the galaxies more-or-less simultaneously over the past 9 billion years. Faber et al. (2007) discuss these issues in detail. A corollary is that the progenitors of coreless ellipticals likely were more similar to present-day galaxies than were the progenitors of core ellipticals. The latter may have been different from all galaxies seen today.

Why did the E – E dichotomy arise? The key observations are: (8) core-boxy ellipticals often are radio-loud whereas coreless-disky ellipticals are not, and (9) core-boxy ellipticals contain X-ray gas whereas coreless-disky ellipticals do not (Bender et al. 1989). Figure 4 brings result (9) up-to-date. KFCB suggest that the hot gas keeps dry mergers dry and protects giant ellipticals from late star formation. This is the operational solution to the above "maintenance problem". However, the trick is to keep the gas hot. It is well known that X-ray gas cooling times are short. KFCB review evidence that the main heating mechanism may be energy feedback from accreting BHs (the AGNs of observation 8); these may also have quenched star formation after ~ 1 Gyr. Many details of this picture require work (Cattaneo et al. 2009). Cosmological gas infall is an additional heating mechanism (Dekel & Birnboim 2006). Nevertheless, Figure 4 provides a crucial connection between X-ray gas, AGN physics, and the E – E dichotomy.

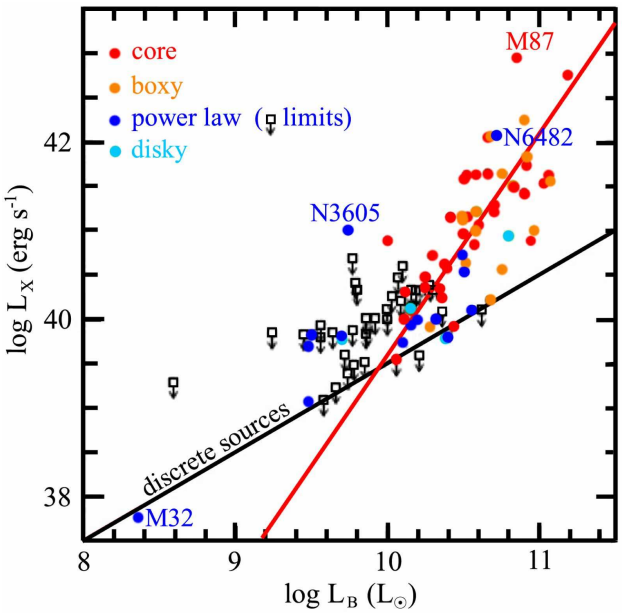

Figure 4. Observed X-ray emission versus galaxy luminosity (KFCB; adapted from Fig. 9 of Ellis & O'Sullivan 2006). Detections are color-coded according to the E – E dichotomy (see the key). The black line is an estimate of the contribution from discrete sources. The red line is a bisector fit to the core-boxy points. Core and coreless ("power law") Es overlap in luminosity, but most core galaxies do and most coreless galaxies do not contain hot gas.

"Bottom line:" In essence, only giant, core ellipticals and their progenitors are massive enough to contain hot gas that helps to engineer the E – E dichotomy.

Acknowledgments. I thank Ralf Bender, Mark Cornell, and David Fisher for fruitful collaboration. This work was supported by NSF grant AST-0607490.

References

Bender, R. 1988, A&A, 193, L7
Bender, R., Burstein, D., & Faber, S. M. 1992, ApJ, 399, 462
Bender, R., et al. 1989, A&A, 217, 35
Binggeli, B. 1994, in ESO/OHP Workshop on Dwarf Galaxies, ed. G. Meylan & P. Prugniel (Garching: ESO), 13
Binggeli, B., & Cameron, L. M. 1991, A&A, 252, 27
Cappellari, M., et al. 2007, MNRAS, 379, 418
Carollo, C. M. 1999, ApJ, 523, 566
Cattaneo, A., et al. 2009, Nature, submitted
Chung, A. et al. 2007, ApJ, 659, L115
Davies, R. L., et al. 1983, ApJ, 266, 41
Dekel, A., & Birnboim, Y. 2006, MNRAS, 368, 2
Dekel, A., & Silk, J. 1986, ApJ, 303, 39
Djorgovski, S., & Davis, M. 1987, ApJ, 313, 59
Djorgovski, S., de Carvalho, R., & Han, M.-S. 1988, in The Extragalactic Distance Scale, ed. S. van den Bergh & C. J. Pritchet (San Francisco: ASP), 329
Ellis, S. C., & O'Sullivan, E. 2006, MNRAS, 367, 627
Emsellem, E., et al. 2007, MNRAS, 379, 401
Faber, S. M., et al. 1987, in Nearly Normal Galaxies: From the Planck Time to the Present, ed. S. M. Faber (New York: Springer), 175

Faber, S. M., et al. 1997, AJ, 114, 1771
Faber, S. M., et al. 2007, AJ, 665, 265
Ferrarese, L., et al. 2006, ApJS, 164, 334
Fisher, D. B., & Drory, N. 2008, AJ, 136, 773
Gavazzi, G., et al. 2005, A&A, 430, 411
Gebhardt, K., et al. 1996, AJ, 112, 105
Graham, A. W., & Guzmán, R. 2003, AJ, 125, 2936
Ho, L. C., Ed. 2004, Carnegie Observatories Astrophysics Series, Vol. 1, Coevolution of Black Holes and Galaxies (Cambridge: Cambridge University Press)
Hopkins, P. F., et al. 2006, ApJS, 163, 1
Hopkins, P. F., Cox, T. J., Dutta, S. N., Hernquist, L., Kormendy, J., & Lauer, T. R. 2009a, ApJS, 181, 135
Hopkins, P. F., Lauer, T. R., Cox, T. J., Hernquist, L., & Kormendy, J. 2009b, ApJS, 181, 486
Hopkins, P. F., Cox, T. J., & Hernquist, L. 2008, ApJ, 689, 17
Hopkins, P. F., Hernquist, L., Cox, T. J., Keres, D., & Wuyts, S. 2009c, ApJ, 691, 1424
Jerjen, H., & Binggeli, B. 1997, in The Second Stromlo Symposium: The Nature of Elliptical Galaxies, ed. M. Arnaboldi, et al. (San Francisco: ASP), 239
Joseph, R. D., & Wright, G. S. 1985, MNRAS, 214, 87
Kormendy, J. 1977, ApJ, 218, 333
Kormendy, J. 1985, ApJ, 295, 73
Kormendy, J. 1987, in Nearly Normal Galaxies: From the Planck Time to the Present, ed. S. M. Faber (New York: Springer), 163
Kormendy, J. 1989, ApJ, 342, L63
Kormendy, J. 1999, in Galaxy Dynamics: A Rutgers Symposium, ed. D. Merritt, J. A. Sellwood, & M. Valluri (San Francisco: ASP), 124
Kormendy, J., & Bender, R. 1996, ApJ, 464, L119
Kormendy, J., & Fisher, D. B. 2008, in Formation and Evolution of Galaxy Disks, ed. J. G. Funes, S. J. & E. M. Corsini (San Francisco: ASP), 297
Kormendy, J., Fisher, D. B., Cornell, M. E., & Bender, R. 2009, ApJS, 182, 216 (KFCB)
Kormendy, J., & Kennicutt, R. C. 2004, ARA&A, 42, 603
Kormendy, J., et al. 1994, in ESO/OHP Workshop on Dwarf Galaxies, ed. G. Meylan & P. Prugniel (Garching: ESO), 147
Lauer, T. R., et al. 1995, AJ, 110, 2622
Lauer, T. R., et al. 2005, AJ, 129, 2138
Lauer, T. R., et al. 2007, ApJ, 664, 226
Mihos, J. C., & Hernquist, L. 1994, ApJ, 437, L47
Moore, B., Lake, G., & Katz, N. 1998, ApJ, 495, 139
Moore, B., et al. 1996, Nature, 379, 613
Nieto, J.-L., Bender, R., & Surma, P. 1991, A&A, 244, L37
Robertson, B., et al. 2006, ApJ, 641, 21
Sandage, A., Binggeli, B., & Tammann, G. A. 1985, in ESO Workshop on the Virgo Cluster of Galaxies, ed. O.-G. Richter & B. Binggeli (Garching: ESO), 239
Sanders, D. B., et al. 1988, ApJ, 325, 74
Schweizer, F. 1990, in Dynamics and Interactions of Galaxies, ed. R. Wielen (New York: Springer), 60
Sérsic, J. L. 1968, Atlas de Galaxias Australes (Cordoba: Obs. Astr., Univ. de Cordoba)
Silk, J., & Rees, M. J. 1998, A&A, 331, L1
Steinmetz, M., & Navarro, J. F. 2002, NewA, 7, 155
Strateva, I., et al. 2001, AJ, 122, 1861
Thomas, D., et al. 2005, ApJ, 621, 673
Toomre, A. 1977, in The Evolution of Galaxies and Stellar Populations, ed. B. M. Tinsley & R. B. Larson (New Haven: Yale University Observatory), 401
Tremblay, B., & Merritt, D. 1996, AJ, 111, 2243
White, S. D. M., & Rees, M. J. 1978, MNRAS, 183, 341

Wirth, A., & Gallagher, J. S. 1984, ApJ, 282, 85

GALAXY EVOLUTION: EMERGING INSIGHTS AND FUTURE CHALLLENGES
ASP Conference Series, Vol.
@jourvol, © 2009
S. Jogee, I. Marinova, L. Hao, and G. A Blanc

Stellar Populations and Mass-to-Light Ratios Throughout the Fundamental Plane

Genevieve J. Graves

UCO/Lick Observatory, Santa Cruz, CA 95064

Abstract. We demonstrate that the stellar populations of early type galaxies span a 2-D space, which means that their star formation histories form a two-parameter family. This two-parameter family maps onto a cross section through the Fundamental Plane (FP), suggesting a strong correlation between the present day structure of a galaxy and its past star formation history. The observed stellar population differences translate into $M_\star/L$ variations that are too small to explain either the tilt of the FP or its thickness. This implies that the tilt and thickness of the FP are driven by systematic variations in either the central dark matter fraction in galaxies or in the IMF with which they form stars. Furthermore, because star formation histories can be mapped onto locations in FP-space, the variations in central dark matter fraction or IMF differences must be correlated with differences in the galaxies' star formation histories.

1. Introduction

In the three-dimensional (3-D) parameter space defined by effective radius (R_e), velocity dispersion (σ), and effective surface brightness (I_e), early type galaxies are observed to lie on a relatively tight 2-D plane called the Fundamental Plane (FP; Djorgovski & Davis 1987; Dressler et al. 1987). The FP can be understood as a manifestation of the virial plane predicted for relaxed systems, which takes the form $R_e \propto \sigma^2 I_e^{-1}$ under the assumption that the dynamical mass-to-light ratio ($M_{\rm dyn}/L$) is constant. However, the observed FP is tilted from the virial plane and has finite thickness (Dressler et al. 1987; Djorgovski & Davis 1987; Jørgensen et al. 1996), indicating that $M_{\rm dyn}/L$ must vary both along the plane and through its thickness (Faber et al. 1987).

There are multiple physical process that could contribute to the observed variations in $M_{\rm dyn}/L$: variations in the dynamical structure of galaxies (e.g., non-homology), variations in the baryonic to dark matter ratio enclosed within R_e, variations in the intial mass function (IMF) with which the galaxies formed their stars, and variations in the stellar population. We write these as

$$\frac{M_{\rm dyn}}{L} = \frac{M_{\rm dyn}}{M_{\rm tot}} \times \frac{M_{\rm tot}}{M_\star} \times \frac{M_\star}{M_{\star,IMF}} \times \frac{M_{\star,\rm IMF}}{L}. \quad (1)$$

In this formulation, $M_{\rm dyn}/M_{\rm tot}$ represents the difference between the total mass of the galaxy ($M_{\rm tot}$) within R_e and the dynamical mass as estimated from the virial scaling relation ($M_{dyn} \propto \sigma^2 R_e$). This term thus encapsulates variations in the dynamical structure of galaxies. Variations in dark matter fraction will affect the ratio between total mass and stellar mass ($M_{\rm tot}/M_\star$), while stellar population differences will affect $M_\star/L$. We break this latter term into two

pieces: $M_{\star,\mathrm{IMF}}/L$ derived from stellar population properties (which necessarily assumes a particular IMF), and $M_\star/M_{\star,\mathrm{IMF}}$, which encapsulates possible IMF variation. Any, or indeed all of these four effects may contribute to the total variation in M_{dyn}/L that is observed in the tilt and thickness of the FP.

We have recently completed a study mapping the stellar population properties of early type galaxies in the color-magnitude diagram (Graves et al. 2009a, hereafter Paper I) and throughout the 3-D FP space defined by σ, R_e, and I_e (Graves et al. 2009b, hereafter Paper II). In the latter work, we find that the stellar populations of early type galaxies are strongly dependent on two FP parameters: σ and I_e, when variation in I_e is expressed as residuals from the FP in the I_e dimension ($\Delta \log I_e$). Interestingly, the third parameter R_e does not appear to correlate with stellar population properties. This implies that early type galaxy star formation histories form a two parameter family and are independent of R_e.

In this conference proceeding, we present the 2-D family of stellar population properties and illustrate that these properties map onto a cross-section through the FP. The observed stellar population variations imply variations in $M_{\star,\mathrm{IMF}}/L$ both along the FP (contributing to the FP tilt) and through the thickness of the FP. However, these variations are not enough to explain the observed variations in M_{dyn}/L either along or through the thickness of the plane.

2. Stellar Population Trends in FP Space

2.1. The Data

The data presented here are a subset of the data in Papers I and II and we refer the reader to those works for details. Briefly, ∼16,000 galaxies are selected from the Sloan Digital Sky Survey (SDSS; York et al. 2000) spectroscopic Main Galaxy Sample (Strauss et al. 2002) in a limited redshift range ($0.04 < z < 0.08$). We select quiescent galaxies by requiring that their spectra contain no optical emission lines. Galaxies selected in this way populate the red sequence in a color-magnitude diagram (see Paper I); the small number of color outliers are excluded from this analysis.

The 3-D FP space used in this work is defined by $\log \sigma$, $\log R_e$, and $\log I_e$, where R_e is measured from de Vaucouleurs fits to the SDSS r-band photometry and where I_e is defined as $I_e = L_r/2\pi R_e^2$. Bins are defined in absolute space in $\log \sigma$ and $\log R_e$. For the third dimension, we fit the FP and measure the distance between $\log I_e$ and the best-fit FP to define $\Delta \log I_e$. Galaxies are sorted into bins in $\log \sigma$–$\log R_e$–$\Delta \log I_e$ space and their spectra are stacked to create a high S/N average spectrum for each bin (the grid has six bins in $\log \sigma$, five bins in $\log R_e$, and three bins in $\Delta \log I_e$ for a total of 90 average spectra). This produces a characteristic spectrum for each point in FP space.

2.2. The 2-D Family of Stellar Populations

The stacked spectra are run through the stellar population code *EZ_Ages* (Graves & Schiavon 2008) to measure mean light-weighted stellar population ages, as well as element abundances [Fe/H], [Mg/H], and [Mg/Fe] (the latter is simply [Mg/H]−[Fe/H]). These stellar population properties are then mapped

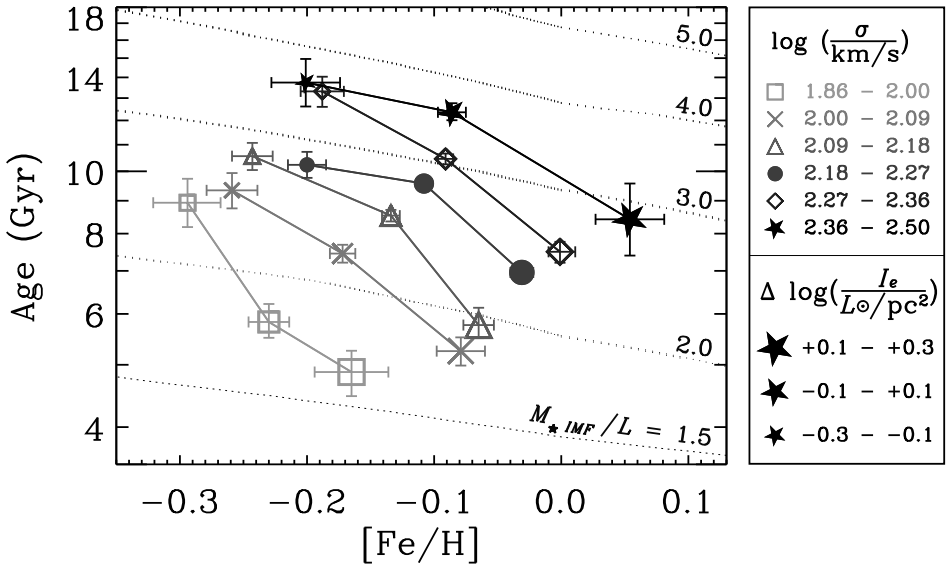

Figure 1. Age and [Fe/H] as measured in the stacked spectra. Dotted lines indicate lines of constant $M_{\star,\mathrm{IMF}}/L$ from the BC03 stellar population models. The stellar population properties of early type galaxies form a 2-D family. Age and [Fe/H] increase with increasing σ, while age and [Fe/H] are anti-correlated at fixed σ such that lower-surface brightness galaxies are older and Fe-poor compared to their higher-surface brightness counterparts.

through FP space. In Paper II, we show that none of the stellar population properties depend strongly on R_e; the star formation histories of these galaxies are independent of their physical size. To simplify the parameter space presented in this work, were therefore show results only for galaxies in the central bin in R_e, with $0.3 < \log(R_e/\mathrm{kpc}) < 0.5$. This results in a sample of 18 stacked spectra, binned in $\log\sigma$ and $\Delta\log I_e$. Results for other values of R_e are nearly identical.

Figure 1 shows the derived mean light-weighted age and [Fe/H] for each of the stacked spectra. Galaxies clearly form a two-parameter family in this space. This indicates that the star formation histories of the galaxies are also a two-parameter family. The first dimension of this two-parameter space has been known for some time; star formation histories scale with galaxy mass. In Figure 1, both age and [Fe/H] are correlated with σ such that higher-σ galaxies have older ages and higher [Fe/H] than lower-σ, in agreement with previous work (Trager et al. 2000; Bernardi et al. 2003b; Thomas et al. 2005; Nelan et al. 2005; Smith et al. 2007; Graves et al. 2007).

However, Figure 1 confirms that there is a second parameter affecting galaxy star formation histories: age and [Fe/H] are *anti-correlated* at fixed σ. This anti-correlation was first identified by Trager et al. (2000) and recently corroborated by Smith et al. (2008). The advance made here is the discovery that this anti-correlation is driven by I_e residuals from the FP. This discovery links the second parameter of galaxy star formation histories to their central surface brightness properties. We will return to this point in §3.

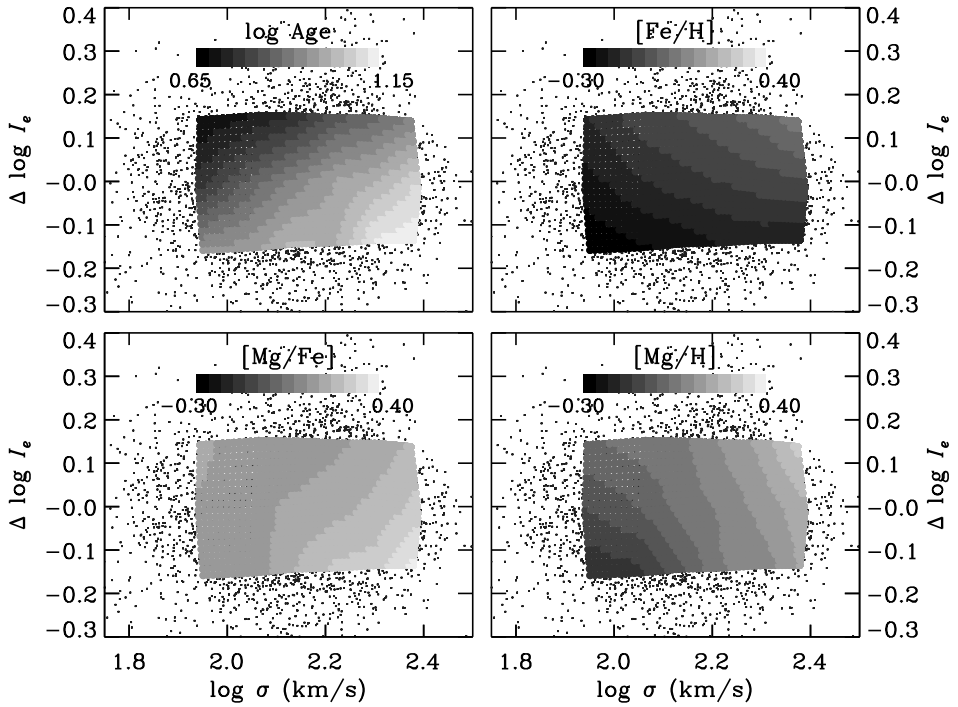

Figure 2. Stellar population properties mapped onto a cross-section through the FP. Individual galaxy σ and $\Delta \log I_e$ values are plotted as gray points. The overplotted grayscale contours show the mean stellar population properties for the binned spectra, with values indicated by the grayscale bars in each panel. Age and [Mg/Fe] behave similarly, with the oldest and most [Mg/Fe]-enhanced galaxies found at *high* σ and *low* $\Delta \log I_e$. [Fe/H] and [Mg/H] exhibit different behavior, showing the highest abundances for galaxies with *high* σ and *high* $\Delta \log I_e$. This is consistent with galaxies at fixed σ having experienced different durations of star formation (see text).

Figure 1 also conclusively ends the debate on two issues. *The age–[Fe/H] anti-correlation at fixed σ must be real*, rather than due to correlated errors in the stellar population modelling process. Correlated errors could not reproduce the observed dependence of stellar population properties on $\Delta \log I_e$. *The thickness of the FP must be real.* Galaxies that fall slightly above or below the main FP in surface brightness have systematically different stellar populations than those in the center on the FP and are thus genuinely different objects. Measurement errors in σ, R_e, or I_e cannot produce this effect (Paper II).

2.3. Mapping Stellar Populations onto Cross-sections Through the FP

Figure 1 demonstrates that age and [Fe/H] must map onto a *cross-sectional slice* through the FP at fixed R_e. These mappings are shown explicitly in Figure 2, along with those for [Mg/H] and [Mg/Fe]. Each panel shows a cross-section through the FP at $\log(R_e/\mathrm{kpc}) \sim 0.4$. Overlaid on the individual galaxy data are grayscale contours that indicate the stellar population properties of the galaxies

at each point in FP space. The grayscale contours are produced by interpolating between the values derived for the 18 stacked spectra.

These maps show the strong dependence of all stellar population properties on σ. Age, [Fe/H], [Mg/Fe], and [Mg/H] all increase with increasing σ. Indeed, σ appears to be the dominant parameter in determining early type galaxy star formation histories (Trager et al. 2000, Paper I, Paper II). The standard explanations for the observed trends are by now familiar. High-σ galaxies have deeper gravitational potential wells and are thus better able to retain metals ejected by supernovae, resulting in larger values of [Fe/H] and [Mg/H]. Also, galaxies with high values of σ formed their stars at earlier times and more rapidly than those at low σ. The high values of [Mg/Fe] observed in high-σ galaxies reveal a paucity of elements that are predominantly produced by supernovae type Ia (e.g., Fe) as compared to those produced mostly by supernovae type II (e.g., Mg), suggesting a short timescale for star formation (Worthey et al. 1992).

The maps in Figure 2 confirm that there is a second parameter affecting galaxy star formation histories, because the various population properties show different dependences on $\Delta \log I_e$ at fixed σ. Applying the same reasoning that is invoked to explain stellar population trends with σ, we propose that these variations at fixed σ are due to differences in the *duration* of star formation. In a "staged" star formation scenario (e.g., Noeske et al. 2007b) where all galaxies of the same mass (or in this case σ) start forming stars at the same time, those galaxies which shut down star formation earlier than others at the same σ will have: (1) older mean ages, (2) higher [Mg/Fe] due to lack of time for SN Ia enrichment, (3) lower [Fe/H], again due to lack of time for SN Ia enrichment, and (4) similar [Mg/H] because the galaxies have similar potential well depth. This is observed in Figure 2 for low-$\Delta \log I_e$ galaxies compared to high-$\Delta \log I_e$ galaxies. The scenario holds particularly well in the high-σ regime, where significant variations are seen in [Mg/Fe] and the variations in [Mg/H] are small.

3. Mass-to-light Ratios in FP Space

3.1. The Tilt of the FP

Having determined the typical stellar population properties for galaxies everywhere in FP space, we can now return to the question of mass-to-light ratios. From the measured values of mean age and [Fe/H], it is possible to predict the expected values of $M_{\star,\mathrm{IMF}}/L$ throughout FP space. In Figure 1, the dotted lines show lines of constant $M_{\star,\mathrm{IMF}}/L$ from Bruzual & Charlot (2003, hereafter BC03) stellar population models. Using these models to compute $M_{\star,\mathrm{IMF}}/L$ for each of the stacked spectra, we can compare the results with values of M_{dyn}/L that correspond to the bins in FP space. Figure 3 shows $M_{\star,\mathrm{IMF}}/L$ (left panel) and M_{dyn}/L (right panel) as functions of σ for the stacked spectra.

If there were no tilt between the FP and the virial plane, M_{dyn}/L would be flat with σ. Instead, it increases significantly. Some of this increase is due to systematic differences in the stellar populations, as manifested in the increase of $M_{\star,\mathrm{IMF}}/L$ with σ. However, M_{dyn}/L increases more strongly with σ than does $M_{\star,\mathrm{IMF}}/L$, in agreement with numerous previous authors (e.g., Dressler et al.

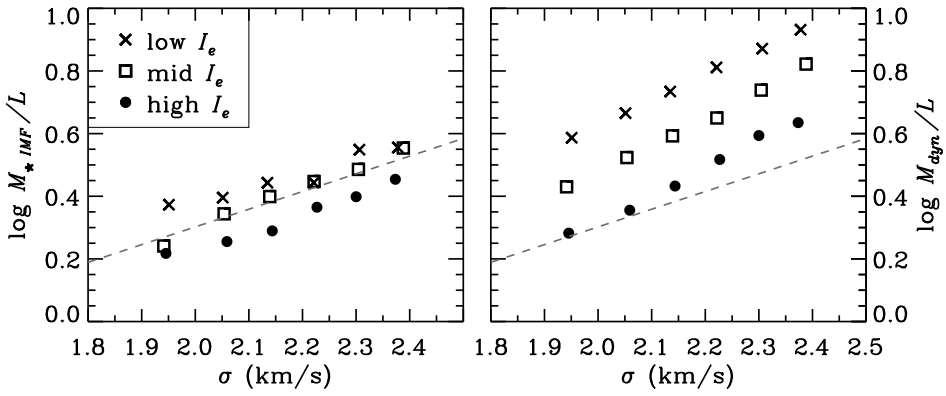

Figure 3. A comparison of $M_{\star,\mathrm{IMF}}/L$ and M_{dyn}/L as functions of σ. The dashed line in both panels shows a fit of $M_{\star,\mathrm{IMF}}/L$ onto σ. If the FP were not tilted, M_{dyn}/L would be flat with σ. It is clear that $M_{\star,\mathrm{IMF}}/L$ variations contribute to the variation in M_{dyn}/L with σ but are inadequate to explain the full tilt of the FP. There is also less variation in $M_{\star,\mathrm{IMF}}/L$ than in M_{dyn}/L at fixed σ. This requires structural non-homology, variations in central dark matter fraction, or variations in the IMF both as a function of σ and among galaxies at fixed σ to explain the observed variation in M_{dyn}/L.

1987; Prugniel & Simien 1996; Pahre et al. 1998). This indicates that one of the other terms in equation 1. must also increase with σ.

Two recent studies suggest that there is surprisingly little variation in $M_{\mathrm{dyn}}/M_{\mathrm{tot}}$ among early type galaxies. Both Cappellari et al. (2006), using integral field unit data from the SAURON survey to construct sophisticated dynamical mass models, and Bolton et al. (2008), using mass models from strong lensing data, find that their independent mass estimates agree surprisingly well with the simple $M_{\mathrm{dyn}} \propto \sigma^2 R_e$ virial proscription over a galaxy sample that spans several orders of magnitude in mass. If $M_{\mathrm{dyn}}/M_{\mathrm{tot}}$ is relatively constant for early type galaxies and stellar population effects cannot explain the full tilt of the FP, then either $M_{\mathrm{tot}}/M_\star$ (i.e., the central dark matter fraction) or $M_\star/M_{\star,\mathrm{IMF}}$ (i.e., the IMF) must vary systematically as a function of σ.

3.2. The Thickness of the FP

The increase in $M_{\star,\mathrm{IMF}}/L$ with σ is not enough to account for the tilt of the FP. Figure 3 shows that it is also not enough to account for the *thickness* of the FP. Galaxies in the sample were binned by $\log\sigma$ and $\Delta\log I_e$. As can be seen in the right panel of Figure 3, binning by $\Delta\log I_e$ is essentially equivalent to binning in $\Delta\log M_{\mathrm{dyn}}/L$ at fixed σ. This is because

$$\frac{M_{\mathrm{dyn}}}{L} \propto \frac{\sigma^2 R_e}{\pi R_e^2 I_e} \propto \frac{\sigma^2}{R_e I_e}. \tag{2}$$

For a fixed bin in σ and R_e, variations in M_{dyn}/L therefore correspond to variations in I_e.

While variations in $M_{\star,\mathrm{IMF}}/L$ produce some spread at fixed σ, it is not enough to account for the observed spread in M_{dyn}/L. In fact, the spread in

$M_{\star,\rm IMF}/L$ at fixed σ shown in Figure 3 is an *overestimate* of the true variation, due to the very simple (single burst) star formation histories that were assumed. More realistic, extended star formation histories will tend to raise the lowest values of $M_{\star,\rm IMF}/L$ without changing the higher values, both tightening and flattening the trend with σ. This implies that variations in central dark matter fraction or IMF must exist through the *thickness* of the FP as well as *along* it.

The close correspondence between $\Delta \log I_e$ and $\Delta \log M_{\rm dyn}/L$ means that this variation can be treated as the second parameter affecting star formation histories. We have just argued that galaxies with lower $\Delta \log I_e$ have higher $\Delta M_{\rm dyn}/L$, much of which is contributed by higher values of $M_{\rm tot}/M_\star$ or $M_\star/M_{\star,\rm IMF}$. But these are also the same galaxies that have shorter duration star formation (§2.3.). The data therefore point to a physical process in galaxy formation that both truncates star formation at early times and also leads to higher central dark matter fractions or top-heavy IMFs.

Acknowledgments. Funding for the creation and distribution of the SDSS Archive has been provided by the Alred P. Sloan Foundation, the Participating Institutions, the National Aeronautics and Space Administration, the National Science Foundation, the US Dept. of Energy, the Japanese Monbukagakusho, and the Max-Planck Society. The SDSS website is http://www.sdss.org.

References

Bruzual, G. & Charlot, S. 2003, MNRAS, 344, 1000 (BC03)
Bernardi, M., et al. 2003, AJ, 125, 1882
Bolton, A. S., Treu, T., Koopmans, L. V. E., Gavazzi, R., Moustakas, L. A., Burles, S., Schlegel, D. J., & Wayth, R. 2008, ApJ, 684, 248
Cappellari, M., et. al. 2006, MNRAS, 366, 1126
Djorgovski, S. & Davis, M. 1987, ApJ, 313, 59
Dressler, A., Lynden-Bell, D., Burstein, D., Davies, R. L., Faber, S. M., Terlevich, R., & Wegner, G. 1987, ApJ, 313, 42
Faber, S. M., Dressler, A., Davies, R. L., Burstein, D., & Lynden-Bell, D. 1987, in Nearly Normal Galaxies, ed. S. M. Faber, 175–183
Graves, G. J., Faber, S. M., & Schiavon, R. P. 2009a, ApJ, 693, 486 (Paper I)
Graves, G. J., Faber, S. M., & Schiavon, R. P. 2009, ApJ, 698, 1590 (Paper II)
Graves, G. J., Faber, S. M., Schiavon, R. P., & Yan, R. 2007, ApJ, 671, 243
Graves, G. J. & Schiavon, R. P. 2008, ApJS, 177, 446
Jørgensen, I., Franx, M., & Kjaergaard, P. 1996, MNRAS, 280, 167
Nelan, J. E., Smith, R. J., Hudson, M. J., Wegner, G. A., Lucey, J. R., Moore, S. A. W., Quinney, S. J., & Suntzeff, N. B. 2005, ApJ, 632, 137
Noeske, K. G., et al. 2007, ApJ, 660, L47
Pahre, M. A., Djorgovski, S. G., & de Carvalho, R. R. 1998, AJ, 116, 1591
Prugniel, P. & Simien, F. 1996, A&A, 309, 749
Smith, R. J., Lucey, J. R., & Hudson, M. J. 2007, MNRAS, 381, 1035
Smith, R. J., Lucey, J. R., & Hudson, M. J. 2008, in IAU Symposium 245, Formation and Evolution of Galaxy Bulges, ed. M. Bureau, E. Athanassoula & B. Barbury (Cambridge: Cambridge University Press), 411
Strauss, M. A., et al. 2002, AJ, 124, 1810
Thomas, D., Maraston, C., Bender, R., & Mendes de Oliveira, C. 2005, ApJ, 621, 673
Trager, S. C., Faber, S. M., Worthey, G., & González, J. J. 2000, AJ, 120, 165
Worthey, G., Faber, S. M., & Gonzalez, J. J. 1992, ApJ, 398, 69
York, D. G., et al. 2000, AJ, 120, 1579

GALAXY EVOLUTION: EMERGING INSIGHTS AND FUTURE CHALLLENGES
ASP Conference Series, Vol.
@jourvol, © 2009
S. Jogee, I. Marinova, L. Hao, and G. A Blanc

Mapping the Galaxy with Photometric Surveys: Insights from SDSS and Future Prospects

Mario Jurić[1] and Željko Ivezić[2]

[1]*Institute for Advanced Study, 1 Einstein Drive, Princeton, NJ 08540 USA*

[2]*Department of Astronomy, University of Washington, Box 351580, Seattle, WA 98195 USA*

Abstract. The Sloan Digital Sky Survey (SDSS) produced accurate, multi-band, deep photometric sample of $\sim 10^8$ stars over about one quarter of the sky. These measurements enabled photometric metallicity estimates for F and G stars accurate to $\sim$0.2 dex, as well as estimates of proper motions from astrometric comparison with the Palomar Observatory Sky Survey, accurate to about 3-5 mas/yr. For main sequence stars, photometric distance estimates are sufficiently precise ($\sim$10%) to directly map their three-dimensional distribution out to distances of $\sim$15 kpc, making this data set an exquisite tool for Galactic structure studies. We summarize the key results and lessons of recent SDSS efforts in this area (Jurić et al. 2008; Ivezić et al. 2008a), and discuss what further progress can be expected from the Large Synoptic Survey Telescope (LSST). LSST will obtain similar imaging data as SDSS, but to about 5 magnitudes deeper limit and over twice as large sky area.

1. Introduction

A major objective of modern astrophysics is to understand when and how galaxies formed, and how they have evolved since then. Our own galaxy, the Milky Way, provides a unique opportunity to study a galaxy by measuring and analyzing the properties of a large number of individual stars. As these stars can be studied in great detail, their characterization provides clues about galaxy formation process that cannot be extracted from observations of distant galaxies.

Historically, Milky Way surveys have suffered from lack of data, having instead to rely on sparse samples and analytic density laws to derive and characterize the results (e.g., Bahcall & Soneira 1980). But large, deep, and uniform datasets, exemplified by the Sloan Digital Sky Survey (York et al. 2000, hereafter SDSS), have shifted the emphasis from model fitting toward multi-dimensional mapping. Such model-free maps were instrumental in characterizing the overall smooth distribution of stars in the Galaxy (Jurić et al. 2008), as well as revealing a number of coherent, localized substructures (Newberg et al. 2002; Rocha-Pinto et al. 2003; Jurić et al. 2008) that would have been missed or misinterpreted by pencil-beam surveys. Interestingly, some of these structures have been found in the disk (Newberg et al. 2002), suggesting a more complex disk assembly history than previously suspected (Kazantzidis et al. 2008).

Here we review and summarize the results of recent works by Jurić et al. (2008, hereafter J08) and Ivezić et al. (2008a, hereafter I08) using SDSS data. A common aspect of both papers is the *model-free mapping* approach: the use of photometric distance estimates sufficiently precise (∼10%) to directly map the three-dimensional distribution of stars and their physical properties. We further extrapolate these results to illustrate what can be expected from the next generation of imaging surveys, such as Pan-STARRS (Kaiser et al. 2002) and the Large Synoptic Survey Telescope (Ivezić et al. 2008b).

2. Mapping the Milky Way with SDSS

Table 1. The SDSS Galactic Model: Exponential thin/thick disk and power law halo model parameters fitted from a dataset of ∼ 50 million main-sequence stars observed in 6,500 deg^2 of the sky. The second column lists the uncorrected best-fit values, and the third column lists the values corrected for unresolved binarity and the Malmquist bias. The units for Z_0, L_1, H_1, L_2, and H_2 are pc. See J08 for details.

Parameter	Fitted	Best fit	Error estimate
Z_0	25		20%
L_1	2150	2600	20%
H_1	245	300	20%
f	0.13	0.12	10%
L_2	3261	3600	20%
H_2	743	900	20%
f_h	0.0051		25%
q	0.64		$\lesssim 0.1$
n	2.77		$\lesssim 0.2$

Using photometric data for 50 million stars from SDSS Data Release 4, J08 have constructed 3-dimensional maps (data cubes) of the stellar number density distribution for 19 narrow color bins spanning mid-F to early M spectral types. As the bin color is varied from the reddest to the bluest, the subsamples cover distances ranging from 100 pc to 15 kpc. Distance to each star is estimated using a maximum likelihood implementation of photometric parallax method, and stars are binned and counted in small 3-dimensional pixels whose size depends on dynamical range provided by each color bin and Poisson noise limits (typically there are 250,000 pixels per map). Examples of 2-dimensional projections of the resulting maps are shown in Figure 1.

Such maps make a powerful tool for studying the Milky Way's stellar number density distribution. Traditional methods for modeling stellar counts must adopt a large number of poorly known functions (e.g., the IMF, mass-luminosity relationship, the luminosity function, and analytic density laws for the postulated components such as disks, bulge and halo, etc). Instead, the maps shown in Figure 1 can be constructed and examined without any of these

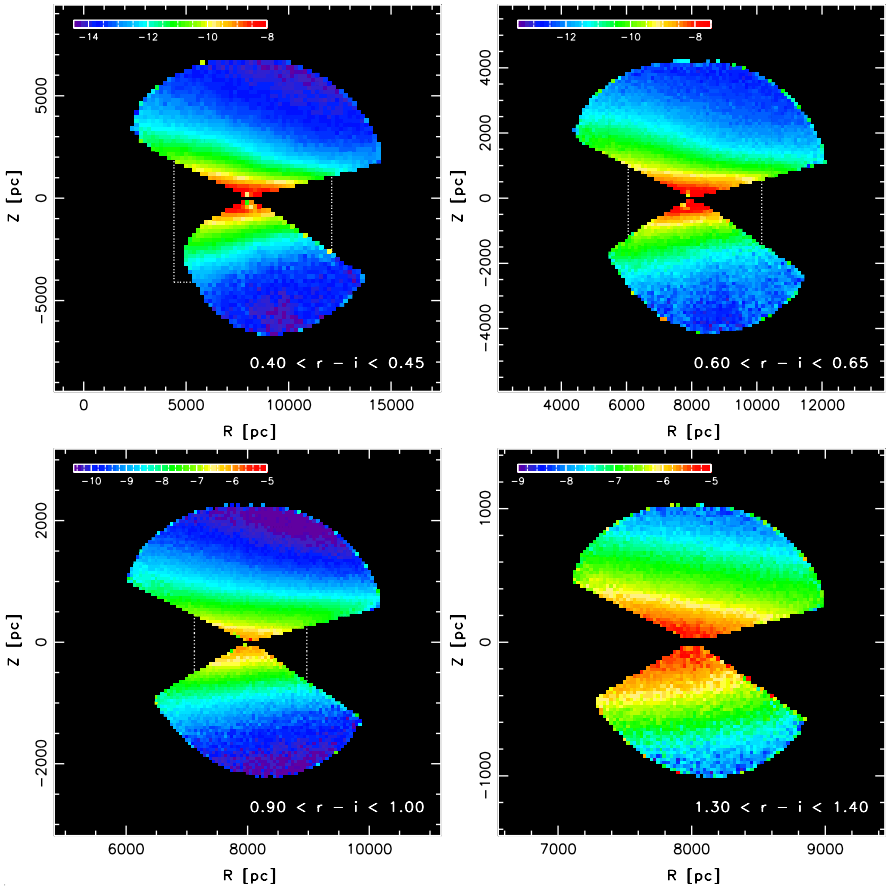

Figure 1. The stellar number density as a function of Galactic cylindrical coordinates R (distance from the axis of symmetry) and Z (distance from the plane of the Sun), for different $r-i$ color bins as marked in each panel (J08). The density is shown on a logarithmic scale, and coded from blue to red as shown in the legend (black pixels are regions without the data). Each pixel value is the median for all polar angles. Note that the distance scale varies from panel to panel. The color bins shown correspond to late K through early M dwarfs.

assumptions, making conclusions drawn from their analysis significantly more robust.

3. Modeling the Galactic Stellar Number Density Distribution

While halo substructure has been known for a while (e.g., Ivezić et al. 2000; Yanny et al. 2000; Vivas et al. 2001; Majewski 1993, and references therein) the SDSS maps analyzed by J08 demonstrate that the thin and thick disk density is similarly complex and permeated by localized substructures. This makes the analysis and description of the underlying smooth large-scale Galactic density distribution a non-trivial task.

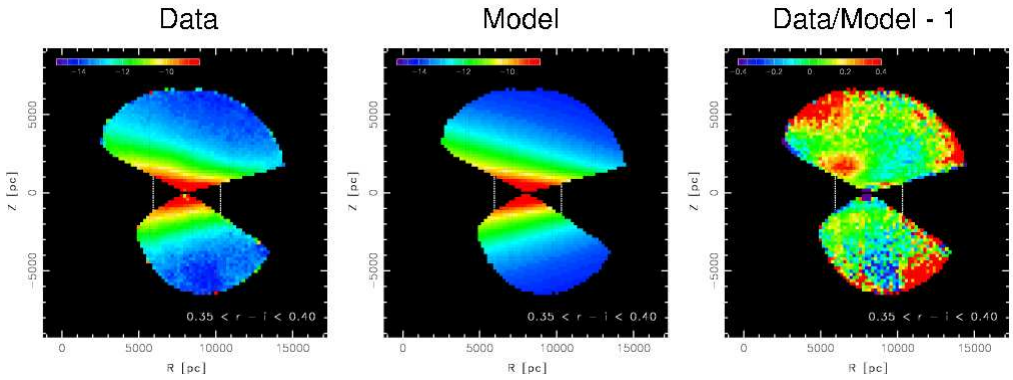

Figure 2. The left panel shows the measured stellar number density as a function of Galactic cylindrical coordinates for stars with $0.35 < r - i < 0.40$. The middle panel shows the best-fit smooth model taken from J08, and the right panel the normalized (data-model) difference. Note the large overdensities visible in the right panel.

Nevertheless, using custom fitting algorithms to detect and remove clumpy substructure, in J08 we fit the gross behavior of Galactic stellar number density distribution with Bahcall-Soneira type models (two exponential disks, power-law halo). The best-fit parameters are given in Table 1. They successfully describe the stellar number density distribution to $r \sim 21$ mag over $6,500$ deg^2 of the sky. The dataset used to constrain these best-fit parameters is 400 times larger than in any previously published analysis. The large distance limit and large sky area break most degeneracies inherent in the multi-parameter model, to which pencil beam studies are very susceptible.

The low-contrast substructure is difficult to see in maps such as Figure 1, but becomes readily discernible in maps of model fit residuals (Figure 2). These clumps are detected in different color bins at different apparent magnitude ranges, but all translate to *same spatial positions*. This consistency strongly argues that the detected overdensities are not artefacts of the adopted photometric parallax relation and are indeed real.

3.1. Mapping the Distribution of Stellar Metallicity and Kinematics

Encouraged by the demonstrated feasibility of direct mapping as the method of choice for analysis of large-scale photometric samples, I08 used it to obtain an unbiased, three-dimensional, volume-complete metallicity distribution of ∼2.5 million F/G stars at heliocentric distances of up to ∼8 kpc. SDSS spectroscopic metallicity was used to calibrate a photometric metallicity indicator based on the $u-g$ and $g-r$ colors, and an explicit metallicity dependence term, calibrated using globular clusters, was added to the photometric parallax relation. This study also had a kinematic component, with velocities deduced from SDSS-POSS proper motion. I08 found that

- The metallicity distribution function (MDF) of the halo and its kinematics are clearly distinct and separate from those of the disk (see Figure 3).

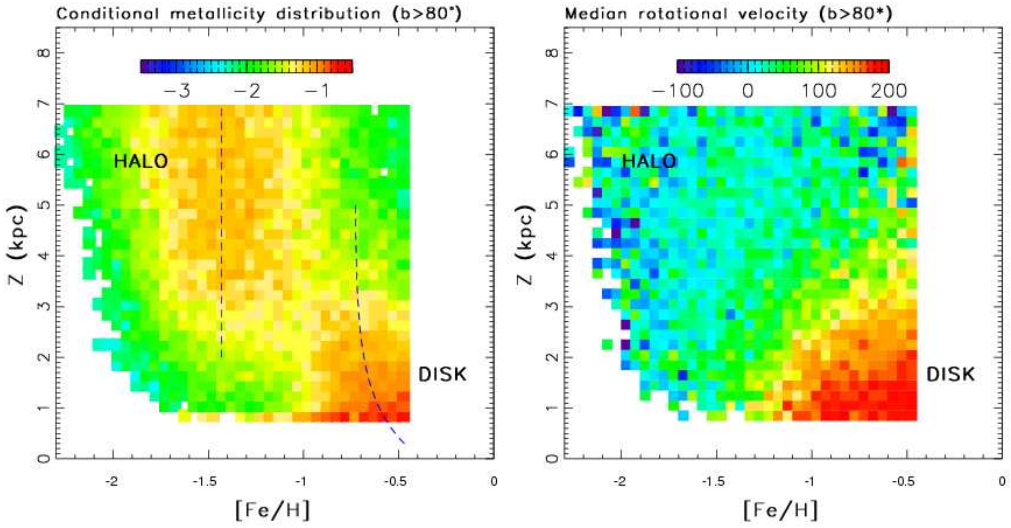

Figure 3. The left panel shows the full metalicity distribution, as a function of the distance from the Galactic plane, for about 60,000 stars within 10 degrees from the North Galactic Pole (I08). The distribution is displayed on a logarithmic scale and color-coded as shown in the inset. Two distinct Galaxy components, halo and disk, are evident. High-metallicity disk stars dominate close to the plane, while low-metallicity halo stars dominate beyond 3 kpc from the plane. The dashed lines mark the median metallicity for each component. The median metallicity for disk stars shows a gradient, while halo stars have spatially invariant metallicity distribution. These two components with distinct metallicity distributions also have different kinematics. The right panel shows the median rotational velocity component for the same stars as in the left panel. The velocity is determined from displacements of stars on the sky over half a century that lapsed between the Palomar Observatory Sky Survey (POSS) in the 1950s and SDSS. The high-metallicity disk stars have large rotational velocity (about 200 km s^{-1}, see the inset), while the low-metallicity halo stars display behavior consistent with no net rotation. The rotational velocity for disk stars decreases with the distance from the Galactic plane, while it is constant for halo stars, similarly to the behavior of their metallicity distributions.

- The median metallicity of the disk exhibits a clear vertical (with respect to the Galactic plane; Z) gradient. The MDF of the disk at $Z > 0.5$ kpc is consistent with no gradient in the radial direction ($6 < R/\mathrm{kpc} < 10$). The spatial variation of the median metallicity does not follow the distribution of stellar number density.

- Disk stars show a rotational velocity gradient with distance Z from the Galactic plane. However, there is no correlation between the metallicity and rotational velocity of stars at $Z > 0.4$kpc, in apparent conflict with traditional thin/thick disk decomposition.

- The Monoceros stream is seen as a structure with different metallicity distribution than its surroundings.

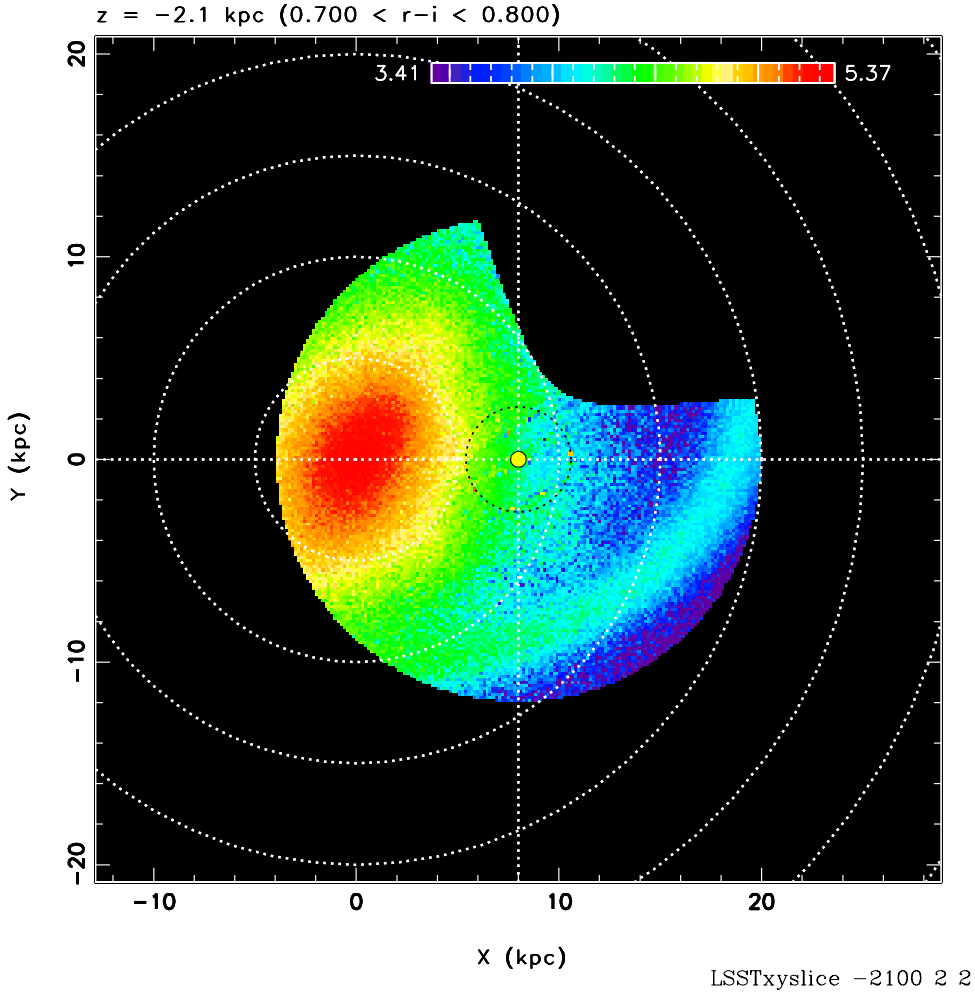

Figure 4. LSST View of the Inner Galaxy. A plane-parallel slice through a simulated three-dimensional map of stellar number density (stars kpc^{-3}, log scale) taken at Z=-2.1 kpc (south of the Galactic plane). The simulation includes a SDSS-like model of instrumental and methodological uncertainties, and is directly comparable to Figs. 12-14 of Jurić et al. (2008). The projected positions of the Galactic center and the Sun are at X=Y=0 and X=8kpc, Y=0, respectively. The stars were distributed according to the J08 density law, with the addition of an inner triaxial halo/bulge/bar component, and a nearly plane-parallel Monoceros-like tidal stream in the outer regions. Only data at Galactic latitudes $b > 10$ is shown. The missing piece in the first quadrant is due to the $\delta < 34.5°$ limit of the survey.

3.2. Expectations for the Future: The LSST

The Large Synoptic Survey Telescope, (LSST; Ivezić et al. 2008b), will be a large, wide-field ground-based system designed to obtain multiple images covering the sky visible from its location at Cerro Pachón, Chile. The current baseline design, with an 8.4m (6.7m effective) primary mirror, a 9.6 deg^2 field of view, and

a 3,200 Megapixel camera, will allow about 10,000 square degrees of sky to be covered using pairs of 15-second exposures in two photometric bands every three nights on average. The system is designed to yield high image quality as well as superb astrometric and photometric accuracy. The survey area will include 30,000 deg^2 with $\delta < +34.5^\circ$, and will be imaged multiple times in six bands, *ugrizy*, covering the wavelength range 320–1050 nm. About 90% of the observing time will be devoted to a deep-wide-fast survey mode which will observe a 20,000 deg^2 region about 1000 times in six bands during anticipated 10 years of operations. These data will result in databases including about 20 billion objects, and will serve the majority of science programs.

LSST will produce a massive and exquisitely accurate photometric and astrometric dataset for about 10 billion Milky Way stars. The coverage of the Galactic plane will yield data for numerous star-forming regions, and the y band data will penetrate through the interstellar dust layer. Photometric metallicity measurements will be available for about 200 million main-sequence F/G stars which will sample the halo to distances of 100 kpc (I08). No other existing or planned survey will provide such a massive and powerful dataset to study the outer halo (including Gaia which is flux limited at $r = 20$, and Pan-STARRS which will not have the u band). The LSST in its standard surveying mode will be able to detect RR Lyrae variables (pulsating stars and standard candles) and classical novae (exploding stars and standard candles) at a distance of 400 kpc and hence explore the extent and structure of our own halo out to half the distance to the Andromeda galaxy. Thus, the LSST will enable studies of the distribution of main-sequence stars beyond the presumed edge of the Galaxy's halo, of their metallicity distribution throughout most of the halo, and of their kinematics beyond the thick disk/halo boundary.

Acknowledgments. We thank the Institute of Advanced Study, the University of Washington and the Kavli Institute for Theoretical Physics for generous support (NSF PHY05-51164). M. Jurić gratefully acknowledges support from the NSF grant PHY-0503584. Ž. Ivezić acknowledges support by NSF grant AST-0707901, and NSF grant AST-0551161 to LSST for design and development activity.

References

Bahcall, J.N. & Soneira, R.M. 1980, ApJSS, 44, 73
Ivezić, Ž., Goldston, J., Finlator, K., et al. 2000, AJ, 120, 963
Ivezić, Ž., Sesar, B., Jurić, M., et al. 2008a, ApJ, 684, 287 (I08)
Ivezić, Ž., Tyson, J.A., Allsman, R, et al. 2008b, arXiv:0805.2366
Jurić, M., Ivezić, Ž., Brooks, A., et al. 2008, ApJ, 673, 864 (J08)
Kaiser, N., et al. 2002, Proceedings of the SPIE, 4836, 154
Kazantzidis, S., Bullock, J. S., Zentner, A. R., Kravtsov, A. V., & Moustakas, L. A. 2008, ApJ, 688, 254
Majewski, S.R. 1993, ARA&A, 31, 575
Newberg H.J., Yanny, B., Rockosi, C., et al. 2002, ApJ, 569, 245
Rocha-Pinto, H. J., Majewski, S. R., Skrutskie, M. F., & Crane, J. D. 2003, ApJ, 594, L115
Vivas, A.K., Zinn, R., Andrews, P., et al. 2001, ApJ, 554, L33
Yanny, B., Newberg, H. J., Kent, S., et al. 2000, ApJ, 540, 825
York, D. G., et al. 2000, AJ, 120, 1579

GALAXY EVOLUTION: EMERGING INSIGHTS AND FUTURE CHALLLENGES
ASP Conference Series, Vol.
@jourvol, © 2009
S. Jogee, I. Marinova, L. Hao, and G. A Blanc

The Star Formation Histories of the M31 and M33 Spheroids

Thomas M. Brown

Space Telescope Science Institute, 3700 San Martin Drive, Baltimore, MD 21218 USA

Abstract. I review the observational constraints on the star formation histories in the spheroids of M33 and M31, the other two spiral galaxies in the Local Group. M33 does not possess a traditional bulge; instead, it has a small nuclear region hosting stars with a wide range of ages. The star formation history of the M33 halo is poorly constrained, but composite spectra of its halo globular clusters imply a wide age spread of 5–7 years, while the presence of RR Lyrae stars in the halo implies at least some of the population is ancient. Although it is possible to obtain the detailed star formation history of the M33 halo via deep photometry, this has not been done to date. M31 hosts a traditional bulge that is apparently dominated by stars older than 10 Gyr. Deep photometry of the M31 halo demonstrates that it hosts both a population of ancient metal-poor stars and a significant population extending to younger ages and high metallicity, apparently due to its active merger history.

1. Introduction

The Local Group hosts three spiral galaxies: the Milky Way, M31, and M33. The Milky Way and M31 are the only massive galaxies in the Local Group, and there are indications that M31 is more representative of massive spirals than the Milky Way (e.g., Hammer et al. 2007). While M33 is the third most massive galaxy in the Local Group, it is a distant third (van den Bergh 2000), and it is representative of the most common type of spiral galaxy in the local universe (see Marinoni et al. 1999). Because M31 and M33 are at respective distances of 770 kpc (Freedman & Madore 1990) and 860 kpc (Sarajedini et al. 2006), we can obtain photometry of their resolved stellar populations and thus constrain their star formation histories at a fidelity exceeding that possible in the Milky Way, where such studies of the field population are often hampered by distance and reddening uncertainties. Here, I review the observational constraints on the spheroid (bulge and halo) populations of these galaxies.

2. Age Constraints

Spheroids are generally dominated by stars older than 1 Gyr. In such populations, changes with age are less dramatic than they are for younger systems. The best age diagnostics come from photometry reaching low-mass ($\sim$0.8 $M_{\odot}$) main sequence (MS) stars; such photometry enables the reconstruction of the complete star formation history with an age resolution of $\sim$1 Gyr, but it is difficult to obtain such photometry outside the Milky Way

system, due to crowding and depth limitations. Age constraints are also available through photometry of later evolutionary phases, such as the horizontal branch (HB), asymptotic giant branch (AGB), and red giant branch (RGB); relative to MS stars, these brighter stars can be detected in more distant and crowded regions, but the age resolution is poorer, allowing one to distinguish between young (<3 Gyr), intermediate-age (3–8 Gyr), and old (>8–13 Gyr) stars.

3. M33 Spheroid

The existence of a spheroid in M33 has been controversial for decades. While the galaxy does not appear to have a bulge, it definitely possesses a halo. I discuss these components in turn below.

3.1. M33 Bulge

M33 apparently does not possess a bulge in the classical sense of that term (Bothun 1992), although this has been the subject of debate (e.g., Minniti et al. 1993). Semantics aside, the galaxy hosts a small nucleus that can be fit with a bulge profile that dominates within $\sim 0.1'$ of the galaxy center (Stephens & Frogel 2002). In a K vs. $V-K$ color-magnitude diagram (CMD) of the brightest stars in the nucleus, Stephens & Frogel (2002) find young, intermediate-age, and old stars with a mean metallicity [Fe/H]$=-0.26$. It is not possible to obtain photometry of the low-mass MS stars in the nucleus with any observatory in operation or in development, so the constraints on the star formation history will be poor for the foreseeable future.

3.2. M33 Halo

The existence of a halo in M33 was also controversial in the past, such that the galaxy was sometimes referred to as a "pure disk" galaxy. However, in recent years a preponderance of evidence demonstrated beyond any doubt that M33 hosts a stellar halo. Although some regions of the disk have *Hubble Space Telescope (HST)* photometry reaching the stellar MS (Program 10190; PI Garnett), the halo-dominated regions beyond the disk have not been imaged at sufficient depth, so the star formation history of the M33 halo remains poorly constrained.

Chandar et al. (2002) kinematically segregated the stellar clusters of M33 into disk and halo components. Unresolved photometry and spectroscopy of the clusters enabled a rough age estimate that is prone to degeneracies between blue MS stars and blue HB stars. The young clusters in the sample have motions consistent with disk membership, but the old clusters show a much larger velocity dispersion, implying that 85% belong to the halo and 15% belong to the disk (Figure 1). The clusters with halo kinematics have a spread in relative ages of 5–7 Gyr, much greater than the globular cluster system in the Milky Way halo. Subsequent photometry of one globular cluster in the sample was sufficiently deep to demonstrate that its blue spectrum is due to the presence of blue MS stars and not blue HB stars, proving its age is 5–8 Gyr than the other globular clusters in their sample, but unfortunately the cluster cannot be kinematically assigned to either the disk or halo (Chandar et al. 2006).

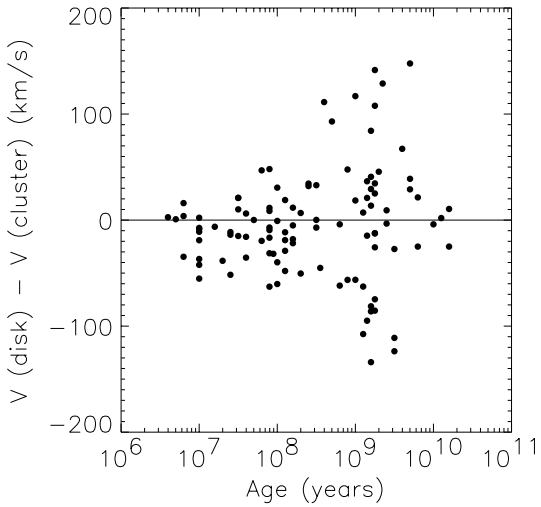

Figure 1. Difference between local disk velocity and measured cluster velocity as a function age in M33 clusters (Chandar et al. 2002), where cluster age is estimated from integrated photometry and spectroscopy. The spread in age for globular clusters in the M33 halo is much larger than it is for such clusters in the Galactic halo. Plot provided courtesy of R. Chandar.

Sarajedini et al. (2006) found evidence for a halo using 64 RR Lyrae variables they identified in the galaxy. They estimated reddenings from their minimum $V - I$ colors and metallicities from their periods. The resulting distributions of reddening and metallicity imply they belong to two distinct populations, associated with the disk and halo, providing evidence for these components in the field that complements the evidence in clusters (above). RR Lyrae stars are only present in ancient (>10 Gyr) populations, implying that both the M33 disk and halo host at least some ancient stars. In the [Fe/H] distribution for the halo RR Lyrae stars, the peak is at −1.3, although the metallicities of the RR Lyrae stars are not necessarily representative of the underlying population, because metallicity affects the HB temperature distribution and thus the fraction of HB stars falling in the instability strip.

McConnachie et al. (2006) also found evidence for a halo field population. From spectroscopy of 280 stars, they were able to segregate their sample into three components using both kinematics and metallicity: the halo, the disk, and a third unknown component possibly associated with a stellar stream. The halo component exhibits a mean [Fe/H] of −1.5 and a velocity dispersion of ∼50 km s^{-1}, but the data provide no age constraints.

Using star counts of RGB and AGB stars along the minor axis, Teig (2008) found a break in the surface brightness profile at 11 kpc, where the profile changes from that of an exponential disk to a power-law halo (see also Teig et al. 2009). The CMD of these bright stars implies the halo population is dominated by stars older than 3 Gyr with a mean [Fe/H] of −1.2. This is in good agreement with the CMD of Brooks et al. (2004), who obtained V and I photometry in the halo outskirts and found a mean [Fe/H] of −1.24.

The next logical step in the investigation of the M33 halo is deep photometry reaching its low-mass MS stars. This is the only way to unambiguously characterize the age distribution in the field population. While such photometry has been obtained in multiple regions of the M31 halo with *HST* (discussed below), the M33 halo remains unexplored, with very loose constraints on its star formation history.

4. M31 Spheroid

While M31 certainly has both a bulge and a halo, the distinction between these components is somewhat muddled in the literature. Historically, studies of the bulge and halo were driven by the appearance of M31 in wide-field shallow imaging (e.g., Walterbos & Kennicutt 1988), with "bulge" studies generally focusing on the region within a kpc of the center, and "halo" studies focusing on regions beyond 10 kpc on the minor axis. However, subsequent studies showed that the spheroid looks like a bulge out to ∼20 kpc in both its surface-brightness profile (Pritchet & van den Bergh 1994) and metallicity distribution (Mould & Kristian 1986; Durrell et al. 1994, 2001). It was only recently discovered that the surface-brightness profile transitions to a power-law (Guhathakurta et al. 2005; Irwin et al. 2005) and the metallicity drops by ∼1 dex (Kalirai et al. 2006) beyond 20 kpc, as expected for a halo. For consistency with historical studies, I will refer to all regions beyond 10 kpc on the minor axis as "halo" despite the persistence of some bulge-like properties out to 20 kpc.

4.1. M31 Bulge

Two fields in the M31 bulge were recently imaged in the near-IR at high resolution using adaptive optics on Gemini North (Davidge et al. 2005), resolving the upper 4–5 mag of the RGB and AGB. The resulting H and K CMDs are consistent with a population dominated by stars at an age of ∼10 Gyr, with a metallicity near solar, although the best-fit models include a minority intermediate-age component that may be spurious (Olsen et al. 2006). As with the center of M33, no observatory in operation or development is capable of obtaining the detailed star formation history of the M31 bulge, because crowding precludes photometry of the low-mass MS stars.

4.2. M31 Halo

Until the past decade, studies of the resolved stellar populations in the M31 halo generally focused on the metallicity distribution (e.g., Mould & Kristian 1986; Durrell et al. 1994, 2001). Metallicity distributions were usually fit by assuming an old age (>10 Gyr) and then comparing the stars on the AGB and RGB to isochrones or globular cluster templates, although some studies were deep enough to reach the HB (e.g., Holland et al. 1996). Although the RGB, AGB, and HB distributions are, in principle, sensitive to age in broad age bins (as noted above), several factors prevented these studies from exploring the age distribution, including photometric scatter, insufficient star counts, and contamination from foreground Milky Way dwarfs.

When the Advanced Camera for Surveys (ACS) was installed on *HST* in 2002, it became possible to obtain photometry of low-mass MS stars in the M31

halo, enabling the exploration of both the metallicity and age distributions. Brown et al. (2003) imaged a field 11 kpc from the nucleus on the southeast minor axis, obtaining photometry of 250,000 stars down to $V \sim 30.5$ mag in bands similar to V and I (Figure 2). By providing a large number of stars with small photometric errors on the low-mass MS, the catalog was immune to contamination from foreground Milky Way dwarfs. The resulting fit to the CMD found a wide age range in addition to the wide metallicity range that was already known, and speculated that this was due to a significant merger or series of smaller mergers in the galaxy. In the best-fit model (Brown et al. 2006), ∼40% of the stars are younger than 10 Gyr and more metal-rich than 47 Tuc ([Fe/H] = –0.7), with significant numbers of stars down to ages of 2 Gyr. Besides the field population, there is evidence from integrated colors and spectroscopy that the M31 globular cluster system also extends to intermediate ages (Puzia et al. 2005; Beasley et al. 2005).

The recent wide-field imaging surveys of M31 clearly show that it has undergone a violent merger history (Ferguson et al. 2002; Ibata et al. 2007), including a giant stellar stream resulting from the tidal debris of a recent merger event (Ibata et al. 2001). Subsequent studies demonstrated that the inner spheroid of M31 (within ∼15 kpc) is polluted by material stripped from progenitor satellite of the giant stellar stream. This evidence includes N-body simulations of the satellite disruption that reproduce the morphology of the major substructures in the galaxy (Fardal et al. 2007), kinematical surveys that confirm the motions in the N-body simulations (Gilbert et al. 2007), and followup ACS imaging of the giant stellar stream that shows strong similarities between the star formation histories of the stream and inner spheroid (Figure 2; Brown et al. 2006).

Given the discovery that the M31 halo becomes more like a halo beyond 20 kpc, a subsequent ACS survey explored regions on the minor axis further out, at 21 kpc (in the transition region; Brown et al. 2007) and 35 kpc (where the spheroid clearly exhibits a halo surface brightness profile and metallicity; Brown et al. 2008). Compared to the field at 11 kpc, these fields host far fewer stars at ages younger than 8 Gyr, but the populations clearly do not represent a classical halo formed via monolithic collapse at early times (Figure 2); in the best-fit model, ∼30% of the stars are younger than 10 Gyr, and only ∼10% of the stars are ancient (≥12 Gyr) and metal-poor ([Fe/H]≤–1.5). All regions of the halo explored to date are consistent with a history whereby the galaxy forms over a prolonged period of hierarchical merging.

5. Summary

M33 possesses a halo but not a traditional bulge. This halo exhibits secondary evidence for intermediate-age populations, such as a halo globular cluster system spanning a wide age range in integrated spectroscopy (Chandar et al. 2002), but the age distribution in the M33 halo has not been constrained via photometry of the low-mass MS stars, as done in M31. Thus, our understanding of the star formation history in the M33 halo is in a state similar to that found in M31 prior to the advent of the *HST* ACS. For years, M31 was assumed to host an old halo of age >10 Gyr. The M31 halo has now been probed in multiple locations along

the minor axis, spanning the regions where the halo looks more like a bulge and where it looks more like a traditional halo, but in all of these regions it exhibits an extended star formation history (Brown et al. 2006, 2007, 2008). The M33 halo remains the last spiral galaxy halo unexplored via photometry of its low-mass MS stars, leaving its star formation history poorly constrained. Appropriately deep imaging of the M33 halo should be obtained during the remaining *HST* mission, or it may be many years before such data can be obtained again.

Acknowledgments. I am grateful to my collaborators on the *HST*/ACS M31 observing programs for their contributions to those projects, and to R. Chandar for useful discussions and suggestions.

References

Beasley, M.A., Brodie, J.P., Strader, J., Forbes, D.A., Proctor, R.N., Barmby, P., & Huchra, J.P. 2005, AJ, 129, 1412
Bothun, G.D. 1992, AJ, 103, 104
Brooks, R.S., Wilson, C.D., & Harris, W.E. 2004, AJ, 128, 237
Brown, T.M., et al. 2008, ApJ, 658, L121.
Brown, T.M., et al. 2007, ApJ, 658, L95
Brown, T.M., et al. 2006, ApJ, 652, 323
Brown, T.M., et al. 2003, ApJ, 592, L17
Chandar, R., Bianchi, L., Ford, H.C., & Sarajedini, A. 2002, ApJ, 564, 712
Chandar, R., Puzia, T.H., Sarajedini, A., & Goudfrooij, P. 2006, ApJ, 646, L107
Davidge, T.J., Olsen, K.A.G., Blum, R., Stephens, A.W., & Rigaut, F. AJ, 129, 201
Durrell, P.R., Harris, W.E., & Pritchet, C.J. 1994, AJ, 108, 2114
Durrell, P.R., Harris, W.E., & Pritchet, C.J. 2001, AJ, 121, 2557
Fardal, M.A., Guhathakurta, P., Babul, A., & McConnachie, A.W. 2007, MNRAS, 380, 15
Ferguson, A.M.N, Irwin, M.I., Ibata, R.A., Lewis, G.F., & Tanvir, N.R. 2002, ApJ, 124, 1452
Freedman, W.L., & Madore, B.F. 1990, ApJ, 365, 186
Gilbert, K.M., et al. 2007, ApJ, 669, 245
Guhathakurta, P., et al. (2005), preprint (astro-ph/0502366)
Hammer, F., Puech, M., Chemin, L., Flores, H., & Lehnert, M. D. 2007, ApJ, 662, 322
Holland, S., Fahlman, G.G., & Richer, H.B. 1996, AJ, 112, 1035
Ibata, R., Irwin, M., Lewis, G., Ferguson, A.M.N., & Tanvir, N. 2001, Nature, 412, 49
Ibata, R., Martin, N.F., Irwin, M., Chapman, S., Ferguson, A.M.N., Lewis, G.F., & McConnachie A.W. 2007, ApJ, 671, 1591
Irwin, M.J., Ferguson, A.M.N., Ibata, R.A., Lewis, G.F., & Tanvir, N.R. 2005, ApJ, 628, L105
Kalirai, J.S., et al. (2006), ApJ, 648, 389
Marinoni, C., Monaco, P., Giuricin, G., & Costantini, B. 1999, ApJ, 521, 50
McConnachie, A.W., et al. 2006, ApJ, 647, L25
Minniti, D., Olszewski, E.W., & Rieke, M. 1993, ApJ, 410, L79
Moulds, J., & Kristian, J. 1986, ApJ, 305, 591
Olsen, K.A.G., Blum, R.D., Stephens, A.W., Davidge, T.J., Massey, P., Strom, S.E., & Rigaut, F. 2006, AJ, 132, 271
Puzia, T.H., Perrett, K.M., & Bridges, T.J. 2005, A&A, 434, 909
Pritchet, C.J., & van den Bergh, S. 1994, AJ, 107, 1730
Sarajedini, A., Barker, M.K., Geisler, D., Harding, P., & Schommer, R. 2006, ApJ, 132, 1361
Stephens, A.W., & Frogel, J.A. 2002, AJ, 124, 2023
Teig, M. 2008, PASP, 120, 474

Teig, M., Smecker-Hane, T., & Hood, M.A. 2009, in prep.
van den Bergh, S. 2000, PASP, 112, 529
Walterbos, R.A.M., & Kennicutt, R.C. 1988, A&A, 61, 86

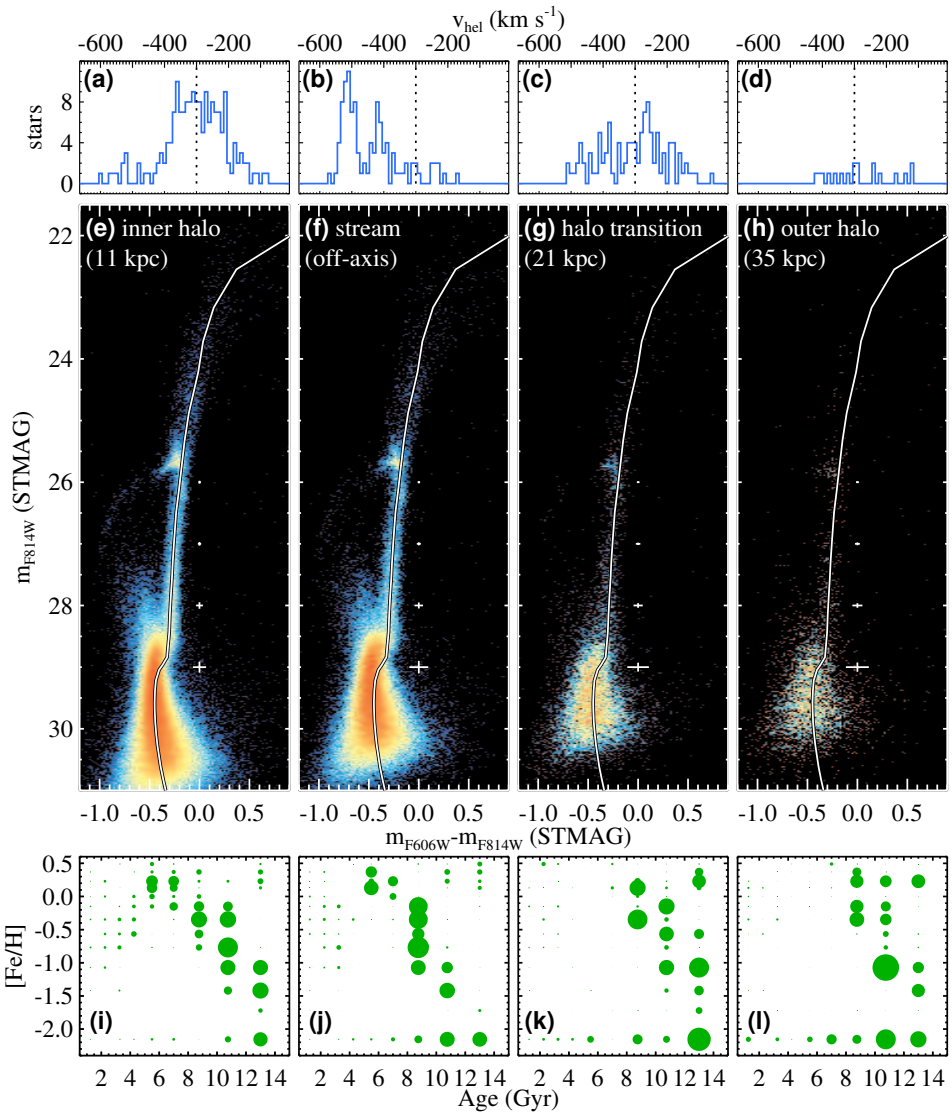

Figure 2. Radial velocities (top row; dotted line is M31 systemic velocity), CMDs (middle row; curve shows 47 Tuc ridge line for comparison), and star formation histories (bottom row; area of circles proportional to weight in fit) for four regions in the M31 halo (Brown et al. 2003, 2006, 2007, 2008). The three regions on the minor axis (at 11, 21, and 35 kpc) show a kinematically hot population at the M31 systemic velocity, while the off-axis field shows the kinematically cold stream plunging into M31 toward us from behind the galaxy. Despite their distinct kinematic profiles, the CMDs and associated star formation histories for the 11 kpc field and the stream are very similar, due to the inner halo being polluted by debris from the stream's progenitor (Brown et al. 2006; Fardal et al. 2007; Gilbert et al. 2007). Although the fields further out on the minor axis do not include significant numbers of stars as young and metal-rich as those found in the 11 kpc and stream fields, all of the halo fields exhibit an extended star formation history, consistent with expectations from hierarchical merging.

GALAXY EVOLUTION: EMERGING INSIGHTS AND FUTURE CHALLLENGES
ASP Conference Series, Vol.
@jourvol, © 2009
S. Jogee, I. Marinova, L. Hao, and G. A Blanc

M31's Giant Southern Stream: Constraints on the Progenitor's Mass, Phase, and Rotation

Mark Fardal,[1] Puragra Guhathakurta,[2] Karoline Gilbert,[2,3] Arif Babul,[4] Cara Dodge,[5] Martin Weinberg,[1] and Yu Lu[1]

Abstract. We use N-body simulations to investigate the origin of the Giant Southern Stream in M31. Our model suggests the stream resulted from the disruption of a large satellite galaxy less than 1 Gyr ago, and connects it to other debris structures in M31's halo. The stream pumps a significant fraction of the progenitor's mass into M31's outer reaches, demonstrating the ongoing buildup of galaxy stellar halos. Rotating models give better fits to the observed stream structure than spherical models, adding a constraint on the progenitor's nature. We use Bayesian sampling of the simulations to get a preliminary estimate of the progenitor's initial mass $M_{\rm sat} = (3.5 \pm 0.5) \times 10^9 {\rm M}_\odot$, which would make it one of the most massive Local Group galaxies. We find its current orbital phase to be 1.1 ± 0.1 radial periods past disruption, suggesting any intact remnant lies against the NE portion of M31's disk.

1. Introduction

Maps of red giants in M31's halo reveal a stellar stream projecting from M31's southern side (Ibata et al. 2001). This giant southern stream (GSS) has now been observed in exquisite detail. Continued mapping efforts (Ferguson et al. 2002; Irwin et al. 2005; Ibata et al. 2007) show this stream extends to a projected distance of 100 kpc, while photometric distances from the red giant tip show the stream's far end lies behind M31, for a total stream radius of about 150 kpc. Spectroscopy in multiple fields along the GSS show it to be cold, and reveal how quickly it speeds up as it falls into M31's center (Ibata et al. 2004; Guhathakurta et al. 2006; Kalirai et al. 2006).

This stream opens up several lines of investigation. How much of the abundant tidal debris in and around M31 can be attributed to a single disruption event that produced the GSS, and which specific features? Can we use the cold phase-space track of this stellar stream to measure M31's halo potential? And finally, what was the nature of the object that produced the stream?

[1]Dept. of Astronomy, University of Massachusetts, Amherst, MA 01003, USA

[2]UCO/Lick Observatory, Dept. of Astronomy & Astrophysics, Univ. of California, 1156 High St., Santa Cruz, CA 95064, USA

[3]Department of Astronomy, Box 351580, University of Washington, Seattle, WA 98195, USA

[4]Dept. of Physics & Astronomy, University of Victoria, Elliott Building, 3800 Finnerty Rd., Victoria, BC, V8P 1A1, Canada

[5]Astronomy Department, Smith College, Clark Science Center, Northampton, MA 01060, USA

2. Model for Stream and Shelves

Our scenario (Fardal et al. 2007) supposes a diffuse dwarf galaxy is disrupted at pericenter, and the first wrap of the orbit makes the stream. A second wrap of the orbit makes the NE Shelf, as suggested by its similar color (Ferguson et al. 2002). A third wrap of the orbit produces the fainter W Shelf, which again has a similar color. Building on our earlier modeling work (Geehan et al. 2006; Fardal et al. 2006), we first fit our semi-analytic orbital model to reproduce the stream and constrain its next wrap to lie near the NE shelf. Using this trajectory, we produce an N-body simulation that closely resembles the morphology of the observations. The model also reproduces the distance, velocity, and velocity dispersion of the GSS, as well as a set of planetary nebulae and RGB stars with "counter-rotating" velocities on the NE side, against M31's disk.

This model is supported by the subsequent spectroscopic discovery of a faint cold minor-axis component (Gilbert et al. 2007), which matches the predicted position and kinematics of the fourth wrap of the orbit. Also, in deep HST/ACS observations, the stellar population in fields predicted to be stream-dominated by the model shows a good match to the GSS population itself (Richardson et al. 2008).

3. Mass and Phase Constraints

Our semi-analytic orbit modeling does not constrain the mass or the orbital phase of the progenitor, and we used a crude estimate of the stream mass to compare our N-body model to observations. Here, we compare the red giant star-count map (Irwin et al. 2005) directly to N-body simulations, using the Markov chain sampling algorithm Differential Evolution within the UMass Bayesian Inference Engine (BIE) to sample the entire parameter space.

We convert this map from counts to mass, rebin it to reduce noise, and select GSS and W shelf regions which constrain the trailing and leading streams. Exploring the full 7-d parameter space of orbital parameters and mass with N-body simulations is still in progress. To demonstrate the method, we fit five orbital parameters as a function of orbital phase, using the semi-analytic orbital model. Then we explore the remaining 2-d space of orbital phase and mass.

The resulting sample yields an initial stellar mass of $(3.5 \pm 0.5) \times 10^9 \mathrm{M}_\odot$. (This formal error is certainly underestimated, due to the omission of the orbital dimensions and systematic error in the mass-to-light ratio). This estimate makes the progenitor one of the most massive Local Group galaxies, next in line after the LMC. The high mass agrees perfectly with the stream's high metallicity of -0.5, which was initially something of a puzzle (Font et al. 2006).

We find the current orbital phase to be $F_\mathrm{p} = 1.1 \pm 0.1$, i.e. whatever remains of the progenitor's core has most likely just completed one orbital wrap since disruption, and lies against the NE portion of M31's disk. This may explain why no remnant of the progenitor is obvious.

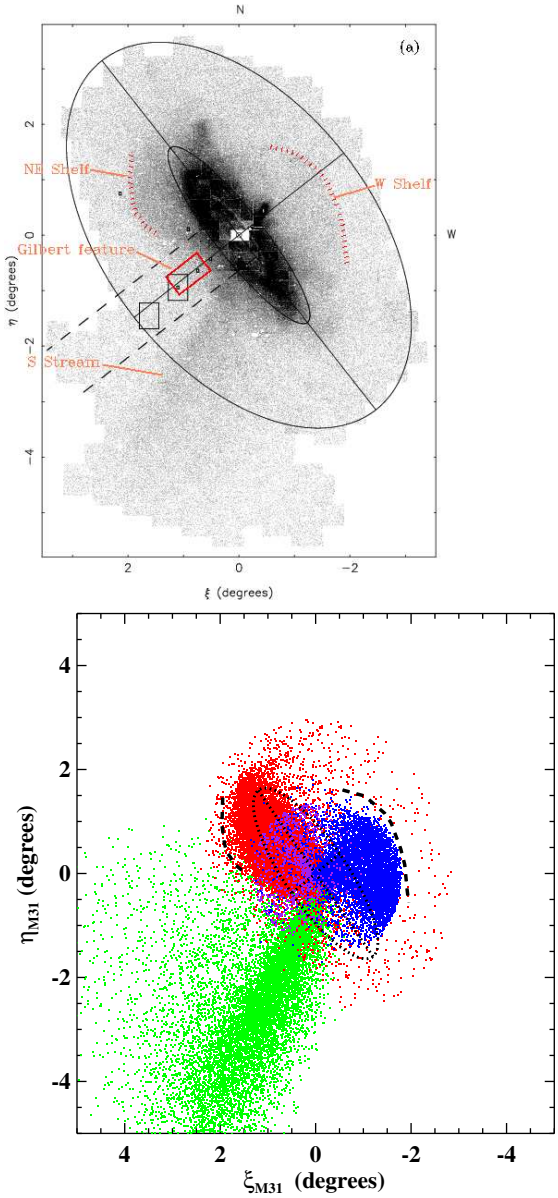

Figure 1. *Left:* Map of RGB count density, from Irwin et al. (2005), reprinted by kind permission of the American Astronomical Society. The edges of the NE and W shelves are marked with red dotted lines. *Right:* Simulation of the GSS from Fardal et al. (2007) (showing only particles associated with the GSS, not M31 itself). The simulation star particles are color-coded according to the number of orbital wraps they have performed since the main disruption event: green for < 1 (GSS), red for 1–2 (NE shelf), blue for 2–3 (W shelf), and purple for > 3.

4. Clues to the progenitor's internal structure

Our modeling so far does not reproduce the very skewed profile of the observed GSS, which has a sharp falloff to the NE and a more gradual decline to the

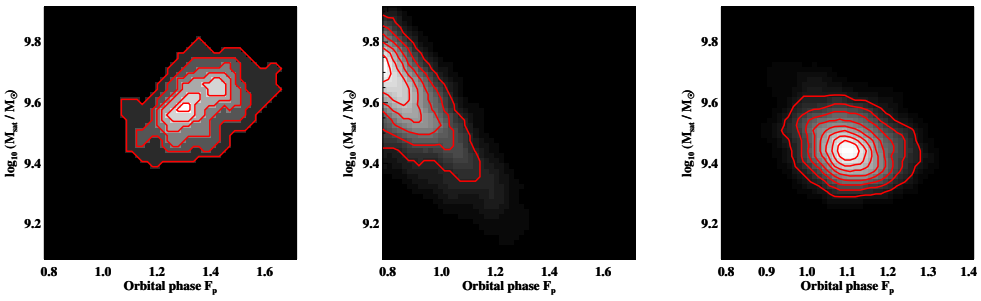

Figure 2. Probability distribution of the mass and progenitor orbital phase (relative to its disruption point), as constrained by the RGB counts map in the GSS and W shelf regions. *Left:* Using GSS constraint only. *Center:* Using W shelf constraint only. *Right:* Final distribution with both constraints.

SW (McConnachie et al. 2003). Consistent with this, very little GSS debris is found in minor axis spectroscopic fields (Gilbert et al. 2007). This indicates some physics is missing from our progenitor models so far.

We now test rotating progenitors, in contrast to the simple spherical models used above. We use hot exponential disks or Kuzmin-Kutuzov models with 12 evenly spaced orientations, all starting in the same orbit as in § 2. We compare our models to the observed skew, and to updated spectroscopy on the minor axis (Fardal et al. 2008, Gilbert et al. 2009, in preparation). A few models pass these tests, all of them "right-handed frisbee" orbits (spinning like a flying disk tossed overhand over M31's center). This success implies a coherently rotating progenitor, like a disk galaxy. It was not gas-rich recently though, since the stream stellar population is old (Brown et al. 2006a,b). The galaxy may thus have been more like a dwarf lenticular or a rotating dE than a typical spiral.

This evidence for rotation suggests testing a radial metallicity gradient as found in disk galaxies. Starting with a plausible disk gradient, the final skymap shows a gradient in the same sense and amount as found in the GSS (Ibata et al. 2007): the "cocoon" to the SW has lower metallicity by ~ 0.2 dex than the "core" to the NE, while the gradient is weak along the stream's path (Fardal et al. 2008). Thus the observed gradient is again suggestive of a disk-like progenitor. The discrepant orbits and metallicities of the outermost stars in this experiment suggest caution in deciding which debris features are associated with the GSS.

Acknowledgments. We thank Tom Quinn and Joachim Stadel for their N-body code PKDGRAV, and Josh Barnes for his N-body utility ZENO.

References

Brown, T. M., Smith, E., Guhathakurta, P., Rich, R. M., Ferguson, H. C., Renzini, A., Sweigart, A. V., & Kimble, R. A. 2006a, ApJ, 636, L89

Brown, T. M., Smith, E., Ferguson, H. C., Guhathakurta, P., Renzini, A., Sweigart, A. V., & Kimble, R. A. 2006b, ApJ, 652, 323

Fardal, M. A., Babul, A., Geehan, J. J., & Guhathakurta, P. 2006, MNRAS, 366, 1012

Fardal, M. A., Guhathakurta, P., Babul, A., & McConnachie, A. W. 2007, MNRAS, 380, 15

Fardal, M. A., Babul, A., Guhathakurta, P., Gilbert, K. M., & Dodge, C. 2008, ApJ, 682, L33
Font, A. S., Johnston, K. V., Guhathakurta, P., Majewski, S. R., & Rich, R. M. 2006, AJ, 131, 1436
Ferguson, A. M. N., Irwin, M. J., Ibata, R. A., Lewis, G. F., & Tanvir, N. R. 2002, AJ, 124, 1452
Geehan, J. J., Fardal, M. A., Babul, A., Guhathakurta, P. 2006, MNRAS, 366, 996
Gilbert, K. M., et al. 2007, ApJ, 668, 245
Guhathakurta, P., et al. 2006, AJ, 131, 2497
Ibata, R., Irwin, M. J., Ferguson, A. M. N., Lewis, G., & Tanvir, N. 2001, Nature, 412, 49
Ibata, R., Chapman, S., Ferguson, A. M. N., Irwin, M., Lewis, G., & McConnachie, A. 2004, MNRAS, 351, 117
Ibata, R., Martin, N. F., Irwin, M., Chapman, S., Ferguson, A. M. N., Lewis, G. F., & McConnachie, A. W. 2007, ApJ, 671, 1591
Irwin, M. J., Ferguson, A. M. N., Ibata, R. A., Lewis, G. F., & Tanvir, N. R. 2005, ApJ, 628, L105
Kalirai, J. S., Guhathakurta, P., Gilbert, K. M., Reitzel, D. B., Majewski, S. R., Rich, R. M., & Cooper, M. C. 2006, ApJ, 641, 268
McConnachie, A. W., Irwin, M. J., Ibata, R. A., Ferguson, A. M. N., Lewis, G. F., & Tanvir, N. 2003, MNRAS, 343, 1335
Richardson, J. C., et al. 2008, AJ, 135, 1998

GALAXY EVOLUTION: EMERGING INSIGHTS AND FUTURE CHALLLENGES
ASP Conference Series, Vol.
@jourvol, © 2009
S. Jogee, I. Marinova, L. Hao, and G. A Blanc

GALEX Observations of Disk and Bulge-Dominated Galaxies

D. Schiminovich and the GALEX Science Team

Columbia University

Abstract. We present some highlights of the Galaxy Evolution Explorer mission, particularly those relevant to the evolution of disk and bulge-dominated galaxies. We briefly describe new results on star-formation in the extended outer parts of disks, star-formation laws, disks on the star-forming sequence of galaxies and massive UV luminous galaxies forming stars at elevated rates. We also discuss efforts to probe star-formation and AGN feedback in bulge-dominated galaxies.

1. Introduction

Star forming regions emit copious amounts of ultraviolet light, and although some of that light is eventually re-radiated by dust in the IR, a typical star-forming galaxy in the universe emits 10-50% of its bolometric luminosity in the UV. The Galaxy Evolution Explorer (GALEX) was launched in April 2003 and has been performing nested imaging surveys in the space ultraviolet (1300-2800Å) in order to study star formation in galaxies in the nearby and distant universe, trace the star formation history of the universe and investigate the physical mechanisms responsible for driving galaxy evolution (Martin et al. 2005). After five years in orbit, GALEX has been used to address many of these questions, with many of the results having been published as part of two Astrophysical Journal Letters and Supplement Special Issues. In this review we present some highlights, particularly those relevant to the evolution of disk and bulge-dominated galaxies.

2. GALEX Observations of Disk-Dominated Galaxies

Extended UV disks One of the most unique discoveries of GALEX has been the observation of low surface brightness, extended UV features around many normal disk galaxies. While extended star-forming regions had already been identified (Ferguson et al. 1998), the survey speed and low surface brightness sensitivity of GALEX has yielded a much larger sample of extended star forming regions in the outer parts of galaxies (e.g., Thilker et al. 2007). A star forming region producing stars at a constant rate with uniform IMF is expected to generate a nearly constant ratio of ionizing to non-ionizing UV photons. However, several XUV disks, including M83 (Thilker et al. 2005) and NGC 4625 (Gil de Paz et al. 2005), have been shown to be Hα deficient, suggesting that the standard assumptions are not valid. Recent work presents possible evidence that Hα deficiency in low surface brightness star-forming regions could be evidence for a varying IMF

(e.g., Meurer et al. 2009), density bounded ionization (e.g., Elmegreen & Hunter 2006) or a signature of a complex, rather than continuous, star formation history (e.g., Gogarten et al. 2009).

In Thilker et al. (2007), a sample of 189 nearby disk galaxies were observed as part of the GALEX Nearby Galaxy Survey (see Gil de Paz et al. 2007, for the full atlas) and used to explore the nature and incidence of the XUV disk phenomenon in the local universe (D<40 Mpc). Within this sample the incidence was 10-20%, and although the total SFR in XUV disks is small compared to the SFR of the main disk, the extended star formation itself suggests the presence of a larger reservoir of gas, and may be linked to accretion of material from the IGM. On-going efforts are expected to further quantify the incidence of XUV disks, search for low-level star formation in early-type galaxies (e.g., Donovan et al. 2009) and groups (e.g., discovery in the Leo Ring, Thilker et al. 2009) and develop a physical model for outer-disk star formation, as discussed below.

Star Formation Laws Star formation rates derived from the UV and other wavelengths can be combined with gas measures to investigate how star formation is triggered in different galactic environments (Kennicutt 1998). The SINGS and THINGS surveys (Kennicutt et al. 2003; Walter et al. 2008) in particular have produced a powerful new database for studying these local and global star formation relations. Some of the highlights have included a detailed assessment of the Schmidt-Kennicutt law on local and global scales and using HI and CO as tracers of the atomic and molecular (H_2) component of the gas reservoir and in particular the molecular Schmidt law that suggests a nearly constant star formation efficiency across the sample (Bigiel et al. 2008). There is evidence from these observations of a "knee" in the relation, which appears close to the atomic vs. molecular "transition" in the galaxy, where there is a shift in the dominance of gas phases. Theoretical work is now focused on understanding why star formation becomes less efficient at low gas surface densities (Krumholz & McKee 2005) and what causes the HI-H_2 transition (e.g., Gnedin et al. 2009).

Star-formation at or beyond the break in the Schmidt-Kennicutt relation has been explored recently by Boissier et al. (2007), who investigated radial profiles of star-formation thresholds using UV vs. Hα tracers. Boissier et al. (2007) found that UV light decreases with radius less-sharply than the Hα—possibly suggesting a weaker break in the law—though this result might also be linked to the observed Hα deficiency in some XUV disks, noted above. Wyder et al. (2009) has investigated the star formation law at low density and confirms the presence of the knee, also finding that UV can trace very low SFR surface densities in LSB disks.

UV Luminous Galaxies At the other extreme is a population in the local universe of UV-selected, intensely star-forming galaxies (UV luminous galaxies or UVLGs: Heckman et al. 2005; Hoopes et al. 2007; Overzier et al. 2008). Notable are the most intense, super-compact UVLGs with SFR surface densities and total SFRs similar to those in high-redshift LBGs. There are few other examples in the local universe of intense, unobscured star formation in massive galaxies, thus the UVLG sample is ideal for understanding how and why these SFR episodes occur. HST imaging reveals that the vast majority of these galaxies show signs of interaction, suggesting that mergers are triggering the

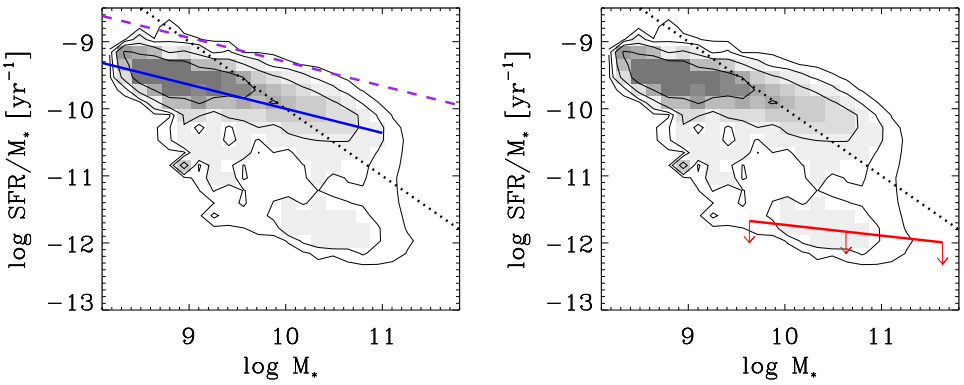

Figure 1. Specific star formation rate vs. Stellar Mass distribution ($1/V_{max}$-weighted) in a sample of SDSS galaxies at $z \sim 1$ Solid lines show location of "Star-forming sequence" (blue, right) and "Red sequence" (red, left). Galaxies above the dashed purple line show a star formation excess (SFX). The black dotted line corresponds to SFR = 1 $M_\odot$ yr^{-1}. Non-SF galaxies may have $SFR/M_\star$ below the red line, which corresponds to an upper limit set by the small contribution of UV light from evolved stars.

star-formation event (Overzier et al. 2008). Integral field spectroscopy (in Hα *and* Pα) obtain velocity dispersions consistent with this hypothesis, although other less-violent "secular" processes might also be at work (Basu-Zych et al. 2009).

Star-Forming Sequence Extremes of star-formation can only be identified in relation to the properties of the full galaxy population. The UV-optical color-magnitude diagram (Wyder et al. 2007), and the derived $SFR/M_\star$ vs. $M_\star$ relation (calibrated using dust corrections from, e.g., Johnson et al. 2007), shown in Figure 1, has enabled the study of scaling relations of disk and bulge-dominated galaxies (Schiminovich et al. 2007). Up until a threshold stellar mass, the galaxy population appears to follow a scaling relation of SFR $\propto M_\star^{2/3}$ (Schiminovich et al. 2007; Salim et al. 2007). As shown in Figure 2, disk-dominated galaxies fall tightly on this "star-forming sequence", while bulge-dominated galaxies show significant scatter across a range of stellar masses. As we discuss in the next section, some bulge-dominated galaxies show residual SFRs that put them near (even on, or above) the star-forming sequence. Considerable work is now being devoted to understanding how and why galaxies transition to become "red and dead", but only recently have we been able to use the galaxy distribution itself, and physically-derived timescales to explore the "flow" of galaxies as they evolve in SFR and M_* (Martin et al. 2007; Schiminovich et al. 2007).

Noeske et al. (2007) has shown that the slope of the star-forming sequence persists out to z$\sim$1, though with an elevated intercept, suggesting that the increase in SFR vs. z may occur uniformly in galaxies of all masses. Somerville et al. (2008) has been able to match the z 0 $SFR/M_\star$ vs. $M_\star$ relation using semi-analytic models that incorporate AGN feedback, while Conroy & Wechsler

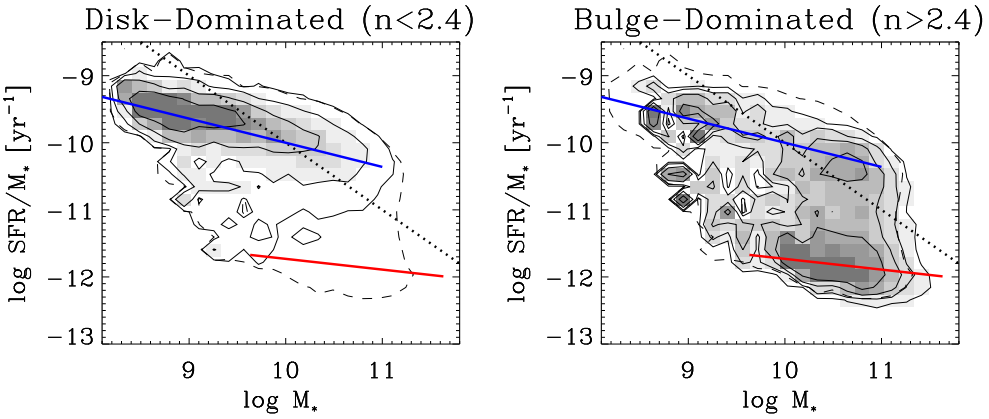

Figure 2. $SFR/M_\star$ vs. $M_\star$ distribution for subsamples split by Sersic index: n_i. $n_i < 2.4$ (*left*) and $n_i > 2.4$ (*r ight*).

(2009) has used the sequence and its evolution to investigate the relationship between star formation and halo mass in a simple, observationally-motivated halo occupation model without feedback. While the detailed properties of the star-forming sequence are providing sensitive new constraints on these models, further work is needed to explore exactly why star formation in a typical disk-dominated galaxy follows these scaling relations and how it evolves (see e.g., Davé 2008).

3. GALEX Observations of Bulge-Dominated Galaxies

UV Optical Colors and Residual Star Formation Bulge-dominated galaxies are known to populate the red-sequence, and generally have low $SFR/M_\star$ although a fraction do show residual SF, and in some cases have SFRs consistent with the galaxies on the star-forming sequence. Most evolved stars do not produce significant amounts of UV light, but a fraction, particularly low-mass, helium-burning extreme horizontal branch stars are thought to dominate the UV luminosity of non-star-forming red galaxies. Yi et al. (2005) studied the UV color-magnitude relation in early-type galaxies and found that some galaxies show UV-light in excess of what can be explained by the evolved component, and that this excess might correspond to present to past-averaged SFRs of 1-10%. The implication of this result is that even with contamination from evolved stars, the UV can trace very low levels of star-formation in these relatively passive galaxies. (For an interesting perspective on the information that ultraviolet measurements add to optical-NIR data see Blanton & Roweis 2007). Improved models of the predicted UV light from the evolved component (which may vary as a function of galaxy properties), and better constraints on the dust attenuation in bulge-dominated galaxies should allow unprecedentedly low measures of trace star formation. Low level SF may result from the recycling of gas from stellar mass loss back into stars of but it could also be a signature of massive galaxy growth through recent accretion of gas and stellar mass.

For example Kaviraj et al. (2007) found that galaxies with $NUV - r < 5.5$ are extremely likely to have experienced recent star formation and that in a sample of SDSS early-type galaxies at $z < 0.11$ more than 30% of early type galaxies have experienced this (>1%) growth over the past Gyr. They suggest find that this residual star formation is consistent with a model of growth through mergers and that galaxies with $NUV - r < 5$ cannot result from star formation that originates in gas produced by stellar mass loss.

Donas et al. (2007) made progress by investigating the origin of the UV colors of early-type galaxies using a sample selected from RC3. A correlation was found between the $NUV - V$ and $B - V$ colors of ellipticals and lenticulars, but significant scatter was observed for $FUV - V$ vs $B - V$ colors. They speculated that the correlation with the NUV light is likely due to a color-metallicity relationship, where the NUV light is modulated by line blanketing of light from stars near the main-sequence turnoff (see also Rich et al. 2005). On the other hand, the scatter in the FUV is likely due to an EHB or other evolved component plus low-level recent SF that does not show up in the $B - V$ color. The combination of these effects (line blanketing, residual SF) can lead to different manifestations of the "UV upturn" in early-type galaxies.

Blue to Red: Green Valley Evolution Residual star formation represent be the fading embers of a once-active galaxy or it may signal an episode of rejuvenation. Studies of the evolving galaxy population show that the red sequence has grown in stellar mass since z∼1, and although disagreement remains regarding the rate of growth as a function of stellar mass, these observations together with the decline of the global SFR density suggest a progressive quenching of star formation for galaxies on the star-forming sequence (e.g., Bell et al. 2007; Faber et al. 2007). As galaxies evolve from an active blue SF to a passive red, non-SF stage they pass through the "green valley" where they may show quenched star formation histories and residual SF.

Martin et al. (2007) used the measurements of the number density of green valley galaxies (taken from the UV-optical color magnitude diagram) and a quenching timescale based on a combination of UV-optical color and spectral line indices, to determine the rate of evolution, or flow of galaxies through the green valley. This evolution relies on the assumption that there is not a significant population of galaxies making the reverse trajectory, but initial results produce a mass flux through the green valley consistent with red sequence growth rates. In Schiminovich et al. (2007) we took a slightly different tack, and—based a standard merger quenching model (e.g., Hopkins et al. 2006) galaxies showing a brief star formation *excess* (SFX) were soon to be quenched and would fall off of the star-forming sequence. Calculations based on the volume density of SFX galaxies and relevant merging/quenching timescales were also consistent with red sequence growth over a range of stellar masses. Including only the bulge-dominated SFX galaxies could already explain a significant fraction of the growth, possibly linking the star formation excess with morphological transformation. Clearly there are considerable uncertainties with these techniques, but they offer alternate methods for measuring the evolution of galaxies over time and provide insight into the mechanisms driving this evolution.

Connection Between SF and AGN As discussed above, theoretical work has suggested a possible link between the quenching of star formation and the onset of AGN activity. Martin et al. (2007); Salim et al. (2007) find that a significant fraction of green valley or residual SF galaxies harbor a detectable AGN. Using ages determined using UV-NIR spectral energy distributions Schawinski et al. (2007) found evidence for a 1 Gyr evolutionary sequence (in age) that evolves from star-forming, through an AGN phase and finally to quiescence. They claim that the most likely explanation is that star-formation is suppressed by AGN activity. Kauffmann et al. (2007) identify similar trends but reach slightly different conclusions by investigating "triangular correlations" between the stellar age in the inner vs. outer parts of a galaxy and AGN activity. Galaxies with either AGN activity *or* young stellar ages in the central regions possess younger stellar populations in the outer parts. Conversely, galaxies with redder outer regions are less likely to have AGN activity or young stellar populations in their centers. One conclusion that might be drawn from this is that recent star formation in the outer parts of galaxies is a signature of a gas reservoir that might feed the grown of an AGN or new SF activity in a galaxy's central regions. In this case, such a galaxy might transition back towards the star-forming sequence through growth by progressive accretion of gas in this nearby reservoir.

4. Further Work

Numerous outstanding questions are being addressed by current and future surveys that incorporate GALEX data. For disk-domionated galaxies: Do we understand SF at low density and low metallicities? Is the IMF constant? What is the connection between SF at low density/metallicity and star formation in primordial galaxies? For bulge-dominated galaxies: How can we refine SFRs (and dust corrections) for the complete population, particularly for bulge-dominated galaxies with significant old populations? Where is residual SF occurring in massive galaxies? Does this tell us anything about BH growth, quenching and/or new disk formation and rejuvenation? Over the full population: Do we have the right physical models for what is driving the star formation histories of galaxies (triggers/quenching)? Can we show that redshift evolution of $SFR/M_\star$ vs. $M_\star$ is consistent with the inferred star formation histories of the full galaxy population? GALEX is continuing to operate and will addressed many of these questions as part of its extended mission surveys, particularly the Galactic Cap surveys that extend its Medium Imaging (and Nearby Galaxy) Surveys over the full extragalactic sky. Many of the results discussed above will also benefit tremendously from the last HST servicing mission (high-resolution imaging and UV spectroscopy), and the next generation of optical/NIR imaging and spectroscopic surveys.

Acknowledgments. D.S. would like to acknowledge the hard work and contributions from the members of the GALEX science and implementation team as well as the numerous associated investigators who have helped to make the mission a success. We would also like to thank Shardha Jogee and the conference organizers. The *Galaxy Evolution Explorer* is a NASA Small Explorer, launched in April 2003. We gratefully acknowledge NASA's support

for construction, operation, and science analysis for the GALEX mission, developed in cooperation with the Centre National d'Etudes Spatiales of France and the Korean Ministry of Science and Technology.

References

Basu-Zych, A. R., et al. 2009, ApJ, 699, L118
Bell, E. F., Zheng, X. Z., Papovich, C., Borch, A., Wolf, C., & Meisenheimer, K. 2007, ApJ, 663, 834
Bigiel, F., Leroy, A., Walter, F., Brinks, E., de Blok, W. J. G., Madore, B., & Thornley, M. D. 2008, AJ, 136, 2846
Blanton, M. R., & Roweis, S. 2007, AJ, 133, 734
Boissier, S., et al. 2007, ApJS, 173, 524
Brinchmann, J., Charlot, S., White, S. D. M., Tremonti, C., Kauffmann, G., Heckman, T., & Brinkmann, J. 2004, MNRAS, 351, 1151
Conroy, C., & Wechsler, R. H. 2009, ApJ, 696, 620
Davé, R. 2008, MNRAS, 385, 147
Donas, J., et al. 2007, ApJS, 173, 597
Donovan, J. L., et al. 2009, AJ, 137, 5037
Elmegreen, B. G., & Hunter, D. A. 2006, ApJ, 636, 712
Faber, S. M., et al. 2007, ApJ, 665, 265
Ferguson, A. M. N., Wyse, R. F. G., Gallagher, J. S., & Hunter, D. A. 1998, ApJ, 506, L19
Gil de Paz, A., et al. 2007, ApJS, 173, 185
Gil de Paz, A., et al. 2005, ApJ, 627, L29
Gnedin, N. Y., Tassis, K., & Kravtsov, A. V. 2009, ApJ, 697, 55
Gogarten, S. M., et al. 2009, ApJ, 691, 115
Heckman, T. M., et al. 2005, ApJ, 619, L35
Hoopes, C. G., et al. 2007, ApJS, 173, 441
Hopkins, P. F., Somerville, R. S., Hernquist, L., Cox, T. J., Robertson, B., & Li, Y. 2006, ApJ, 652, 864
Johnson, B. D., et al. 2007, ApJS, 173, 377
Kauffmann, G., et al. 2007, ApJS, 173, 357
Kaviraj, S., et al. 2007, ApJS, 173, 619
Kennicutt, R. C., Jr. 1998, ARA&A, 36, 189
Kennicutt, R. C., Jr., et al. 2003, PASP, 115, 928
Krumholz, M. R., & McKee, C. F. 2005, ApJ, 630, 250
Martin, D. C., et al. 2005, ApJ, 619, L1
Martin, D. C., et al. 2007, ApJS, 173, 342
Meurer, G. R., et al. 2009, ApJ, 695, 765
Noeske, K. G., et al. 2007, ApJ, 660, L47
Overzier, R. A., et al. 2008, ApJ, 677, 37
Rich, R. M., et al. 2005, ApJ, 619, L107
Salim, S., et al. 2007, ApJS, 173, 267
Schawinski, K., Thomas, D., Sarzi, M., Maraston, C., Kaviraj, S., Joo, S.-J., Yi, S. K., & Silk, J. 2007, MNRAS, 382, 1415
Schiminovich, D., et al. 2007, ApJS, 173, 315
Somerville, R. S., Hopkins, P. F., Cox, T. J., Robertson, B. E., & Hernquist, L. 2008, MNRAS, 391, 481
Thilker, D. A., et al. 2005, ApJ, 619, L79
Thilker, D. A., et al. 2007, ApJS, 173, 538
Thilker, D. A., et al. 2009, Nat, 457, 990
Walter, F., Brinks, E., de Blok, W. J. G., Bigiel, F., Kennicutt, R. C., Thornley, M. D., & Leroy, A. 2008, AJ, 136, 2563

Wyder, T. K., et al. 2007, ApJS, 173, 293
Wyder, T. K., et al. 2009, ApJ, 696, 1834
Yi, S. K., et al. 2005, ApJ, 619, L111

GALAXY EVOLUTION: EMERGING INSIGHTS AND FUTURE CHALLLENGES
ASP Conference Series, Vol.
@jourvol, © 2009
S. Jogee, I. Marinova, L. Hao, and G. A Blanc

Galactic Bulges: the SAURON Perspective

Jesús Falcón-Barroso,[1] Reynier F. Peletier,[2] Roland Bacon,[3]
Michele Cappellari,[4] Roger L. Davies,[4] P. Tim de Zeeuw,[5,6]
Eric Emsellem,[3] Davor Krajnović,[4] Harald Kuntschner,[7]
Richard M. McDermid,[8] Marc Sarzi,[9] Remco C. E. van den Bosch,[10]
and Glenn van de Ven[11]

Abstract. We present results on the study of 24 bulges of Sa galaxies observed with the integral-field unit SAURON at the William Herschel Telescope. Here we review some of the main features observed in our maps in terms of their kinematics and stellar populations, and unveil a rather complex picture in which the centers of spiral galaxies are made of several components: one (or more) thin, disclike component, often containing recent star formation, and another, elliptical-like component, consisting of old stars and rotating more slowly, dominating the light above the plane.

1. Introduction

Historically, the light in the centers of lenticular and spiral galaxies has been thought to be dominated by an elliptical galaxy-like object surrounded by a generally larger disk. This simple picture led over the years to the conclusion that galactic bulges are nothing but scaled-down versions of elliptical galaxies.

[1]European Space and Technology Centre, Keplerlaan 1, 2200 AG Noordwijk, The Netherlands

[2]Kapteyn Astronomical Institute, University of Groningen, NL-9700 AV Groningen, The Netherlands

[3]Université de Lyon 1, CRAL, Observatoire de Lyon, 9 av. Charles André, 69230 Saint-Genis Laval, France

[4]Sub-Department of Astrophysics, University of Oxford, Denys Wilkinson Building, Keble Road, Oxford OX1 3RH, United Kingdom

[5]ESO, Karl-Schwarzschild-Str 2, 85748 Garching, Germany

[6]Sterrewacht Leiden, Leiden University, Postbus 9513, 2300 RA Leiden, The Netherlands

[7]Space Telescope European Coordinating Facility, European Southern Observatory, Karl-Schwarzschild-Str. 2, 85748 Garching, Germany

[8]Gemini Observatory, Northern Operations Centre, 670 N. Aohoku Place, Hilo, Hawaii 96720 USA

[9]Centre for Astrophysics Research, University of Hertfordshire, Hatfield, Herts AL10 9AB, United Kingdom

[10]McDonald Observatory, University of Texas, Austin, TX 78712, USA

[11]Institute for Advanced Study, Einstein Drive, Princeton, NJ 08540, USA

Indeed, at the time, most observations pointed in this direction, showing that they shared rather similar morphology (e.g., Caon, Capaccioli, & D'Onofrio 1993; Andredakis, Peletier, & Balcells 1995), and stellar populations to low luminosity ellipticals (e.g., Fisher, Franx, & Illingworth 1996; Peletier & Balcells 1996). Their kinematics appear to be consistent with that of small oblate systems (e.g., Kormendy & Illingworth 1982; Davies & Illingworth 1983). Despite the marked difference between these central regions and the outer parts of their surrounding disks, color images show a, perhaps surprisingly, smooth transition between the bulge and disk component (Balcells & Peletier 1994; Peletier & Balcells 1997), with bulge and inner disk colours that are very similar.

An important breakthrough in the study of galactic bulges happened with the discovery that some of them displayed kinematics typically associated to disks (Kormendy 1993). At the same time, the traditional view of old stellar populations (Falcón-Barroso, Peletier, & Balcells 2002; Jablonka, Martin, & Arimoto 1996), got also disputed as samples started to grow (Prugniel, Maubon, & Simien 2001; Proctor & Sansom 2002; Thomas & Davies 2006). It looks as if a consensus has been reached in the rather complex picture that bulges can contain several structural and kinematical components which might have formed through very different mechanisms (see Kormendy & Kennicutt 2004 for a detailed review).

In this contribution we will discuss, based on integral-field observations, our view of galactic bulges, with the aim to shed some light on the reasons for the disparity of opinions in previous works and bring us somewhat closer to understanding the nature of bulges. The results presented here are fully expanded in two main papers of the SAURON series (Falcón-Barroso et al. 2006; Peletier et al. 2007).

2. The SAURON Survey

In the context of the SAURON survey (de Zeeuw et al. 2002) of early-type galaxies, we have obtained integral-field observations for 24 Sa spiral galaxies. The full sample is completed by additional observations of 48 elliptical and lenticular galaxies. The sample aims to contain a set of representative galaxies in the local volume (up to ~ 30 Mpc), selecting an equal number of galaxies in the field and cluster environment for each morphological type. For this purpose we use the SAURON spectrograph, mounted at the William Herschel Telescope in La Palma, which delivers 1431 spectra over a two-dimensional contiguous field of view of $33'' \times 41''$ with a spatial separation of $\sim 1''$. Observations cover the narrow range between 4800 and 5380Å, which includes a number of important stellar absorption lines (e.g., Hβ, Fe5015, Mgb, Fe5270) and also potential emission lines (Hβ λ4861, [O III] $\lambda\lambda 4959, 5007$, [N I] $\lambda\lambda 5198, 5200$).

We derive the stellar kinematics and remove the contribution of nebular emission from the spectra in the way described in Falcón-Barroso et al. (2006). The stellar population parameters (i.e., line-strength indices, but also ages, metallicities and abundance ratios) were then determined by assuming they could be represented by a single-age, single metallicity population (Peletier et al. 2007). Models of Vazdekis (1999) were used for this purpose. While this approach is not completely valid for these spiral systems, which are expected to

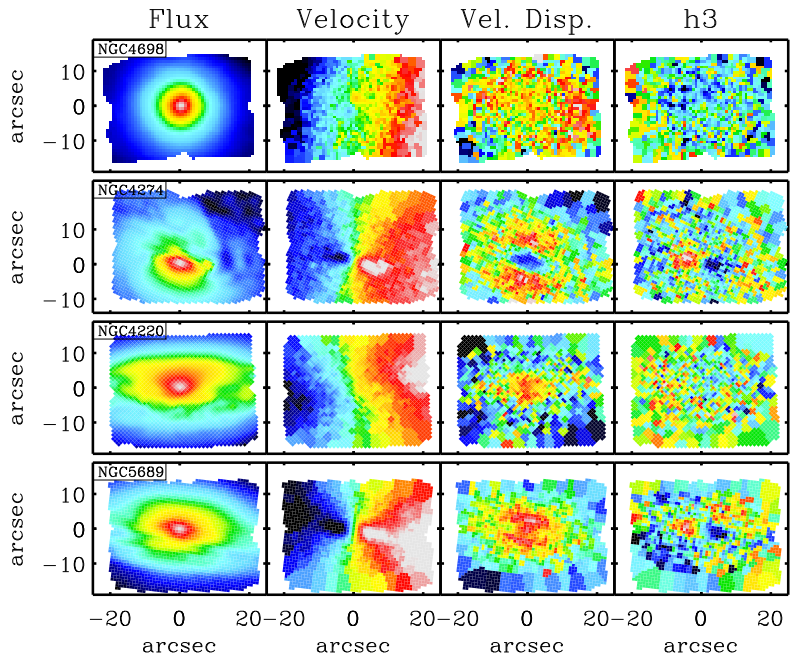

Figure 1. Stellar kinematics of four galaxies in the SAURON sample of Sa galaxies. For each galaxy we plot the integrated flux, line-of-sight velocity, velocity dispersion and h_3 Gauss-Hermite moment. In this set of galaxies, NGC 4220 illustrates a case with no evidence for a kinematic inner component.

have experienced a more continuous star formation history (e.g., Ganda et al. 2007), it provides a reasonable first-order approximation.

3. Stellar and Ionised-Gas Kinematics

The stellar kinematic maps of our galaxies display a variety of substructures in the central regions. We illustrate this variety in Figure 1 using four galaxies in our sample representative of the whole set of 24. The left panels show the integrated light of the galaxies within our field-of-view, obtained by collapsing all the spectra in our datacubes along the wavelength direction. The second and subsequent rows present the line-of-sight stellar velocity, velocity dispersion, and h_3 Gauss-Hermite moment maps. Inner components (e.g., disks or rings) leave a particular imprint in these maps. They are usually identified by the pinching of the isovelocities in the inner regions, which is also accompanied by a decrease of the velocity dispersion (i.e., sigma-drop) and an anti-correlated h_3 parameter at the same locations. The vast majority of these decoupled components in our sample appear to be aligned with the major axis of the galaxy and tend to be associated with dust disks or rings seen in unsharped masked images. A few cases, however, contain inner components whose rotation is about a different axis to that of the main body of the galaxy (i.e., the main disk). Signatures for the decoupling in these cases are most prominent in the velocity maps (usually

as a twist of the zero velocity curve in the inner regions), and not so much on the velocity dispersion (see NGC 4698 in Figure 1). Overall we find that 13 out of 24 galaxies (52%) display clear signatures of kinematically distinct structures. Despite the high fraction, the true value could be even higher as the detection of these components can be hampered by inclination (i.e., as it is more difficult to detect them at face-on configurations), but also by a limited spatial sampling and the sample selection.

The ionised-gas kinematics in our sample is, in general, rather regular and shares the sense of rotation of the stellar kinematics. A few cases depart from this simple description (see Falcón-Barroso et al. 2006): NGC 4772 and NGC 5953, where the gas in certain regions rotates almost perpendicularly to the stars; NGC 7742, where the gas counter-rotates with respect to the stars; NGC 4383, which displays mean velocities confined in a jet-like structure; NGC 4369, that shows no well defined rotation axis, possibly due to the patchy nature of the gas distribution, and NGC 3623, where the gas traces spiral arm structure. In all cases, however, and as already found by other authors (see Goudfrooij et al. 1994) there is a good correspondence between the presence and spatial morphology of the dust with that of the ionised gas.

4. Stellar Populations Diagnostics

In addition to the stellar and ionised-gas kinematics, our data also allow us to explore the stellar populations across the central region of our galaxies.

4.1. Mg*b*–σ Relation with Central Apertures

One of the most studied relations linking kinematics and stellar populations is the Mg*b* vs. σ relation (Terlevich et al. 1981). In this diagram early-type galaxies define a very tight sequence down to low velocity dispersions (Falcón-Barroso et al. 2002). Deviations from the relation are usually understood in terms of the presence of young populations. Previous studies of this relation for galactic bulges show a range of results. Some of them conclude that bulges follow closely the relation defined by ellipticals and S0s (Bender, Burstein, & Faber 1993; Jablonka et al. 1996; Falcón-Barroso et al. 2002). Others show that galactic bulges can be very young and therefore scatter from the main relation (Prugniel et al. 2001; Proctor & Sansom 2002; Thomas & Davies 2006).

In Figure 2, we show the Mg*b* vs. σ relation for our sample. We use measurements obtained within the central $1.2''$ for the 24 Sa galaxies and $R_{\rm e}/8$ for the sample of E/S0 galaxies in the SAURON survey (Kuntschner et al. 2006). The black line is the least-squares fit to the ellipticals and S0 galaxies in Coma of Jorgensen, Franx, & Kjaergaard (1996). In the figure it appears that the relation defined by the E and S0 acts as an upper envelope for the Sa galaxies. The Sa galaxies show a variety of behaviours with some bulges being as old as ellipticals, and therefore sharing similar places in the relation, and others scatter significantly from it, which would imply that they are significantly younger than galaxies in the Coma cluster. It is worth noting that there are several S0 galaxies in the SAURON sample that are also far away from the main relation, sitting in the same location as the spirals with the lowest Mg*b* values. This interpretation is

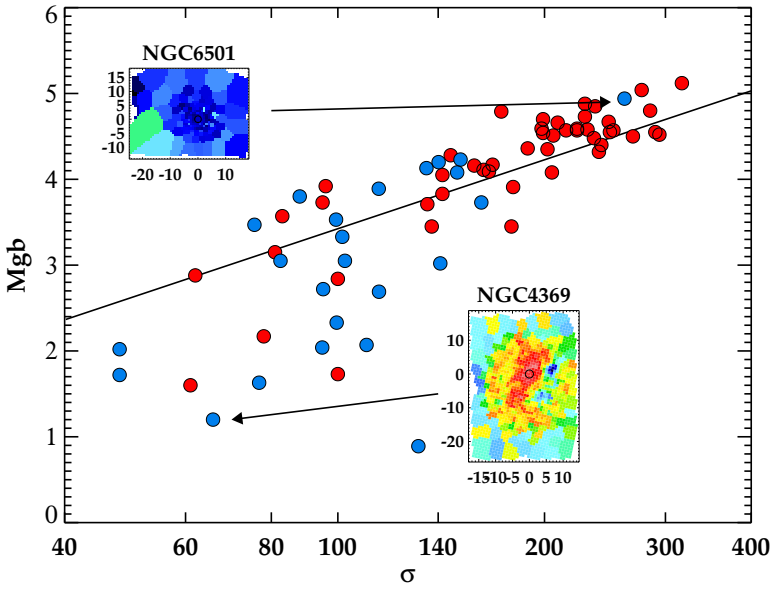

Figure 2. Mgb–σ relation for the 24 Sa galaxies in the SAURON sample (blue solid points). Red points denote the 48 ellipticals and lenticulars in the sample. In the insets we present the Hβ line-strength maps of two Sa galaxies: one on the main relation define by E/S0 and another (young) one deviating from it. The small circle in the maps marks the aperture used to derived the plotted measurements.

confirmed by the Hβ line-strength maps shown in the inset for two representative cases in each regime.

4.2. Kinematic Components on the Mgb–σ Relation

Our integral-field data allows us to study populations in two dimensions, and it is therefore possible to study in detail the particular stellar composition of the kinematically decoupled inner components and relate them to that of their surroundings. Here we will use again the Mgb vs. σ relation to illustrate where the different components fall in this diagram.

We do this in Figure 3 using the same galaxies highlighted in Figure 1. In the figure, for each galaxy, we plot the Mgb and σ measured at different locations within the galaxies. In our sample we can distinguish four types of behaviours or trends as a function of radius for our galaxies. The first case is illustrated with NGC 4698. In this system variations along radius in Mgb and σ are such that all the points stay within the relation defined by ellipticals. A second class of objects are those where star formation is taking place intensively across the whole galaxy (e.g., NGC 4369). Here no matter where you look in the galaxy points will scatter down from the main relation. A third type of objects contains those in which star formation takes place only in a confined location at the center of the galaxy (NGC 4293). In those, the Mgb of this star forming structure (typically an inner disk in our sample) is rather low. As we

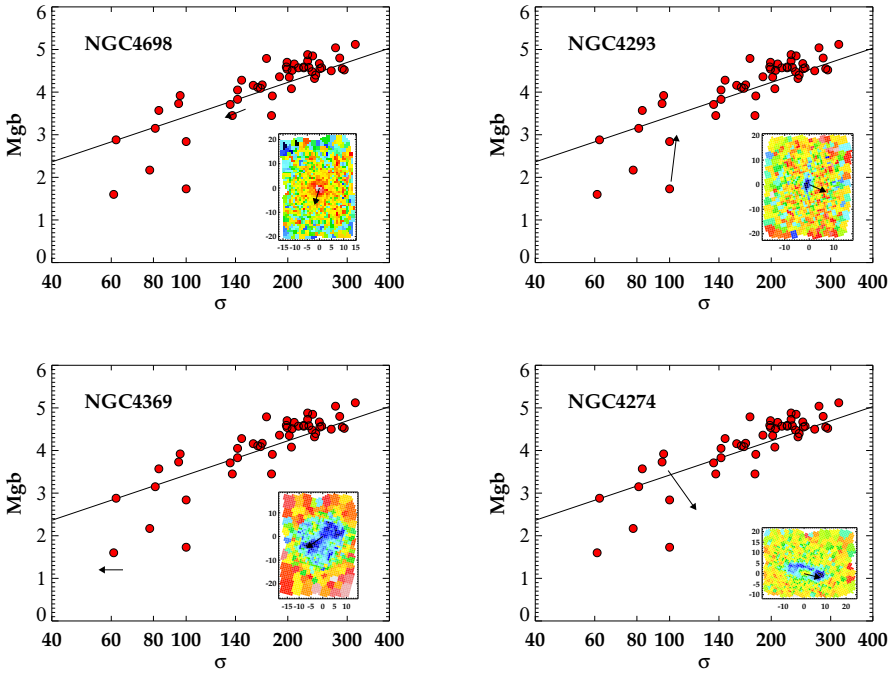

Figure 3. Mg*b*–σ relation for four representative Sa galaxies in the SAURON sample with distinct Mg*b* index morphology. Red points denote the 48 ellipticals and lenticulars in the sample for reference. The insets present the Mg*b* line-strength map for each galaxy. The arrows mark the variation of the index as we move from one region to another in the line-strength map (see insets).

move away from the center to the outer parts, one can see that the other regions behave more like the intermediate-age/old E/S0. The final group is conformed by galaxies displaying circumnuclear star formation. One of the most prominent examples in our set of galaxies is NGC 4274. For this galaxy the center is old and lies on the relation, while the star forming region deviates from it.

5. Our View of Galactic Bulges

With the results presented in the previous section in mind, it becomes much clearer the reason for the disparity of results in the literature in terms of the stellar populations of galactic bulges. The way the samples have been selected imposes a strong bias on the results. It turns out that those studies that focussed on highly inclined samples concluded that bulges are old. These studies excluded on purpose the very central regions of their long slit data to avoid dust and disk contamination. On the other hand, studies with no particular bias on the inclination of the galaxies concluded that bulges are young. In the light of our

results above this is because these authors were probing the innermost regions of the galaxies, where young inner disks or nuclear rings may reside.

Given the complexity of bulges, it is interesting to understand their nature and evolution. There are a few recent attempts to classify bulges in terms of their likely formation scenario based on the number and type of components they contain. Kormendy & Kennicutt (2004) divides bulges in 'classical' (those with $r^{1/4}$ light profiles and pressure-supported kinematics, which would have formed through interactions), and pseudo-bulges, which are flattened and display disk-like kinematics. This second group is thought to form through secular processes. A different classification is provided by Athanassoula (2005), who pleads for three categories: classical bulges, which are the product of monolithic collapse or mergers, disk-like bulges, which form through gas infall to the central regions of the galaxies and subsequent star formation, and peanut-shaped bulges, which are parts of a bar seen in edge-on galaxies.

Our two-dimensional data has contributed in this field to clarify some of the disparities manifest in the past literature on the subject, and emphasises the fact that the central light of Sa galaxies (i.e., their bulges) can consist of several components: one which is old, elliptical-like, and slowly rotating, and another more flattened, disk-like component containing often young stellar populations.

Acknowledgments. JFB is grateful to the organizers for the financial support and for a very stimulating and enjoyable meeting.

References

Athanassoula E., 2005, MNRAS, 358, 1477
Andredakis Y. C., Peletier R. F., Balcells M., 1995, MNRAS, 275, 874
Balcells, M. & Peletier, R. F. 1994, AJ, 107, 135
Bender R., Burstein D., Faber S. M., 1993, ApJ, 411, 153
Caon N., Capaccioli M., D'Onofrio M., 1993, MNRAS, 265, 1013
Davies R. L., Illingworth G., 1983, ApJ, 266, 516
de Zeeuw, P.T., et al., 2002, MNRAS, 329, 513
Falcón-Barroso, J., Peletier, R. F., & Balcells, M. 2002, MNRAS, 335, 741
Falcón-Barroso J., et al., 2006, MNRAS, 369, 529
Fisher D., Franx M., Illingworth G., 1996, ApJ, 459, 110
Ganda K., et al., 2007, MNRAS, 380, 506
Goudfrooij, P., Hansen, L., Jorgensen, H. E., & Norgaard-Nielsen, H. U. 1994, A&AS, 105, 341
Jablonka P., Martin P., Arimoto N., 1996, AJ, 112, 1415
Jorgensen I., Franx M., Kjaergaard P., 1996, MNRAS, 280, 167
Kormendy J., Illingworth G., 1982, ApJ, 256, 460
Kormendy J., 1993, in IAU Symp. 153, p. 209
Kormendy, J., & Kennicutt, R. C., Jr. 2004, ARA&A, 42, 603
Kuntschner H., et al., 2006, MNRAS, 369, 497
Peletier R. F., Balcells M., 1996, AJ, 111, 2238
Peletier R. F., Balcells M., 1997, New Astronomy, 1, 349
Peletier R.F., et al., 2007, MNRAS, 279, 445
Proctor R. N., Sansom A. E., 2002, MNRAS, 333, 517
Prugniel P., Maubon G., Simien F., 2001, A&A, 366, 68
Terlevich R., Davies R. L., Faber S. M., Burstein D., 1981, MNRAS, 196, 381
Thomas D., Davies R. L., 2006, MNRAS, 366, 510
Vazdekis A., 1999, ApJ, 513, 224

GALAXY EVOLUTION: EMERGING INSIGHTS AND FUTURE CHALLLENGES
ASP Conference Series, Vol.
@jourvol, © 2009
S. Jogee, I. Marinova, L. Hao, and G. A Blanc

The Properties of Local Barred Disks in the Field and Dense Environments: Implications for Galaxy Evolution

Irina Marinova,[1] Shardha Jogee,[1] Fabio D. Barazza,[2]
Amanda Heiderman,[1] Meghan E. Gray,[3] Marco Barden,[4]
Christian Wolf,[5] Chien Y. Peng,[6,7] David Bacon,[8] Michael Balogh,[9]
Eric F. Bell,[10] Asmus Böhm,[4,11] John A. R. Caldwell,[12] Boris Häußler,[3]
Catherine Heymans,[13] Knud Jahnke,[10] Eelco van Kampen,[4] Kyle Lane,[3]
Daniel H. McIntosh,[14,15] Klaus Meisenheimer,[10] Sebastian F. Sánchez,[16]
Rachel Somerville,[10] Andy Taylor,[13] Lutz Wisotzki,[11] and
Xianzhong Zheng[17]

Abstract. Stellar bars are the most efficient internal drivers of disk evolution because they redistribute material and angular momentum within the galaxy and dark matter halo. Mounting evidence suggests that processes other than major mergers, such as minor mergers, secular processes driven by bars, and clump coalescence, as well as smooth accretion, play an important role in galaxy evolution since $z = 2$. As a key step toward characterizing this evolution and constraining theoretical models, we determine the frequency and properties of bars in the local Universe in both field and cluster environment, based on three of our studies: Marinova & Jogee (2007), Barazza, Jogee, & Marinova (2008)

[1]Department of Astronomy, University of Texas at Austin, 1 University Station C1400, Austin, TX 78712-0259, USA

[2]Laboratoire d'Astrophysique, École Polytechnique Fédéralede, Lausanne, Switzerland

[3]School of Physics and Astronomy, The University of Nottingham, Nottingham, UK

[4]Institute for Astro- and Particle Physics, University of Innsbruck, Innsbruck, Austria

[5]Department of Astrophysics, University of Oxford, Oxford, UK

[6]NRC Herzberg Institute of Astrophysics, Victoria, Canada

[7]Space Telescope Science Institute, Baltimore, MD, USA

[8]Institute of Cosmology and Gravitation, University of Portsmouth, Portsmouth, UK

[9]Department of Physics and Astronomy, University Of Waterloo, Ontario, Canada

[10]Max-Planck-Institut für Astronomie, Heidelberg, Germany

[11]Astrophysikalisches Insitut Potsdam, Potsdam, Germany

[12]University of Texas, McDonald Observatory, Fort Davis, TX, USA

[13]Scottish Universities Physics Alliance, Institute for Astronomy, University of Edinburgh, UK

[14]Department of Astronomy, University of Massachusetts, Amherst, MA, USA

[15]Department of Physics, University of Missouri-Kansas City, Kansas City, MO

[16]Centro Hispano Aleman de Calar Alto, Almeria, Spain

[17]Purple Mountain Observatory, Chinese Academy of Sciences, Nanjing, China

and Marinova et al. (2009). Among field spirals of intermediate Hubble types in the OSU survey, we find using ellipse fitting that the bar fraction is 44% in the optical and 60% in the NIR, giving an extinction correction factor of approximately 1.4 at $z \sim 0$. Using data from the Abell 901/902 cluster system at $z \sim 0.165$ from the HST ACS survey STAGES, we find that the optical bar fraction is a strong trend of both absolute magnitude and host bulge-to-total ratio, increasing for galaxies that are brighter and/or more disk-dominated. The latter trend is also found in the field from SDSS. For bright early types and faint late types the optical bar fraction in the cluster is similar to that in the field. We find that between the core region and the virial radii of the clusters the optical bar fraction is not a strong function of local environment density. We discuss the implications of our results in the context of theoretical models of the impact of bars on galaxy evolution.

1. Introduction

Recent results suggest that major mergers play a less important role in driving galaxy evolution since $z \sim 2$ than previously thought. In particular, studies have shown that non-interacting galaxies dominate the star formation rate (SFR) density over the past ~ 8 Gyr (Jogee et al. 2009; Wolf et al. 2005; Bell et al. 2005) and that more quiescent processes, such as minor mergers, smooth accretion (Dekel et al. 2009; Kereš et al. 2009), and internal secular evolution driven by bars and clump coalescence (Elmegreen, Bournaud, & Elmegreen 2008), have played a major role in building the bulges of present-day spirals (Weinzirl et al. 2009). There is also evidence for massive disks at $z \sim 2$ with high SFRs but showing no indications of major mergers (Shapiro et al. 2008; Genzel 2009).

The most efficient internal driver of disk galaxy evolution are stellar bars. Bars redistribute angular momentum between the disk and dark matter (DM) halo, funneling gas to the central regions of galaxies. The large central gas concentrations trigger intense starbursts (Sakamoto et al. 1999; Jogee et al. 2005; Sheth et al. 2005), and are thought to build pseudobulges (Kormendy & Kennicutt 2004).

HST ACS surveys show that strong bars are present out to $z \sim 1$ (Jogee et al. 2004; Sheth et al. 2008). A key step in characterizing the role played by stellar bars in driving disk evolution since $z \sim 1$ is to determine the frequency and properties of barred galaxies in the local Universe in the field and in dense environments. We summarize here results from three of our studies: Marinova & Jogee (2007; hereafter MJ07), Barazza, Jogee, & Marinova (2008; hereafter BJM08), and Marinova et al. and the STAGES collaboration (2009; hereafter M09). Our results provide a low-redshift reference point for ACS surveys out to $z = 1$ in rest-frame optical and for WFC3 and JWST surveys out to $z \sim 3$ in the rest-frame NIR. In addition, we aim to set constraints on theoretical models of bar formation and evolution in a cosmological context.

2. Field Galaxies at $z \sim 0$

In MJ07, we fit the B and H images of 180 spirals from the OSU Bright Spiral Galaxy Survey (OSUBSGS; Eskridge et al. 2002), which is dominated

by early to intermediate-type spirals (Sab to Sc). We determine the frequency and characterize the structural properties of bars in *nearby field galaxies at optical and NIR wavelengths*. For field galaxies at $z \sim 0$, we find a bar fraction of $60\% \pm 6\%$ in the near-infrared H band, and $44\% \pm 6\%$ in the optical B band (MJ07). Our results in the NIR agree with those of Laurikainen et al. (2004) and Menéndez-Delmestre et al. (2007). This result reinforces the notion that many bars are obscured at optical wavelengths by dust and star formation, and gives an obscuration factor of ~ 1.4 at $z \sim 0$. It also suggests that at $z \sim 1$ where the average SFR and SFR density are 4–10 times higher than at $z = 0$ (e.g., Lilly et al. 1996; Le Floc'h et al. 2005; Jogee et al. 2009), the optical bar fraction can be lowered by an even larger factor due to obscuration.

In BJM08, we ellipse-fit the r-band images of ~ 3000 galaxies in the low-redshift subsample of SDSS (Blanton et al. 2005). This sample complements MJ07 as it is dominated by faint, late-type spirals (e.g., Sc to Sd). Using this much larger sample, we also find an optical bar fraction of ~ 48–52% averaged over all spirals, with a trend of higher optical bar fraction in disk-dominated systems (BJM08). Our results are in agreement with other studies of local spirals at optical wavelengths (Aguerri et al. 2009; Reese et al. 2007).

3. Properties of Barred Cluster Galaxies and Implications for Bar Evolution

To explore the properties of barred disks in dense environments we use the Space Telescope A901/2 Galaxy Evolution Survey (STAGES; Gray et al. 2009), which consists of ~ 800 bright galaxies in the Abell901/902 cluster system at $z \sim 0.165$, imaged with HST ACS. Photometric redshifts, luminosities, and masses (Borch et al. 2006) are available based on the COMBO-17 survey (Wolf et al. 2004). We identify and characterize bars through ellipse-fitting, and other morphological features (clumpyness, prominence of bulge) through visual classification. Figure 1 shows examples of some barred disks in the A901/902 cluster system.

We select disk galaxies using visual classification, single component Sérsic cut ($n \leq 2.5$), and a blue-cloud cut. We find that the latter two methods miss 31% and 51%, respectively, of visually-identified disks, particularly the many red, bulge-dominated disk galaxies in clusters. This underscores that the widely used methods of color or Sérsic cuts for selecting samples of disk or spiral galaxies fail direly in clusters. However, the optical bar fraction in the cluster is $\sim 30\%^{+10\%}_{-3\%}$ for all three methods of disk selection (M09).

In the field, the bar fraction varies with Hubble type or B/D, and color (Odewahn 1996; Aguerri et al. 2009, BJM08). Thus, in the clusters, we explore $f_{\rm bar-opt}$ as a function of host galaxy properties such as the prominence of the bulge and $M_{\rm V}$. We visually classify disk galaxies as those with prominent bulges (bulge+disk) and those that appear bulgeless (pure disk). We find that the optical bar fraction rises in brighter galaxies and those that appear to have no significant bulge component. Within a given absolute magnitude bin, $f_{\rm bar-opt}$ is higher in visually-selected disk galaxies that have no bulge as opposed to those with bulges. Conversely, for a given visual morphological class, $f_{\rm bar-opt}$

rises at higher luminosities (Table 1). *The latter result is a new insight into the relationship between bars and the B/D of their host disks.*

Table 1. Optical bar fraction in the A901/902 clusters as a function of morphology and absolute magnitude.

M_V range	bulge+disk	pure disk
$-18 \geq M_V > -19$	13%±4% (8/63)	39%±8% (16/41)
$-19 \geq M_V > -20$	19%±4% (17/88)	59%±9% (16/27)
$-20 \geq M_V > -21$	40%±6% (29/73)	63%±17% (5/8)
$-21 \geq M_V > -22$	63%±8% (22/35)	—

The result that $f_{\rm bar-opt}$ rises toward disk-dominated galaxies may be interpreted in the context of bar formation models. If bars form and grow through swing amplification, a large bulge that leads to an inner Lindblad resonance (ILR) may inhibit bar formation by cutting off the feedback loop. We also find that for a particular morphological class, $f_{\rm bar-opt}$ rises for brighter galaxies. Athanassoula (2002) finds that the distribution of the halo mass is the most influential factor dictating the evolution of the bar. Bars in more halo-dominated simulations develop more slowly than bars embedded in disks that are massive compared to the halo in the inner regions. However, these bars tend to become stronger because the live DM halo acts as a sink for angular momentum transferred out by the bar. In the context of these simulations, one would expect bars to form and grow more slowly in galaxies with higher DM fraction, namely in fainter galaxies. This is in agreement with our results. However, we find no trend of stronger bars (higher ellipticity) at lower luminosities.

4. Optical Bar Fraction as a Function of Environment Density

To characterize local density within the Abell 901/902 cluster system, we use four indicators: the distance from the nearest cluster center, projected surface mass density κ (Heymans et al. 2008), projected galaxy number density (Wolf, Gray, & Meisenheimer 2005), and ICM density from x-ray emission. We find that between the core and the virial radius of the clusters at *intermediate density*, the bar fraction does not depend strongly on environment density (Figure 2; M09).

We also compare the results from the STAGES cluster study to the field. Using our results at $z \sim 0$ from the OSU sample (MJ07) and results from the SDSS for $z \sim 0.01$–0.04 (Aguerri et al. 2009), we find that for bright early Hubble types, as well as faint late-type systems with no evident bulge, the cluster optical bar fraction at $z \sim 0.165$ *at intermediate densities* is comparable within a factor of 1.2 to that of field galaxies (M09).

Theoretical models of bar formation in a cosmological context, suggest that interaction with the halo sub-structure induces bars (Romano-Díaz et al. 2008). Since this substructure is present in all environments, these models imply a similar bar fraction across a large range of environment densities, which is consistent with our results comparing the field and intermediate densities.

Within the dense cluster cores, *at the highest environment density*, we cannot reach a firm conclusion about the behavior of the bar fraction because of low number statistics, projection effects, and different trends from the different density indicators. However, we note that some previous studies that use visual classifications to characterize bars and radial velocities to indicate galaxy position within the cluster, find an enhancement in the optical bar fraction toward the cores of Coma and Virgo (Thompson 1981; Andersen 1996). This may seem counterintuitive given that bulge-dominated galaxies prevail in the cores of clusters and our result that such galaxies host a lower bar fraction. However, it is possible that the increased number of high-speed encounters between galaxies in cluster cores compensate for this drop by inducing bars.

Acknowledgments. I.M., S.J., and A.H. acknowledge support from NSF grant AST 06-07748, NASA LTSA grant NAG5-13063, as well as HST G0-10395.

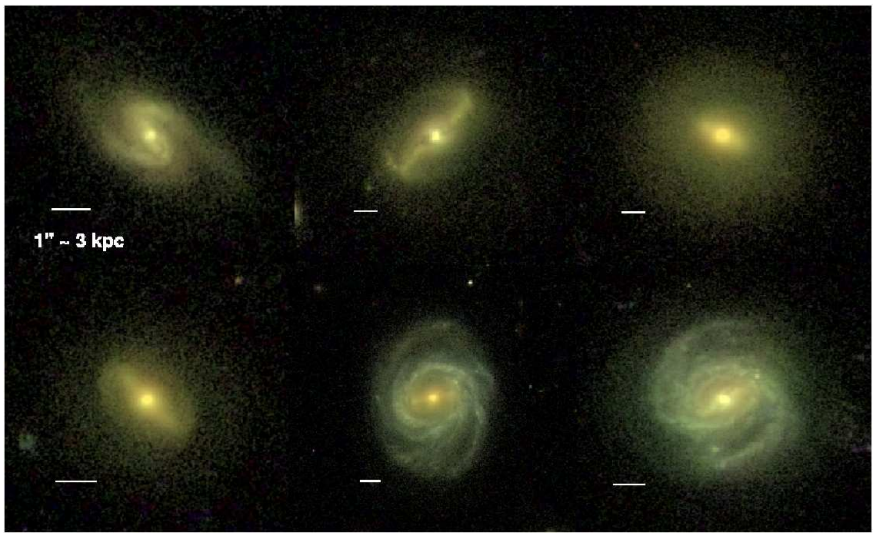

Figure 1. Examples of barred disks in the A901/902 cluster system.

References

Aguerri, J. A. L., Méndez-Abreu, J., & Corsini, E. M. 2009, A&A, 495, 491
Andersen, V. 1996, AJ, 111, 1805
Athanassoula, E. 2002, ApJ, 569, L83
Barazza, F. D., Jogee, S., & Marinova, I. 2008, ApJ, 675, 1194 (BJM08)
Bell, E. F., et al. 2005, ApJ, 625, 23
Blanton, M. R., et al. 2005, AJ, 129, 2562
Borch, A., et al. 2006, A&A, 453, 869
Dekel, A., et al. 2009, Nat, 457, 451
Elmegreen, B. G., Bournaud, F., & Elmegreen, D. M. 2008, ApJ, 688, 67
Eskridge, P. B., et al. 2002, ApJS, 143, 73
Genzel, R. 2009, Nat, 457, 388
Gray, M. E., et al. 2009, MNRAS, 393, 1275
Heymans, C., et al. 2008, MNRAS, 385, 1431
Jogee, S., et al. 2004, ApJ, 615, L105

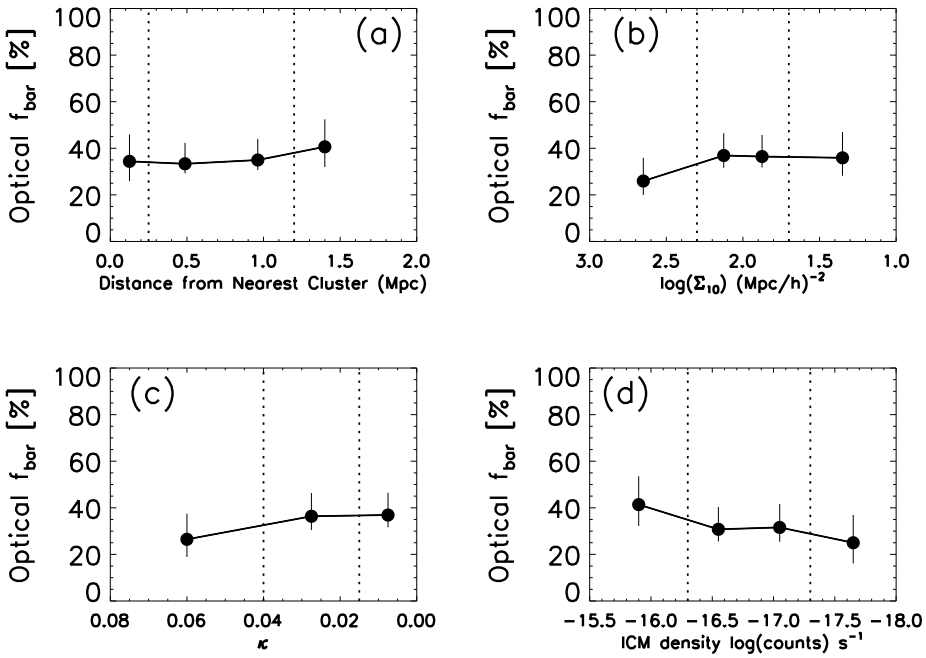

Figure 2. Optical bar fraction as a function of local environment density (§ 4) using different indicators. The dashed vertical lines separate the core, outer, and outskirt regions of the clusters. (adapted from M09)

Jogee, S., Scoville, N., & Kenney, J. D. P. 2005, ApJ, 630, 837
Jogee, S., et al. 2009, ApJ, 697, 1971
Kereš, D., Katz, N., Fardal, M., Davé, R., & Weinberg, D. H. 2009, MNRAS, 395, 160
Kormendy, J., & Kennicutt, R. C., Jr. 2004, ARA&A, 42, 603
Laurikainen, E., Salo, H., Buta, R., & Vasylyev, S. 2004, MNRAS, 355, 1251
Le Floc'h, E., et al. 2005, ApJ, 632, 169
Lilly, S. J., Le Fevre, O., Hammer, F., & Crampton, D. 1996, ApJ, 460, L1
Marinova, I., & Jogee, S. 2007, ApJ, 659, 1176 (MJ07)
Marinova, I., et al. 2009, ApJ, 698, 1639 (M09)
Menéndez-Delmestre, K., Sheth, K., Schinnerer, E., Jarrett, T. H., & Scoville, N. Z. 2007, ApJ, 657, 790
Odewahn, S. C. 1996, ASP Conf. Ser. 91: IAU Colloq. 157: Barred Galaxies, ed. R. Buta, D. A. Crocker & B. G. Elmegreen (San Francisco: ASP), 30
Reese, A. S., Williams, T. B., Sellwood, J. A., Barnes, E. I., & Powell, B. A. 2007, AJ, 133, 2846
Romano-Díaz, E., Shlosman, I., Heller, C., & Hoffman, Y. 2008, ApJ, 687, L13
Sakamoto, K., Okumura, S. K., Ishizuki, S., & Scoville, N. Z. 1999, ApJ, 525, 691
Shapiro, K. L., et al. 2008, ApJ, 682, 231
Sheth, K., Vogel, S. N., Regan, M. W., Thornley, M. D., & Teuben, P. J. 2005, ApJ, 632, 217
Sheth, K., et al. 2008, ApJ, 675, 1141
Thompson, L. A. 1981, ApJ, 244, L43
Weinzirl, T., Jogee, S., Khochfar, S., Burkert, A., & Kormendy, J. 2009, ApJ, 696, 411
Wolf, C., et al. 2004, A&A, 421, 913

Wolf, C., Gray, M. E., & Meisenheimer, K. 2005, A&A, 443, 435
Wolf, C., et al. 2005, ApJ, 630, 771

GALAXY EVOLUTION: EMERGING INSIGHTS AND FUTURE CHALLLENGES
ASP Conference Series, Vol.
@jourvol, © 2009
S. Jogee, I. Marinova, L. Hao, and G. A Blanc

Bars in Field and Cluster Galaxies at Intermediate Redshifts

Fabio D. Barazza, [1] Pascale Jablonka, [1,2] and the EDisCS collaboration

Abstract. We present the first study of large-scale bars in clusters at intermediate redshifts ($z = 0.4 - 0.8$). We compare the properties of the bars and their host galaxies in the clusters with those of a field sample in the same redshift range. We use a sample of 945 moderately inclined disk galaxies drawn from the EDisCS project. The morphological classification of the galaxies and the detection of bars are based on deep HST/ACS $F814W$ images. The total optical bar fraction in the redshift range $z = 0.4 - 0.8$, averaged over the entire sample, is 25%. This is lower than found locally, but in good agreement with studies of bars in field environments at intermediate redshifts. For the cluster and field subsamples, we measure bar fractions of 24% and 29%, respectively. In agreement with local studies, we find that disk-dominated galaxies have a higher bar fraction than bulge-dominated galaxies. We also find, based on a small subsample, that bars in clusters are on average longer than in the field and preferentially found close to the cluster center, where the bar fraction is somewhat higher than at larger distances.

1. Introduction

Bars are believed to be very important with regard to the dynamical and secular evolution of disk galaxies, particularly in redistributing the angular momentum of the baryonic and dark matter components of disk galaxies. Theory and n-body simulations predict that this redistributions is characterized by the transfer of angular momentum to the outer disk. As a result, gas is driven inside the corotation radius toward the center of the disk, which can trigger starbursts (Sakamoto et al. 1999; Bournaud & Combes 2002; Jogee et al. 2005) and contribute to the formation of disky bulges (Kormendy & Kennicutt 2004).

While it is still unknown why a specific disk galaxy hosts a bar and an apparently similar galaxy is unbarred, it is clear that a significant fraction of bright disk galaxies appears barred in optical observations (Eskridge et al. 2000; Reese et al. 2007; Marinova & Jogee 2007; Barazza et al. 2008). This result is mainly based on samples of disk galaxies in field environments, whereas studies of bars in cluster galaxies are rather rare. In general it is found that the fraction of barred disks in clusters or groups is roughly the same as in the field (van den Bergh 2007; Marinova et al. 2009), suggesting that the denser environment does not significantly affect bar formation. On the other hand, Thompson (1981) and Andersen (1996) present evidence that barred galaxies in the Coma and Virgo clusters are more concentrated toward the cluster centers than unbarred disks.

[1]Laboratoire d'Astrophysique, EPFL, Observatoire de Sauverny, CH-1290 Versoix, Switzerland

[2]Université de Genève, Observatoire de Sauverny, CH-1290 Versoix, Switzerland

We present results of the first study of bars in clusters at intermediate redshifts and investigate the impact of the cluster environment on bar formation and evolution. We use a sample of disk galaxies from the ESO distant cluster survey (EDisCS, White et al. 2005). Using the available I-band HST/ACS images we identify and characterize bars, based on quantitative criteria. We look for relations between barred and unbarred galaxies and their environment for a subsample, for which spectroscopic redshifts and reliable cluster membership determinations are available.

2. Sample and method

The EDisCS project has assembled three-band optical VLT deep photometry, deep NTT/SOFI near-infrared imaging, and optical VLT/FORS2 spectroscopy for 26 optically selected and spectroscopically confirmed galaxy structures between redshifts 0.39 and 0.96 (Halliday et al. 2004; Milvang-Jensen et al. 2008). Additional HST/ACS images in the $F814W$ filter were acquired for 10 fields containing the most distant clusters. Galaxies in these 10 fields, regardless of whether they are cluster members or group/field galaxies, and with $I < 23$ mag constitute our basic sample. ¿From this sample we select all galaxies with Hubble types S0–Sm/Im based on visual classification (Desai et al. 2007) and in the redshift range $z = 0.4 - 0.8$, which ensures to remain in the rest-frame optical (1906 objects). Results based on the separation between cluster and field galaxies are based on a subsample, for which spectroscopic redshifts and therefore a reliable cluster or field allocation is available (459 objects).

Our method to find bars relies on the fact that the isophotes of bars in moderately inclined disk galaxies (i.e. with disk inclination $i < 60°$) have much higher ellipticities than the isophotes of the underlying disk. The ellipticities of the isophotes are derived by fitting ellipses to the surface brightness distribution of the disks using the IRAF task 'ellipse'. The corresponding profiles of ellipticity (ϵ) and position angle (P.A.) are investigated based on two quantitative criteria: (1) ϵ increases steadily to a global maximum higher than 0.25, while the P.A. value remains constant (within 10°), and (2) ϵ then drops by at least 0.1 and the P.A. changes at the transition between the bar to the disk region. Galaxies meeting these two criteria have been classified as barred.

3. Results

The optical bar fraction of the entire sample (including field and cluster galaxies) is $\sim 25\%$. This is significantly lower than is typically found in optical studies of *local* galaxies (Eskridge et al. 2000; Reese et al. 2007; Marinova & Jogee 2007; Barazza et al. 2008), but in good agreement with studies of galaxies in field environments at intermediate redshifts (Jogee et al. 2004; Elmegreen et al. 2004; Sheth et al. 2008). For the spectroscopically confirmed cluster sample, we obtain $\sim 24\%$, and for the corresponding field sample, we derive $\sim 29\%$. These values agree within the uncertainties with the result for the complete sample and indicate that the frequency of bars in clusters is almost identical to that in the field. Figure 1 shows the optical bar fraction of the entire sample as a function of Hubble type (top left) and effective radius (r_e, bottom left). The effective radius

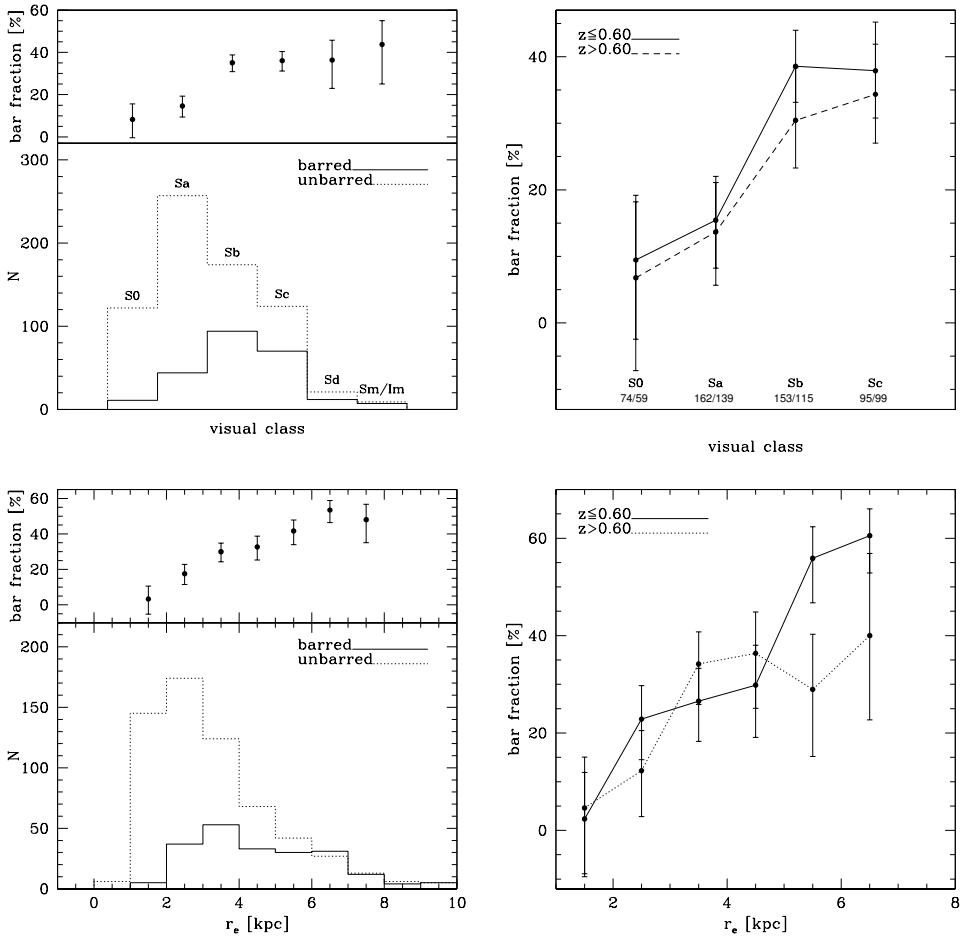

Figure 1. *Top Left* : The number of barred and unbarred galaxies in the entire sample as a function of Hubble type and the corresponding bar fraction. *Top Right* : The bar fraction as a function of Hubble type for two redshift bins. *Bottom Left* : The number of barred and unbarred galaxies in the entire sample as a function of effective radius (r_e). *Bottom Right* : The bar fraction as a function of r_e for two redshift bins.

defines the area, which contains half of the total galaxy light. The bar fraction increases towards later Hubble types and disks with larger effective radii. This indicates that disk-dominated galaxies are more likely to be barred than bulge-dominated galaxies. This results is in good agreement with two recent SDSS studies also based on Hubble types and effective radius (Barazza et al. 2008; Aguerri et al. 2009). The right panels of Figure 1 show the same as the left panels, but separated into a low and high redshift bin. The relations remain roughly the same showing that the relative bar fractions of the different Hubble types do not change significantly with look-back time. The distribution of the barred galaxies within the clusters shows two interesting features represented in Figure 2. The left panel shows that the largest bars are preferentially found close to the cluster centers and the right panel indicates that the bar fraction

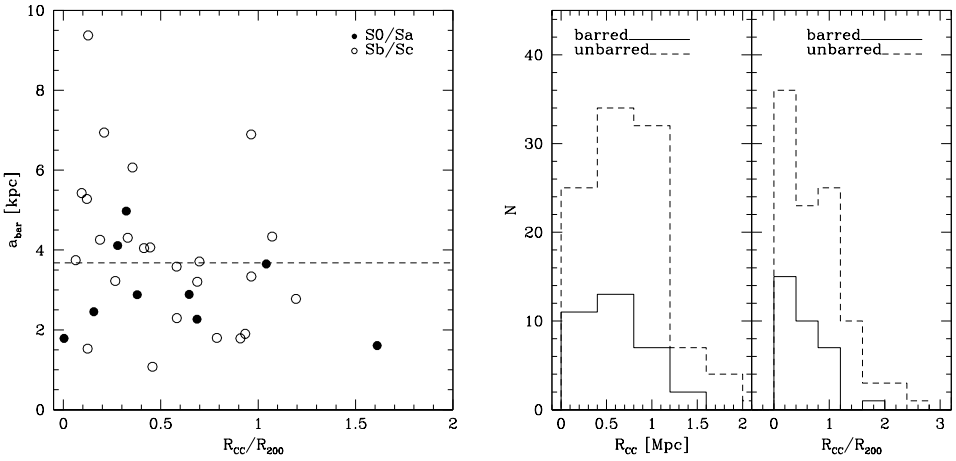

Figure 2. *Left* : The bar size as a function of normalized clustercentric distance for the spectroscopic cluster subsample (R_{200} is a measure of the virial radius). The dashed line indicates the mean bar size for this sample of 3.68 kpc. *Right* : The distribution of the disk galaxies with respect to the clustercentric distance (left) and the normalized clustercentric distance (right) for the spectroscopic subsample.

is somewhat larger near the cluster centers than at larger radii. For the R_{CC} distribution, the bar fraction declines from 31% in the central bin to 18% at ~ 1 Mpc. For the R_{CC}/R_{200} distribution, the corresponding values are 29% in the central bin and 22% at R_{200}. We have to stress though that the sample used is rather small, but we can safely say that barred galaxies do not avoid the cluster center.

The question whether internal or external factors are more important for bar formation and evolution cannot be answered definitely. On the one hand, the bar fraction and properties of cluster and field samples of disk galaxies are quite similar, indicating that internal processes are crucial for bar formation. On the other hand, we find evidence that cluster centers are favorable locations for bars, which suggests that the internal processes responsible for bar growth are supported by the typical interactions taking place in such environments.

References

Andersen, V. 1996, AJ, 111, 1805
Aguerri, J. A. L., Méndez-Abreu, J., & Corsini, E. M. 2009, A&A, 495, 491
Barazza, F. D., Jogee, S., & Marinova, I. 2008, ApJ, 675, 1194
Bournaud, F., & Combes, F. 2002, A&A, 392, 83
Desai, V., et al. 2007, ApJ, 660, 1151
Elmegreen, B. G., Elmegreen, D. M., & Hirst, A. C. 2004, ApJ, 612, 191
Eskridge, P. B., et al. 2000, AJ, 119, 536
Halliday, C., et al. 2004, A&A, 427, 397
Jogee, S., Scoville, N., & Kenney, J. D. P. 2005, ApJ, 630, 837
Jogee, S., et al. 2004, ApJ, 615, L105
Kormendy, J., & Kennicutt, R. C., Jr. 2004, ARA&A, 42, 603
Marinova, I., & Jogee, S. 2007, ApJ, 659, 1176

Marinova, I., et al. 2009, ApJ, 698, 1639
Milvang-Jensen, B., et al. 2008, A&A, 482, 419
Reese, A. S., Williams, T. B., Sellwood, J. A., Barnes, E. I., & Powell, B. A. 2007, AJ, 133, 2846
Sakamoto, K., Okumura, S. K., Ishizuki, S., & Scoville, N. Z. 1999, ApJ, 525, 691
Sheth, K., et al. 2008, ApJ, 675, 1141
Thompson, L. A. 1981, ApJ, 244, L43
van den Bergh, S. 2007, AJ, 134, 1508
White, S. D. M., et al. 2005, A&A, 444, 365

GALAXY EVOLUTION: EMERGING INSIGHTS AND FUTURE CHALLLENGES
ASP Conference Series, Vol.
@jourvol, © 2009
S. Jogee, I. Marinova, L. Hao, and G. A Blanc

Detection of a Distinct Pseudobulge Hidden Inside the "Box-Shaped Bulge" of NGC 4565

John C. Barentine and John Kormendy

University of Texas at Austin, Department of Astronomy, 1 University Station, C1400 Austin, TX 78712, USA

Abstract. N-body simulations show that "box-shaped bulges" of edge-on galaxies are not bulges at all: they are bars seen side on. The two components that we readily see in edge-on Sb galaxies like NGC 4565 are a disk and a bar. But face-on SBb galaxies always show a disk, a bar, and a (pseudo)bulge. Where is the (pseudo)bulge in NGC 4565? We use archival Hubble Space Telescope K-band images and *Spitzer* Space Telescope 3.6 μm wavelength images to penetrate the dust in NGC 4565. We find a high surface brightness central stellar component that is clearly distinct from the boxy bar and from the galaxy's disk. Its minor-axis profile has a Sérsic index of 1.33 ± 0.12, so it is a pseudobulge. The pseudobulge has the smallest scale height ($\sim$90 pc) of any component in the galaxy. This is in contrast to a scale height of $\sim$740 pc for the boxy bar plus thin disk. The disky pseudobulge is also much less luminous than the boxy bar, so the true pseudobulge-to-total luminosity ratio of the galaxy is much less than previously thought. We infer that the (pseudo)bulge-to-total luminosity ratios of edge-on galaxies with box-shaped bulges have generally been overestimated. Therefore more galaxies than we have recognized contain little or no evidence of a merger-built classical bulge. This presents a challenge to our picture of galaxy formation by hierarchical clustering, because it is difficult to grow big galaxies without also making a big classical bulge. Solving the puzzle of the "missing pseudobulge" in NGC 4565 further increases our confidence that we understand box-shaped bulges correctly as edge-on bars. This in turn supports our developing picture of the formation of pseudobulges—both edge-on bars and disky central components—by secular evolution in isolated galaxies.

1. Motivation

Hierarchical clustering of galaxies dominated their evolution in the early Universe but is currently yielding to internal, slow ("secular") evolution. The evolution of galaxies via interactions with collective phenomena like bars and spiral structure is well-established (Kobulnicky & Kewley 2004). N-body simulations suggest that bars heat up in the axial direction and explain the morphology of so-called "box-shaped" bulges of some edge-on galaxies (Combes & Sanders 1981). These secular processes drive gas toward the galactic center, building to high densities and often triggering starbursts. In the process, bulge-like ("pseudobulge") structures are produced mimicking "classical" (i.e., merger-built) bulges. These structures are easy to identify in nearly face-on objects such as NGC 4608, a normal, early-type barred galaxy shown in Figure 1. The disk, bar and pseudobulge are clearly discernible in this image. To what extent are these same components seen in (nearly) edge-on galaxies?

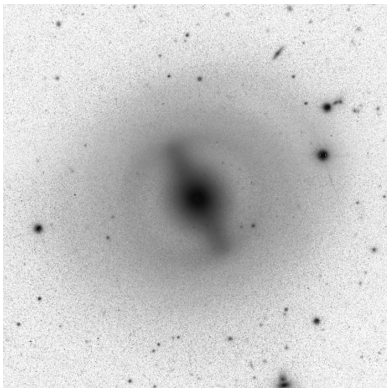

Figure 1. The nearly face-on SB0 galaxy NGC 4608 in a *gri* composite image from the Sloan Digital Sky Survey.

An edge-on galaxy with a box-shaped bulge that we can use to check this is NGC 4565. Short-wavelength imagery shows a prominent dust lane in NGC 4565 that may hide interior structures due to the shallow viewing angle. Infrared images of this galaxy penetrate the dust and show the disk and the edge-on bar manifesting as a box-shaped bulge. Using infrared data from the *Spitzer* Space Telescope and Hubble Space Telescope (HST), we set out to (1) search for the underlying pseudobulge that our picture of secular evolution tells us should exist, and (2) determine the scale heights for the various components of the galaxy.

2. Method

In edge-on galaxies, extinction at optical wavelengths is large along the sightline through the highly inclined disk. Observations in infrared solve this problem. We used 3.6 μm *Spitzer*/IRAC archive images to see through the dust and measure the minor axis light profile of NGC 4565. The imagery is shown in Figure 2 with stretches emphasizing the box-shaped bulge (top) and the central pseudobulge (bottom). We supplemented the *Spitzer* data at small radii with NICMOS F160W imagery from the HST archive; the higher spatial resolution of the NICMOS data allowed us to measure the Sérsic index of the pseudobulge. Profiles were measured by taking vertical cuts along the minor axis of NGC 4565 after registering the HST and *Spitzer* images. Surface photometry was done using these cuts, from which we performed a three-component decomposition into a central Sérsic function for the pseudobulge, another Sérsic function for the boxy bulge, and an outer exponential. The data and fits are shown in Figure 3.

3. Results

We find that the innermost component of the decomposition is best fit by a profile with Sérsic index $n = 1.33 \pm 0.12$, consistent with a pseudobulge rather than a classical bulge (Fisher & Drory 2008). Excluding the faint thick disk

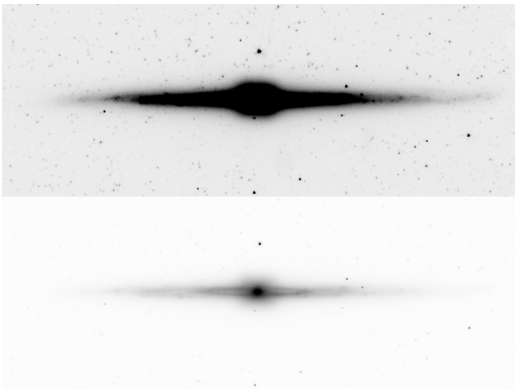

Figure 2. *Spitzer*/IRAC 3.6 μm image of NGC 4565 presented in two different stretches, emphasizing the boxy bar (top) and the inner ring and pseudobulge (bottom).

and halo, the thickest parts of the galaxy are in decreasing order of thickness: the edge-on bar, the thin disk, and the pseudobulge. The boxy bar and thin disk have a combined scale height of $10\farcs5$ ($\sim$740 pc at a distance of 14.5 Mpc; Wu et al. 2002), while the pseudobulge scale height is only $1\farcs2$ ($\sim$90 pc). Wu et al. (2002) fit a profile to the "bulge" in NGC 4565, defining this structure as what remained after subtracting fitted profiles for the disks and halo. Their fitted scale height for the structure we interpret as a pseudobulge is 0.65 kpc. Our value compares favorably with theirs, but they fitted an exponential rather than a Sérsic function to their optical data and claim that photometry alone cannot resolve uncertainty about whether the box structure is a bar or not. We assert that when the real bulge in NGC 4565 is revealed to be a pseudobulge, interpretation of the structures becomes more straightforward.

Simien & de Vaucouleurs (1986) find the bulge-to-total light ratio $B/T = 0.4$ for NGC 4565, but B refers to the boxy bar—not the pseudobulge within. Figure 2 shows that the pseudobulge is clearly less luminous than the boxy structure. If NGC 4565 were seen face-on, light from the apparent box-shaped bulge would be recognized as a bar and would lead to a lower B/T value. Previously measured B/T ratios of edge-on galaxies with box-shaped bulges are probably overestimates given this reasoning.

4. Conclusions

The interpretation of boxy bulges in edge-on galaxies as signature of bars is more believable if we find pseudobulges like those associated with bars in face-on galaxies. Our discovery of the pseudobulge in NGC 4565, distinct from the box-shaped bar previously thought to be the bulge, increases confidence in our picture of secular evolution. Furthermore, B/T ratios in edge-on galaxies with boxy bulges are smaller than previously believed. Published B/T values for most edge-on galaxies must be inconsistent with those derived for their face-on counterparts. Finally, overestimates of B/T in edge-on galaxies present a problem with respect to CDM galaxy formation. The disk of NGC 4565 rotates

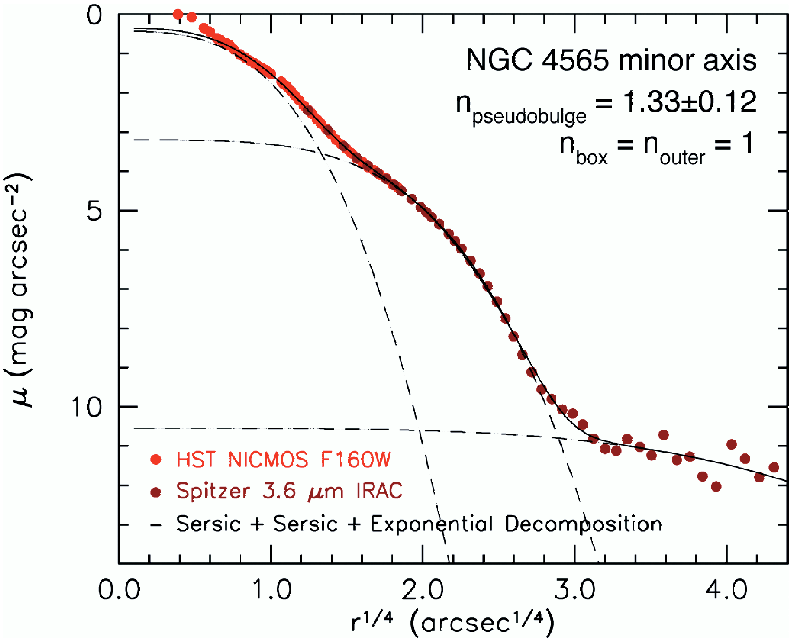

Figure 3. The measured brightness profile of the center of NGC 4565 along the minor axis from HST/NICMOS F160W (circles) and *Spitzer*/IRAC 3.6 μm data (triangles). The dashed lines show a decomposition of the profile into components in order of increasing radius: the pseudobulge (Sérsic), box-shaped bar (Sérsic), and outer disk (exponential). The solid line is the sum of the components.

at 255 $\pm$ 10 km s^{-1} interior to the outer warp (Rupen 1991); it has thus grown to great mass while showing no evidence for a major merger. It is difficult to reconcile these observations in the context of a hierarchically clustering universe.

Acknowledgments. These results are based on observations made with the *Spitzer* Space Telescope, which is operated by the Jet Propulsion Laboratory, California Institute of Technology under a contract with NASA. Additional data from the NASA/ESA Hubble Space Telescope were used, obtained from the data archive at the Space Telescope Institute, operated by the association of Universities for Research in Astronomy, Inc. under the NASA contract NAS 5-26555. This work was supported by the National Science Foundation under grant AST-0607490. The image of NGC 4608 was furnished by David W. Hogg, Michael R. Blanton, and the Sloan Digital Sky Survey Collaboration.

References

Combes, F. & Sanders, R. H. 1981, A&A, 96, 164
Fisher, D. B. & Drory, N. 2008, AJ, 136, 773
Kormendy, J. & Kennicutt, Jr., R. C. 2004, ARA&A, 42, 603
Rupen, M. P. 1991, AJ, 102, 48
Simien, F. & de Vaucouleurs, G. 1986, ApJ, 302, 564
Wu, H., et al. 2002, AJ, 123, 1364

GALAXY EVOLUTION: EMERGING INSIGHTS AND FUTURE CHALLLENGES
ASP Conference Series, Vol.
@jourvol, © 2009
S. Jogee, I. Marinova, L. Hao, and G. A Blanc

Simulations of Long-Lived Double-Barred Galaxies

Juntai Shen[1] and Victor P. Debattista[2]

[1]*Department of Astronomy, University of Texas, Austin, Texas 78712, USA.*

[2]*Centre For Astrophysics, University of Central Lancashire, Preston, UK PR1 2HE*

Abstract. Many barred galaxies harbor small-scale secondary bars in the center. The evolution of such double-barred galaxies is still not well understood, partly because of a lack of realistic N-body models with which to study them. Here we report the generation of such systems in the presence of rotating pseudobulges. We demonstrate with high mass and force resolution collisionless N-body simulations that long-lived secondary bars can form spontaneously without requiring gas, contrary to previous claims. We find that secondary bars rotate faster than primary ones. The rotation is not rigid: the secondary bars pulsate, with their amplitude and pattern speed oscillating as they rotate through the primary bars. This self-consistent study supports previous work based on orbital analysis in the potential of two rigidly rotating bars. We also characterize the density and kinematics of the N-body simulations of the double-barred galaxies, compare with observations to achieve a better understanding of such galaxies. The pulsating nature of secondary bars may have important implications for understanding the central region of double-barred galaxies.

1. Introduction

Recent imaging surveys have revealed the frequent existence of nuclear bars in a large number of barred galaxies, e.g., Erwin & Sparke (2002) found that double-barred galaxies are surprisingly common: at least one quarter of their sample of 38 early-type optically-barred galaxies harbor small-scale secondary bars. They found that a typical secondary bar is about 12% the size of its primary counterpart. The facts that inner bars are also seen in near-infrared (e.g. Mulchaey, Regan, & Kundu 1997; Laine et al. 2002), and they are often found in gas-poor S0s indicate that most of them are stellar structures. Results from these surveys also show inner bars are at a random angle relative to the primary bars, implying that they are probably dynamically independent structures. Shlosman et al. (1989) invoked multiple nested bars to channel gas inflow into galactic centers to feed AGN, in a similar fashion as the primary bar drives gas inward. However, recent work suggests that this mechanism may not be as efficient as originally hoped (e.g. Maciejewski et al. 2002).

Simulations offer the best way to understand double barred systems. However, the decoupled nuclear bars that formed in early simulations did not last long. For example, the most long-lived nuclear bar in Friedli & Martinet (1993) lasted for less than two turns of the primary bar, corresponding to about 0.4 Gyr, which is far too short to explain the observed abundance of nested

bars. Furthermore, their models usually require substantial amounts of gas to form and maintain these nuclear bars. Heller, Shlosman, & Athanassoula (2007a,b) reported that nested bars form in a quasi-cosmological setting, but the amplitudes of the bars also seem to weaken rapidly after most of gas has formed stars (Heller et al. 2007a). Petitpas & Wilson (2004) found that 4 out of 10 double-barred galaxies contain very little molecular gas in the nuclear region. These clues suggest that large amounts of molecular gas may not be necessary to maintain central nuclear bars.

On the side of orbital studies, Maciejewski & Sparke (1997, 2000) discovered a family of loop orbits that may form building blocks of long-lived nuclear stellar bars (also Maciejewski & Athanassoula 2007). Their studies are very important for understanding double barred galaxies, but their models are not fully self-consistent, since nested bars in general cannot rotate rigidly through each other (Louis & Gerhard 1988). So fully self-consistent N-body simulations are still needed to check if their main results still hold when the non-rigid nature of the bars is taken into account.

Here we demonstrate that long-lived secondary bars can form in purely collisionless N-body simulations, when a rotating pseudobulge is introduced in the model (also Debattista & Shen 2007; Shen & Debattista 2009). The nuclear bars in our work are distinctly bars, and do not have a spiral shape. We show that the behavior of our models are in good agreement with the loop orbit predictions of Maciejewski & Sparke (2000). We also analyze the photometrical and kinematical properties of high resolution models. Our theoretical results can also be compared to the observed 2-D kinematics of some double-barred galaxies, to achieve a better understanding of the dynamics of the secondary bars.

2. Model Setup

Our high-resolution simulation consists of a live disk and bulge component. We do not include a halo component for simplicity, also because secondary bars are very small-scale phenomena in galactic centers where visible matter is dominant. The initial disk has the exponential surface density profile and Toomre's $Q \sim 2.0$. The bulge was generated using the method of Prendergast & Tomer (1970) as described in Debattista & Sellwood (2000), where a distribution function is integrated iteratively in the global potential, until convergence. The bulge has the mass of $M_{\rm b} = 0.2M_{\rm d}$. The bulge set up this way is un-rotating, we then give the rotation of the bulge by simply reversing the negative azimuthal velocities of all bulge particles into the same positive values. We have checked that systems set up this way are in very good virial equilibrium.

3. Results

Figure 1 shows the projected double-barred model (at $t = 405$ when the two bars are nearly perpendicular) with an ordinary orientation: the system is inclined at $i = 45^\circ$ with the line of nodes (LON) of $\psi_{\rm nuc} = 45^\circ$ relative to the secondary bar major axis. The surface density image and contours resemble many observed

double-barred systems, such as NGC 2950, even though we did not deliberately set out to match it.

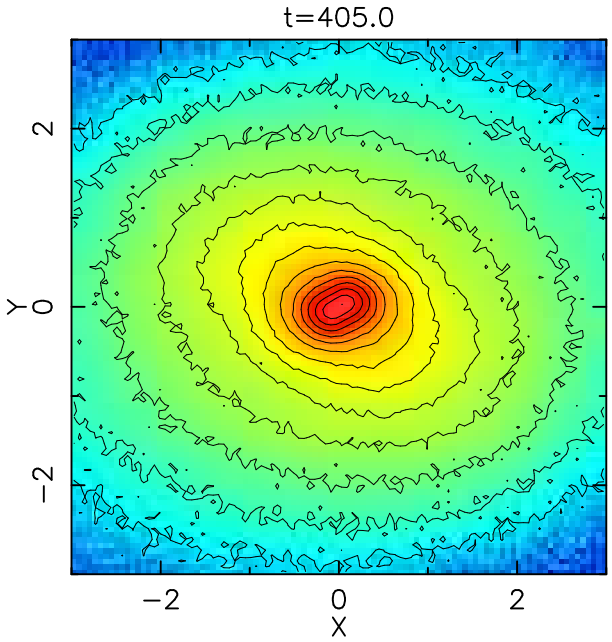

Figure 1. The double-barred model at $t = 405$ projected to $i = 45°$ and $\psi_{\rm nuc} = 45°$ with all particles shown. The model bears a passing resemblance to NGC 2950.

Figure 2 shows the behavior of the azimuthally averaged Ω, $\Omega \pm \kappa/2$, and the location of the Lindblad resonances of the bars at around $t = 400$. As shown in Debattista & Shen (2007), the pattern speeds of the bars, especially that of the secondary, vary as they rotate through each other: the secondary bar rotates slower than average when the two bars are perpendicular, and faster when the bars are parallel. The patten speed bands shown in Figure 2 reflect such variations. Clearly the pattern speed of the secondary bar oscillates much more than that of the primary.

We also analyzed the line-of-sight velocity distribution (LOSVD) by measuring the mean velocity $\overline{v}$ and velocity dispersion σ. Departures from a Gaussian distribution are parameterized by Gauss-Hermite moments (Gerhard 1993; van der Marel & Franx 1993; Bender, Saglia, & Gerhard 1994). The second order term in such an expansion is related to the dispersion. h_3 measures deviations that are asymmetric about the mean, while h_4 measures the lowest order symmetric deviations from Gaussian (negative for a "flat-top" distribution, and positive for a more peaked one).

The most striking feature in Figure 3 is that the twist of the kinematic minor axis (i.e. $v_{\rm los} = 0$) in the secondary bar region is weak (see the mean velocity maps in Figure 3a, 3b). The kinematic minor axis is almost perpendicular to the inclination axis, although there is a small but noticeable twisted pinch near the kinematic minor axis in the nuclear region. The weak central twist is mainly due to the relatively large velocity dispersion, especially in the central region

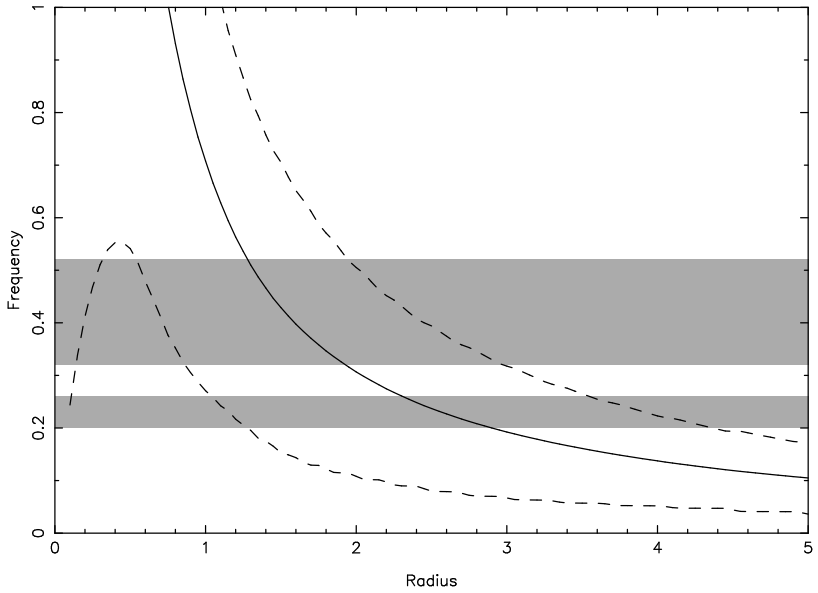

Figure 2. Frequencies as a function of radius at around $t = 400$ for run D, calculated based on the azimuthally averaged gravitational attraction. The full-drawn line shows the curve of the circular angular frequency Ω and the dashed curves mark $\Omega \pm \kappa/2$, where κ is the epicyclic frequency. The two shaded bands show the oscillational ranges of the bar pattern speeds (the upper band is for the secondary bar and the lower one is for the primary).

(likewise at $t = 20$ when only the small nuclear bar exists, the stellar twist is stronger than at $t = 405$, but still quite small compared to the expected twist in gaseous kinematics). On the other hand, the twist of the kinematic *major* axis is more prominent in the central region. Moiseev, Valdés, & Chavushyan (2004) found the stellar kinematic minor axis hardly twists from the PA of the disk in their sample with the most reliable kinematics, leading them to question whether nuclear photometric isophotal twists represent *bona fide* dynamically decoupled secondary bars. We demonstrate that an authentic decoupled secondary bar may indeed produce a very weak twist of the kinematic minor axis in the stellar velocity field. So a central stellar velocity map without a strong twist as in Moiseev et al. (2004) does not necessarily exclude the existence of a decoupled nuclear bar.

The general agreement between our simulations and observations of double barred galaxies gives us confidence that the simulations are capturing the same dynamics as in nature. This is especially remarkable because secondary bars are not merely scaled down versions of primary bars, but have distinctly different kinematic properties. In the absence of self-consistent simulations, earlier orbit-based models could not directly confront the challenge from observations which found such differences. This demonstrates the advantage of finally being able to simulate stellar double-barred galaxies, which had been puzzling for so long.

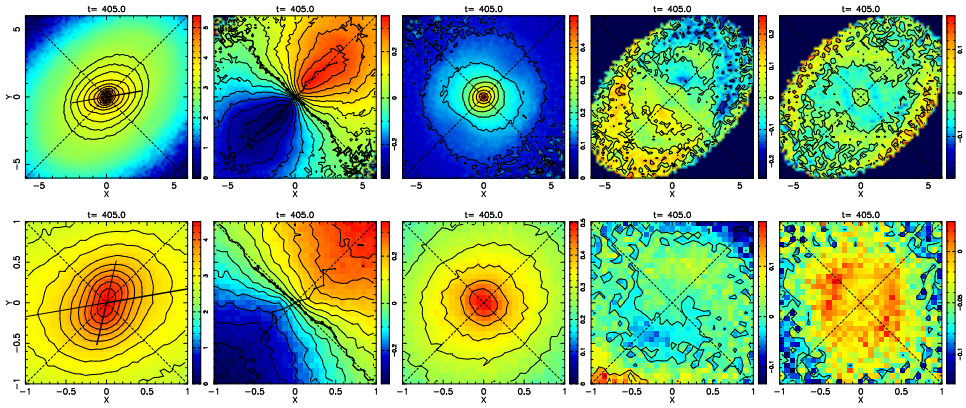

Figure 3. Photometrical and kinematic maps of our double-barred model. For each row from left to right are the projected surface density, mean velocities, velocity dispersion, h_3, and h_4 maps. (a): Row 1, the double-barred model at $t = 405$ inclined at 45° with the LON of 45° relative to the primary bar major axis; (b): Row 2, close-up view of (a). One of the dashed lines represents the line of nodes (45°), while the other dashed is the anti-LOS (135°).

References

Bender, R., Saglia, R. P., & Gerhard, O. E. 1994, MNRAS, 269, 785
Debattista, V. P., & Sellwood, J. A. 2000, ApJ, 543, 704
Debattista, V. P., & Shen, J. 2007, ApJ, 654, L127
Erwin, P., & Sparke, L. S. 2002, AJ, 124, 65
Friedli, D., & Martinet, L. 1993, A&A, 277, 27
Gerhard, O. E. 1993, MNRAS, 265, 213
Heller, C. H., Shlosman, I., & Athanassoula, E. 2007a, ApJ, 657, L65
Heller, C. H., Shlosman, I., & Athanassoula, E. 2007b, ApJ, 671, 226
Laine, S., Shlosman, I., Knapen, J. H., & Peletier, R. F. 2002, ApJ, 567, 97
Louis, P. D., & Gerhard, O. E. 1988, MNRAS, 233, 337
Maciejewski, W., & Athanassoula, E. 2007, MNRAS, 380, 999
Maciejewski, W., & Sparke, L. S. 1997, ApJ, 484, L117
Maciejewski, W., & Sparke, L. S. 2000, MNRAS, 313, 745
Maciejewski, W., Teuben, P. J., Sparke, L. S., & Stone, J. M. 2002, MNRAS, 329, 502
Moiseev, A. V., Valdés, J. R., & Chavushyan, V. H. 2004, A&A, 421, 433
Mulchaey, J. S., Regan, M. W., & Kundu, A. 1997, ApJS, 110, 299
Petitpas, G. R., & Wilson, C. D. 2004, ApJ, 603, 495
Prendergast, K. H., & Tomer, E. 1970, AJ, 75, 674
Shen, J., & Debattista, V. P. 2009, ApJ, 690, 758
Shlosman, I., Frank, J., & Begelman, M. C. 1989, Nat, 338, 45
van der Marel, R. P., & Franx, M. 1993, ApJ, 407, 525

GALAXY EVOLUTION: EMERGING INSIGHTS AND FUTURE CHALLLENGES
ASP Conference Series, Vol.
@jourvol, © 2009
S. Jogee, I. Marinova, L. Hao, and G. A Blanc

Beyond the *Best-Fit* Parameter: New Insight on Galaxy Structure Decomposition from GALPHAT

Ilsang Yoon, Martin D. Weinberg and Neal S. Katz

Department of Astronomy, University of Massachusetts, Amherst, USA

Abstract. We introduce a novel image decomposition package, GALPHAT, that provides robust estimates of galaxy surface brightness profiles using Bayesian Markov Chain Monte Carlo. The GALPHAT-determined posterior distribution of parameters enables us to assign rigorous statistical confidence levels to maximum a posteriori estimates and to test complex galaxy formation and evolution hypotheses. We describe the GALPHAT algorithm, assess its performance using test image data, and demonstrate that it has sufficient speed for production analysis of a large galaxy sample. Finally we briefly introduce our ongoing science program to study the distribution of galaxy structural properties in the local universe using GALPHAT.

1. What and Why is GALPHAT?

Large photometric and spectroscopic surveys of galaxies (e.g., SDSS, York et al. 2000 and 2MASS, Skrutskie et al. 2006) continue to provide vast ensembles of galaxy images, but rigorous conclusions about galaxy formation and evolution hypotheses based on the full volume of information present serious computational and algorithmic challenges. For example, parametric models are widely used to derive galaxy structural parameters: brightness, size, profile shape and ellipticity. A recent study (Allen et al. 2006) presented a bulge-disc decomposition for 10^4 nearby galaxies. However, an accurate decomposition is stymied by degeneracies in the parameter estimation itself. A Sérsic profile has 8 parameters, and the topology of the likelihood function in this high-dimensional parameter space is too complex to visualize and hard to characterize robustly. In most previous galaxy decomposition analyses, the uncertainties of derived model parameters have not been carefully characterized. The correlations of physical properties and structural parameters of galaxies are usually assessed through *scatter* plots of the *best-fit* parameters (e.g., maximum a posteriori estimates with formal inverse Hessian variance estimates). These correlations are subject to strong contamination by underlying systematic correlations of each model parameter.

A Bayesian approach to parameter inference and hypothesis testing naturally addresses these difficulties. The probability of model parameters (M) for a given data set (D), $P(M|D)$, is related to the probability of the data given the model (the likelihood), $P(D|M)$, and prior probability of the model, $P(M)$, through Bayes theorem:

$$P(M|D) = \frac{P(D|M)P(M)}{P(D)} = \frac{P(D|M)P(M)}{\int P(D|M)P(M)dM} \quad (1)$$

In our galaxy decomposition problem, M is the vector of parameters describing the model and D is the image data. For a high-dimensional model space, direct integration is infeasible, and one resorts to Markov Chain Monte Carlo (MCMC) methods. Although costly, sampling the posterior using MCMC returns a robust estimate of the model parameters. From this distribution, one may also define a *best-fit* parameter value and confidence bounds, but the real power in this approach is the natural description by the posterior distribution of any intrinsic correlation between model parameters. This power comes at a cost: Bayesian MCMC requires much more computation time than χ^2 minimization. To make this feasible for present-day surveys with large numbers of galaxies, we present a novel image decomposition package GALPHAT (GALaxy PHotometric ATtributes[1]) which uses a state-of-the-art Bayesian computation software package BIE (Bayesian Inference Engine[2]) for sampling MCMC efficiently and incorporates an optimized image processing algorithm to reduce the likelihood evaluation time. We will introduce the algorithm, test its performance, and present science using GALPHAT in the following sections.

2. The GALPHAT Algorithm

Given a parameter vector M, GALPHAT produces a likelihood function for an image (pixel data, mask, PSF, background) and the BIE samples the posterior for a prior distribution using an MCMC algorithm. The BIE provides a choice of MCMC algorithm depending on the complexity of the problem. To date, we have found that a multiple chain algorithm with tempering (Geyer & Thompson 2005) is a good compromise between speed and flexibility. For the tests described here, GALPHAT models the galaxy surface brightness using multiple 2D Sérsic profiles with arbitrary ellipticities and position angles. For computational efficiency, GALPHAT pre-generates two-dimensional cumulative distributions of Sérsic profile with many different n using a rigorous error tolerance. By assigning pixel values by table interpolation, GALPHAT generates a model image with arbitrary axis ratio b/a. Image rotation is done in Fourier space using three shear operations; a rotation matrix is decomposed into three sequential shear matrices in the X, Y, and X directions and then each shear operation is carried out using the Fourier shift theorem (Larkin, Oldfield, & Klemm 1997). Then, the model image is convolved with a given PSF and an adjustable flux pedestal with a spatial gradient is added to model the sky background. GALPHAT uses a Poisson likelihood function to describe the photon counting process. A more detail description of the algorithm will be published in upcoming method papers Yoon et al. (2009) and Weinberg et al. (2009).

---

[1]GALPHAT web page: `http://sites.google.com/site/galphat/galphat`

[2]For more information, see `http://www.astro.umass.edu/BIE` and Weinberg et al. (2009)

3. GALPHAT Performance Test Using Synthetic Galaxy Images

For a given signal-to-noise ratio S/N, we generate an ensemble of 100 synthetic Sérsic profile galaxy images over a wide range of magnitude, effective radius r_e, Sérsic index n, axis ratio $q = b/a$ and position angle. The parameter posterior distribution for each individual galaxy is sampled using MCMC and summed to obtain the ensemble distribution of structural parameter for a given S/N. We define S/N as the ratio of the total flux from the source and the noise within galaxy r_e.

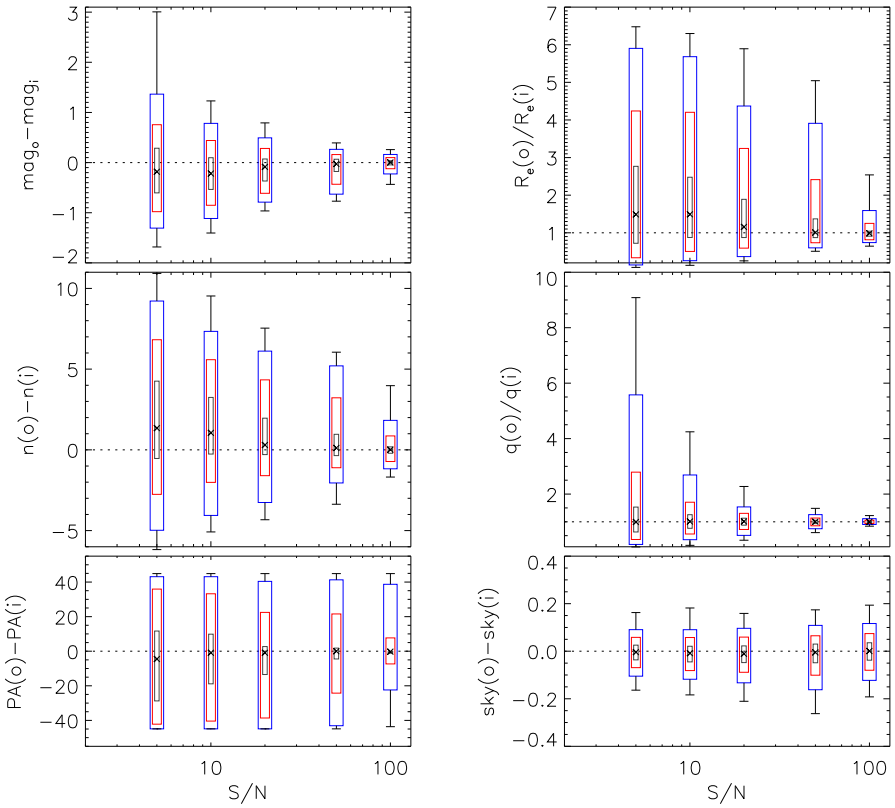

Figure 1. The differences between GALPHAT posterior medians (cross) and the true input values for a given S/N. Boxes with different sizes are 68.3 (small), 95.4 (medium) and 99.7% (large) CL. The GALPHAT inference is very robust over all S/N. However magnitude, r_e and n are slightly biased if S/N ≤ 10 and the posteriors of n and r_e have a tail toward large values. Also when galaxy S/N is low, the axis ratio q, if it is small, has a probability of overestimation, which leads to skewed distribution with tail.

GALPHAT successfully recovers the input parameter values. FIGURE 1 shows the GALPHAT posterior median (cross) and 68.3, 95.4 and 99.7% confidence level (CL) with increasing box size and minimum and maximum values (end bars). The posterior distributions of r_e and q are scaled by their input parameters and all other distributions are differenced from the input parameters.

GALPHAT posterior is consistent and encloses true input parameter within 68.3% CL even in the case of low S/N ≤ 10.

MCMC convergence may be slow in high-dimensional parameter spaces owing to the complexity of the likelihood function. We have found it productive to iteratively add image information using a hierarchy of successively aggregated images. Beginning with the most aggregated image (Level 0) one computes the posterior, $P(\theta|D_0)$. The posterior for the next level (Level 1) is $P(\theta|D_1) \propto P(\theta|D_0)[P(D_1|\theta)/P(D_0|\theta)]$ and so on. Using this hierarchical data structure, GALPHAT reduces the run time by factors of two, depending on the level of aggregation, by accelerating convergence. Also, the BIE checkpoints the full state of the simulation, efficiently enabling the posterior distribution to be augmented at a later date.

GALPHAT can be run on either a single CPU or in a cluster environment. TABLE 1 provides GALPHAT runtimes for a simple one-component decomposition. Of course, in addition to computing hardware, the time for your parameter estimate will depend on image size, characteristics of the model, the MCMC algorithm, the convergence diagnostic method, and the required number of posterior samples. More detailed results will be shown in the methods paper (Yoon et al. 2009).

Table 1. WALL CLOCK TIME FOR GALPHAT

Image	samples	CPU	Processors	Level	runtime
200 by 200 single Sérsic	20,000	AMD Athlon(tm) MP 1800+ 1533 MHz	8	1	2 hr
200 by 200 single Sérsic	20,000	AMD Athlon(tm) MP 1800+ 1533 MHz	8	2	40 min

4. Ongoing Science Program Using GALPHAT

We are currently performing a bulge+disk model decomposition of 2MASS K_s band selected galaxies with $7 < K_s < 11$ to derive luminosity functions for each component in the present day Universe. We will investigate the effect of environment on these distributions. From these, we can compare to mass assembly histories predicted from hierarchical galaxy formation theories.

Acknowledgments. We thank Dr. Daniel McIntosh and Mr. Yicheng Guo for useful discussions and providing sample images in early stage of this work. This work has been supported in part by the NSF Grant IIS 0611948 and by the NASA AISR Program Grant NNG06GF25G.

References

Allen, P. D., et al. 2006, MNRAS, 371, 2
Geyer, C. J., & Thompson, E. A. 2005, JASA, 90, 909
Larkin, K. G., Oldfield, M. A., & Klemm, H. 1997, Optics Communications
Skrutskie, M., et al. 2006, AJ, 131, 1163

Weinberg, M. D., et al. 2009, in preparation
Yoon, I., et al. 2009, in preparation
York, D., et al. 2000, AJ, 120, 1579

GALAXY EVOLUTION: EMERGING INSIGHTS AND FUTURE CHALLLENGES
ASP Conference Series, Vol.
@jourvol, © 2009
S. Jogee, I. Marinova, L. Hao, and G. A Blanc

Analytical Galactic Models with Mild Cusps

Tanja Rindler-Daller

Institut für Theoretische Physik, Universität zu Köln, Zülpicher Strasse 77, 50937 Cologne, Germany

Abstract. High-resolution observations of early-type galaxies have shown that their nuclear surface brightness and corresponding stellar mass densities are characterized by cusps. We present a new class of spherical analytical potential-density pairs describing mild cuspy centres. We study isotropic and anisotropic models of Osipkov-Merritt type. The associated distribution functions and intrinsic velocity dispersions can be represented analytically in a unified way in terms of hypergeometric functions for a large range of parameters. This allows for an easy comparison of these important quantities for underlying mass densities having varying degrees of central cuspiness or radial falloff.

1. Introduction

In the past two decades, it has been established by observations that the nuclear surface brightness and corresponding stellar mass densities of early-type galaxies are characterized by cusps. The construction of galactic models incorporating cuspy centres has therefore been an active part of theoretical modeling. Analytical spherical models with cusps have been presented e.g. in Dehnen (1993), Tremaine et al. (1994), Zhao (1996) and more recently in Baes & Dejonghe (2004) and Buyle, Hunter & Dejonghe (2007). However, many models in the literature, which are able to capture varying cusp strengths, are rather inflexible with regard to the outer falloff behaviour or vice versa. This note is a summary of Rindler-Daller (2009), where we present a spherical model family which allows more flexibility in the central as well as in the outer radial shape of the stellar mass density. We start from a family of non-singular, quite general potentials for the stellar component. All further intrinsic quantities can be calculated analytically, notably the distribution functions, for which an analytical representation for a large range not mere for a little subset of parameters is possible, providing thus a straightforward study of the relation between the cuspiness of the density and the behaviour of the corresponding intrinsic velocity dispersion and distribution function, than it would be without analytical expressions at hand. To this aim, we consider an isotropic as well as an anisotropic parametrization of our models. The family presented below is able to model the cuspy centres of massive early-type galaxies and nucleated dwarf elliptical galaxies. Our models may also serve as useful input for numerical studies on the time-dependent evolution of galactic nuclei.

2. Potential-Density Pair

We adopt the following family of spherical (relative) potentials

$$\Psi(r) = \frac{b^{\alpha\gamma}}{(b^\alpha + r^\alpha)^\gamma} \tag{1}$$

with b a positive number, and $\Psi(r) \sim r^{-\alpha\gamma}$ as $r \to \infty$. We choose the slope parameters according to $0 < \alpha \leq 2$ and $\gamma > 0$. The corresponding *self-consistent* mass density to (1) is

$$\rho(r) = \frac{b^{\alpha\gamma+2}}{1+\alpha} \frac{(1+\alpha)b^\alpha + (1-\alpha\gamma)r^\alpha}{r^{2-\alpha}(b^\alpha + r^\alpha)^{\gamma+2}}, \tag{2}$$

which is positive for $\alpha\gamma \leq 1$ and this restriction is imposed throughout. For $\alpha = 2$, the central density is finite. Otherwise, there is a cusp with $\rho(r) \sim r^{-2+\alpha}$. For large r, the density goes like $\rho(r) \sim r^{-2-\alpha\gamma}$. The above family includes a lot of known models as special cases: For instance, the Plummer model is recovered by setting $\alpha = 2, \gamma = 1/2$. For $\alpha = 1$, the Hernquist (1990) model follows for $\gamma = 1$. Other special cases obtained in the literature include $\alpha = 1/2, \gamma = 2$ and $\alpha = 1, \gamma = \beta - 3$ with $\beta \leq 4$, see Zhao (1996). In order to recover the cusps of the models of Dehnen (1993) and Tremaine et al. (1994), one had to put $\alpha = 1/n, n \in \mathbf{N}$. On the other hand, the outer falloff is recovered by setting $\gamma = 1/n$. Both conditions at once can not be fulfilled to recover the full models of the above authors. However, we note that those models do not include mild cusps with $0 < 2 - \alpha < 1$ whereas our density does. The associated cumulative mass function to (1) goes for large radii as $M(r) \sim r^{1-\alpha\gamma}$, therefore only models with $\alpha\gamma = 1$ have a finite total mass. In terms of the circular velocity, this amounts to $v_c \sim r^{-\alpha\gamma/2}$ for large r, hence the circular velocity is Keplerian only for $\alpha\gamma = 1$, and decreases more slowly for $\alpha\gamma < 1$. In the limit $\alpha\gamma \to 0$ it becomes constant. However, for any fixed product $\alpha\gamma \in (0, 1)$, the increase in the cumulative mass function is not as severe as it is for instance for the familiar logarithmic potential of Binney (1981) where $M(r) \sim r$ for large r. Due to its ability to reproduce constant or rising mass and velocity profiles at large radii, the above potential may be also useful for modeling dark matter structures. However, we restrict to self-consistent models and then the drawback of unbounded $M(r)$ must be relieved in practice by adopting an appropriate cutoff radius r_* with $M(r) = M_*$ for $r \geq r_*$.

The projected quantities follow straightforwardly, but must be determined numerically for our model family (1) - (2), except in the case of flat density cores $\alpha = 2$, where analytical expressions can be derived. Concerning the surface brightness associated to (2), it can be easily shown that they rise steeply with decreasing α as the projected radius tends to zero, since then there is more stellar mass concentrated in the nuclear region and this behaviour is more pronounced for larger values of γ.

3. Distribution Functions and Intrinsic Velocity Dispersions

We consider isotropic models with the distribution function depending on the relative energy $\mathcal{E} = -E$ as well as anisotropic Osipkov-Merritt models, where it

depends on $\mathcal{E}$ and the angular momentum L via $Q = \mathcal{E} - L^2/(2r_a^2)$ (see Merritt 1985; Osipkov 1979), where the anisotropy radius r_a is a free parameter and $\beta(r) = r^2/(r_a^2 + r^2)$, hence the models are isotropic in the centres.

As is shown in Rindler-Daller (2009), the corresponding distribution functions (DFs) can be determined analytically in terms of Beta functions and general hypergeometric series provided that $2/\alpha = n, 1/\gamma = m$ and $2/(nm) \leq 1$ with $n, m \in \mathbf{N}$. In case of the flat core models $\alpha = 2$, the only restriction on the value of γ, however, is to be $\leq 1/2$.

In Fig.1, we show plots of the isotropic and anisotropic DFs, $f(\mathcal{E})$ and $f_a(Q)$, respectively, for four models. The depth of the central potential well is finite, $\Psi(0) = \mathcal{E}_{max} = 1$ and, as a result, the distribution functions $f(\mathcal{E})$ diverge for $\mathcal{E} \to 1$. It can be seen that the models are mostly affected by α. As $\mathcal{E} \to 1$, a steeper inner cusp corresponds to a stronger divergence in this limit because the system is then dominated by stars at small radii where the cusp dominates and this effect is therefore hardly affected by γ. On the other hand, the decrease of $f(\mathcal{E})$ as $\mathcal{E} \to 0$ is larger for small values of γ. This is more pronounced if α is small as well because then the model is more centrally concentrated as a result of the cusp.

Likewise, the increase of $f_a(Q)$ for $Q \to 1$ is dominated by the cusp parameter α and the reason is the same as in the isotropic case. On the other hand, for fixed α the parameter γ controls essentially the degree of the anisotropy in the sense that the model is more anisotropic for small values of γ. Overall, the distribution functions do not decrease as rapidly for $Q \to 0$ as do the isotropic ones. It can also be easily shown that the models approach the isotropic behaviour for large $r_a > b$, as expected. In contrast, for $r_a < b$ the anisotropic signature in $f_a(Q)$ dominates over a wider range in Q, whereas the increase for $Q \to 1$ remains quite unaffected.

As is shown in Rindler-Daller (2009), all intrinsic velocity dispersions (IVs), isotropic as well as anisotropic ones, can be calculated analytically in terms of special hypergeometric functions. However, due to page limits we cannot plot them here. The isotropic IVs converge to zero as $r^{2\alpha}$ for $r \to 0$ if $\alpha < 2$. This sounds counterintuitive, but it is a typical behaviour of such models as long as no additional central black hole potential is added (e.g. Tremaine et al. 1994). For $\alpha = 2$, they are asymptotically constant, as expected. Moreover, the overall shape is flatter for increasing cuspiness. It can be shown that the projected velocity dispersions exhibit the same overall behaviour.

The anisotropic IVs decrease more slowly for small values of γ, i.e. for more anisotropic models. Concerning the overall shape, it can be shown that the tangential IVs fall off more rapidly for $r > b$ than the radial ones. For increasing cuspiness, the shape of both velocity dispersions becomes flatter, although this behaviour is much less pronounced than it is for the isotropic models.
The presence of a central point mass potential, mimicking a massive black hole, is also studied for the isotropic models. It can be shown that the velocity dispersions rise steeply at small radii for increasing black hole mass at fixed α which, in the same time, leads to higher values of the velocity dispersion at larger radii.

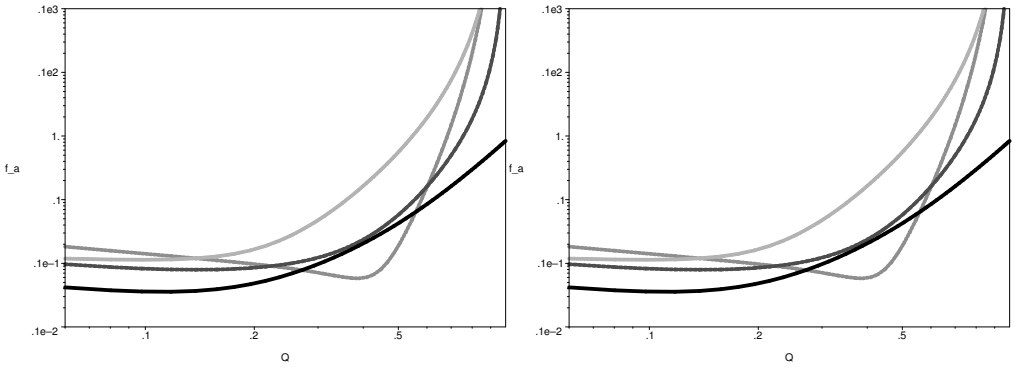

Figure 1. Log-log plots of the isotropic and anisotropic distribution functions for the models $\alpha = 2, \gamma = 1/3$ (black solid), $\alpha = 1, \gamma = 1/2$ (black dashed), $\alpha = 2/3, \gamma = 1$ (light grey), $\alpha = 1/2, \gamma = 1/2$ (dark grey); $G = 1 = b,\ r_a = 2$

4. Conclusions

In this note, we considered a family of non-singular potentials falling off as $1/r$ or more slowly at large radii. The associated self-consistent mass density incorporates flat or cuspy nuclear regions and shows a flexible falloff behaviour at large distances from the centre. The distribution functions and intrinsic velocity dispersions for the isotropic as well as for the anisotropic models can be represented analytically in terms of hypergeometric functions. This allows for a straightforward comparison between models of varying cuspiness and outer falloff in the mass density. It is shown that the anisotropy affects the distribution functions only outside the central parts where they do not fall off as rapidly as the isotropic ones, whereas the increase for large arguments is dominated by the cusp parameter in both cases. Moreover, the velocity dispersions decrease more rapidly for the less anisotropic models and their shape is flatter for increasing cuspiness.

References

Baes M., & Dejonghe H. 2004, MNRAS, 351, 18
Binney J. 1981, MNRAS, 196, 455
Buyle P., Hunter C., & Dejonghe H. 2007, MNRAS, 375, 773
Dehnen W. 1993, MNRAS, 265, 250
Hernquist L. 1990, ApJ, 356, 359
Merritt D. 1985, AJ, 90, 1027
Osipkov L.P. 1979, Sov.Astron.Lett., 5, 42
Rindler-Daller T. 2009, MNRAS, 396, 997
Tremaine S., Richstone D.O., Byun Y.-I., Dressler A., Faber S.M., Grillmair C., Kormendy J., Lauer T.R. 1994, AJ,107(2),634
Zhao H. 1996, MNRAS, 278, 488

GALAXY EVOLUTION: EMERGING INSIGHTS AND FUTURE CHALLLENGES
ASP Conference Series, Vol.
@jourvol, © 2009
S. Jogee, I. Marinova, L. Hao, and G. A Blanc

A Shared Tully-Fisher Relation for Spirals and S0 Galaxies

M. J. Williams, M. Bureau, and M. Cappellari

Sub-department of Astrophysics, University of Oxford, Denys Wilkinson Building, Keble Road, Oxford OX1 3RH, United Kingdom

Abstract. We measure the positions of the Tully-Fisher relations of a sample of 14 lenticular galaxies (S0s) and 14 spirals. We use two measures of rotational velocity. One is derived directly from observed spatially-resolved stellar kinematics and the other from the circular velocities of mass models that include a dark halo and whose parameters are constrained by detailed kinematic modelling. Contrary to the naive expectations of theories of S0 formation, we find no significant difference between the Tully-Fisher relations of the two sample when plotted as functions of both brightness and stellar mass.

1. Introduction

The Tully-Fisher (TF) relation is a widely-used and strong correlation between the maximum rotational velocity of spiral galaxies and their total magnitude. It follows naturally from the assumption that spiral galaxies have similar surface brightnesses profiles and approximately equal dynamical mass-to-light ratios for a given mass.

Many authors have argued that at least some S0 galaxies are the faded direct descendants of spiral galaxies (e.g. Dressler 1980; Dressler et al. 1997). Environmental processes such as strangulation (e.g. Larson et al. 1980) or ram-pressure stripping (e.g. Gunn & Gott 1972) may have stripped these galaxies of their gas and left them unable to form stars. This process should make only a slight change to their dynamical masses, but a significant change to their luminosities. Regardless of the particular mechanism by which S0s form, they are therefore generally expected to have higher mass-to-light ratios than spirals on average. They should therefore therefore have fainter luminosities for a given rotational velocity and lie below the TF relation defined by spiral galaxies.

Here we seek to test this prediction using long-slit stellar kinematics and detailed mass models for a sample of S0 galaxies and a control sample of spiral galaxies. A secondary goal is to investigate whether the size of the offset between the S0 and spiral TF relations (if one exists) changes when we plot a TF-like relation which uses mass rather than luminosity, as expected from the S0 formation mechanisms discussed above.

2. Data and Models

We use a sample of 14 early spirals (Sa and Sb) and 14 S0s. All of the galaxies are close to edge-on. Many of them have boxy bulges, which are believed to be bars viewed side-on (e.g. Kuijken & Merrifield 1995; Bureau & Freeman 1999).

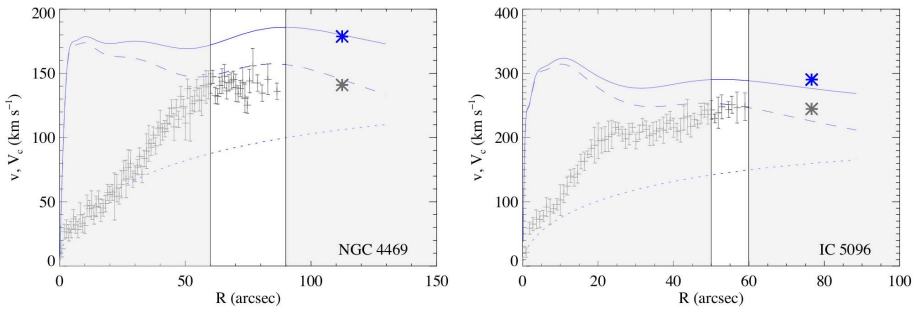

Figure 1. Example rotation curves. The data points show the observed line-of-sight velocities. The lines show the total circular velocities of the axisymmetric mass models (solid), the stellar components (dashed line) and dark halo components (dotted line). The kinematic quantities used in this work, v and V_c, are the mean of the data points and model in the unshaded radial region, chosen to be the flat region of the observed rotation curve. They are shown here as large stars.

The bar should not, however, affect the present results because we use maximum rotational velocities well outside of the bar regions and the bar fraction in the sample (≈ 75 per cent) is representative of that in the spiral galaxy population (≈ 65 per cent, see, e.g., Sheth et al. 2008 and references therein).

The major-axis long-slit stellar kinematic observations are presented in Chung & Bureau (2004). These data were observed and reduced identically for the spirals and S0s. We measure the maximum observed rotation velocity v directly from the stellar kinematics by taking the mean of the data points in the flat region of the rotation curve. Two sample rotation curves are shown in Figure 1.

In Williams et al. (2009) we modelled the mass distribution of each galaxy by assuming they are composed of an axisymmetric stellar component with a constant mass-to-light ratio and an NFW dark halo (Navarro et al. 1997). We determined the two parameters of the mass models (the stellar mass-to-light ratio and total halo mass) by comparing the observed second velocity moment to that predicted by solving the Jeans equations assuming a constant anisotropy (Cappellari 2008).

We compute the circular velocity curves of the galaxies from these models. Circular velocity is of course free from the effects of projection and asymmetric drift, which is particularly important when comparing S0s and spirals, because S0s have greater pressure support. We characterize the circular velocity by a single value V_c by taking its average at the same radii that were used to measure the maximum observed rotational velocity (see Figure 1).

We adopt errors in the observed velocity of half the difference between the approaching and receding sides. The uncertainties in the circular velocity curves are due to the errors in the parameters of the mass model, described in Williams et al. (2009).

We use total absolute magnitudes M_K at K-band derived from apparent magnitudes (and errors) taken from the 2MASS Extended Source Catalog (Skrutskie et al. 2006) and distances (and errors) from the NASA/IPAC

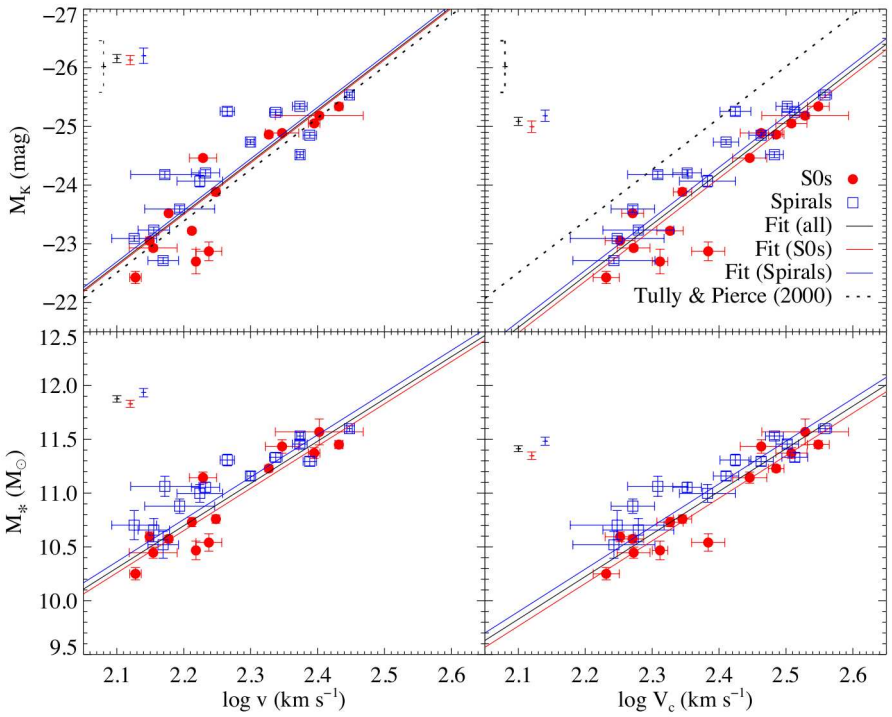

Figure 2. TF-like plots for our samples. Spirals are shown as blue squares and S0s as red triangles. We show power law fits of the form $M_{\rm K} = a + b(\log v - 2.5)$ for the two samples as red and blue lines, and a fit to all 28 galaxies as a solid black line. We show $1\,\sigma$ confidence intervals on a for each sample in the top-left of each plot. The TF relation for spirals found by Tully & Pierce (2000) is also shown as a dashed black line in the upper plots.

Extragalactic Database. K-band is chosen to minimize the effects of obscuration by dust, which can be significant in edge-on systems at optical wavelengths. We convert these to stellar masses M_* using the best-fitting stellar mass-to-light ratios presented in Williams et al. (2009).

We present four TF-like plots derived from the above quantities in Figure 2. We first plot the maximum observed rotational velocity and model circular velocity against the total magnitude to provide both a purely observed TF relation and one which eliminates asymmetric drift. We also plot both velocities against the stellar mass of the system, M_*.

It is important to note that at no point in this analysis do we do anything that might systematically affect the S0s in the sample differently to the spirals.

3. Discussion

In neither of the TF-like plots showing measures of velocity against measures of magnitude (upper panes of Figure 2) do we see a significant difference between the spirals and S0s. This is demonstrated by the error bars in the top-left corner

of each plot, which show the $1\,\sigma$ confidence interval of a in fits to each sample, assumed to be of the form $M_{\rm K} = a + b(\log v - 2.5)$. We fixed the gradients of the individual fits in the upper panels at -8.78, as found by Tully & Pierce (2000).

When we use circular velocity as the measure of rotation, which avoids the effects of asymmetric drift (top-right pane of Figure 2), there is still no significant difference between the TF relations of the S0s and spirals. Both samples (S0s *and* spirals), however, are significantly offset from the TF relation found by Tully & Pierce (2000), which is derived from unresolved HI kinematics (single-dish spectra).[1] This offset is in the same sense and of approximately the same size ($\approx +1$ mag or $+0.1$ dex in velocity) as that found by Bedregal et al. (2006) for their sample of S0s only.

There is a marginal change in the offset between the two samples in the change from magnitude to stellar mass (lower panels), although this could be due to a different slope in the best fits of the two samples. In this work we fixed the gradients of each fit to M_* to the shared gradient of the two samples (3.92 as a function of $\log v$ and 3.96 for $\log V_{\rm c}$).

In conclusion, we find no evidence that S0s lie in a different region of the luminosity/mass–rotational velocity plane than spirals. Present models of S0 formation, which our observations seem to contradict, are nevertheless extremely appealing, so we emphasize that we merely report an observational result and not an astrophysical interpretation. Future work will head in two directions: firstly, we will further attempt to determine the origin of the offset between our TF relations and that of Tully & Pierce (2000) as well as the difference between our findings and those of Bedregal et al. (2006). Secondly, we will characterize the statistical significance of the (lack of) offset and the scatter in TF plots of our samples at both K-band and B-band, and seek to interpret the results within the context of models of galaxy evolution.

References

Bedregal A. G., Aragón-Salamanca A., Merrifield M. R., 2006, MNRAS, 373, 1125
Bureau M., Freeman K. C., 1999, AJ, 118, 126
Cappellari M., 2008, MNRAS, 390, 71
Chung A., Bureau M., 2004, AJ, 127, 3192
Dressler A., 1980, ApJ, 236, 351
Dressler A., et al., 1997, ApJ, 490, 577
Gunn J. E., Gott J. R. I., 1972, ApJ, 176, 1
Kuijken K., Merrifield M. R., 1995, ApJL, 443, L13
Larson R. B., Tinsley B. M., Caldwell C. N., 1980, ApJ, 237, 692
Navarro J. F., Frenk C. S., White S. D. M., 1997, ApJ, 490, 493
Sheth K., et al., 2008, ApJ, 675, 1141
Skrutskie M. F., et al., 2006, AJ, 131, 1163
Tully R. B., Pierce M. J., 2000, ApJ, 533, 744
Williams M. J., Bureau M., Cappellari M., 2009, MNRAS, submitted

[1] We follow Bedregal et al. (2006) in shifting the Tully & Pierce (2000) K-band TF relation by -0.207 mag to match our adopted $H_0 = 70\,{\rm km\,s^{-1}\,Mpc^{-1}}$.

GALAXY EVOLUTION: EMERGING INSIGHTS AND FUTURE CHALLLENGES
ASP Conference Series, Vol.
@jourvol, © 2009
S. Jogee, I. Marinova, L. Hao, and G. A Blanc

The Morphological Type Dependence of K-band Luminosity Functions

Nick Devereux and Paul Hriljac

Embry-Riddle Aeronautical University, Prescott, AZ

S. P. Willner and M. L. N. Ashby

Harvard-Smithsonian Center for Astrophysics

C. N. A. Willmer

University of Arizona

Abstract. Differential 2.2μm (K-band) luminosity functions are presented for a complete sample of 1570 nearby ($V_{\rm gsr}\leq$3000 km s^{-1}, where $V_{\rm gsr}$ is the velocity measured with respect to the Galactic Standard of Rest), bright ($K\leq$10 mag), galaxies segregated by visible morphology. The K-band luminosity function for late-type spirals follows a power law that rises towards low luminosities whereas the K-band luminosity functions for ellipticals, lenticulars and bulge-dominated spirals are peaked with a fall off at both high and low luminosities. However, each morphological type (E, S0, S0/a-Sab, Sb-Sbc, Sc-Scd) contributes approximately equally to the overall K-band luminosity density in the local universe, and by inference, the stellar mass density as well.

1. Introduction

The Two Micron All Sky Survey (2MASS, Skrutskie et al. 2006) constitutes a unique resource that has been exploited in recent years to produce near-infrared luminosity functions for galaxies with ever greater precision (Cole et al. 2001; Kochanek et al. 2001; Bell et al. 2003; Eke et al. 2005; Jones et al. 2006). The K-band luminosity function provides a key constraint in understanding galaxy evolution in the context of Lambda Cold Dark Matter (ΛCDM) cosmology by virtue of the fact that the zero redshift K-band luminosity function traces the stellar mass accumulated in galaxies at a wavelength where interstellar extinction is minimal (Devereux, Becklin & Scoville 1987; Bell & de Jong 2001; Bell et al. 2003).

The current paradigm, constrained, in part by the K-band luminosity function (e.g., Benson et al. 2003) has galaxy disks forming through a combination of cold gas accretion and feedback (e.g., Dutton 2009) with bulges resulting from mergers (e.g., Masjedi, Hogg & Blanton 2008). Thus, the diversity of visible morphologies seen today among galaxies represents the culmination of multiple evolutionary paths. These end points in galaxy evolution are captured in a taxonomy devised by Hubble (1936) and refined by de Vaucouleurs (1959), that is based on the relative prominence of the stellar bulge and the degree of resolution of the spiral arms.

Nearby galaxies were identified using HYPERLEDA; a web-based interface (http://leda.univ-lyon1.fr) that provides access to the Principal Galaxy Catalog (Paturel et al. 2003). The 2MASS counterparts were identified on the basis of positional coincidence with the Extended Source Catalog (XSC, Jarrett et al. 2000) A volume-limited sample was defined for further study, hereafter the $K10/3000$ sample, comprising 1604 galaxies with $K \leq 10$ mag, $V_{\rm gsr} \leq 3000$ km s^{-1}, and $|b| > 10$ degrees. The adopted K-band magnitudes are those measured within the 20 mag arcsec^{-2} elliptical isophote; the parameter k_m_k20fe in the 2MASS XSC.

The principal aim of this project, described in more detail in Devereux et al. (2009), is to use nearby galaxies to define the first benchmark K-band luminosity functions for galaxies segregated by visible morphology. The luminosity function calculation employs the non-parametric maximum likelihood method of Choloniewski (1986). Our study improves on Marzke et al. (1994, 1998); Bingelli, Sandage & Tammann (1988); Efstathiou, Ellis, & Peterson (1988); Kochanek et al. (2001) and Bell et al. (2003) by limiting the sample to include only nearby galaxies, which have the most reliable morphological assignments, and by using the most recent galaxy distance determinations in conjunction with near infrared K-band magnitudes that correlate with stellar mass.

2. Morphological Type Dependence of the K-band Luminosity Function

Figure 1 shows that galaxies of different morphological type have different luminosity functions and no type mimics the shape of the total luminosity function. Ellipticals dominate the space density at high luminosities, whereas late-type (Sc - Scd) spirals dominate the space density at low luminosities. Lying between these two extremes are the lenticular galaxies and the bulge-dominated spirals (S0/a - Sbc).

The *total* K-band luminosity density, calculated by integrating the total luminosity function yields $(5.8 \pm 1.2) \times 10^8$ h L$_\odot$ Mpc^{-3}. Elliptical galaxies contribute $\sim$16$\pm$3% of the total. Lenticulars and bulge-dominated spirals combined contribute $\sim$68$\pm$14% of the total, or $\sim$22$\pm$4% for each sub-group (S0, S0/a-Sab, Sb-Sbc). Finally, the late-type spirals contribute $\sim$16$\pm$3% of the total. *Overall, to a good approximation, one could say that each Hubble type (E, S0, S0/a-Sab, Sb-Sbc, Sc-Scd) contributes equally to the overall K-band luminosity density in the local universe.* Using information provided in Bell et al. (2003), one can predict that the M/L ratio measured in the K-band will not vary systematically by more than $\sim$7% between E and Scd galaxies. Consequently, each morphological type contributes approximately equally to the stellar mass density as well.

As far as the shape of the luminosity functions, late-type spirals follow a power law that rises towards low luminosities, whereas the ellipticals, lenticulars and bulge-dominated spirals (S0/a - Sbc) are peaked with a fall off at both high *and* low luminosities. Our results concerning the morphological type dependence of K-band luminosity functions differ from previous studies. Kochanek et al. (2001) and Bell et al. (2003) divided their sample into just two broad categories;

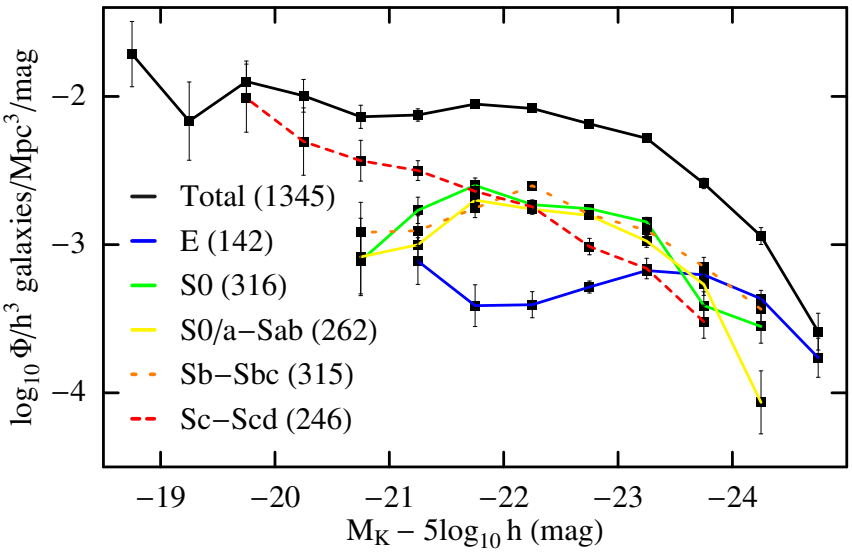

Figure 1. *K*-band isophotal luminosity functions for 1345 galaxies in the *K*10/3000 sample segregated by visible morphology. The error bars reflect statistical uncertainties only. The binning procedure inherent to the Choloniewski method excludes some galaxies which is why the total number of galaxies is not the sum of the number of galaxies within each Hubble type, and why the total number of galaxies in the plot is less than the total in the sample.

early and *late*, based on visual classifications and the SDSS light concentration index. They found little difference in form between the luminosity functions for the different types, which reflect that of the total luminosity function. Our results, based on a more comprehensive segregation according to the visual morphological classification scheme of de Vaucouleurs (1959), reveal significant differences between the luminosity functions for the different types, none of which mimic the shape of the total luminosity function.

3. Discussion

Our principal new result is that *the shape of the K-band luminosity functions depend significantly on galaxy visible morphology.* It may be more than a coincidence that the functional forms distinguish between *bulge* dominated and *disk* dominated systems. Evidently, there are at least two quite distinct galaxy formation mechanisms at work to produce the diversity of morphological types seen in the local universe. The next step, of course, is to establish what the formation mechanisms are exactly, which will require modeling the *differential* luminosity functions in the context of hierarchical clustering scenarios (e.g., Cole et al. 2000; Benson et al. 2003).

Semi-analytic models have already revealed that a combination of cold gas accretion (Weinberg et al. 2004) and feedback (Oppenheimer, & Davé

2006) can flatten the slope of the halo mass function to match that seen for galaxy disks. Such models are also able to reproduce the peaked luminosity functions observed for ellipticals and bulge-dominated spirals by incorporating major mergers (Barnes & Hernquist 1992; Hopkins et al. 2008). Thus, there is promise that the morphological dichotomy revealed by the K-band luminosity functions may be understood within the context of ΛCDM cosmology (Benson 2008, private communication). On the other hand, dwarf ellipticals pose a problem; even though they may be structurally related to their more luminous counterparts (Kormendy et al. 2009), our results show that they have a distinct luminosity function as noted previously by Bingelli, Sandage & Tammann (1988).

References

Barnes, J.E., & Hernquist, L. 1992, ARA&A, 30, 705
Bell, E.F., McIntosh, D.H., Katz, N., & Weinberg, M.D. 2003, ApJS, 149, 289
Bell, E.F., & de Jong, R.S. 2001, MNRAS, 312, 497
Benson, A.J., Bower, R.G., Frenk, C.S, Lacey, C.G., Baugh, C.M., & Cole, S. 2003, ApJ, 599, 38
Bingelli, G.A., Sandage, A., & Tammann, B., 1988 ARA&A, 26, 509
Choloniewski, J., 1986, MNRAS, 223,1
Cole, S., et al. 2000, MNRAS, 319, 168
Cole, S., et al. 2001, MNRAS, 326, 255
de Vaucouleurs, G. 1959, *Handbuch der Physik*, Vol. 53 (Berlin: Springer), 275
Devereux, N.,et al. 2009, ApJin press, (arXiv:0905.3825)
Devereux, N.A., Becklin, E.E., & Scoville, N.Z. 1987, ApJ, 312, 529
Dutton, A. A. 2009, MNRAS, 396, 121
Efstathiou, G., Ellis, R. S., Peterson, B. A. 1988, MNRAS, 232, 431
Eke, V.R., Baugh, C.M., Cole, S., Frenk, C.S., King, H.M., Peacock, J.A. 2005, MNRAS, 362, 1233
Hopkins, P.F., Cox, T.J., Keres, D.,& Hernquist, L. 2008, ApJS, 175, 390
Hubble, E., 1936, Realm of the Nebulae (New Haven: Yale University Press)
Jarrett, T. H., Chester, T., Cutri, R., Schneider, S., Skrutskie, M., Huchra, J. P. 2000 AJ, 119, 2498
Jones, D.H.; Peterson, B.A., Colless, M., & Saunders, W. 2006, MNRAS, 369, 25
Kochanek, C. S., et al. 2001, ApJ, 560, 566
Kormendy, J., Fisher, D.B., Cornell, M.E., & Bender, R., 2009, ApJS, in press (arXiv:0810.1681)
Marzke, R.O., Da Costa, L.N., Pellegrini, P.S., Willmer, C.N.A., & Geller, M.J. 1998, ApJ, 503, 617
Marzke, R.O., Geller, M.J., Huchra, J.P., & Corwin, H.G. 1994, AJ, 108, 437
Masjedi, M., Hogg, D.W., & Blanton, M.R. 2008, ApJ, 679, 260
Oppenheimer, B. D., & Davé, R. 2006, MNRAS, 373, 1265
Paturel, G., Petit, C., Prugniel, Ph., Theureau, G., Rousseau, J., Brouty, M., Dubois, P., Cambrsy, L. 2003, A&A, 412, 45
Skrutskie, M.F., et al. 2006, AJ, 131, 1163
Weinberg, D.H., Davé, R., Katz, N., & Hernquist, L. ApJ, 601, 1

GALAXY EVOLUTION: EMERGING INSIGHTS AND FUTURE CHALLLENGES
ASP Conference Series, Vol.
@jourvol, © 2009
S. Jogee, I. Marinova, L. Hao, and G. A Blanc

Dynamical Models of the Dark Halo of Elliptical Galaxy NGC 6702

Amy Forestell & Karl Gebhardt

Department of Astronomy, University of Texas, 1 University Station C1400, Austin, TX 78712, USA

Abstract. Our current picture of the universe says that galaxies are surrounded by massive dark matter halos in which they formed. Cosmological simulations have become detailed enough to model individual galaxy formation yet observational signatures of dark matter in elliptical galaxies are still difficult to measure. Tracers such as planetary nebulae have been used to probe the outer parts of galaxies where dark matter is thought to dominate. We present line-of-sight velocity distributions of elliptical galaxy NGC 6702 obtained with long-slit spectroscopy from the Hobby-Eberly Telescope. We then use axisymmetric orbit-superposition models to match possible dark matter distributions to our kinematic data. Previously we used this technique to show that elliptical galaxy NGC 821 contains dark matter and that it is not in the expected NFW profile shape. Our results for NGC 6702 show that dark matter is needed to explain the data yet we can not constrain the shape of the dark matter halo.

1. Data

Long-slit spectra were taken with the Hobby-Eberly Telescopes Low-Resolution Spectrograph over fourteen nights from April to October 2002 for a total of 7.4 hours along the major axis and 4.6 hours along the minor axis. Our spectra cover a wavelength range from 4300-7300Å with a resolving power of 1300. The CCD frame has a plate scale of $0.47''$/pix spatially and 2 Å/pix spectrally. The observations are reduced using standard procedures and we obtain a nonparametric line-of-sight velocity distribution (LOSVD) be deconvolving the galaxy spectrum with a set of stellar template spectra. The uncertainty of each velocity bin is obtained from Monte Carlo simulations. We use the full nonparametric velocity distribution in our dynamical modeling, however we plot the first four Gauss-Hermite moments in Figure 1.

2. Dynamical Models

We use axisymmetric orbit superposition models based on the method of Schwarzschild (1979) as used in Gebhardt et al. (2000). First a surface brightness profile is converted to luminosity density using an assumed edge-on inclination. This luminosity density is converted to a mass density using a mass-to-light ratio ($M/L_{\rm V}$) that is constant over the galaxy. A spherically symmetric dark halo density profile is added to the stellar density and this total mass density gives the galaxy's gravitational potential. Next individual stellar orbits are run for a significant number of orbital times in the specified potentials. The galaxy is

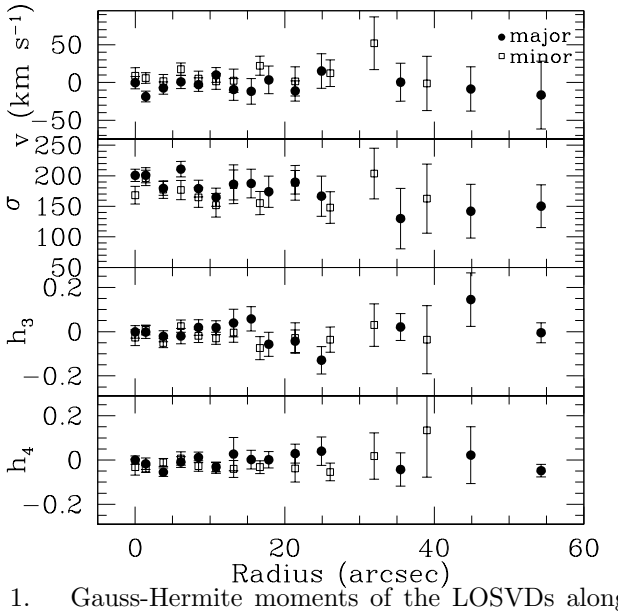

Figure 1. Gauss-Hermite moments of the LOSVDs along the major axis (solid circles) and minor axis (open squares).

divided spatially into cells, and the amount of time that an orbit spends in a cell represents the mass contributed by that orbit. Finally the orbits are combined with nonnegative weights to find the best-fitted superposition to match the data LOSVDs and the light profile. This process is repeated for different dark halo density profiles and $M/L_{\rm V}$ values to find the halo potential that best fits the data, as determined by χ^2.

3. Results

We use both NFW (Navarro et al. 1996) and Logarithmic Potential halos to characterize the dark matter in the galaxy. The NFW halo is given by

$$\rho(r) = \frac{\rho_{\rm crit}\ \delta_{\rm c}}{(r/r_{\rm s})(1+r/r_{\rm s})^2} \tag{1}$$

where $r_{\rm s}$ is the scale radius of the halo and $\rho_{\rm crit} = 3H^2/8\pi G$ is the critical density. Throughout this paper we refer to $\rho_{\rm crit}\delta_{\rm c}$ as the scale density. The characteristic overdensity $\delta_{\rm c}$ is approximately related to a concentration parameter c by

$$\delta_{\rm c} = \frac{\Delta_{\rm vir}}{3}\frac{c^3}{\ln(1+c) - c/(1+c)}. \tag{2}$$

We vary both the concentration and scale radius, although there is a known correlation between them.

Figure 2 shows the χ^2 grids in $M/L_{\rm V}$, radius, and density for each of the NFW halo models.

The Logarithmic Potential halo is given by

$$\rho(r) = \frac{v_{\rm c}^2}{4\pi G}\frac{3r_{\rm c}^2 + r^2}{(r_{\rm c}^2 + r^2)^2} \tag{3}$$

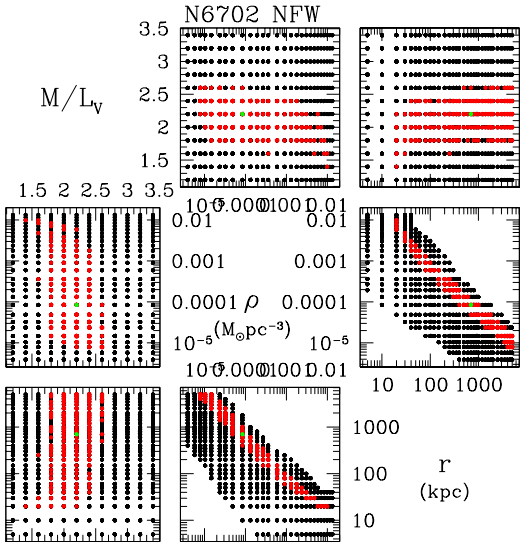

Figure 2. χ^2 grid in $M/L_{\rm V}$, radius, and density for each of the NFW halo models.

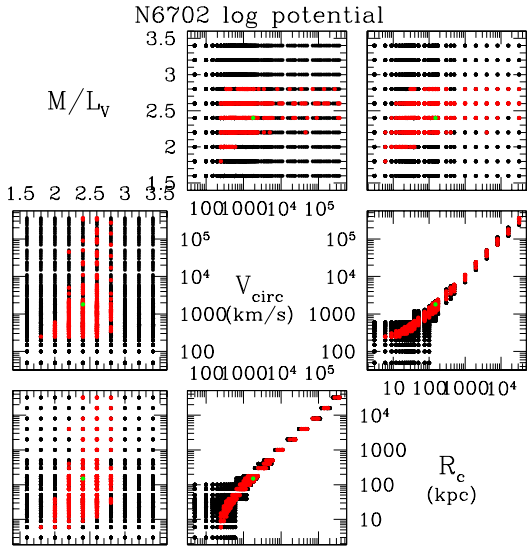

Figure 3. χ^2 grid in $M/L_{\rm V}$, radius, and circular velocity for each of the logarithmic potential halo models.

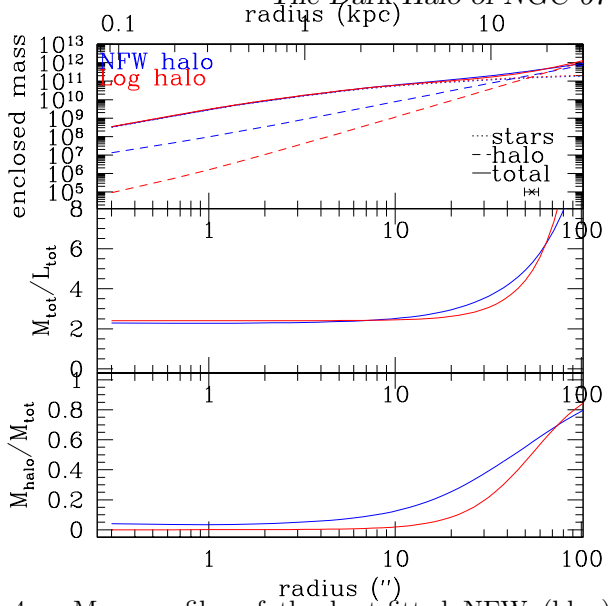

Figure 4. Mass profiles of the best-fitted NFW (blue) and logarithmic potential (red) halos.

Figure 3 shows the χ^2 grids in M/L_V, radius, and circular velocity for each of the logarithmic potential halo models.

The properties of the best-fitted models with no halo, NFW halo, and logarithmic potential halo are given in Table 1. The mass profiles of the best-fitted NFW and logarithmic potential halos are shown in 4. We find that that dark matter is necessary to explain the observations of NGC 6702, yet we are unable to constrain the shape of the dark matter profile for this galaxy.

Table 1. Best-Fitted Halo Model Results

Halo	χ^2	M/L_V	Halo parameters	M_{tot} $10^{11}M_\odot$	M_{stars} $10^{11}M_\odot$	M_{halo} $10^{11}M_\odot$
No halo	113.2	3.2 ± 0.2	...	2.24	2.24	0.00
Log halo	99.11	$2.4^{+0.5}_{-0.7}$	r=1800 kpc v=150 km/s	3.45	1.68	1.77
NFW halo	99.06	$2.2^{+0.4}_{-0.8}$	c=2.0 $\rho = 8.48 \times 10^{-5} M_\odot/pc^3$ r=700 kpc	3.73	1.54	2.19

References

Gebhardt, K., et al. 2000, AJ, 119, 1157
Navarro, J. F., Frenk, C. S., & White, S. D. M. 1996, ApJ, 462, 563
Schwarzschild, M. 1979, ApJ, 232, 236

GALAXY EVOLUTION: EMERGING INSIGHTS AND FUTURE CHALLLENGES
ASP Conference Series, Vol.
@jourvol, © 2009
S. Jogee, I. Marinova, L. Hao, and G. A Blanc

Stellar Velocity Profiles and Line-Strengths out to Four Effective Radii in the Early-Type Galaxy NGC 3379

A. Weijmans[1], M. Cappellari[2], P. T. de Zeeuw[3,1], E. Emsellem[4], J. Falcón-Barroso[5], H. Kuntschner[3], R. M. McDermid[6], R. C. E. van den Bosch[7], and G. van de Ven[8]

[1]*Sterrewacht Leiden, Leiden University, Postbus 9513, 2300 RA Leiden, the Netherlands [weijmans@strw.leidenuniv.nl]*
[2]*Sub-Department of Astrophysics, University of Oxford, Denys Wilkinson Building, Keble Road, Oxford OX1 3RH, UK*
[3]*ESO, Karl-Schwarzschild-Str 2, 85748 Garching, Germany*
[4]*CRAL, University of Lyon, 9 Avenue Charles André, 69230 Saint Genis Laval, France*
[5]*ESTEC, Postbus 299, 2200 AG Noordwijk, the Netherlands*
[6]*Gemini Observatory, Northern Operations Centre, 670 N. A'ohoku Place, Hilo, Hawaii 96720 USA*
[7]*McDonald Observatory, University of Texas, Austin, TX 78712, USA*
[8]*IAS, Einstein Drive, Princeton, NJ 08540, USA*

Abstract. We describe a new technique to measure stellar kinematics and line-strengths at large radii in nearby galaxies. Using the integral-field spectrograph SAURON as a 'photon-collector', we obtain spectra out to four effective radii (R_e) in the early-type galaxy NGC 3379. By fitting orbit-based models to the extracted stellar velocity profile, we find that $\sim 40\%$ of the total mass within 5 R_e is dark. The measured absorption line-strengths reveal a radial gradient with constant slope out to 4 R_e.

1. Introduction

Although the presence of dark matter dominated haloes around spiral galaxies is well established (see e.g. van Albada et al. 1985), little is known about the dark haloes around early-type galaxies. Large regular H I discs or rings, whose kinematics are often used to constrain the properties of dark haloes, are rare in these systems (though see Franx, van Gorkom, & de Zeeuw 1994; Weijmans et al. 2008), so that we are forced to use other tracers of the gravitational potential.

Here we use stellar kinematics obtained with the integral-field spectrograph SAURON (Bacon et al. 2001) at large radii in the elliptical (E1) galaxy NGC 3379 to model its dark halo. This galaxy is of intermediate luminosity ($M_B = -20.57$) and has a half-light or effective radius R_e of 42 arcsec, which corresponds to 2.1 kpc at its distance of 10.3 Mpc.

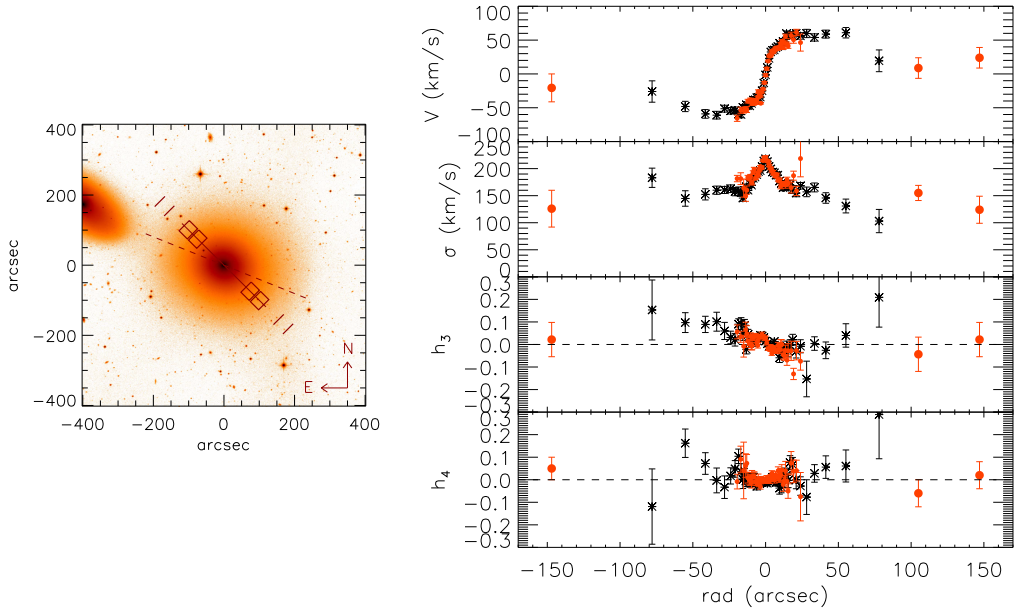

Figure 1. Left: Positions of our observed fields in NGC 3379. The red boxes denote each SAURON field-of-view. The skylenslets (short thick lines) are aligned with the long side of the SAURON field, at a distance of two arcminutes. The dashed line denotes the major axis of NGC 3379. The underlying V-band image was obtained with the 1.3-m McGraw-Hill Telescope at MDM Observatory. Right: LOSVD of NGC 3379 out to 4 R_e. The black stars are long-slit data from Statler & Smecker-Hane (1999) and the central dots are SAURON observations obtained in the original survey (Emsellem et al. 2004). The dots at large radii are our new observations, and double the spatial extent of the data.

2. Method

We centered SAURON at 2.6 and 3.5 R_e on both sides of the nucleus of NGC 3379, close to its major axis (see Fig. 1, left panel). A single spectrum of one lenslet is dominated by noise at these large radii, but adding all spectra of all lenslets together we obtained in three out of our four fields sufficient signal-to-noise to measure the stellar absorption line-strengths and the line-of-sight velocity distribution (LOSVD) up to the fourth Gauss-Hermite moment h_4. This last parameter is necessary to break the well-known mass-anisotropy degeneracy when modeling the dark halo (e.g. Gerhard 1993).

3. Results

We measured the LOSVD using the penalized pixel fitting method (pPXF) by Cappellari & Emsellem (2004). The resulting LOSVD (Figure 1, right panel) shows a smooth continuation of existing stelllar kinematic measurements (Statler & Smecker-Hane 1999).

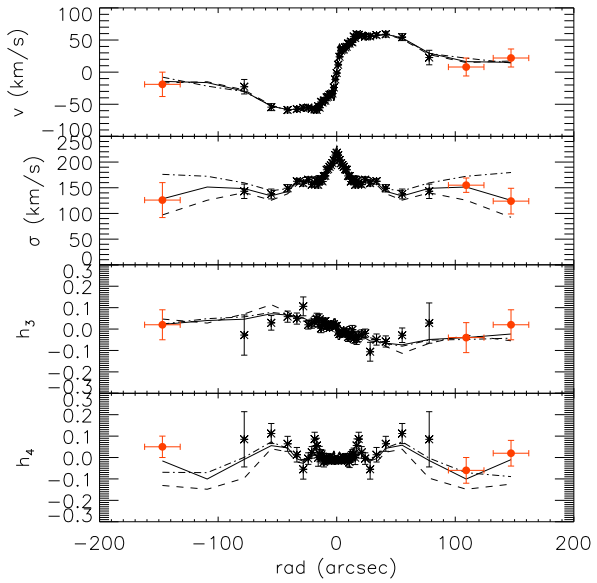

Figure 2. Best-fit model (solid line) overplotted on datapoints. The stars are (symmetrized) long-slit data from Statler & Smecker-Hane (1999) and the dots are our datapoints (horizontal error bars indicate the width of the SAURON field-of-view). Also shown are a model without a dark halo (dashed line) and a model with a ten times too massive halo (dot-dashed line). These models do not fit the observed dispersion and h_4 profiles.

We use a Schwarzschild model (van den Bosch et al. 2008; van de Ven, de Zeeuw, & van den Bosch 2008) to fit our measurements, including the central SAURON field of the original survey (Emsellem et al. 2004) and the long-slit data of Statler & Smecker-Hane (1999). The black hole mass and the (nearly axisymmetric) shape of the stellar distribution of NGC 3379 are taken from van den Bosch (2008). We model the spherical dark halo with an NFW profile (Navarro, Frenk, & White 1996) with a concentration $c = 10$ (Bullock et al. 2001). Our best-fit model is shown in Fig. 2, and has a total halo mass M_{200} of 1.0×10^{12} $M_\odot$, which corresponds to 10 times the total stellar mass of NGC 3379.

We obtained line-strength measurements following the procedures outlined in Kuntschner et al. (2006). We find that the slope of the line-strength gradients remains constant out to at least 4 R_e, although our values of Fe5015 are not consistent with this trend (Fig. 3). Plotting our measurements on the stellar population models of Thomas, Maraston, & Bender (2003), we find that the stellar halo population is old ($\sim$ 12 Gyr) and metal-poor (below 20% solar).

4. Conclusion

We showed that by using SAURON as a 'photon collector', we can measure both the stellar velocity profile and absorption line-strengths out to large radii in early-type galaxies. We presented our measurements of NGC 3379 and modeled its dark halo. In our best-fit model, 41% of the total mass within 5 R_e is dark.

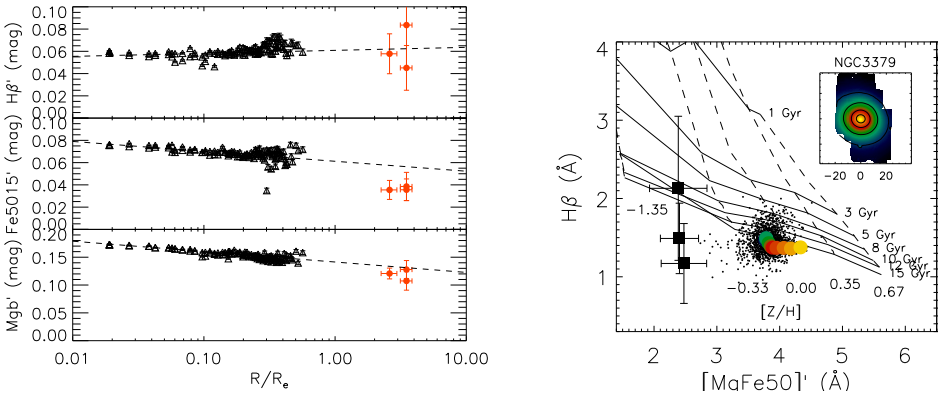

Figure 3. Left: Line-strength gradients (from top to bottom: Hβ, Fe5015 and Mg b, in magnitudes) out to 4 R_e in NGC 3379. Triangles denote SAURON data from the original survey (Kuntschner et al. 2006), filled dots our new measurements. Right: Hβ index against [MgFe50]$'$, overplotted on the stellar population models of Thomas et al. (2003). Black dots show measurements from the SAURON survey, while the grey dots are averaged along isophotes (see inset for scale). Squares denote our measurements at large radii.

We will present more elaborate modeling of the dark halo of NGC 3379 and comparisons with literature values in a forthcoming paper (Weijmans et al. in prep.), as well as a comparable dataset and analysis for the elliptical galaxy NGC 821.

Acknowledgments. It is a pleasure to thank the organisers for a stimulating and fruitful conference. We gratefully acknowledge Chris Benn, Eveline van Scherpenzeel, Richard Wilman and the ING staff for support on La Palma. The SAURON observations were obtained at the William Herschel Telescope, operated by the Isaac Newton Group in the Spanish Observatorio del Roque de los Muchachos of the Instituto de Astrofísica de Canarias.

References

Bacon, R., et al. 2001, MNRAS, 326, 23
Bullock, J.S., Kolatt, T.S., Sigad, Y., Somerville, R.S., Kravtsov, A., Klypin, A.A., Primack, J.R., & Dekel, A. 2001, MNRAS, 321, 559
Cappellari, M., & Emsellem, E. 2004, PASP, 116, 138
Emsellem, E., et al. 2004, MNRAS, 352, 721
Franx, M., van Gorkom, J.H., & de Zeeuw, P.T. 1994, ApJ, 436, 642
Gerhard, O.E. 1993, MNRAS, 265, 213
Kuntschner, H., et al. 2006, MNRAS, 369, 497
Navarro, J.F., Frenk, C.S., & White, S.D. 1996, ApJ, 462, 563
Statler, T.S., & Smecker-Hane, T. 1999, AJ, 117, 839
Thomas, D., Maraston, C., & Bender, R. 2003, MNRAS, 339, 897
van Albada, T.S., Bahcall, J.N., Begeman, K., & Sancisi, R. 1985, ApJ, 295, 305
van den Bosch, R.C.E. 2008, PhD thesis, Leiden University
van den Bosch, R.C.E., van de Ven, G., Verolme, E.K., Cappellari, M., & de Zeeuw, P.T. 2008, MNRAS, 385, 647
van de Ven, G., de Zeeuw, P.T., & van den Bosch, R.C.E. 2008, MNRAS, 385, 614
Weijmans, A., Krajnović, D., van de Ven, G., Oosterloo, T.A., Morganti, R., & de Zeeuw, P.T. 2008, MNRAS, 383, 1343

Part II

History and Impact of Galaxy Mergers

GALAXY EVOLUTION: EMERGING INSIGHTS AND FUTURE CHALLLENGES
ASP Conference Series, Vol.
@jourvol, © 2009
S. Jogee, I. Marinova, L. Hao, and G. A Blanc

Merger History of Galaxies and Disk+Bulge Formation

Sadegh Khochfar

Max-Planck Institute for Extraterrestrial Physics, Giessenbachstrasse D-85748 Garching, Germany

Abstract. We discuss the transitions of galaxy morphologies within the CDM paradigm under the assumption of bulge formation in mergers and disk growth via cooling of gas and subsequent star formation. Based on the relative importance of these two competing processes it is possible to make predictions on the expected morphological mix of galaxies. In particular we here discuss the generation of massive disk galaxies with low bulge-to-total mass ratios. Our results indicate that it is difficult to generate enough massive disk galaxies with $B/T < 0.2$ via major mergers and subsequent disk re-growth, if during the major merger progenitor disks get disrupted completely. On average low B/T galaxies must have had there last major merger at $z \geq 2$. The main limiting factor is the ability to re-grow massive disks at late times after the last major merger of a galaxy. Taking into account the contribution from minor mergers ($4 \geq M_1/M_2$, $M_1 \geq M_2$) to the formation of bulges, we recover the right fraction of massive low B/T disk galaxies, indicating that minor mergers play an important role in the formation of massive low B/T disk galaxies.

1. Introduction

The close resemblance of elliptical galaxies and *classical* bulges has lead to the widely accepted assumption that they have the same origin. Profiles of elliptical galaxies and bulges are nicely fit by Sersic-laws. The fact that super-massive black holes in bulges also follow the fundamental $M_\bullet$-σ-relation (Sarzi et al. 2001) provides further evidence for a common formation scenario of elliptical galaxies and classical bulges.

Early work by Toomre & Toomre (1972) showed that elliptical galaxies can be the result of a major merger between two spiral galaxies. Subsequent numerical simulations showed that indeed various properties of elliptical galaxies and classical bulges can be recovered from simulations that use cosmological self-consistent initial orbital parameters (Khochfar & Burkert 2006) for merging systems (see e.g. Barnes & Hernquist 1992; Naab & Burkert 2003; Naab et al. 2006; Jesseit et al. 2007). As a consequence it should be possible to generalize results for the formation of elliptical galaxies to the formation of classical bulges and to speak more general of the formation of spheroids (Khochfar & Silk 2006). E.g. it has been predicted that massive spheroids form in dry major mergers of elliptical galaxies, and that intermediate mass spheroids form as a result of a major merger between an elliptical and a spiral galaxy (Khochfar & Burkert 2003; Naab et al. 2006). Khochfar & Silk (2006) find that this is indeed the case for ellipticals as well as bulges.

Bulges are embedded in large stellar disks in contrast to elliptical galaxies which poses the question if they really can have the same origin. The ΛCDM paradigm offers a natural way for the transition from elliptical galaxies to bulges of early-type spirals via the accretion of a new disk in the aftermath of a major merger (Kauffmann et al. 1999; Springel & Hernquist 2005). As Khochfar & Burkert (2001) show the predicted merger rate of galaxies in the ΛCDM paradigm is in fair agreement with the observed one which allows to test robustly the transition in Hubble types due to the growth of a new stellar disk. Hence the properties of bulges like e.g. the isophotal shape (Khochfar & Burkert 2005) will initially be set by the properties of the progenitor elliptical galaxy.

2. Model

We use semi-analytical modeling of galaxy formation to predict the star burst and quiescent components of elliptical galaxies. The dark matter history is calculated using the merger tree proposed by Somerville & Kolatt (1999) with a mass resolution of $2 \times 10^9 M_\odot$. The baryonic physics within these dark matter halos is calculated following recipes presented in Khochfar & Burkert (2005) and Khochfar & Silk (2006). In our simulation, we assume that elliptical galaxies form whenever a major merger ($M_1/M_2 \leq 4$ with $M_1 \geq M_2$) takes place. We assume that during this process all the cold gas which was in the progenitor disks will be consumed in a central starburst, adding to the spheroid mass, and that all stars in the progenitor disks will be scattered into the spheroid too. Furthermore we allow the stars of satellite galaxies in minor mergers to also contribute to the spheroid. During the evolution of a galaxy, we keep track of the origins of all stars brought into the spheroid and attribute them to two categories, starburst and quiescent, where the first incorporates stars formed during a starburst in a major merger and the latter includes stars previously formed in a disk and added to the spheroid during a major merger. Each star will carry along its label and not change it, which means that if a star was made in a merger of two progenitor galaxies and the remnant of that merger participated in another merger, the star will still contribute to the merger component of the final remnant. For more modeling details, we refer the reader to Khochfar & Silk (2006) and references therein. Please note that our simulation does not include AGN-feedback (Schawinski et al. (2006)) or environmental effects (Khochfar & Ostriker 2008) that have influence on the most massive galaxies.

3. Results

3.1. Build-up of bulges

Ongoing mergers constantly transfer disk stars to spheroids in the universe. If this process is more efficient than star formation in disks one is to expect an increase in the fraction of stars in spheroids over cosmic time. However, the merger rate is a strong decreasing function with redshift (Khochfar & Burkert 2001) and at late times disk growth overtakes merging. In the left panel of Figure 1 the fraction of stars in spheroids as a function of redshift and galaxy mass is shown. At early times the most massive galaxies, $M_* > M_{\rm c} \sim 3 \times 10^{10}$ M$_\odot$ are

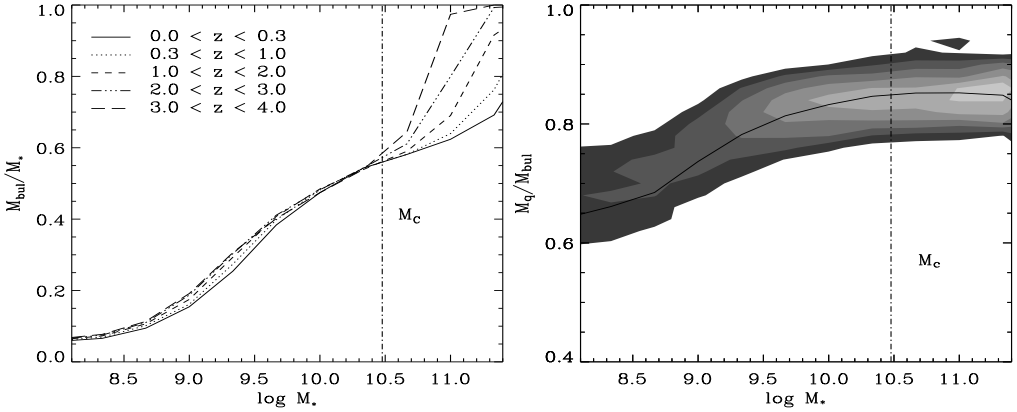

Figure 1. Left panel: Fraction of stars in galaxies of a given mass that reside in spheroids at various redshifts. Right panel: Quiescent fraction of stars in spheroids as a function of galaxy mass. The solid line shows the median of the distribution. The dot-dashed line indicates the critical mass scale $M_{\rm c}$

all elliptical galaxies and only at late times massive spiral galaxies appear. This is related to the gradual transformation of gas into stars in disks in contrast to the violent and fast transformation of gas into stars during major mergers and the ability of halos at high-z to accrete gas efficiently onto their central galaxy on approximately halo dynamical times (e.g., Kereš et al. 2005; Khochfar et al. 2007; Ocvirk et al. 2008; Khochfar & Silk 2008b). Many of the intermediate massive elliptical galaxies that formed at high redshift continue to grow disks to become bulges of present day spiral galaxies.

The right panel of Figure 1 shows the quiescent fraction of bulge stars as a function of galaxy mass. The quiescent fraction increases gradually until roughly $M_{\rm c}$ where it becomes constant at ~ 0.85. Most of the stars in bulges therefore originated from disks of progenitor galaxies or satellite galaxies. Khochfar & Silk (2006) report the number of minor satellite mergers exceeds that of major mergers by an order of magnitude and is therefore one important driver for a high quiescent fraction in bulges. For massive bulges in addition mostly dry major mergers cause the quiescent fraction to stay constant and not to change much (see also Khochfar & Silk 2008a), which explains the behavior at the high mass end.

Numerical simulations by Springel & Hernquist (2005) show that dissipation accompanied by starbursts during major mergers leads to a population of stars that is more centrally concentrated than the scattered disk stars once they relaxed to a spheroid at the end of the merger. In our simulations we identified those centrally concentrated stars with the starburst component and the less concentrated previous disk stars with the quiescent component of bulges. Khochfar & Silk (2006b) propose based on these two components a simple model in which the size of galaxies scales with the amount of dissipation during their formation and that is able to reproduce the size-evolution of early-type galaxies. In the left panel of Figure 3 we show the expected size evolution of bulges as a function of their mass and formation time, i.e. we show the ratio of the present day effective radius of bulges, $r_{\rm e,local}$, to that of bulges at higher redshifts.

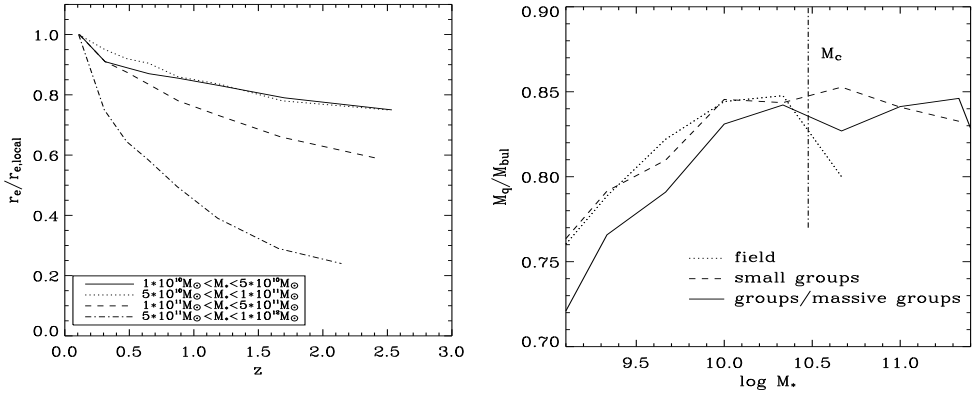

Figure 2. Left panel: size ratio between spheroids of the same mass at high redshift and locally. Right panel: quiescent fraction of stars in bulges as a function of galaxy mass and environment.

Massive bulges that formed early are most likely to have had a significant amount of dissipation involved during their formation, because the gaseous disk only had enough time to transform a small portion of the gas into stars. In contrast the size-evolution for small bulges is not very strong, as there is only a small difference in the amount of dissipation.

The right panel of the same figure shows the quiescent fraction in bulges as a function of galaxy mass and environment. For galaxies more massive than $M_{\rm c}$ the quiescent fraction does not depend on the environment. Only for galaxies below $M_{\rm c}$ we find an environmental dependence which reflects itself in a larger quiescent fraction for field galaxies. The reason for this is mainly buried in the larger amount of dissipation that is involved in the formation of bulges that end up in high density environments. These galaxies form in general earlier and therefore the amount of dissipation is larger during major mergers.

Observations of core phase-space densities in spiral galaxies reveal that they are several order of magnitudes lower than those of elliptical galaxies of the same mass (Carlberg 1986). A possible solution to this problem is dissipation during starburst that can increase the phase space density in the remnant. If the centers of early-type spirals are dominated by bulges this suggest that bulges and ellipticals of the same mass must have had different amounts of dissipation during their formation. Indeed our simulations suggest that the quiescent fraction in bulges of spiral galaxies is higher than that of ellipticals of the same mass, which could explain the observations.

3.2. Bulge-to-total stellar mass ratios of disk galaxies

Using above prescriptions it is possible to investigate the distribution of bulge-to-total (B/T) stellar mass ratios within our SAM and compare them to recent observations of Weinzirl et al. (2009). The left of Figure 3 shows that our model significantly underestimate the fraction of low B/T bulges for massive late-type galaxies with $\rm M_* \geq 10^{10}$ $\rm M_\odot$ if we only consider bulges that had at least one major merger during their history. The main reason for this result becomes

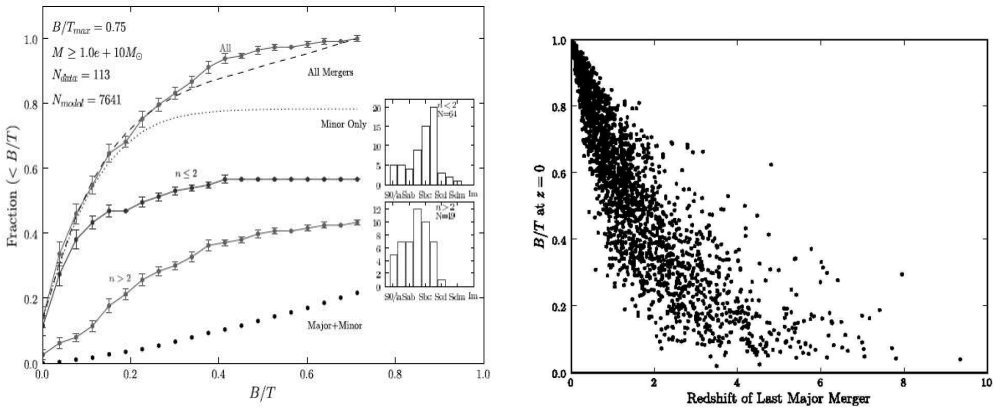

Figure 3. Left panel: Cumulative fraction of disk galaxies with bulge-to-total ratios less B/T. The small dotted line *minor only* refers to model bulges formed from only minor mergers and the big dotted line labeled *major+ minor* to bulges that had at least one major merger in their history. Solid black and grey line shows the observed disk galaxies with bulges having Sersic index $N \leq 2$ and $n > 2$, respectively. Right panel: B/T of galaxies as a function of the redshift when they had their last major merger (figures from Weinzirl et al. 2009)

clearer by looking at the B/T ratio of galaxies as a function of the time of their last major merger that led to the disruption of the disk (right part of Figure 3). It appears that only those galaxies that experienced a major merger before $z \geq 2$ significantly contribute to low B/T galaxies. These galaxies were the only ones that had enough time to re-grow a massive disk after it was destroyed in the major merger. As mentioned earlier satellite mergers are by far more frequent than major mergers. In that respect they are able to contribute to the build up of bulges, especially low mass bulges. In our simple model we add the stars of the satellite to the bulge component of the host in minor mergers ($M_1/M_2 \geq 4$, $M_1 \geq M_2$). The small dotted line in the left panel of Figure 3 shows the prediction for bulges only build up via minor mergers. The majority of bulges made in this way live in low $B/T < 0.2$ bulges, while those made in major mergers have $B/T \geq 0.2$. Adding the bulges that have experienced major mergers as well reproduces the overall distribution of observed bulges quite well. There are however, some interesting discrepancies. The fraction of large B/T galaxies is increasing too steep as a function of B/T compared to the observations. This can be traced back to possibly too efficient destruction of disk during major mergers in our model. Recent work by Hopkins et al. (2009) showed that disks can actually survive major mergers if they are very gas-rich. This indeed could also explain the missing fraction of intermediate B/T galaxies that are missing in our current model. The main results however, that minor merger have a significant contribution to systems with low B/T also holds in a model with modified disk destruction (Hopkins et al. 2009).

4. Conclusions

In this paper we discussed how the merger history of galaxies affects their morphology in terms of disks and bulges. We showed that in a model where disks get disrupted in major mergers the majority of stars ending up in a bulge are actually made in progenitor disks. Only $15-40\%$ of stars in present day spheroids, bulges and ellipticals, are made from starbursts in gas-rich mergers. Thus we would argue that the main mode of star formation is in disks and not in starbursts triggered by galaxy interactions. Furthermore, we find that the fraction of stars made in starburst increases as a function of redshift due to dissipation playing a more important role at high z. Cooling times of gas are short resulting in large quantities of unprocessed gas in progenitor disks that can be transformed into stars during major mergers. Taking into account the amount of dissipation during merger and the amount of satellite mergers it is possible to recover the size-evolution of early-type galaxies with time. Massive early-type galaxies at low redshift have had many mergers with satellite galaxies that puffed them up to become larger in size over time. In contrast massive early-type galaxies at high redshift did form from a single very gas-rich merger leaving behind a compact remnant.

When considering the growth of bulges from major mergers we find that the fraction of massive disk galaxies with $B/T < 0.2$ is far too low compared to the observations. In addition the fraction of galaxies with $B/T > 0.2$ increases to steep as function of B/T. Latter is possibly due to a too simplified model for the effects on progenitor disks by major mergers. Our model assumes a total destruction which has been recently shown to be not necessarily the case. As a consequence we might underestimate intermediate B/T ratios and overestimate high B/T ratios. Independent of that however, we find that the bulges of the $B/T < 0.2$ population of disk galaxies can be associated with a series of minor mergers forming them in our model. Assuming that satellites contribute their stars to the bulge of the host galaxy we find a steep rise in the fraction of low B/T galaxies in agreement with recent observations. Combining both, bulges formed by minor mergers only and those by at least one major merger and a series of minor mergers, we recover the overall trend in the fraction of disk galaxies as a function of B/T. Though these are promising results future work will have to show what the role of minor mergers in the formation of bulges is, and how it reflects on other properties like e.g. the bar fraction in disk galaxies.

Acknowledgments. I would like to thank Tim Weinzirl & Shardha Jogee for many useful discussions.

References

Barnes, J. E., & Hernquist, L. 1992, ARA&A, 30, 705
Carlberg, R. G. 1986, ApJ, 310, 593
Hopkins, P. F., Cox, T. J., Younger, J. D., & Hernquist, L. 2009, ApJ, 691, 1168
Hopkins, P. F., et al. 2009, arXiv:0901.4111
Jesseit, R., Naab, T., Peletier, R. F., & Burkert, A. 2007, MNRAS, 376, 997
Kauffmann, G., et al. 1999, MNRAS, 303, 188
Kereš, D., Katz, N., Weinberg, D. H., & Davé, R. 2005, MNRAS, 363, 2
Khochfar, S., & Burkert, A. 2001, ApJ, 561, 517
Khochfar, S., & Burkert, A. 2003, ApJ, 597, L117

Khochfar, S., & Burkert, A. 2005, MNRAS, 359, 1379
Khochfar, S., & Silk, J. 2006a, MNRAS, 370, 902
Khochfar, S., & Silk, J. 2006b, ApJ, 648, L21
Khochfar, S., & Burkert, A. 2006c, A&A, 445, 403
Khochfar, S., Silk, J., Windhorst, R. A., & Ryan, R. E., Jr. 2007, ApJ, 668, L115
Khochfar, S., & Ostriker, J. P. 2008, ApJ, 680, 54
Khochfar, S., & Silk, J. 2008a, arXiv:0809.1734
Khochfar, S., & Silk, J. 2008b, arXiv:0812.1183
Naab, T., & Burkert, A. 2003, ApJ, 597, 893
Naab, T., Khochfar, S., & Burkert, A. 2006, ApJL, 636, L81
Naab, T., Jesseit, R., & Burkert, A. 2006, MNRAS, 372, 839
Ocvirk, P., Pichon, C., & Teyssier, R. 2008, MNRAS, 390, 1326
Sarzi, M., Rix, H.-W., Shields, J. C., Rudnick, G., Ho, L. C., McIntosh, D. H., Filippenko, A. V., & Sargent, W. L. W. 2001, ApJ, 550, 65
Schawinski, K., et al. 2006, Nature, 442, 888
Somerville, R. S., & Kolatt, T. S. 1999, MNRAS, 305, 1
Springel, V., & Hernquist, L. 2005, ApJ, 622, L9
Toomre, A., & Toomre, J. 1972, ApJ, 178, 623
Weinzirl, T., Jogee, S., Khochfar, S., Burkert, A. & Kormendy, J. 2009, ApJ, 696, 41

GALAXY EVOLUTION: EMERGING INSIGHTS AND FUTURE CHALLLENGES
ASP Conference Series, Vol.
@jourvol, © 2009
S. Jogee, I. Marinova, L. Hao, and G. A Blanc

Galaxy Mergers and Secular Evolution over the Last 10 Gyr

Shardha Jogee

Department of Astronomy, University of Texas at Austin, 1 University Station C1400, Austin, TX 78712-0259, USA

Abstract. In the hierarchical ΛCDM framework of galaxy evolution, galaxy mergers, tidal interactions, secular evolution, and smooth accretion constitute the most important mechanisms for redistributing the mass and angular momentum of galaxies. The relative importance of these mechanisms depends on the epoch being considered. I will review mounting evidence, which suggests that since $z \sim 2$, the evolution of spirals is not dominated by major mergers, but is instead *a more quiescent one*. I discuss the main results from Jogee et al. (2009) on the frequency of galaxy mergers and their impact on star formation since $z \sim 1$, based on *HST* ACS, Combo-17, and Spitzer 24 μm data in the GEMS survey. Finally, I discuss observational constraints on stellar bars as drivers of secular evolution since $z \sim 1$ and prospects for future progress.

1. Introduction

Contemporary galaxy formation models combine the well-established Λ Cold Dark Matter cosmology with baryonic physics in order to provide a general framework for galaxy evolution. However, the predictions on how galaxies evolve are not unique, and the timescales and mechanisms through which the main baryonic components of galaxies – bulges, bars, and disks – assemble remain hotly debated.

Major mergers, minor mergers, and stellar bars are three of the most important mechanisms for redistributing the mass and angular momentum of galaxies, and their relative importance depends on the epoch being considered. At redshifts $z > 2$, corresponding to look-back times $T_{\rm back} > 10.4$ Gyr [1], observations and theory suggest that galaxy evolution is dominated by violent major mergers (e.g., Steinmetz & Navarro 2002; Conselice et al. 2003; Patton et al. 2000; Le Fevre et al. 2000). However, over $z \sim 0$–1, mounting evidence suggests that the evolution of disks was not dominated by major mergers, but was instead *a more quiescent one*. The evidence includes the absence of any strong morphological disturbances in the galaxies producing most of the ultraviolet (UV) (Wolf et al. 2005) and infra-red

[1]We assume throughout a flat cosmology with $\Omega_M = 1 - \Omega_\Lambda = 0.3$ and H_0 =70 km s^{-1} Mpc^{-1}.

2. Galaxy mergers and their impact on star formation

The merger history of galaxies impacts the mass assembly (e.g., Dickinson et al. 2003), star formation history, AGN activity (e.g., Springel. et al. 2005b) and structural evolution of galaxies. The merger rate/fraction at $z > 1$ remains highly uncertain, owing to relatively modest volumes and bandpass shifting effects, but with a general trend towards higher merger fractions at higher redshifts Even the merger rate at $z < 1$ has proved hard to robustly measure for a variety of reasons, ranging from small samples in early studies, to different methods on large samples in later studies.

In Jogee et al. (2008a,b), we have performed a complementary and comprehensive observational estimate of the frequency of interacting galaxies over $z \sim 0.24$–0.80 (lookback times of 3–7 Gyr), and the impact of interactions on the star formation (SF) of galaxies over this interval. Our study is based on *HST* ACS, COMBO-17, and Spitzer 24 μm data from the GEMS survey. We use a large sample of $\sim$ 3600 ($M \geq 1 \times 10^9$ $M_\odot$) galaxies and $\sim$ 790 high mass ($M \geq 2.5 \times 10^{10}$ $M_\odot$) galaxies for robust number statistics. Two independent methods are used to identify strongly interacting galaxies: a tailored visual classification system complemented with spectrophotometric redshifts and stellar masses, as well as the CAS merger criterion ($A > 0.35$ and $A > S$; Conselice 2003), based on CAS asymmetry A and clumpiness S parameters. This allows one of the most extensive comparisons to date between CAS-based and visual classification results. We set up this visual classification system so as to target interacting systems whose morphology and other properties suggest they are a recent merger of mass ratio $M1/M2 > 1/10$. While many earlier studies focused only on major mergers, we try to constrain the frequency of minor mergers as well, since they dominate the merger rates in ΛCDM models. Some of our results are outlined below.

(1) Among $\sim$ 790 high mass galaxies, *the fraction of visually-classified interacting systems over lookback times of 3–7 Gyr ranges from 9% ± 5% at $z \sim 0.24$–0.34, to 8% ± 2% at $z \sim 0.60$–0.80, as averaged over every Gyr bin.(Fig. 1a).* These systems appear to be in merging or post-merger phases, and are candidates for a recent merger of mass ratio $M1/M2 > 1/10$. Similar results on the interaction fraction are reported by Lotz et al. (2008). The lower limit on the major ($M1/M2 > 1/4$) merger fraction ranges from 1.1% to 3.5% over $z \sim 0.24$–0.80. The corresponding lower limit on the minor ($1/10 \leq M1/M2 < 1/4$) merger fraction ranges from 3.6% to 7.5%. This is the first, albeit approximate, empirical estimate of the frequency of minor mergers over the last 7 Gyr.

(2) For an assumed value of ~ 0.5 Gyr for the visibility timescale, it follows that *each massive ($M \geq 2.5 \times 10^{10}$ $M_\odot$) galaxy has undergone $\sim$ 0.7 mergers of mass ratio > 1/10 over the redshift interval $z \sim 0.24$–0.80.* Of these, we estimate that 1/4 are major mergers, 2/3 are minor mergers, and the rest are ambiguous cases of major or minor mergers. The corresponding merger rate R is a few $\times 10^{-4}$ galaxies Gyr^{-1} Mpc^{-3}. Among $\sim$ 2840 blue cloud galaxies of mass $M \geq 1.0 \times 10^9$ $M_\odot$, similar results hold.

(3) We compare our empirical merger rate R for high mass ($M \geq 2.5 \times 10^{10}$ $M_\odot$) galaxies to predictions from different ΛCDM-based simulations of galaxy

evolution, including the halo occupation distribution (HOD) models of Hopkins et al. (2007); semi-analytic models (SAMs) of Somerville et al. (2008), Bower et al. (2006), and Khochfar & Silk (2006); and smoothed particle hydrodynamics (SPH) cosmological simulations from Maller et al. (2006). To our knowledge, such extensive comparisons have not been attempted to date, and are long overdue. *We find qualitative agreement between the observations and models, with the (major+minor) merger rate from different models bracketing the observed rate, and showing a factor of five dispersion* (Fig. 1b). One can now anticipate that in the near future, improvements in both the observational estimates and model predictions will start to rule out certain merger scenarios and refine our understanding of the merger history of galaxies.

(4) The idea that galaxy interactions generally enhance the star formation rate (SFR) of galaxies is well established from observations (e.g., Joseph & Wright 1985; Kennicutt et al. 1987) and simulations (e.g., Hernquist 1989; Mihos & Hernquist 1994, 1996; Springel, Di Matteo & Hernquist 2005b). However, simulations cannot uniquely predict the factor by which interaction enhance the SF activity of galaxies over the last 7 Gyr, since both the SFR and properties of the remnants in simulations are highly sensitive to the stellar feedback model, the bulge-to-disk (B/D) ratio, the gas mass fractions, and orbital geometry (e.g., Cox et al 2006; di Matteo et al. 2007). Thus, empirical constraints are needed. Among ~ 3600 intermediate mass ($M \geq 1.0 \times 10^9\ M_\odot$) galaxies, we find that *the average SFR of visibly interacting galaxies is only modestly enhanced compared to non-interacting galaxies over $z \sim 0.24$–0.80* (Fig. 1c). This result is found for SFRs based on UV, UV+IR, and UV+stacked-IR data. This modest enhancement is consistent with the results of di Matteo et al. (2007) based on numerical simulations of several hundred galaxy collisions.

(5) The SF properties of interacting and non-interacting galaxies since $z < 1$ are of great astrophysical interest, given that the cosmic SFR density is claimed to decline by a factor of 4 to 10 since $z \sim 1$ (e.g., Lilly et al. 1996; Ellis et al 1996; Hopkins 2004; Pérez-González et al. 2005; Le Floc'h et al. 2005). We therefore set quantitative limits on the contribution of obviously interacting systems to the UV-based and UV+IR-based SFR density over $z \sim 0.24$–0.80. Among ~ 3600 intermediate mass ($M \geq 1.0 \times 10^9\ M_\odot$) galaxies, we find that *visibly interacting systems only account for a small fraction ($< 30\%$) of the cosmic SFR density over lookback times of ~ 3–7 Gyr ($z \sim 0.24$–0.80; Fig. (1d)).* Our result is consistent with that of Wolf et al. (2005) over a smaller lookback time interval of ~ 6.2–6.8 Gyr. In effect, our result suggests that *the behavior of the cosmic SFR density over the last 7 Gyr is predominantly shaped by non-interacting galaxies, rather than strongly interacting galaxies.* This suggests that the observed decline in the cosmic SFR density since $z \sim 0.80$ is largely the result of a shutdown in the SF of non-interacting galaxies.

3. Secular evolution and bars out to $z \sim 1$

Recent ACS studies show that prior to applying any correction for obscuration and redshift-dependent systematic effects, the directly observed optical fraction of strong (ellipticity ¿0.4) bars (Jogee et al. 2004; Sheth et al. 2008; Fig. 2a) and of strong and weak bars (Elmegreen et al. 2004; Zheng et al. 2005; Sheth et

al. 2008; Fig. 2b) in bright galaxies show a decrease by a factor between ~ 1.5 to ~ 2.3 between $z \sim 0.2$ and $z \sim 1$. However, interpretations differ on whether the observed variation is due in large part to systematic effects, such as the loss of spatial resolution and the rising obscuration by dust and star formation with redshift (Jogee et al. 2004; Marinova & Jogee 2007; Barazza et al. 2008), or reflects an intrinsic decline (Sheth et al. 2008) in the true bar fraction.

The decreasing spatial resolution alone can cause the optical bar fraction to artificially drop by a by a factor of 1.3 between $z \sim 0$ to $z \sim 1$ (e.g., Marinova & Jogee 2007, Barazza et al. 2008; Fig. 2c). The obscuration of bars by star formation and dust can further mask bars at optical wavelengths: even at $z \sim 0$ this effect already causes a factor of 1.3 loss in optically-visible bars (Marinova & Jogee 2007), and this loss factor X is expected to rise with redshift out to $z \sim 1$, since the average SFR and SFR density rises by a factor of 3 to 10 between $z \sim 0$ and $z \sim 1$ (e.g., Lilly et al .1996; Le Floc'h et al. 2005; Jogee et al. 2009). The amount by which X rises with z is presently unknown and constitutes the largest uncertainty.

Thus, at the present time, the data allow for three possibilities: the true bar fraction in bright galaxies may show a moderate decline below a factor of 2, a constant value, or even a rise out to $z \sim 1$. In order to constrain X and help distinguish between the three possibilities, we need future work in the rest-frame NIR with WFC3 and JWST so as to trace optically-obscured bars of intermediate size (Fig. 2d).

Acknowledgments. S. J. acknowledges support from the National Aeronautics and Space Administration (NASA) LTSA grant NAG5-13063, NSF grant AST-0607748, and *HST* grants G0-10395 from STScI, which is operated by AURA, Inc., for NASA, under NAS5-26555.

References

Abraham, R. G.,Merrifield, M. R., Ellis, R. S.,et al. 1999,MNRAS, 308, 569
Barazza, F. D., Jogee, S., & Marinova, I. 2008a, ApJ, 675, 1194 (BJM08)
Böker, T. Laine, S., van der Marel, R. P., et al. 2002, AJ, 123, 1389
Bower, R. G., Benson,A. J., Malbon, R., et al. 2006, MNRAS, 370, 645
Conselice, C. J. 2003, ApJs, 147, 1
Cox, T. J., Jonsson, P., Primack, J. R., & Somerville, R. S.2006, MNRAS, 373, 1013
Dickinson, M., Papovich, C., Ferguson, H. C., & Budavári, T.2003, ApJ, 587, 25
Di Matteo, P., Combes, F., Melchior, A.-L., & Semelin, B.2007, A&A, 468, 6
Hernquist, L.1989, Nature, 340, 687
Hernquist, L. & Mihos, J. C.1995, ApJ, 448, 41
Hopkins et al. 2007, ApJ, submitted (arXiv:0706.1243)
Jogee, S. 1999, Ph.D. thesis, Yale University
Jogee, S., Shlosman, I., Laine, S., et al. 2002, ApJ, 575, 156
Jogee, S., Scoville, N., & Kenney, J. D. P.2005, ApJ, 630, 837
Jogee S. 2006, in Lecture Notes in Physics, Vol. 693, Physics of Active Galactic Nuclei at all Scales, ed. D. Alloin, R. Johnson & P. Lira (Berlin/Heidelberg: Springer), 143
Jogee, S., et al. 2009, ApJ, 697, 1971
Joseph, R. D., & Wright, G. S.1985, MNRAS, 214, 87
Kautsch, S. J., Grebel, E. K., Barazza, F. D., & Gallagher, J. S., III 2006, A&A, 445, 765

Kennicutt, R. C.,Jr., Roettiger, K. A., Keel, W. C., van der Hulst, J. M., & Hummel, E.1987, AJ, 93, 1011
Khochfar, S., &Burkert, A.2005, MNRAS, 359, 1379
Khochfar, S., & Silk, J.2006, MNRAS, 370, 902
Kormendy, J. 1993, in IAU Symposium 153, Galactic Bulges, ed. H. Dejonghe & H. J. Habing (Dordrecht: Kluwer), 209
Kormendy, J., & Kennicutt, R. C.2004, ARAA, 42, 603
Le Floc'h, E., et al.2005, ApJ, 632, 169
Lilly, S. J., Le Fevre, O., Hammer, F., & Crampton, D.1996, ApJl, 460, L1
Lotz, J. M., et al.2008, ApJ, 672, 177
Maller, A. H., Katz, N., Kereš, D., Davé, R., & Weinberg, D. H.2006, ApJ, 647, 763
Mihos, J. C., & Hernquist, L.1994, ApJ, 437, 611
Mihos, J. C., & Hernquist, L.1996, ApJ, 464, 641
Navarro, J. F., & Steinmetz, M.2000, ApJ, 538, 477
Pérez-González, P. G., et al.2005, ApJ, 630, 8
Quinn, P. J., Hernquist, L., & Fullagar, D. P.1993, ApJ, 403, 74
Rix, H., et al.2004, ApJs, 152, 163
Sheth, K., et al. 2008, ApJ, 675, 1141
Somerville, R.S., Hopkins, P. F., Cox, T.J., et al. 2008, MNRAS, accepted
Somerville, R. S., & Primack, J. R.1999, MNRAS, 310, 1087
Springel, V., & Hernquist, L.2005, ApJl, 622, L9
Springel, V., et al.2005a, Nature, 435, 629
Springel, V., Di Matteo, T., & Hernquist, L.2005b, MNRAS, 361, 776
Steinmetz, M., & Navarro, J. F.2002, NewA, 7, 155
Weinzirl, T., Jogee, S., Khochfar, S., Burkert, A. & Kormendy, J. 2009, ApJ, 696, 41
Wolf, C., et al.2005, ApJ, 630, 771

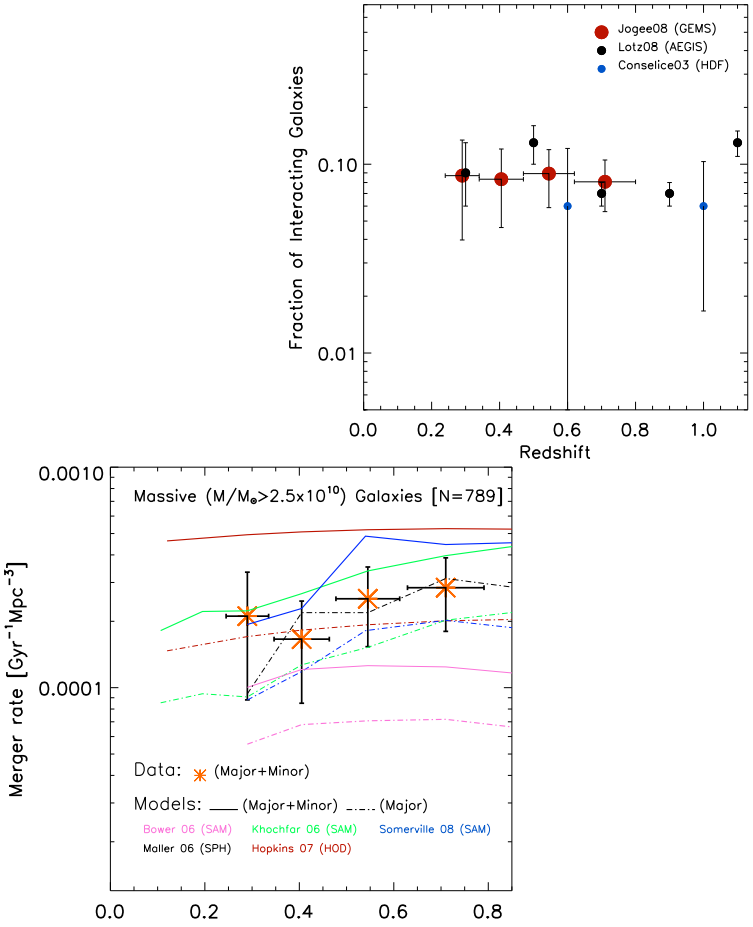
Jogee08 (GEMS)
Lotz08 (AEGIS)
Conselice03 (HDF)
Fraction of Interacting Galaxies
0.10
0.01
0.0
0.2
0.4
0.6
0.8
1.0
Redshift
Massive (M/M$_\odot$>2.5x10^{10}) Galaxies [N=789]
Merger rate [Gyr^{-1}Mpc^{-3}]
0.0010
0.0001
Data: (Major+Minor)
Models: (Major+Minor) (Major)
Bower 06 (SAM)
Khochfar 06 (SAM)
Somerville 08 (SAM)
Maller 06 (SPH)
Hopkins 07 (HOD)
0.0
0.2
0.4
0.6
0.8

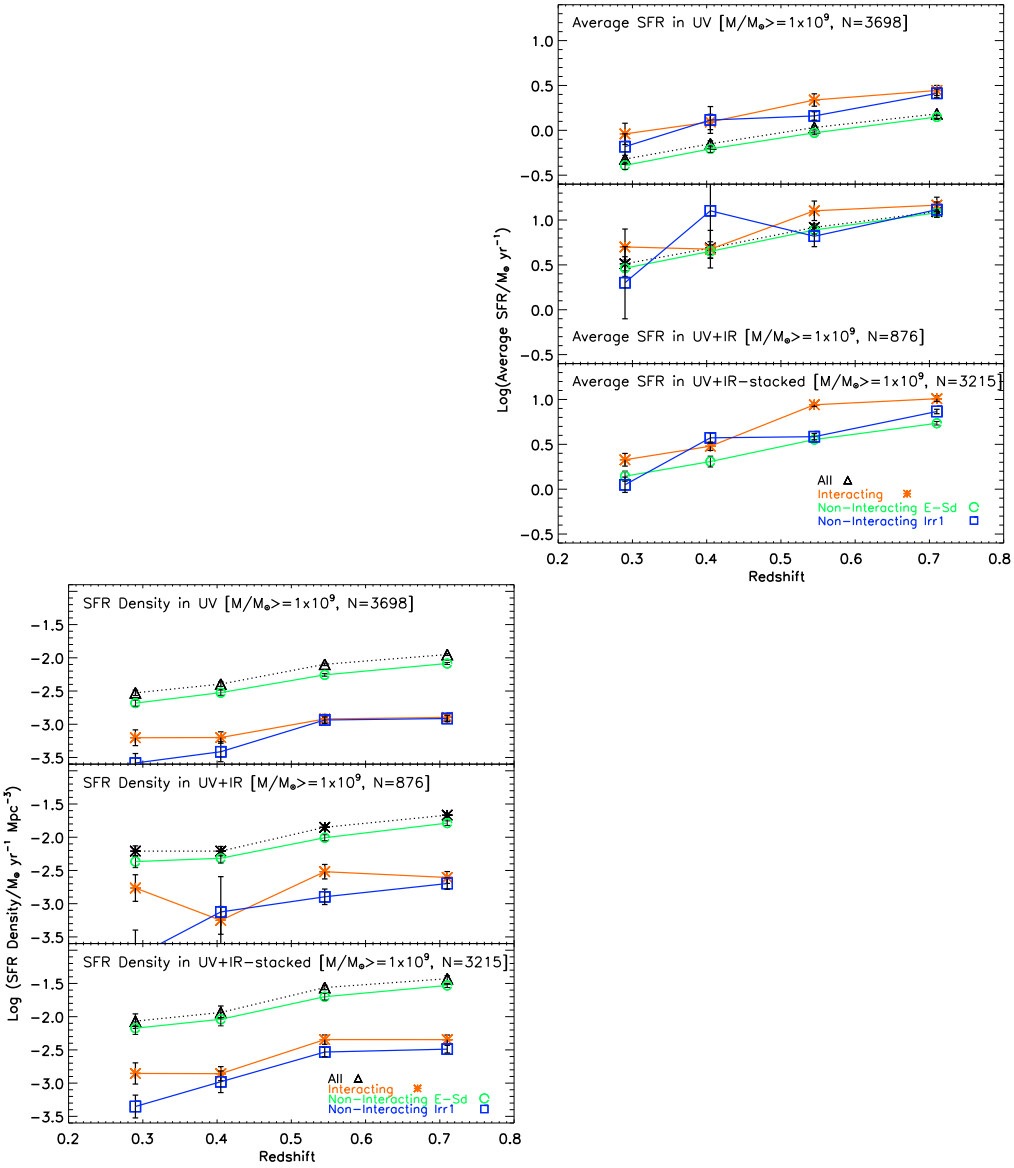

Fig. 1a (Top Left): We show the observed fraction of interacting/merging galaxies from Lotz et al. (2008), Jogee et al. (2009), and Conselice (2003). among high mass galaxies is compared to the rate of (major+minor) mergers (solid lines) predicted by different ΛCDM-based models of galaxy evolution. **Fig. 1c (Lower Left):** The average SFR of interacting and non-interacting galaxies are compared. The average UV-based SFR (top panel; based on 3698 galaxies), average UV+IR-based SFR (middle panel; based on only the 876 galaxies with 24um detections), and average UV+IR-stacked SFR (based on 3215 galaxies with 24um coverage) are shown. In all there cases, the average SFR of interacting galaxies is only modestly enhanced compared to non-interacting E-Sd galaxies over $z \sim 0.24$–0.80 (lookback time $\sim$ 3–7 Gyr). **Fig. 1d (Lower Right):** As in. 2c, but now showing the SFR density of galaxies. In all bins, interacting

galaxies only contribute a small fraction (typically below 30%) of the total SFR density. [All figures are adapted from Jogee et al (2009)]

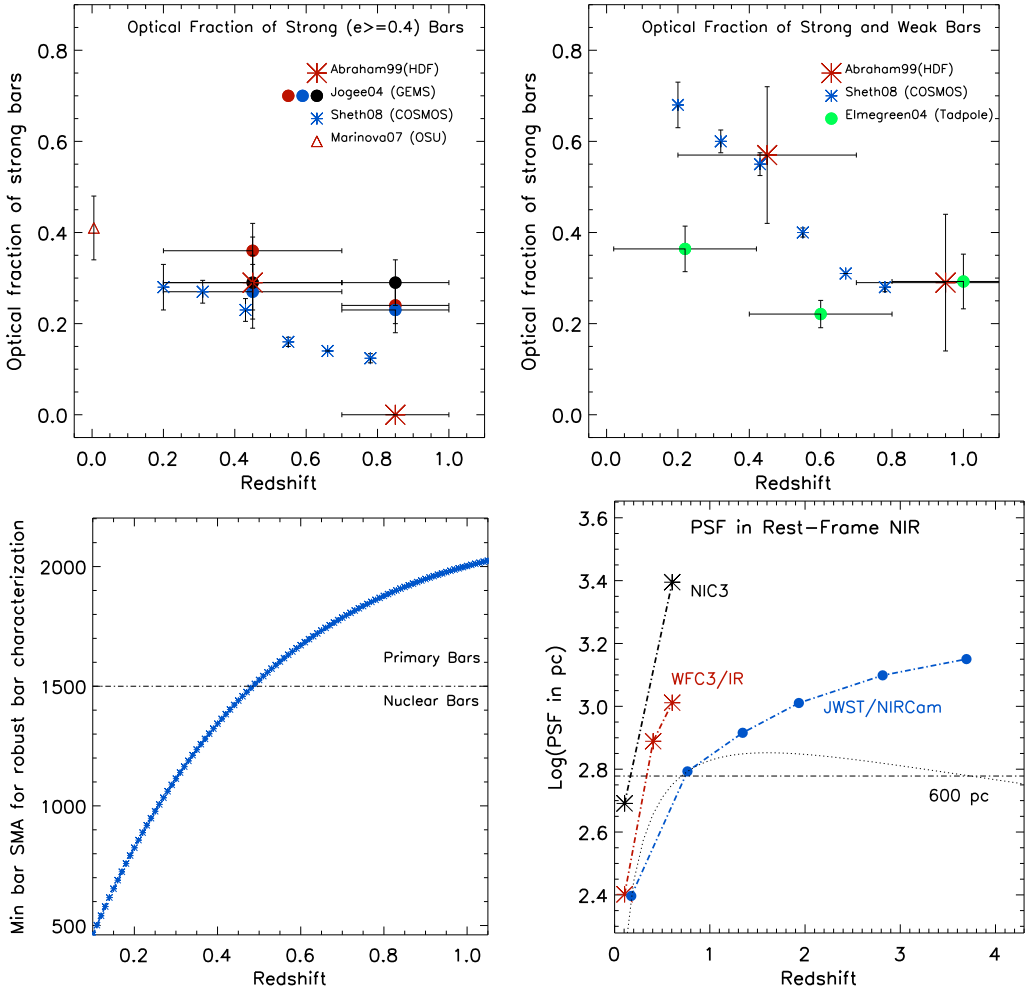

Fig. 1a (Top Left): The observed rest-frame optical fraction of *strong (ellipticity $e \geq 0.4$)* bars as a function of redshift is shown for the studies by Abraham et al.(1999), Jogee et al. (2004), Marinova & Jogee (2007), and Sheth et al. (2008). The data points for Abraham et al. (1999) are based on their Figure 4, which shows that the fraction of strong bars with $e \geq 0.4$ (or $(b/a)^2 \leq 0.36$) falls from 9/31 ($29\% \pm 10\%$) over The red, black, and blue filled circles for Jogee et al. (2004) show the results obtained using three commonly used techniques (based on Sérsic cuts, rest-frame color cuts, and concentration indices) to identify spiral galaxies. **Fig. 1b (Top Right):** As in 1a, but showing the observed rest-frame optical fraction of *(strong+weak)* bars, with no ellipticity cuts applied. **Fig. 1c (Lower Left):** We show the minimum semi-major axis ($a_{\rm min}$) that a bar must have so that it can be robustly characterized using ellipse-fitting and the quantitative criteria in Jogee et al. (2004). We increasingly lose primary bars with a in the range of 1.5 to 2.0 kpc at $z > 0.5$. **Fig. 1d (Lower Right):** Future observations in the rest-frame NIR with WFC3 and JWST will enable us to trace optically-obscured primary bars of intermediate sizes, at the resolution (PSF) shown.

GALAXY EVOLUTION: EMERGING INSIGHTS AND FUTURE CHALLLENGES
ASP Conference Series, Vol.
@jourvol, © 2009
S. Jogee, I. Marinova, L. Hao, and G. A Blanc

Too Few to be Relevant: Major Merger Statistics up to $z \sim 1$

Carlos López-Sanjuan,[1] Marc Balcells,[1] Pablo G. Pérez-González,[2] Guillermo Barro,[2] César Enrique García-Dabó,[1,3] Jesús Gallego,[2] and Jaime Zamorano[2]

Abstract. We study the evolution of galaxy structure and of the major merger fraction since $z \sim 1$ to present in GOODS-S field for $M_{\rm B} \leq -20$ and $M_\star \geq 10^{10}\ M_\odot$ selected galaxies. We segregate the galaxies into early-type galaxies (ET, E/S0/Sa), and late-type galaxies (LT, Sb–Irr) by their position in the concentration–asymmetry plane, while we pick up high asymmetric sources as disk–disk major merger remnants. We find that the early-type fraction ($f_{\rm ET}$) rises with cosmic time in both samples. However, the number density evolution is very different: the decrease in the total number density of $M_{\rm B} \leq -20$ galaxies since $z = 1$ is due to the decrease in the late-type population, while the increase in the total number density of $M_\star \geq 10^{10}\ M_\odot$ in the same redshift range is due to early-type evolution. This suggests that we need a structural transformation between late-type galaxies that form stars actively and early-type galaxies in which the stellar mass is located. Comparing the observed evolution with the disk–disk major merger rate in GOODS-S, we infer that only $\sim 17\%$ of the early-type galaxies that appear since $z = 1$ can be explained by these kinds of mergers, suggesting that minor mergers and secular evolution are the main processes in the structural evolution of $M_\star \geq 10^{10}\ M_\odot$ galaxies since $z \sim 1$.

1. Introduction

It is known that more massive galaxies are the first to form their stars and populate the mass function, being in place at $z \sim 1$. This is the called the 'downsizing' scenario (Cowie et al. 1996): several massive galaxies experienced most of their star formation at early times and were passive by $z \sim 1$, and many among the less massive galaxies experienced extended star formation histories (Bundy et al. 2006; Pérez-González et al. 2008). This fact is a challenge to the popular hierarchical Λ-CDM models, in which more massive dark matter halos are the final stage of successive mergers of smaller halos. However, the treatment of the baryonic component is still unclear and only accessible via models (Bower et al. 2006; De Lucia & Blaizot 2007). In this framework, the role of galaxy mergers in the buildup of the red sequence and their relative importance in the evolution of the galaxy properties, e.g., morphology, mass, and color, is an important open question.

[1]Instituto de Astrofísica de Canarias, Calle Vía Láctea s/n, E-38205 La Laguna, Tenerife, Spain

[2]Departamento de Astrofísica y Ciencias de la Atmósfera, Universidad Complutense de Madrid, Madrid, Spain

[3]European South Observatory, Karl-Schwarzschild-Strasse 2, D-85748 Garching, Germany

In this work we summarize preliminary results about the redshift evolution of the disk–disk major merger fraction, $f_{\rm m}^{\rm mph}$, and the early/late type fraction in B-band luminosity and mass selected samples up to $z \sim 1$ in GOODS-S. We use $H_0 = 70$ km s^{-1} Mpc^{-1}, $\Omega_{\rm M} = 0.3$, and $\Omega_\Lambda = 0.7$ throughout. All magnitudes are Vega unless noted otherwise.

2. Data

Galaxies were selected from the merged photometric catalog of *Spitzer* IRAC selected sources in GOODS-S published by Pérez-González et al. (2008). This catalog has 9676 IRAC sources detected in 225 arcmin^2. The catalog is 75% complete down to [3.6] $\sim$ 23.5 (AB), and includes spectroscopic redshifts and photometric data in a variety of bands from the UV to the MIR, including GALEX (UV), HST ACS ($F435W, F606W, F775W, F850LP$), VLT ISAAC ($J, H, K$), *Spitzer* IRAC (3.6, 4.5, 5.4, 8.5 μm), *Spitzer* MIPS (24 μm), *Chandra* (X-ray) and COMBO-17 filters. We have used the photometric redshifts, absolute magnitudes, and stellar masses presented in Pérez-González et al. (2008)[1]. We took two different samples: one comprises 1122 sources with $M_{\rm B} \leq -20$, while another comprises 982 objects with $M_\star > 10^{10}\ M_\odot$.

3. Asymmetry Index

We use the asymmetry index A (Abraham et al. 1996) to identify recent merger systems which are very distorted, and in combination with the concentration index C (Abraham et al. 1994) to classify our galaxies as early/late type (§ 5). On the basis of asymmetry measurements on images of nearby merger remnants, previous merger fraction determinations have taken a system to be a major merger remnant if its asymmetry index is $A > A_{\rm m}$, with $A_{\rm m} = 0.35$ (Conselice 2003). Note that this criterion applies to disk–disk mergers only.

The asymmetry index measured on survey images systematically varies with the source redshift due to the loss of spatial resolution with z and cosmological dimming. In our work we treated this bias by artificially redshifting all the source images to a representative common redshift, which we chose as $z_{\rm d} = 1$. The degradation procedure is explained in detail in López-Sanjuan et al. (2009a) and López-Sanjuan et al. (2009b, hereafter L09). We obtained the concentration index C of the sources in the same way. The final obtained concentrations and asymmetries referred to $z_{\rm d} = 1$ provide a homogeneous data set that permits consistent morphological studies in the GOODS-S field.

How does degradation affect the local merger criterion $A > A_{\rm m} = 0.35$? We assumed that $A_{\rm m}(z) = A_{\rm m}(0) + \delta_{\rm A} z = 0.35 + \delta_{\rm A} z$, where the degradation rate $\delta_{\rm A}$ is the statistical descent of asymmetry with redshift (see L09 for details). We obtained $\delta_{\rm A} = -0.05$ for luminosity and mass-selected samples. Finally, we used $A_{\rm m}(1) = 0.35 - 0.05 = 0.3$.

[1] See `http://t-rex.fis.ucm.es/~pgperez/Proyectos/databaseuse.en.html` for details.

4. Merger Fraction Determination

Following Conselice (2006a), the merger fraction by morphological criteria is $f_{\rm m}^{\rm mph} = N_{\rm m}/N_{\rm tot}$, where $N_{\rm m}$ is the number of the distorted sources in the sample with $A > A_{\rm m}$, and $N_{\rm tot}$ is the total number of sources in the sample. In López-Sanjuan, García-Dabó, & Balcells (2008) they developed a maximum likelihood (ML) method that yields the most probable value of $f_{\rm m,k}^{\rm mph}$ in $[z_{\rm k}, z_{\rm k+1}]$ interval taking into account not only the z and A values, but also their experimental errors. In addition, the ML method provides a reliable estimate of the 68% confidence interval of $f_{\rm m,k}^{\rm mph}$. Using synthetic catalogs, López-Sanjuan et al. (2008) also show that the experimental errors tend to smooth an initial distribution described by $f_{\rm m,k}^{\rm mph}$, due to spill-over of sources to neighboring bins. This leads to a $\sim$ 30–100% overestimate of the galaxy merger fraction in typical observational cases. In addition, thanks to the use of the ML method, they accurately recover the initial merger fractions: the input and ML method merger fraction difference is $\sim$ 1% even when experimental errors are as large as the bin size.

5. Structural Classification

We segregated our galaxies in bulge-dominated galaxies (E/S0/Sa, named early types), and in disk-dominated galaxies and irregulars (Sb–Irr, named late types) by their position in the concentration–asymmetry plane (C–A). In Figure 1 we show the distribution in the C–A plane of the 757 sources with $M_{\rm B} \leq -20$ and $0.35 < z < 1.1$, that present a clear bimodality (Zamojski et al. 2007; Conselice, Yang, & Bluck 2009). We assigned early-type galaxies to the less asymmetric, more concentrated peak, while late-type galaxies to the asymmetric, less concentrated peak (Ilbert et al. 2006): we took as separation the line $A = 0.3C - 0.75$. In Figure 1 we also see the disk–disk major merger area, $A > 0.3$. To obtain unbiased early/late type fractions in function of redshift we used the ML method in the calculation.

6. Results

6.1. Merger Fraction Evolution

We obtain lower values than in previous asymmetry merger fraction studies, $f_{\rm m}^{\rm mph} < 0.06$ (López-Sanjuan et al. 2009b). On the other hand, our merger fractions are in good agreement with those expected by the Jogee et al. (2009) eye-ball study, $f_{\rm m}^{\rm mph} = 0.03 \pm 0.01$. Parameterizing the merger fraction evolution as $f_{\rm m}^{\rm mph}(z) = f_{\rm m}^{\rm mph}(0)(1+z)^{\rm m}$, we obtain that $f_{\rm m}^{\rm mph}(z, M_{\rm B} \leq -20) = 0.013(1+z)^{1.8}$, while $f_{\rm m}^{\rm mph}(z, M_\star \geq 10^{10}\ M_\odot) = 0.001(1+z)^{5.4}$. This different evolution becomes similar when we compute the disk–disk major merger rate, $\Re_{\rm m}^{\rm mph}$ (see Lotz et al. 2008a, for details): $\Re_{\rm m}^{\rm mph}(z, M_{\rm B} \leq -20) \propto (1+z)^{3.3}$, while $\Re_{\rm m}^{\rm mph}(z, M_\star > 10^{10}\ M_\odot) \propto (1+z)^{3.5}$. In the merger rate determination we assumed a merger timescale $T_{\rm m,A} = 0.475 \pm 0.125$ Gyr (Conselice 2006a; Lotz et al. 2008b).

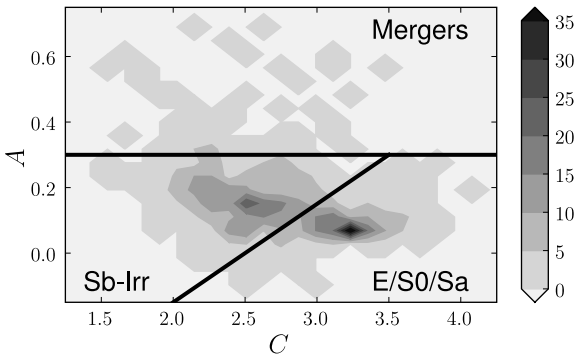

Figure 1. Bimodal distribution of $M_{\rm B} \leq -20$ sources with $0.35 < z < 1.1$ in the concentration–asymmetry plane. We mark three areas in the figure: early-type galaxies (E/S0/Sa), late-type galaxies (Sb–Irr), and disk–disk major mergers ($A > 0.3$).

6.2. Structural Evolution in GOODS-S

We find that the fraction of early-type galaxies increases with cosmic time in both samples, while the fraction of late-types decreases. More interesting is the evolution in number density, Figure 2. We see that for $M_{\rm B} \leq -20$ galaxies, late-type number density decreases with time, while early-type number density is nearly constant. Because descent in *total* number density of $M_{\rm B} \leq -20$ galaxies since $z \sim 1$ is due to the star formation fading, this result suggests that star formation at $z < 1$ is located in late-type galaxies, in agreement with Bell et al. (2005) and Jogee et al. (2009). On the other hand, the increase in the number density of $M_\star \geq 10^{10}\ M_\odot$ galaxies is due to the increase in the early-type population. Hence, we need a structural transformation from late-type galaxies, where stars are forming, to early-type galaxies, where the stellar mass is located, as suggested by Bell et al. (2007). The question is, can disk–disk major mergers drive this structural transformation?

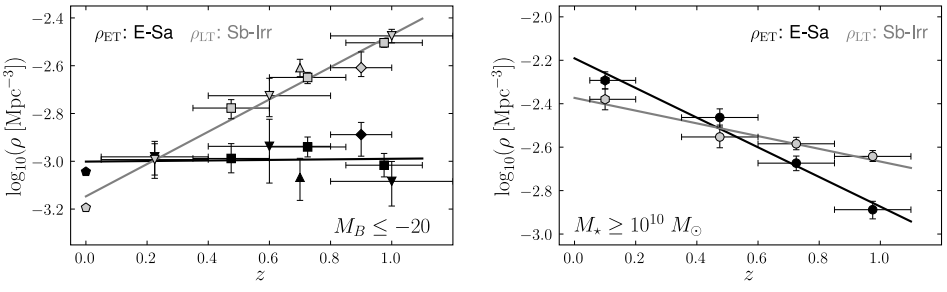

Figure 2. Number density evolution of early-type (black) and late-type galaxies (gray) in GOODS-S. *Left*: Results for $M_{\rm B} \leq -20$ galaxies. Squares are from our work, diamonds from Lotz et al. (2008a), triangles from Scarlata et al. (2007), inverted triangles from Ilbert et al. (2006), and pentagons from Conselice (2006b). *Right*: Results for $M_\star \geq 10^{10}\ M_\odot$ galaxies. Circles are from our work, while hexagons are from Mandelbaum et al. (2006).

6.3. The Role of Major Mergers in Structural Evolution Since $z \sim 1$

If we integrate the disk–disk major merger rate since $z = 1$ to the present (§ 6.1), and assume that all remnants of this kind of mergers are early-type galaxies (Hopkins et al. 2008), we obtain the number density of new early-type galaxies that comes from disk–disk major mergers, $\rho_{\rm ET,m}$. Comparing $\rho_{\rm ET,m}$ with the observed number density of *total* new early-type galaxies that appear since $z = 1$, $\rho_{\rm ET,new}$, we infer that $17^{+12}_{-8}\%$ of $\rho_{\rm ET,new}$ can be explained by disk–disk major mergers (López-Sanjuan et al., in prep.) This implies that we need other mechanisms, i.e., minor mergers or secular evolution, to explain the structural evolution of galaxies since $z = 1$.

Acknowledgments. We dedicate this work to the memory of our six IAC colleagues and friends who met with a fatal accident in Piedra de los Cochinos, Tenerife, in February 2007, with a special thanks to Maurizio Panniello, whose teachings of `python` were so important for this work. We thank S. Jogee for a stimulating and challenging meeting. This work was supported by the Spanish Programa Nacional de Astronomía y Astrofísica through project number AYA2006-12955.

References

Abraham R. G., Valdes F., Yee H. K. C., van den Bergh S., 1994, ApJ, 432, 75
Abraham, R. G., van den Bergh, S., Glazebrook, K., Ellis, R. S., Santiago, B. X., Surma, P., & Griffiths, R. E. 1996, ApJS, 107, 1
Bell, E. F., et al. 2005, ApJ, 625, 23
Bell, E. F., Zheng, X. Z., Papovich, C., Borch, A., Wolf, C., & Meisenheimer, K. 2007, ApJ, 663, 834
Bower, R. G., Benson, A. J., Malbon, R., Helly, J. C., Frenk, C. S., Baugh, C. M., Cole, S., & Lacey, C. G. 2006, MNRAS, 370, 645
Bundy, K., et al. 2006, ApJ, 651, 120
Conselice C. J., 2003, ApJS, 147, 1
Conselice C. J., 2006a, ApJ, 638, 686
Conselice C. J., 2006b, MNRAS, 373, 1389
Conselice C. J., Yang C., Bluck A. F. L., 2009, MNRAS, 361
Cowie L. L., Songaila A., Hu E. M., Cohen J. G., 1996, AJ, 112, 839
De Lucia G., Blaizot J., 2007, MNRAS, 375, 2
Hopkins P. F., Hernquist L., Cox T. J., Dutta S. N., Rothberg B., 2008, ApJ, 679, 156
Ilbert, O., et al. 2006, A&A, 453, 809
Jogee, S., et al. 2009, ApJ, 697, 1971
López-Sanjuan, C., et al. 2009a, ApJ, 694, 643
López-Sanjuan C., et al., 2009b, ArXiv 0905.2765
López-Sanjuan C., García-Dabó C. E., Balcells M., 2008, PASP, 120, 571
Lotz, J. M., et al. 2008a, ApJ, 672, 177
Lotz J. M., Jonsson P., Cox T. J., Primack J. R., 2008b, MNRAS, 391, 1137
Mandelbaum R., Seljak U., Kauffmann G., Hirata C. M., Brinkmann J., 2006, MNRAS, 368, 715
Pérez-González P. G., et al., 2008, ApJ, 675, 234
Scarlata, C., et al. 2007, ApJS, 172, 406
Zamojski, M. A., et al. 2007, ApJS, 172, 468

GALAXY EVOLUTION: EMERGING INSIGHTS AND FUTURE CHALLLENGES
ASP Conference Series, Vol.
@jourvol, © 2009
S. Jogee, I. Marinova, L. Hao, and G. A Blanc

Are Mergers so Good at Triggering Starbursts?

Aday R. Robaina,[1] Eric F. Bell,[1] Rosalind E. Skelton,[1] Daniel H. McIntosh,[2] Rachel Somerville,[3] and STAGES collaboration

[1]*Max-Planck-Institut für Astronomie, Königstuhl 17, D-69117 Heidelberg, Germany*
[2]*Dept. of Physics, UMKC, Kansas City, MO 64110, USA*
[3]*Space Telescope Science Institute, Bloomberg 516, Baltimore, USA*

Abstract. Observations and simulations tell us that major galaxy interactions can lead to intense bursts of star formation. In order to constrain models and understand the fraction of stellar mass formed in mergers, it is of interest, however, to determine the *average* enhancement of star formation rate in major mergers. We apply two-point correlation function techniques, supplemented with morphlogical classifications to two deep cosmological surveys (ECDFS/GEMS and A901-2/STAGES) using COMBO-17 redshifts, colors and stellar masses plus IR-derived SFRs from *Spitzer*. For a sample of galaxies at $0.4 < z < 0.8$ we find a mild average enhancement $\epsilon = 1.50 \pm 0.25$ of the SFR of massive ($M_* \geq 10^{10}\mathrm{M}_\odot$) star-forming galaxies caused by major merging out to projected distances of $\sim 40\,\mathrm{kpc}$. Using these results, we find that less than 10% of star formation at $z \sim 0.6$ is *triggered directly* by major mergers and interactions; star formation triggered by major mergers does not significantly impact the growth of stellar mass at $z < 1$.

1. Introduction

It has been known for some time that at least a fraction of mergers and interactions lead to dramatically-enhanced star formation (SF) (Sanders et al. 1988; Barton et al. 2000; Lambas et al. 2003; Barton et al. 2007). Following the discovery of luminous and ultra-luminous infrared galaxies (LIRGs and ULIRGs respectively) it became clear that the highest-intensity star formation events were invariably hosted by merging galaxies (Sanders et al. 1988). In a more statistical way, many authors (Barton et al. 2000; Lambas et al. 2003; Barton et al. 2007; Li et al. 2008) have found an anticorrelation between the degree of enhancement in the star formation and the separation between two galaxies in a pair.

Furthermore, simulations of interacting galaxies which explicitly include gas and star formation models have shown that changes in the potential well and collisions lead to wide-scale shocking and compression of gas, resulting in significant enhancement in star formation(; Mihos & Hernquist 1996; Di Matteo et al. 2007; Cox et al. 2008).

Beyond the effect on individual galaxies, for a number of applications the parameter of interest is the average enhancement in star formation triggered by merging. In the present work we try to address statistically the problem of

the SF enhancement in major galaxy interactions and answer a simple question: What fraction of the stellar mass is created by major galaxy mergers?

2. The Method

The goal of this work is to explore the star formation rate in major mergers between massive galaxies, both during the pre-merger interaction and after the coalescence of the nuclei. To track the star formation in pre-coalesence interactions and mergers, we chose to study a stellar mass–limited sample with a lower mass cut of $M_\star = 10^{10}\mathrm{M}_\odot$ and a limiting observed magnitude of $m_R = 23.5$ in the redshift slice of $0.4 < z \leq 0.8$. In addition to this stellar mass cut, we choose only galaxies that fall into the footprint of the ACS surveys GEMS and STAGES and from those, only the ones that are inside the region covered by *Spitzer*. These criteria result in a final sample of 2551 galaxies.

The method used to find the enhancement in the star formation activity, as well as the exhaustive description of the redshifts, SFRs, stellar masses, morphological classes and other quantities used here are extensively explained in Robaina et al. (in prep.), Wolf et al. (2003) and references therein. Here we briefly explain the main body of our methodology and refer the reader to that paper for further information.

2.1. 2-point Marked Correlation Function

In this work, we choose to explore the enhancement of star formation triggered by galaxy merging using weighted projected two-point correlation function techniques (Davis & Peebles 1983; Beisbart & Kerscher 2000). We made this choice for two reasons. Firstly, redshift uncertainties from COMBO-17, or indeed any redshift survey, necessitate the use of projected correlation functions to explore the properties of close physical pairs of galaxies (Bell et al. 2006). Secondly, even if one had accurate spectroscopic redshifts, the use of correlation function formalism is a convenient mathematical framework in which to discuss the phenomenon robustly (Li et al. 2008).

The projected correlation function $w(r_\mathrm{p})$ is the integral along the line of sight of the real-space correlation function:

$$w(r_\mathrm{p}) = \int_{-\infty}^{\infty} \xi([r_\mathrm{p}^2 + \pi^2]^{1/2}) d\pi, \tag{1}$$

where r_p is the distance between the two galaxies projected on the plane of sky and π the line-of-sight separation. A typical estimator for this unweighted correlation function is $w(r_\mathrm{p}) = \Delta(DD/RR - 1)$, where Δ is the path length being integrated over, DD is the histogram of separations between real galaxies and RR is the histogram of separations between galaxies in a randomly-distributed catalogue.

In order to perform the weighted statistics we choose to use an additive weight, this is, the weight of the pair is the sum of the weights of the individual galaxies ($w_{i,j} = w_i + w_j$). The weights we use are the SFR and the specific SFR (SFR/M_*) of the galaxies, and the estimator we use to calculate the

enhancement $E(r_{\rm p})$ is:

$$E(r_{\rm p}) = \frac{PP/DD}{\langle P_{ij} \rangle}, \tag{2}$$

where PP is the histogram of the separations weighted with the SFR (or specific SFR) of the pairs and $\langle P_{ij} \rangle$ is the average value of the weight used across the sample (see Robaina et al. in prep., for a deeper explanation).

As we are interested in major galaxy interactions we impose a stellar-mass ratio criteria. All the pairs we consider here have a mass ratio between 1:1 and 1:4. We run two different analysis: the first is the autocorrelation of star forming galaxies and the second is a cross-correlation in which the primary galaxy is defined to be forming stars and the secondary galaxy can be every other galaxy in the sample, star forming or not.

2.2. Visual Morphologies

A challenge encountered when constructing a census of SF in pairs and mergers is accounting for systems with separations of < 2" (the radius within which we can no longer separate two massive galaxies using COMBO-17 ; Bell et al. 2006). We attempt to complete the census of close physical pairs by including visually-classified interacting pairs of galaxies, or merger remnants, into the sample in the $< 15\,$kpc bins.

In order to track star formation in very close pairs and merger remnants, we decided to include only visually-classified merging systems with a mass $> 2 \times 10^{10} {\rm M}_{\odot}$: i.e. the minimum possible mass of a merger between two galaxies of $10^{10} {\rm M}_{\odot}$ each.

A visual inspection of the galaxy sample was carried out by four independent human classifiers in order to identify morphological signatures of gravitational interactions. We assigned every object to one of four groups as follows: 1) Isolated galaxies, 2) Major close interactions and 3) Merger remnants.

Galaxies in group 1 are included in the two point correlation function analysis as isolated galaxies, and any SF triggered by major interactions is accounted for by that method. As we have four different classifications for every object (one given by each human classifier), we randomly assign one of them, calculate the average value of the weight we are using and repeat the process a number of times. This approach presents the clear advantage that the morphology of every object is weighted with *the four* classifications given. This means that objects with not-so-clear morphologies are not just assigned to one category when we calculate the SFR (or specific SFR) enhancement, reducing the chances of a wrong measure due to an incorrect morphology estimate.

3. Results

In Figure 1 we show the main findings of this work. The specific SFR in galaxy pairs is mildly but clearly enhanced with respect to the average SSFR in the sample out to separations of $\sim 40\,$kpc. We interpret this as clear evidence that major galaxy interactions trigger, on average, weak bursts of star formation. This result is not in contradiction with the extreme starbursts seen in ULIRGs

and LIRGS if, as the simulations predict, the most intense bursts of star formation last only for $\sim 100\,\mathrm{Myr}$ (Di Matteo et al. 2007; Cox et al. 2008).

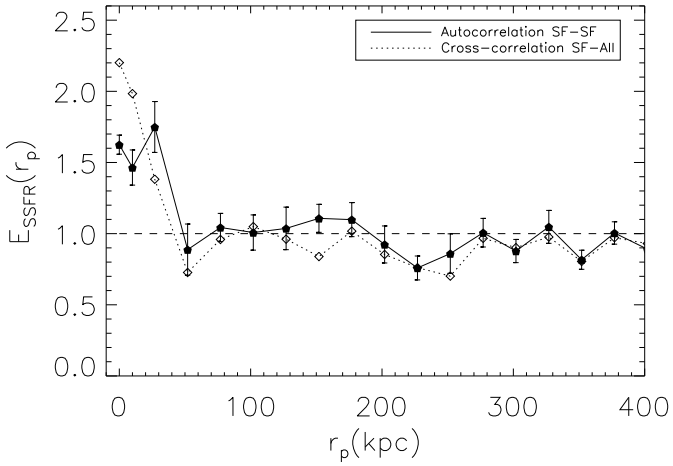

Figure 1. Specific SFR enhancement as a function of the projected separation between two galaxies. A clear enhancement is present in galaxy pairs and mergers below 40 kpc in both the autocorrelation of star forming galaxies and the cross-correlation between star formers and all galaxies in the sample. We use proper coordinates as the process of interest is fully decoupled from the Hubble flow. Figure taken from Robaina et al. (in prep.).

If we repeat the same exercise with the SFR instead of the SSFR we also recover a mild enhancement. Taking into account both SFR and SSFR enhancements we find an average value in pairs $r_\mathrm{p} < 40\,\mathrm{kpc}$ of $\epsilon = 1.50 \pm 0.25$ in the case of the SF-SF autocorrelation and $\epsilon = 1.80 \pm 0.30$ for the SF-All cross-correlation.

Our result is in extremely good agreement with the enhancement found by Li et al. (2008) in the local Universe (SDSS) and also with that of Lin et al. (2007) at $0.75 < z < 1.1$ and Jogee et al. (2009) at $0.24 < z < 0.8$. The lack of significant difference between our results and both the $z = 0.1$ and $z = 1$ results, despite the factors of several difference between the star formation rates of galaxies between $z = 1$ and $z = 0$ (see, e.g., Hopkins 2004; Zheng et al. 2007) is interesting, and points to a picture in which at least the average enhancement of star formation appears to scale reasonably linearly with the 'pre-existing' star formation in the population.

3.1. What fraction of SFR is *directly* triggered by major interactions?

Once we have the average enhancement in SFR, it is relatively easy to calculate the fraction of the SFR which is directly triggered by major galaxy interactions. We note that the average SFR in *all pairs* in our sample (limited to have $> 10^{10}\mathrm{M}_\odot$, be in pairs with mass ratios between 1 : 1 and 4 : 1, and have

24μm fluxes $> 83\mu$Jy and/or be blue) is $SFR_{\rm typical,pair} = 16.4 \pm 0.7 {\rm M}_\odot {\rm yr}^{-1}$. The total SFR in the 38 ± 5 recognizable merger remnants is $753 \pm 97 {\rm M}_\odot {\rm yr}^{-1}$. Thus, we can calculate the total SFR in all pairs with separations $< 40\,$kpc:

$$\frac{N_{\rm gal} f_{\rm pair,proj} 0.5 \epsilon SFR_{\rm typical,pair} + SFR_{\rm remnants}}{N_{\rm gal} 0.5 SFR_{\rm typical,pair}} = 16 \pm 3\% \,{\rm or}\, 18 \pm 4\% \qquad (3)$$

for the SF–SF ($\epsilon = 1.5 \pm 0.25$) and SF–All ($\epsilon = 1.8 \pm 0.3$) correlations respectively.

But the total amount of SF in major interactions is a poor proxy for the *directly* triggered fraction. Instead, it is a fairer exercise to isolate the *excess* star formation in pairs, attributing this to triggering by interactions. Substracting from the interacting galaxies the SF that would happen anyway in the quiescent mode (without mergers), we obtain a triggered fraction of $4 \pm 2\%$ or $6 \pm 3\%$, again depending on whether one refers to the SF–SF or the SF–All case.

4. Summary

- SF activity is weakly enhanced by major galaxy interactions in massive galaxies at $0.4 < z < 0.8$. We find an enhancement of $\epsilon = 1.50 \pm 0.25$ for the autocorrelation of star forming galaxies and $\epsilon = 1.80 \pm 0.30$ for the cross-correlation between star formers and all galaxies in the sample.
- This enhancement is in good agreement with other estimates at $z = 0.1$ and $z = 1$, pointing to a picture in which the enhancement scales linearly with the quiescent SF activity in the population.
- Knowing the average enhancement in SF and the fraction of galaxies undergoing interactions, we find that only $6 \pm 3\%$ of the SF is *directly* triggered by galaxy interactions. Put differently, star formation triggered by major interactions does not significantly impact the growth of stellar mass at $z < 1$.

References

Barnes, J.E. & Hernquist, L. 1996, ApJ, 471, 115
Barton, E.J., Geller, M.J. & Kenyon, S.J. 2000, ApJ, 530, 660
Barton, E. J. et al. 2007, ApJ, 671, 1538
Beisbart, C., & Kerscher, M. 2000, ApJ, 545, 6
Bell, E.F. et al. 2006, ApJ, 652, 270
Cox, T. J.et al. 2008, MNRAS, 384, 386
Davis, M. & Peebles, P.J.E. 1983, ApJ, 267,465
Di Matteo, P. et al. 2007, A&A, 468, 61
Hopkins, A.M. 2004, ApJ, 615, 209
Jogee, S., et al. 2009, ApJ, 697, 1971
Lambas, D.G. et al. 2003, MNRAS, 346, 1189
Li, C. et al. 2008, MNRAS, 385, 1903
Lin, L. et al. 2007, ApJ, 660,L51
Mihos, J.C. & Hernquist, L. 1996, ApJ, 464, 641
Sanders, D. B. et al. 1988, ApJ, 325, 74
Wolf, C. et al. 2003, A&A, 401, 73

Zheng, X. Z. et al. 2007, ApJ, 661, L41

GALAXY EVOLUTION: EMERGING INSIGHTS AND FUTURE CHALLLENGES
ASP Conference Series, Vol.
@jourvol, © 2009
S. Jogee, I. Marinova, L. Hao, and G. A Blanc

The Millennium Simulation Compared to Observations of $z \approx 2$ Galaxies

Shy Genel

Max Planck Institut für extraterrestrische Physik, Giessenbachstrasse, D-85748 Garching, Germany

Abstract. Recent observations of UV-/optically selected, massive star forming galaxies at $z \approx 2$ indicate that their mass assembly and star formation history is dominated by continuous rapid gas accretion and internal secular evolution, rather than by major mergers. We use the Millennium Simulation to gain insights on these observations. We find that even for halos not undergoing major mergers the mass accretion rates are plausibly sufficient to account for the high star formation rates observed in $z \approx 2$ disks. At the same time, the fraction of major mergers in the Millennium Simulation is sufficient to account for the submillimeter galaxies (SMGs), in support of observational evidence that these are major mergers. Following these populations in the simulation to $z = 0$, we find that subsequent mergers are not frequent enough to convert all $z \approx 2$ turbulent disks into late-type galaxies. Therefore, internal evolution must play an important role in the evolution of a significant fraction of $z \approx 2$ galaxies to $z = 0$.

1. Introduction

In the CDM model of hierarchical structure formation mergers are believed to play an important role in galaxy formation and evolution. However, there is growing evidence that a smoother growth mode may also be important for the baryonic mass assembly and star formation history at high redshift.

As part of the SINS survey (Förster Schreiber et al. 2006; N. M. Förster Schreiber et al. 2009 in preparation), integral field spectroscopy of more than 50 UV-/optically selected $z \approx 2$ star forming galaxies show a preponderance of thick gas-rich rotating disks and only a minority of major mergers (Förster Schreiber et al. 2006; Genzel et al. 2006, 2008; Shapiro et al. 2008). In contrast, SMGs are probably short-lived maximum-starburst galaxies undergoing dissipative major mergers (Tacconi et al. 2006, 2008; Bouché et al. 2007). Table 1 summarises key properties of these $z \approx 2$ galaxy samples.

How do these observations fit into the concordance cosmological model? Can the continuous rapid star formation observed in the SINS galaxies be achieved without the presence of major mergers? Are there enough mergers to account for the observed merging SMGs?

Here we use the cosmological dark matter (DM) Millennium Simulation (Springel et al. 2005) to investigate the possible roles of major mergers versus smoother accretion in galaxy formation at $z \approx 2$. The full details of our analysis and our results appear in Genel et al. (2008).

2. Analysis of the Millennium Simulation

The Millennium Simulation is a cosmological N-body simulation. It follows 2160^3 DM particles of mass $8.6 \times 10^8 h^{-1}\mathrm{M}_\odot$ in a box $500h^{-1}$Mpc on a side. There are 64 snapshots, with $\approx$ 300Myr intervals at $z \sim< 3$. The cosmology is ΛCDM, with $\Omega_m = 0.25$, $\Omega_\Lambda = 0.75$, $\Omega_b = 0.045$, $h = 0.73$, $n = 1$ and $\sigma_8 = 0.9$.

Structures in the simulation are identified first by constructing Friends-of-Friends (FOF) groups (Davis et al. 1985), which represent DM halos. Second, substructures are identified using SUBFIND (Springel et al. 2001). Merger trees (which have been made public by the Virgo Consortium: http://www.mpa-garching.mpg.de/millennium) were constructed based on the *subhalos*.

To determine the halo merger rate, new trees based on *halos* should be constructed (Fakhouri & Ma 2008; Genel et al. 2009). However, to derive merger fractions and mass growth rates, we must consider the physical durations of mergers, information that is absent from the original trees.

We identify a merger whenever two or more halos have a common descendant. However, at this time the halos are not necessarily already physically merging, since they may still be well separated. To account for that, we track the distances between the subhalo descendants of the original FOF groups and define the start point of the merger as the last snapshot at which this distance is still larger than the sum of the virial radii of the original halos.

After a merger begins, one halo becomes a substructure within the other. This subhalo typically dissolves in a resolution-dependant way and the completion of the merger cannot be reliably determined. To overcome this, we estimate the duration of mergers T_{merger}, and define their end point as T_{merger} after the start point. We estimate the durations using an orbit-averaged form of the fitting function of Boylan-Kolchin et al. (2008). The accretion rate associated with each merger equals the amount of accreted mass divided by the merger duration.

To summarise, we construct new halo-based merger trees, where each halo also holds information about internal on-going mergers. The accretion rates associated with those mergers are summed up to obtain the total accretion rate onto the halo in question. The merger mass ratio is determined by the masses of the FOF groups just prior to the appearance of a common FOF group descendant. If a halo is undergoing a merger with a mass ratio between $3:1$ and $1:1$, it is labelled as undergoing a major merger.

3. Results - Galaxies at $z \approx 2$

Fig. 1 (*left*) shows halo number densities (*shaded*) and major merger fractions (*red*) as functions of halo mass and DM accretion rate for $z \approx 2.2$. It shows that the major merger fraction is an increasing function of *specific* DM accretion rate ($\frac{\dot{M}_{\mathrm{DM}}}{M_{\mathrm{halo}}}$), as both quantities increase towards the upper-left direction of the plane.

To compare our results to observed galaxies, we convert DM accretion rate ($\dot{M}_{DM}$) into SFR in the central galaxy of the halo ($\dot{M}_*$) using the baryonic fraction $\eta_B = 0.18$ and an effective star formation efficiency ϵ:

$$\dot{M}_* = \eta_B \times \epsilon \times \dot{M}_{DM}. \quad (1)$$

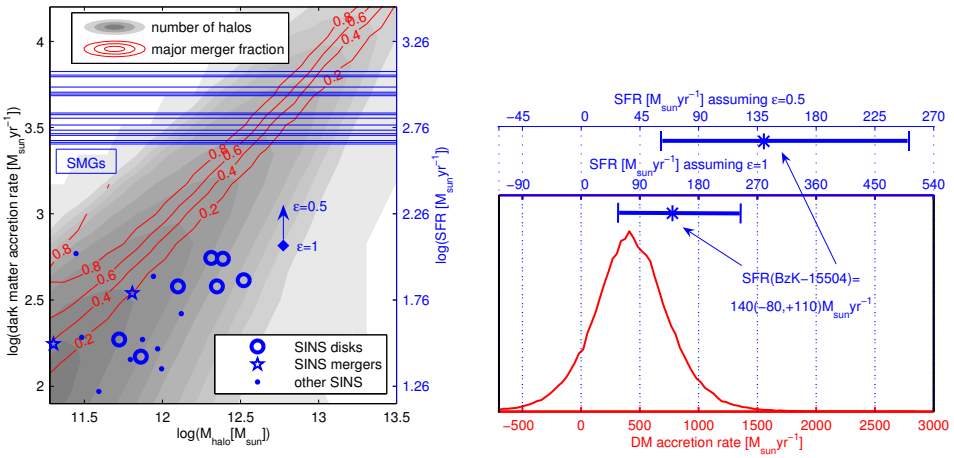

Figure 1. *Left:* The distribution (*shaded*) of $z \approx 2.2$ halos in the DM accretion rate (left y-axis) versus halo mass plane. Also major merger fractions are displayed (*red*). Associated SFRs are indicated (right y-axis) assuming an effective star formation efficiency $\epsilon = 1$ in eq. 1. SINS galaxies at $2 < z < 2.5$ are indicated as disks (*circles*) or mergers (*stars*) based on the Shapiro et al. (2008) classification, and others (*points*) not investigated by Shapiro et al. (2008). Their SFRs are based on their $H\alpha$ fluxes corrected for extinction using $A_{H\alpha} = 0.8$. Their halo masses were determined by assuming that the observed disk maximum rotation velocity is equal to the circular velocity of the halo (Förster Schreiber et al. 2006), and only galaxies with $M_{\rm halo} > 10^{11.25}{\rm M}_\odot$ are included. The SFRs for the SMGs are shown as the horizontal lines in the upper part of the figure (because the SMGs are compact, their halo masses cannot be reliably inferred from the observed gas motions). The *left* y-axis indicates what DM accretion rates are needed to account for the observed SFRs when assuming $\epsilon = 1$. The arrow indicates the shift in the galaxy positions if $\epsilon = 0.5$. *Right:* The distribution of DM accretion rates for halos with masses $(1.2 \pm 0.3) \times 10^{12}{\rm M}_\odot$ at $z \approx 2.4$ (corresponding to the halo mass and redshift of BzK-15504), which are not undergoing a major merger. The SFRs on the upper axes are given assuming effective star formation efficiencies $\epsilon = 1$ and $\epsilon = 0.5$. The measured SFR of $140(-80, +110){\rm M}_\odot{\rm yr}^{-1}$ in BzK-15504 is indicated by the asterisks and error bars.

In the 'cold flow' regime ($M_{\rm halo} \sim< 10^{12}{\rm M}_\odot$; Birnboim & Dekel 2003; Kereš et al. 2005; Ocvirk et al. 2008; **?**) eq. 1 is a plausible measure of the baryonic accretion rate. In that regime, the cold gas is fed via filaments directly into the halo center and onto the galaxy. For major mergers ϵ may even exceed 1, because the star formation burst they trigger can be shorter than the DM halo merger time scale.

3.1. SINS Galaxies

On Fig. 1 (*left*) we overplot the SINS galaxies. If $\epsilon \sim> 0.5$ is assumed, the host halos of SINS galaxies with $M_{\rm halo} > 10^{11.25}{\rm M}_\odot$ lie in the region where most halos of their mass are concentrated. Furthermore, for $\epsilon \sim> 0.5$ the expected mass accretion rates are sufficient to account for the observed SFRs. Also, the predicted major merger fraction is small ($\sim< 0.5$), consistent with observations.

The computed number density of halos with $M \approx 10^{11.5} - 10^{12}\mathrm{M}_{\odot}$ is a few times higher than the observed number density of the galaxies the SINS sample is drawn from (Table 1). Possibly, the observed galaxies have typically high $M_{\rm gal}/M_{\rm halo}$, with other halos of comparable mass hosting fainter undetected galaxies. Also, some of the halos in this mass range may have already developed virial shocks that quench star formation.

In should be noted that our estimated major merger duration $T_{\rm merger}$ equals $\approx 350 - 1000$Myr at $z \approx 2.2$, depending on the mass ratio. This is similar to the "observable" galaxy merger timescale often found in the literature (e.g. Conselice 2006; Lotz et al. 2008). Therefore, it is reasonable to consider directly the halo merger fraction and to infer the galaxy merger fraction from it.

Genzel et al. (2006) studied BzK-15504 with high resolution using adaptive optics, and concluded that it was a large disk with no sign of a recent/ongoing major merger, and a SFR of $140(-80, +110)\mathrm{M}_{\odot}\mathrm{yr}^{-1}$. Others have found similar systems. Fig. 1 (*Right*) shows that for halos not undergoing major mergers, and with masses equal to the estimated halo mass of BzK-15504, the typical DM accretion rate is $\approx 450\mathrm{M}_{\odot}\mathrm{yr}^{-1}$, i.e. the typical SFR assuming $\epsilon = 1$ is $\approx 80\mathrm{M}_{\odot}\mathrm{yr}^{-1}$. About 15% of such halos have SFRs exceeding the $140\mathrm{M}_{\odot}\mathrm{yr}^{-1}$ observed in BzK-15504. Considering the uncertainty in the measured SFR, the implied DM accretion rate is consistent with theoretical expectations for ϵ as low as ≈ 0.5.

We conclude that high star formation rates and large abundances of non-major merger massive disks at $z \approx 2$ are consistent with expectations from ΛCDM simulations if accretion is in the 'cold flow' regime and the star formation efficiency is high.

3.2. SMGs

For $\epsilon \approx 1$, the observed SFRs of the SMGs imply DM accretion rates of $\approx 2500 - 6000\mathrm{M}_{\odot}\mathrm{yr}^{-1}$ (Fig. 1, *left*). Masses of halos with accretion rates in this range that are undergoing major mergers obey a log-normal distribution with a mean $\approx 3 \times 10^{12}\mathrm{M}_{\odot}$ and $\sigma \approx 0.25$dex. Also, their number density is $\approx 5 \times 10^{-5}\mathrm{Mpc}^{-3}$. This is only slightly larger than the observed SMG density (Table 1), and supports the conclusions of Tacconi et al. (2006, 2008) that the SMGs are major mergers. If the SMG phase is shorter than the halo merger duration, such that $\epsilon > 1$, the implied number density is not much altered, but lower halo masses are found. E.g., if the SMG phase lasts only 100Myr, the mean halo mass is $\approx 10^{12}\mathrm{M}_{\odot}$, in which case SMGs could be members of the UV-/optically selected galaxy populations that have recently experienced a dissipative major merger.

4. Results - Fates of SINS Galaxies at $z = 0$

For halos with initial masses typical of the SINS galaxies' halos, $\approx 40\%$ will be accreted via minor mergers by more massive halos (representing groups or clusters). The other $\approx 60\%$ remain "main branch" halos to $z = 0$. Of these, $\approx 1/3$ do not undergo any future major merger, and grow to a mass $10^{11.8}\mathrm{M}_{\odot} \lesssim M \lesssim 10^{12.5}\mathrm{M}_{\odot}$ at $z = 0$. Thus, these may evolve via secular evolution into bulges (Genzel et al. 2008) and later possibly grow a new disk.

Table 1. Properties of galaxy samples at $z \approx 2$

Galaxy sample	SFR $[M_\odot yr^{-1}]$	Halo mass $[M_\odot]$	Comoving number density $[h_{0.7}^3 Mpc^{-3}]$	Major merger fraction
SINS	$\approx 30 - 300$	$10^{11.84} v_{200}^3 \times (\frac{1+z}{3.2})^{-1.5} h_{0.7}^{-1}$	$1 - 2.2 \times 10^{-4}$	≈ 0.3
SMGs	$\approx 750 \pm 300$	-	$1 - 2 \times 10^{-5}$	≈ 1

5. Summary

We have constructed new halo merger trees from the Millennium Simulation. Our trees account for merger durations, and we use them to identify halos undergoing mergers and to extract DM accretion rates. We show that the high star formation rates observed in rotating disks at $z \approx 2$ are plausibly consistent with the DM accretion rates expected for halos not undergoing major mergers. Given the measured star formation rates of SMGs, and the observationally supported assumption that they are undergoing major mergers, we infer their likely halo masses. Major mergers cannot lead to the complete transformation of the $z \approx 2$ disks to $z = 0$ ellipticals. Therefore, secular/internal processes are likely important in the evolution of these high-redshift populations to present time.

Acknowledgments. I thank my thesis advisor, Reinhard Genzel, and all of the SINS team members, for their valuable contributions to the work presented here. I also thank the conference organisers for giving me the opportunity to present these results. The Millennium Simulation databases used in this paper and the web application providing online access to them were constructed as part of the activities of the German Astrophysical Virtual Observatory.

References

Birnboim, Y., & Dekel, A. 2003, MNRAS, 345, 349
Bouché, N. et al. 2007, ApJ, 671, 303
Boylan-Kolchin, M., Ma, C.-P., & Quataert, E. 2008, MNRAS, 383, 93
Conselice, C. J. 2006, ApJ, 638, 686
Davis, M., Efstathiou, G., Frenk, C. S., & White, S. D. M. 1985, ApJ, 292, 371
Dekel, A., Birnboim, Y., Engel, G. et al. 2009, Nat, 457, 451
Fakhouri, O., & Ma, C.-P. 2008, MNRAS, 359
Förster Schreiber, N. M. et al. 2006, ApJ, 645, 1062
Genel, S. et al. 2008, ApJ, 688, 789
Genel, S., Genzel, R., Bouché, N., Naab, T., & Sternberg, A. 2009, ApJ, submitted
Genzel, R. et al. 2008, ApJ, 687, 59
—. 2006, Nat, 442, 786
Kereš, D., Katz, N., Weinberg, D. H., & Davé, R. 2005, MNRAS, 363, 2
Lotz, J. M., Jonsson, P., Cox, T. J., & Primack, J. R. 2008, MNRAS, 391, 1137
Ocvirk, P., Pichon, C., & Teyssier, R. 2008, MNRAS, 390, 1326
Shapiro, K. L. et al. 2008, ApJ, 682, 231
Springel, V. et al. 2005, Nat, 435, 629
Springel, V., White, S. D. M., Tormen, G., & Kauffmann, G. 2001, MNRAS, 328, 726
Tacconi, L. J. et al. 2008, ApJ, 680, 246

—. 2006, ApJ, 640, 228

GALAXY EVOLUTION: EMERGING INSIGHTS AND FUTURE CHALLLENGES
ASP Conference Series, Vol.
@jourvol, © 2009
S. Jogee, I. Marinova, L. Hao, and G. A Blanc

How Do Disks Survive Mergers?

Philip F. Hopkins

Department of Astronomy, University of California Berkeley, Berkeley, CA 94720

Abstract. We develop a physical model for how galactic disks survive and/or are destroyed in interactions. Based on dynamical arguments, we show gas primarily loses angular momentum to internal torques in a merger. Gas within some characteristic radius (a function of the orbital parameters, mass ratio, and gas fraction of the merging galaxies), will quickly lose angular momentum to the stars sharing the perturbed disk, fall to the center and be consumed in a starburst. A similar analysis predicts where violent relaxation of the stellar disks is efficient. Our model allows us to predict the stellar and gas content that will survive to re-form a disk in the remnant, versus being violently relaxed or contributing to a starburst. We test this in hydrodynamic simulations and find good agreement as a function of mass ratio, orbital parameters, and gas fraction, in simulations spanning a wide range in these properties and others, including different prescriptions for gas physics and feedback. In an immediate sense, the amount of disk that re-forms can be understood in terms of well-understood gravitational physics, independent of details of ISM gas physics or feedback. This allows us to explicitly quantify the requirements for such feedback to (indirectly) enable disk survival, by changing the pre-merger gas content and distribution. The efficiency of disk destruction is a strong function of gas content: we show how and why sufficiently gas-rich major mergers can, under general conditions, yield systems with small bulges ($B/T < 0.2$). We provide prescriptions for inclusion of our results in semi-analytic models.

1. Outline

In Hopkins et al. (2009b), we attempt to derived a general physical model for how disks survive and/or are destroyed in mergers and interactions. The model describes both the dissipational and dissipationless components of the merger, and allows us to predict, for a given arbitrary encounter, the stellar and gas content of the system that will be dissipationlessly violently relaxed, dissipationally lose angular momentum and form a compact central starburst, or survive (without significant angular momentum loss or violent relaxation) to re-form a disk. We show that, in an immediate (short-term) sense, the amount of stellar or gaseous disk that survives or re-forms following a given interaction can be understood purely in terms of simple, well-understood gravitational physics. Knowing these physics, the model allows us to accurately predict the behavior in full hydrodynamic numerical simulations across as a function of the merger mass ratio, orbital parameters, pre-merger cold gas fraction, and mass distribution of the gas and stars, in simulations which span a wide range of parameter space in these properties as well as prescriptions for gas physics, stellar and

AGN feedback, halo and initial disk structural properties, redshift, and absolute galaxy masses.

Gas, in mergers, primarily loses angular momentum to internal gravitational torques (from the stars in the same disk) owing to asymmetries in the galaxy induced by the merger (on the close passages and final coalescence of the secondary, during which phase the potential also rapidly changes, scattering and violently relaxing the central stellar populations of the stellar disk).[1] Hydrodynamic torques and the direct torquing of the secondary are second-order effects, and inefficient for all but pathological orbits.

For these reasons, many processes and details that are important cosmologically (systematically changing e.g., the pre-merger disk gas fractions) – in some sense setting the initial conditions for our idealized study of what happens in mergers – do not alter the basic dynamical behavior within the mergers themselves, and therefore do not change our conclusions.

Figure 1 summarizes our results for the ensemble of our simulations. We compare the fraction of the baryonic galaxy mass in the merger remnant that is in a surviving post-merger disk to that predicted by our simple model scalings, and find good agreement over the entire range in disk and bulge mass fractions sampled, with surprisingly small scatter given the complexity of behavior in mergers. We highlight several of the parameter studies, showing that – for fixed mass ratio, orbital parameters, and gas content *at the time of the final merger*, none of these choices systematically affect our predictions (note that these are not the only parameters varied – the complete list is discussed in Hopkins et al. (2009b), but it is representative). That is not to say they cannot affect them indirectly, by e.g., altering how much gas is available at the time of merger – but it emphasizes that the processes we model and use to form our predictions, the processes that dominate violent relaxation and the loss of angular momentum in gas in mergers, are fundamentally dynamical.

This allows us to make robust, accurate physical predictions independent of the (considerable) uncertainty in feedback physics and sub-resolution physics of the ISM. Regardless of how those physics alter the "initial" conditions, they do not change basic dynamical processes, and so do not introduce significant uncertainties in our model.

In turn, this means that we can use our model to understand just why and how feedback is important for the cosmological survival of disks. Why, in short, have various works (see e.g., Springel & Hernquist 2005; Robertson et al. 2006a; Governato et al. 2007) concluded that strong feedback is essential for enabling disk survival in mergers? Our results show that it is not that feedback somehow makes the disk more robust to the dynamical torques within the merger, in any instantaneous sense. These torques, at least within the critical radii where the gravitational perturbation from the merger is large and in resonance, are sufficiently strong that any reasonable feedback prescription is a dynamically negligible restoring force. Rather, feedback has two important

[1] We note that although these asymmetries are often described as "bars" or "bar-like," there are a number of properties of the non-axisymmetric distortions induced in mergers that make them – at least over the short relaxation timescale of the merger – dynamically distinct from traditional bar instabilities in isolated systems.

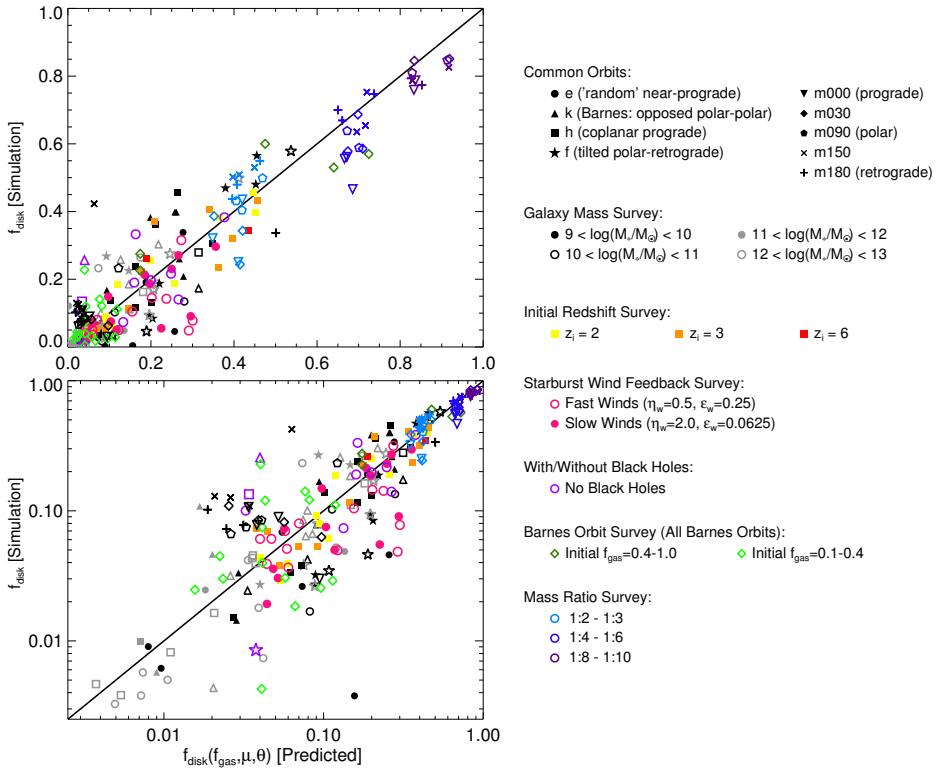

Figure 1. Summary of our comparison between simulations and analytic model for the mass of disks in merger remnants as a function of appropriate orbital parameters, merger mass ratio, and pre-merger cold gas content. We plot our model prediction versus the simulation remnant disk fraction for all ~ 400 full hydrodynamic merger simulations considered in this paper (shown in both a linear and logarithmic scale). Symbols encode some of the parameter studies we consider: orbital parameters, galaxy masses, initial merger redshift, choice of feedback prescription, merger mass ratio, and presence or absence of black holes, as labeled. For each subset of simulations, we sample a wide range in initial and pre-merger gas fractions $f_{\rm gas} = 0 - 1$. Solid line is a one-to-one relation. In all cases, our predictions agree well with the simulations, with no systematic offsets owing to any of the parameters we have varied. At high $f_{\rm disk}$, our predictions are accurate to an absolute uncertainty $\sim 0.05 - 0.10$ in $f_{\rm disk}$. At low $f_{\rm disk} < 0.1$, our predictions are accurate to a factor $\sim 2-3$ (down to $f_{\rm disk} < 1\%$, where it is difficult to reliably identify disks in the remnant).

effects that fundamentally alter the conditions in the merger: first, it allows the galaxy to retain much higher gas content going into the merger. Without feedback from e.g., star formation and supernovae contributing to heating and pressurizing the ISM and redistributing gas spatially, isolated gas-rich disks may be unstable to fragmentation. Even if fragmentation is avoided, it is well-known that star formation in simulations proceeds efficiently under these conditions. This would leave the disks essentially pure stars (even for idealized simulations beginning with $\sim 100\%$ gas disks; see e.g., Springel et al. 2005) by the time of the merger, which guarantees that a major merger will inevitably violently relax the stars (this is a simple collisionless mixing process, and under such circumstances is inescapable). With large gas fractions, however, the system relies on stripping angular momentum from the gas to form new bulge stars, which in turn relies on internal torques from induced asymmetries in the stellar disk. If the gas fractions are sufficiently large, there is little stellar disk to do any such torquing, and the gas survives largely intact.

Second, feedback from supernovae and stellar winds moves the gas to large radii, where it does not feel significant torques from the merger. The most efficient torquing is driven by the internal stellar disk of the galaxy, and as such is most efficient at torquing gas within small radii (this can be thought of as analogous to the well-known co-rotation condition for isolated disk bars). If star formation-driven feedback has blown much of the gas to large radii, then there is little gas inside the radius where torques can efficiently strip angular momentum, yielding little induced starburst and largely preserving the gas disk at large radii.

A number of interesting consequences are immediately apparent. First, it is a well-known problem that theoretical models systematically overpredict the abundance and mass fractions of bulges in (especially) low-mass galaxies. This is true even in e.g., semi-analytic models, which are not bound by resolution requirements and can adopt a variety of prescriptions for behavior in mergers. However, it is also well-established observationally that disk gas fractions tend to be very high in this regime, with large populations of gas-dominated disks at $M_* \ll 10^{10}\,M_\odot$ (Bell & de Jong 2001; Kannappan 2004; McGaugh 2005). Our models predict that bulge formation should, therefore, be strongly suppressed in precisely the regime required by observations. For e.g., disks with $M_* < 10^9\,M_\odot$ where observations suggest typical gas fractions $\sim 60-80\%$, our results show that even a 1:1 major merger would typically yield a remnant with only $\sim 30\%$ bulge by mass – let alone a more typical 1:3-1:4 mass-ratio merger, which should yield a remnant with $< 20\%$ bulge. That is not to say that it is impossible to form a bulge-dominated system at these masses, but it should be much more difficult than at high masses, requiring either unusually gas-poor systems, violent merger histories, or rarer merging orbits that are more efficient at destroying disks. Low-mass systems, when a proper dynamical model of bulge formation in mergers is considered, should have lower bulge-to-disk ratios – by factors of several, at least – than have been assumed and modeled in previous theoretical models.

Second, the importance of this suppression owing to gas content in disks will be even more significant at high redshifts. Observations suggest (see e.g., Erb et al. 2006) that by $z \sim 2$, even systems with masses near $\sim L_*$ ($M_* \sim 10^{10}-10^{11}\,M_\odot$) may have gas fractions as high as $f_{\rm gas} \sim 0.6$. In this

regime, the same argument as above should apply, dramatically suppressing the ability of mergers to destroy disks. Moreover, since most of the mass density is near L_*, this can change not just the behavior in a specific mass regime but significantly suppress the global mass density of spheroids, modifying the predicted redshift history of bulge formation.

Third, our models imply that a large fraction of bulges and disks survive mergers together, rather than being formed entirely separately. It is often assumed that classical bulges – being similar to small ellipticals in most of their properties – were formed initially in major mergers, as entirely bulge-dominated systems, and then accreted new gaseous and stellar disks at later times. Although nothing in our modeling would prevent this from happening, our analytic and simulation results generically lead to the expectation that a large (perhaps even dominant) fraction of the bulge population did *not* form in this manner, but rather formed *in situ* from minor mergers or less efficient major mergers (in e.g., very gas-rich systems). Observations tracing the evolution of disk components, kinematics, and morphology in the last $\sim 10\,$Gyr increasingly suggest that such co-formation or disk regeneration scenario is common (see e.g., Hammer et al. 2005; Conselice et al. 2005; Flores et al. 2006; Puech et al. 2008, and references therein). In short, a system with a mass fraction $\sim 0.1-0.2$ in a bulge could be the remnant of an early, violent major merger (when the system was ~ 0.1 times its present mass) with a re-accreted disk, or could be the remnant of a typical (low to intermediate gas fraction) 1:10-1:5 mass ratio minor merger, or could even be the remnant of a gas-rich major merger (mass ratio $< 1:3$, if $f_{\rm gas}$ is sufficiently large).

Based on a simple comparison of typical merger histories, we would actually expect that the minor merger mechanism should be most common, but all may be non-negligible. Fundamentally, the physics forming the bulge (torquing the gas within some radius owing to internal asymmetries and violently relaxing stars within a corresponding radius) are the same in all three cases, and moreover other indicators such as their stellar populations will be quite similar (in all cases, the bulge will appear old: this is both because the central stars in even present-day disks are much older than those at more typical radii, and because in any case star formation will cease within the bulge itself, as opposed to the ongoing star formation in the disk, and stellar population age estimates are primarily sensitive to the amount of recent or ongoing star formation; see e.g., Trager et al. 2000). This is also not to say that mergers are the only means of producing bulges. Secular evolution of e.g., barred disks probably represents an increasingly important channel for bulge evolution in later-type and more gas-rich systems (see e.g., Christodoulou et al. 1995; Sheth et al. 2003; Mayer & Wadsley 2004; Debattista et al. 2004; Jogee et al. 2004; Kormendy & Kennicutt 2004; Marinova & Jogee 2007), and may even be related (albeit through longer timescales of "isolated," post-merger evolution and different physics) to initial bar formation or "triggering" in mergers.

Our results are also of direct interest to models of spheroid formation in ellipticals and S0 galaxies. It is increasingly clear that embedded sub-components – constituting surviving gaseous and stellar disks – are both ubiquitously observed and critical for theoretical models to match the detailed kinematics and isophotal shapes of observed systems (Naab et al. 2006; Cox et al. 2006a,b; Robertson et al. 2006b; Jesseit et al. 2007; Hopkins et al. 2009a, 2008).

We have developed a model that allows us to make specific predictions for how disks survive mergers, including both the survival of some amount of the pre-merger stellar disks and the post-merger re-formation of disks and rotationally supported components from gas that survives the merger without losing most of its angular momentum.

Figure 1 shows that we can extend these predictions with reasonable accuracy to surviving rotational systems containing as little as $\sim 1\%$ of the remnant stellar mass, comparable to small central subcomponents and subtle features giving rise to e.g., slightly disky isophotal shapes (see e.g., Ferrarese et al. 1994; Lauer et al. 2005; McDermid et al. 2006). Owing to the combination of resolution requirements and desire to understand the fundamental physics involved, most theoretical studies of these detailed properties of ellipticals have been limited to idealized studies of individual mergers. Our results allow these to be placed in a more global context of cosmological models and merger histories. Moreover, our models allow the existence of such features (or lack thereof) to be translated into robust constraints on the possible merger histories and gas-richness of spheroid-forming mergers. Further, Hopkins et al. (2009a, 2008), studied how the dissipational starburst components arising in gas-rich mergers are critical to explaining the observed properties and scaling relations of ellipticals, and how these components can both be extracted from and related to observed elliptical surface brightness profiles.

These points relate to a number of potentially testable predictions of our models. These include the in situ formation of bulges from various types of mergers, and possible associated stellar population signatures, the presence of embedded disks in ellipticals, and how their sizes and mass fractions scale with e.g., the masses and formation times of ellipticals (and how this relates to gas fractions and stellar populations in observed disks). In general, for similar merger histories, the increasing prevalence of later type galaxies (S0's and S0a's) at lower masses where disks are characteristically more gas rich is a natural consequence of our predictions here. To the extent that these processes also give rise to disk heating and/or increasing velocity dispersions in disks, or changing kinematics in both disks and bulges, then there should be corresponding relationships between galaxy shapes, kinematics, and bulge-to-disk ratios along the Hubble sequence.

Acknowledgments. We thank Shardha Jogee for helpful conversations and for organizing the conference at which this work was presented. This work was supported in part by NSF grants ACI 96-19019, AST 00-71019, AST 02-06299, and AST 03-07690, and NASA ATP grants NAG5-12140, NAG5-13292, and NAG5-13381, and by the W. M. Keck Foundation.

References

Bell, E. F., & de Jong, R. S. 2001, ApJ, 550, 212
Christodoulou, D. M., Shlosman, I., & Tohline, J. E. 1995, ApJ, 443, 551
Conselice, C. J., Bundy, K., Ellis, R. S., Brichmann, J., Vogt, N. P., & Phillips, A. C. 2005, ApJ, 628, 160
Cox, T. J., Di Matteo, T., Hernquist, L., Hopkins, P. F., Robertson, B., & Springel, V. 2006a, ApJ, 643, 692

Cox, T. J., Dutta, S. N., Di Matteo, T., Hernquist, L., Hopkins, P. F., Robertson, B., & Springel, V. 2006b, ApJ, 650, 791
Debattista, V. P., Carollo, C. M., Mayer, L., & Moore, B. 2004, ApJ, 604, L93
Erb, D. K., Steidel, C. C., Shapley, A. E., Pettini, M., Reddy, N. A., & Adelberger, K. L. 2006, ApJ, 646, 107
Ferrarese, L., van den Bosch, F. C., Ford, H. C., Jaffe, W., & O'Connell, R. W. 1994, AJ, 108, 1598
Flores, H., Hammer, F., Puech, M., Amram, P., & Balkowski, C. 2006, A&A, 455, 107
Governato, F., Willman, B., Mayer, L., Brooks, A., Stinson, G., Valenzuela, O., Wadsley, J., & Quinn, T. 2007, MNRAS, 374, 1479
Hammer, F., Flores, H., Elbaz, D., Zheng, X. Z., Liang, Y. C., & Cesarsky, C. 2005, A&A, 430, 115
Hopkins, P. F., Cox, T. J., Dutta, S. N., Hernquist, L., Kormendy, J., & Lauer, T. R. 2009a, ApJS, 181, 135
Hopkins, P. F., Cox, T. J., & Hernquist, L. 2008, ApJ, 689, 17
Hopkins, P. F., Cox, T. J., Younger, J. D., & Hernquist, L. 2009b, ApJ, 691, 1168
Jesseit, R., Naab, T., Peletier, R. F., & Burkert, A. 2007, MNRAS, 376, 997
Jogee, S., et al. 2004, ApJ, 615, L105
Kannappan, S. J. 2004, ApJ, 611, L89
Kormendy, J., & Kennicutt, Jr., R. C. 2004, ARA&A, 42, 603
Lauer, T. R., et al. 2005, AJ, 129, 2138
Marinova, I., & Jogee, S. 2007, ApJ, 659, 1176
Mayer, L., & Wadsley, J. 2004, MNRAS, 347, 277
McDermid, R. M., et al. 2006, MNRAS, 373, 906
McGaugh, S. S. 2005, ApJ, 632, 859
Naab, T., Jesseit, R., & Burkert, A. 2006, MNRAS, 372, 839
Puech, M., et al. 2008, A&A, 484, 173
Robertson, B., Bullock, J. S., Cox, T. J., Di Matteo, T., Hernquist, L., Springel, V., & Yoshida, N. 2006a, ApJ, 645, 986
Robertson, B., Cox, T. J., Hernquist, L., Franx, M., Hopkins, P. F., Martini, P., & Springel, V. 2006b, ApJ, 641, 21
Sheth, K., Regan, M. W., Scoville, N. Z., & Strubbe, L. E. 2003, ApJ, 592, L13
Springel, V., Di Matteo, T., & Hernquist, L. 2005, MNRAS, 361, 776
Springel, V., & Hernquist, L. 2005, ApJ, 622, L9
Trager, S. C., Faber, S. M., Worthey, G., & González, J. J. 2000, AJ, 119, 1645

GALAXY EVOLUTION: EMERGING INSIGHTS AND FUTURE CHALLLENGES
ASP Conference Series, Vol.
@jourvol, © 2009
S. Jogee, I. Marinova, L. Hao, and G. A Blanc

The Impact of Minor Galaxy Mergers

T. J. Cox
Harvard–Smithsonian Center for Astrophysics
60 Garden St., Cambridge MA, 02143 USA

Abstract. It is now well accepted that galactic structure is directly influenced by its past merger history. Unfortunately, despite a considerable amount of effort, there is still not a complete mapping between the full ensemble of merger histories and the resultant galactic structure. This proceeding describes efforts to better understand certain routes in this mapping using numerical simulations of galaxy interactions. In particular, we outline the generic events that occur during the interaction and merger of unequal mass galaxies, so-called minor galaxy mergers, briefly focusing on the induced star formation and the morphological evolution induced by a minor merger. Some implications for the formation and evolution of bulges and the persistence of thin galactic disks is discussed.

1. Introduction

While the last several decades have yielded a wonderfully successful model for the overall composition and large–scale evolution of our Universe from the Big Bang to the present (and even into the future), an equally comprehensive effort to understand the formation and evolution of galaxies has produced just as many questions as answers, a large number of which were addressed at one point or another during the four wonderful days of this conference.

The many open questions regarding the formation and evolution of galaxies persist in spite of a well understood and very successful framework for structure formation. A key element of this framework is that structure forms hierarchically, i.e., small objects form first and grow via mergers with other objects. The hierarchical growth of structure, in combination with numerous observations of galaxies that show the tell–tale signs of interaction motivate the notion that galactic structure is a direct byproduct of the past history of hierarchical (i.e., merger) formation.

While study of the effects of mergers between equal–mass galaxies, so–called major merger, has evolved into a mature field, the study of unequal–mass, minor mergers, is still in its infancy. Such a focus of effort and understanding lies in direct contrast to the relative abundance of such mergers in ΛCDM – mergers between unequal–mass galaxies are far more abundant than mergers between systems of equal mass (see, e.g., Fakhouri & Ma 2008, Hopkins et al. 2009b, and references therein). This proceeding will provide a necessarily brief outline of efforts to rectify this discrepancy. These efforts employ state-of-the-art numerical models to understand the star formation, black hole growth, and morphological transformation of galaxies when undergoing unequal-mass, minor mergers.

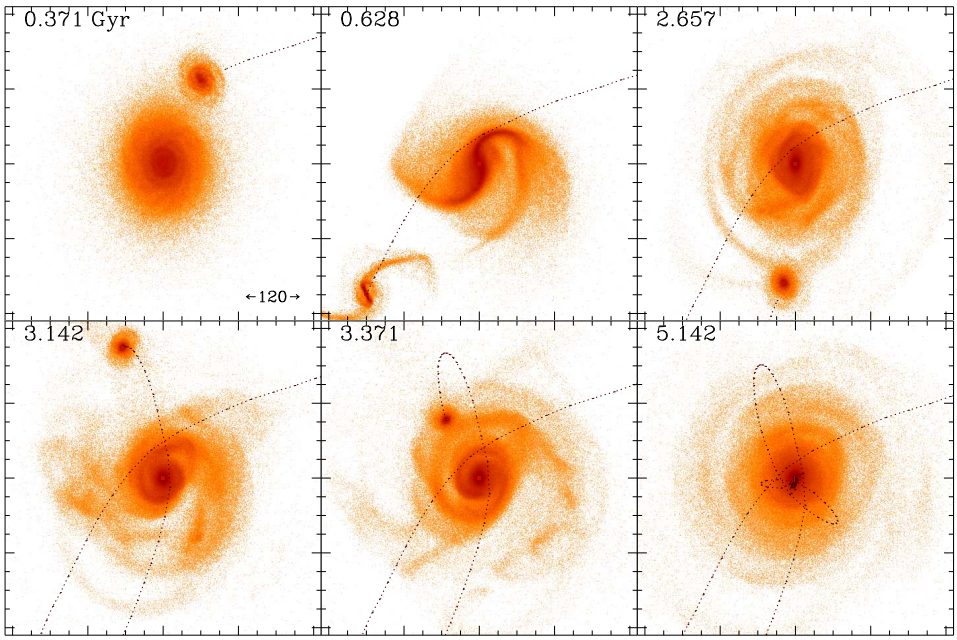

Figure 1. The projected stellar mass distribution for a representative 1:8 minor galaxy merger. In this interaction, the satellite approaches on a close parabolic orbit. Each panel shows a 120 kpc box centered on the primary galaxy. The time, in Gyr, is displayed on the upper–left of each panel and the satellite trajectory is demarked for clarity.

2. Numerical Models

To study the influence of minor galaxy mergers, we employ numerical simulations that follow the interaction and merger of idealized galaxy models. Such techniques have become invaluable to study the complex, non–linear, and often interrelated astrophysical phenomena that come into play during the formation and evolution of galaxies.

The construction and simulation of these galaxy models is described in detail in a number of published papers (Hernquist 1993, Springel 2000, Springel et al. 2005, Cox et al. 2006a,b, and references therein). While we briefly outline the numerical methods here, we refer the interested reader these works for a more complete description. All numerical experiments use the publically available N-body/SPH evolutionary code GADGET2 (Springel 2005). The code includes a recipe for star formation that is designed to match observations (Kennicutt 1998), a model for the multi–phase interstellar medium that includes stellar feedback (Springel & Hernquist 2003), and an accreting black hole and its associated feedback (Springel et al. 2005).

The simulations track the interaction between a primary galaxy and a satellite of smaller mass, an example of which is shown in Fig. 1. The primary galaxy is an approximate model for the Milky Way, a Sb galaxy with a total mass of $\sim 1.4 \times 10^{12}\ M_{\odot}$, bulge–to–disk ratio of 1:4, baryonic mass fraction of

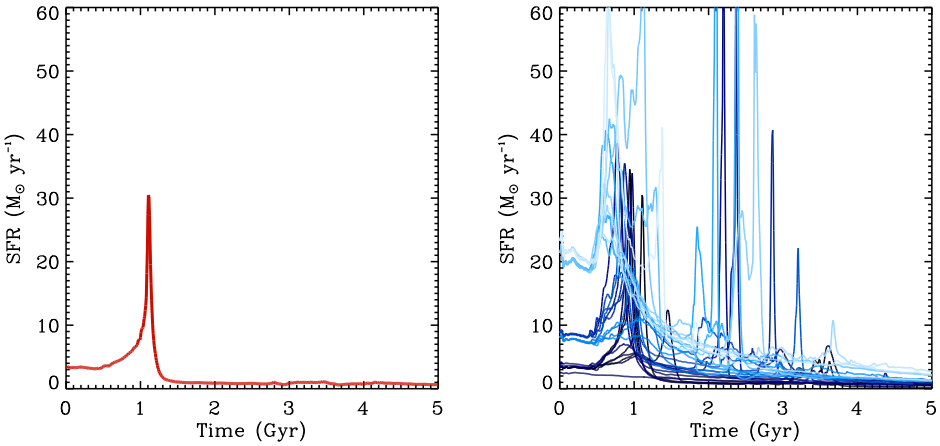

Figure 2. Star-formation rate during minor galaxy mergers. The plot on the left displays the star–formation history for the encounter shown in Fig. 1. A merger–induced starburst at T≈ 1.0 Gyr is clearly triggered by the first passage of the smaller satellite. Subsequent passages and the final merger do no have the right conditions to trigger bursts of star formation. The plot on the right shows the star–formation history of 32 independent interactions in which the structure of the progenitors and the interacting orbit has been varied. This plot demonstrates the wide variety of star–formation histories possible during minor galaxy encounters.

0.05, and gas fraction of 0.2. The satellite galaxies are one–third, one–eighth, and one–twentieth the mass of the primary. For simplicity, the structures of the satellites are identical to that of the primary, although future experiments will employ models with properties selected to match observed mass trends (see, e.g., Cox et al. 2008).

Once equilibrium galaxy models are constructed, two galaxies are placed on a parabolic orbit and allowed to interact and merge (see Fig. 1). While the set of simulations performed to date do not represent a complete survey of the entire parameter space of galaxy interactions, a large number of different galaxy models and interacting orbits have been investigated. Simulations include models that vary the galaxy properties (bulge, gas content), as well as models that vary the interacting orbit (radial, such as those that are expected to be cosmologically common (Khochfar & Burkert 2006), large angular momentum, and bound orbits).

3. Star Formation

Observational studies (see, e.g., Larson & Tinsley 1978, Sanders & Mirabel 1996, Barton et al. 2000, Borne et al. 2000, Jogee et al. 2009, and references therein) as well as theoretical modeling (e.g., Mihos & Hernquist 1994a,b, Springel 2000, Cox et al. 2006a, 2008, and references therein) both indicate that galaxy mergers induce periods of enhanced star formation. Fig. 2 demonstrates this explicitly. While the strength and duration of merger–induced

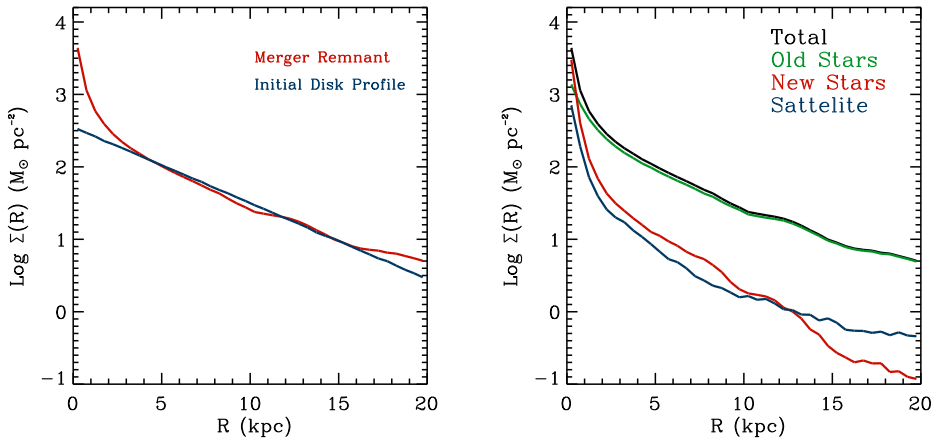

Figure 3. Projected surface mass profile for a minor merger remnant viewed face–on. The profile on the left is the same 1:8 merger remnant that is shown in Figs. 1 and 2. The profile of the remnant is compared to the progenitor (bulge–less) disk. A clear excess of surface density (a bulge) is produced by the minor merger. On the right is the surface density of the minor merger remnant decomposed by origin. The bulge surface density at small radii ($\leq$ 1 kpc) is primarily composed of "new stars," which are formed as a result of the merger–induced gaseous inflows. Outside of this radius, the surface density is entirely dominated by "old stars," which are stars that existed prior to the beginning of the simulation. For the 1:8 merger remnant shown here, the accreted satellite contributes very little mass density at all radii.

star formation is still uncertain (Cox et al. 2006a, Noeske et al. 2007) a basic theoretical understanding of the structural and orbital properties that influence the starburst has emerged (Barnes & Hernquist 1996, Hopkins et al. 2009a).

Merger–induced star formation is a result of perturbations to the internal disk kinematics. These perturbations, when resonant with internal disk motions, induced bar–like structures in the disk, and result in radial inflows of gas (Barnes & Hernquist 1996, Hopkins et al. 2009a). Thus, the stronger the tidal disturbance, or the more efficiently it can induce resonances, the stronger the merger–induced star formation.

Of primary import to this process is the mass of the perturbing satellite (e.g., Mihos & Hernquist 1994a,b, di Matteo et al. 2007, Cox et al. 2008). Major mergers will invariably lead to enough resonances that a burst of star formation results. For mergers between galaxies with a mass ratio above 1:3, i.e., minor mergers, the strength (or even existence) of merger–induced star formation depends upon a number of structural (bulge–to–disk ratio, disk size) and orbital parameters (spin–orbit orientation, distance of closest approach) which influence the efficiency of a satellite perturber to induce a starburst (see Fig. 2 for a demonstration of the wide variety of star–formation histories during a galaxy minor merger). Close–passage, prograde orbits between bulge–less galaxies are the most efficient at inducing nuclear inflows of gas and therefore star formation (see Hopkins et al. 2009a for a detailed outline of these dependencies).

While a considerable quantity of the interstellar medium is converted to stars during a galaxy interaction (depending upon the efficiency), there are several other outcomes possible. Black hole growth consumes a small quantity of gas ($< 1\%$ of the total interstellar medium) resulting in remnants that are consistent with the observed bulge mass – black hole mass relation (Younger et al. 2008b, Johansson et al. 2009). Owing to collisional shocks, gas can be heated to $\geq 10^{5-6}$ K. Gas can also be heated to this temperature by feedback from either star formation or black hole growth or both (Cox et al. 2004, Cox et al. 2006b). Hot gas will eventually expand out of the central regions and, if it is energetic enough, will exit the system in the form of a large–scale galactic outflow. If the gas does not have enough energy, it will come to rest in a static halo of hot gas. Outflowing gas also has the potential to mix with the nearby intergalactic medium, either outside of the galaxy, or as it is accreting onto the system. This reservoir of gas, as well as any left over cold interstellar medium from the merger (such as progenitor disk gas at large radii) may contribute to rebuilding (or growing) the disk after the merger (Barnes 2002, Robertson et al. 2006b, Keres & Hernquist 2009).

4. Bulge Formation

It is well established that the remnants of major galaxy mergers bear a striking resemblance to early–type galaxies. Numerical experiments have shown that the surface brightness profiles, colors and color gradients, kinematics, and fine structure of simulated major merger remnants are akin to elliptical galaxies (see, e.g., Naab & Trujillo 2006, Naab et al. 2006, Cox et al. 2006a,b, Robertson et al. 2006a, Hopkins et al. 2008a, and references therein). These results, and the similarities between galactic bulges and ellipticals, have supported the notion that bulges are the relics of major mergers in which a galactic disk has subsequently formed.

It is unclear, however, whether major mergers are the only mechanism to form galactic bulges. In fact, secular processes have long been considered the likely route to form psuedobulges (see Kormendy & Kennicutt 2004 for an extensive review). But what role do minor mergers play, if any? Minor mergers may present an attractive scenario for bulge building because they are far more ubiquitous than major mergers and also far less destructive to the galactic disk.

In light of this, the remnants of simulated minor mergers have been analyzed in numerous studies, all of which find the growth of a central mass concentration (e.g., Aguerri et al. 2001, Bournaud et al. 2004, 2005, 2007, Eliche–Moral et al. 2006, Naab & Trujillo 2006, Younger et al. 2007). Fig. 3 shows a typical surface brightness profile for a 1:8 merger remnant, and clearly demonstrates a newly formed bulge–like mass concentration. Fig. 3 also identifies its origin. Namely, within the central $\sim$ 1 kpc the surface density is dominated by "new stars" - stars formed as a result of merger–induced gaseous inflows. Beyond the inner $\sim$kpc, the surface density is dominated by "old stars" – stars that were originally in the disk of the primary. From $\sim$4-16 kpc, the profile is clearly disk–like and nearly unchanged from that of the progenitor. Inside of 4 kpc, the surface density of "old stars" is distinctly increased as a result of the merger. It is also interesting to note that the cannibalized satellite is sub–dominant at

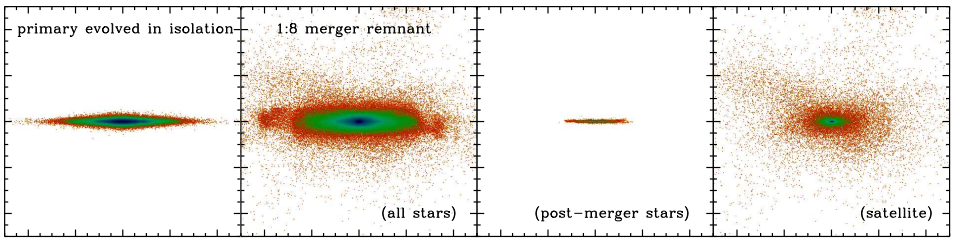

Figure 4. Edge-on view of the same 1:8 minor merger remnant as shown in Figs. 1, 2, and 3. For reference, the left–most panel shows the primary disk evolved in isolation. The post–merger remnant is shown in the second panel and this remnant is further decomposed into stars that were formed subsequent to the minor merger in the third panel and the accreted satellite in the right–most panel.

all radii, even though most of the satellite material has effectively plunged to the center of the merger remnant (see both Fig. 3, and the images presented in Fig. 4). However, this might not be the case when the mass ratio is much smaller than 1:8.

Some insight into which mergers are responsible for bulge formation also come from semi–empirical, or semi–analytic models that follow the hierarchical growth of structure (see, e.g., Khochfar & Silk 2006, Somerville et al. 2008, Hopkins et al. 2009b). In a recent study Hopkins et al. 2009b deduced that, by mass, bulge formation is dominated by major mergers, with a non–negligible ($\sim$ 30%) contribution from minor mergers. Furthermore, they find that this delineation is mass dependent; galaxies of smaller mass are more likely to have their bulge built from a minor merger. While much can be learned from these statistical studies, it is also important to identify bulge formation mechanisms in a case by case basis, clearly outlining the generic properties of bulges formed via various scenarios. Clearly, there is still much work to be done in this regard. In particular, there have been claims (Eliche–Moral et al. 2006, Younger et al. 2008b) that bulges which result from minor mergers are structurally more akin to psuedobulges than classical bulges. Additional study is required to understand whether a kinematic analysis yields a similar result, and how robust this conclusion is to a more extensive survey of parameter space.

5. The Impact on Galaxy Disks

While minor mergers may be responsible for the growth of a bulge, it is clear that they do so while still leaving some amount of the disk structure in tact. Fig. 4 shows this explicitly by viewing the merger remnant edge–on and demonstrating that the morphology is still distinctly disk–like.

A number of studies have pointed out the tension between the heating and thickening of galaxy disks owing to a single minor merger and the observed abundance of extremely thin bulgeless disks (e.g., Ostriker & Tremaine 1975, Toth & Ostriker 1990, Walker et al. 1996, Kazantzidis et al. 2008, Purcell et al. 2009). How do these structures survive a hierarchical formation? While more

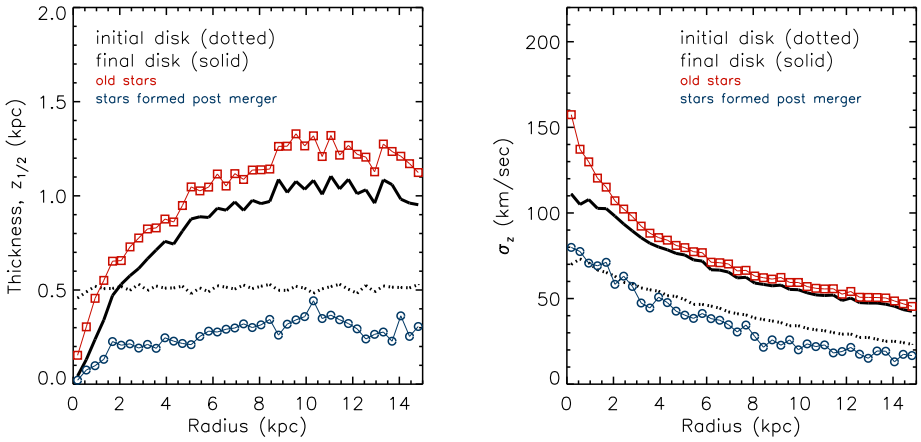

Figure 5. The thickness (left) and vertical velocity dispersion (right) of the same 1:8 minor merger remnant as shown in Figs. 1-4. For reference, the dotted black shows quantities for the primary disk evolved in isolation. The merger remnant is shown by a solid black line, which is further decomposed into "old stars" that were formed prior to the merger, and "new stars" that were formed after the merger. It is clear that the surviving gaseous disk grows a thin and cold stellar disk.

realistic assumptions about the orbits of infalling satellites may alleviate some of this concern (Hopkins et al. 2008b), the presence of a gaseous disk, which can dissipate energy and maintain its thin and cold structure, may be the ultimate solution to this problem (Hopkins et al. 2009a, Moster et al. 2009).

Figure 5 shows the influence of gas on the thickening and heating of a galactic disk owing to a single minor merger. Clearly, the stars that form post–merger are thin and cold, but (as also pointed out by Moster et al. 2009) they are subdominant by mass and thus the disk is still strongly affected by the satellite accretion. It is therefore still unclear whether gaseous dissipation will resolve the tension of thin disks observed in a hierarchical universe. Will more gas help? How does continual gas accretion and infall influence the evolution? Does this result depend upon the structure of the disk? satellite? orbit?

While the last decade has rapidly increased our understanding of the role that mergers play in the hierarchical formation of structure, it is safe to say that we still have a long way to go. As a final comment, we note that it would be ideal to have independent observational probes to directly test the numerical merger models. One such intriguing possibility is "fine" stellar structures produced by groups of stars inhabiting unique regions of phase space. The Monoceros Ring may be just such a structure within our own galaxy (Younger et al. 2008a). Time will tell how ubiquitous such features are, and just what they are telling us.

Acknowledgments. We thanks the organizers of this conference for an exciting week in Austin and many stimulating discussion. Furthermore, I apologize for the delinquency in submitting these proceedings.

References

Aguerri J. A. L., Balcells M., Peletier R. F., 2001, A&A, 367, 428.
Barnes J. E, 2002, MNRAS, 333, 481.
Barnes J. E & Hernquist L., 1996, ApJ, 471, 115.
Barton E. J., Geller M. J., Kenyon S. J., 2000, ApJ, 530, 660.
Borne K. D., Bushouse H.., Lucas R. A., Colina L., 2000, ApJ, 529, L77.
Bournaud F., Combes F., Jog C. J., 2004, A&A, 418, L27.
Bournaud F., Jog C. J., Combes F., 2005, A&A, 437, 69.
Bournaud F., Jog C. J., Combes F., 2007, A&A, 476, 1179.
Cox T. J., et al., 2004, ApJ, 650, L791.
Cox T. J., Jonsson P., Primack J. R., Somerville R. S., 2006a, MNRAS, 373, 1013.
Cox T. J., et al., 2006b, ApJ, 650, 791.
Cox T. J., et al., 2008, MNRAS, 384, 386.
di Matteo P., Combes F., Melchoir A. L., Semelin B., 2007, A&A, 468, 61.
Eliche–Moral M. C. et al., 2006, A&A, 457, 91.
Fakhouri O., & Ma C. P., 2008, MNRAS, 386, 577.
Hernquist L., 1993, ApJS, 86, 389.
Hernquist L., & Mihos J. C., 1994a, ApJ, 425, L13.
Hernquist L., & Mihos J. C., 1994b, ApJ, 431, L9.
Hopkins P. F., et al., 2008a, ApJ, 679, 156.
Hopkins P. F., et al., 2008b, ApJ, 688, 757.
Hopkins P. F., Cox T. J., Younger J. D., Hernquist L., 2009a, ApJ, 691, 1168.
Hopkins P. F. et al., 2009b, ApJ, 691, 1168.
Jogee S., et al., 2009, ApJ, 697, 1971.
Johansson P., Naab T. & Burkert, A., 2009, MNRAS, 690, 802.
Kazantzidis S. et al., 2008, ApJ, 688, 254.
Kennicutt R., 1998, ApJ, 498, 541.
Keres D., & Hernquist L., 2009, ApJ, 700, L1.
Khochfar S., & Burkert A., 2006, A&A, 445, 403.
Khochfar S., & Silk J., 2006, MNRAS, 370, 902.
Kormendy J., & Kennicutt R. C., 2004, ARA&A, 42, 603.
Larson R. B, & Tinsley B. M., 1978, ApJ, 219, 46.
Moster B. P. et al., 2009, submitted to MNRAS(astro-ph/0906.0764).
Naab T., Jesseit R., Burkert A., 2006, MNRAS, 372, 839.
Naab T., & Trujillo I., 2006, MNRAS, 369, 625.
Noeske K. G. et al., 2007, ApJ, 660, L43.
Ostriker J. P. & Tremaine S. D., 1975, ApJ, 202, L113.
Purcell C. W., Kazantzidis S., Bullock S., 2009, ApJ, 694, 98.
Robertson B. E. et al., 2006a, ApJ, 641, 21.
Robertson B. E. et al., 2006b, ApJ, 645, 986.
Sanders, D. B, Mirabel, I. F., 1996, ARA&A, 34, 749.
Somerville R. S. et al., 2008, MNRAS, 391, 481.
Springel, V. 2000, MNRAS, 312, 859.
Springel, V. 2005, MNRAS, 364, 1105.
Springel, V., Hernquist, L., 2003, MNRAS, 339, 289.
Springel V., Di Matteo T., Hernquist L., 2005b, MNRAS, 361, 776.
Toth G., Ostriker J. P., 1992, ApJ, 389, 5.
Walker I. R., Mihos J. C., Hernquist L., 1996, ApJ, 460, 121.
Younger J. D., Cox T. J., Seth A. C., Hernquist L., 2007, ApJ, 670, 269.
Younger J. D. et al., 2008a, ApJ, 676, L21.
Younger J. D., Hopkins P. F., Cox T. J., Hernquist L., 2008b, ApJ, 686, 815.

GALAXY EVOLUTION: EMERGING INSIGHTS AND FUTURE CHALLLENGES
ASP Conference Series, Vol.
@jourvol, © 2009
S. Jogee, I. Marinova, L. Hao, and G. A Blanc

Invisible Major Mergers: Why the Definition of a Galaxy "Merger Ratio" Matters.

Kyle R. Stewart

Center for Cosmology, Department of Physics and Astronomy, The University of California at Irvine, Irvine, CA, 92697, USA

Abstract. The mapping between dark matter halo mass, galaxy stellar mass, and galaxy cold gas mass is not a simple linear relation, but is influenced by a wide array of galaxy formation processes. We implement observationally-normalized relations between dark matter halo mass, stellar mass, and cold gas mass to explore these mappings, with specific emphasis on the correlation between different definitions of a major galaxy merger. We always define a major merger by a mass ratio $m/M > 0.3$, but allow the masses used to *compute* this ratio to be defined in one of three ways: dark matter halo masses, galaxy stellar masses, or galaxy baryonic masses (stars and cold gas). We find that the merger ratio assigned to any particular merger event depends strongly on which of these masses is used, with the mapping between different mass ratio definitions showing strong evolution with halo mass and redshift. For example, major dark matter mergers (> 0.3) in small galaxies ($M_{\rm DM} < 10^{11} M_{\odot}$) typically correspond to very minor *stellar* mergers ($< 1/20$). These mergers contain significant dark matter mass, and should cause noticable morphological disruption to the primary galaxy, even though there is no observable bright companion. In massive galaxies, there is an opposite effect, with bright companion galaxies corresponding to only minor dark matter mergers. We emphasize that great care must be taken when comparing mergers based on different mass ratio definitions.

1. Introduction

In the cold dark matter (CDM) model of structure formation, galaxy mergers are believed to play an important role in galaxy evolution. Typically, these mergers are divided into two categories. "Minor" mergers (with mass ratios $< 1/3$) are often thought to trigger moderate bursts of increased star formation and/or morphological disturbances, as well as contributing to the deposition of diffuse light components of galaxies. "Major" mergers (with mass ratios $> 1/3$) are likely to influence stronger morphological disturbances responsible for the transformation from disk-dominated to bulge-dominated morphologies, in addition to triggering stronger starburst and AGN activity.

Despite this commonly adopted distinction between major and minor mergers at merger mass ratios of $\sim 1/3$, there is still ambiguity in what mass is used to *define* this ratio. Theoretical investigations of dark matter halo merger rates typically define merger ratios in terms of dark matter halo masses, which is the most theoretically robust prediction from cosmological N-body simulations (e.g., Stewart et al. 2008, and references within). However, because estimates of dark matter halo masses are difficult to obtain observationally, it is also

common to define merger ratios by comparing the stellar masses or the total baryonic masses of galaxies.

In attempting to compare theoretically derived merger statistics (in terms of dark matter mass ratios) to observational investigations of galaxy mergers (in terms of stellar or galaxy mass ratios), it is important to understand the mapping between these definitions. Galaxy merger rates, for example, are quite sensitive to the merger mass ratio being considered (Stewart et al. 2009a). In order to explore the fundamental differences between major mergers as defined by dark matter halo, stellar, and galaxy merger ratios, we adopt a semi-empirical methodology to estimate the stellar and cold gas content of dark matter halos as a function of halo mass and redshift. We give a very brief overview of this method before presenting our findings, but we refer reader to Stewart et al. (2009b) for a more in-depth discussion of this method.

2. Assigning Baryons and Defining Masses

In order to assign stars to our halos, we assume a monotonic relationship between halo mass and stellar mass. Using this technique, provided we know $n_g(> M_{\rm star})$ (the cumulative number density of galaxies with stellar mass more massive than $M_{\rm star}$) we may determine the associated dark matter halo population by finding the halo mass above which the number density of halos (including subhalos) matches that of the galaxy population, $n_h(> M_{\rm DM}) = n_g(> M_{\rm star})$. Specifically, we adopt the relation found by Conroy & Wechsler 2008 (interpolated from the data in their Figure 2). Of course, a simple relation of this kind cannot be correct in detail, but in an average sense, it provides a good characterization of the relationship between halo mass and galaxy stellar mass that must hold in order for LCDM to reproduce the observed universe.

In order to reasonably assign gas to the central galaxies within our halos, we quantify observationally-inferred relations between gas fraction and stellar mass. Specifically, we characterize the data from McGaugh 2005 (disk-dominated galaxies at $z = 0$) and Erb et al. 2006 (UV-selected galaxies at $z \sim 2$) with a relatively simple function of stellar mass and redshift (see Stewart et al. 2009b), and find that this adopted characterization is also consistent with a number of other observationally motivated works (e.g., Kannappan 2004; Baldry et al. 2008).

Using this prescription to estimate the stellar and cold gas content of dark matter halos as a function of halo mass and redshift, we define three different means of identifying the mass of a galaxy (and thus, define merger mass ratios):

1. The mass (or mass ratio) of each dark matter halo, $(m/M)_{\rm DM}$. We will refer to these as the *DM mass (ratio)* of a galaxy (merger).

2. The mass (mass ratio) of the stellar mass of each dark matter halo's central galaxy, $(m/M)_{\rm star}$. We refer to this definition as the *stellar mass (ratio)*.

3. The mass (mass ratio) of the total baryonic mass of each dark matter halo's central galaxy, $(m/M)_{\rm gal}$. In this case, we define a galaxy's baryonic mass as a combination of its stellar mass and cold gas mass ($M_{\rm gal} \equiv M_{\rm star} + M_{\rm gas}$). We refer to this definition as the *galaxy mass (ratio)*.

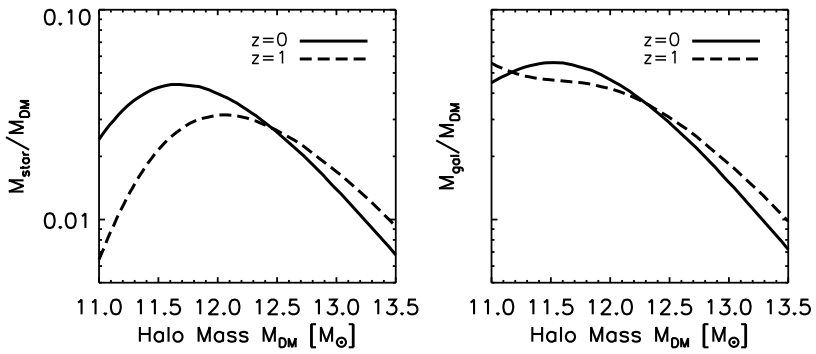

Figure 1. A comparison of the baryonic properties of a central galaxy to its dark matter halo mass. *Left:* Ratio of stellar mass to dark matter halo mass, as a function of halo mass. *Right:* Ratio of total baryonic mass (stars and cold gas) to halo mass, as a function of halo mass. In both panels, the solid and dashed lines correspond to $z = 0$ and $z = 1$, respectively. Note that these relations vary significantly with halo mass and redshift.

Using these mass definitions, we show the stellar and galaxy mass of a dark matter halo's central galaxy as a function of halo mass (and normalized by halo mass) in Figure 1, where solid and dashed lines represent galaxies at $z = 0$ and $z = 1$, respectively. We emphasize that these mass fractions are a strong function of halo mass, and evolve with redshift. Assumptions of a constant mass-to-light ratio (or more specifically, a constant stellar mass to DM mass ratio: $M_{\rm star} = fM_{\rm DM}$), which are common in semi-analytic formalisms, will ignore the significant evolution with halo mass and redshift shown in this figure.

3. Mapping Between Mass Ratios

We explore the various mappings between major mergers using different mass definitions in Figure 2. In the top panels we focus on mergers with $(m/M)_{\rm DM} = 0.3$ (henceforth *major DM mergers*), with the dashed and dotted lines showing the corresponding stellar and galaxy mass ratios of these mergers. In the bottom panels, we instead focus on *major stellar mergers*, defined by $(m/M)_{\rm star} = 0.3$. In these panels, the solid and dotted lines corresponding to the DM and galaxy mass ratios of these mergers. The left and right panels show relations at $z = 0$ and $z = 1$, respectively.

We emphasize that, in general, the DM mass ratio between two galaxies is *not* the same as the stellar (or galaxy) mass ratio. Specifically, major DM mergers (top panels) correspond to stellar mass ratios ranging from $\sim 5 - 60\%$ $(5 - 50\%)$ and galaxy mass ratios of $\sim 20 - 60\%$ $(35 - 50\%)$ for $10^{11-13} M_\odot$ halos at $z = 0$ (1). Similarly, major stellar mergers (bottom panels) correspond to DM mass ratios from $\sim 10 - 55\%$ $(15 - 65\%)$ and galaxy mass ratios of $\sim 30 - 45\%$ $(75 - 35\%)$ for $10^{11-13} M_\odot$ halos at $z = 0$ (1). Indeed, the *only* broad regime

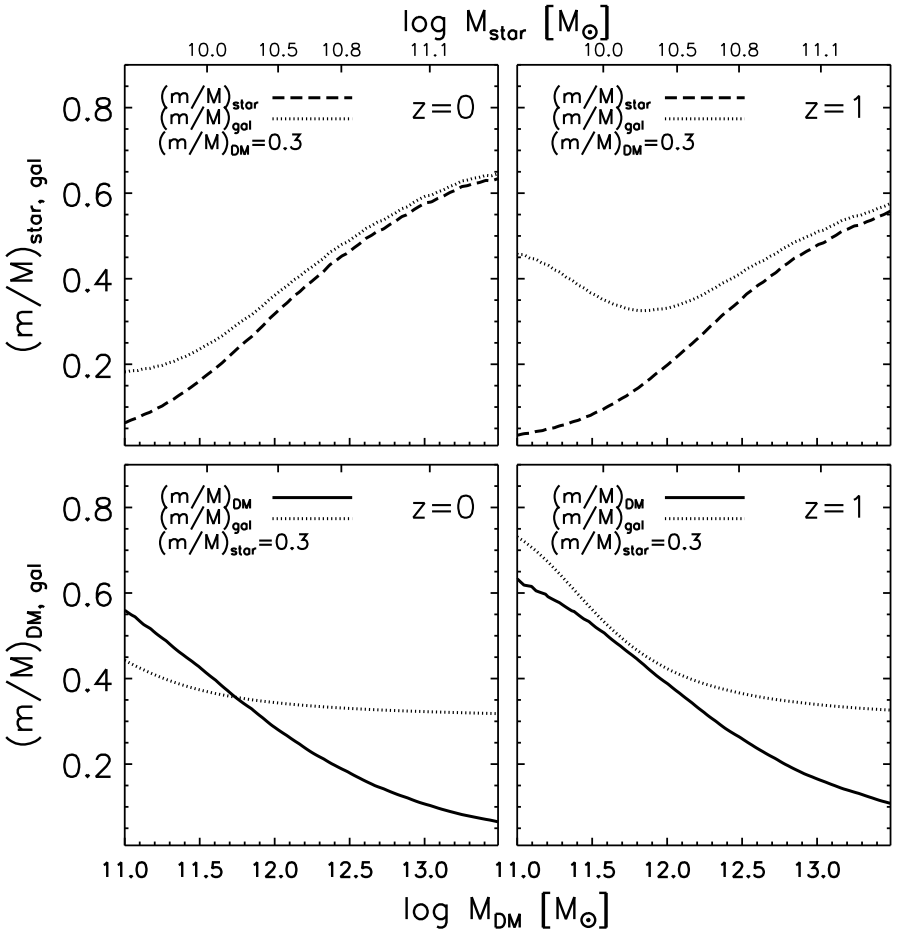

Figure 2. Conversion between major merger ratios defined by dark matter halo mass ($M_{\rm DM}$), stellar mass ($M_{\rm star}$), or galaxy (baryonic) mass ($M_{\rm gal}$). In the top panels, the dashed and dotted lines show the stellar and galaxy mass ratios of major DM mergers with $(m/M)_{\rm DM} = 0.3$, as a function of halo mass (lower axis) and stellar mass (top axis). Similarly, the solid and dotted lines in the bottom panels show the DM and galaxy mass ratios corresponding to major stellar mergers with $(m/M)_{\rm star} = 0.3$. The left and right panels give these relations at $z = 0$ and $z = 1$, respectively.

where different mass definitions result in similar merger ratios is for stellar and galaxy merger ratios of massive galaxies, where galaxy gas fractions are typically low enough that $M_{\rm star} \sim M_{\rm gal}$.

Note that in low mass galaxies ($M_{\rm DM} < 10^{11} M_\odot$) major DM mergers should contain stellar mass ratios $< 1/20$. The secondary (smaller) galaxy in these mergers contain significant mass in dark matter, and should be capable of triggering severe morphological disruption in the primary galaxy, but they are observationally "invisible," with negligible luminous content with respect to the

primary. The existence of these "invisible" major mergers is a robust, testable prediction of LCDM.

4. Example Consequence: Measuring the Merger Rate

While theoretical investigations into dark matter halo merger rates define mergers by DM mass ratios, observed merger rates (specifically, those based on close-pair counts of galaxies) typically select pairs based on luminosity (stellar mass), and should thus constitute major *stellar* mergers. The mapping between stellar and DM mass ratios has two important qualitative effects in this case. First, for smaller halos, major DM mergers should correspond to substantially smaller stellar mass ratios, and may not be distinguishable as a luminous close-pair when observed (ie. faint/invisible major mergers). Second, for massive halos, some observed close-pairs with comparable luminosities (major stellar mergers) may correspond to substantially smaller *DM* mass ratios, and would be counted as *minor* (not major) mergers in theoretical predictions from N-body simulations (ie. bright minor mergers).

For a more quantitative analysis, we adopt the fitting function for dN/dt from Stewart et al. 2009a (Table 1, infall, "simple fit"), which provides the rate of mergers more massive than $(m/M)_{\rm DM}$ into dark matter halos of mass $M_{\rm DM}$ (per halo, per Gyr) as a function of redshift, mass, and mass ratio. For $10^{11}M_{\odot}$ dark matter halos and DM merger ratios $> 30\%$ at $z = 0 - 1$, the merger rate increases from $\sim 0.015 - 0.070$. Now consider an identical halo mass, but for mergers selected on *stellar* mass ratios $> 30\%$, corresponding to a DM mass ratio of $\sim 7\%$ (4%) at $z = 0$ (1). Because of the minor DM mergers being considered, this selection would result in an artificial increase of the observed merger rate by a factor of $3 - 4$ compared to DM merger rates ($\sim 0.05 - 0.30$ from $z = 0 - 1$), with a redshift evolution that is too steep (and does not appear to fit well to $dN/dt \propto (1+z)^{\alpha}$; see Stewart et al. 2009a). Thus, using different mass ratios to define mergers has a substantial effect on predictions of galaxy merger rates, and great care must be taken when comparing studies of galaxy or halo mergers, if the merger mass ratios have been defined by different criterion.

Acknowledgments. KRS thanks Shardha Jogee and the conference organizers for an excellent conference with a thought provoking program.

References

Baldry, I. K., Glazebrook, K., & Driver, S. P., 2008 MNRAS, 388, 945
Conroy, C., & Wechsler, R. H. 2009, ApJ, 696, 620
Erb, D. K., Steidel, C. C., Shapley, A. E., Pettini, M., Reddy, N. A., & Adelberger, K. L., 2006 ApJ, 646, 107
Kannappan, S. J., 2004, ApJ, 611, L89
Maller, A. H., Astronomical Society of the Pacific Conference Series, 396, 251
McGaugh, 2005, ApJ, 632, 859
Stewart, K. R., Bullock, J. S., Wechsler, R. H., Maller, A. H. and Zentner, A. R., 2008 ApJ, 683, 597
Stewart, K. R., Bullock, J. S., Barton, E. J., & Wechsler, R. H. 2009, ApJ, 702, 1005
Stewart, K. R., Bullock, J. S., Wechsler, R. H., & Maller, A. H. 2009, ApJ, 702, 307

GALAXY EVOLUTION: EMERGING INSIGHTS AND FUTURE CHALLLENGES
ASP Conference Series, Vol.
@jourvol, © 2009
S. Jogee, I. Marinova, L. Hao, and G. A Blanc

Galactic Disk Transformation via Massive Satellite Accretion Events

Chris W. Purcell[1], Stelios Kazantzidis[2], and James S. Bullock[1]

Abstract. Accretion events involving the infall of a massive satellite galaxy ($M_{\rm sat} \sim 10^{11} M_{\odot}$) onto a stellar disk in a Galactic-scale host halo ($M_{\rm host} \sim 10^{12} M_{\odot}$) are both cosmologically common and capable of inducing significant morphological and dynamical changes in the primary system. We review the work of Purcell et al. (2009) in which, for the first time, the destruction of a cold and thin Milky Way analogue disk is demonstrated in the context of these common accretion events. Using high-resolution simulations, in both the collisionless regime and in hydrodynamical experiments, we show that the resultant disk scale heights are typically larger, and the stellar dynamical temperature significantly hotter, than that of the Galactic thick disk. We conclude that in order for the Milky Way to be as thin and cold as it is today, the accretion history of the Galaxy must have been unusually quiescent compared to median ΛCDM expectations.

1. Introduction

If the ΛCDM cosmology represents the correct model of structure formation in the universe, then the process of building disk galaxies like the Milky Way must be fraught with accretion events involving subhalos massive enough to affect the morphology and kinematics of the host galaxy. The question of disk survival has been of persistent interest to the galaxy formation community (Toth & Ostriker 1992; Hopkins et al. 2008), but only recently have numerical techniques advanced to the point of allowing high-resolution, fully self-consistent experiments involving cosmologically-motivated initial conditions.

Perhaps the most relevant scale of interest to the question of disk stability is the regime of massive accretion events involving the infall of satellite galaxies with mass ratio $M_{\rm sat}$:$M_{\rm host} \sim$ 1:10. This mode of mass delivery represents the dominant means by which ΛCDM halos grow on all scales (Purcell et al. 2007), and cosmological simulations indicate that $\sim 70\%$ of Galaxy-sized halos ($M_{\rm host} \sim 10^{12} M_{\odot}$) have accreted a subhalo with mass $M_{\rm sat} \sim 10^{11} M_{\odot}$ in the past 10 Gyr (Stewart et al. 2008). Less massive satellite accretion events are ubiquitous and do not destroy the thin primary disk (Kazantzidis et al. 2008), while more massive mergers are quite rare and known to be catastrophically destructive to the galaxies involved. Given the wide range of observational

[1]Center for Cosmology, Department of Physics and Astronomy, The University of California, Irvine, CA 92697 USA; cpurcell@uci.edu, bullock@uci.edu

[2]Center for Cosmology and Astro-Particle Physics; and Department of Physics; and Department of Astronomy, The Ohio State University, Columbus, OH 43210 USA; stelios@mps.ohio-state.edu

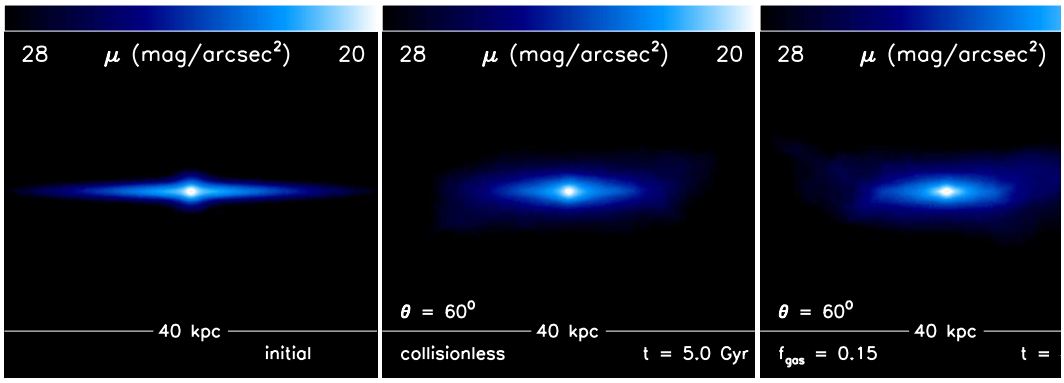

Figure 1. Surface brightness maps, assuming $M_\star/L = 3$, for the initial galaxy model as well as the endstates involving prograde satellite galaxy infall with an orbital inclination of 60° for three cases: $f_{\rm gas} = 0$ (collisionless), $f_{\rm gas} = 0.15$, and $f_{\rm gas} = 0.45$ as described in §2.

evidence that the large majority of Galactic-scale halos in the universe host stellar systems with disk-dominant morphology (*e.g.*, van den Bosch et al. 2007; Park et al. 2007), the 1:10 accretion regime therefore represents the crucial scale for disk survivability.

Here, we briefly review the work of Purcell et al. (2009, hereafter PKB09), in which the authors perform a suite of focused, high-resolution collisionless simulations designed to emulate the impact of 1:10 satellite galaxies on Galactic-analogue disks. In addition, we present a selection of results from a resimulation campaign involving a full treatment of hydrodynamics and ISM physics, in order to determine the effect of a substantial disk of cold gas on the morphological and dynamical transformations brought about during these massive accretion events.

2. Methods

For a more complete methodological description of the simulation campaign, we refer the reader to PKB09 for the collisionless experiments and to Kazantzidis, Purcell & Bullock (2009, in preparation) for more detail regarding the hydrodynamical resimulations. Briefly, we instantiate a primary galaxy designed to match the observed properties of the Milky Way today (with $M_{\rm host} \simeq 10^{12} M_\odot$), according to the fully self-consistent distribution functions advanced by Widrow et al. (2008); the initial sech^2 scale height of the disk is 430 pc, and the total stellar mass $M_\star = 4.5 \times 10^{10} M_\odot$ including the material in the disk as well as the central bulge.

The satellite galaxy we construct for the fiducial accretion scenario emulates a subhalo with mass $M_{\rm sat} \simeq 10^{11} M_\odot$ that is well-fitted by an NFW profile with concentration $c_{\rm vir} = 14$ at redshift $z = 0.5$. Embedding a stellar spheroid with Sérsic index $n \simeq 0.5$ and mass $M_\star \simeq 2.2 \times 10^9 M_\odot$ according to the abundance-matching prescription of Conroy & Wechsler (2009), we initialize

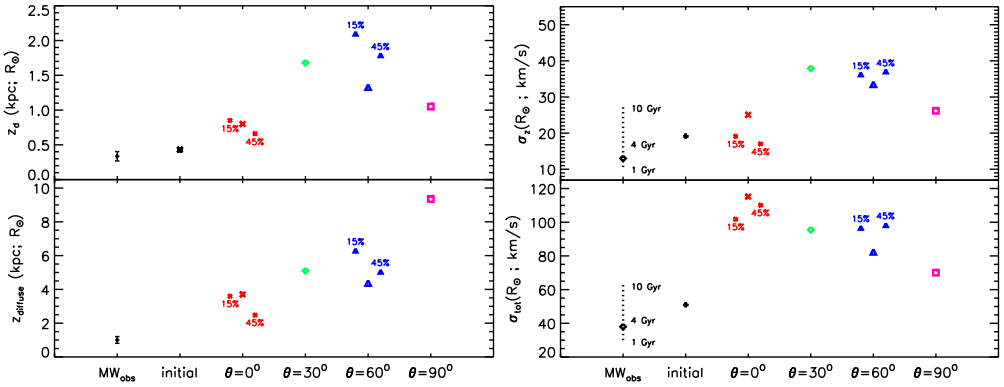

Figure 2. Morphological and dynamical measurements of the initial thin disk and final thick disks following each satellite infall with orbital inclination θ. In each panel, the observational values for the Milky Way are presented for comparison; in the *left* panel the two-component decomposition of Jurić et al. (2008) is shown next to the fits for each simulation as described in §3., while in the *right* panel we display the kinematics for the solar neighborhood stars (as drawn from Nordström et al. 2004). The small points in the 0° and 60° columns denote the results for the simulations with $f_{\rm gas} = 15\%$ and 45% as marked.

the accretion event by placing the subhalo roughly 120 kpc from the center of the host halo, and assigning it an initial velocity vector drawn from the median infall parameters found in the cosmological simulations of Benson (2005). We examine a range of prograde orbital inclination angles: $\theta = 0°, 30°$, and 60°, as well as a polar infall with $\theta = 90°$ and no tangential velocity component. As a test case, we also simulate a retrograde orbit with $\theta = 60°$ in the collisionless suite of experiments.

In our simulations involving a full treatment of hydrodynamics, we convert a significant fraction $f_{\rm gas}$ of the initial stellar disk mass into a cold and thin gaseous component with the same density structure as the original disk. We investigate two gas fractions, $f_{\rm gas} = 0.15$ and $f_{\rm gas} = 0.45$, in each of two infall inclinations, $\theta = 0°$ and 60°. Our hydrodynamical prescription includes atomic cooling and the star formation algorithm of Katz (1992), as well as a supernova feedback implementation based on the blast-wave model of Stinson et al. (2006); this set of parameters produces realistic disk galaxies in large-scale cosmological simulations (Governato et al. 2007).

3. Results and Discussion

In Figure 1, we show surface brightness visualizations of the initial galaxy model as well as the resultant stellar systems following a prograde accretion event with $\theta = 60°$, for the three cases $f_{\rm gas} = 0$ (collisionless), 0.15, and 0.45. The heavy thickening undergone during the event is apparent; much stellar mass originally near the mid-plane of the disk has now been ejected to heights larger than a few kpc. To quantify this morphological change, and to capture

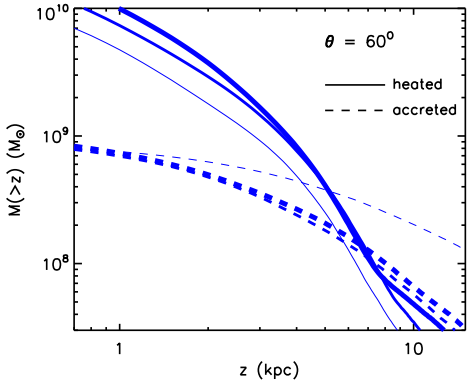

Figure 3. The cumulative amount of stellar mass above a height z from the disk plane, for prograde subhalo infalls with $\theta = 60°$, as contributed by heated disk stars (*solid*) as well as accreted satellite stars (*dashed*). Line thicknesses correspond to gas fraction values: $f_{\rm gas} = 0$ (*thin*), 0.15 (*medium*), and 0.45 (*thick*).

the remnant thick disk as well as the faint material at large distances from the plane, we fit a two-component profile along the minor axis, *i.e.*, $\Sigma(z) = \Sigma_{\rm d}\,{\rm sech}^2(z/z_{\rm d}) + \Sigma_{\rm diffuse}\,{\rm sech}^2(z/z_{\rm diffuse})$. As shown in the left panels of Figure 2, typical values of the minimal scale height $z_{\rm d}$ are inconsistent with even the thick disk of the Galaxy (which has scale height ~ 0.9 kpc, according to Jurić et al. 2008); thus our claim that the initially thin disk has been destroyed.

In addition to the severe thickening undergone by our galactic systems during the simulated accretion events, the transfer of orbital kinetic energy from the satellite causes extensive dynamical heating of the primary disk. Even substantial thin-disk regrowth due to the presence of a massive gas disk cannot cool these heated stars, yielding predictions based on our resultant velocity ellipsoids that are more robust with respect to variance in our sub-grid physical prescriptions. In the right panels of Figure 2, we compare the vertical and total velocity dispersion of our thick disks to that of the stars observed in the solar neighborhood by Nordström et al. (2004). Note that all but the oldest and hottest local stellar populations are still significantly colder than the heated disks we produce; the addition of a cold, star-forming gas disk serves to mitigate this effect in the planar satellite infall, but exacerbates the heating in the accretion event with $\theta = 60°$. Similarly, the scale heights we obtain are noticeably smaller for the $\theta = 0°$ infalls involving non-zero $f_{\rm gas}$ than for their collisionless counterpart, but significantly larger for the simulated high-latitude accretion events.

The behavior of the hydrodynamical disks betrays the fact that a stellar disk's susceptibility to violent destruction during satellite infall is strongly dependent on not only the orbital parameters of the subhalo, but also the vertical restoring force available to the stars in the disk. Upon impact, a significant fraction of the cold gas is ejected to large distances from the disk plane, effectively lowering the total baryonic mass near the plane. This reduction in the restoring force makes the disk less able to maintain a thin self-

gravitating state. The strength of this effect correlates with the vertical orbital energy deposited into the disk material by the subhalo, and thus also with the infall inclination angle θ; high-latitude accretion events yield resultant scale heights and velocity dispersions that are larger than those in their collisionless counterpart simulations, while the planar infall (which deposits no vertical energy) results in smaller morphological and dynamical measurements for the hydrodynamical case. We explore these interpretations further in Kazantzidis, Purcell & Bullock (2009, in preparation). It appears that the role of gas may play a more complex role in satellite-disk interactions than typically considered by efforts to address whether thin and cold galaxies like the Milky Way must have unusually quiescent accretion histories in order to survive.

Acknowledgments. We would like to thank Larry Widrow and John Dubinski for kindly making available the software used to set up the primary galaxy models. CWP and JSB are supported by National Science Foundation (NSF) grants AST-0607377 and AST-0507816, and the Center for Cosmology at UC Irvine. SK is supported by the Center for Cosmology and Astro-Particle Physics at The Ohio State University.

References

Benson, A. J. 2005, MNRAS, 358, 551
Conroy, C., & Wechsler, R. H. 2009, ApJ, 696, 620
Governato, F., Willman, B., Mayer, L., Brooks, A., Stinson, G., Valenzuela, O., Wadsley, J., & Quinn, T. 2007, MNRAS, 374, 1479
Hopkins, P. F., Hernquist, L., Cox, T. J., Younger, J. D., & Besla, G. 2008, ApJ, 688, 757
Jurić, M. et al. 2008, ApJ, 673, 864
Katz, N. 1992, ApJ, 391, 502
Kazantzidis, S., Bullock, J. S., Zentner, A. R., Kravtsov, A. V., & Moustakas, L. A. 2008, ApJ, 688, 254
Nordström, B. et al. 2004, A&A, 418, 989
Park, C., Choi, Y.-Y., Vogeley, M. S., Gott, J. R. I., & Blanton, M. R. 2007, ApJ, 658, 898
Purcell, C. W., Bullock, J. S., & Zentner, A. R. 2007, ApJ, 666, 20
Purcell, C. W., Kazantzidis, S., & Bullock, J. S. 2009a, ApJ, 694, L98
Stewart, K. R., Bullock, J. S., Wechsler, R. H., Maller, A. H., & Zentner, A. R. 2008, ApJ, 683, 597
Stinson, G., Seth, A., Katz, N., Wadsley, J., Governato, F., & Quinn, T. 2006, MNRAS, 373, 1074
Soubiran, C., Bienaymé, O., & Siebert, A. 2003, A&A, 398, 141
Toth, G. & Ostriker, J. P. 1992, ApJ, 389, 5
van den Bosch, F. C. et al. 2007, MNRAS, 376, 841
Widrow, L. M., Pym, B., & Dubinski, J. 2008, ApJ, 679, 1239

GALAXY EVOLUTION: EMERGING INSIGHTS AND FUTURE CHALLLENGES
ASP Conference Series, Vol.
@jourvol, © 2009
S. Jogee, I. Marinova, L. Hao, and G. A Blanc

The Impact of Mergers on the Survival and Abundance of Disk-Dominated Galaxies

Jun Koda, Miloš Milosavljević, and Paul R. Shapiro

Department of Astronomy, Texas Cosmology Center, University of Texas, 1 University Station C1400, Austin, TX 78712.

Abstract. We study the formation of disk-dominated galaxies in a ΛCDM universe. Their existence is considered to be a challenge for the ΛCDM cosmology, because galaxy mergers isotropize stellar disks and trigger angular momentum transport in gas disks, thus fostering the formation of central stellar spheroids. Here, we postulate that the formation of stellar spheroids from gas-rich disks is controlled by two parameters that characterize galaxy mergers, the mass ratio of merging dark matter halos, and the virial velocity of the larger merging halo. We utilize merger histories generated from realizations of the cosmological density field to calculate the fraction of dark matter halos that have avoided spheroid formation, and compare the derived statistics with the spheroid occupation fractions in surveys of nearby galaxies. We find, for example, that the survival rate of disk-dominated galaxies in ΛCDM is just high enough to explain the observed fractional representation of disk-dominated galaxies in the universe if the only mergers which lead to central spheroid formation are those with mass ratios $M_2/M_1 > 0.3$ and virial velocities $V_{\rm vir,1} > 55$ km s^{-1}. We discuss the physical origin of this criterion, and show that the dependence of the disk-dominated fraction on galaxy mass provides a further test of the merger hypothesis.

1. Introduction

Disk-dominated galaxies with little or no bulge are frequently cited as a challenge to the ΛCDM cosmology (e.g. Kautsch et al. 2006). In ΛCDM cosmology, galaxy-hosting halos grow hierarchically by mergers. Major mergers destroy disks and create elliptical galaxies/classical bulges. On the other hand, pseudobulges are thought to be created by secular evolution, not by major mergers (Kormendy & Kennicutt 2004). We consider what the requirements for bulge-forming mergers must be in order for the merger history of galactic halos in ΛCDM to account statistically for the observed fraction of galaxies today which are "disk-dominated" – i.e., those with either no bulge or only a pseudobulge. [For additional details, see, Koda et al. (2009).]

2. A Simple Merger Hypothesis

We explore a simple model in which bulge formation due to merger is controlled by two parameters, mass ratio $\mu = M_2/M_1 (\leq 1)$ and the virial velocity of the larger halo, $V_{\rm vir,1}$. The hypothesis of the model is that a bulge forms if and only if, $\mu > \mu_{\rm crit}$ and $V_{\rm vir,1} > V_{\rm vir,crit}$. (1)

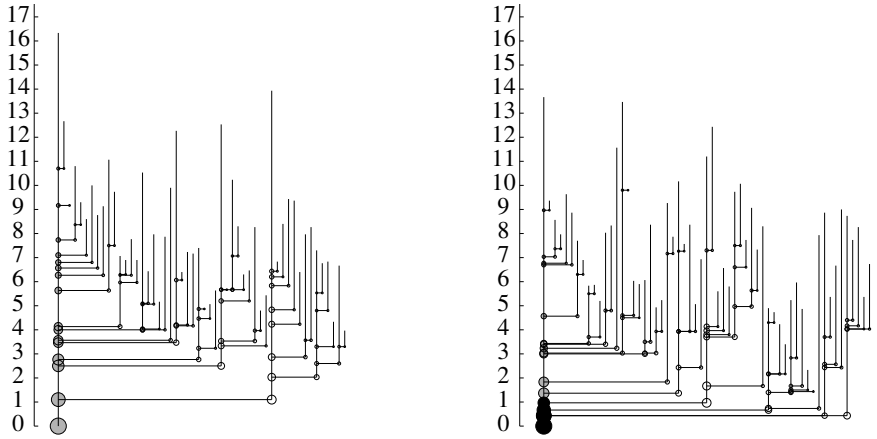

Figure 1. Examples of merger trees. Gray circles represent disk-dominated galaxies and black circles represent galaxies with classical bulges, respectively, under a bulge-forming criterion $\mu_{\rm crit} = 0.3$, $V_{\rm vir,crit} = 55$ km s^{-1}. Radii of circles are proportional to $M^{1/3}$. Mergers with $\mu < 0.05$ are not plotted in the figure. Vertical axis label is redshift.

Motivation: Mergers which make bulges are generally assumed to require a merging-halo mass ratio, μ, above some threshold, $\mu_{\rm crit}$, consistent with N-body and some hydro simulations (e.g., Bournaud, Jog, & Combes 2005; Cox et al. 2008). We hypothesize here an additional dependence on $V_{\rm vir,1}$, the virial velocity of the larger halo. The virial velocity characterizes gas dynamical effects. Bulge formation requires angular-momentum transport, which strong shocks can promote. Shock-induced radiative cooling and compression also promote gravitational instability. The strength of merger shocks is characterized by the Mach number $\mathcal{M} \propto V_{\rm vir}$. If the IGM was pre-heated by reionization, gas pressure can prevent gas from collapsing into galaxies ("Jeans-mass filtering," Shapiro et al. 1994) if the virial velocity is too low. The threshold value of this Jeans-mass filtering is uncertain ($\sim 30 - 80$ km s^{-1}, e.g., Okamoto et al. 2008, and references therein). Mergers of pre-existing stellar systems with $\mu > \mu_{\rm crit}$ still require $V_{\rm vir,1} > V_{\rm vir,crit}$ to make enough stars before merger (i.e., star formation requires gaseous baryons but halos may not retain if $V_{\rm vir}$ too low).

Method: Merger Tree. We generate merger trees for the galactic halos in a comoving box 40 Mpc on a side, using a publicly available code PINOCCHIO (Monaco et al. 2002) based on Lagrangian perturbation theory. The code gives halo masses and their merger histories that are in good agreement with N-body simulations, but with less computation. We follow the most massive progenitor of each halo, in mass range $5 \times 10^{10} M_\odot < M < 10^{12} M_\odot$, and check the bulge-forming condition (Eq. 2.) for all mergers (see Figure 1). We assume that a halo hosts a disk-dominated galaxy if none of its mergers satisfies the bulge formation criterion. We vary $\mu_{\rm crit}$ and $V_{\rm vir,crit}$ to see which critical values are consistent with the observed fraction of disk-dominated galaxies.

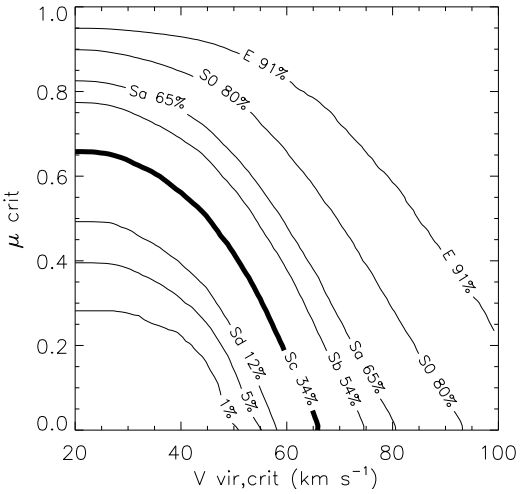

Figure 2. The fraction of disk-dominated galaxies that results from bulge formation criteria characterized by the critical merger mass ratio, $\mu_{\rm crit}$, and the critical virial velocity of the larger halo at merger, $V_{\rm vir,crit}$. The points along the bold contour "Sc 34%" (e.g., $\mu_{\rm crit} = 0.3, V_{\rm vir,crit} = 55$ km s^{-1}) constitutes our theoretical expectation for the bulge-forming threshold criteria that is compatible with observation (See § 3.).

3. Results and Conclusion

Figure 2 shows the fraction of galaxies without classical bulge (disk-dominated galaxies) as a function of the bulge formation criterion ($\mu_{\rm crit}, V_{\rm vir,crit}$), which is the result of the model described in § 2. Some of the contours are also labeled by the morphological type of galaxy in the *Tully Catalogue* [1] such that the observed fraction of galaxies of that morphological type or later equals the theoretical fraction of disk-dominated galaxies. We assume that galaxies of type Sc and later are the disk-dominated population. Fraction of Sc or later is 34% in the Tully subsample, which is also consistent with other observations (e.g., Kautsch et al. 2006; Barazza et al. 2008). So, the ($\mu_{\rm crit}, V_{\rm vir,crit}$)-values for which our bulge formation hypothesis predicts the observed disk-dominated-galaxy fraction 34% are shown by the bold contour in Figure 2, labelled "Sc 34%," e.g., $\mu_{\rm crit} = 0.3, V_{\rm vir,crit} = 55$ km s^{-1}. Somewhat smaller $\mu_{\rm crit}$ and larger $V_{\rm vir,crit}$, or vice versa, are also plausible. However, $V_{\rm vir,crit}$ cannot be larger than 65 km s^{-1} because it will overproduce disk-dominated galaxies.

In order to explain the observed fraction of disk-dominated galaxies within ΛCDM cosmology, we propose a bulge-forming criterion such that only those mergers with $M_2/M_1 > \mu_{\rm crit} \sim 0.3$ and $V_{\rm vir,1} > V_{\rm vir,crit} \sim 55$ km s^{-1} form bulges. The validity of this bulge formation criterion needs to be confirmed by further study of low-mass mergers ($V_{\rm vir,1} \sim 30 - 60$ km s^{-1}) by, e.g., hydro

[1] http://haydenplanetarium.org/universe/duguide/exgg_tully.php

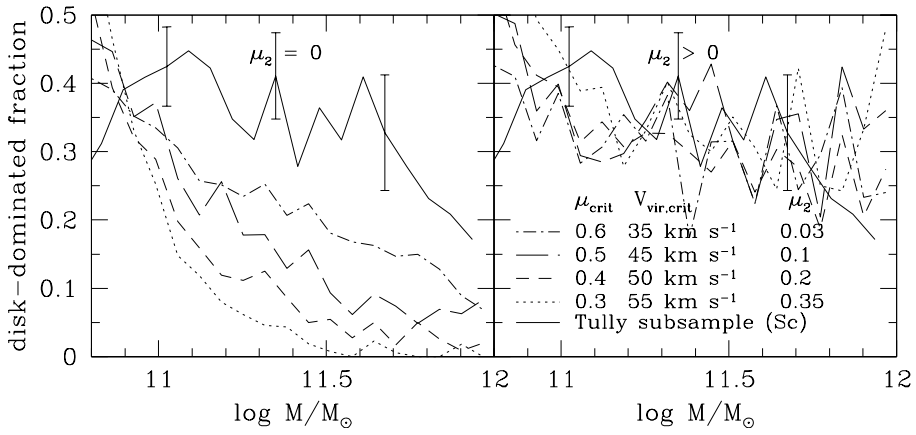

Figure 3. Disk-dominated fraction as a function of galaxy-hosting halo mass for the two-parameter model ($\mu_{\rm crit}, V_{\rm crit}$) (*left panel*) and the three-parameter model with additional parameter μ_2 (*right panel*), in which we assume that a merger remnant would not be observed as a classical bulge if its mass were smaller than μ_2 times present halo mass. Solid line is the observed fraction of Sc and later in the Tully subsample. Our model with only two parameters (*left*) does not agree with the observed mass dependence, but the agreement becomes reasonably good by introducing the third parameter μ_2 (*right*).

simulations. The mass dependence of the disk-dominated fraction (Figure 3) can be explained, too, if merger remnants which are small compared to the present halo mass are too small to be observed as a classical bulge. Future surveys of bulgeless/pseudobulged galaxy fraction as a function of mass would be useful for determining the bulge-formation criterion and testing this hypothesis.

Acknowledgments. We would like to thank Shardha Jogee for detailed comments, and John Kormendy for inspiring and illuminating discussions. This work was supported in part by NSF grant AST-0708795 to M. M., and NASA ATP grants NNG04G177G, NNX07AH09G, SAO TM8-9009X, and NSF grant AST-0708176 to P. R. S.

References

Barazza, F. D., Jogee, S., & Marinova, I. 2008, ApJ, 675, 1194
Bournaud, F., Jog, C. J., & Combes, F. 2005, A&A, 437, 69
Cox, T. J., Jonsson, P., Somerville, R. S., Primack, J. R., & Dekel, A. 2008, MNRAS, 384, 386
Kautsch, S. J., Grebel, E. K., Barazza, F. D., & Gallagher, J. S., III 2006, A&A, 445, 765
Koda, J., Milosavljević, M., & Shapiro, P. R. 2009, ApJ, 696, 254
Kormendy, J., & Kennicutt, R. C., Jr. 2004, ARA&A, 42, 603
Monaco, P., Theuns, T., & Taffoni, G. 2002, MNRAS, 331, 587
Okamoto, T., Gao, L., & Theuns, T. 2008, MNRAS, 390, 920
Shapiro, P. R., Giroux, M. L., & Babul, A. 1994, ApJ, 427, 25

GALAXY EVOLUTION: EMERGING INSIGHTS AND FUTURE CHALLLENGES
ASP Conference Series, Vol.
@jourvol, © 2009
S. Jogee, I. Marinova, L. Hao, and G. A Blanc

Galaxy Mergers in the A901/902 Supercluster with STAGES

Amanda Heiderman,[1] Shardha Jogee,[1] Irina Marinova,[1] Eelco van Kampen,[9,17] Marco Barden,[9] Chien Y. Peng,[5,6] Catherine Heymans,[12] Meghan E. Gray,[2] Eric F. Bell,[4] David Bacon,[7] Michael Balogh,[8] Fabio D. Barazza,[3] Asmus Böhm,[10] John A.R. Caldwell,[16] Boris Häußler,[2] Knud Jahnke,[4] Kyle Lane,[2] Daniel H. McIntosh,[13] Klaus Meisenheimer,[4] Sebastian F. Sánchez,[11] Rachel Somerville,[4] Andy Taylor,[12] Lutz Wisotzki,[10] Christian Wolf,[14] and Xianzhong Zheng,[15]

Abstract. We investigate galaxy mergers in the A901/902 supercluster at $z \sim 0.165$, based on *HST* ACS F606W, COMBO-17, *Spitzer* 24μm, XMM-

[1]Department of Astronomy, University of Texas at Austin, 1 University Station C1400, Austin, TX 78712-0259, USA

[2]School of Physics and Astronomy, The University of Nottingham, University Park, Nottingham NG7 2RD, UK

[3]Laboratoire d'Astrophysique, École Polytechnique Fédéralede Lausanne (EPFL), Observatoire, CH-1290 Sauverny, Switzerland

[4]Max-Planck-Institut für Astronomie, Königstuhl 17, D-69117, Heidelberg, Germany

[5]NRC Herzberg Institute of Astrophysics, 5071 West Saanich Road, Victoria, V9E 2E7, Canada

[6]Space Telescope Science Institute, 3700 San Martin Drive, Baltimore, MD 21218, USA

[7]Institute of Cosmology and Gravitation, University of Portsmouth, Hampshire Terrace, Portsmouth, PO1 2EG, UK

[8]Department of Physics and Astronomy, University Of Waterloo, Waterloo, Ontario, N2L 3G1, Canada

[9]Institute for Astro- and Particle Physics, University of Innsbruck, Technikerstr. 25/8, A-6020 Innsbruck, Austria

[10]Astrophysikalisches Insitut Potsdam, An der Sternwarte 16, D-14482 Potsdam, Germany

[11]Centro Hispano Aleman de Calar Alto, C/Jesus Durban Remon 2-2, E-04004 Almeria, Spain

[12]The Scottish Universities Physics Alliance (SUPA), Institute for Astronomy, University of Edinburgh, Blackford Hill, Edinburgh, EH9 3HJ, UK

[13]Department of Physics, 5110 Rockhill Road, University of Missouri-Kansas City, Kansas City, MO 64110, USA

[14]Department of Physics, Denys Wilkinson Building, University of Oxford, Keble Road, Oxford, OX1 3RH, UK

[15]Purple Mountain Observatory, National Astronomical Observatories, Chinese Academy of Sciences, Nanjing 210008, PR China

[16]University of Texas, McDonald Observatory, Fort Davis, TX 79734, USA

[17]ESO, Karl-Schwarschild-Str. 2, D-85748, Garching bei München, Germany

Newton X-ray, and gravitational lensing maps, as part of the STAGES survey. We utilize two methods to identify interacting galaxies in A901/902: visual classification and quantitative CAS parameters. In this article, we summarize our results for the frequency, distribution, color, and star formation rates of mergers, compared to non-interacting galaxies in A901/902. We also compare our results to other studies of clusters and groups, as well as theoretical predictions.

1. Introduction and Sample Selection

Understanding the effects of environment on galaxy evolution at various epochs remains a challenge. Cluster galaxies may differ from field galaxies due to high initial densities leading to early collapse. Furthermore, the relative importance of galaxy interactions (e.g., galaxy harassment, tidal interactions, minor mergers, and major mergers) and galaxy-ICM interactions (e.g, ram pressure stripping and compression) are likely to differ between cluster and field environments.

In order to constrain how galaxies evolve in cluster environments, we present a study based on the STAGES survey of the Abell 901/902 supercluster (Gray et al. 2009). The survey covers a $0.5^\circ \times 0.5^\circ$ field, and includes high resolution ($0.1''$, corresponding to $\sim$280 pc at $z \sim 0.165$[1]) *HST* ACS F606W images, along with COMBO-17, *Spitzer* 24μm, XMM-Newton X-ray data, and gravitational lensing maps (Heymans et al. 2008). The STAGES survey is complemented with accurate spectrophotometric redshifts down to $R_{\rm Vega}$ $\sim$24 from the COMBO-17 survey (Wolf et al. 2004), and stellar masses (Borch et al. 2006). Star formation rates (SFR) are derived from the COMBO-17 UV and *Spitzer* 24μm data (Bell et al. 2007).

Our supercluster sample consists of 893 bright ($R_{\rm Vega} \leq 24$), intermediate mass ($M_* > 10^9$ $M_\odot$) galaxies. We restrict our sample to bright, intermediate mass galaxies in order to be complete in stellar mass, to limit the field contamination lever to $\leq$20%, and to ensure that the analysis focuses on bright galaxies whose features are generally well resolved by the ACS PSF of $0.1''$.

2. Method of Indentifing Mergers in A901/902

We identified mergers by visually classifying galaxies using the F606W images, using a physically-driven classification scheme similar to that used in Jogee et al. (2009). Our classification scheme consists of 5 main visual classes: Mergers of types 1, 2a, and 2b, and Non-Interacting systems of type Symmetric and Irr-1, defined as follows:

(1) 'Type 1 Mergers': systems that host *externally triggered* distortions, similar to those produced in simulations of major mergers with mass ratio ($M_1/M_2 > 1/4$), and minor mergers with ($1/10 < M_1/M_2 \leq 1/4$). Such distortions include arcs, shells, ripples, tidal tails, large tidal debris, extremely asymmetric light distributions, double nuclei inside a common body, tidal bridges of light, and galaxies enclosed within a distorted envelope.

(2) 'Type 2a Mergers' and 'Type 2b Mergers': Type 2 systems have

[1]We assume in this paper a flat cosmology with $\Omega_M = 1 - \Omega_\Lambda = 0.3$ and H_0 =70 km s^{-1} Mpc^{-1}.

separation ($d < 10$ kpc) in the ACS images, and properties that suggest they are in the late phase of a merger or mass ratio $M_1/M_2 > 1/10$. Type 2a mergers are unresolved by the ground based COMBO-17 survey ($1.5''$ at $z = 0.165$) and thus have only one redshift and stellar mass, while type 2b mergers are resolved into two separate systems. The Type 2b mergers must have one pair member with $M_* \geq 10^9 M_\odot$, and a companion that satisfies two conditions: (a) a mass ratio in the range $1/10 < M_1/M_2 \leq 1/1$ and (b) a redshift such that the difference between redshifts ($z_1 - z_2$) is less or equal to the 1-sigma redshift error for our sample. By restricting our mergers to those that show morphological distortions, and using the above condition for type 2b mergers, we reduce the number of false projection pairs in our sample.

(3) Non-interacting Irr-1' galaxies: these exhibit *internally triggered* asymmetries, typically on scales of a few hundred parsecs, generally due to stochastic star formation and/or low rotational to random motions.

(4)) Non-interacting Symmetric' galaxies: these are relatively undistorted and are not associated with an overlapping companion.

For our final sample, we identify 20 mergers with morphological distortions and 866 non-interacting galaxies (123 Irr-1 and 743 Symmetric).

3. Summary of Results

Below, we summarize our results from Heiderman et al. (2009):

- Using visual classification, the fraction of mergers is 20/886 or 0.023±0.007 among bright, intermediate mass galaxies in A901/902. The estimated fraction of likely major mergers ($1/4 < \mathrm{M_1/M_2} \leq 1$) is 0.01±0.004%, likely minor mergers ($1/10 < \mathrm{M_1/M_2} \leq 1/4$) 0.006±0.003%, and 0.007±0.003 are classified as ambiguous major or minor mergers.

- We use the CAS code (Conselice et al. 2000) to derive the concentration (C), asymmetry (A), and clumpiness (S) parameters from the F606W images. If the CAS criterion (A>S and A>0.35), is used instead of visual classification, the fraction of strongly distorted galaxies is 18/886 or 0.02±0.006. We find that 7/18 (39±14%) of the CAS mergers are non-interacting systems which tend to be dusty and highly inclined. The remaining 11/18 (61±17%) of CAS mergers are visually classified as mergers.

- We compare our visually-based merger fraction in A901/902 to those found in other clusters and groups out to $z \sim 0.08$ (Fig. 1b). The low merger fractions among intermediate mass (10^9 to a few $\times 10^{10} M_\odot$) or intermediate luminosities ($L < L^*$) galaxies in the A901/902 clusters and other low redshift clusters are consistent with predictions from hierarchical models. However, we cannot yet test the predicted rate of evolution of the merger fraction with redshfit. Data on the merger fraction among $L \leq L^*$ cluster galaxies, based on our study and three other published studies, allow for a wide spectrum of scenarios, ranging from no evolution to evolution by a factor of $\sim$5 over $z \sim 0.17$ to 0.4.

- We define different regions in A901/902 clusters by computing the projected galaxy number density (n) for our sample as a function of clustocentric radius (R), assuming a spherical distribution. We consider the cluster core to be at $R \leq 0.25$ Mpc, where n rises steeply, the 'outer region' is between the core and average virial radius (0.25 Mpc $< R \leq 1.2$), and the 'outskirt region' is 1.2 Mpc $< R \leq 2.0$ Mpc. Mergers are found to lie outside the cluster core (Fig. 1a), although the timescale for collisions and close encounters is shortest in the core (< 1 Gyr). We suggest that this is due to the large velocity dispersion (700 to 900 km s^{-1}) of galaxies in the core. Such a dispersion makes it less likely that a close encounter between two galaxies culminates into a merger or a disruptive interaction associated with a large amount of tidal heating.

  We suggest two possible reasons why mergers might populate the region between the core and cluster outskirt: (1) In many clusters, the velocity dispersion of galaxies falls between the core and outer region, due to the *intrinsic* velocity dispersion profile (VDP) of such clusters. In the case of the A901/902 clusters, due to the low number statistics and the influence of members of neighboring clusters on the VDPs, we cannot tell whether the velocity dispersion falls in the outer regions, or remains flat. (2) Another possibility is that interacting galaxies are part of groups or are field galaxies that may currently be accreting along filaments into the A901/902 clusters. To quantify whether this might be the case, we compare the data to model predictions from simulations of the STAGES A901/A902 supercluster (van Kampen et al. 2009, in prep). The larger merger density and fraction that we observe between the cluster core and the virial radius is close to those predicted in typical *group overdensities*. This supports the scenario that mergers may be part of a group or the field population accreting into the A901/902 clusters.

- Out of the 20 morphologically distorted merger remnants and merging pairs in the sample, 16/20 (80±18%) lie on the blue cloud and 4/20 (20±10%) are in the red sample. The fraction of mergers that lie on the blue s is twice as high as the fraction of non-interacting galaxies (294/866 or 34±7%) on the blue cloud. This suggests that mergers are preferentially blue compared to non-interacting galaxies. This effect may be due to the enhanced recent star formation in mergers (see below) and/or due to the possibility that the mergers are part of group and field galaxies accreting onto the cluster.

- The average UV-based and combined UV and *Spitzer* 24μm (UV + IR) star formation rates of mergers are typically enhanced by only a modest factor of $\sim$2 and $\sim$1.5, respectively, compared to the non-interacting galaxies (i.e., Symmetric + Irr-1). A similar result is reported in the field at $z = 0.2 - 0.8$ by Jogee et al. (2009) and in mixed environments by Robaina et al. (2009, submitted). This modest enhancement is consistent with the theoretical predictions of di Matteo et al. (2007), based on a recent statistical study of several hundred simulated galaxy collisions. Our results of a modest enhancement and a low merger fraction culminate in

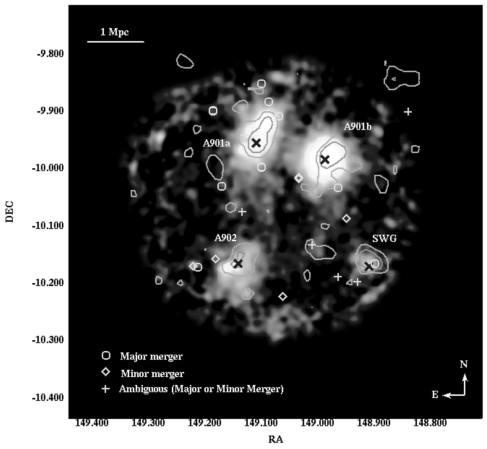

(a) The distribution of interacting galaxies in A901/902 overlaid on the ICM density map. Contours show peaks in dark matter distribution. Figure adapted from Heiderman et al. (2009).

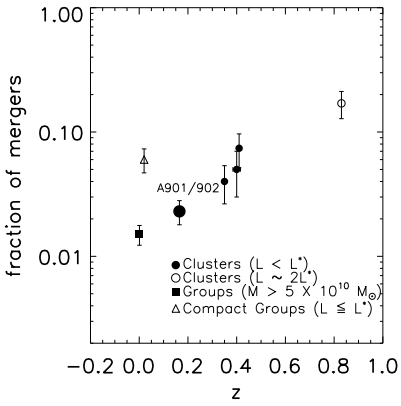

(b) Comparisons of our observed merger fraction to other studies of clusters and groups. The large filled circle is the A901/901 clusters from this study. Figure adapted from Heiderman et al. (2009).

Figure 1.

our finding that mergers contribute only ∼10% of the total SFR density of the A901/902 clusters.

Acknowledgments. AH and SJ acknowledge support from NSF grant AST-0607748, LTSA grant NAG5-13063, HST-GO-11082, and HST-GO-10861 from STScI, which is operated by AURA, Inc., for NASA, under NAS5-26555.

References

Bell, E., et al. 2007, ApJ, 663, 834
Borch, A., et al. 2006, A&A, 453, 869
Conselice, C., Bershady, M. A., & Jangren, A. 2000, 529, 886
Gray, M. E. , et al. 2009, MNRAS, 393,1275
Heiderman, A. L., Jogee, S., Marinova, I., and STAGES collaboration, 2009, ApJ, submitted.
Heymans, C., et al. 2008, MNRAS, submitted.
Jogee, S., Miller, S., Penner, K., Skelton, R. E., Conselice, C. J., Somerville, R. S., and the GEMS collaboration, 2009, ApJ, 697, 1971
di Matteo, P., et al., 2007, A&A, 468, 61
Robaina, A., et al., 2009, ApJ, submitted.
Van Kampen, E., et al., 2009, in preparation.
Wolf, C., et al. 2004, A&A, 421, 913
Wolf, C., et al., 2009, MNRAS, 393, 1302

GALAXY EVOLUTION: EMERGING INSIGHTS AND FUTURE CHALLLENGES
ASP Conference Series, Vol.
@jourvol, © 2009
S. Jogee, I. Marinova, L. Hao, and G. A Blanc

Numerical Simulations of Hot Halo Gas in Galaxy Mergers

Manodeep Sinha and Kelly Holley-Bockelmann

Department of Physics and Astronomy, Vanderbilt University, 6301 Stevenson Center, Nashville, TN 37235

Abstract. Galaxy merger simulations have explored the behavior of gas within a galactic disk, yet the dynamics of hot gas within the galaxy halo has been neglected. We report on the results of high-resolution hydrodynamic simulations of colliding galaxies with hot halo gas. We find that: *(i)* A strong shock is produced in the galaxy halos before the first passage, increasing the temperature of the gas by almost an order of magnitude to $\sim 10^{6.3}$ K. *(ii)* The X-ray luminosity of the shock is strongly dependent on the gas fraction. It is $\gtrsim 10^{39}$ erg/s for gas fractions larger than 10%. *(iii)* The hot diffuse gas in the simulation also produces X-ray luminosities as large as 10^{42} erg/s, contributing to the total X-ray background in the Universe. *(iv)* Approximately 10–20% of the initial gas mass is unbound from the galaxies for equal-mass mergers, while 3–5% of the gas mass is released for the 3:1 and 10:1 mergers. This unbound gas ends up far from the galaxy and can be a feasible mechanism for metal enrichment of the WHIM. We use an analytical halo merger tree to estimate the fraction of gas mass lost over the history of the Universe.

1. Introduction

Galaxy formation models have long predicted the existence of an extended reservoir of hot halo gas around spiral galaxies (White & Rees 1978; White & Frenk 1991). In that scenario, gas falling into the dark matter potential shock-heats to virial temperature and subsequently cools over a characteristic time-scale. This gas cools via thermal Bremsstrahlung and atomic line emission processes, with the majority of the radiation occurring in the soft X-ray band with an expected luminosity $L_{\rm X} \propto v_{\rm circ}^5$. Thus, the effect of mass on the halo luminosity is extremely non-linear and attempts to observe the halos in the X-ray are biased towards very massive halos. Consequently, until very recently (Pedersen et al. 2006), there had not been any significant detection of extra-planar gas in quiescent spiral galaxies although there are numerous such examples in starburst galaxies (e.g., Strickland et al. 2002). Given the existence of hot halo gas, it is important to include such a component in the simulations of galaxy mergers. However, none of the galaxy merger simulations performed so far explicitly included the hot gas in the galactic halo.

One of the outstanding issues in large scale structure formation is the understanding of the evolution of the warm-hot inter-galactic medium (WHIM)—a major component in the baryon budget of the universe, containing more than 50% of the baryons at $z = 0$. The metallicity distribution in the WHIM is non-homogeneous with higher (over)density regions containing a larger fraction of the metals (e.g., Cen & Ostriker 1999; Davé & Oppenheimer 2007). Historically,

SN feedback and starburst-assisted superwinds have been invoked to address this issue but the effect of SN feedback alone is about an order of magnitude smaller than the required metal pollution of the WHIM (Ferrara, Pettini, & Shchekinov 2000) and requires some other mechanism to mix metals on length scales of the order of inter-galactic distances. Gnedin & Ostriker (1997) suggest galaxy mergers as a viable method for the ejection of metal enriched gas into the WHIM that can work in addition to regular SN feedback and superwinds. Thus, our set of simulations will also explore how galaxy mergers can supply the WHIM.

We have undertaken a set of 36 simulations using GADGET-2 (Springel, Yoshida, & White 2001; Springel 2005): 27 of these are elliptical encounters between galaxies with mass ratios 1:1, 3:1 and 10:1 with impact parameters of $\sim$ 2 kpc, 22 kpc and 110 kpc. The galaxies have gas fractions of 1%, 10% and 18%. In addition, we have simulated another 9 mergers with hyperbolic encounters between equal-mass galaxies. This total set gives us a crude sampling of the 4-parameter space of galaxy mergers contain mass ratios, impact parameters, gas fraction and orbital types. We refer the reader to Sinha & Holley-Bockelmann (2009a) for details on the simulations.

2. X-Rays from Shocked Halo Gas

From our simulations, we see that $L_{\rm X}$ and shock $L_{\rm X}$ increases with increasing mass of colliding halos and decreasing impact parameters. Larger initial velocities do result in larger $L_{\rm X}$; however, if the hot gas fraction drops too much, as it does in the case of some of the hyperbolic mergers, the X-ray emission can get reduced. We find that the hot halo gas shock-heats to temperatures $\sim 10^{6.3}$ K in equal-mass mergers and $\sim 10^{6}$ K in unequal-mass mergers. This is reflected in a strong temperature jump in the regions between the two colliding galaxies (see Figure 1), well before pericenter passage, and persists until the first pass. The strongest shocks, and correspondingly the largest X-ray luminosities due to shocked gas, are created after the pericenter passage. For gas fractions greater than 10%, this $L_{\rm X}$ from shocks remains above observable thresholds of $\sim 10^{39}$ erg/s for at least a period of $\sim$ 300 Myrs, and thus should be detectable in ongoing mergers with *Chandra* and *XMM-Newton*.

3. Unbound Gas in the Universe from Mergers

A fraction of the gas is unbound (up to $\sim$ 20%) and resides $\gtrsim$ 1 Mpc from the remnant. This unbinding occurs in multiple stages, with most of the gas freed during the first pass. This unbound gas can even come from the metal-rich central region of the progenitor galaxies. We find that the amount of unbound gas can be described as a linear function of the impulse and use an Extended Press-Schechter (EPS) merger tree to calculate the amount of gas freed by galaxy mergers over the history of the Universe.

To estimate the total fraction of gas released by mergers, we construct a series of analytic halo merger trees using a publicly available EPS code from (Parkinson, Cole, & Helly 2008). We assume that a galaxy merger with a mass ratio greater than $\eta_{\rm min}$ unbinds 10% of the original gas content of the halos. We refer the reader to Sinha & Holley-Bockelmann (2009b) for further

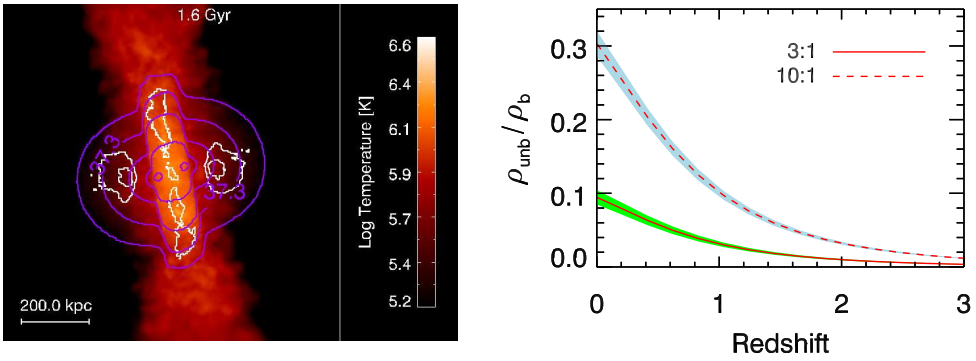

Figure 1. *Left:* Temperature projection for the 18% gas fraction for a hyperbolic equal-mass merger with an impact parameter of 2.3 kpc. This run has the highest X-ray emission and largest unbound material. The X-ray contours are in the darker shade and the unbound material is shown by white contours. Most of the unbound material comes from two distinct regions: the far lobes of the galaxy and the shocked front in between the galaxies *Right*: The evolution with redshift of the gas mass lost as a fraction of baryon density in the Universe ρ_b. The solid and the dashed line shows the evolution for 3:1 and 10:1 mergers respectively. The shaded region shows the 1-σ deviation at each redshift from 100 realizations.

details about the semi-analytic recipe. Figure 1 shows the redshift evolution of the unbound gas mass compared to the total baryon content of all the haloes for $\eta_{\rm min} = 0.1$ and 0.3. For $\eta_{\rm min} = 0.1$ and 0.3, about 30% and 10% of all the baryons in the Universe gets ejected respectively. Since observations show that $\sim 60\%$ of the baryons should be in the WHIM (Fukugita & Peebles 2004; Allen et al. 2002), we find that more than half of the "missing" baryons can be ejected from galaxies by mergers if each merger with $\eta \geq 0.1$ releases 10% of the baryons.

4. Discussion

In our simulations we find that the X-ray emission from shocks increases as the merger gets more violent. So the best bet to detect the shock signature of the hot halo gas during mergers would be to locate major mergers between Milky-Way-type galaxies that are happening in the local universe. Such systems would produce significant X-rays from the hot halo and the shock-heated interface if the galaxies are to be observed in the initial stages of the merger. Compared to the merger timescale, an observable X-ray shock is ~ 20 times shorter. During the merger, the hot gas itself also radiates and can have an X-ray luminosity of $\sim 10^{42}$ erg/s for galaxies with a gas fraction as low as 10%. Herein lies the difficulty of detecting the shocked gas: the shocked gas is ~ 1000 times less luminous than the non-shocked gas. To observe such X-ray shocks from mergers, one would have to look for a signal 3 orders of magnitude smaller than the global X-ray level; *and* the effect only lasts for a timescale that is an order of magnitude shorter than the merger.

We show that it is possible for a significant portion of the WHIM to be produced by gas ejected from galaxies during mergers. Our semi-analytic

prescription shows that up to 50% of the hot halo gas in haloes of mass 10^8–$10^{13}\,M_\odot$ can be ejected by mergers. While we do not include the more numerous smaller halos in the semi-analytic calculation, numerical simulations have shown that such galaxies are quite susceptible to feedback effects from galaxy winds and SNe (Mac Low & Ferrara 1999; Cen & Ostriker 2006; Kobayashi, Springel, & White 2007) with up to 80% of the baryons ejected from galaxies of mass $\lesssim 10^{11}\,M_\odot$ (Kobayashi et al. 2007) by SNe feedback alone. Our results imply that this merger mechanism, which acts preferentially in massive galaxies, may work in tandem with other processes to remove gas from galaxies and enrich the WHIM.

Acknowledgments. MS would like to thank the organizers for a wonderful conference. We thank the GALFORM team for making the EPS code publicly available. This work was conducted in part using the resources of the Advanced Computing Center for Research and Education at Vanderbilt University, Nashville, TN.

References

Allen, S. W., Schmidt, R. W., & Fabian, A. C. 2002, MNRAS, 334, L11
Cen, R. & Ostriker, J. P. 1999, ApJ, 519, L109
Cen, R., & Ostriker, J. P. 2006, ApJ, 650, 560
Davé, R. & Oppenheimer, B. D. 2007, MNRAS, 374, 427
Fukugita, M., & Peebles, P. J. E. 2004, ApJ, 616, 643
Ferrara, A., Pettini, M., & Shchekinov, Y. 2000, MNRAS, 319, 539
Gnedin, N. Y. & Ostriker, J. P. 1997, ApJ, 486, 581
Kobayashi, C., Springel, V., & White, S. D. M. 2007, MNRAS, 376, 1465
Mac Low, M.-M. & Ferrara, A. 1999, ApJ, 513, 142
Parkinson, H., Cole, S., & Helly, J. 2008, MNRAS, 383, 557
Pedersen, K., Rasmussen, J., Sommer-Larsen, J., Toft, S., Benson, A. J., & Bower, R. G. 2006, New Astronomy, 11, 465
Sinha, M. & Holley-Bockelmann, K. 2009, MNRAS, 768
Sinha, M. & Holley-Bockelmann, K. 2009, MNRAS, submitted
Springel, V. 2005, MNRAS, 364, 1105
Springel, V., Yoshida, N., & White, S. D. M. 2001, New Astronomy, 6, 79
Strickland, D. K., Heckman, T. M., Weaver, K. A., Hoopes, C. G., & Dahlem, M. 2002, ApJ, 568, 689
White, S. D. M. & Frenk, C. S. 1991, ApJ, 379, 52
White, S. D. M. & Rees, M. J. 1978, MNRAS, 183, 341

GALAXY EVOLUTION: EMERGING INSIGHTS AND FUTURE CHALLLENGES
ASP Conference Series, Vol.
@jourvol, © 2009
S. Jogee, I. Marinova, L. Hao, and G. A Blanc

The Effect of Dry Mergers on the Color–Magnitude Relation

Rosalind E. Skelton,[1] Eric F. Bell,[1] and Rachel S. Somerville[1,2]

[1]*Max-Planck-Institut für Astronomie, Königstuhl 17, D-69117 Heidelberg, Germany*
[2]*Space Telescope Science Institute, 3700 San Martin Drive, Baltimore, MD 21218*

Abstract. We investigate the effect of gas-poor (so-called "dry") mergers on the color–magnitude relation (CMR) of early-type galaxies through a simple toy model and compare with low-z observations from the Sloan Digital Sky Survey (SDSS). The observed red sequence shows a tilt towards bluer colors and a decrease in scatter at the bright end. These characteristics are predicted by our model, based on merger trees from a semi-analytic model of galaxy formation. We assume galaxies move onto a "creation red sequence" when they undergo major gas-rich mergers. Subsequent dry mergers move galaxies along the relation by increasing their mass, but also make them slightly bluer. This occurs because bright galaxies are most likely to merge with one of the more numerous fainter and consequently bluer galaxies that lie further down the relation. Bright galaxies undergo a higher fraction of dry mergers than faint galaxies, which causes a change in the slope of the CMR. A more realistic model that includes scatter in the initial relation shows that dry merging causes a tightening of the CMR towards the bright end. The small scatter in the observed CMR thus cannot be used to argue against significant mass growth from dry merging.

1. Introduction

Galaxies can be separated into two main classes, occupying different regions in color–magnitude space (Strateva et al. 2001; Blanton et al. 2003). The gas-rich, star-forming galaxies form a broad distribution known as the blue cloud. The early-type or spheroidal galaxies are gas-poor and have low levels of star formation. These galaxies lie along a tight color–magnitude (or mass) relation known as the red sequence, which is driven to first order by a metallicity–mass relation (Faber 1973; Kodama & Arimoto 1997; Gallazzi et al. 2006). The amount of mass in red galaxies has approximately doubled since $z \sim 1$ (e.g., Bell et al. 2004; Faber et al. 2007) whereas the mass in the blue cloud remains roughly constant. Galaxy merging is thought to play an important role in moving galaxies from the blue cloud onto the red sequence, through morphological transformation (e.g., Toomre 1977; Barnes & Hernquist 1996) and the quenching of star formation. The most massive ellipticals are more likely to build up from mergers between galaxies which already lie on the CMR, however. Such mergers are observed in the local Universe (e.g., van Dokkum 2005; Bell et al. 2006; McIntosh et al. 2008) but the resulting mass growth is difficult to constrain. The rate at which they occur is uncertain, to a large extent

due to the uncertainty in merging time-scale, and indirect means of measuring it, through the evolution of the mass–size relation (van der Wel et al. 2008) or number density (e.g., Faber et al. 2007; Cool et al. 2008, and references therein) for example, are thus far inconclusive.

The CMR provides a further avenue to explore, with both the slope and scatter giving insight into the formation history of elliptical galaxies. The relation is generally assumed to be linear, though there is some evidence for a change in slope with magnitude (e.g., Baldry et al. 2004; Ferrarese et al. 2006). Previous work on the scatter in the CMR suggested that ellipticals formed at high redshifts, evolving passively thereafter (Bower, Kodama, & Terlevich 1998, BKT98 hereafter) though recent models allow for the continuous build-up of the red sequence through the quenching of blue cloud galaxies (Harker et al. 2006; Ruhland et al. 2009). BKT98 argued that the amount of mass growth due to dry merging was limited to a factor of 2–3 because such mergers would cause a flattening of the relation and an increase in scatter, contradicting the small scatter measured in clusters such as Coma. In this contribution we show that the CMR for local field galaxies from the SDSS has a change in slope (§ 2). We attribute this effect to dry mergers, using a simple toy model to investigate how they influence the red sequence (§ 3). Further details can be found in Skelton, Bell, & Somerville (2009).

2. Observations

We select a subsample of galaxies from the SDSS Data Release 6 (DR6, Adelman-McCarthy et al. 2008) using the New York University Value-Added Galaxy Catalog (NYU-VAGC; Blanton et al. 2005). We choose galaxies in a thin redshift slice ($0.0375 < z < 0.0625$) with Galactic extinction corrected (Schlegel, Finkbeiner, & Davis 1998) Petrosian magnitudes $m_{\rm r} < 17.77$ (72646 objects). This range in redshift provides a significant number of bright galaxies but is narrow enough to avoid the need for volume and evolution corrections. We use the Sérsic magnitudes provided in the NYU-VAGC as an estimate of total magnitude and the SDSS model magnitudes, determined with an equivalent aperture in all bands, as the most reliable estimator of color. We k-correct to rest-frame $z = 0.1$ bandpasses using `kcorrect_v4_1` (Blanton & Roweis 2007). To isolate the red sequence we apply a cut in concentration of $C \geq 2.6$, where $C = R_{90}/R_{50}$ with R_{90} and R_{50} the radii enclosing 90% and 50% of the Petrosian flux, respectively. The remaining sample contains 29017 galaxies and is complete for $M_{\rm r} \lesssim -18.3$ mag.

The CMD for these galaxies (upper left panel of Fig. 1) shows a change in slope with magnitude, flattening at the bright end. We fit a Gaussian function to the distribution of colors in each magnitude bin of 0.25 mag and fit straight lines to the means above and below $M_{\rm r} = -21$ mag. The faint-end fit given by ${}^{0.1}(g-r) = 0.10 - 0.04\,{}^{0.1}M_{\rm r}$ and average scatter (0.046 mag) are used as the input creation red sequence for the model, as described below.

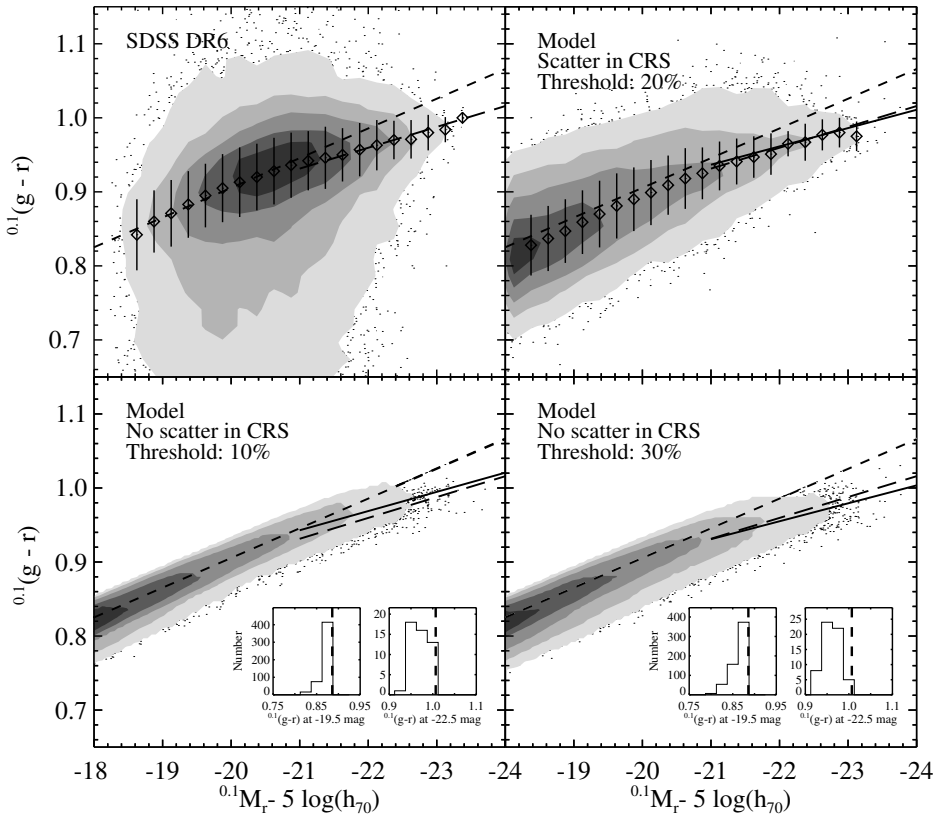

Figure 1. The upper left panel shows the CMD of galaxies with concentrations of $C \geq 2.6$ from the SDSS DR6. The upper right panel shows the red sequence for a model which includes scatter in the CRS, with a gas fraction threshold of 20%. The mean and scatter of Gaussian fits are shown as diamonds and bars. The lower panels show models with gas fraction thresholds of 10 and 30% with no scatter in the initial relation. In all panels the contours enclose 2, 10, 25, 50 and 75% of the maximum value. The short dashed lines show the fit to the observed means for magnitudes fainter than $M_{\rm r} = -21$ mag, extended over the whole magnitude range to illustrate the change in slope at the bright end. Long dashed and solid lines show the fit to the bright end ($M_{\rm r} < -21$ mag) of the observed and model relations respectively. The inset histograms show the distribution of colors in two magnitude bins 0.1 mag wide, centered on $^{0.1}M_{\rm r} = -19.5$ and $^{0.1}M_{\rm r} = -22.5$ mag.

3. A Toy Model for Dry Merging

We use a simple toy model to isolate the effect of dry merging on the colors of galaxies on the red sequence, taking a similar approach to BKT98. We differ in that we use galaxy merger histories from an up-to-date model of galaxy formation for all haloes with $\log_{10}[M_{\rm halo}/M_{\odot}] > 11.7$, rather than just cluster-sized haloes. Furthermore, we suppose that major wet mergers quench star formation and move galaxies onto a "creation red sequence" (CRS), whereas the

BKT98 model assumes the red sequence is in place at some formation epoch. Galaxy merger trees and the masses and gas fractions of galaxies are extracted from the semi-analytic galaxy formation model (SAM) of Somerville et al. (2008) embedded in the ΛCDM hierarchical framework.

We consider major mergers with mass ratios[1] between 1:1 and 1:4 to be sufficient at quenching star formation if either of the progenitor galaxies has a cold gas fraction[2] above some threshold. In order to compare directly with observations we have used the measured faint-end slope and zeropoint of the observed red sequence to specify the remnant's color ($^{0.1}(g-r) = 0.10 - 0.04^{0.1}M_{\rm r}$, short dashed lines in Fig. 1). The magnitude of the remnant galaxy is found from the total stellar mass of the two progenitors using the M/L ratio of low-z red sequence galaxies produced by the SAM ($^{0.1}M_{\rm r} = 2.87 - 2.22\log_{10}[M_*/M_\odot]$). Subsequent dry merging produces remnant galaxies with colors and magnitudes determined by the simple combination of the progenitor colors and magnitudes. A more realistic model includes scatter in the CRS, with the width of the relation given by the average observed scatter for faint galaxies (0.046 mag).

In Fig. 1 we compare the observed red sequence (upper left panel) with the CMR produced by the model, using gas fraction thresholds ranging from 10 to 30%. A linear regression to the bright end ($M_{\rm r} < -21$ mag) of the model distribution is shown as a solid line in each case. There is a clear tilt towards a shallower slope for bright galaxies, with the slope and break point sensitive to the chosen gas fraction threshold. The observed bright-end slope is bracketed by models with thresholds of 10% and 30% (lower panels). The inset histograms show that the distribution peaks on the CRS (dashed line) in the faint bins because most of these galaxies have not had dry mergers. In contrast, most bright galaxies have undergone dry mergers and are predicted to lie significantly bluewards of the CRS at the present day. A lower gas fraction threshold results in more wet merger remnants lying directly on the CRS, thus the slope at the bright end changes less dramatically and the break occurs at brighter magnitudes. The upper right panel shows the resulting red sequence for the model with scatter in the CRS and a gas fraction threshold of 20%. We fit a Gaussian to the color distribution in each magnitude bin of 0.25 mag, as for the observations. The slope at the bright end decreases in the same way as for the models without scatter, while the relation becomes tighter towards the bright end. The small fraction of dry mergers taking place at all magnitudes result in a small zeropoint offset.

4. Conclusions

The existence of a tight CMR over a wide range in magnitude has been used to argue against the importance of dry mergers because they were expected to increase the scatter and flatten the relation (BKT98). We show that the CMR

[1]The mass used is the total baryonic mass plus the dark matter mass within twice the characteristic NFW scale radius (see Somerville et al. 2008 for details).

[2]Cold gas fraction is defined as the ratio of cold gas to total baryonic mass.

for local field galaxies from the SDSS has a change in slope at the bright end and that a toy model for dry merging in an hierarchical Universe produces a red sequence that is consistent with these observations. In models without scatter dry mergers shift galaxies at the bright end towards bluer colors and increase the width of the relation. There is little change at the faint end because most mergers occurring there are wet. This results in a change in slope rather than a flattening of the whole relation, predicted by BKT98. They assumed that the red sequence formed at a given time and that subsequent merging at all stellar masses was dry, moving the entire population bluewards, whereas we associate the build-up of the red sequence with merging events. The change in slope and magnitude at which the break occurs depend strongly on the assumption of a gas fraction threshold below which mergers are assumed to be dry. Thresholds of 10% and 30% bracket the observed relation. Including scatter in the CRS, we find a reduction in scatter at the bright end as a consequence of the central limit theorem. The scatter in the observed relation is slightly smaller than in the model, however we have not accounted for differences in age or metallicity. We have assumed the CRS has the same scatter as the faint end of the observed red sequence, which has a contribution from the aging of the stellar populations (Gallazzi et al. 2006), thus the scatter could be even smaller than predicted if dry mergers occur soon after the arrival of galaxies on the red sequence.

Acknowledgments. RES would like to thank the conference organisers for a very interesting and well-run workshop. This work makes use of the Sloan Digital Sky Survey (http://www.sdss.org/).

References

Adelman-McCarthy, J. K., et al. 2008, ApJS, 175, 297
Baldry, I. K., Glazebrook, K., Brinkmann, J., Ivezić, Ž., Lupton, R. H., Nichol, R. C., & Szalay, A. S. 2004, ApJ, 600, 681
Barnes, J. E. & Hernquist, L. 1996, ApJ, 471, 115
Bell, E. F. et al. 2004, ApJ, 608, 752
Bell, E. F., et al. 2006, ApJ, 640, 241
Blanton, M. R., et al. 2003, ApJ, 594, 186
Blanton, M. R., et al. 2005, AJ, 129, 2562
Blanton, M. R. & Roweis, S. 2007, AJ, 133, 734
Bower, R. G., Kodama, T., & Terlevich, A. 1998, MNRAS, 299, 1193
Cool, R. J., et al. 2008, ApJ, 682, 919
Faber, S. M. 1973, ApJ, 179, 731
Faber, S. M., et al. 2007, ApJ, 665, 265
Ferrarese, L., et al. 2006, ApJS, 164, 334
Gallazzi, A., Charlot, S., Brinchmann, J., & White, S. D. M. 2006, MNRAS, 370, 1106
Harker, J. J., Schiavon, R. P., Weiner, B. J., & Faber, S. M. 2006, ApJ, 647, L103
Kodama, T. & Arimoto, N. 1997, A&A, 320, 41
McIntosh, D. H., Guo, Y., Hertzberg, J., Katz, N., Mo, H. J., van den Bosch, F. C., & Yang, X. 2008, MNRAS, 388, 1537
Ruhland, C., Bell, E. F., Häußler, B., Taylor, E. N., Barden, M., & McIntosh, D. H. 2009, ApJ, 695, 1058
Schlegel, D. J., Finkbeiner, D. P., & Davis, M. 1998, ApJ, 500, 525
Skelton, R. E., Bell, E. F., & Somerville, R. S. 2009, ApJ, 699, L9
Somerville, R. S., Hopkins, P. F., Cox, T. J., Robertson, B. E., & Hernquist, L. 2008, MNRAS, 391, 481

Strateva, I., et al. 2001, AJ, 122, 1861
Toomre A. 1977 in Evolution of Galaxies and Stellar Populations, ed. B. M. Tinsley, R. B. Larson, (New Haven: Yale University Observatory), 401
van der Wel, A., Holden, B. P., Zirm, A. W., Franx, M., Rettura, A., Illingworth, G. D., & Ford, H. C. 2008, ApJ, 688, 48
van Dokkum, P. G. 2005, AJ, 130, 2647

GALAXY EVOLUTION: EMERGING INSIGHTS AND FUTURE CHALLLENGES
ASP Conference Series, Vol.
@jourvol, © 2009
S. Jogee, I. Marinova, L. Hao, and G. A Blanc

A Dynamical Miss: A Study of the Discrepancy Between Optical and Infrared Kinematics in Mergers

Barry Rothberg

Naval Research Laboratory, Code 7211, 4555 Overlook Ave SW, Washington D.C. 20375

Abstract. Recently, controversy has erupted over whether gas-rich spiral-spiral mergers are capable of forming m^* ellipticals. Measurements of $\sigma_\circ$ from the 2.29μm CO band-head for local LIRG/ULIRGs, suggest they are not. IR-bright mergers are often cited as the best candidates for forming massive ellipticals, so the recent observations have raised doubts about both the Toomre Merger Hypothesis and the fundamental assumptions of Λ-CDM galaxy formation models. However, kinematics obtained with the Calcium II Triplet at 8500 Å suggest mergers are forming $m \geq m^*$ ellipticals. In this work, we show that kinematics derived from the CO stellar absorption band-head leads to a significant underestimation of the masses of LIRGs/ULIRGs. This is primarily due to the presence of a young population affecting CO band-head measurements.

1. Introduction

In the local universe, Luminous and Ultra-luminous Infrared Galaxies (LIRGs & ULIRGs) have long been proposed as ideal candidates for forming massive elliptical galaxies (Kormendy & Sanders 1992). They contain vast quantities of molecular gas and most show evidence of recent or ongoing merging activity, along with relatively high star-formation rates. Observations of these and other advanced mergers have long suggested that their luminosities are equivalent to or greater than massive elliptical galaxies (Schweizer 1982, 1996; Hibbard & van Gorkom 1996; Rothberg & Joseph 2004, hereafter Paper I).

The arguments *against* LIRGs/ULIRGs, and mergers in general forming L^* or m^* elliptical galaxies are based on kinematic arguements. Until recently, kinematic studies of LIRGs/ULIRGs have used the infrared CO stellar absorption lines at 1.6μm and 2.29μm to measure central velocity dispersions ($\sigma_\circ$). These stellar band-heads are prominent in late-type stars and lie within observable infrared atmospheric windows.

$\sigma_{\circ,\mathrm{CO}}$ have been previously measured for $\sim$ 60 LIRGs/ULIRGs and two non-LIRG/ULIRG merger remnants (Doyon et al. 1994; Shier, Rieke, & Rieke 1994; Shier & Fischer 1998; James et al. 1999; Genzel et al. 2001; Tacconi et al. 2002; Dasyra et al. 2006), yielding a median $\sigma_\circ \sim 150$ km s^{-1}, far less than an m^* elliptical galaxy.

Lake & Dressler (1986) used the Mg*Ib* ($\lambda \sim 5200$ Å) and Ca II triplet ($\lambda \sim 8500$ Å, hereafter CaT) to measure $\sigma_\circ$ in a sample of 13 visually selected mergers, producing a median of $\sigma_\circ = 200$ km s^{-1}. Rothberg & Joseph (2006), hereafter Paper II, measured $\sigma_\circ$ for 38 optically selected single-nuclei merger

remnants, including 10 LIRGs and 2 ULIRGs, using the CaT absorption lines and found a median $\sigma_\circ = 211$ km s^{-1} for the entire sample and a median of 196 km s^{-1} for the LIRGs/ULIRGs.

In Paper II, *K*-band photometry from Paper I was combined with $\sigma_{\circ,\mathrm{CaT}}$ to test whether and where merger remnants lie on the *K*-band Fundamental Plane (Pahre et al. 1998). Most of the merger remnants did lie on or within the scatter of the Fundamental Plane. A small number of predominantly LIRG/ULIRG remnants sat offset from the Fundamental Plane in a tail-like feature, (see Figure 1 in Paper II). The offset was due to high surface brightness ($<\mu_\mathrm{K}>_\mathrm{eff}$), not small $\sigma_\circ$, suggesting the presence of a younger IR-bright population.

Paper II also demonstrated that the CO band-head produced consistently *smaller* $\sigma_\circ$ for LIRGs/ULIRGs than CaT. This suggested previous infrared studies may have *underestimated* their masses. Unfortunately, to date, *all* published $\sigma_{\circ,\mathrm{CaT}}$ and $\sigma_{\circ,\mathrm{CO}}$ of remnants lie within the above-mentioned tail-like offset from the *K*-band Fundamental Plane, making it difficult to separate whether the discrepancy is related to galaxy properties or problems with one of the stellar lines. Silge & Gebhardt (2003) (hereafter SG03) first noted that in their sample of 25 (mostly S0) early-type galaxies, a signficant fraction also showed $\sigma_{\circ,\mathrm{CO}} < \sigma_{\circ,\mathrm{Optical}}$. The largest discrepancies were found in S0s. They proposed that dust enshrouded stellar disks, visible only in the IR produced smaller $\sigma_{\circ,\mathrm{CO}}$.

2. Sample Selection and Observations

An E0 and 6 non-LIRG/ULIRG merger remnants found to lie on the Fundamental Plane were observed in queue mode with the Gemini Near-Infrared Spectrograph (GNIRS) on Gemini-South (Program GS-2007A-Q-17, P.I. Rothberg) using the Short Camera with the 111 l/mm grating and $0''.3 \times 99''$ slit ($R \sim 6200$). Observations were centered on the ^{12}CO(2,0) 2.29μm band-head. Previously published optical and infrared spectroscopic data were also used (see Papers I and II for details), bringing the total to 8 non-LIRG and 6 LIRG merger remnants. All $\sigma_\circ$ were either extracted or corrected (for data from the literature) to a 1.53 h^{-1} kpc central aperture.

Low-resolution ($R \sim 1200$) spectra were obtained with SpeX on the NASA Infrared Telescope Facility for 11 merger remnants. Observations were made using the short cross-dispersed mode ($0.8\mu\mathrm{m} < \lambda < 2.4\mu\mathrm{m}$, $R \sim 1200$) with the $0''.5 \times 15''$ slit. These observations were used to measure Brackett γ (Brγ) equivalent widths (EW) and supplement measurement of CO indices for published $\sigma_{\circ,\mathrm{CO}}$.

A comparison sample of 23 pure elliptical galaxies was assembled from the literature to look for the same discrepancy between $\sigma_{\circ,\mathrm{Optical}}$ and $\sigma_{\circ,\mathrm{CO}}$ observed in merger remnants and SG03. All $\sigma_\circ$ obtained from the literature were corrected to a 1.53 h^{-1} kpc aperture.

3. Comparison between Optical and Infrared $\sigma_\circ$

Figure 1 shows a three-panel comparison among the LIRG merger remnants (*left*), non-LIRG merger remnants (*center*) and elliptical galaxies (*right*). The

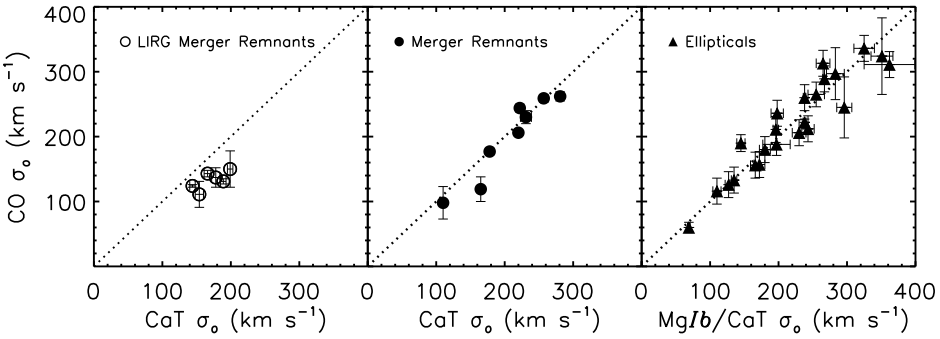

Figure 1. Comparison between $\sigma_{\circ,\mathrm{Optical}}$ and $\sigma_{\circ,\mathrm{CO}}$ for LIRG (*left*) and non-LIRG (*center*) merger remnants and elliptical galaxies (*right*). The overplotted dotted line represents $\sigma_{\circ,\mathrm{Optical}} = \sigma_{\circ,\mathrm{CO}}$.

data were fit with a double weighted least-squares fit to compare with a slope of unity to search for discrepancies in $\sigma_\circ$. Both the non-LIRG merger remnants and the elliptical galaxies have a slope within 1σ of unity, while the the LIRG merger remnants yield a slope of 0.24 ± 0.1.

4. $\sigma_\circ$ Variations Compared with Stellar Populations

In Paper II it was postulated that the CaT and CO stellar features were probing two different stellar populations; the former probing older, late-type giants contributed from the progenitor spirals, and the latter sensitive to young Red Supergiants (RSGs) or Asymptotic Giant Branch (AGB) stars formed during the merger. A direct way to test this is to measure EWs of the CaT and CO features and compare those with stellar populations models in order to age-date each population. The premise is that the younger stellar populations are created within a disk formed when gas from the progenitor spirals dissipates towards the barycenter of the merger (see Barnes 2002). At *K*-band, the light from this population dominates during certain epochs (Maraston 2005, hereafter M05).

Figure 2 shows stellar population models from M05 (*solid lines*) for a simple burst population with a Salpeter IMF and solar metallicity for the CaT* and CO indices. CaT* EWs and $\mathrm{CO}_{\mathrm{phot}}$ indices were measured for each merger remnant and used in conjunction with the models to age-date each remnant as plotted. In some cases, the measured indices intersected multiple points in the models. The degeneracy was broken by measuring the EW of the Paschen triplet (PaT) absorption lines (near 8500 Å) and comparing with predicted values from M05, or measuring the EWs of Brγ emission (2.165μm) and comparing with predicted values from Starburst99 (Leitherer et al. 1999). In some cases the degeneracy for CO ages could not be broken due to the absence of Brγ. Double values are plotted in Figure 2 with a dotted line connecting them.

Overplotted in Figure 2 (*right*) next to each merger remnant are the fractional $\sigma_\circ$ differences $(\sigma_{\circ,\mathrm{CaT}} - \sigma_{\circ,\mathrm{CO}})/\sigma_{\circ,\mathrm{CaT}}$. The LIRG merger remnants show larger fractional differences than the non-LIRG remnants (except NGC

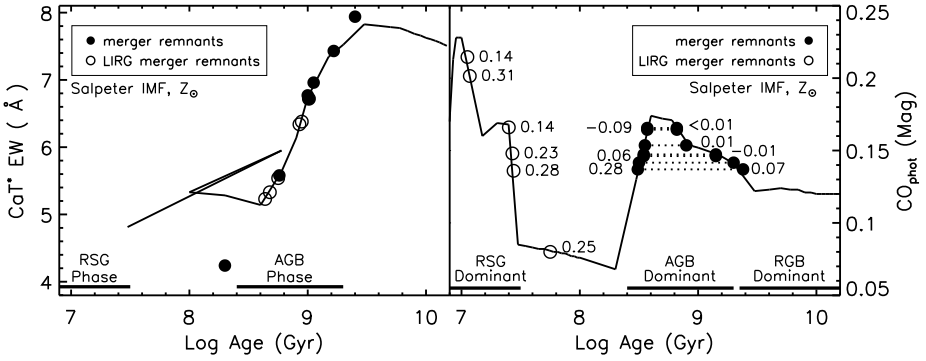

Figure 2. Stellar population models from M05 (*solid lines*) for CaT* (*left*) and CO (*right*) indices. Overplotted are 6 LIRG merger remnants (*open circles*) and 7 non-LIRG merger remnants (*filled circles*). RSG and AGB phases are noted along with when phases dominate the *K*-band light. The numbers in the right panel are $(\sigma_{\circ,\mathrm{CaT}} - \sigma_{\circ,\mathrm{CO}})/\sigma_{\circ,\mathrm{CaT}}$. Dotted lines indicate degenerate age results.

7252). The results in Figure 2 appear to support the premise that the presence of young populations are responsible for the smaller $\sigma_\circ$ observed in LIRGs. The final test will be to confirm whether these young populations reside in rotating disks located within the central few kpc of the LIRG/ULIRG merger remnant using spatially resolved spectroscopic observations of the CO band-head.

References

Barnes, J. E. 2002, MNRAS, 333, 481
Dasyra, K. M., Tacconi, L. J., Davies, R. I., Naab, T., Genzel, R., Lutz, D., Sturm, E., Baker, A. J., Veilleux, S., Sanders, D. B., & Burkert, A. 2006, ApJ, 651, 835
Doyon, R., Wells, M., Wright, G. S., Joseph, R. D., Nadeau, D., & James, P. A. 1994, ApJ, 437, L23
Genzel, R., Tacconi, L. J., Rigopoulou, D., Lutz, D., & Tecza, M. 2001, ApJ, 563, 527
Hibbard, J. E. & van Gorkom, J. H. 1996, AJ, 111, 655
James, P., Bate, C., Wells, M., Wright, G., & Doyon, R. 1999, MNRAS, 309, 585
Kormendy, J. & Sanders, D. B. 1992, ApJ, 390, L53
Lake, G. & Dressler, A. 1986, ApJ, 310, 605
Leitherer, C., Schaerer, D., Goldader, J. D., Delgado, R. M. G., Robert, C., Kune, D. F., de Mello, D. F., Devost, D., & Heckman, T. M. 1999, ApJS, 123, 3
Maraston, C. 2005, MNRAS, 362, 799
Pahre, M. A., de Carvalho, R. R., & Djorgovski, S. G. 1998, AJ, 116, 1606
Rothberg, B. & Joseph, R. D. 2004, AJ, 128, 2098
—. 2006, AJ, 131, 185
Schweizer, F. 1982, ApJ, 252, 455
—. 1996, AJ, 111, 109
Shier, L. M., Rieke, M. J., & Rieke, G. H. 1994, ApJ, 433, L9
Shier, L. M. & Fischer, J. 1998, ApJ, 497, 163
Silge, J. D. & Gebhardt, K. 2003, AJ, 125, 2809

Tacconi, L. J., Genzel, R., Lutz, D., Rigopoulou, D., Baker, A. J., Iserlohe, C., & Tecza, M. 2002, ApJ, 580, 73

Part III

Star Formation

GALAXY EVOLUTION: EMERGING INSIGHTS AND FUTURE CHALLLENGES
ASP Conference Series, Vol.
@jourvol, © 2009
S. Jogee, I. Marinova, L. Hao, and G. A Blanc

CDM Substructure Problem and Star Formation in Dwarf Halos

Andrey Kravtsov

Department of Astronomy & Astrophysics,
Kavli Institute for Cosmological Physics,
The University of Chicago

Abstract. During the last decade cosmological simulations have convincingly demonstrated that virialized regions of Cold Dark Matter (CDM) halos are filled with a multitude of dense, gravitationally-bound clumps. These dark matter *subhalos* are central regions of halos that survived strong gravitational tidal forces and dynamical friction during the hierarchical sequence of merging and accretion via which the CDM halos form. Comparisons with observations revealed that there is a glaring discrepancy between abundance of subhalos and luminous satellites of the Milky Way and Andromeda as a function of their circular velocity or bound mass within a fixed aperture. This large discrepancy, which became known as the "substructure" or the "missing satellites" problem, begs for an explanation. In this contribution I briefly review the progress made during the last several years in exploring different physical explanations of the problem, focusing on the explanations in the framework of the CDM paradigm of structure formation. I also argue that in addition to UV heating and supernova feedback we need to carefully examine the role of inefficient star formation in low surface density, low metallicity environments of dwarf halos in suppressing their efficiency to form luminous components.

1. Introduction

A decade ago cosmological simulations of increasingly higher resolution were used to demonstrate that virialized regions of Cold Dark Matter (CDM) halos are filled with a multitude of dense, gravitationally-bound clumps. These dark matter *subhalos* are central regions of halos that survived strong gravitational tidal forces and dynamical friction during the hierarchical sequence of merging and accretion via which the CDM halos form. Comparisons with observations revealed that there is a glaring discrepancy between abundance of subhalos and luminous satellites of the Milky Way and Andromeda as a function of their circular velocity or bound mass within a fixed aperture. The manifestly different observed satellite populations around galaxies of different luminosities and expected approximately self-similar populations of satellite subhalos around halos of different mass is known as the *substructure problem* (Kauffmann et al. 1993; Klypin et al. 1999; Moore et al. 1999, see Kravtsov 2009 for a recent review).

Although dozens of new satellite galaxies were discovered during the last decade (Willman et al. 2005; Belokurov et al. 2006, 2007; Zucker et al. 2006a,b; Irwin et al. 2007; Koposov et al. 2007; Walsh et al. 2007; Geha et al. 2009), and hundreds additional faint satellites expected to exist within the virial radius of

the Milky Way (Tollerud et al. 2008; Willman 2009), this does not necessarily mean that the substructure problem has been "alleviated," as was often claimed recently. Indeed, the most recent simulations show that more than 100,000 subhalos of mass $m_{\rm sub} > 10^5 M_\odot$ should exist in the Milky Way (Diemand et al. 2008; Springel et al. 2008). The substructure problem stated in the actual *numbers* of satellites is therefore alive and well and has not been alleviated in the least. It still begs for an explanation.

One possible way to account for the differences of the predicted and observed abundances of galactic satellites is to assume that ΛCDM model is incorrect on the small scales probed by the dwarf galactic satellites either because the power spectrum is suppressed on small scales compared to the amplitude of the CDM models (Kamionkowski & Liddle 2000; Colín et al. 2000; Bode et al. 2001; Zentner & Bullock 2003; Colín et al. 2008) and/or dark matter is not exactly collisionless, as assumed in the CDM (Spergel & Steinhardt 2000; Moore et al. 2000). These scenarios, however, both run into contradiction with other observational properties of galaxies and clusters (Kochanek & White 2000; Yoshida et al. 2000; Miralda-Escude 2000; Gnedin & Ostriker 2001) and are now strongly disfavored by observational evidence indicating that dark matter self-interaction is weak (Clowe et al. 2006) and small-scale power is present in the fluctuation spectrum of our universe (Abazajian 2006; Seljak et al. 2006). There is thus no compelling reason yet to think that the observed properties of galactic satellite populations are more naturally reproduced in these models.

A more natural explanation for the substructure problem most likely lies in the (uncertain) physics of galaxy formation. After all, a similar problem exists for objects of larger masses and luminosities if we compare the slope of the luminosity function and the halo mass function (Gonzalez et al. 2000; Baldry et al. 2008) or the predicted and observed abundance of galaxies in the nearby low density "field" regions (Tikhonov & Klypin 2009). In the subsequent discussion, I will therefore focus on the galaxy formation scenarios accounting for the substructure problem within the ΛCDM model.

2. Gas accretion and galaxy formation in dwarf halos

Several plausible physical processes can suppress gas accretion and star formation in dwarf dark matter halos. The cosmological UV background, which reionized the Universe at $z > 6$, heats the intergalactic gas and establishes a characteristic time-dependent minimum mass for halos that can accrete gas (Thoul & Weinberg 1996; Quinn et al. 1996; Gnedin & Hui 1998; Kitayama & Ikeuchi 2000; Gnedin 2000; Dijkstra et al. 2004; Hoeft et al. 2006; Okamoto et al. 2008). This mass is redshift dependent (Gnedin 2000; Kravtsov et al. 2004; Hoeft et al. 2006; Okamoto et al. 2008) and scales approximately as $M_{\rm c} \approx 2\times10^9 \exp(-5.4z/z_{\rm re}) h^{-1}\,{\rm M}_\odot$, where $z_{\rm re}$ is the redshift of reionization (O. Gnedin, private comm.).

UV radiation that permeates the universe after the epoch of reionization (or before in regions around bright UV sources) may photoevaporate gas out of dwarf halos (Barkana & Loeb 1999; Shaviv & Dekel 2003; Shapiro et al. 2004). The gas can also be blown away by the first generation of supernovae (Dekel

& Silk 1986; Mac Low & Ferrara 1999; Dekel & Woo 2003; Mashchenko et al. 2008, see, however, Marcolini et al. 2006).

At the same time, the ionizing radiation may quickly dissociate molecular hydrogen, the only efficient coolant for low-metallicity gas in such halos, and prevent star formation even before the gas is completely removed (Haiman et al. 1997). Even if the molecular hydrogen is not dissociated, cooling rate in halos with virial temperature $T_{\rm vir} < 10^4$ K is considerably lower than in more massive halos (Haiman et al. 2000) and we can therefore expect the formation of dense gaseous disks and star formation suppressed in such halos.

Finally, even if the gas is accreted and cools in small-mass halos, it is not guaranteed that it will form stars if gas does not reach metallicities and surface densities sufficient for efficient formation of molecular gas and subsequent star formation (Kravtsov et al. 2004; Kaufmann et al. 2007; Tassis et al. 2008; Robertson & Kravtsov 2008; Gnedin et al. 2009).

The combined effect of galaxy formation suppression processes listed above is likely to leave most of dark matter halos with masses $<$ few $\times\, 10^9\ M_\odot$ dark, and could have imprinted a distinct signature on the properties of the dwarf galaxies that did manage to form stars before reionization. In fact, if all these suppressing effects are as efficient as is usually thought, it is quite remarkable that galaxies such as the recently discovered ultra-faint dwarfs exist at all. One possibility extensively discussed in the literature is that they managed to accrete a certain amount of gas and form stars before the universe was reionized (Bullock et al. 2000; Somerville 2002; Benson et al. 2002; Gnedin & Kravtsov 2006; Moore et al. 2006; Madau et al. 2008; Koposov et al. 2009; Busha et al. 2009).

Direct cosmological simulations do show that dwarf galaxies forming at $z > 6$ bear striking resemblance to the faint dwarf spheroidal galaxies orbiting the Milky Way (Ricotti & Gnedin 2005; Bovill & Ricotti 2009; Ricotti 2009) and their predicted abundance around the Milky Way is consistent with estimates of the abundance of the faintest satellites (Gnedin & Kravtsov 2006). Alternatively, some authors argued (Stoehr et al. 2002, 2003; Hayashi et al. 2003; Peñarrubia et al. 2008) that observed dwarf satellite galaxies could be in much more massive subhalos than was indicated by simple estimates of dynamical masses and circular velocities using stellar velocity dispersions. In this case, the relatively large halo mass could allow an object to resist the suppressing effects of the UV background.

Cosmological simulations also clearly show that the subhalos found within virial radii of larger halos at $z = 0$ have on average lost significant amount of mass and have been considerably more massive in the past (Kravtsov et al. 2004; Nagai & Kravtsov 2005; Giocoli et al. 2008). The dramatic loss of mass occurs due to the tidal forces that subhalos experience as they orbit in the potential of their host halo. A significant fraction of the luminous dwarf satellites therefore can be associated with those subhalos that have been substantially more massive in the past and hence more resilient against galaxy formation suppressing processes. Such subhalos could have had a window of opportunity to form their stellar systems even if the subhalos they are embedded in today have relatively small mass (Kravtsov et al. 2004).

Overall, diversity of possible evolutionary histories of the host halos of dwarf galaxies and a large variety of potential galaxy formation suppression processes operating during each evolutionary path imply a diversity of dwarf

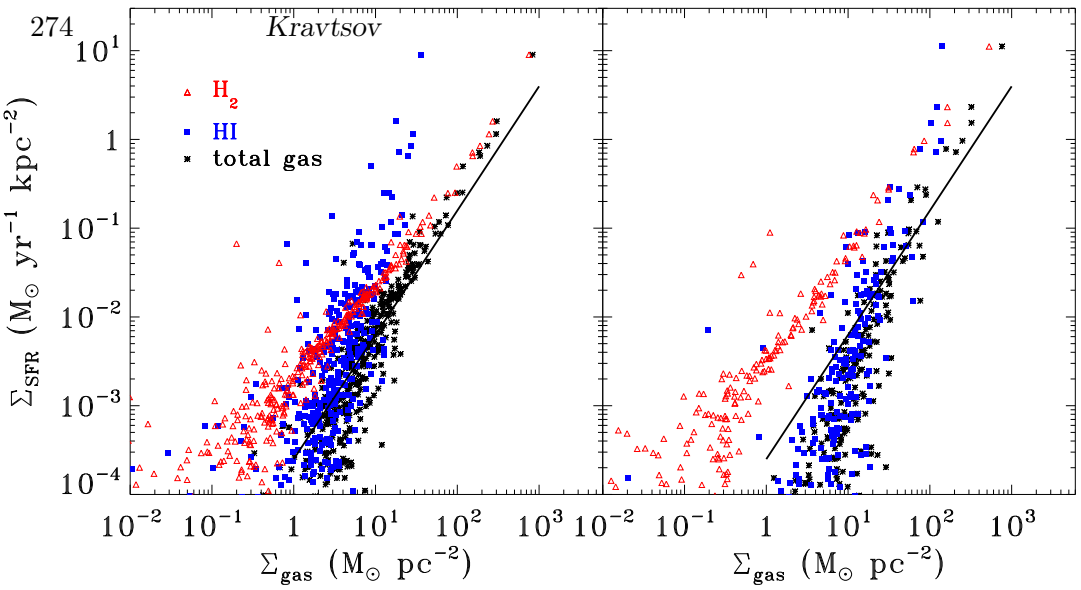

Figure 1. Sensitivity of the Kennicutt-Schmidt relation to metallicity. The two panels show results of a calculation in which star formation in cosmological simulations of galaxy formation is based on molecular gas and metallicity of the gas was kept at solar value (left panel) and 0.1 solar (right value). The star formation and gas surface densities are averaged over level 3 cells (corresponding, at $z = 4$, to a proper scale of 3.2 kpc). Star formation rates are averaged over 30 Myrs. Each point corresponds to a different level 3 cell in the simulation at $z = 4$. Red triangles: molecular gas; blue squares: atomic gas; black stars: total gas (no He). Solid line shows the best fit relation of Kennicutt (1998, with the slope of 1.4).

galaxy properties, such as star formation histories, and this is indeed borne out by observations (e.g., Orban et al. 2008). As emphasized by Orban et al. (2008), one of the key processes that needs to be understood in order to connect evolutionary histories of satellite dark matter halos to observed satellite dwarf galaxies is star formation in the low-metallicity (and hence low dust), low gas surface density disks of dwarf galaxies. In the remaining part of this contribution I will focus on our recent efforts to make progress in this direction.

3. Inefficient star formation in dwarf halos

The standard approach in models of galaxy formation is to assume a recipe for conversion of gas into stars based on the empirical correlations observed for local galaxies (the Kennicutt-Schmidt, hereafter KS, relations: Schmidt 1959; Kennicutt 1998). While this approach is no doubt reasonable, one limitation is that these relations have only been studied relatively well for nearby massive or star bursting galaxies. There is, however, a growing body of evidence that the relations for galaxies of lower surface brightness and/or metallicity may be quite different (see, e.g., Robertson & Kravtsov 2008, for references and discussion and the recent study by Bigiel et al. 2008). Bigiel et al. (2008), for example, show that for the gas surface densities of dwarf galaxies the gas consumption time scale is longer than the Hubble time ($> 10 - 20$ Gyrs) compared to the

consumption time of ≈ 2 Gyrs for the surface densities typical for the inner regions of L_* galaxies. This means that dwarf halos would be able to convert only a small fraction of their cold gas into stars even in the absence of any other suppressing processes.

Theoretically, the longer gas consumption time scales in the low metallicity gas at low surface densities is due to difficulty of forming cold, dense, molecular regions in such environments (e.g., Kravtsov 2003; Schaye 2001; Krumholz et al. 2009; Gnedin et al. 2009). Indeed, the transition from atomic to fully molecular gas depends strongly on the local gas metallicity and dissociating UV flux (Elmegreen 1989, 1993; Schaye 2001; Pelupessy et al. 2006; Krumholz et al. 2009; Gnedin et al. 2009). Thus, for example, we expect that in low metallicity galaxies gas becomes fully molecular (and thereby conducive to star formation) at higher gas density compared to more massive, higher metallicity systems.

This means that on the global scale of a galaxy gas may be converted into stars at a slower rate per unit mass of gas or, in other words, the star formation efficiency is lower, even if the density distribution of ISM is the same. Not only is this regime applicable to dwarf or low surface brightness galaxies today, but also to the majority of progenitors of massive galaxies at high redshifts. This is illustrated in Figure 1, which shows the Kennicutt-Schmidt relation between surface density of star formation rate and gas in cosmological simulations of galaxy formation. The simulations incorporate a novel star formation recipe based on molecular gas, as described by Gnedin et al. (2009). The two panels show relations measured in identical simulations in which gas metallicity was fixed to the solar value (left panel) and ten times smaller value (right panel). The relation of star formation with the total surface density of gas is shown with black symbols. Red and blue points show relations with atomic and molecular hydrogen separately. Comparison of the star formation rate at densities typical for nearby dwarf galaxies, $\Sigma_{\rm gas} \approx 1-10\,{\rm M}_\odot\,{\rm pc}^{-2}$ (e.g., Bigiel et al. 2008), clearly shows that star formation rate is smaller by a factor of at least $\sim 5-10$ in the low metallicity case.

The lower efficiency of gas conversion into stars in small mass halos at high redshifts may have profound implications for galaxy evolution from shaping the faint end of the luminosity function to the morphological mix of galaxies. Traditionally, in cosmological simulations and semi-analytic models the efficiency of star formation in $< L_*$ galaxies is suppressed by supernova feedback. However, the efficiency of such suppression is not clear and in many observed dwarf galaxies star formation is inefficient without obvious signs of active feedback. We argue that a similar suppression can be provided by the inherent difficulty of building self-shielding molecular regions within low-density, low-metallicity ISM of smaller galaxies (Gnedin et al. 2009). Exploring the effects of this new "metallicity feedback" is an interesting avenue of research in the near future.

Acknowledgments. I would like to thank the organizing committee for organizing a great and stimulating conference. This work was funded by the NSF grants AST-0507666, and AST-0708154. The research was also partially supported by the Kavli Institute for Cosmological Physics at the University of Chicago through grant NSF PHY-0551142 and an endowment from the Kavli Foundation. I have made extensive use of the NASA Astrophysics Data System and arXiv.org preprint server during writing of this paper.

References

Abazajian, K. 2006, Phys.Rev.D, 73, 063513
Baldry, I. K., Glazebrook, K., & Driver, S. P. 2008, MNRAS, 388, 945
Barkana, R. & Loeb, A. 1999, ApJ, 523, 54
Belokurov, V., Zucker, D. B., Evans, N. W., & et al. 2006, ApJ, 647, L111
—. 2007, ApJ, 654, 897
Benson, A. J., Frenk, C. S., Lacey, C. G., Baugh, C. M., & Cole, S. 2002, MNRAS, 333, 177
Bigiel, F., Leroy, A., Walter, F., Brinks, E., de Blok, W. J. G., Madore, B., & Thornley, M. D. 2008, AJ, 136, 2846
Bode, P., Ostriker, J. P., & Turok, N. 2001, ApJ, 556, 93
Bovill, M. S. & Ricotti, M. 2009, ApJ, 693, 1859
Bullock, J. S., Kravtsov, A. V., & Weinberg, D. H. 2000, ApJ, 539, 517
Busha, M. T., Alvarez, M. A., Wechsler, R. H., Abel, T., & Strigari, L. E. 2009, ApJ submitted (arXiv/0901.3553)
Clowe, D., Bradač, M., Gonzalez, A. H., Markevitch, M., Randall, S. W., Jones, C., & Zaritsky, D. 2006, ApJ, 648, L109
Colín, P., Avila-Reese, V., & Valenzuela, O. 2000, ApJ, 542, 622
Colín, P., Valenzuela, O., & Avila-Reese, V. 2008, ApJ, 673, 203
Dekel, A. & Silk, J. 1986, ApJ, 303, 39
Dekel, A. & Woo, J. 2003, MNRAS, 344, 1131
Diemand, J., Kuhlen, M., Madau, P., Zemp, M., Moore, B., Potter, D., & Stadel, J. 2008, Nat, 454, 735
Dijkstra, M., Haiman, Z., Rees, M. J., & Weinberg, D. H. 2004, ApJ, 601, 666
Elmegreen, B. G. 1989, ApJ, 338, 178
—. 1993, ApJ, 411, 170
Geha, M., Willman, B., Simon, J. D., Strigari, L. E., Kirby, E. N., Law, D. R., & Strader, J. 2009, ApJ, 692, 1464
Giocoli, C., Tormen, G., & van den Bosch, F. C. 2008, MNRAS, 386, 2135
Gnedin, N. Y. 2000, ApJ, 542, 535
Gnedin, N. Y. & Hui, L. 1998, MNRAS, 296, 44
Gnedin, N. Y. & Kravtsov, A. V. 2006, ApJ, 645, 1054
Gnedin, N. Y., Tassis, K., & Kravtsov, A. V. 2009, ApJ, 697, 55
Gnedin, O. Y. & Ostriker, J. P. 2001, ApJ, 561, 61
Gonzalez, A. H., Williams, K. A., Bullock, J. S., Kolatt, T. S., & Primack, J. R. 2000, ApJ, 528, 145
Haiman, Z., Abel, T., & Rees, M. J. 2000, ApJ, 534, 11
Haiman, Z., Rees, M. J., & Loeb, A. 1997, ApJ, 476, 458
Hayashi, E., Navarro, J. F., Taylor, J. E., Stadel, J., & Quinn, T. 2003, ApJ, 584, 541
Hoeft, M., Yepes, G., Gottlöber, S., & Springel, V. 2006, MNRAS, 371, 401
Irwin, M. J., Belokurov, V., Evans, N. W., & et al. 2007, ApJ, 656, L13
Kamionkowski, M. & Liddle, A. R. 2000, Physical Review Letters, 84, 4525
Kauffmann, G., White, S. D. M., & Guiderdoni, B. 1993, MNRAS, 264, 201
Kaufmann, T., Wheeler, C., & Bullock, J. S. 2007, MNRAS, 382, 1187
Kennicutt, Jr., R. C. 1998, ApJ, 498, 541
Kitayama, T. & Ikeuchi, S. 2000, ApJ, 529, 615
Klypin, A., Kravtsov, A. V., Valenzuela, O., & Prada, F. 1999, ApJ, 522, 82
Kochanek, C. S. & White, M. 2000, ApJ, 543, 514
Koposov, S., de Jong, J. T. A., Belokurov, V., Rix, H.-W., Zucker, D. B., Evans, N. W., Gilmore, G., Irwin, M. J., & Bell, E. F. 2007, ApJ, 669, 337
Koposov, S. E., Yoo, J., Rix, H.-W., Weinberg, D. H., Macciò, A. V., & Escudé, J. M. 2009, ApJ, 696, 2179
Kravtsov, A. V. 2003, ApJ, 590, L1
—. 2009, Advances in Astronomy submitted (arXiv/0906.3295

Kravtsov, A. V., Gnedin, O. Y., & Klypin, A. A. 2004, ApJ, 609, 482
Krumholz, M. R., McKee, C. F., & Tumlinson, J. 2009, ApJ, 693, 216
Mac Low, M.-M. & Ferrara, A. 1999, ApJ, 513, 142
Madau, P., Kuhlen, M., Diemand, J., Moore, B., Zemp, M., Potter, D., & Stadel, J. 2008, ApJ, 689, L41
Marcolini, A., D'Ercole, A., Brighenti, F., & Recchi, S. 2006, MNRAS, 371, 643
Mashchenko, S., Wadsley, J., & Couchman, H. M. P. 2008, Science, 319, 174
Miralda-Escude, J. 2000, ArXiv/0002050
Moore, B., Diemand, J., Madau, P., Zemp, M., & Stadel, J. 2006, MNRAS, 368, 563
Moore, B., Gelato, S., Jenkins, A., Pearce, F. R., & Quilis, V. 2000, ApJ, 535, L21
Moore, B., Ghigna, S., Governato, F., Lake, G., Quinn, T., Stadel, J., & Tozzi, P. 1999, ApJ, 524, L19
Nagai, D. & Kravtsov, A. V. 2005, ApJ, 618, 557
Okamoto, T., Gao, L., & Theuns, T. 2008, MNRAS, 390, 920
Orban, C., Gnedin, O. Y., Weisz, D. R., Skillman, E. D., Dolphin, A. E., & Holtzman, J. A. 2008, ApJ, 686, 1030
Peñarrubia, J., McConnachie, A. W., & Navarro, J. F. 2008, ApJ, 672, 904
Pelupessy, F. I., Papadopoulos, P. P., & van der Werf, P. 2006, ApJ, 645, 1024
Quinn, T., Katz, N., & Efstathiou, G. 1996, MNRAS, 278, L49
Ricotti. 2009, Advances in Astronomy, this volume
Ricotti, M. & Gnedin, N. Y. 2005, ApJ, 629, 259
Robertson, B. E. & Kravtsov, A. V. 2008, ApJ, 680, 1083
Schaye, J. 2001, ApJ, 562, L95
Schmidt, M. 1959, ApJ, 129, 243
Seljak, U., Makarov, A., McDonald, P., & Trac, H. 2006, Physical Review Letters, 97, 191303
Shapiro, P. R., Iliev, I. T., & Raga, A. C. 2004, MNRAS, 348, 753
Shaviv, N. J. & Dekel, A. 2003, MNRAS submitted, `astro-ph/0305527`
Somerville, R. S. 2002, ApJ, 572, L23
Spergel, D. N. & Steinhardt, P. J. 2000, Physical Review Letters, 84, 3760
Springel, V., Wang, J., Vogelsberger, M., Ludlow, A., Jenkins, A., Helmi, A., Navarro, J. F., Frenk, C. S., & White, S. D. M. 2008, MNRAS, 391, 1685
Stoehr, F., White, S. D. M., Springel, V., Tormen, G., & Yoshida, N. 2003, MNRAS, 345, 1313
Stoehr, F., White, S. D. M., Tormen, G., & Springel, V. 2002, MNRAS, 335, L84
Tassis, K., Kravtsov, A. V., & Gnedin, N. Y. 2008, ApJ, 672, 888
Thoul, A. A. & Weinberg, D. H. 1996, ApJ, 465, 608
Tikhonov, A. V. & Klypin, A. 2009, MNRAS, 395, 1915
Tollerud, E. J., Bullock, J. S., Strigari, L. E., & Willman, B. 2008, ApJ, 688, 277
Walsh, S. M., Jerjen, H., & Willman, B. 2007, ApJ, 662, L83
Willman, B. 2009, Advances in Astronomy, this volume
Willman, B., Blanton, M. R., West, A. A., & et al. 2005, AJ, 129, 2692
Yoshida, N., Springel, V., White, S. D. M., & Tormen, G. 2000, ApJ, 544, L87
Zentner, A. R. & Bullock, J. S. 2003, ApJ, 598, 49
Zucker, D. B., Belokurov, V., Evans, N. W., & et al. 2006a, ApJ, 650, L41
—. 2006b, ApJ, 643, L103

GALAXY EVOLUTION: EMERGING INSIGHTS AND FUTURE CHALLLENGES
ASP Conference Series, Vol.
@jourvol, © 2009
S. Jogee, I. Marinova, L. Hao, and G. A Blanc

Fossil Signatures of the Reionization Epoch in the Galactic Halo

Piero Madau

University of California Santa Cruz

Abstract. The *Via Lactea II* simulation of a Milky Way-sized dark matter halo resolves over 50,000 gravitationally bound clumps orbiting today within the virialized region of the main host. More than 2,000 of these surviving subhalos have one or more "progenitors" with $M > 10^6 M_\odot$ at redshift $z > 11$, i.e. massive enough for their gas to have cooled via excitation of H_2 and fragmented prior to the epoch of cosmological reionization. If such progenitors were able to convert a fraction of their gas content into very metal-poor stars with a Salpeter initial mass function (IMF), their low-mass stellar populations would still be shining today with a visual magnitude $M_V = 6.7$ per solar mass of initial stars. Assuming a universal baryon fraction, we show that mean star formation efficiencies as low as 0.1% in progenitors $\ll 10^8 M_\odot$ would overproduce the abundance of the faint Galatic dwarf spheroidals observed by the Sloan Digital Sky Survey. Star formation at first light must have occurred either with an IMF lacking stars below $0.9 M_\odot$, or was intrinsically very inefficient in small dark matter halos.

1. Introduction

Galaxy halos are one of the crucial testing grounds for structure formation scenarios, as they contain the imprints of past accretion events, from before the epoch of reionization to the present. In the standard ΛCDM concordance cosmology, objects like the halo of our Milky Way are assembled via the hierarchical merging and accretion of many smaller progenitors. Subunits collapse at high redshift, are dense, and have cuspy density profiles, and when they merge into larger hosts they are able to resist tidal disruption. Galaxy halos today are teeming with tens of thousands of surviving "subhalos" down to mass scales as small as globular clusters (Diemand et al. 2008). Several tests of this fundamental prediction have been proposed: the substructure population may be detectable via flux ratio anomalies in strong gravitational lenses (Metcalf & Madau 2001), through its effects on stellar streams (Ibata et al. 2002), or via γ-rays from dark matter annihilation in their cores (Bergstrom et al. 1999). The predicted subhalo counts vastly exceed the number of known satellites of the Milky Way, a "substructure problem" that has been the subject of many recent studies. While a full characterization of this discrepancy is hampered by luminosity bias in the observed satellite luminosity function (LF) (Koposov et al. 2008), it is generally agreed that cosmic reionization may offer a plausible solution to the apparent conflict between the Galaxy's relatively smooth stellar halo and the extremely clumpy cold dark matter distribution. In the simplest version of this hypothesis, photoionization heating after reionization

breakthrough reduces the star forming ability of newly forming halos that are not sufficiently massive to accrete intergalactic gas (e.g. Bullock et al. 2000; Somerville 2002; Kravtsov et al. 2004; Ricotti & Gnedin 2005; Moore et al. 2006; Strigari et al. 2007; Simon & Geha 2007; Madau et al. 2008).

In this talk I will take a slightly different approach and focus instead on the sources of reionization itself. I will use the one billion particle *Via Lactea II* simulation to constrain the character of star formation (initial mass function and efficiency of gas conversion into stars) at first light, i.e. in subgalactic halos prior to the epoch of reionization. The starting point of this investigation is the finding that $> 2,000$ bound clumps that survive today in the *Via Lactea II* halo have early progenitors that were massive enough for their gas to cool via excitation of molecular hydrogen and fragment before reionization breakthrough. If low-mass stars formed in the process, their hosts would be shining today as faint Milky Way satellites.

2. Via Lactea II

The *Via Lactea II* simulation, one of the highest-precision calculation of the assembly of the Galactic CDM halo to date (Diemand et al. 2008), offers a unique opportunity for a systematic investigation of the fossil records of reionization in the halo of the Milky Way. *Via Lactea II* employs just over one billion $4,100 M_\odot$ particles to model the formation of a $M_{200} = 1.9 \times 10^{12} M_\odot$ Milky-Way size halo and its substructure. It resolves 50,000 subhalos today within the host's $r_{200} = 402$ kpc (the radius enclosing an average density 200 times the mean matter value). The *Wilkinson Microwave Anisotropy Probe (WMAP)* 5-year data require the universe to be fully reionized by $z = 11.0 \pm 1.4$ (Dunkley et al. 2009). Assuming that the region around the Milky Way was reionized at about the same epoch of the universe as a whole, we can trace the progenitors of present-day surviving substructure back to a redshift > 11, i.e. before star formation was quenched by photoheating. We link a descendant "A" at $z = 0$ to a progenitor "B" at $z > 11$ if "A" contains more than 10 particles from "B" and more than any other descendant of "B". Thus a descendant can have more than one progenitor, but a progenitor is linked to at most one descendant. We include in our analysis only progenitors that either survive individually during the hierarchical clustering process or contribute to a gravitationally-bound descendant at $z = 0$. About 10,000 "first generation" systems above $10^6 M_\odot$ are totally disrupted by tidal forces: for half of them all of their particles lie today within r_{200} and contribute to the smooth stellar halo. Figure 1 shows the cumulative mass functions of progenitors and parents. We track forward in time 4,500 of these early minihalos into 2,300 descendants today.

3. Star formation at first light

Cosmological hydrodynamics simulations of structure formation in a ΛCDM universe have found that in the early collapse of $\gtrsim 10^6 M_\odot$ systems, enough H_2 is produced to cool the gas and allow star formation within a Hubble time (e.g. Abel et al. 2002; Bromm et al. 2002). Figure 1 shows that a few hundred progenitors are above the "atomic cooling" mass threshold of $\sim 3 \times 10^7 M_\odot$

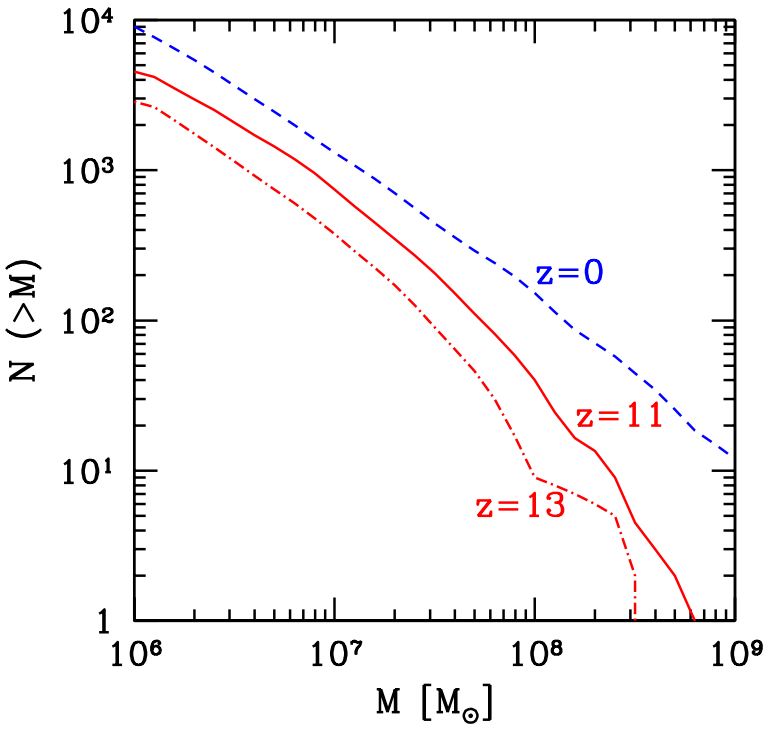

Figure 1. *Via Lactea II* cumulative substructure mass function at different epochs. *Solid curve:* All 4,500 progenitor halos with $M > 10^6 M_\odot$ at $z \gtrsim 11$ that contribute to a gravitationally bound descendant (2,300 of them) today within r_{200}. *Dot-dashed curve:* same for the 2,900 $M > 10^6 M_\odot$ progenitors at $z = 13$. Also shown for comparison is the mass function of all *Via Lactea II* subhalos at the present epoch (*dashed curve*).

($T_{\rm vir} \gtrsim 10^4\,{\rm K}$), where gas can cool and fragment via excitation of hydrogen Lyα. Numerical studies also suggest that, while primordial stars were likely very massive and formed in isolation at $z \gtrsim 20$ (e.g. O'Shea & Norman 2007), low-mass second-generation stars can form as soon as a minimum pre-enrichment level of $Z = 10^{-5\pm1}\,Z_\odot$ is reached (e.g. Schneider et al. 2002). The existence of $0.8 M_\odot$ extremely iron-deficient stars in the halo of the Milky Way (Christlieb et al. 2002; Frebel et al. 2005) indicates that low-mass star formation was possible at very-low metallicities (e.g. Tumlinson 2007). In order to constrain the number of low-mass stars that lit up dark matter halos before reionization, our default model makes a number of simplifying assumptions: 1) all progenitor hosts above $M(z \gtrsim 11) = 10^6 M_\odot$ have a gas content given by the universal baryon fraction, $M_{\rm gas} = (\Omega_b/\Omega_m) M = 0.17\,M$; 2) at $z \gtrsim 11$ a fraction f_* of this gas is turned into very metal-poor stars with $Z = Z_\odot/200$ (the lowest metallicity allowed by Bruzual & Charlot's 2003 stellar population synthesis models) and a standard Salpeter initial mass function (IMF) in the range $0.1 < m_* < 100 M_\odot$. The star formation efficiency is independent of M; 3) star formation is suppressed at later

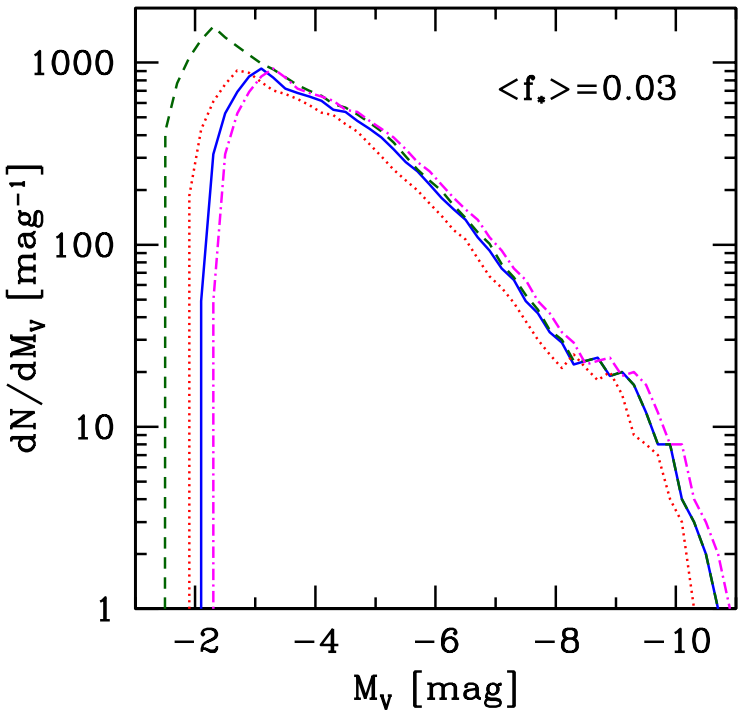

Figure 2. The luminous fossil remnants of reionization. *Solid curve:* present-day LF of all *Via Lactea II* subhalos that had one or more progenitor with $M > 10^6 M_\odot$ at $z \gtrsim 11$. At this epoch, a fraction f_* of the gas content of each progenitor is turned instantaneously into stars with a Salpeter IMF and metallicity $Z = Z_\odot/200$. *Dashed curve:* same for $M > 5 \times 10^5 M_\odot$. *Dot-dashed curve:* same for a Chabrier (2003) IMF. *Dotted curve:* same for $Z = Z_\odot/5$. In all the above cases visual magnitudes at age 13.7 Gyr have been calculated using Bruzual & Charlot's (2003) models.

epochs in all progenitors and their descendants; 4) primordial stellar systems are deeply embedded in progenitor minihalos and remain largely unaffected by tidal stripping even if their hosts are not. The complete tidal disruption of a host, however, also destroys its stellar system.

We are now in the position to construct the present-day LF of the fossil remnants of reionization in the halo of the Milky Way. According to Bruzual & Charlot (2003), a stellar population undergoing an instantaneous burst will be shining at age 13.7 Gyr with a visual magnitude per solar mass in stars of 6.7 mag (Salpeter IMF, $Z = Z_\odot/200$). The steep LF of *Via Lactea II* first-generation halos predicted in this case is shown in Figure 2 for $\langle f_* \rangle = 0.03$. Luminous remnants are distributed between $M_V = -2$ and $M_V = -10$, and there are more than two hundred relatively bright objects with $M_V < -6$, i.e. as bright as Boötes. A mean star formation efficiency three times smaller would shift this curve 1.2 mag to the left. The cutoff at faint magnitudes simply

reflects our assumption that clumps below $M(z \gtrsim 11) = 10^6 M_\odot$ never form stars: the effect of lowering this mass threshold by a factor of two is also shown for comparison. Note that implausibly increasing the metallicity of early stars to $Z = Z_\odot/5$ would only shift the curve 0.3 mag to the left (Bruzual & Charlot 2003). Similarly, a Chabrier (2003) IMF in the same mass range instead of Salpeter has only a small (0.2 mag) brightening effect.

4. Constraints from the SDSS

Over the last two years, the Sloan Digital Sky Survey (SDSS) has doubled the number of known Milky Way dwarf spheroidals (dSphs) brighter than $M_V = -2$ (e.g. Belokurov et al. 2007). An accurate estimate of the total number of dwarfs requires a correction to the observed LF that accounts for completeness limits and that depends on the unknown intrinsic spatial distribution of sources. Rather than producing an "unbiased" list of Galactic satellites as in Tollerud et al. (2008), we apply here the completeness limit of the SDSS DR5 to our predicted fossil remnants in *Via Lactea II* (Fig. 2) to construct an artificial DR5 sample of luminous first-generation substructure. As computed by Koposov et al. (2008) (and fitted by Tollerud et al. 2008), the maximum accessible distance beyond which an object of magnitude M_V will go undetected by the SDSS is

$$r_{\rm max} = \left(\frac{3}{4\pi f_{\rm DR5}}\right)^{1/3} 10^{(-0.6M_V - 5.23)/3}\,{\rm Mpc}, \qquad (1)$$

where $f_{\rm DR5} = 0.194$ is the fraction of the sky covered by DR5. Therefore, only subhalos brighter than $M_V = -6.6$ will be detected all the way to r_{200}: first-generation remnants with $M_V = -4$ will be included in the sample only if they are closer than 120 kpc. (The above detection limit applies to objects with surface brightness $\lesssim 30$ mag arcsec^{-2}, i.e. we are implicitly assuming that our luminous progenitors are less diffuse than this.) As a first order correction we also assume that subhalos within $r_{\rm max}$ are detected with 100% efficiency, and account for the partial sky coverage of SDSS by multiplying the number of detectable subhalos by $f_{\rm DR5}$. The resulting cumulative LF $N_{\rm DR5}(< M_V)$ is plotted in Figure 3 for values of $\langle f_* \rangle$ that decrease from 3% down to 3×10^{-4}. In this range, the faint-end of the predicted LF is dominated by the remnants of $10^6 - 10^7 M_\odot$ progenitors. For an efficiency of 1%, SDSS should have detected ~ 150 first-generation systems brighter than $M_V = -2$, while only a dozen are actually observed. The known Milky Way satellites are also plotted for comparison: these include the SDSS eleven dwarfs with $M_V < -2$ (including Leo T which, at a distance of 417 kpc, lies just outside r_{200}) as well as the eleven (times $f_{\rm DR5}$ to correct for the partial sky coverage) classical (pre-SDSS) bright satellites. *Clearly, mean star formation efficiencies as low as 0.1% in progenitors below* $10^7 M_\odot$ *would overproduce the abundance of ultra-faint dSphs.* The mean efficiency of star formation must actually scale with halo mass in order to reproduce the observations with first-generation remnants. This is because a constant efficiency translates into a steep LF that follows the steep mass function of CDM field halos. By contrast, the 23 known satellites of the Milky Way have a flat LF and shine with luminosities ranging from about a thousand to a billion times solar. The dashed curve in Figure 3 shows a toy

model with a mass-dependent efficiency, $\langle f_* \rangle = (0.02, 0.0025, 0)$ for M in the range $M = (> 7 \times 10^7, 3.5 \times 10^7\text{-}7 \times 10^7, < 3.5 \times 10^7 M_\odot)$. Note how the data allow efficiencies of order 1% only above the atomic cooling threshold. Our results are not extremely sensitive to the assumed reionization epoch: a case in which only the remnants of progenitor minihalos at $z \gtrsim 13$ are shining today with $\langle f_* \rangle = 0.0005$ produces a fossil LF similar to the $z \gtrsim 11$, $\langle f_* \rangle = 0.0003$ case.

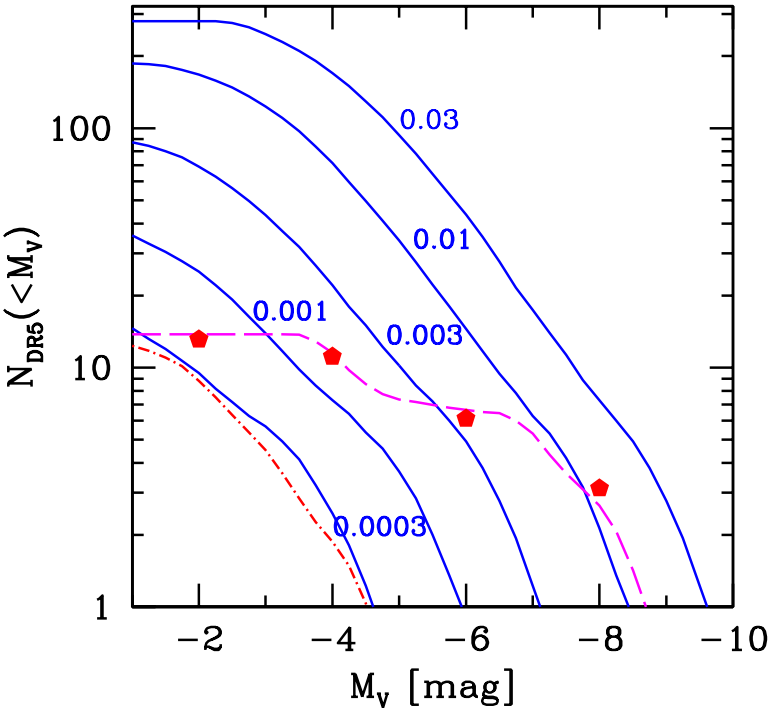

Figure 3. *Via Lactea II* first-generation ($z \gtrsim 11$) subhalos detectable today by the SDSS DR5. All curves assume $M > 10^6 M_\odot$, a Salpeter IMF, and $Z = Z_\odot/200$. The data points are taken from the compilation of Tollerud et al. (2008). *Labelled solid curves:* $\langle f_* \rangle = 0.03, 0.01, 0.003, 0.001, 0.0003$. *Dashed curve:* mass-dependent star formation efficiency, $\langle f_* \rangle = (0.02, 0.0025, 0)$ for M in the range $(> 7 \times 10^7, 3.5 \times 10^7\text{-}7 \times 10^7, < 3.5 \times 10^7 M_\odot)$. Also plotted for comparison is the LF of the remnants of $z = 13$ halos with $\langle f_* \rangle = 0.0005$ (*short dot-dashed curve* at the bottom).

5. Summary

The first-generation stars that formed in small-mass subgalactic halos well beyond redshift 10 likely contributed significantly to the reheating of the intergalactic medium. The detailed thermal and ionization history of the universe during the formative early stages at $z > 10$ depends on the

power-spectrum of density fluctuations on small scales, the stellar IMF and star formation efficiency, a complex network of poorly understood feedback mechanisms, and remains one of the crucial missing links in galaxy formation and evolution studies. Results from one billion particle dark matter simulations are allowing for the first time a systematic study of the fossil signatures of the pre-reionization epoch in the Galactic halo and of the baryonic building blocks of today's galaxies. In this talk I have traced the progenitors of present-day surviving substructure back to a time prior to reionization breakthrough, i.e. before star formation was quenched by an external UV background. We have then populated early-forming minihalos with very metal-poor stars following a Salpeter IMF, and looked at the photometric properties today of their 2,300 descendants within r_{200}. We have shown that even star formation efficiencies as low as 0.1% in progenitor minihalos below $10^7 M_\odot$ would overproduce the abundance of Galatic dSphs observed by the SDSS. This value should be regarded as an upper limit since luminous dSphs are known to have formed a fraction of their stars after reionization (e.g. Orban et al. 2008). It is also meant to be taken as a mean value, since an alternative possibility is to allow stars to form efficiently in a small fraction of minihalos at some given mass and to suppress star formation in the remainders, rather than reducing the efficiency across the board. Note that the parameter f_* is degenerate with the baryon fraction: if the gas content of early virialized structure was smaller than the universal value (as found, e.g., by O'Shea & Norman 2007), then our limits on the star formation efficiency would be correspondingly higher.

It is possible to test a posteriori the main assumption underlying our calculations, i.e. that early *Via Lactea II* progenitors were populated with "pre-reionization" stellar systems. In the simulated high-resolution volume, there are 17,700 $M > 10^6 M_\odot$ subhalos at $z \gtrsim 11$, spread over a comoving volume of 78 Mpc^3 containing a total mass of $M_{\rm DM} = 3.5 \times 10^{12} M_\odot$. Stars distributed according to a Salpeter IMF produce during their lifetime $f_\gamma \approx 4,000$ Lyman continuum photons per stellar proton, of which only a fraction $f_{\rm esc}$ will escape into the intergalactic medium (IGM). The total stellar mass in these early-forming progenitors is $M_* = 3.6 \times 10^{10} \langle f_* \rangle M_\odot$. Hydrogen photoionization requires $(1 + N_{\rm rec})$ photons above 13.6 eV per atom, where $N_{\rm rec}$ is the number of radiative recombinations over a Hubble time. The total mass of intergalactic gas that can be kept ionized is then $M_{\rm ion} = f_\gamma M_* f_{\rm esc}/(1 + N_{\rm rec})$. The condition $M_{\rm ion} < (\Omega_b/\Omega_m)\, M_{\rm DM}$ then implies $\langle f_* \rangle < 0.004\, [(1 + N_{\rm rec})/f_{\rm esc}]$, where the factor in square brackets is of order 10 or so. The low star formation efficiencies derived here appear then to be consistent with the idea that the region around the Milky Way was reionized at $z \lesssim 11$ by external radiation, before stars in the Local Group formed in sufficient numbers (Weinmann et al. 2007).

It seems fair to conclude that star formation at first light must have occurred either with an IMF lacking stars below $0.9 M_\odot$, or was intrinsically very inefficient in small dark matter halos. If the former, this may be an indication of an upward shift in the mass scale of the IMF at early cosmological times owing, e.g., to the hotter cosmic microwave background (Larson 2005). If the latter, our results may be viewed as another hint (see Strigari et al. 2008) of a minimum scale in galaxy formation, below which supernova feedback (Dekel & Silk 1986) and/or

H_2 photodissociation by a Lyman-Werner background (Haiman et al. 1997) sharply suppress star formation.

References

Abel, T., Bryan, G., & Norman, M. L. 2002, Science, 295, 93
Belokurov, V., et al. 2007, ApJ, 654, 897
Bergstrom, L., Edsjo, J., Gondolo, P., & Ullio, P. 1999, PhRvD, 59, 043506
Christlieb, N., et al. 2002, Nature, 419, 904
Bromm, V., Coppi, P. S., & Larson, R. B. 2002, ApJ, 564, 23
Bruzual, G., & Charlot, S. 2003, MNRAS, 344, 1000
Bullock, J. S., Kravtsov, A. V., & Weinberg, D. H. 2000, ApJ, 539, 517
Chabrier, G. 2003, ApJ, 586, L133
Dekel, A., & Silk, J. 1986, ApJ, 303, 39
Diemand, J., Kuhlen, M., & Madau, P. 2007, ApJ, 657, 262
Diemand, J., Kuhlen, M., Madau, P., Zemp, M., Moore, B., Potter, D., & Stadel, J. 2008, Nature, 454, 735
Dunkley, J., et al. 2009, ApJS, 180, 306
Dutton, A. A., van den Bosch, F. C., Dekel, A., & Courteau, S. 2007, ApJ, 654, 27
Frebel, A., et al. 2005, Nature, 434, 871
Haiman, Z., Rees, M. J., & Loeb, A. 1997, ApJ, 476, 458
Ibata, R. A., Lewis, G. F., Irwin, M. J., & Quinn, T. 2002, MNRAS, 332, 915
Klypin, A., Zhao, H., & Somerville, R. S. 2002, ApJ, 573, 597
Koposov, S., et al. 2008, ApJ, 686, 279
Kravtsov, A. V., Gnedin, O. Y., & Klypin, A. A. 2004, ApJ, 609, 482
Larson, R. B. 2005, MNRAS, 359, 211
Madau, P., Diemand, J., & Kuhlen, M. 2008, ApJ, 679, 1260
Metcalf, R. B., & Madau, P. 2001, ApJ, 563, 9
Moore, B., Diemand, J., Madau, P., Zemp, M., & Stadel, J. 2006, MNRAS, 368, 563
Orban, C., Gnedin, O. Y., Weisz, D. R., Skillman, E. D., Dolphin, A. E., & Holtzman, J. A. 2008, ApJ, 686, 1030
O'Shea, B. W., & Norman, M. L. 2007, ApJ, 654, 66
Ricotti, M., & Gnedin, N. Y. 2005, ApJ, 629, 259
Schneider, R., Ferrara, A., Natarajan, P., & Omukai, K. 2002, ApJ, 571, 30
Simon, J. D., & Geha, M. 2007, ApJ, 670, 313
Somerville, R. S. 2002, ApJ, 572, L23
Strigari, L. E., Bullock, J. S., Kaplinghat, M., Simon, J. D., Geha, M., Willman, B., & Walker, M. G. 2008, Nature, 454, 1096
Strigari, L. E., Bullock, J. S., Kaplinghat, M., Diemand, J., Kuhlen, M., & Madau, P. 2007, ApJ, 669, 676
Tollerud, E. J., Bullock, J. S., Strigari, L. E., & Willman, B. 2008, ApJ, 688, 277
Tumlinson, J. 2007, ApJ, 665, 1361
Weinmann, S. M., Macció, A. V., Iliev, I. T., Mellema, G., & Moore, B. 2007, MNRAS, 381, 367

GALAXY EVOLUTION: EMERGING INSIGHTS AND FUTURE CHALLLENGES
ASP Conference Series, Vol.
@jourvol, © 2009
S. Jogee, I. Marinova, L. Hao, and G. A Blanc

Star Formation Histories and Stellar Mass Growth out to $z > 1$

Kai G. Noeske

W.M. Keck Foundation Postdoctoral Fellow

Harvard-Smithsonian Center for Astrophysics

Abstract. The deepest multi-wavelength surveys now provide measurements of star formation in galaxies out to $z > 1$, and allow to reconstruct its history for large parts of the galaxy population. I review recent studies, which have consistently revealed a picture where galaxy star formation rates and their evolution are primarily determined by galaxy mass. Unless they undergo a quenching of their star formation, galaxies of similar masses have very similar star formation histories, which turn out to be relatively smooth: star formation rates decline with redshift in a primarily gradual manner, while typical starburst episodes have only a modest amplitude that barely evolves.

I discuss how the found relations and their redshift evolution can provide an observed reference star formation history as a function of galaxy mass.

The observed amplitudes and timescales of galaxy star formation are not fully reproduced by current theoretical models, and are a promising testbed to improve the assumed baryon physics. However, measurements of star formation rates in distant galaxies need to be treated with caution. Near-future data, methods and instruments will help us to improve on calibrations and sensitivities for high redshift star formation.

1. Star Formation and the Deep Multi-Wavelength Surveys

Star formation (SF) is responsible for most of those galaxy properties that we can currently measure out to high z: luminosities, spectral energy distributions, morphologies. Understanding the history and physics of SF is fundamental for the understanding of baryons in galaxies, and also for many other fields of astrophysics: the cosmic evolution of gas and metals, the extragalactic background light, and cosmological tests that rely on galaxies' clustering and number densities to illuminate the evolution of Dark Matter structure.

Studies of SF histories have been dramatically advanced by the recent arrival of deep, multi-wavelength surveys like GOODS, AEGIS and COSMOS. Their sensitivity allows to observe all galaxies down to masses below typical $L^\star$ systems out to $z > 1$, providing a comprehensive picture of their evolution. Their variety of multi-wavelength data, especially the Spitzer IRAC and MIPS $24\mu m$ data, have much improved the measurements of SF rates (SFR) and stellar masses ($M_\star$) in distant galaxies, where dust extinction corrections are challenging to measure (e.g. Daddi et al. (2007)).

In the following, I summarize the first broad-brushed, but comprehensive and new picture of SF in field galaxies that the deep surveys have just revealed: SF was predominantly not driven by an evolution of strong starbursts, but

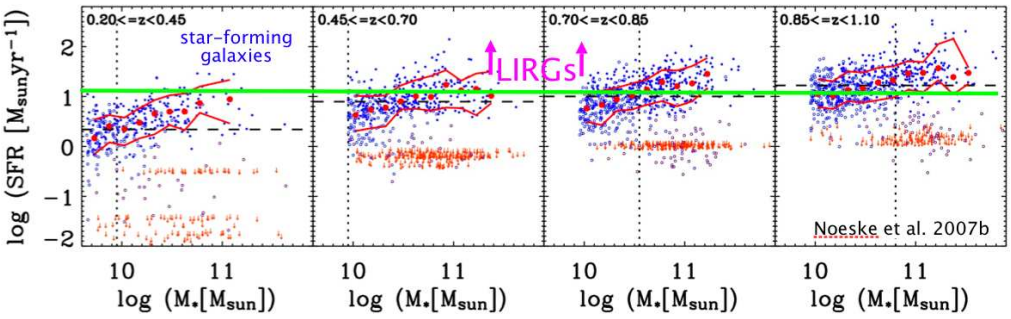

Figure 1 Log(SFR) vs log($M_\star$) for 2905 galaxies in AEGIS, in the $M_\star$ range where the data are $> 80\%$ complete. See Noeske et al. (2007a) for details. The *dotted vertical line* marks $> 95\%$ completeness. *Filled blue circles:* Combined SFR from MIPS 24μm and DEEP2 emission lines. *Open blue circles:* No 24μm detection, blue $U - B$ colors, SFR from extinction-corrected emission lines. *Purple circles:* as open blue circles, but red $U - B$ colors, mostly LINER/AGN candidates. *Orange down arrows:* No robust detection of $f(24\mu\text{m})$ or emission lines; conservative SFR upper limits shown. There is a distinct "Main Sequence" formed by fiducial SF galaxies (open and filled blue circles); galaxies with little or no SF lie below this sequence. Red circles: median of log(SFR) in mass bins of 0.15 dex for Main Sequence galaxies (blue circles). Red lines include 34% of Main Sequence galaxies above and 34% below the median of log(SFR), $\pm 1\sigma$ in the case of a normal distribution. *Horizontal black dashed line:* SFR corresponding to the 24μm 80% completeness limit at the center of each z bin. 24μm-detected galaxies above the *green line* are LIRGs.

gradually declining on mass-dependent scales (Noeske et al. 2007a,b; Elbaz et al. 2007; Daddi et al. 2007). This picture ties together some separate key results of the preceding decade, that (i) the comoving SF rate (SFR) density of the Universe has decreased by about an order of magnitude since $z = 1$ (Madau et al. 1996; Hopkins 2004), (ii) that many distant galaxies had high SFR that are unusual today, and (iii) that the average SF history of galaxies is a strong function of their mass (Cowie et al. 1996; Heavens et al. 2004; Juneau et al. 2005), a phenomenon dubbed "Downsizing" (Cowie et al. 1996).

Most of the following discussion is based on the AEGIS survey (Davis et al. 2007). For more details, see (Noeske et al. 2007a,b).

2. A Star Formation Rate-Stellar Mass Relation ("Galaxy Main Sequence") out to $z \sim 2$

The evolution of SFR as a function of $M_\star$ and z is summarized in Figure 1, adapted from Noeske et al. (2007a). Shown are data from the AEGIS survey from $z = 0.2$ to 1.1. SFR are derived from Spitzer $24\mu m$ photometry and DEEP2 emission lines (Weiner et al. 2007), $M_\star$ from optical DEEP2 and NIR photometry (Bundy et al. 2006). For other SFR tracers and calibrations, the results are consistent, with small quantitative systematic differences.

The star-forming galaxies (blue symbols, predominantly late type morphologies, mostly blue $(U - B)$ colors) segregate from those with no measurable SF (red symbols; early types; red $(U - B)$ colors) and the galaxies with weak emission lines that are likely to have some residual SF (Schiminovich

et al. 2007) or to be LINER/AGN-powered (purple; mostly early types; red $(U-B)$ colors). See the caption of Figure 1 or Noeske et al. (2007a).

Importantly, the SF galaxies form a defined relation between SFR and $M_\star$ over the whole z range, with a spread in SFR at a given $M_\star$ and z that is crudely log-normal with a 1σ width of $\lesssim 0.3$ dex (after correction for minimal estimates of SFR errors) at all z. Such a relation had been known at $z \sim 0.1$ (Brinchmann et al. 2004), and its existence to $z > 1$ (Noeske et al. 2007a) was confirmed by Elbaz et al. (2007). Recently, Daddi et al. (2007) reported this relation with a similar spread in SFR at $z \sim 2$. Detailed studies at $z \sim 0.1$ are given in Schiminovich et al. (2007) and Salim et al. (2007). While the scatter in SF remains roughly constant at all observed z, the above authors find the SFR at a given $M_\star$ to decrease by a factor of $\sim 6(20)$ from $z = 1(2)$ to 0 (Noeske et al. 2007a; Elbaz et al. 2007; Daddi et al. 2007).

For reasons explained in Section 4., we nicknamed the SFR-$M_\star$ relation the "Galaxy Main Sequence (GMS)".

3. Implications of the Galaxy Main Sequence: A New Picture of Star Formation in Field Galaxies since $z \sim 2$.

The surprising persistence of an equally sharp relation between SFR and $M_\star$ out to $z \sim 2$, or over 10 Gyr in lookback time, has profound implications for SF in field galaxies over most of the cosmic time. These were first discussed in Noeske et al. (2007a) (and already in part in Zamojski et al. (2007)), and pertain only to star-forming galaxies on the SFR-$M_\star$ relation (and in the z-dependent $M_\star$ range where we are complete), not to those where SF was shut down by still debated processes (cf. Faber et al. (2007)).

1) Galaxies of equal mass must have had similar SF histories, else the scatter in SFR along the GMS would increase with time. The smoothness of the dependence of SFR on $M_\star$ suggests that we observe a generic mode of galaxy-wide star formation, possibly dominated by the same set of few physical processes over several decades in galaxy mass.

2) The 1σ spread of SFR at a given $M_\star$ and z is $\lesssim \pm 0.3$ in log(SFR), and remains roughly equally narrow out to $z \sim 2$. This finding limits the amplitude and duty cycles of typical variations in SFR that galaxies can have experienced over the past 10 Gyr: statistically, a galaxy spent 2/3 of its time within a factor of 2 of its typical SFR at that z. If some galaxies underwent stronger variations, causing much of the observed scatter, then the remaining majority of galaxies must have had even smoother SF histories. These limits on SFR variations constrain the effect of galaxy interactions on galaxy SFRs; they are consistent with theoretical predictions of the influence of frequent minor interactions (Somerville et al. 2001), and constrain the longer-term $(10^8 - 10^9\,\mathrm{yr})$ enhancement of SFR (e.g. Cox et al. (2006)) by major mergers to a modest factor.

3) The factor by which the SFR along the GMS have decreased since ~ 2 (see Section 2.) is much larger than the amplitude of typical SFR variations. The *dominant* process in the evolution of SF over the past 10 Gyr was hence *a gradual decline of SFR in individual galaxies*, with at most modest variations that were superposed on that smooth decline. It is especially noteworthy that these SFR variations seem to have the *same relative amplitude* (factor) at all

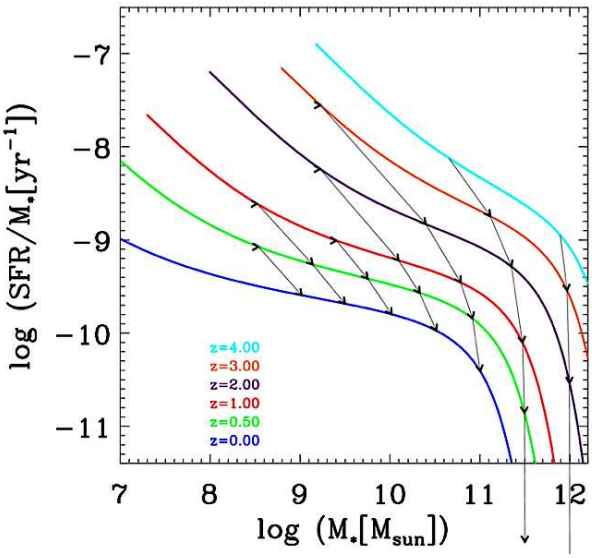

Figure 3 Isochrones in the log(specific SFR) - log(stellar mass) plane for the mass-dependent τ models presented in Noeske et al. (2007b). Isochrones range from $z = 0$ to 4 from bottom to top; the arrows are evolutionary tracks for galaxies of different masses. Note the substantial stellar mass growth due to SF over time: galaxy properties cannot simply be compared for galaxies of equal stellar mass at different z, but require corrections for this mass growth (Noeske et al. 2009, in preparation).

z: out to $z \sim 2$, episodic SF variations or starbursts played a minor, barely evolving role in the SF history of the Universe, and of typical galaxies. This result is contrary to the formerly popular hypothesis that the evolution of SF might be driven by increasingly frequent strong starbursts at higher z.

The effect of galaxy interactions on SFR has now been measured for galaxies in major and minor mergers, and close pairs (Lin et al. (2007); Robaina et al. (2009), and this conference; Jogee et al. (2009), and this conference). These studies have consistently shown a mild enhancement of SFR: SFR distributions of interacting samples are shifted to $\lesssim 2\times$ larger values than those of isolated control samples. This limits the fraction of $M_\star$ formed at intermediate z to $\lesssim 10\%$ (Robaina et al. (2009), and this conference).

Finally, Figure 1 (green line) reveals the origin of the strong number density increase of Luminous Infrared Galaxies (LIRGs) with z: apparently, galaxies become IR-luminous due to their generic, gradual evolution of star formation, where SFR (and hence likely their dust extinction) increase with z. This supports studies (Bell et al. 2005; Melbourne et al. 2005) that found LIRGs at intermediate z to have mostly regular, disk-like morphologies and suggested that LIRGs are a universal phase in the intrinsic, gradual evolution of many galaxies.

4. The Galaxy Main Sequence: The Stellar Main Sequence - Equivalent for Galaxies

The results I summarized in Section 2. reveal a fundamental role of the SFR-$M_\star$ relation: because galaxies of equal mass have similar SF histories, they must evolve along similar tracks in the SFR - $M_\star$ plane. The SFR - $M_\star$ relation at a given z must therefore mark the point on each mass-dependent evolutionary track across the galaxy mass spectrum at that z: it is an *isochrone* cutting across the evolutionary tracks at a given time. See Figure 2, where this is shown for the equivalent case of specific SFR vs $M_\star$ at different z.

This is analog to another important isochrone in astrophysics - the Hertzsprung-Russell Diagram, which is a superposition of the mass-dependent stellar evolutionary tracks. In this picture, the galaxies' SFR-$M_\star$ relation is the analog of the stellar main sequence, where regular, active evolution, driven by the same set of physical processes in an undisturbed system, proceeds until a change in physics moves the object to its red late stages and passive end stadium (the "red and dead" galaxies). Incidentally, the galaxies' '"Main Sequence Turnoff" occurs systematically earlier for more massive galaxies (e.g. Bundy et al. (2006)), similar to stars.

These similarities led us to adopt the term "Galaxy Main Sequence", and the GMS is as fundamental to the understanding of galaxy evolution as the stellar MS to stellar physics: from the GMS at different z, we can recover the mass-dependent SF histories of galaxies. In Noeske et al. (2007b), we presented a first simple, parametric approach: The evolution of the GMS was modeled by simple, smooth model SF histories, justified by the dominance of the smoothly declining component of SF histories (Section 2.). We chose exponential SF histories ("τ models"), given their previous success for many applications; both parameters, the e-folding time τ and the "formation redshift" z_f where SF begins, were allowed to depend on the galaxies' "baryonic mass" as power laws [1]. This model reproduces the evolution of SFR and $M_\star$ on the GMS up to $z = 1.1$ remarkably well, and can attribute the scatter of SFR along the GMS to scatter in SF history parameters at a given mass (see Noeske et al. (2007b), Figure 1), suggesting an even smaller role of episodic or bursty SF. These τ models are the first parametrization of the mass-dependent SF histories of galaxies.

Figure 2 shows the τ models (colored lines) in the specific SFR (SFR normalized by $M_\star$) vs $M_\star$ plane. It is equivalent to the SFR-$M_\star$ plane, essentially with the MS rotated clockwise. For illustration, the model GMS is extrapolated out to $z = 4$; note that the models are only constrained by data to $z \sim 1$. The evolutionary tracks (black arrows) reveal substantial mass growth due to SF with redshift for all but the most massive galaxies, also found by independent methods (Conroy et al. 2007; Zheng et al. 2007). Comparing galaxies of equal $M_\star$ at different z is therefore generally not justified: one may compare very different objects. Instead, one needs to compare galaxies on the same evolutionary track, i.e. apply a mass correction that can for the first time be inferred from the τ models discussed above, or future refined parametrizations.

5. A Delayed Onset of Efficient Star Formation in Less Massive Galaxies

Interestingly, the τ model fits required both τ and z_f to be mass-dependent: Less massive galaxies had not only longer τ, i.e. a slower decline of SF, SF being less efficient and having lower initial SFRs; they also had systematically

[1] Note that the mass in Noeske et al. (2007b) is the "baryonic mass" of a closed box model. Since galaxies are not closed boxes, this mass will depend in a complicated way on the galaxies' actual (baryonic/dark/total/dynamical) masses. This "mass" merely acts as a dummy parameter to generate evolutionary tracks that correctly reproduce the data on SFR and $M_\star$ vs z, by keeping track of the stellar mass growth due to a SF history. These tracks can however easily be linked to actual stellar masses at any observable z, through the $M_\star$ they generate at a given z.

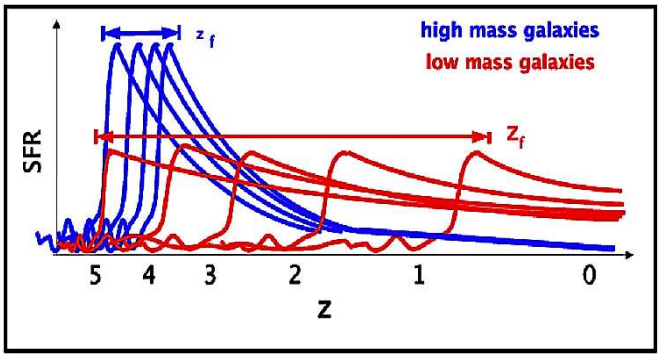

Figure 3 Simplified cartoon sketch of the concept of *"staged galaxy formation"* (Noeske et al. 2007b): In massive galaxies, SF declines on short timescales and begins to be efficient at high z. In less massive galaxies, SF declines not only more slowly; many low mass galaxies are also inefficient at forming stars at high z and attain sustained efficient SF only at lower z.

later z_f, equivalent to a later onset of SF. The observed "Downsizing" in SF galaxies is apparently a combination of both phenomena.

The late z_f are required to account for the high specific SFR (SFR/$M_\star$) of a majority of sub-$L_\star$ galaxies at $z \gg 0$ (see Figure 2 in Noeske et al. (2007b). These imply "doubling times" much shorter than the age of the Universe, i.e. these galaxies cannot have formed stars at their observed rate without overproducing their stellar mass. The usual explanation for high specific SFR, starburst events on top a lower SFR history, is not physical because a majority of all such galaxies would need to simultaneously undergo a stochastic event, and is also in contradiction with other observations - see Noeske et al. (2007a) for details. In a substantial fraction - but not necessarily all - of less massive galaxies, SF must hence have been inefficient at early times and only attained sustained efficiency later than in more massive galaxies (cf. Figure 3).

This mass-dependence of the onset of efficient SF, dubbed "Staged Galaxy Formation" (Noeske et al. 2007b), is consistent with the observed presence of very old stars — roughly a Hubble time — in the majority of Local Group dwarf galaxies and other resolved systems. Our data on SF to $z \sim 1$ only indicate that SF was inefficient, not absent, in less massive galaxies, allowing for some old stars; (ii) efficient SF only needs to delayed in the majority, but not all of such galaxies; (iii) our data do not probe galaxies down to true dwarf masses.

This systematic delay of efficient of SF in less massive galaxies is not likely to be an artifact of SFR measurement errors. It is consistent with statistical studies of galaxy SF histories from independent methods - the evolution of stellar mass functions and the fossil record in stellar populations of low z galaxies; cf. Conroy et al. (2007), especially Figure 6; Zheng et al. (2007); Panter et al. (2007).

6. Constraints to Galaxy Formation Models, and Uncertainties of SFR Measurements

The various data on SFR and $M_\star$ out to $z > 2$ have become an important testbed for theoretical work on galaxy formation, and help to improve the treatment of the complicated and numerically expensive baryon physics. Current models of galaxy populations do generally reproduce the SFR-$M_\star$ relation with a slope and scatter similar to the observed one (Elbaz et al. 2007; Daddi et al. 2007; Davé et al. 2008).

Two types of discrepancies seem however to be universal between the data and models: On the one hand, models underpredict the redshift evolution of SFR for galaxies on the GMS. It is currently debated whether this results from systematic errors in SFR measurements at high z, problems of model physics, or both (Elbaz et al. 2007; Daddi et al. 2007; Davé et al. 2008). On the other hand, the delay of efficient SF in less massive galaxies is not correctly reproduced by current models (Cirasuolo et al. 2008; Marchesini et al. 2008; Fontanot et al. 2009). Found from independent data and methods (Section 5.), this difference is probably physical and likely due to not yet fully understood baryonic physics (Neistein et al. 2006) that renders SF or its fueling processes inefficient at early times in low mass halos.

While observed galaxy SFR across most of the cosmic time have provided new key information for many purposes, considerable work is still necessary (and underway!) to improve their calibrations and systematics (see, e.g. Salim et al. (2009)), improve restframe IR coverage with Herschel, ALMA and JWST. In addition, systematics like the adopted stellar IMF and extinction curves can be tested from non-standard derivations of SFR (Conroy et al. 2007; Chen et al. 2009).

Acknowledgments. This work received funding through grants from the W.M. Keck Foundation, NASA and NSF and is based on observations with the W.M. Keck Telescope, the Hubble Space Telescope, the Spitzer Space Telescope, the Galaxy Evolution Explorer, the Canada France Hawaii Telescope, and the Palomar Observatory.

References

Bell, E. F., et al. 2005, ApJ, 625, 23
Brinchmann, J., Charlot, S., White, S. D. M., Tremonti, C., Kauffmann, G., Heckman, T., & Brinkmann, J. 2004, MNRAS, 351, 1151
Bundy, K., et al. 2006, ApJ, 651, 120
Chen, Y.-M., Wild, V., Kauffmann, G., Blaizot, J., Davis, M., Noeske, K., Wang, J.-M., & Willmer, C. 2009, MNRAS, 393, 406
Cirasuolo, M., McLure, R. J., Dunlop, J. S., Almaini, O., Foucaud, S., & Simpson, C. 2008, arXiv:0804.3471
Conroy, C., Wechsler, R. H., & Kravtsov, A. V. 2007, ApJ, 668, 826
Cowie, L. L., Songaila, A., Hu, E. M., & Cohen, J. G. 1996, AJ, 112, 839
Cox, T. J., Jonsson, P., Primack, J. R., & Somerville, R. S. 2006, MNRAS, 373, 1013
Daddi, E., et al. 2007, ApJ, 670, 156
Davé, R. 2008, MNRAS, 385, 147
Davis, M., et al. 2007, ApJ, 660, L1
Elbaz, D., et al. 2007, A&A, 468, 33
Faber, S. M., et al. 2007, ApJ, 665, 265
Fontanot, F., De Lucia, G., Monaco, P., Somerville, R. S., & Santini, P. 2009, MNRAS, 987
Heavens, A., Panter, B., Jimenez, R., & Dunlop, J. 2004, Nat, 428, 625
Hopkins, A. M. 2004, ApJ, 615, 209
Jogee, S., et al. 2009, ApJ, 697, 1971
Lin, L., et al. 2007, ApJ, 660, L51
Juneau, S., et al. 2005, ApJ, 619, L135
Madau, P., Ferguson, H. C., Dickinson, M. E., Giavalisco, M., Steidel, C. C., & Fruchter, A. 1996, MNRAS, 283, 1388

Marchesini, D., van Dokkum, P. G., Forster Schreiber, N. M., Franx, M., Labbe', I., & Wuyts, S. 2008, arXiv:0811.1773
Melbourne, J., Koo, D. C., & Le Floc'h, E. 2005, ApJ, 632, L65
Neistein, E., van den Bosch, F. C., & Dekel, A. 2006, MNRAS, 372, 933
Noeske, K. G., et al. 2007a, ApJ, 660, L43
Noeske, K. G., et al. 2007b, ApJ, 660, L43
Panter, B., Jimenez, R., Heavens, A. F., & Charlot, S. 2007, MNRAS, 378, 1550
Robaina, A. R., et al. 2009, arXiv:0907.3728
Salim, S., et al. 2007, ApJS, 173, 267
Salim, S., et al. 2009, ApJ, 700, 161
Schiminovich, D., et al. 2007, ApJS, 173, 315
Somerville, R. S., Primack, J. R., & Faber, S. M. 2001, MNRAS, 320, 504
Weiner, B. J., et al. 2007, ApJ, 660, L39
Zamojski, M. A., et al. 2007, ApJS, 172, 468
Zheng, Z., Coil, A. L., & Zehavi, I. 2007, ApJ, 667, 760

GALAXY EVOLUTION: EMERGING INSIGHTS AND FUTURE CHALLLENGES
ASP Conference Series, Vol.
@jourvol, © 2009
S. Jogee, I. Marinova, L. Hao, and G. A Blanc

The Molecular Gas Content of Massive Spirals at $z = 1.5$

Emanuele Daddi

CEA, Laboratoire AIM - CNRS - Université Paris Diderot, Irfu/SAp, Orme des Merisiers, F-91191 Gif-sur-Yvette, France

Abstract. Following our seminal discovery with IRAM-PdBI of giant molecular gas reservoirs inside two typical, near-IR selected galaxies at $z = 1.5$ (Daddi et al. 2008), we have now observed a total of six $z = 1.5$ galaxies in CO[2-1] and detected all of them. Observations of CO[3-2] in one source strikingly revealed the presence of Milky Way like, low-excitation gas. Higher resolution CO[2-1] observations for two galaxies revealed 10 kpc size, galaxy wide gas extension. The star-formation efficiency for all galaxies resembles that of local spirals. These new results have profound consequences on our understanding galaxy formation and evolution and open major prospective for IRAM and EVLA science that can be already performed before the coming of ALMA.

1. Introduction

A characterization of the molecular gas content inside distant galaxies, the primary ingredient to star formation, is crucial to empirically map the physical processes leading to the formation and evolution of galaxies. This is best probed through the detection of redshifted emission lines of CO. At high redshift, CO lines have been until recently detected only for extreme objects such as bright ($S_{850\mu m} > 5$ mJy) submm-selected galaxies (SMGs; e.g., Genzel et al. 2005; Neri et al. 2003; Greve et al. 2005) and QSOs (e.g., Walter et al. 2003; Maiolino et al. 2007; Riechers et al. 2006). These extreme objects are rare, and presumably non-representative of the typical star forming galaxies at the epoch of galaxy assembly $1 < z < 3$ (e.g., Dickinson et al 2003).

As a groundbreaking result from IRAM, we have recently demonstrated (Daddi et al. 2008) that more typical galaxies are also within reach of detailed investigations already with existing facilities. We observed in a pilot project (Q076) two massive $z \sim 1.5$ galaxies with the IRAM Plateau de Bure Interferometer, searching for the redshifted emission lines from the CO [2-1] transition in the 3mm window and detected both of them. These have been the first CO detection ever of normal near-IR selected, unlensed galaxies in the distant Universe.

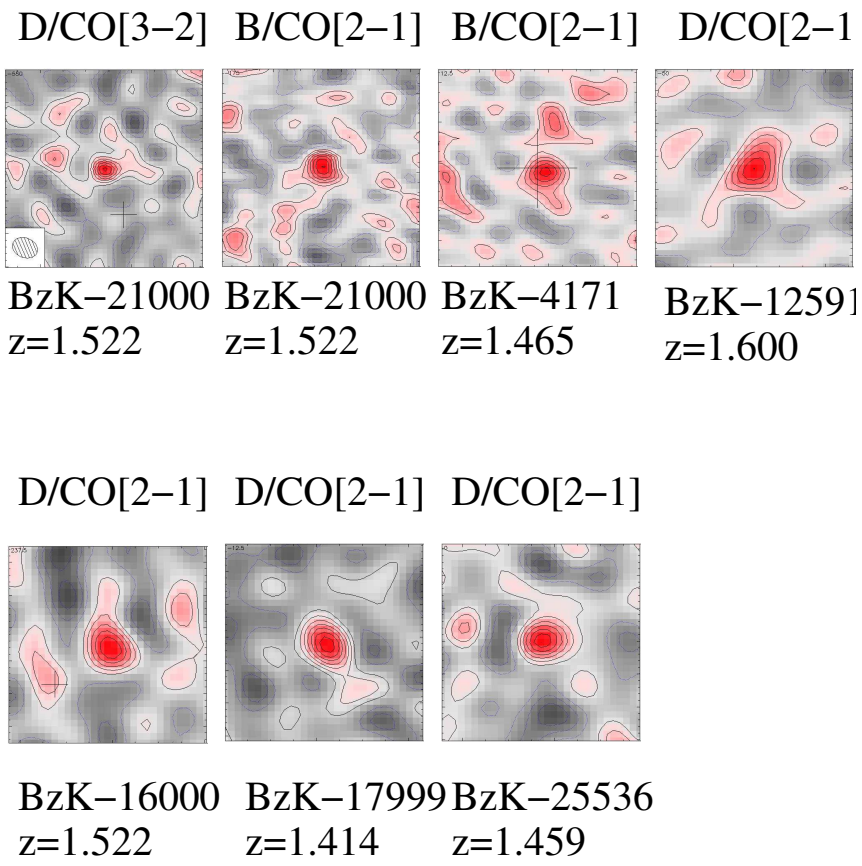

Figure 1. CO detections of the BzK galaxies in our sample. The top labels report the configuration used with IRAM PdBI and the CO transition observed. Bottom labels report the source name and redshift. See Daddi et al. (2008) for the maps of the two original CO[2-1] detections in D-conf for BzK-21000 and BzK-4171. Crosses indicate a 2″ scale at phase center (in some galaxy the pointing was offset from the BzK to allow a reduced attenuation at the position of secondary targets; some of the data were in fact presented in Daddi et al. 2009ab).

2. Low-excitation galaxy-wide gas reservoirs inside typical high-z galaxies

Following these initial discoveries, further observations with the IRAM PdBI have allowed us additional step forwards, allowing much increased understanding of the nature of star formation inside normal disk galaxies at high redshifts:

2.1. Massive high-z galaxies are virtually all hosting giant gas reservoirs

So far, we have observed 6 massive galaxies at $z \sim 1.4$–1.6 in the CO[2-1], securely detecting all of them (Fig. 1). These targets were selected in the near-IR K(2.2μm)-band (sensitive to the stellar mass) and pre-identified as $z \sim 1.5$–2 sources using the BzK technique (Daddi et al. 2004) which is

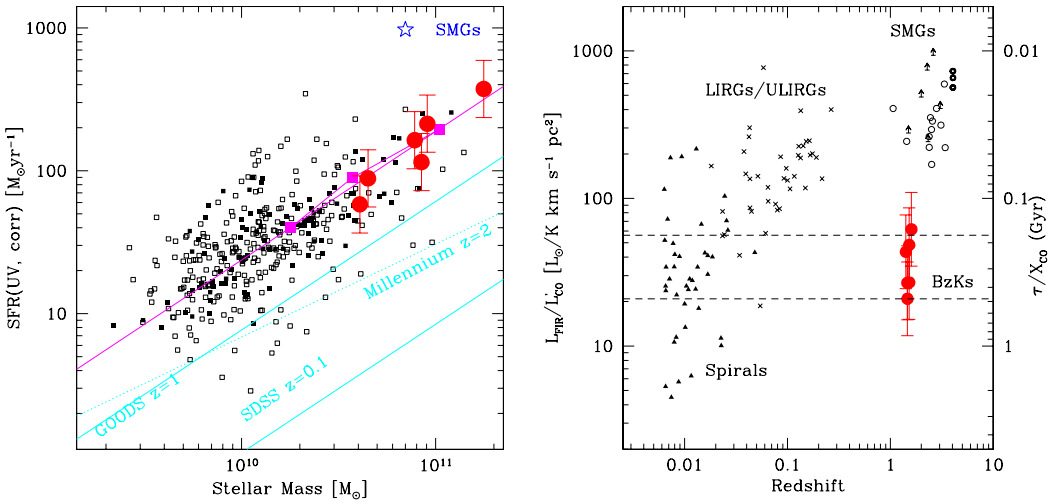

Figure 2. **Left:** the 6 CO detected massive galaxies (red) lie on the stellar mass-SFR correlation (from Daddi et al. 2007 and scaled to a Chabrier IMF) and are typical massive objects at $z \sim 1.5$. **Right:** the star formation efficiency ($\propto L_{\rm FIR}/L'_{rmCO}$) of the 6 CO detected BzK galaxies is similar to that of local spirals and the Milky Way, implying gas exhaustion timescales 10 times longer than in distant SMGs.

based on optical and near-IR colors (i.e., they were *not* pre-selected by means of large $L_{\rm IR}$ or alike). Their stellar mass $\sim$ 0.5–3$\times10^{11} M_\odot$ and SFR $\sim$ 50–300 $M_\odot$ yr^{-1} are typical of bright $K < 20$ BzK selected galaxies placing these sources on top of the $z \sim 2$ mass-SFR correlation (Fig. 2), as opposed to the SFR $\sim 1000-2000$ $M_\odot$ yr^{-1} for SMG which are outliers of the same correlation. These are amongst the most massive $z \sim 1.5$–2 near-IR selected galaxies with ongoing star-formation, but fully typical otherwise, in term of their colors, $E(B-V)$, stellar population properties, etc. Their UV rest-frame morphology shows disk-like galaxies with bright clumps from star formation (Fig. 4), typical of objects at these redshifts. The CO luminosities are ten times larger than what would be predicted by the non-linear correlation between CO luminosity and FIR (Solomon & van den Bout 2005), which appears when combining observations of local spirals with the more highly excited, more luminous systems with more dense gas like local ULIRGs and distant SMGs. The stellar mass to molecular gas mass in our sample is fairly constant, within a factor of 2. Together with our 100% detection rate, this very convincingly demonstrates that virtually all massive high-z galaxies with star formation are very gas rich. Further increasing the sample size is not thus the highest priority next step in this newly opened research field.

2.2. Star formation proceeds at low efficiency

The $L_{\rm FIR}$ to $L_{\rm CO}$ ratios observed in these galaxies (Fig. 2) confirm that star formation at ULIRG rates can be sustained over very long timescales, perhaps up to 0.5–1 Gyr, implying that long-lasting secular evolution is a primary channel

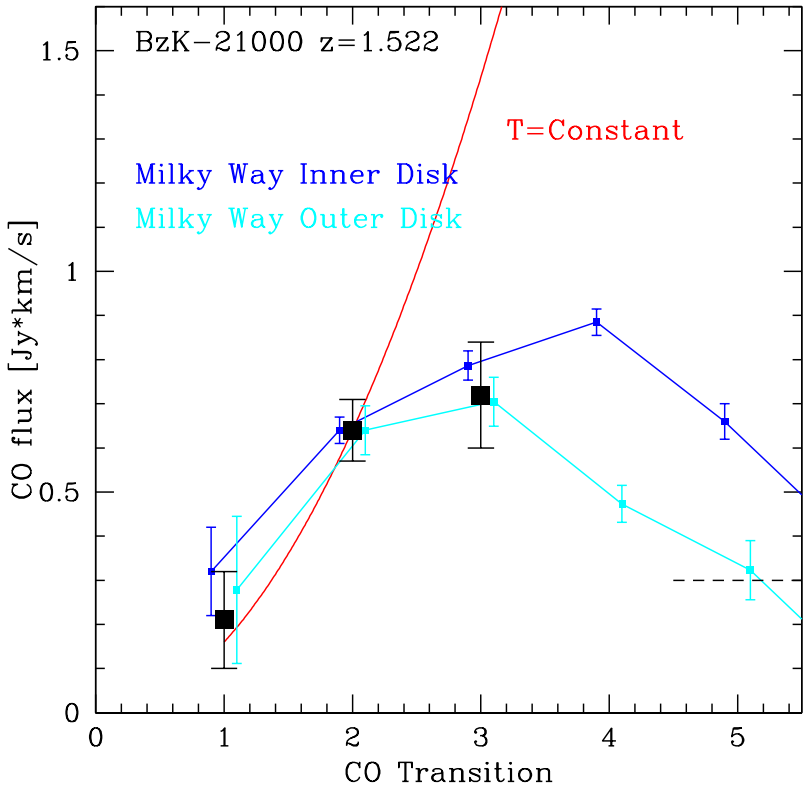

Figure 3. The CO transitions SED of BzK-21000 at $z = 1.522$, from IRAM and the VLA, reveal cold gas excitation properties comparable to the Milky Way and local spirals (Dannerbauer et al. 2009). Such low excitation gas is seen here at high-z for the first time.

for the formation of massive galaxies (Daddi et al. 2005; 2007ab). The SFR of these CO detected sources has been measured by comparing luminosities in the radio continuum (all have reliable detections in our VLA maps), mid-IR and UV, and we conclude with high confidence that it is not strongly overestimated. Direct measurements of their bolometric luminosities will soon be available thanks to ultradeep Herschel observations of the GOODS-North field (PI Elbaz). These accurate measurements of the bolometric luminosities are crucial for a solid interpretation of these findings, and will be uniquely available in the GOODS fields to the necessary depths. We conclude that we have now unveiled *the* major star formation mode for massive high-z sources.

2.3. Discovery of spatially extended, giant gas reservoirs

The re-observations of the two Daddi et al. (2008) sources in CO[2-1] in B-configuration have allowed us a robust detection of both with 1.2″ beam FWHM (Fig. 1; Daddi et al. 2009 in preparation). Analysis of the combined B and D-configuration visibility tables shows obviously extended emission, and allows

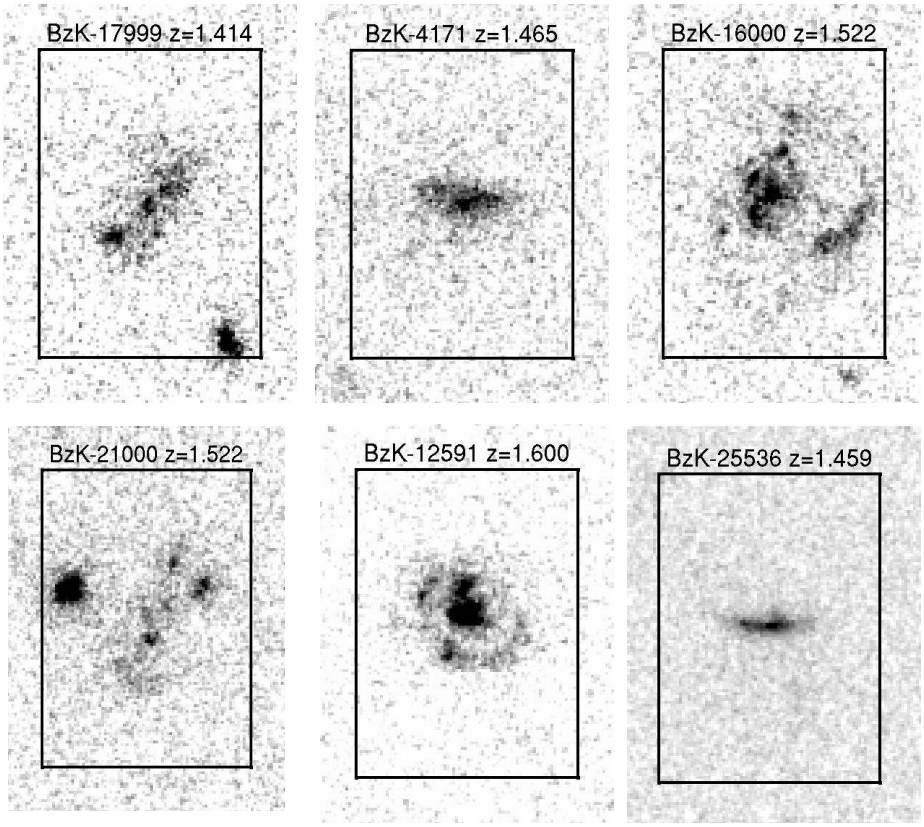

Figure 4. Hubble Space Telescope imaging with the ACS camera and F850LP filter of the 6 CO[2-1] detected galaxies. Boxes are 2x3″

us to obtain solid size estimates for both galaxies of FWHM$\sim 8 \pm 2$ kpc from circular Gaussian fits. While these are just crude size estimates, much higher S/N would be needed to reveal in detail the morphology of CO, this is still the first evidence so far of cosmological sources with such large extensions in the CO emission. The combined B- and D-conf datasets allow much higher S/N spectra of CO[2-1] to be obtained (Fig. 5), revealing the velocity FWHM of the systems and velocity resolved structures like double peaks, pronounced central minima, etc, allowing us to estimate dynamical masses.

2.4. The gas excitation is Milky-Way like

The CO[3-2] and [2-1] fluxes are nearly the same for BzK-21000. Observations of CO[1-0] with the VLA in BzK-21000 and 4171 yielded only 2.5–3σ fluxes which nevertheless imply twice larger L'_{CO} than estimated from CO[2-1]. This implies very low excitation CO SEDs (Fig. 3; Dannerbauer et al. 2009) consistent to the Milky-Way disk (Fixsen et al. 1996), something unprecedentedly seen at high redshift where gas is found to be thermalised up to at least the $J = 3$ transition (Weiß et al. 2007). With star-formation efficiencies and CO excitation properties being similar to local spirals and the Milky Way, it is likely that a Milky-Way type X_{CO} conversion apply to these sources. This would imply molecular gas

reservoirs of $\sim 10^{11} M_{\odot}$ (even neglecting atomic gas) and $f_{\rm gas} \gtrsim 0.6$, consistent with dynamical estimates.

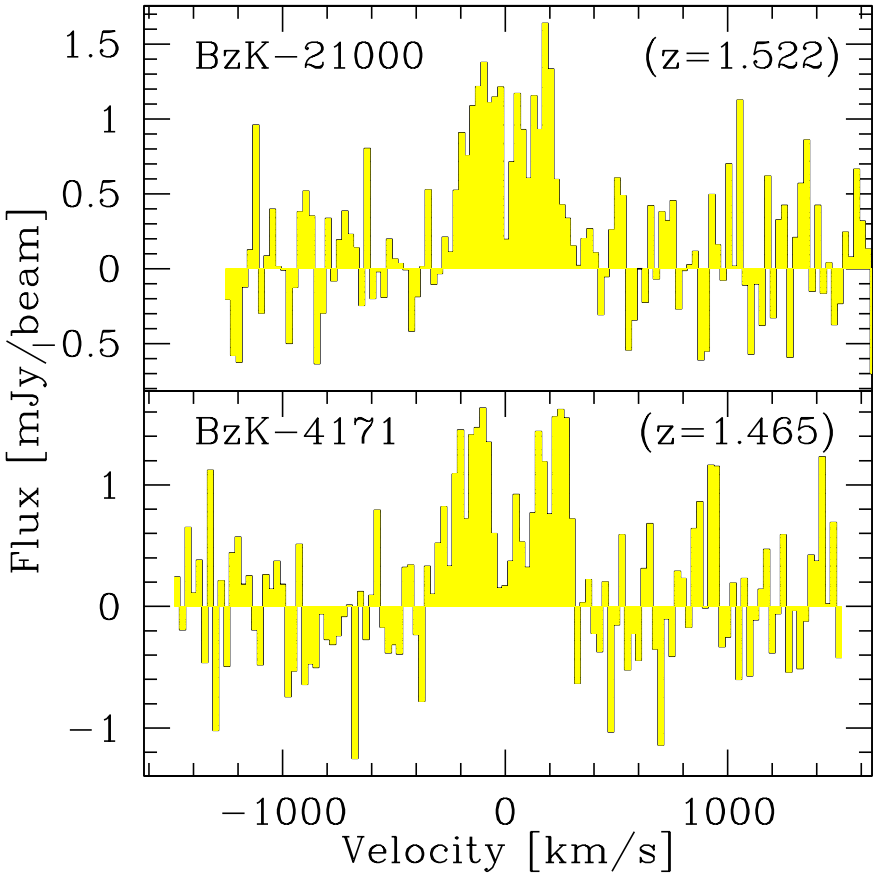

Figure 5. Coadded B-conf and D-conf CO[2-1] spectra of two of the BzK galaxies from our survey, binned at a resolution of 25 km/s. A double horn profile, typical of rotating disks, is clearly detected for BzK-4171 and possible for BzK-21000.

3. Conclusions

We believe that all these findings will have profound implications on our understanding of the physical processes leading to galaxy formation and evolution, with galaxies passing from being predominantly gas dominated to being mostly stars, and are crucial for the planning of ALMA and future facilities for which normal high-z galaxies are high-priority targets. However, some of our major results are still strongly limited by poor statistics: only two galaxies have a CO size estimate and only for one galaxy a CO ratio and thus an excitation estimate is available. Observations of multiple CO transitions in more galaxies and high resolution CO observations from IRAM and EVLA can and should be

obtained for such galaxies in the next few years, paving the way to the arrival of ALMA.

Acknowledgments. I would like to acknowledge the contribution of all collaborators in this work, including in particular H. Dannerbauer, M. Dickinson, D. Elbaz, F.Walter, C. Carilli, D. Riechers, G. Morrison and M. Krips. I acknowledge the funding support of French ANR under contracts ANR-07-BLAN-0228 and ANR-08-JCJC-0008.

References

Daddi, E., et al. 2004, ApJ, 617, 746
Daddi, E., et al. 2005, ApJ, 631, L16
Daddi, E., et al. 2007a, ApJ, 670, 156
Daddi, E., et al. 2007b, ApJ, 670, 173
Daddi, E., et al. 2008, ApJL, 673, 21
Daddi, E., et al. 2009a, ApJ, 694, 1517
Daddi, E., et al. 2009b, ApJ, 695, L176
Dannerbauer, H., et al. 2008, ApJ, 698, L178
Dickinson, M., et al. 2003, ApJ, 587, 25
Fixsen et al. 1999, 526, 207
Genzel, R., et al. 2005, in Multiwavelength Mapping of Galaxy Formation and Evolution, ed. A. Renzini & R. Bender (Berlin/Heidelberg: Springer-Verlag), 112
Neri, R., et al. 2003, ApJ, 597, L113
Greve, T. R., et al. 2005, MNRAS, 359, 1165
Maiolino, R., et al. 2007, A&A, 472, L33
Riechers et al. 2006 ApJ 650 604
Solomon, P. M. & Vanden Bout 2005, ARA&A, 43, 677
Tacconi, L., et al. 2008, ApJ, 680, 246
Walter, F., et al. 2003, Nat, 424, 406
Weiß A., Downes D., Neri R., Walter F., Henkel C., Wilner D. J., Wagg J., & Wiklind T., 2007, A&A, 467, 955

GALAXY EVOLUTION: EMERGING INSIGHTS AND FUTURE CHALLLENGES
ASP Conference Series, Vol.
@jourvol, © 2009
S. Jogee, I. Marinova, L. Hao, and G. A Blanc

A Steep Faint-End Slope of the UV Luminosity Function at $z \sim 2-3$: Implications for the Missing Stellar Mass Problem

Naveen A. Reddy[1,2]

Abstract.
We use the deep ground-based optical photometry of the Lyman Break Galaxy (LBG) Survey to derive robust measurements of the faint-end slope (α) of the UV luminosity function (LF) at redshifts $1.9 \leq z \leq 3.4$. Our sample includes $>$ 2000 spectroscopic redshifts and $\approx$ 31000 LBGs in 31 spatially-independent fields over a total area of 3261 arcmin^2. These data allow us to select galaxies to $0.07L^*$ and $0.10L^*$ at $z \sim 2$ and $z \sim 3$, respectively. A maximum-likelihood analysis indicates steep values of $\alpha(z=2) = -1.73 \pm 0.07$ and $\alpha(z=3) = -1.73 \pm 0.13$. This result is robust to luminosity-dependent systematics in the Lyα equivalent width and reddening distributions, is similar to the steep values advocated at $z \gtrsim 4$, and implies that $\approx 93\%$ of the unobscured UV luminosity density at $z \sim 2-3$ arises from sub-L^* galaxies. We find a factor of $8-9$ increase in the star formation rate density between $z \sim 6$ and $z \sim 2$, due to both a brightening of L^* and an increasing dust correction proceeding to lower redshifts. Combining the UV LF with stellar mass estimates suggests a relatively steep low mass slope of the stellar mass function at high redshift. We show that the previously observed discrepancy between the integral of the star formation history and stellar mass density measurements at $z \sim 2$ may be reconciled by accounting for the lower attenuation of UV-faint galaxies relative to their brighter counterparts, the stellar mass contributed by UV-faint galaxies, and subjecting the stellar mass and star formation rate density estimates to the same limiting luminosity.

1. Introduction

Taken at face value, the integral of the star formation history implies stellar mass densities that are a factor of $2-5$ times larger than the values measured at redshifts $z \gtrsim 1$, commonly refered to as the "missing stellar mass" problem (Wilkins et al. 2008). Several explanations have been put forth to resolve the discrepancy, including an evolution of the star formation rate and stellar mass calibrations typically used at high redshift, or an evolution in the IMF such that it was more top-heavy (or bottom-light) in the past (e.g., Davé et al. 2008). In this contribution, we focus on two additional systematics that may also be important for comparisons between the integrated star formation history and stellar mass density measurements, namely luminosity-dependent

[1]National Optical Astronomy Observatory, 950 N. Cherry Ave., Tucson, AZ 85719

[2]Hubble Fellow

dust corrections and the contribution of UV-faint galaxies to the budget of stellar mass at high redshift.

We start our investigation with a robust measurement of the UV luminosity function (LF) at $z \sim 2-3$. UV emission is a direct tracer of massive star formation, modulo the effects of dust. UV observations of high redshift galaxies are not generally limited by spatial resolution and the deepest observations are up to a factor of $\approx$ 2000 times more sensitive than those at infrared and longer wavelengths. The combination of resolution, sensitivity, and the accessibility of UV wavelengths over almost the entire age of the Universe makes the UV LF a unique tool in assessing the star formation history in a consistent manner. The relative efficiency of UV-dropout selection has enabled a number of investigations of the UV LF at high redshifts based on photometrically-selected samples (Steidel et al. 1999; Adelberger & Steidel 2000; Yan & Windhorst 2004; Bunker et al. 2004; Dickinson et al. 2004; Bouwens et al. 2007; Sawicki & Thompson 2006; Reddy et al. 2008; Ouchi et al. 2004; Beckwith et al. 2006; Yoshida et al. 2006).

Apart from the uncertainties that can be constrained from photometry alone, such as photometric errors and field-to-field variations, spectroscopy is a critical means of quantifying several important systematics that can affect the LF. These include contamination from low redshift objects and high redshift AGN/QSOs, attenuation of UV emission due to the opacity of the intergalactic medium (IGM), and the perturbation of galaxy colors due to Lyα, reddening, and the stellar population ages of galaxies. The relevance of these systematic effects is underscored by the fact that while there are numerous studies of the UV LF, the results have been inconsistent, both at low ($z \lesssim 3$; e.g., Reddy et al. 2008; Le Fèvre et al. 2005) and at high ($z \gtrsim 4$; Beckwith et al. 2006; Bouwens et al. 2007) redshifts.

In practice, high redshift spectroscopic surveys have been limited to UV-bright galaxies, but our knowledge of the properties of these bright galaxies can be used to understand the systematic effects that can affect our computation of the faint-end slope of the UV LF. We provide a brief description of the survey of star-forming galaxies at $z \sim 2-3$ and the computation of the UV LF taking into account some of the systematics mentioned above. We proceed then to discuss the implications of our results on the UV LF for the dust corrected star formation rate densities at $z \sim 2-3$, the budget of stellar mass at these redshifts, and a possible resolution for the problem of missing stellar mass.

2. Sample

The data that form the basis for our computation of the UV LF are from the Lyman Break Galaxy (LBG) survey discussed in Steidel et al. (2003, 2004). Galaxies are selected via their rest-frame UV colors using the LBG or "BX" color criteria. At present, the survey includes 31000 photometrically-selected galaxies spread across 31 spatially-independent fields across the sky over a total area of 0.9 square degrees. While the spectroscopic sample of $>$ 2000 galaxies with $1.9 \leq z_{\rm spec} < 3.4$ is limited to galaxies with $\mathcal{R} < 25.5$, the photometric sample includes galaxies as faint as $\mathcal{R} \sim 27.0$. Full details on the 31 fields of

the survey and the photometry and spectroscopy are provided in Steidel et al. (2003, 2004) and Reddy et al. (2008); Reddy & Steidel (2009).

3. UV Luminosity Functions at $z \sim 2-3$

Our calculation of the luminosity function uses a maximum-likelihood method that takes advantage of the full photometric sample of LBGs and takes into account a number of non-uniform sources of error including photometric error. The fractions of star-forming galaxies and AGN at low redshifts, as well as AGN/QSOs at the redshifts of interest, as determined from the spectroscopic sample, are used to correct the number counts when computing the LF for star-forming galaxies between $1.9 \leq z < 3.4$. The details of the initial computation of the UV LF to our spectroscopic limit of $\mathcal{R} = 25.5$ is provided in Reddy et al. (2008). To extend these results to the faint-end of the UV LF, we ran detailed simulations of the how the systematic effects induced by Lyα emission and luminosity-dependent reddening affect our incompleteness corrections at the faint-end. These results are presented in Reddy & Steidel (2009). Our final determinations of the UV LFs at $1.9 \leq z < 2.7$ and $2.7 \leq z < 3.4$ are shown in Figure 1.

Our determinations of the bright-end of the UV LFs to $M(1700\ \text{Å}) = -18.83$ and -19.52 at $z \sim 2$ and $z \sim 3$, respectively, incorporate data over 3261 arcmin^2 in 31 spatially-independent fields. Data from 22 fields and 2239 arcmin^2 are used to constrain the LFs at $-18.83 \leq M(1700\ \text{Å}) < -18.33$ and $-19.52 \leq M(1700\ \text{Å}) < -19.02$ at $z \sim 2$ and $z \sim 3$, respectively. Finally, data from 6 fields and 317 arcmin^2 are used to constrain the LF in the faintest magnitude bin to $M(1700\ \text{Å}) = -17.83$ and -18.52 at $z \sim 2$ and $z \sim 3$, respectively. Based on these data, we find best-fit faint-end slopes of $\alpha(z = 2) = -1.73 \pm 0.07$ and $\alpha(z = 3) = -1.73 \pm 0.13$, using data extending to $0.07L^*_{z=2}$ and $0.1L^*_{z=3}$. Within the errors, the UV LFs at $z \sim 2$ and $z \sim 3$ are indistinguishable. However, comparing our results with those at higher redshifts points to a significant evolution of the UV LF that can be accommodated by a brightening of L^* from $z \sim 6$ to $z \sim 2$. The faint-end slope of the UV LF is essentially constant and steep between these redshifts (Figure 2).

4. Luminosity-Dependent Dust Corrections

The UV LF can be integrated to determine the UV luminosity density. Using an appropriate estimate of the average dust correction applicable for the sample then allows one to estimate the bolometric luminosity or star formation rate density. The canonical extinction correction of $4-5$ has been shown to be valid only for UV-bright galaxies with $\mathcal{R} < 25.5$ (Steidel et al. 1999; Reddy & Steidel 2004; Reddy et al. 2006). These galaxies are bright enough where spectroscopy combined with multi-wavelength observations in the mid-IR and Hα allow us to constrain robustly their dust luminosities (Reddy et al. 2006). Using physically motivated models, Reddy & Steidel (2009) argue that the dust attenuation in UV-faint galaxies is likely to be lower than for their UV-bright counterparts. Hence, the mean attenuation correction applied to the UV luminosity density will depend on how far one integrates down the UV LF to obtain that luminosity

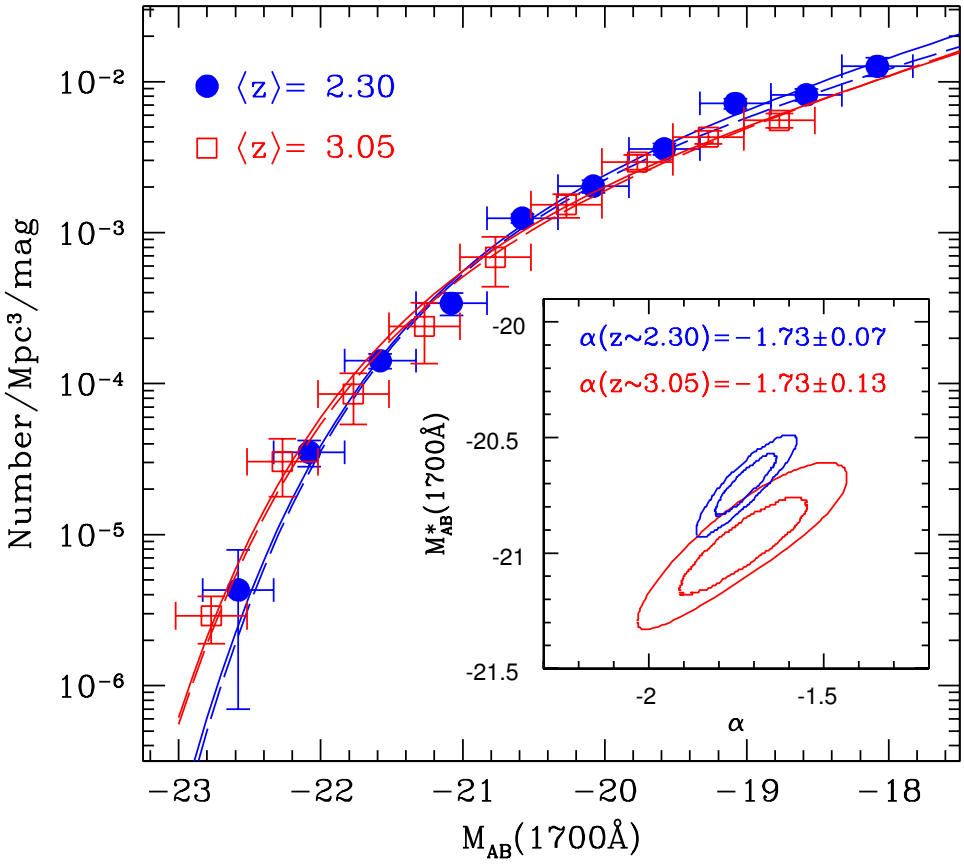

Figure 1. Rest-frame UV luminosity functions of star-forming galaxies at $1.9 \leq z < 2.7$ (*circles*) and $2.7 \leq z < 3.4$ (*squares*), along with the best-fit Schechter functions. The 68% and 95% likelihood contours between M^* and α for our final determinations of the LFs are shown in the inset panel.

density. The luminosity-dependent reddening model, motivated by observations of the UV spectral slope as a function of UV luminosity, implies that when integrated to zero luminosity, the inferred total luminosity density is a factor of ~ 2 lower than what one would infer assuming a constant $4-5$ dust correction (Reddy & Steidel 2009).

5. Stellar Mass Contribution of UV-faint Galaxies at $z \sim 2$

The correlation between star formation rate and stellar mass, and the fact that UV faint galaxies are less reddened than their UV bright counterparts, implies than UV-faint galaxies are also likely to have lower stellar masses than their brighter counterparts. Despite their lower masses, however, such UV-faint galaxies host a stellar mass density that is comparable to that measured for the most massive galaxies at $z \sim 2$ (Reddy & Steidel 2009; van Dokkum et al. 2006). The study of van Dokkum et al. (2006) implies a stellar mass density above 10^{11} $M_\odot$ of $(1.64 \pm 0.45) \times 10^{-4}$, in units of the critical density.

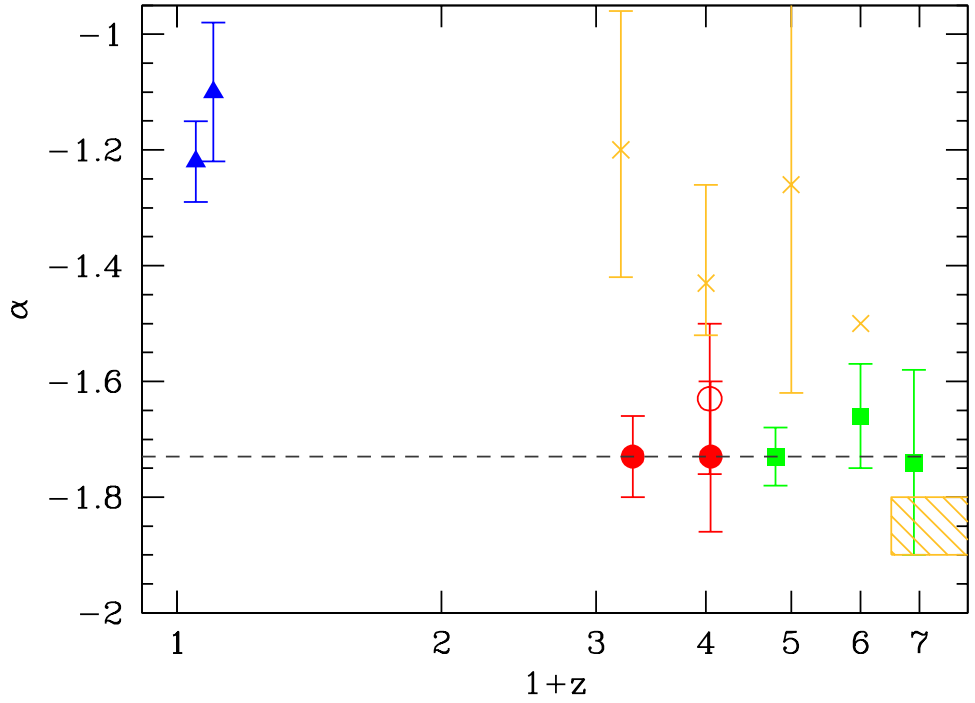

Figure 2. Faint-end slope α as a function of redshift, including our determination at $z \sim 2-3$ (*filled circles*), and those from the literature (Steidel et al. 1999; Bouwens et al. 2007; Ryan et al. 2007).

The value for optically bright galaxies ($\mathcal{R} < 25.5$) and masses $< 10^{11}$ $M_\odot$ is $(3.72 \pm 0.28) \times 10^{-4}$. Finally, the value for optically-faint galaxies ($\mathcal{R} \geq 25.5$) with masses $< 10^{11}$ $M_\odot$ is $(2.06 \pm 0.26) \times 10^{-4}$. This value is restricted to those galaxies that are brighter than 0.08 L^*. From these calculations, we see that UV-faint galaxies contribute significantly to the stellar mass density of galaxies with $L > 0.08$ L^*, making up a larger fraction that the most massive galaxies at these redshifts. We note that stellar mass density measurements based on ground-based near-IR surveys are almost never deep enough to properly sample the low mass end of the stellar mass function at high redshift, and invariably (and incorrectly) suggest that most of the stellar mass density at high redshift is hosted by the most massive galaxies.

6. Comparison of the Integrated Star Formation History and Stellar Mass Density Measurement

It has been suggested recently that our understanding of how galaxies form stars and build up their stellar mass may be seriously flawed based on the observation of missing stellar mass at high redshift. It seems prudent to assess whether such a discrepancy is due to some flaw in our understanding of galaxy evolution, or if it can be attributed to unaccounted systematics. Our observational capabilities make it possible to constrain the luminosity function of galaxies that are significantly fainter than L^*, the characteristic luminosity defined by

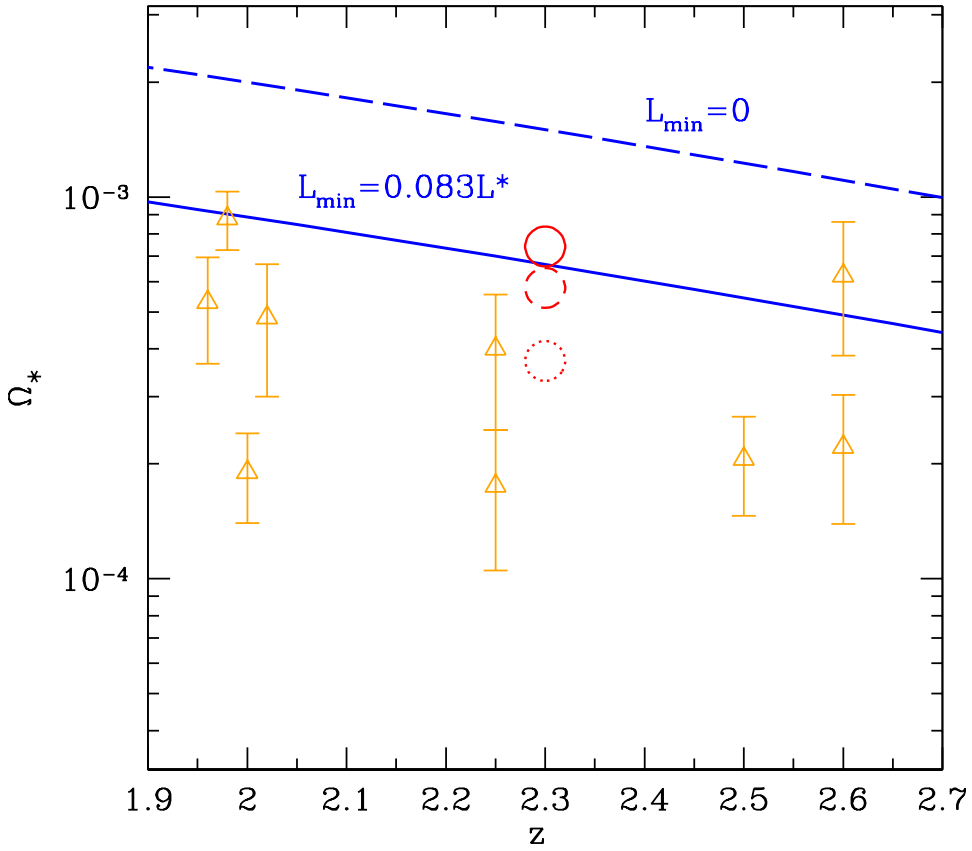

Figure 3. Stellar mass density measurements at $1.9 < z < 2.7$ (*open triangles*) from the following sources: Rudnick et al. (2003); Dickinson et al. (2003); Drory et al. (2005); Pozzetti et al. (2007); Fontana et al. (2003, 2006). All of these studies constrain the stellar mass density over areas that are significantly smaller than the almost 1 square degree probed in this study, and most rely on photometric redshifts. Our estimates at $z \sim 2.3$ are shown by the large circles: *dotted* shows the estimate for UV-bright ($\mathcal{R} \leq 25.5$) galaxies with $M_* < 10^{11}$ $M_\odot$; *dashed* shows the estimate including UV-faint galaxies with $M_* < 10^{11}$ $M_\odot$ to a faint limit of $M_{\rm AB}(1700) = -18.0$; and *solid* denotes the total contribution including massive ($M_* > 10^{11}$ $M_\odot$) galaxies. The stellar mass density inferred by integrating the star formation history to a limit of $0.08L^*$ (same as that used to compute the stellar mass density) is denoted by the solid line. For comparison, the dashed line shows the result when integrating the SFH to zero luminosity.

the "knee" of the luminosity function. Separately, however, observerations are generally insensitive to the low mass slope of the stellar mass function. An underestimation of the low mass contribution to the stellar mass density may therefore be partly responsible for the claimed discrepancy between the integral of the star formation history and stellar mass density measurements. In the previous section, we estimated the total stellar mass contributed by all galaxies with luminosities > 0.08 L^*, and those with stellar masses $> 10^{11}$ $M_\odot$. In order to compare this stellar mass density to the integral of the star formation history,

we must subject the latter to the *same* limiting luminosity of 0.08 L*, keeping in mind that L^* evolves with redshift.

Figure 3 shows the integral of the star formation history (in units of the critical density, Ω^*), both to a limiting luminosity of 0.083 L* and to zero luminosity, along with previous determinations of the stellar mass densities at these redshifts. Our estimate of the total stellar mass density contributed by galaxies with $L > 0.083$ L* (*solid circle*) is in excellent agreement with the integral of the star formation history when the latter is subjected to the same limiting luminosity. This calculation demonstrates the importance of accounting for the observationally well-motivated systematics of a luminosity dependent dust correction and the stellar mass contributed by UV faint galaxies, while adopting the same limiting luminosity. By accounting for these effects, we are able to resolve completely the discrepancy between the integral of the star formation history and the stellar mass density at the very epoch ($z \sim 2$) where the discrepancy was claimed to reach its maximum. Clearly, any reasonably complete description of galaxy evolution must account for the population of the UV faint galaxies that contribute significantly to both the luminosity and stellar mass densities at these redshifts.

Acknowledgments. Support for N. A. R. was provided by NASA through the Hubble Fellowship grant HST-HF-01223.01 awarded by the Space Telescope Science Institute, which is operated by the Association of Universities for Research in Astronomy, Inc., for NASA, under contract NAS 5-26555.

References

Adelberger, K. L. & Steidel, C. C. 2000, ApJ, 544, 218
Beckwith, S. V. W., et al. 2006, AJ, 132, 1729
Bouwens, R. J., et al. 2007, ApJ, 670, 928
Bunker, A. J., et al. 2004, MNRAS, 355, 374
Davé, R. 2008, MNRAS, 385, 147
Dickinson, M., et al. 2003, ApJ, 587, 25
Dickinson, M., et al. 2004, ApJ, 600, L99
Drory, N., et al. 2005, ApJ, 619, L131
Fontana, A., et al. 2003, ApJ, 594, L9
Fontana, A., et al. 2006, A&A, 459, 745
Le Fèvre, O., et al. 2005, Nat, 437, 519
Ouchi, M., et al. 2004, ApJ, 611, 660
Pozzetti, L., et al. 2007, A&A, 474, 443
Reddy, N. A. & Steidel, C. C. 2004, ApJ, 603, L13
—. 2009, ApJ, 692, 778
Reddy, N. A., et al. 2006, ApJ, 644, 792
Reddy, N. A., et al. 2008, ApJS, 175, 48
Rudnick, G., et al. 2003, ApJ, 599, 847
Ryan, Jr., R. E., et al. 2007, ApJ, 668, 839
Sawicki, M. & Thompson, D. 2006, ApJ, 642, 653
Steidel, C. C., et al. 1999, ApJ, 519, 1
Steidel, C. C., et al. 2003, ApJ, 592, 728
Steidel, C. C., et al. 2004, ApJ, 604, 534
van Dokkum, P. G., et al. 2006, ApJ, 638, L59
Wilkins, S. M., Trentham, N., & Hopkins, A. M. 2008, MNRAS, 385, 687
Yan, H. & Windhorst, R. A. 2004, ApJ, 612, L93
Yoshida, M., et al. 2006, ApJ, 653, 988

GALAXY EVOLUTION: EMERGING INSIGHTS AND FUTURE CHALLLENGES
ASP Conference Series, Vol.
@jourvol, © 2009
S. Jogee, I. Marinova, L. Hao, and G. A Blanc

Submillimeter Galaxies

Andrew W. Blain

Caltech, Pasadena, CA91125, USA

Abstract. The Universe was a more exciting place at moderate to high redshifts $z \sim 3$, after reionization took place, but before the present day galaxy properties were firmly established. From a wide variety of directions, we are gaining insight into the Universe at these epochs. Less gas was sequestered into stars and had been ejected into the interstellar medium as weakly emitting, slowly cooling debris, because a significant amount of star formation and supermassive blackhole growth in active galactic nuclei (AGNs) was still to occur. Furthermore, the processes that shape today's galaxies were at work, and can be seen in real time with the appropriate tools. The most active regions of galaxies at these redshifts are deeply obscured at ultraviolet and optical wavelengths by an opaque interstellar medium (ISM) that absorbs most of their radiation, and then re-emits at far-infrared (IR) wavelengths. This emission provides us with a very powerful probe of the regions within galaxies where the most intense activity takes place; both their total energy output, and from spectroscopy, about the physics and chemistry of the atomic and molecular gas that fuels, hides and surrounds these regions. This information is unique, but not complete: radio, mid- and near-IR, optical and X-ray observations each provide unique complementary views. Nevertheless, probing the obscured Universe, with the Atacama Large (Sub-)Millimeter Array (ALMA), *James Webb Space Telescope (JWST)*, *Herschel Space Observatory*, *Wide Field Infrared Survey Explorer (WISE)*, and missions and telescopes that are not yet in construction, like an actively cooled sub-10-m class IR space telescope and a 25-m class ground-based submillimeter/THz telescope (CCAT) will provide a more complete picture of in which neighborhoods, by what means and how quickly the most vigorous bursts of activity take place.

1. Introduction

Even in the local Universe, the bulk of the energy from young stars and AGN is reprocessed by the absorption of optical and UV radiation into the far-IR waveband. The dust and gas responsible are also crucial for cooling gas clouds until they can be accreted onto a protostar or start to fuel an AGN. Even in our relatively quiescent galaxy, in which the luminosity from young stars is three orders of magnitude less than in the most extreme objects (e.g. Coppin et al. 2009), large area surveys of the galactic plane have revealed complex filamentary structure, and provide evidence for the effects of turbulence and magnetic fields, and strong feedback processes from the effects of supernovae and photo-ionization. New features of star formation and feedback are being revealed using both wide-field surveys and more and more powerful interferometers that can probe to angular scales of 10's of AU.

The degree of obscured activity increases with redshift: a larger fraction of all galaxies exceed today's typical luminosity, while the total rate of energy production per unit comoving volume rises by a factor of up to forty (Blain et al. 1999), with a significant excess of power in the far-IR as compared with the optical at $z \simeq 2$. The abundance of galaxies that exceed the *s*lightly artificial definition of being 'ultraluminous', that is exceeding a total luminosity of $10^{12}\,L_{\odot}$, is greater by a factor of over a hundred (see Pope et al. 2009).

2. Discovery of distant ultraluminous infrared galaxies

The first extremely luminous distant objects, the QSOs were discovered by virtue of unusual colors, enabled by powerful spectral features at optical wavelengths. Some of these AGN-powered sources are accompanied by powerful mid- to far-IR emission (e.g Priddey et al. 2008). In fact, when their X-ray emission spectrum is quenched and hardened by gas within the host galaxy, the energy is absorbed by the ISM and appears at far-IR wavelengths. The serendipitous and systematic sifting of the great mine of order 20,000 galaxies discovered at far-IR wavelengths by *IRAS*, the first space-borne all-sky survey in the mid 1980's, revealed a series of extreme galaxies lurking at high redshifts (e.g. Soifer et al. 1994; Irwin et al. 1998), further highlighting the overall importance of far-IR astrophysics, and the existence of powerful galaxies with substantial emission from dust. A decade after the *IRAS* survey was completed, the *FIRAS* instrument on the *COBE* satellite, alongside a very precise measurement of the CMB spectrum (Mather et al. 1990), detected the spectral signature of the sea of unresolved background radiation emitted by the ISM of the sum of all the galaxies throughout cosmic time (Puget et al. 1996).

The presence of more distant galaxies was confirmed with deeper space-borne observations from the *Infrared Space Observatory (ISO)*, and in much greater detail in the soon-to-be-completed cryogenic of the *Spitzer Space Telescope* mission. The modest resolution of space-borne telescopes allows different classes of distant galaxies to be found through atmospheric windows at longer submillimeter wavelengths, where the effect of redshifting the pseudo-thermal spectral peak of galaxies' emission ensures that even galaxies at $z > 5$ can be detected as easily as at $z \sim 1$ for the same SED. On order to rise above the confusion limit, by virtue of their very detection, these submm-selected galaxies (SMGs) are in the ultraluminous class.

The lack of huge samples of very luminous dust-enshrouded galaxies owes to the difficulty of detecting low-energy photons, in the presence of noise from detectors, the atmosphere and in some experiments, to foreground emission from zodiacal dust and the ISM in the Milky Way. A variety of imaging detectors have been fielded in mm/submm-wave atmospheric windows to detect these galaxies: SCUBA, MAMBO, SHARC-2, BOLOCAM and its sister AzTEC, LABOCA and soon SCUBA-2 and MKIDCam.

The description of far-IR or submm-selected galaxies is strictly empirical, as some are very luminous QSOs (e.g. Walter et al. 2009), while others are reasonably bright in optical continuum and emission lines, and some powerful jet-emitting radio galaxies are also powerful emitters of thermal radiation into the far-IR. Others, with similar far-IR properties, however, are extremely faint

with at most only the barest hint of a mutliwavelength counterpart. At $z > 4$, this is especially true, as increasing luminosity distance, decreasing surface brightness, and sampling of increasingly blue continuum all make it tougher to identify counterparts to SMGs at higher redshifts. Systematic redshift surveys are starting to reveal a handful of these most distant examples (e.g. Schinnerer et al. 2008).

3. Existing follow-up studies

The first ultraluminous distant galaxies were identified and pursued for follow-up using existing archive data, and were generally most successful in well-studied deep fields, including rich lensing clusters (Smail et al. 1997, 2002). Substantial (5–20 arcsec) positional uncertainty is imposed due to the large primary beam of single-dish telescopes at long wavelengths, especially as submm telescopes use a pointing model for location rather than reference objects in the field. Deep optical and near-IR imaging inevitably throws up several candidates to match a $z \sim 3$ object. Without a more certain position, obtaining a redshift to enable further study is difficult. Mm/submm-wave spectrometers are becoming available, and future multi-feed instruments could offer a realistic spectral survey capability

Finding redshifts The wide-field high-resolution imaging capability of large radio interferometers allowed the very deep continuum emission, associated with syncrotron emission from electrons accelerated either by supernovae, or additional sources in AGN to provide insight into the positions of likely counterparts (Chapman et al. 2005). With 0.5-deg-wide fields, excellent relative astrometry and sub-arcsec positional accuracy, the combination of deep radio imaging and submm maps has enabled multiobject optical spectroscopy to find a whole range of redshifts. The requirement of a radio detection, and successful optical identification of a redshift, via either emission lines or an array of absorption against an escaping ultraviolet continuum imposes selection effects. Nevertheless, the confirmation that a majority of the SMG population is found at $z < 3$ provides useful insight. The ability to rule out the likelihood of a low-redshift SMG (or one with a cool SED) based on the absence of a radio detection has lead to substantial, but expensive) progress in deep mm-wave interferometer observations to provide precise positions, where excellent multiwavelength surveys can highlight the properties of potential counterparts at the highest redshifts (Younger et al. 2007; Wang et al. 2009).

Follow-up study using molecular line instruments, near-IR spectrographs where lines are found at frequencies that are not blocked by the atmosphere, has provided an excellent preliminary view of the range of properties of galaxies identified and highlighted by way of their far-IR properties (see Tacconi et al. 2008). Near-IR adaptive-optics imaging, mid-IR spectroscopy and X-ray spectroscopy are also enabled or assisted by redshift information.

Inferring total luminosities The smooth modified-blackbody SED of submm-selected galaxies means that a single-band observation provides a relatively poor measure of their total luminosity, especially as their redshift distribution is broad. For a particular color, or set of colors, that reveal the shape of the

broadband spectrum in the observer's frame, an accurate value of $T/(1+z)$ can be inferred, where T is a luminosity-averaged dust temperature; however, in the absence of a known redshift, there is thus unavoidable uncertainty in the dust temperature and the total luminosity L. Almost all deep submm surveys have been carried out in the 850-μm or 1.1–1.3-mm atmospheric windows, that are still on the Rayleigh–Jeans (RJ) tail of the SEDs of typical submm-selected galaxies, with $T \sim 40\,\mathrm{K}$ and $z \sim 2.5$, and so observations at shorter submm wavelengths are much desired. On the RJ tail, the total luminosity $L \propto ST^{\sim 5}$, and so lifting the temperature-redshift degeneracy is important. The SHARC-2 instrument at the Caltech Submillimeter Observatory (CSO) has been very useful for providing accurate SEDs for high-redshift galaxies, to constrain their luminosities (Kovacs et al. 2006; Coppin et al. 2008). The spread in dust temperatures found in low-redshift *IRAS* galaxies, $20\,\mathrm{K} < T < 60\,\mathrm{K}$ appears to continue out to $z \simeq 2$; however, the fraction of the total luminosity that is emitted by radio synchrotron emission appears to increase by a factor of about 2. This implies that the conditions for supernova-accelerated electrons in distant ULIRGs are substantially different than those reflected in the tight far-IR–radio correlation observed at low redshifts (see Blain et al. 2003).

Inferring the environments and masses of parent haloes Existing submm-wave surveys are too small to fully sample even 100-Mpc-scale structures, which require angular extents of at least 3.5 deg at high redshifts. While a clustering power spectrum can be determined on much smaller scales, if a large sample of galaxies is available, mapping out large-scale features individually requires this large area coverage. Furthermore, to identify examples of the richest clusters and the emptiest voids, perhaps in the process of their formation, it is necessary to image a 10-deg^2 area that includes them. A current problem for determining correlation functions from submm surveys is the modest number of low-significance detections that they include. The broad redshift distribution of detected SMGs also acts to reduce the amplitude of clustering signals. Under an assumed redshift distribution, the apparent clustering signal measured from images so far are not reliable. Where reasonably complete redshift distributions are available for detected galaxies, the presence of line-of-sight structures can be inferred, based on the presence of redshift 'associations' with a relative velocity of less than the maximum dispersion of a cluster ($\sim 1200\,\mathrm{km\,s^{-1}}$) (Blain et al. 2004).

Targetting known areas of interest in order to reveal an overdensity of other less-luminous sources has proved to be a successful way of determining the local density of similar sources in the absence of a wide-field survey (e.g. Greve et al. 2007; Priddey et al. 2008; Chapman et al. 2009).

Understanding power sources The spectrum of almost any distribution of dust grain sizes and constituents differs only in detail, whether affecting the long wavelength pseudo-Rayleigh-Jeans slope of the SED, or the relative fraction of hot to cooler dust, which affects the shape of the mid-IR continuum. As a result, the shape of the far-IR continuum SED, while determining the total luminosity of the objects, includes relatively little diagnostic power of the source of this energy. Multiwavelength studies are then required to highlight the true cause, from X-ray observations (Alexander et al. 2005, 2008, this volume), mid-IR low-resolution

spectroscopy indicating the nature of the smallest molecular-size grains (Valiente et al. 2007; Menendez-Delmestre et al. 2006, 2009a), and moderate-to-high-resolution optical, near-IR and mid-IR spectroscopy (Swinbank et al. 2004; Menendez-Delmestre et al. 2009b). Hard X-ray imaging can be used to reveal the presence of a deeply-enshrouded AGN. The results indicate that, unless a substantial fraction of AGNs are surrounded by an ultra-Compton-thick shroud of gas, that most of the luminosity of existing samples of submm-selected galaxies is produced by star-formation activity, with the ratio of X-ray-to-far-IR luminosity being about an order of magnitude less than that found in the most powerful AGN at low redshifts.

Stellar masses and lifetimes Estimates of the molecular gas mass from CO observations set an excellent limit on the duration of a starburst, subject to uncertainties in the initial mass function (IMF), with a very top-heavy IMF perhaps allowing a great deal of power from a modest mass, with little trace left after the activity is over. The molecular gas mass, assuming a CO-to-H_2 ratio, derived from the line intensity, and compared with the line width, assuming an underlying dynamical model, at present typically either a disk or virialized merger remnant, which differ by a factor of two in mass. The timescale is of order 10^8 years, given typical masses of gas and inferred star-formation rate (Tacconi et al. 2008).

Results so far (Smail et al. 2002; Borys et al. 2005; Hainline et al. 2009), greatly assisted by knowledge of redshifts for individual targets (Chapman et al. 2005), indicate that the stellar masses inferred for known high-redshift ULIRGs could also built up at the current rate of activity in about 10^8 years. The masses further indicate that the descendents of the SMGs should be amongst the most massive galaxies today. Larger samples are necessary to underscore these conclusions, but there is an excellent chance that the detection of high-redshift far-IR luminous galaxies at the current flux limits can point the way to the formation of massive galaxies, and allow us to investigating their formation process and environments.

4. Future surveys for powerful dusty galaxies

The Atacama Large (Sub-)Millimeter Array (ALMA) alma.cl ALMA is perhaps the most revolutionary new telescope in the recent history of astronomy. It represents an unprecedented generational leap in capability: an increase in spatial resolution, sensitivity and image fidelity by at least an order of magnitude. It will produce images of the gas and dust, from the solar neighborhood to the most distant galaxies, that beat the images from *HST* in spatial resolution. Furthermore, all ALMA observations will generate a datacube that contains spatially-resolved velocity information, and which thus will reveal the motions of gas in distant galaxies, leading to the precise determination of masses, dynamical timescales, and assessments of the age/state/remaining lifetime for a galaxy interaction. All the targets so far published from surveys at far-IR and submm wavelengths could be observed in considerable detail by ALMA in a matter of minutes.

Herschel Space Observatory and Planck Surveyor The forthcoming launch of the *Herschel Space Observatory*'s SPIRE and PACS instruments, imagers with some spectroscopic capability, will exploit the low space background, along with the lack of atmospheric noise and absorption, and enable a wide-field survey for bright dusty galaxies, and to determine accurate spectral templates from local galaxies and ULIRGs. These templates should increase significantly the quality of astrophysical diagnostics for low-redshift galaxies that can be compared at high redshifts. *Spitzer*'s IRS spectrograph extended longwards only to 38 μm, and so the only far-IR spectra avalable at present for low-redshift galaxies were obtained by the first generation instruments about Kuiper Airborne Observatory (KAO) and the *Infrared Space Observatory (ISO)*. Complementary to *Herschel*, the BLAST balloon experiment has obtained, and is soon to release images with comparable resolution to those that *Herschel* will obtain, and the all-sky CMB survey by *Planck Surveyor* will highlight some of the most extremely luminous distant galaxies in its 5-arcmin resolution images at wavelengths of 350, 550 and 850 μm.

Cornell–Caltech Atacama Telescope (CCAT) submm.org CCAT is a ground-based 25-m aperture submm-wave telescope, being designed to be capable of observations at 200-μm with good aperture efficiency, to exploit the excellent observing conditions at an altitude of 5612 m from Cerro Chajnantor, 600 m above the ALMA site. The conditions are the site are comparable to those in Antarctica, and a suite of cutting-edge multi-band instruments are specified, to exploit the best of developing imaging and spectroscopic capabilities (Glenn et al. 2008; Hailey-Dunsheath et al. 2008; Bradford et al. 2009). With a 20-arcmin field of view, and excellent observing conditions, the combination of high spatial resolution (3.5 arcsec FWHM at 350 μm), and extreme mapping speed will allow tens of square degrees to be mapped at this wavelength, to a 1-σ depth of order 0.05 mJy in a few hundreds of hours of good weather. These observations will exploit the imaging resolution to avoid source confusion, and find every IR-luminous galaxy brighter than L^* all the way out to the end of reionization (Blain et al. 2009). The surface density of 0.2 (2) mJy galaxies at 350 μm (that corresponds to a luminosity $L \simeq 10^{11(12)}\,\mathrm{L}_\odot$) is about $1.7(0.22) \times 10^5\,\mathrm{deg}^{-2}$ for $z = 3$. This will enable a direct comparison between the multiwavelength properties of brighter far-IR/submm selected galaxies, and typical optically-selected galaxies. It will enable the relationship between the stellar mass and total ongoing star formation rate to be compared, galaxy-by-galaxy, over the full range of environmental densities present in the large-scale structure of the cosmic web of galaxies, all the way out to reionization and beyond.

Wide-Field IR Survey Explorer (WISE) wise.ssl.berkeley.edu The ability to detect galaxies at redshifts $z \sim 1-2$ from *Spitzer* has been demonstrated in the widest area surveys, with even modest quality multiwavelength supporting data. The forthcoming *WISE* mission, scheduled to fly in November 2009, will make an all-sky survey to comparable depth at 24-μm as these wide-field *Spitzer* surveys. Covering the whole sky, the targets from WISE can be sifted to highlight 24-μm-bright targets that are good candidates to be distant ULIRGs (Farrah et al. 2008). This will be easiest in fields with extensive supporting optical and near-IR data, such as SDSS and UKIDSS to preselect by redshift. Nevertheless,

for years after the WISE survey is completed, it will provide a very valuable reference to the mid-IR luminosity of any serendipitous discovery.

5. Conclusions

Some of the most luminous galaxies in the Universe are easiest to recognize at submm wavelengths. Follow-up studies indicate that these are predominantly powered by star formation, and appear to be found preferentially in denser regions of the Universe. Forthcoming instruments will both yield much larger, more representative samples (*Herschel, WISE* & CCAT), and fantastic imaging quality (ALMA).

References

Alexander D. M., et al., 2005 ApJ, 632, 736
Alexander D. M., et al., 2008 AJ, 135, 1968
Alexander D. M. 2009, this volume (arXiv:0901.2927)
Blain A. W. et al., 2002, Phys Rep, vol. 369, 111
Blain A, W. et al. 2003, MNRAS, 338, 733
Blain A. W, et al., 2004, ApJ, 611, 725
Blain A. W. et al., 2009, Astro2010 White Paper (arXiv:0903.1272)
Borys C. et al., 2005, ApJ, 635, 853
Bradford C. M. et al., 2009, ApJ, submitted
Chapman S. et al., 2005, ApJ, 622, 772
Chapman S. et al., 2008, ApJ, 689, 889
Chapman S. et al., 2009, ApJ, 691, 560
Coppin K. et al. 2008, MNRAS, 384, 1597
Coppin K. et al. 2009 MNRAS in press (arXiv:0920.4464)
Farrah D. et al. 2008, ApJ, 677, 957
Hailey-Dunsheath S.et al. 2008, ApJ, 689, 109
Glenn J. G. et al. 2008, SPIE, 7020, 9
Greve T. R. et al. 2007, MNRAS, 382, 48
Hainline L. et al. 2009, ApJ, submitted
Irwin M. et al. 1998, ApJ, 505, 529
Isaak K. et al. 1994, MNRAS, 269, L28
Kovacs A. et al. 2006, ApJ, 650, 592
Mather J. C. et al. 1990, ApJ, 354, L37
Menéndez-Delmestre K. et al., 2007, ApJ, 655, L65
Menéndez-Delmestre K. et al., 2009, ApJ, submitted
Pope A., et al. 2008, ApJ, 689, 127
Priddey R. et al., 2008, MNRAS, 383, 289
Puget J.-L. et al., 1996, A&A, 308, L5
Schinnerer E. et al., 2008, ApJ 689, 883
Smail I. et al., 1997, ApJ, 470, L5
Smail I. et al., 2002, MNRAS, 331, 495
Soifer B. T., et al., 1994, ApJ, 433, L69
Tacconi L. J., et al. 2008, ApJ, 680, 246
Valiente E. et al., 2007, ApJ, 660, 1060
Vieira J. et al., ApJ, submitted
Walter F. et al., 2009, Nat, 457, 699
Wang W.-H. et al., 2009, ApJ, 690, 319
Younger J. D. et al., 2007, ApJ, 671, 1531

GALAXY EVOLUTION: EMERGING INSIGHTS AND FUTURE CHALLLENGES
ASP Conference Series, Vol.
@jourvol, © 2009
S. Jogee, I. Marinova, L. Hao, and G. A Blanc

Galaxy Star Formation in Different Environments

R. E. González and N. D. Padilla

Departamento de Astronomía y Astrofísica, Pontificia Universidad Católica de Chile, Avenida Vicuña Mackenna 4860, Casilla 306, Santiago, Chile

Abstract. We use a semi-analytic model of galaxy formation to study signatures of large-scale modulations in the star formation (SF) activity in galaxies. In order to do this we carefully define local and global estimators of the density around galaxies. The former are computed using a voronoi tessellation technique and the latter by the normalised distance to haloes and voids, in terms of the virial and void radii, respectively. As a function of local density, galaxies show a strong modulation in the SF, a result that is in agreement with those from several authors. When taking subsamples of equal local density at different large-scale environments, we find relevant global effects whereby the fraction of red galaxies diminishes for galaxies in equal local density environments farther away from clusters and closer to voids. In general, the semianalitic simulation is in good agreement with the available observational results, and offers the possibility to disentangle many of the processes responsible for the variation of galaxy properties with the environment; we find that the changes found in samples of galaxies with equal local environment but different distances to haloes or voids come from the variations in the underlying mass function of dark-matter haloes. There is an additional possible effect coming from the stellar ages, indicating that halo assembly also plays a small but significant role in shaping the properties of galaxies, and in particular, hints at a possible spatial correlation in halo/stellar mass ages. An interesting result comes from the analysis of the coherence of flows in different large-scale environments of fixed local densities; the neighbourhoods of massive haloes are characterised by lower coherences than control samples, except for galaxies in filament-like regions, which show highly coherent motions.

1. Data Samples & Density Estimates

We use 68801 galaxies corresponding to the $z = 0$ output of the $SAG2$ semi-analytic code (Lagos, Cora & Padilla 2008) which includes gas cooling, star formation, mechanical and chemical feedback from SN types Ia and II, follows the evolution of a central supermassive black hole, and the corresponding AGN feedback. The underlying numerical simulation corresponds to a LCDM model within a periodic cube of $60h^{-1}$Mpc a side with 256^3 particles, for a mass resolution of $1 \times 10^9 h^{-1}\mathrm{M}_\odot$ per particle.

We select as landmarks for global density estimators haloes with $M > 10^{13}\mathrm{h}^{-1}\mathrm{M}_\odot$, then we label galaxies according to their distance, in terms of r_{200}, to the closest DM halo. We divide galaxies in 4 subsamples at different distances from halo centres, which we will refer to as R_{H1} to R_{H4}. A similar principle applies to voids where their density profiles can be scaled using r_{void} (Padilla et al. 2005), we use these voids to make a second characterisation of global densities

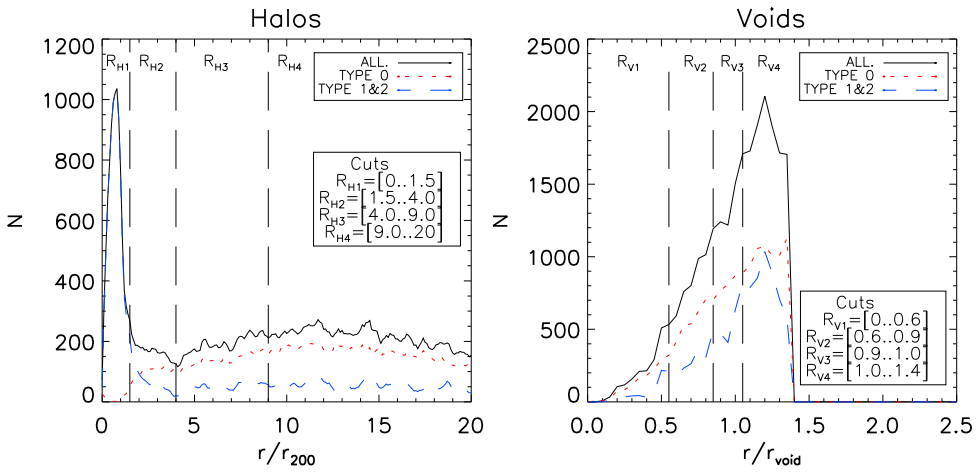

Figure 1. Galaxy distribution vs. normalised distance to halos (left panel), and voids (right panel). The vertical long-dashed lines show the limits between the different global density samples defined in the text.

for the semi-analytic galaxies using $r/r_{\rm void}$. We define 4 distance ranges, referred to as $R_{\rm V1}$ to $R_{\rm V4}$ (See Figure 2).

A choice of local density estimate associated to galaxy-galaxy interactions is the one taking into account the closest neighbors of a galaxy. We use an adaptive local density estimate given by Voronoi Tessellations (VT, Voronoi (1908)). Interpolating this particle density with its neighbors, we obtain a smoothed density field we call Interpolated Voronoi Density (IVD). We compute the IVD field and divide into three subsamples at low, mid & high local densities.

2. Red Galaxy/Starforming Fractions

We compute red galaxy fractions using samples of galaxies located at different halo/void centric distances at fixed local densities, as shown in Figure 2, at increasingly larger distances to halo (left) and void (right) centres. From bottom to top, the lines correspond to bins of increasing local density; each line connects results for samples with equal median IVD. In order to find the origin of this large-scale modulation, we measure the mass function of the host haloes and produce new samples of galaxies taken at random from the simulation box so that the mass functions and local IVD densities of the original samples (defined using limits on both, IVD and global density estimates) are reproduced. We use these random galaxy subsamples as references as to what changes are to be expected in the red galaxy fraction from variations in the local density and the mass function. We make the comparison between random and original samples in Figure 2 (dashed and solid lines, respectively). As can be seen, the underlying mass function is the major(but not the unique, especially for low local density samples) responsible of the large-scale modulation of galaxy fractions.

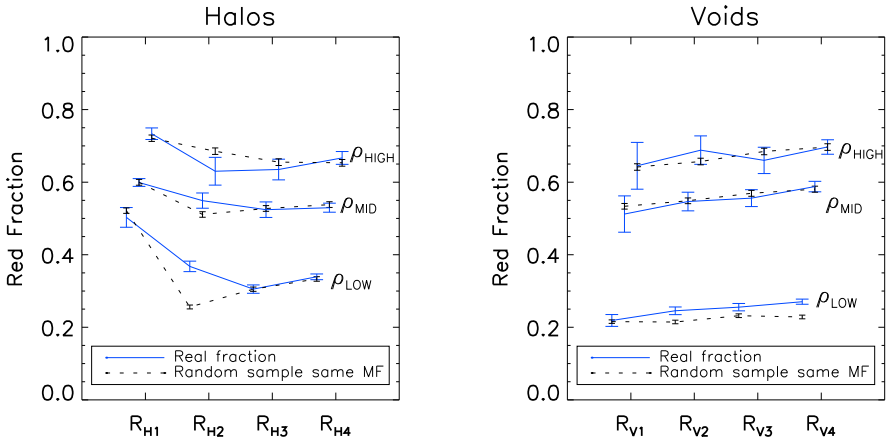

Figure 2. Red Fractions for different halo/void distances and different local density cuts. Blue solid lines: Red Fractions. Black dashed lines: galaxies randomly taken from the simulation to match DM halo mass function and local densities of the parent subsample.

We also study the variation of the fraction of star forming galaxies with the local and global density estimates. We perform this study using the same samples as in the previous sections, and show the results in Figure 3.

There are different possible scenarios to explain the additional changes in galaxy colours and SF fractions to those coming from the mass function. In particular, the literature proposes two possibilities, one related to coherent dynamics of the environments of galaxies and the other to the age of the population of galaxies(See full paper for details).

3. Conclusions

In this paper we have studied large-scale modulations of galaxy colours and SF at different fixed local density environments.

The large-scale structure produces subtle but noticeable effects on the SF of galaxies beyond the local density dependence. We find that the global density has an important impact in colours and SF at low local densities, whereas local galaxy-galaxy interactions may be the major responsible for the variations seen in galaxy colours and SF at higher local density environments, where galaxy-galaxy interactions become important.

In voids we find a large-scale dependence beyond the local density dependence in agreement with Ceccarelli et al. (2008). This dependence weakens at distances larger than a few void radii.

Inside halos, the SF of galaxies is strongly supressed possibly due to the gas depletion processes implemented in the model when galaxies are acquired as new satellites.

Galaxies just outside the virial radius in high density regions (filaments) show indications of infalling motions towards clusters. Additionally, these

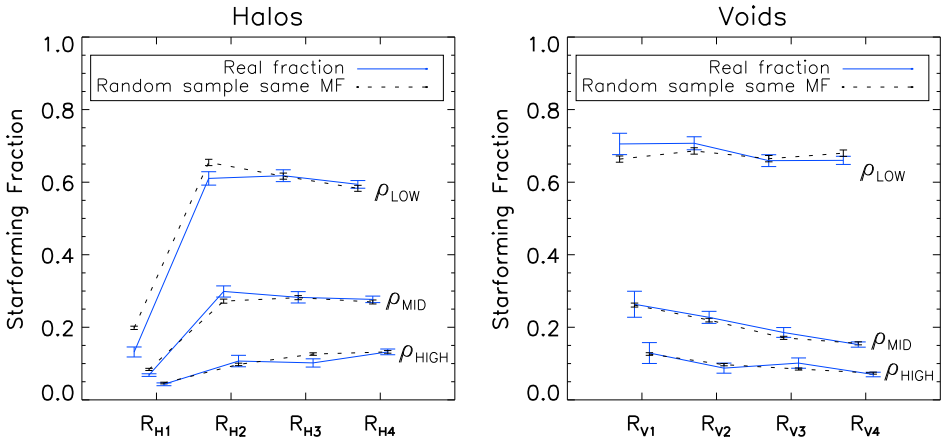

Figure 3. Starforming fraction for different halo/void distances and different local density cuts.

galaxies show traces of enhanced SF activity at intermediate densities, $\rho_{\rm MID}$. Also, for intermediate and high local density environments, galaxies just outside haloes show enhanced SF associated to a higher velocity coherence, in agreement with Porter et al. (2008).

The largest differences in SF fractions in Figure 3 with respect to their corresponding random subsamples are seen for galaxies apparently aproaching void walls from the inner void regions. In this case, the velocity coherence is seen to differ with respect to the associated random sample, although with a low statistical difference.

Our main conclusion is that the large-scale environment affects the galaxy population via variations in the mass function. However, we also find that assembly and large-scale structure are slightly correlated, an effect that could be tested using large observational datasets, providing a new, innovative way to place further constraints on our current paradigm of structure and galaxy formation.

Acknowledgments. This work was supported in part by the FONDAP "Centro de Astrofísica" and Fundación Andes. NP was supported by a Proyecto Fondecyt Regular No. 1071006. RG was supported by CONICYT.

References

Ceccarelli, L., Padilla, N., & Lambas, D. G. 2008, MNRAS, 390, L9
Lagos C., Cora S., Padilla N., 2008, MNRAS, 388, 587.
Padilla N., Ceccarelli L. & Lambas D., 2005 MNRAS, 363, 977
Porter, S. C., Raychaudhury, S., Pimbblet, K. A., & Drinkwater, M. J. 2008, MNRAS, 388, 1152
Voronoi G., 1908, Z. Reine Angew. Math, 134, 198

GALAXY EVOLUTION: EMERGING INSIGHTS AND FUTURE CHALLLENGES
ASP Conference Series, Vol.
@jourvol, © 2009
S. Jogee, I. Marinova, L. Hao, and G. A Blanc

The Chemical Evolution of Intermediate Mass Galaxies over the Last 8 Gyrs

Myriam Rodrigues, Francois Hammer, Hector Flores and Mathieu Puech

GEPI, Observatoire de Paris, CNRS, Universite Paris Diderot, 5 Place Jules Janssen 92190 Meudon, France

Abstract. We have gathered a representative sample of 88 intermediate mass galaxies at $z \sim 0.6$ and have provided robust estimates of their gas phase metallicity based on the strong line method R_{23}. We have found that these galaxies have undergone a strong evolution of their metal content during the last 8 Gyrs. We confirmed the shift about ~ 0.3 dex to lower abundance of the $M - Z$ relation at $z \sim 0.6$ found by Liang et al. (2006). This result shows that the evolution of the gas phase is still active down to $z = 0.4$ and that the close box model is not a valid scenario for local spiral progenitors.

1. Introduction

Around $\sim 70\%$ of intermediate mass galaxies, with stellar mass $M_{\rm stel}$ between 1.45 to $15 \times 10^{10}\, M_{\odot}$ are spiral galaxies in the local Universe. In this work we studied those galaxies at $z \sim 0.6$ which are the likeliest progenitors of the present day spiral galaxies. Results from the ESO large program IMAGES (Intermediate MAss Galaxies Evolution Sequence) show that intermediate mass galaxies have performed a strong evolution of their kinematics and morphological properties since $z \sim 0.6$, see Yang et al. (2008) and Neichel et al. (2008). The evolution of the metal content of the gas in galaxies is a useful tool to disentangle between different scenarios of disk galaxy evolution. In particular the study of the stellar mass-metallicity relation ($M - Z$) can help to constrain the contribution of the several processes taking place during a galaxy lifetime : star-formation history, outflow of gas by SN and stellar winds, and infall of gas by merger or secular accretion. There are several studies of the $M - Z$ relation at different redshifts but the value evolution of the relation is still in debate. See previous work for local galaxies (Tremonti et al. 2004), $0 < z < 1$ (Kobulnicky & Kewley 2004; Savaglio et al. 2005; Liang et al. 2006; Lamareille et al. 2009; Rodrigues et al. 2008), and $z > 1$ (Liu et al. 2008; Erb et al. 2006; Shapley et al. 2004; Maier et al. 2006; Maiolino et al. 2008).

2. Data and Methodology

In the framework of the IMAGES survey, we observed 88 galaxies, with an average redshift of 0.7, in the CDFS. The sample is a complete and representative sample of $M_{\rm stel} > 10^{10}\, M_{\odot}$ galaxies .We have used moderate spectral resolution spectroscopy ($\Delta\lambda = 6.8$Å) at VLT/FORS2 with unprecedent high S/N allowing to remove biases coming from interstellar absorption lines and extinction.

For each galaxy we provided a robust estimate of their gas phase metallicity by using the following methodology :

- Stellar component subtracted from the spectra using Starlight (Cid Fernandes et al. 2005).
- Extinction measured by two methods (Balmer decrement and infrared to optical SFR balance).
- Detection of AGN.
- Estimation of the metallicity from the strong lines method R_{23} and using the relation of Tremonti et al. (2004).
- Determination of the stellar mass from M_K, corrected for red supergiant (Bell et al. 2003) .

3. Evolution of the Metal Content

We compared the metal abundance of 88 distant galaxies with those of local starburst from the SDSS (Tremonti et al. 2004), see Figure 1 left panel. We found that starburst and LIRGs at $z \sim 0.7$ are on average two times less metal rich than local galaxies at the same given mass. We have also compared our results with 4 high-z samples from literature : $1 < z < 1.5$ (Liu et al. 2008), $z \sim 2$ (Shapley et al. 2004), $z \sim 2$ (Erb et al. 2006), and $z \sim 3$ (Maiolino et al. 2008). In Figure 1 right panel, we plotted the metallicity shift from the local relation of the 4 high-z samples as a function of lookback time. We found that the evolution of the metal content in galaxies from local Universe to a lookback time of ~ 12 Gyr is linear.

We compared the observed chemical evolution of the gas with the one predicted by the closed box model. In such a model, the star formation is expected to be very intense at high redshift and then decreases exponentially with time. In fact, at high-z the star formation is fed by the large amount of gas available in galaxies. The production of metals at early epoch is then expected to be very high and the gas is rapidly enriched by metals. Due to the high initial star formation rate, the fraction of gas diminishes rapidly and the star formation rate decreases exponentially with time. The gas is then slowly enriched in metals at intermediate redshift. However, the current observation shows a strong evolution of the metal content from intermediate redshift to local Universe. This evolution is incompatible with the close box model in which galaxies evolve secularly (see Figure 1 right panel). To explain the observed evolution an external supply of gas is required. The input of gas powers the star formation and dilutes metals at the same time. Combining our results with the reported evolution of the Tully-Fisher relation (Puech et al. 2008), we do find that such metal content evolution requires that $\sim 30\%$ of the stellar mass of local galaxies have been formed through an external supply of gas.

This result is in descrepency with the previous work of Savaglio et al. (2005) which claimed that the closed-box model is a good approch to explain the chemical evolution of galaxies. They used observations from the Gemini Deep Deep Survey and the Canada-France-Hawai telescope to determine the

metallicity of 69 intermediate redshift galaxies. They found a small shift of the $M - Z$ relation toward lower metallicities and that massive galaxies have reach high metallicities earlier than low mass galaxies. Based on these observations, they proposed an emperical redshift-dependent $M - Z$ relation combining a simple closed-box model with a SFR that declines more rapidely in more massive galaxies. We suggest that the discrepency between the two works is due to the low S/N quality data and the method applied to correct extinction in Savaglio et al. (2005). The Savaglio et al. (2005) results have been widely used to construct metal content evolution simulation. We are calling for a new generation of modelling able to account for our observations.

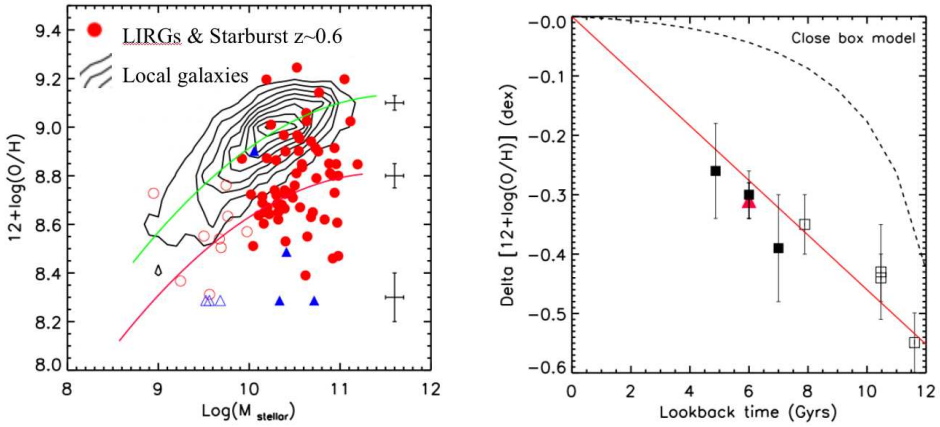

Figure 1. **Left** : Stellar mass-metallicity relation for the SDSS galaxies in contours and dots (Tremonti et al 2004), and the 88 intermediate-z galaxies in circles. Galaxies with masses under the completeness limit $\log M_{\rm stel} < 10$ are plotted with open symbols. Possible AGN are plotted in triangles. The upper line is the best fit of the local $M - Z$ relation and the lower line for the $M - Z$ relation at $z \sim 0.7$. **Right** :The metallicity shift from the local relation as function of the loockback time. The 4 high-z sample are plotted as open squares, the 3 redfhift bins of the IMAGES sample as solid squares and the median of the 3 bins as a triangle. The evolution found by Savaglio et al. (2005) in the frame of a close box model is indicated with dashed line.

4. Similarities Between Local LIRGs and Distant Starbursts

The IMAGES sample has enabled us to investigate several properties of distant starbursts, such as metallicity and star-formation rates, etc. The observations reveal that local LIRGs and distant starbursts/LIRGs share many properties: similar high star-formation efficiency, similar morphologies, dominated by mergers and spirals, same locus in the $M - Z$ relation, and same metal content, see Rodrigues et al. (2008). The only discrepancy between the two populations is their numerical abundance : local LIRGs represent 0.5% of local galaxies while distant LIRGs and starburst account for 20% and 60% of distant galaxies respectively. We suggest that local LIRGs can be the latecomers of the starburst population at $z \sim 0.6$.

As fundamental properties are similar for both local LIRGs and distant starbursts, we may thus wonder whether the two population also have common physical process. For local LIRGs, Rupke, Veilleux, & Baker (2008) have proposed that the encounter between two gas-rich galaxies causes lower metal abundance gas from the outer regions to fall into the merger central regions, providing diluation of the metal abundance and explaining the locus of local LIRGs in the $M - Z$ relation. Independently, Hammer et al. (2005) suggested a scenario in which present spiral galaxies are built by the gradual infall of gas expelled during the first stages of a major merger. Both scenarios are based on supply of unprocessed gas from the outskirt of encounters during a merger. Because distant starburst and LIRGs are common phenomena in the distant Universe, a merger scenario to explain their properties will have a considerable impact on the formation of present-day spirals. Recent simulations indicate that that the majority of gas-rich major merger can reconstruct disk (Hopkins et al. 2009).

References

Bell et al. 2003, ApJS, 149, 289
Cid Fernandes, R., et al. 2005, MNRAS, 358, 363
Erb, D. K., et al. 2006, ApJ, 644, 813
Hammer F., et al. 2005, A&A, 430, 115,
Hopkins et al. 2009, ApJ, 691, 1168
Kobulnicky, H. A., & Kewley, L. J. 2004, ApJ, 617, 240
Lamareille, F., et al. 2009, 495 53
Liang, Y.C., Hammer, F., and Flores, H. 2006, A&A, 447, 113
Liu, X., et al. 2008, ApJ, 678, 758
Neichel, B., et al. 2008, A&A, 484, 159
Maier, C., et al. 2006, ApJ, 639, 858
Maiolino, R., et al. 2008A&A...488..463
Puech, M., et al. 2008, A&A, 484, 173
Rodrigues, M., et al. 2008, A&A, 492, 371
Rupke, D. S. N., Veilleux, S., & Baker, A.J. 2008, ApJ, 674, 172
Savaglio, S., et al. 2005, ApJ, 635, 260
Shapley, A. E., et al. 2004, ApJ, 612, 108
Tremonti, C., et al. 2004, ApJ, 613, 898
Yang, Y., et al. 2008, A&A, 477, 789

GALAXY EVOLUTION: EMERGING INSIGHTS AND FUTURE CHALLLENGES
ASP Conference Series, Vol.
@jourvol, © 2009
S. Jogee, I. Marinova, L. Hao, and G. A Blanc

The First Galaxies: Signatures of the Initial Starburst

Jarrett L. Johnson,[1] Thomas H. Greif,[2] Volker Bromm,[1] Ralf S. Klessen,[2] and Joseph Ippolito[1]

[1]*Department of Astronomy, University of Texas, 1 University Station C1400, Austin, TX 78712, USA*
[2]*Institut für Theoretische Astrophysik, Universität Heidelberg, Albert-Ueberle-Strasse 2, 69120 Heidelberg, Germany*

Abstract. To study the properties of the radiation the first galaxies at $z \geq 10$, as they depend on the dynamical evolution of the galaxies, we carry out cosmological radiation hydrodynamics simulations of Population III (Pop III) starbursts in a dwarf galaxy at $z \sim 12.5$. For different assumptions for the star formation efficiency of the galaxy and for the stellar initial mass function (IMF), we calculate the luminosities and equivalent widths (EWs) of Hα, Lyα, and He II λ1640. We find that photoheating by massive stars causes a strong dynamical response of the gas, which contributes to a weak correlation between luminosity emitted in hydrogen recombination lines and the total mass in stars; however, owing to the low escape fraction of He II-ionizing photons, the luminosity emitted in He II λ1640 is much more strongly correlated with the total stellar mass. The ratio of the luminosities in Lyα and Hα to He II λ1640 is found to be an indicator of the IMF in many cases. The EW of the He II λ1640 emission line is relatively insensitive to dynamical effects, making it an especially reliable indicator of IMF.

1. Introduction

Due to the hard spectra of massive metal-free stars, strong nebular emission in helium recombination lines has been suggested as an observable indicator of a population of such stars (e.g. Oh et al. 2001; Schaerer 2002). We study here the properties of the recombination radiation emitted by the first galaxies with a focus on how the dynamical evolution of the galaxy affects the properties of this radiation. We present high-resolution cosmological radiation hydrodynamics simulations of the production of nebular emission from clusters of primordial stars formed within the first galaxies.

2. The Simulations

To capture the effects of the ionizing radiation emitted by a Pop III stellar cluster within a dwarf galaxy, we approximate the cluster as a point source located at the center of the 9×10^7 $M_\odot$ galaxy in our simulation box at $z = 12.67$. At each timestep, we find both the H II and He III regions generated by the stellar cluster using a ray-tracing technique.

We conduct four simulations, each with a different combination of IMF and total cluster mass. For the IMF, we use either a cluster of 25 $M_\odot$ or 100 $M_\odot$

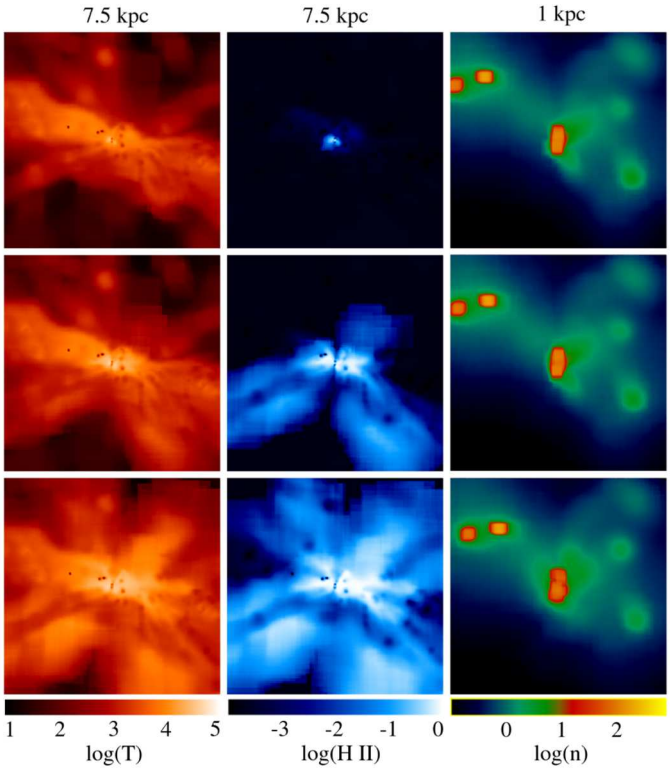

Figure 1. The density-weighted temperature (*left column*), density-weighted H II fraction (*middle column*), and number density (*right column*), surrounding the two hundred fifty 100 $M_\odot$ star cluster, shown at three different times from the prompt formation of the cluster: 500,000 yr (*top row*), 1 Myr (*middle row*), and 3 Myr (*bottom row*). The H II region grows as the density of the gas in the center of the host halo gradually drops in response to the intense photoheating.

Pop III stars. These choices are meant to bracket the expected characteristic mass for Pop III stars formed in the first galaxies, which depending on the cooling properties of the gas may be Pop III.2 stars with masses of order 10 $M_\odot$ or, possibly, Pop III.1 stars with masses perhaps an order of magnitude higher (see e.g. Greif et al. 2008). For each of these IMFs, we vary the total stellar mass in the cluster, choosing either 2.5×10^3 $M_\odot$ or 2.5×10^4 $M_\odot$ for the total mass in stars. These choices correspond to $\sim$ 1 and $\sim$ 10 percent, respectively, of the cold gas available for star formation within the central few parsecs of such a primordial dwarf galaxy. We calculate the ionizing flux from each of these clusters, assuming blackbody stellar spectra at 7×10^4 and 10^5 K and bolometric luminosities of 6×10^4 and 10^6 $L_\odot$, for the 25 and 100 $M_\odot$ stars, respectively.

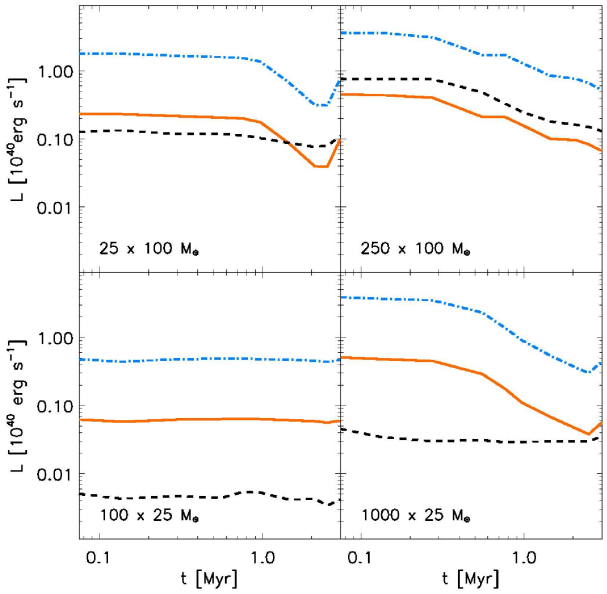

Figure 2. The luminosity of the galaxy, as a function of the time from the prompt formation of the cluster, in three recombination lines: Lyα (*dot-dashed blue*), Hα (*solid red*), and He II λ1640 (*dashed black*). The four panels correspond to our four different choices of IMF and total mass in stars; these are, clockwise from top-left: twenty-five 100 $M_\odot$ stars, two hundred fifty 100 $M_\odot$ stars, one thousand 25 $M_\odot$ stars, and one hundred 25 $M_\odot$ stars.

3. Results

The outcomes of the simulations described above include calculations of the luminosities and equivalent widths of the recombination lines emitted from the dwarf galaxy. We discuss the results of these calculations below.

With the ignition of a stellar cluster at the center of the host halo, the gas surrounding the cluster is photoheated, raising its pressure and leading to its outward expansion. In turn, the overall recombination rate in the host halo drops, allowing the expansion of the H II region. Figure 1 shows the growth of the H II region and the expansion of the gas in the center of the host halo for the two hundred fifty 100 $M_\odot$ cluster.

The evolution of the luminosity in hydrogen recombination lines is shown in Figure 2. Comparing the panels on the left to those on the right, the luminosity in the Lyα and Hα lines, while generally higher for larger total mass in stars, does not scale with the total mass in stars. Overall, because of the temporal evolution of the luminosity in a given line, there is no one-to-one relationship between the total mass in stars, or the star formation rate (SFR), and the luminosity in a given recombination line. Thus, there is likely to be a relatively weak correlation between the SFR and the luminosity in the hydrogen recombination lines emitted from the first dwarf galaxies, owing to the dynamical evolution of the photoionized gas and the escape of ionizing radiation into the IGM. The

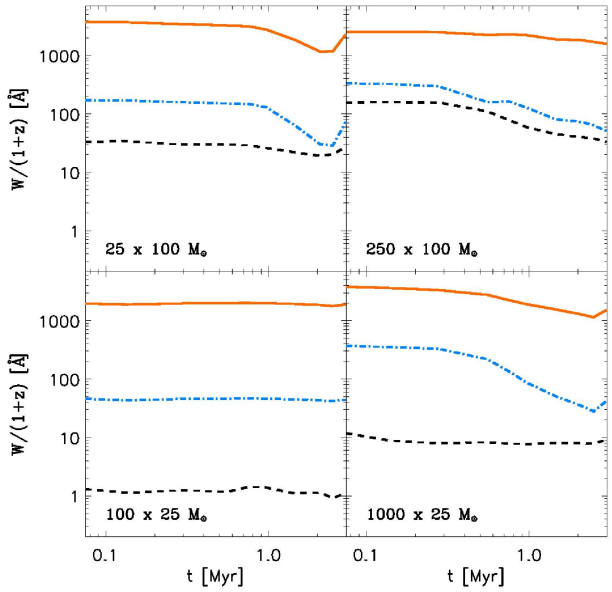

Figure 3. The equivalent widths, as a function of time and redshift z, of the same three recombination lines shown in Fig. 2.

luminosity emitted in He II λ1640 line is generally much more strongly correlated with the total mass in stars, likely making this line a more reliable SFR indicator.

Comparing the top panels of Figure 2 to the bottom panels, it is evident that the ratio of the luminosity emitted in He II λ1640 to that in Hα (or Lyα) can be different depending on the IMF. For the 100 $M_\odot$ star clusters the luminosity in He II λ1640 is comparable to that in Hα, while for the 25 $M_\odot$ star clusters the luminosity in He II λ1640 is up to an order of magnitude lower than in Hα. However, in the latter case the luminosities in these two lines become comparable, revealing some ambiguity in this line ratio as an IMF indicator.

Comparing the EW of Hα in the four panels of Fig. 3, it is clear that it is not strongly dependent on the IMF or on the total mass in stars, varying by at most a factor of three between each of the cases. While showing more variation between the four cases, the EW of Lyα also shows considerable ambiguity as an IMF indicator. The EW of He II λ1640 is, however, a more definitive indicator of IMF, being higher for the clusters of 100 $M_\odot$ stars than for the clusters of 25 $M_\odot$ stars, regardless of the total mass in stars or of the age of the cluster.

Acknowledgments. The simulations presented here were carried out at the Texas Advanced Computing Center.

References

Greif T. H., Johnson J. L., Klessen R. S., Bromm V. 2008, MNRAS, 387, 1021
Oh S. P., Haiman Z., Rees M. J. 2001, ApJ, 553, 73
Schaerer D. 2002, A&A, 382, 28

GALAXY EVOLUTION: EMERGING INSIGHTS AND FUTURE CHALLLENGES
ASP Conference Series, Vol.
@jourvol, © 2009
S. Jogee, I. Marinova, L. Hao, and G. A Blanc

The First Stars: Disk Formation and Fragmentation

Athena Stacy,[1,2] Thomas H. Greif,[3,4] and Volker Bromm[1,2]

[1] *University of Texas at Austin, Department of Astronomy, 1 University Station, C1400 Austin, TX 78712, USA*
[2] *Texas Cosmology Center, University of Texas, Austin, TX 78712, USA*
[3] *Institut für theoretische Astrophysik, Albert-Ueberle Strasse 2, 69120 Heidelberg, Germany*
[4] *Fellow of the International Max Planck Research School for Astronomy and Cosmic Physics at the University of Heidelberg*

Abstract. Protostellar accretion in the early universe and its associated physical processes determined the final masses that were reached by the first stars. The masses of the first stars, in turn, played an important role in determining to what extent the first stars drove early cosmic evolution. We present the results of a continuing study of protostellar accretion at high redshift. These studies were performed using Gadget, a widely-tested three dimensional smoothed particle hydrodynamics (SPH) code. We performed cosmological simulations starting from $z \sim 100$ until the formation of the first minihalo. The mass resolution was then increased, and the evolution of the minihalo was followed up to densities of 10^{12} cm^{-3}. At this point accretion onto the central high density peak, which corresponds to the first protostar, was studied for the following 5000 years. During this 5000-year time period a disk forms around the first protostar, and within this disk several other lower-mass protostars form. The current results represent the no-feedback limit of protostellar accretion onto a star that has formed in an environment uninfluenced by any previous stellar generation. This work, as well as further simulations which will include prescriptions for protostellar feedback, will lead to a much improved determination of the accretion rate and its evolution over the life of the protostar as well as the typical mass of the first stars.

1. Initial Runaway Collapse

Simulations are carried out in a periodic box with size of $100h^{-1}$ kpc (comoving) and initialized with both DM particles and SPH gas particles. This is done in accordance with a ΛCDM cosmology with $\Omega_\Lambda = 0.7$, $\Omega_\mathrm{M} = 0.3$, $\Omega_\mathrm{b} = 0.04$, and $h = 0.7$. We use an artificially large normalization of the power spectrum, $\sigma_8 = 1.4$, to accelerate structure formation in our relatively small box. The simulations were run from $z \sim 100$ until the formation of the first minihalo. The mass resolution was then increased, and the evolution of the minihalo was followed up to densities of 10^{12} cm^{-3}. We then represent these high-density peaks with sink particles, allowing us to follow the mass flow onto the sinks for 5000 yr after the first protostar forms.

As shown in Fig. 1, the results of our calculation up to the point of creation of the first sink particle agree well with previous studies (Bromm & Larson

2004; Yoshida et al. 2006). The gas that collapses into the minihalo is heated adiabatically to ~ 1000 K as it reaches $n \sim 1$ cm^{-3} (panel a). At this point the molecular hydrogen fraction $f_{\rm H_2}$ becomes high enough (panel b) to allow the gas to cool through H_2 rovibrational transitions to a minimum of $T \sim 200$ K, which is reached at $n \sim 10^4$ cm^{-3} (panel a). After the onset of gravitational instability, the gas reaches yet higher densities, and is heated to a maximum of ~ 1000 K once it approaches a density of $\sim 10^8$ cm^{-3}. At this density three-body reactions become important, and the gas is rapidly converted into fully molecular form by $n \sim 10^{12}$ cm^{-3} (panel b, see detailed discussion in Yoshida et al. 2006; Yoshida, Omukai, & Hernquist 2008).

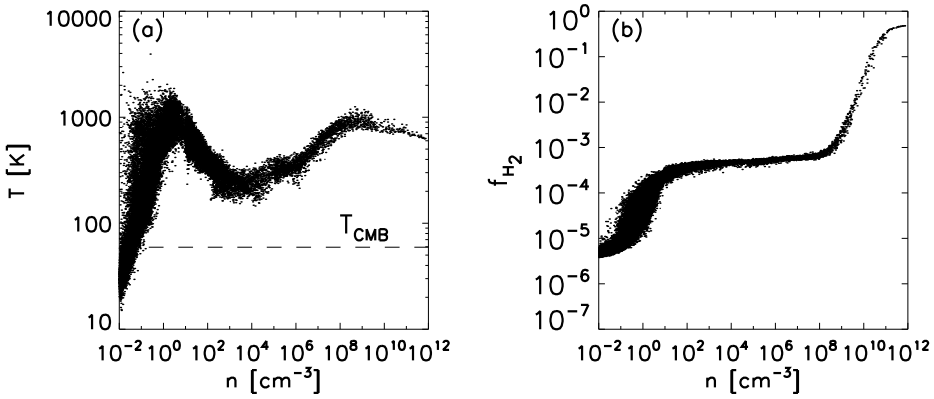

Figure 1. Physical state of the collapsing core. The situation is shown just prior to the formation of the first sink particle. *(a)* Temperature vs. density. *(b)* Molecular hydrogen fraction vs. density.

2. Protostellar Accretion

Particles that reach densities of 10^{12} cm^{-3} are converted into sink particles, which are held constant at that density as they accrete the nearby surrounding gas particles. Fig. 2 shows the density and temperature projections at various times in the simulation over the initial sink's 5000 yr of accretion. As is visible in the top panel of Fig. 2, the central region is evolving into a Keplerian disk ($v_{\rm rot} \propto r^{-1/2}$) by 1000 yr after the first sink has formed, yielding a total star-disk system of $\sim 100\ M_\odot$. The disk spins up as the inner few hundred solar masses infalls towards smaller radii, and thus rotational support increases.

Around 1000 yr after sink formation, the disk becomes unstable to fragmentation. Soon after the disk instability sets in, some spiral structure develops. Several new fragments also form, represented by new sink particles. The spirals and fragments serve to transport angular momentum outward through gravitational torques, allowing the inner gas to accrete onto the sinks.

After the initial sink particle has grown in mass, the surrounding gas divides into two phases—the cool disk particles and the hot particles. This can be seen in the bottom two panels of Fig. 2. Particle heating becomes significant once

the initial sink grows beyond 10 $M_\odot$. At this mass the gravitational force of the sink particle is strong enough to pull gas towards it with velocites sufficiently high to adiabatically heat the gas to a maximum temperature of ~ 7000 K. The main sink is furthermore able to accrete these heated particles as its mass grows beyond 20 $M_\odot$. At 5000 yr after initial formation, the main sink is accreting slightly over 50 percent heated particles. In contrast, the less massive sinks can accrete particles from only the cool disk phase.

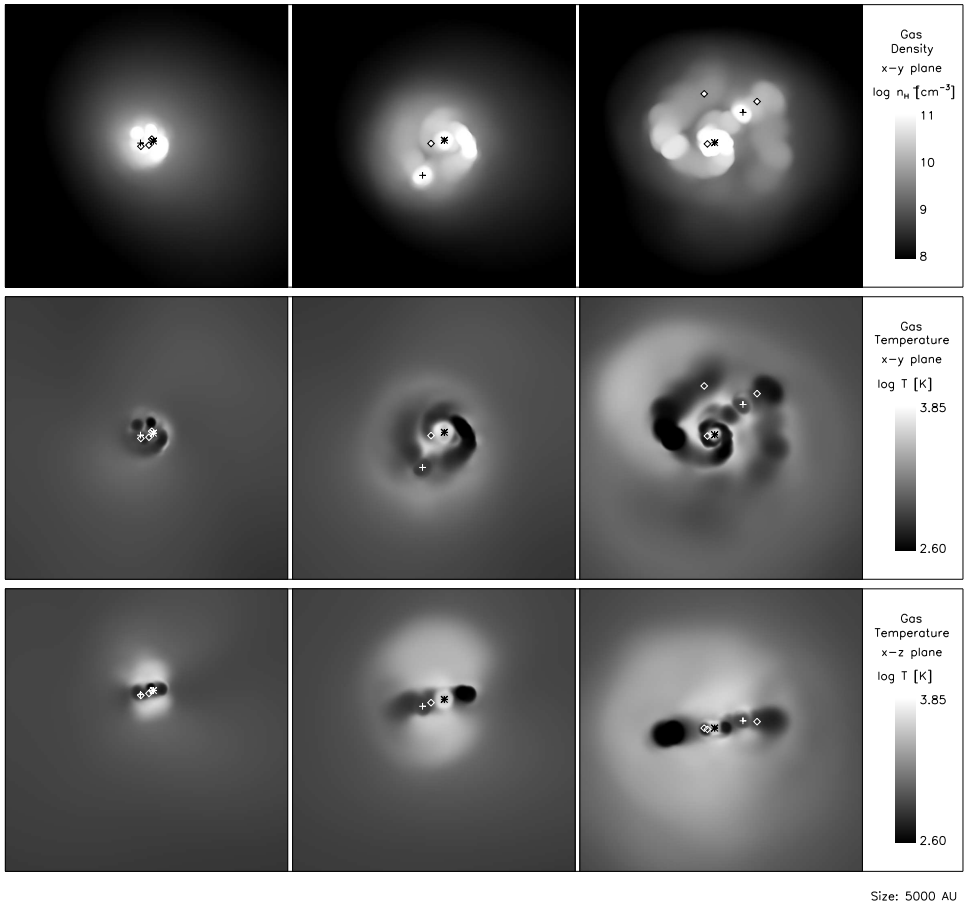

Figure 2. Density and temperature projections of the central high-density region (length 5000 AU) in either the x–y or x–z planes. Asterisks denote the location of the initial and most massive sink. Crosses show the location of the second most massive sink. Diamonds are the locations of the other sinks. Each panel shows projections at 1000 yr (left), 2000 yr (center), and 5000 yr (right) after the initial sink formation.

Fig. 3a shows the growth of the two most massive sink particles over time. We find that the main sink approximately grows as $M \propto t^{0.55}$ (red line). By 5000 yr after sink formation, it has grown to ~ 43 $M_\odot$, only slightly higher than the corresponding result from Bromm & Loeb (2004). Fig. 3b shows

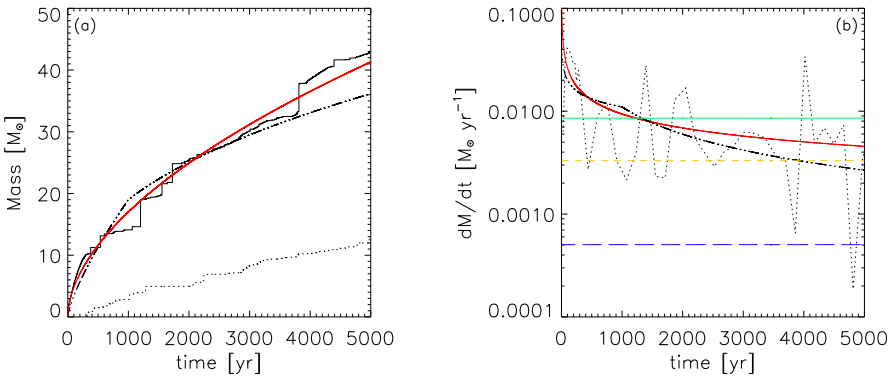

Figure 3. (*a*) Solid line: mass of the first sink particle over time in our calculation. Red line: least-squares powerlaw fit to the sink mass over time. Dash-dot line: result Bromm & Loeb (2004) obtained in their calculation. Dotted line: mass growth of the second largest sink. (*b*) Black dotted line: accretion rate of the main sink particle throughout our calculation. Red line is: powerlaw fit to the mass accretion rate. Solid green line: average accretion rate of the main sink over its 5000 yr of accretion. Black dash-dot line: instantaneous accretion rate found by Bromm & Loeb (2004). Yellow short-dash line and blue long-dash line: Shu accretion rates for isothermal gas at 700 K and 200 K.

the accretion rate onto the most massive sink particle over time (dotted line). The initial accretion rate is $\sim 7\ c_{\rm s}^3/G$ for 700 K gas (short-dash yellow line) and $\sim 50\ c_{\rm s}^3/G$ for 200 K gas (long-dash blue line), where $c_{\rm s}$ is the gas sound speed. These rates are similar to accretion rates expected expected from analytic solutions (Shu 1977; Larson 1969; Penston 1969), and they are furthermore quite similar to the accretion rate found in Bromm & Loeb (2004; dash-dot line).

The accretion rate begins very high and declines as approximately $\dot{M} \propto t^{-0.45}$ (red line in Fig. 3b). If this trend can be extrapolated to later times, the protostar represented by the main sink can easily accrete several hundred solar masses over its main sequence lifespan of $3{\times}10^6$ yr. This work further indicates that the cloud providing the mass for a highly massive Pop III star will also undergo disk formation and fragmentation, leading to binary or mutiple systems with other low or intermediate-mass stars within a minihalo. Future work will explore how protostellar feedback will affect these results.

References

Bromm, V., & Larson, R.B. 2004, ARA&A, 42, 79
Bromm, V., & Loeb, A. 2004, New. Astron., 9, 353
Larson, R. B. 1969, MNRAS, 145, 271
Penston, M. W. 1969, MNRAS, 144, 425
Shu, F. H. 1977, ApJ, 214, 488
Yoshida, N. & Omukai, K., & Hernquist, L., & Able, T. 2006, ApJ, 652, 6
Yoshida, N., Omukai, K., & Hernquist, L. 2008, Sci, 321, 669

Part IV

AGN and Stellar Feedback

GALAXY EVOLUTION: EMERGING INSIGHTS AND FUTURE CHALLLENGES
ASP Conference Series, Vol.
@jourvol, © 2009
S. Jogee, I. Marinova, L. Hao, and G. A Blanc

Missing Halo Baryons and Galactic Outflows

Romeel Davé

University of Arizona

Abstract. We present predictions for galactic halo baryon fractions from cosmological hydrodynamic simulations with a well-constrained model for galactic outflows. Without outflows, halos contain roughly the cosmic fraction of baryons, slightly lowered at high masses owing to pressure support from hot gas. The star formation efficiency is large and increases monotonically to low masses, in disagreement with data. With outflows, the baryon fraction is increasingly suppressed in halos to lower masses. A Milky Way-sized halo at $z = 0$ has about 60% of the cosmic fraction of baryons, so "missing" halo baryons have largely been evacuated, rather than existing in some hidden form. Large halos ($\gtrsim 10^{13} M_\odot$) contain 85% of their cosmic share of baryons, which explains the mild missing baryon problem seen in clusters. By comparing results at $z = 3$ and $z = 0$, we show that most of the baryon removal occurs at early epochs in larger halos, while smaller halos lose baryons more recently. Star formation efficiency is maximized in halos of $\sim 10^{13} M_\odot$, dropping significantly to lower masses, which helps reconcile the sub-L_* slope of the observed stellar and halo mass functions. These trends are predominantly driven by *differential wind recycling*, namely, that wind material takes longer to return to low-mass galaxies than high-mass galaxies. The hot gas content of halos is mostly unaffected by outflows, showing that outflows tend to blow holes and escape rather than deposit their energy into halo gas.

1. Introduction

Everywhere we look, baryons are missing. Globally, observations only account for around half the baryons today (e.g., Fukugita 2004). Simulations indicate that the missing baryons are contained in intergalactic gas at $10^5 < T < 10^7$ K, called the Warm-Hot Intergalactic Medium (WHIM; e.g., Davé et al. 2001). Initially, O VI absorbers seen in quasar spectra were thought to be collisionally-ionized tracers of WHIM gas (Tripp, Savage, & Jenkins 2000). But recent simulations and observations suggest that most intergalactic O VI is actually photo-ionized (Oppenheimer & Davé 2008b, and refs therein), and so the WHIM must be traced using higher ionization lines (e.g., O VII; Nicastro et al. 2005).

Baryons are also missing on galactic scales. Current hierarchical structure formation models predict that baryons do not substantially decouple from dark matter until well inside of halos, hence the expectation is that halos should contain roughly the cosmic fraction of baryons. However, dynamical modeling of the Milky Way's disk and halo reveals that it contains at best half of its cosmic share of baryons in stars and cold gas (Dehnen & Binney 1998; Sommer-Larsen & Dolgov 2001); the same is true of M31 (Klypin, Zhao, & Somerville 2002). This is the "Missing Halo Baryons" problem. Either a substantial portion of the

$\sim L_*$ galaxies' halo baryons are in some heretofore hidden form, or else there has been a sizeable exodus of baryons into the intergalactic medium (IGM). Many models have advocated the former possibility, suggesting by analogy with the WHIM that the missing halo gas is in some warm-hot component (e.g., Fukugita & Peebles 2006; Sommer-Larsen 2006), or cold clouds (Maller & Bullock 2004). However, there is little observational evidence for massive coronae of hot gas around typical spirals (Benson et al. 2000; Wang 2007), and furthermore if all halos contained such coronae, this would substantially overpredict the soft X-ray background (Pen 1999; Wu, Fabian, & Nulsen 2001). Meanwhile, the mass in cold clumps as traced by high velocity clouds is unlikely to be sizeable even in optimistic scenarios (Blitz et al. 1999; Sommer-Larsen 2006). In contrast, Silk (2003) developed an analytic model that argued for a substantial fraction of baryons being removed by galactic outflows. In fact, Silk presciently predicted that such outflows could solve a surprisingly wide range of current dilemmas in galaxy formation, which our simulations have largely confirmed.

Clusters also seem to have a missing baryon problem. In a recent census by Gonzalez, Zaritsky, & Zabludoff (2007), baryons make up $\approx 13\%$ of the mass of the cluster, while the latest WMAP-5 results (Hinshaw et al. 2009) favor a cosmic mean value of $\approx 17\%$. This is a small but persistent discrepancy which could have implications for using clusters as probes of precision cosmology.

In these proceedings we examine the baryonic content of galaxy halos in cosmological hydrodynamic simulations with and without galactic outflows. The outflow model implemented in our simulations is unique in that it matches detailed properties of a wide range of outflow-related observables, including IGM enrichment at various epochs (Oppenheimer & Davé 2006, 2008b, 2009), the galaxy mass-metallicity relation (Finlator & Davé 2008), early galaxy luminosity functions (Davé, Finlator, & Oppenheimer 2006), and intragroup gas enrichment and entropy (Davé, Oppenheimer, & Sivanandam 2008). Even though our modeling of outflows is parameterized and heuristic, these successes suggest that it plausibly moves mass, metals, and energy on large scales in a manner consistent with the real Universe.

2. Halo Baryon Fractions

We run simulations using our modified version of Gadget-2 (Springel 2005), as described in Oppenheimer & Davé (2008a). The runs here employ 2×256^3 particles in volumes of $32h^{-1}$Mpc and $64h^{-1}$Mpc, with our WMAP3-concordant *d-series* cosmology (see Oppenheimer & Davé 2008b). We identify halos using a spherical overdensity algorithm (see Keres et al. 2005), and consider only "resolved" halos with masses $M_h > 128(m_d + m_g)$, where $m_d = (1.6, 12.7) \times 10^8 M_\odot$ and $m_g = (0.34, 2.72) \times 10^8 M_\odot$ are the dark matter and gas particles masses for the $(32, 64)h^{-1}$Mpc volumes, respectively. We run two versions of these simulations: One with no winds, and one with our favored momentum-driven (M-D) wind model that matches a range of data as mentioned above. Outflows are implemented in a probabalistic Monte Carlo fashion by giving kicks to gas particles; details are in Oppenheimer & Davé (2008a).

The fraction of baryons within halos are shown in the top panel of Figure 1. In the no-wind case (blue points, upper swath), halos of Milky Way's size and

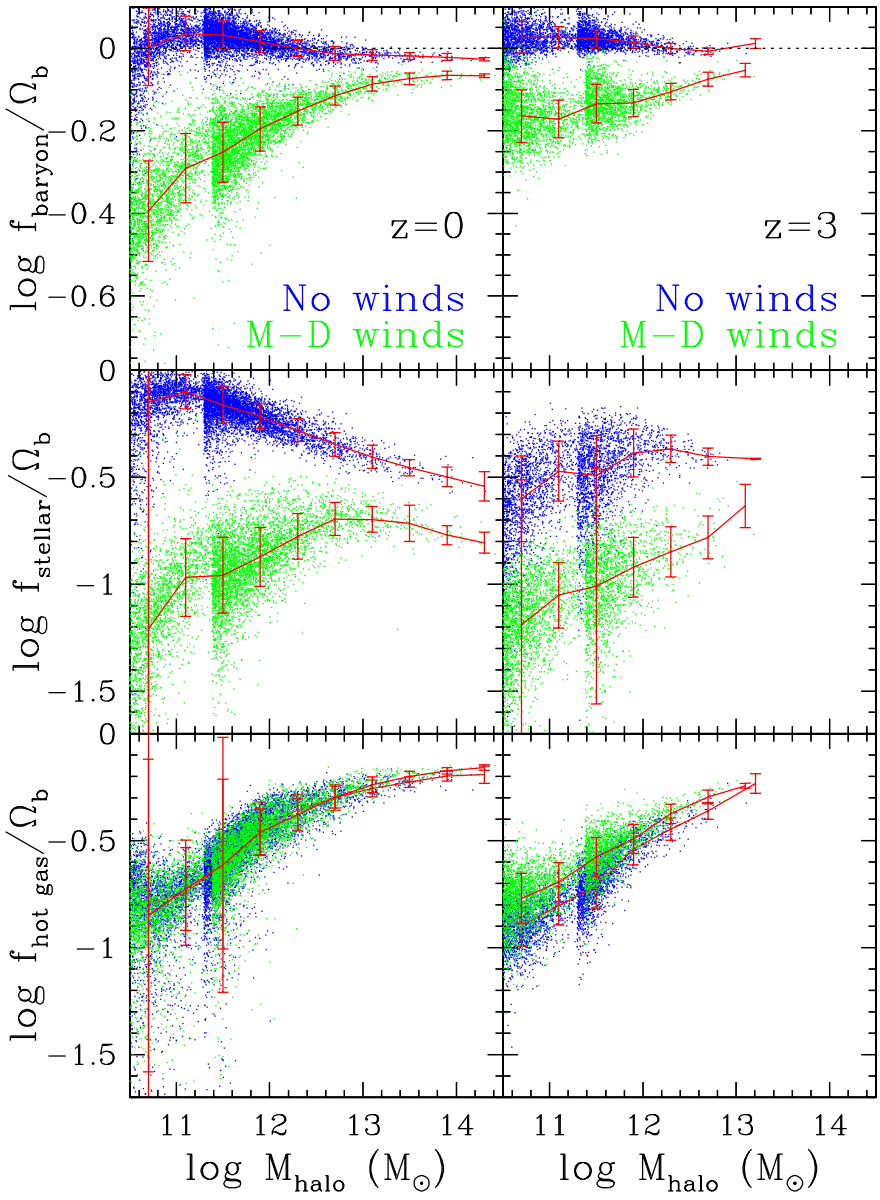

Figure 1. *Top:* Baryon fraction (relative to cosmic mean) as a function of halo mass, for simulations at $z = 0$ (left panels) and $z = 3$ (right), without winds (blue, upper points) and with momentum-driven winds (green, lower points). Dotted line shows the cosmic baryon fraction assumed in our runs. *Middle:* Stellar fractions. *Bottom:* Hot gas ($T > 10^{4.5}$K) fractions. In each panel, the red line shows a running median with 1σ dispersion, and the two groups of points for each model show results from our $32h^{-1}$Mpc and $64h^{-1}$Mpc volumes. Outflows drive out substantial amounts of baryons particularly from low-mass systems, which helps regulate star formation to observed level. In large systems most of the mass loss has already occured by $z = 3$, while in small systems the mass loss occurs later owing to differential wind recycling. Hot gas fractions are a strong function of halo mass, but are not sensitive to outflows. A Milky Way-sized halo today contains about 60% its cosmic share of baryons, of which half is in the form of hot gas, one-third in cool gas, and one-sixth in stars.

below have, as expected, roughly their cosmic share of baryons (shown by the dotted line at $\Omega_b/\Omega_m = 0.044/0.25 = 0.176$). In detail, adiabatic contraction causes the baryon fraction to typically be slightly greater than the cosmic mean. This shows that without any strong feedback, baryons do indeed mostly trace dark matter on halo scales in $\lesssim L_*$ galaxies.

In more massive halos ($M_h \gtrsim 10^{13} M_\odot$), the increasing predominance of hot halo gas (Keres et al. 2008, see also bottom panels of Figure 1) causes pressure support that pushes baryons farther out than the dark matter, and the baryon content is lowered. At the highest masses probed by $z = 0$ ($M_h \sim 10^{14} M_\odot$), this reduction reaches 6%, which is not trivial but still insufficient to explain observed cluster baryon fractions.

Now we consider the M-D wind runs, shown by the lower (green) swath of points. Outflows have a dramatic impact, increasingly so to smaller halo masses. Already by $z = 3$, typical halos ($M_h \sim 10^{11-12} M_\odot$) have had their baryon fraction reduced by $20 - 30\%$ compared to the cosmic mean. At $z = 3$ there is only a mild trend with halo mass, but by $z = 0$ the trend becomes much stronger: Milky Way-sized halos ($M_h \sim 10^{12} M_\odot$) have lost roughly 40% of their baryons, while the smallest halos we probe at $M_h \sim 10^{10.5} M_\odot$ have lost 60%. This indicates that *missing halo baryons have mostly been ejected by outflows.*

Outflows have a noticeable impact on large halos as well. Davé, Oppenheimer, & Sivanandam (2008) showed that outflows add substantial entropy on poor group scales, and this translates into increased pressure support over the no-wind case. With outflows, the most massive ($M_h \gtrsim 10^{13} M_\odot$) halos now contain only 85% of their cosmic share of baryons, and the trend is essentially flat with halo mass. This value is in better agreement with observational estimates (Vikhlinin et al. 2006; Gonzalez, Zaritsky, & Zabludoff 2007).

The falling baryon fraction in low-mass halos is a consequence of wind recycling in our outflow model, i.e. the re-accretion of previously ejected wind material. In Oppenheimer & Davé (2008a), we found that small galaxies push their winds out farther relative to large galaxies (owing primarily to the fact that they reside in less dense surroundings), and as a result the time for winds to be re-accreted onto small systems is longer. At early epochs, recycling is relatively unimportant, because there hasn't been sufficient time to permit substantial re-accretion. The weak trend seen at $z = 3$ owes to the fact that our mass loss rate scales inversely with velocity dispersion in our momentum-driven wind scalings. By $z = 0$, however, the longer recycling times in smaller systems results in much more cumulative mass loss from small halos relative to larger halos. Hence *differential wind recycling is the dominant driver in establishing the baryon fraction trends with halo mass.* As we will see next, it is also critical for regulating the star formation efficiency in smaller systems.

3. Stellar Baryon Fractions

We now separate baryons within each halo into three phases: Stars, cool gas ($T < 10^{4.5}$K), and hot gas ($T > 10^{4.5}$K). Star-forming gas is included in cool gas. The middle and bottom panels of Figure 1 show the baryon fractions in

stars and hot gas, respectively; the remainder is in cool gas (not shown). In this section we examine stellar baryon fractions.

With no outflows, there is a serious overcooling problem: Star formation is far too efficient. In sub-L_* halos, the fraction of baryons in stars approaches 90%, while observed small galaxies have stellar fractions under 10%. Moreover, the trend is wrong; with no winds, smaller galaxies have a higher baryon fraction in stars, while the shallow slope of the stellar mass function below L_* relative to the halo mass function indicates that the stellar mass fraction should be lower in small halos. At group scales, the stellar baryon fraction is down to 25% of the cosmic mean, but that is still too high compared to data as pointed out in Davé, Oppenheimer, & Sivanandam (2008). Of course, these results are not surprising, as it is well known that outflows, particularly at early epochs, are required to suppress overcooling (e.g., Davé, Finlator, & Oppenheimer 2006).

With outflows, the situation improves dramatically. Stellar fractions are reduced to a maximum of $\approx 20\%$ for $\sim 10^{13} M_\odot$ halos, falling to either smaller or larger halos. A Milky Way-sized halo now has a 12% stellar fraction (relative to Ω_b), which is in general agreement with observations of comparable disk galaxies (Hammer et al. 2007). The stellar fraction drops towards lower halo masses, suggesting a flatter stellar mass function compared to the halo mass function, as observed. The slope of the $z = 0$ fit (red line) is approximately $d \log f_* / d \log M_h \approx 0.5$ for $M_h < 5 \times 10^{12} M_\odot$, which when combined with the halo mass function slope of ≈ -2, yields a stellar mass function slope of ≈ -1.5. This is in general agreement with observations of the sub-L_* stellar mass function slope (Baldry, Glazebrook, & Driver 2008), though still too steep; in fact, the faint-end slope turns out to be even shallower, as will be shown in a forthcoming paper. Note that the stellar fraction slope at $z = 3$ is less steep, reflecting the shallower slope in the overall halo baryon fraction (top right panel). Our models naturally yield a flattening of the faint end slope with time.

The qualitative trend of the star formation efficiency having a maximum at some mass and dropping fairly rapidly to low masses, along with the faint end slope evolution, is a direct consequence of differential wind recycling. Without it, the star formation efficiency would continue to increase to small masses, as in the no-wind case. Hence models of galaxy formation must not only include outflows, but must also track the *dynamics* of wind material on its journey through the IGM to properly capture its impact on galaxy evolution.

4. Hot Gas Baryon Fractions

Turning to the hot gas ($T > 30,000$ K) baryon fractions (bottom panels of Figure 1), there is a strong trend of hot gas fraction increasing with halo mass, which is mostly independent of redshift and whether or not outflows are included. In the no-wind case, the hot gas fraction exceeds the stellar fraction (which comprises the vast majority of condensed baryons) at $z = 0$ for $M_h \gtrsim 10^{12.5} M_\odot$. This transition occurs at a somewhat larger mass than found in Keres et al. (2008), likely because our runs include metal-line cooling.

With outflows, the fraction of halo gas in hot form is more substantial, exceeding the stellar fraction in the outflow case at all masses probed here. This is due to the suppression of star formation, rather than an increase in

the amount of hot gas. Relative to the baryon fraction, the hot gas fraction is about one-third of all halo baryons at the smallest masses probed, and increases to three-fourths or more for $M_h \gtrsim 10^{13} M_\odot$. This indicates that there is still a substantial reservoir of baryons in a difficult-to-detect phase within typical galaxies, and indeed X-ray observations do indicate a warm-hot corona around a nearby spiral galaxy (Pedersen et al. 2006). However, the amount of hot gas we predict is still a factor of two to three smaller than in models that place the majority of missing halo baryons into this phase. This roughly translates into up to an order of magnitude reduction in the predicted X-ray flux (as compared to e.g., Benson et al. 2000). Hence the typical non-detection of X-ray halos around spiral galaxies should not be surprising, but deeper observations with future X-ray telescopes should uncover this phase more ubiquitously.

It is noteworthy that our outflows do not significantly increase the amount of hot gas into halos (as seen by comparing to the no-wind case). Winds in our models tend to escape halos without depositing a significant amount of energy along the way via shocks. This is contrary to typical assumptions in analytic or semi-analytic models of outflows (e.g., Dekel & Silk 1986), and simply reflects the fact that in realistic three-dimensional models outflows prefer to blow holes rather than share their energy with ambient gas. This is also consistent with X-ray observations of hot gas around galaxies that indicate they are radiating a small fraction of the supernova energy input (e.g., Wang 2007). Another factor is that outflows are typically quite enriched, so that the gas cooling times are short, and hence even if outflow material is heated it condenses out quickly. At low-z this results in a "halo fountain" that may be the origin of compact high velocity clouds (Wang 2007; Oppenheimer & Davé 2008a).

5. Summary

We have examined halo baryon fraction in cosmological hydrodynamic simulations, comparing models with and without galactic outflows. Our outflow model is heuristic, but is well-constrained to match a variety of galaxy and IGM observations at a range of epochs. We find that these same outflows may help resolve some puzzles regarding the baryonic content of galactic halos.

For low mass halos, outflows remove a significant portion of halo baryons by $z = 0$. The fraction of ejected baryons increases sharply to lower masses, so that $10^{12} M_\odot$ halos have lost 40% of their baryons, and $10^{10.5} M_\odot$ halos 60%. The trend is not as pronounced at $z = 3$, showing that the longer wind recycling times in small galaxies (i.e. differential wind recycling) plays a critical role in suppressing the baryon fractions in small halos between $z = 3 \rightarrow 0$. This may explain why the faint-end slope of the luminosity function becomes shallower with time. By today, this produces a peak in star formation efficiency at $\sim 10^{12.5-13} M_\odot$, above and below which the efficiency falls. Meanwhile, hot gas fractions are mostly unaffected by outflows, showing that outflows do not deposit much of their energy into halo gas, instead preferring to blow holes and escape. A Milky Way-sized halo today has about 60% of its cosmic share of baryons, half of which are in hot gas, one-third in cool gas, and the remainder in stars.

For high mass halos ($M_h \gtrsim 10^{13} M_\odot$), there is a mild suppression of baryon fractions owing to larger pressure support from an increasingly substantial hot gaseous halo. Without winds, the suppression is fairly small ($\approx 5\%$). In our outflow run, conversely, the suppression is much more substantial, $\approx 15\%$, independent of mass, which agrees better with data. This demonstrates that outflows impact even massive halos today. The key is that most of the ejection occurs at early epochs, when those halos were much smaller.

Our implementation of outflows is primarily constrained to match IGM enrichment at $z \sim 2-4$ (e.g., Oppenheimer & Davé 2006). The fact that this model naturally yields observationally-consistent results for halo baryon fractions at $z \sim 0$ is highly encouraging, and represents another significant success for our outflow model based on momentum-driven wind scalings. It may be that we are approaching a heuristic understanding of how outflows operate on extragalactic scales, even though the detailed mechanisms by which outflows are driven out of galaxies remain unclear.

Acknowledgments. RD thanks Shardha Jogee and the organizing committee for an excellent meeting. The simulations were run on UA's SGI cluster.

References

Baldry, I. K., Glazebrook, K., & Driver, S. P. 2008, MNRAS, 388, 945
Benson, A. J., Bower, R. G., Frenk, C. S., & White, S. D. M. 2000, MNRAS, 314, 557
Blitz, L, Spergel, D. N., Teuben, P. J., Hartmann, D., & Burton, B. 1999, ApJ, 514, 818
Davé, R., et al. 2001, ApJ, 552, 473
Davé, R., Finlator, K., & Oppenheimer, B. D. 2006, 370, 273
Davé, R., Oppenheimer, B. D., & Sivanandam, S. 2008, MNRAS, 391, 110
Dehnen, W. & Binney, J. 1998, MNRAS, 294, 429
Dekel, A. & Silk, J. 1986, ApJ, 303, 39
Finlator, K. & Davé, R. 2008, MNRAS, 385, 2181
Fukugita, M. 2004, IAU Symp. 220, ed. S. D. Ryder et al. (San Francisco: ASP), 227
Fukugita, M. & Peebles, P. J. E. 2006, ApJ, 639, 590
Gonzalez, A. H., Zaritsky, & D., Zabludoff, A. I. 2007, ApJ, 666, 147
Hammer, F., Puech, M., Chemin, L., Flores, H., & Lehnert, M. D. 2007, ApJ, 662, 322
Hinshaw, G. et al. 2009, ApJS, 180, 225
Keres, D., Katz, N., Weinberg, D. H., & Davé, R. 2005, MNRAS, 363, 2
Keres, D., Katz, N., Fardal, M., Davé, R., & Weinberg, D. H. 2008, MNRAS, 395,160
Klypin, A., Zhao, H., & Somerville, R. S. 2002, ApJ, 573, 597
Maller, A. & Bullock, J. 2004, MNRAS, 355, 694
Nicastro, F. et al. 2005, Nat, 433, 495
Oppenheimer, B. D., Davé, R. 2006, MNRAS, 373, 1265
Oppenheimer, B. D., Davé, R. 2008a, MNRAS, 387, 577
Oppenheimer, B. D., Davé, R. 2008b, MNRAS, 395, 1875
Oppenheimer, B. D., Davé, R., & Finlator, K. 2009, MNRAS, 396, 729
Pedersen, K., Rasmussen, J., Sommer-Larsen, J., Toft, S., Benson, A. J., & Bower, R. G. 2006, NewA, 11, 465
Pen, U.-L. 1999, ApJ, 510, L1
Silk, J. 2003, MNRAS, 343, 249
Sommer-Larsen, J. & Dolgov, A. 2001, ApJ, 551, 608
Sommer-Larsen, J. 2006, ApJ, 644, L1
Springel, V. 2005, MNRAS, 364, 1105

Tripp, T. M., Savage, B. D., & Jenkins, E. B. 2000, ApJ, 534, L1
Vikhlinin, A. et al. 2006, ApJ, 640, 691
Wang, Q. D. 2007, in Chemodynamics: from first stars to local galaxies, ed. E. Emsellem et al., EAS v.24, 59
Wu, K. K. S., Fabian, A. C., & Nulsen, P. E. J. 2001, MNRAS, 324, 95

GALAXY EVOLUTION: EMERGING INSIGHTS AND FUTURE CHALLLENGES
ASP Conference Series, Vol.
@jourvol, © 2009
S. Jogee, I. Marinova, L. Hao, and G. A Blanc

The Impact of Feedback on Disk Galaxy Scaling Relations

Aaron A. Dutton[1] and Frank C. van den Bosch[2]

[1] *UCO/Lick Observatory, University of California, Santa Cruz, CA 95060*
[2] *Department of Physics and Astronomy, University of Utah, 115 South 1400 East, Salt Lake City, UT 84112-0830*

Abstract. We use a disk formation model to study the effects of galactic outflows (a.k.a. feedback) on the rotation velocity - stellar mass mass - disk size, gas fraction - stellar mass and gas phase metallicity - stellar mass scaling relations of disk galaxies. We show that models without outflows are unable to explain these scaling relations, having both the wrong slopes and normalization. The problem can be traced to the model galaxies having too many baryons. Models with outflows can solve this "over-cooling" problem by removing gas before it has time to turn into stars. Models with both momentum and energy driven winds can reproduce the observed scaling relations. However, these models predict different slopes which, with better observations, may be used to discriminate between these models.

1. Introduction

Galactic outflows are widely observed in galaxies that are undergoing, or have recently undergone, intense star formation: e.g., nearby starburst and IR bright galaxies (Martin 2005); post starburst galaxies at redshift $z \simeq 0.6$ (Tremonti et al. 2007); normal star forming galaxies at redshift $z = 1.4$ (Weiner et al. 2009) and Lyman break galaxies at redshifts $z \simeq 3$ (Shapley et al. 2003). However, whether or not galactic outflows play an important role in determining the properties of galaxies has yet to be determined.

A clue that outflows might play an important role in galaxy formation comes from fact that galaxy formation is inefficient. The galaxy formation efficiency, ϵ_{GF}, defined as the ratio between the galaxy mass (in stars and cold gas) to the total available baryons available to that galaxy (the cosmic baryon fraction times total virial mass of the halo) peaks at $\simeq 33\%$. This has been determined by galaxy-galaxy weak lensing studies (Hoekstra et al. 2005; Mandelbaum et al. 2006), which are independent of ΛCDM, and galaxy-halo number abundance matching (e.g. Conroy & Wechsler 2009), which assumes the ΛCDM halo mass function as a prior.

A low peak galaxy formation is a problem because cooling is expected to be efficient in typical galaxy mass haloes (with virial velocities ranging from $V_{\rm vir} \simeq 60$ to $\simeq 150\,{\rm km\ s^{-1}}$). At low masses (below $V_{\rm vir} \simeq 30\,{\rm km\ s^{-1}}$) cooling is suppressed by UV photo heating, while at high masses (and high virial temperatures) cooling is inefficient due to the physics of radiative cooling. Thus another mechanism is needed to suppress galaxy formation, in the halo mass

regime one would expect it to be highly efficient. Galactic outflows driven by supernova (SN) or young massive stars are the prime candidate, having been successfully invoked in semi-analytic galaxy formation models to explain the shallow faint end of the galaxy luminosity function (e.g. Benson et al. 2003).

1.1. Simple feedback models

The simplest, physically motivated, feedback models can be described by 2 parameters: the mass loading factor, η, defined as the ratio between the mass outflow rate, and the star formation rate; and the wind velocity, $V_{\rm wind}$. These two parameters are related by the mechanism that drives the wind, and the relation between the wind velocity and the escape velocity, $V_{\rm esc}$. Feedback models can be divided into 3 broad categories:

- **Constant Velocity Wind**: Assumes $V_{\rm wind} = const.$, which implies $\eta = const.$ A popular example is that implemented by Springel & Hernquist (2003), which assumes $V_{\rm wind} = 484$ km s^{-1} and $\eta = 2$. This corresponds to 25% of the SN energy being transferred to the wind (i.e. $\epsilon_{\rm FB} = 0.25$).
- **Momentum Driven Wind**: Assumes $V_{\rm wind} = 3\sigma \simeq V_{\rm esc}$, where σ is the velocity dispersion of the galaxy. Momentum conservation implies $\eta = (300/V_{\rm wind})$ (this assumes 100% momentum conservation) (Murray Quataert & Thompson 2005).
- **Energy Driven Wind**: Assumes $V_{\rm wind} = V_{\rm esc}$, energy conservation implies $\eta = \epsilon_{\rm FB}\, 10(300/V_{\rm wind})^2$, where $\epsilon_{\rm FB}$ is the fraction of SN energy that ends up in the outflow (e.g. van den Bosch 2001)

Finlator & Davé (2008) showed that models with the momentum driven wind provide a better match to the stellar mass - gas phase metallicity relation at $z \simeq 2$ than models with a constant velocity energy driven wind, or models without galaxy winds. However, it is not clear that this is a convincing argument against energy driven winds because Finlator & Davé (2008) did not consider an energy driven wind with the same assumption that they made for the momentum driven wind i.e. $V_{\rm wind} \simeq V_{\rm esc}$.

Here we use a semi-analytic disk galaxy formation model to discuss the observational signatures of different feedback models on the scaling relations of disk galaxies. We address the following questions: 1) Can models without outflows explain these relations? 2) Can models with outflow explain these relations? and 3) Can the scaling relations be used to discriminate between different wind models?

2. The Disk Galaxy Formation Model

Here we give a brief overview of the disk galaxy evolution model used in this proceedings. This model is described in detail in Dutton & van den Bosch (2009). The key difference with almost all disk evolution models is that in this model the inflow (due to gas cooling), outflow (due to SN driven winds), star formation rates, and metallicity, are computed *as a function of galacto centric*

radius, rather than being treated as global parameters. The main assumptions that characterize the framework of these models are the following:

1. **Mass Accretion History**: Dark matter haloes around disk galaxies grow by the smooth accretion of mass which we model with the Wechsler et al. (2002) mass accretion history (MAH). The shape of this MAH is specified by the concentration of the halo at redshift zero;

2. **Halo Structure**: The structure of the halo is given by the NFW profile (Navarro, Frenk, & White 1997), which is specified by two parameters: the mass and concentration. The evolution of the concentration parameter is given by the Bullock et al. (2001) model with parameters for a WMAP 5th year cosmology (Macciò et al. 2008);

3. **Angular Momentum**: Gas that enters the halo is shock heated to the virial temperature, and acquires the same distribution of specific angular momentum as the dark matter. We use the angular momentum distributions of the halo as parametrized by Sharma & Steinmetz (2005);

4. **Gas Cooling**: Gas cools radiatively, conserving its specific angular momentum, and forms a disk in centrifugal equilibrium;

5. **Star Formation**: Star formation occurs according to a Schmidt type law on the dense molecular gas, which is computed following Blitz & Rosolowsky (2006);

6. **Supernova Feedback**: Supernova feedback re-heats some of the cold gas, ejecting it from the disk and halo;

7. **Metal Enrichment**: Stars eject metals into the inter stellar medium, enriching the cold gas.

8. **Stellar Populations**: Bruzual & Charlot (2003) stellar population synthesis models are convolved with the star formation histories and metallicities to derive luminosities and surface brightness profiles.

3. Results

3.1. Impact of Feedback on Velocity, Stellar Mass and Disk Size

Fig. 1 shows the impact of feedback on the rotation velocity, stellar mass, and disk size of a galaxy that forms in a halo with virial mass $M_{\rm vir} = 6.3 \times 10^{11} h^{-1} M_{\odot}$, and which has the median halo concentration and angular momentum parameters for haloes of this mass. The green lines show the observed scaling relations from (Dutton et al. 2007 and Shen et al. 2003). The circles show models with feedback efficiency varying from $\epsilon_{\rm FB} = 0$ to 1. The model without feedback results in a galaxy that is too small and which rotates too fast. The upper right panel shows the galaxy mass fraction $m_{\rm gal} = M_{\rm gal}/M_{\rm vir}$, and galaxy spin parameter $\lambda_{\rm gal} = (j_{\rm gal}/m_{\rm gal})\lambda$, where λ is the spin parameter of the halo and $j_{\rm gal} = J_{\rm gal}/J_{\rm vir}$ is the angular momentum fraction of the galaxy, versus the feedback efficiency. This shows that the model

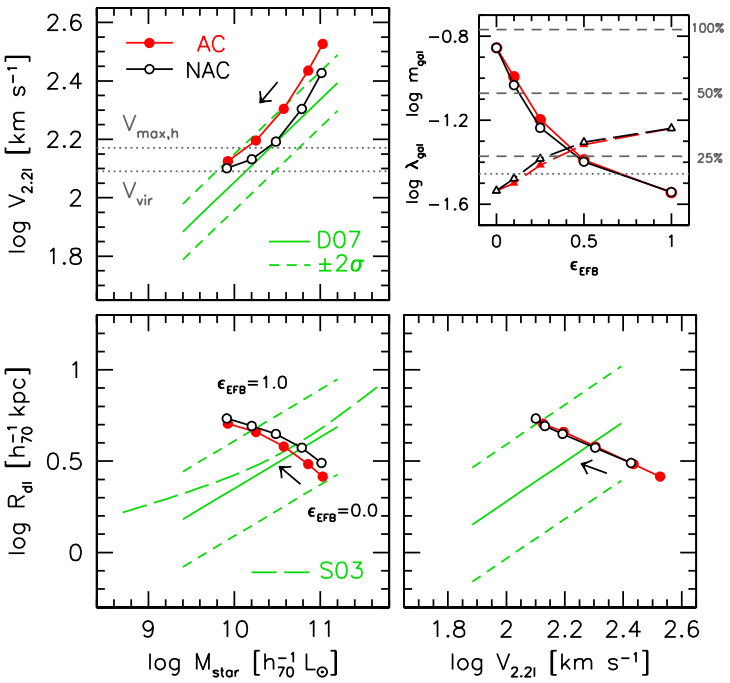

Figure 1. **Dependence of Velocity, Stellar Mass and Disk Size on Feedback:** Effect of feedback efficiency, $\epsilon_{\rm FB}$, for the energy driven wind, on the position of a galaxy with $M_{\rm vir} = 6.3 \times 10^{11} h^{-1} M_\odot$ in the VMR planes. The arrows indicate the direction of increasing $\epsilon_{\rm FB}$. Models with adiabatic contraction are shown with solid red symbols, models without adiabatic contraction are shown as black open symbols. The solid and dashed green lines in show the mean and 2σ scatter of the observed relations from Dutton et al. (2007, D07), assuming a Chabrier IMF. The long dashed green line shows the observed half-light radius stellar mass relation from Shen et al. (2003, S03). The panel in the top right shows the effect of feedback on the galaxy mass fraction, $m_{\rm gal}$ (circles), and galaxy spin parameter, $\lambda_{\rm gal}$ (triangles). The dashed horizontal lines show galaxy formation efficiencies of 100, 50, and 25 percent, the dotted horizontal line shows the spin parameter of the halo. As the feedback efficiency is increased the galaxy mass fraction ($m_{\rm gal}$) decreases, the galaxy spin parameter ($\lambda_{\rm gal}$) increases. This results in the rotation velocity decreasing, the stellar mass decreasing, and the size of the stellar disk increasing.

galaxy without feedback has acquired 85% of the available baryons and 80% of the available angular momentum. The mass and angular momentum fractions are less than unity because cooling is not 100% efficient. The angular momentum fraction is less than the galaxy mass fraction because cooling occurs from the inside-out.

As the feedback efficiency is increased the galaxy stellar mass decreases, disk size increases and the rotation velocity decreases. These changes are primarily driven by the decrease in the galaxy mass fraction, $m_{\rm gal}$, and secondarily by the

increase in the galaxy spin parameter, $\lambda_{\rm gal}$ (upper right panel). The increase in galaxy spin parameter is the result of preferential loss of low angular momentum material, which helps to explain the origin of exponential galaxy disks, which are otherwise not naturally produced in a CDM cosmologies (Dutton 2009).

The upper left panel shows that models with adiabatic contraction (Blumenthal et al. 1986) (red points and lines) rotate too fast for all feedback efficiencies. For a model without adiabatic contraction (open circles and black lines) the zero point of the VM relation is reproduced for feedback efficiencies of $\epsilon_{\rm FB} \simeq 0.1 - 0.5$. In order for our models to produce realistic rotation velocities, in the models that follow we will assume the halo does not contract in response to galaxy formation.

3.2. Impact of feedback on disk sizes, gas fractions and metallicity

Here we discuss the impact of feedback on the scaling relations between disk size, gas fractions and gas phase metallicity with stellar mass. We discuss three feedback models: 1) no feedback; 2) momentum driven feedback; 3) energy driven feedback with $\epsilon_{\rm FB} = 0.25$. For each model we generate a Monte Carlo sample of galaxies, with halo masses logarithmically sampled from $M_{\rm vir} = 10^{10} - 10^{13}\,h^{-1}M_{\odot}$, log-normal scatter in halo spin parameter λ, halo concentration, c, and angular momentum distribution shape, α.

Disk Sizes: The upper panels of Fig. 2 show the disk size- stellar mass relation for our three models. As expected from Fig. 1, the model without feedback produces a size-mass relation with the wrong zero point, but also with the wrong slope. Models with feedback reproduce the zero point of the size-mass relation, but they predict different slopes: 0.26 for the momentum driven wind and 0.14 for the energy driven wind. The energy driven wind predicts a shallower slope because it is more efficient at removing gas from lower mass haloes, which (see Fig. 1) moves galaxies to lower masses and larger sizes. Observationally the correct slope is not clear, with values of 0.24 (Pizagno et al. 2005) and 0.28 (Dutton et al. 2007) and 0.14 (at low masses) to 0.39 (at high masses) from Shen et al. (2003) being reported. Thus a more accurate observational determination of the size-stellar mass relation would provide useful constraints to these models.

Gas Fractions: It has emerged in the last few years (Springel & Hernquist 2005; Hopkins et al. 2009) that the gas fraction of galaxies plays an important role in determining the morphology of galaxies after mergers. In particular galaxies with high gas fractions can re-form their disks after major and intermediate mass mergers. This removes a potential problem for the formation of bulgeless and low bulge fraction galaxies in ΛCDM, where intermediate and major mergers occur in the lifetime of essentially all dark matter haloes.

The middle panels of Fig. 2 show the gas fraction vs. stellar mass relation. The green points show observations from Garnett (2002), with a fit to the mean and scatter of this data shown by the solid and dashed lines. The model without feedback (left) produces galaxies that are too gas poor, especially for lower mass galaxies. This problem is the result of the disks being too small, and hence too high surface density, which results in more efficient star formation. The models with feedback both reproduce the observed relation, with the energy driven wind predicting a higher zero point.

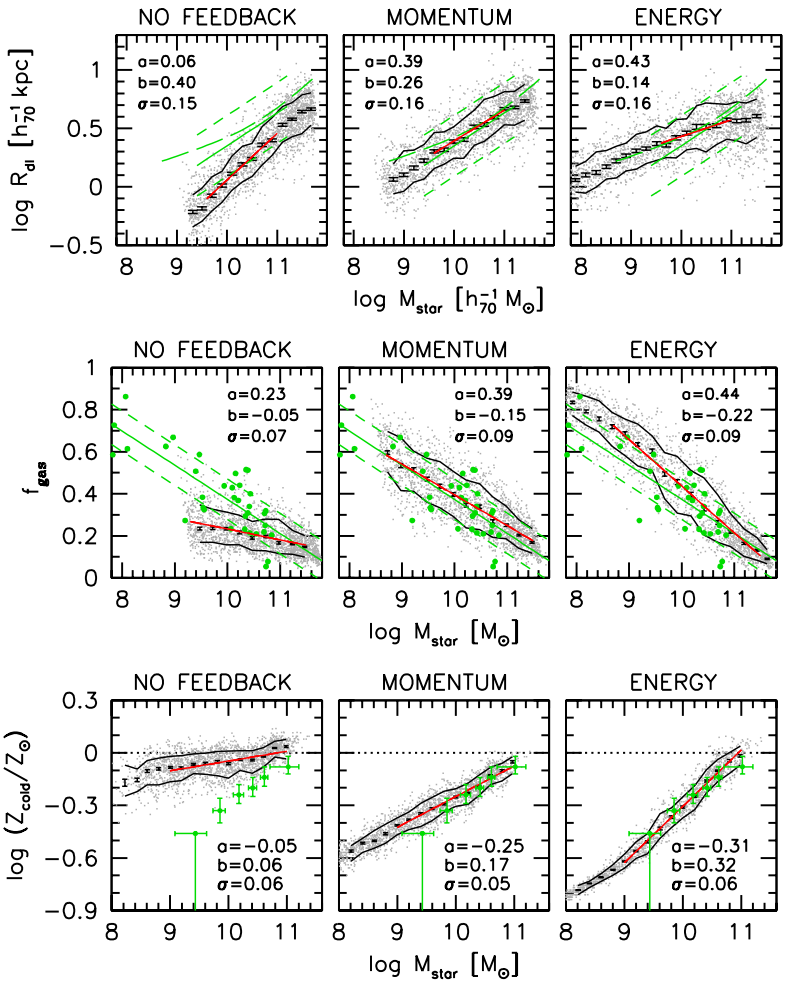

Figure 2. **Dependence of disk size, gas fraction and gas metallicity on feedback.** *Upper panels:* disk size - stellar mass; *Middle panels:* gas fraction - stellar mass, *Lower panels:* gas phase metallicity - stellar mass. The observed relations are given by green lines, points and symbols. The model galaxies are given by grey points, with the black lines showing the 14th and 86th percentiles in stellar mass bins. For the size-mass relation and gas fraction mass scaling relations the data (Dutton et al. 2007; Shen et al. 2003; Garnett 2002) and models are for redshift $z = 0$. For the metallicity-mass relation the data (Erb et al. 2006) and models are for redshift $z = 2.26$. The sizes, gas fractions and metallicities are coupled, and yield different slopes for different feedback models

Mass Metallicity: Finlator & Davé (2008) used the mass metallicity relation at redshift $z \simeq 2$ to argue in favor of momentum driven winds over energy driven winds (of constant velocity). The lower panels of Fig. 2 show the stellar mass - gas metallicity relation at $z = 2.26$. We confirm the result of Finlator & Davé (2008) that models without feedback do not reproduce the mass-metallicity relation, and that models with momentum driven winds provide a good match to the observations. However, we also show that models with

energy driven winds provide a equally good match to the data. The energy and momentum driven winds do predict different slopes: 0.17 for momentum and 0.32 for energy, and thus more accurate observations, and especially to lower stellar masses, may be able to distinguish between these two models.

4. Summary

We have used a semi-analytic disk galaxy formation model to investigate the effects of galaxy outflows on the scaling relations of disk galaxies. We find that

1) None of the scaling relations can be reproduced in models without outflows: model galaxies rotate too fast, are too small, are too gas poor and are too metal rich. These problems are driven by the high baryonic mass fractions of these galaxies.

2) Models with outflows can solve this problem by removing gas from galaxies before it has had time to turn into stars.

3) Models with momentum and energy driven winds provide acceptable fits to the observed disk size-stellar mass, gas fraction stellar mass, and gas metallicity - stellar mass relations. However, these models predict different slopes (due to the different scaling between mass loading factor and wind velocity). Thus more accurate observations will be able to discriminate between these models.

References

Benson, A. J., et al. 2003, ApJ, 599, 38
Blitz, L., & Rosolowsky, E. 2006, ApJ, 650, 933
Blumenthal, G. R., Faber, S. M., Flores, R., & Primack, J. R. 1986, ApJ, 301, 27
Bruzual, G., & Charlot, S. 2003, MNRAS, 344, 1000
Bullock, J. S., et al. 2001, MNRAS, 321, 559
Conroy, C., & Wechsler, R. H. 2009, ApJ, 696, 620
Dutton, A. A., van den Bosch, F. C., Dekel, A., & Courteau, S. 2007, ApJ, 654, 27
Dutton, A. A., & van den Bosch, F. C. 2009, MNRAS, 396, 141
Dutton, A. A. 2009, MNRAS, 396, 121
Erb, D. K., et al. 2006, ApJ, 644, 813
Finlator, K., & Davé, R. 2008, MNRAS, 385, 2181
Garnett, D. R. 2002, ApJ, 581, 1019
Hoekstra, H., et al. 2005, ApJ, 635, 73
Hopkins, P.,F., Cox, T.J., Younger, J.D., & Hernquist, L. 2009, ApJ, 691, 1168
Macciò, A. V., Dutton, A. A., & van den Bosch, F. C. 2008, MNRAS, 391, 1940
Mandelbaum, R., et al. 2006, MNRAS, 368, 715
Martin, C. L. 2005, ApJ, 621, 227
Murray, N., Quataert, E., & Thompson, T. A. 2005, ApJ, 618, 569
Navarro, J. F., Frenk, C. S., & White, S. D. M. 1997, ApJ, 490, 493
Pizagno, J., et al. 2005, ApJ, 633, 844
Shapley, A. E., Steidel, C. C., Pettini, M., & Adelberger, K. L. 2003, ApJ, 588, 65
Sharma, S., & Steinmetz, M. 2005, ApJ, 628, 21
Shen, S., et al. 2003, MNRAS, 343, 978
Springel, V., & Hernquist, L. 2003, MNRAS, 339, 289
Springel, V., & Hernquist, L. 2005, ApJ, 622, L9
Tremonti, C. A., Moustakas, J., & Diamond-Stanic, A. M. 2007, ApJ, 663, L77
van den Bosch, F. C. 2001, MNRAS, 327, 1334

Wechsler, R. H., et al. 2002, ApJ, 568, 52
Weiner, B. J., et al. 2009, ApJ, 692, 187

GALAXY EVOLUTION: EMERGING INSIGHTS AND FUTURE CHALLLENGES
ASP Conference Series, Vol.
@jourvol, © 2009
S. Jogee, I. Marinova, L. Hao, and G. A Blanc

Gravitational Heating, Clumps, Overheating

Yuval Birnboim
Harvard Smithsonian Center for Astrophysics. 60 Garden Street, Cambridge, MA 02138, USA

Abstract. There is no shortage of energy around to solve the overcooling problem of cooling flow clusters. AGNs, as well as gravitational energy are both energetic enough to balance the cooling of cores of clusters. The challenge is to couple this energy to the baryons efficiently enough, and to distribute the energy in a manner that will not contradict observational constraints of metalicity and entropy profiles. Here we propose that if a small fraction of the baryons that are accreted to the cluster halo are in the form of cold clumps, they would interact with the hot gas component via hydrodynamic drag. We show that such clumps carry enough energy, penetrate to the center, and heat the core significantly. We then study the dynamic response of the cluster to this kind of heating using a 1D hydrodynamic simulation with sub-grid clump heating, and produce reasonable entropy profile in a dynamic self-consistent way.

1. Introduction

Galaxy clusters grow by accreting dark matter and baryons from their surroundings. This is partly a continuous process of relatively smooth accretion, and partly via mergers. The existence of a visible, extended X-ray halo as well as limits on the size of the CD galaxy are two indicators that the smooth, continuous accretion is the more pronounced of the two. The baryons that are accreted in this process settle in hydrostatic equilibrium within the cluster's potential well. During this process they achieve virial equilibrium by passing through the virial shock and converting the kinetic energy of the infall to thermal energy. The baryons, at a temperature of a few $keVs$, cool primary by emitting Bremsstrahlung radiation which easily escape the halo and is observed by X-ray telescopes. After de-projection (tomography) of the luminosity and spectrum, radial profiles of temperature and densities are derived, and one can deduce the cooling times of the gas, which, for the centers of cooling flow cluster, is ≤ 1 Gyr, much shorter than the age of typical clusters that, according to ΛCDM formation history (Press & Schechter 1974) should have been in place at $z \geq 1$. Had this gas cooled, *i)* cool gas would have been seen in the halo (no gas below $T = \frac{1}{3}T_{\rm vir}$ is observed), *ii)* a census of all the baryons in galaxies is significantly smaller than amount of gas that was expected to cool from the halo, and *iii)* the star formation within the CD would have been $10^2 - 10^3 M_\odot$ yr^{-1}(two orders of magnitude larger than typically observed). These three contradictions are three manifestations of the overcooling problem of cooling flow clusters. It is highly unlikely that there is a "hidden" baryonic component in cluster halos, so most explanations invoke some kind of heating mechanisms that would balance the cooling, keeping the gas hot and diffuse.

The energies needed to compensate for the rapid cooling of cluster halos are $\sim 10^{45}$ erg s^{-1} which, over the lifetime of the cluster amounts to $\sim 10^{62}$ erg. These required energy rates can originate from AGN emission from the CD (Ciotti & Ostriker 1997, as well as many others), and by gravitational energy. Diffuse baryons falling into a gravitational well convert gravitational energy to kinetic, and ultimately to thermal. This thermal input into the system is usually local, and acts to heat the infalling gas itself. It is necessary to couple this freshly accreted, hot gas, with the central cooling gas. Narayan & Medvedev (2001) have studied conduction and turbulence that could potentially couple the external part to the inner halo. Kim & Narayan (2003), as well as others, deduce that although the amount of energy is sufficient, the conduction coefficient is not enough and turbulence will produce the wrong entropy and metalicity profiles.

In this proceedings, we shall present a novel mechanism of gravitational heating of the central halo gas by the hydrodynamic interactions between cold clumps of accreted gas and the halo gas (Dekel & Birnboim 2008) and (Birnboim & Dekel 2009, in preparation). The structure of this proceeding paper is as follows: First (Section 2.) we show that the accreting gas carries a sufficient rate of energy to compensate for the cooling. Then we model infalling cold clumps, and study the physical processes of their interaction with the diffuse gas, instabilities and survivability (Section 3.). Using this model, we study the valid parameter space of these clumps (Section 4.1.). We further use these insights to construct a sub-grid model for 1D hydrodynamic simulation and present simulations of a cluster with and without such clumps (Section 4.2.). Finally we discuss possible origins of these clumps, and summarize (Section 5.).

2. Energetics

Gas falling from infinity to the virial radius will carry specific energy that correspond to the amount needed for heating itself to the virial temperature. Here we assume that because the gas is clumpy, it can penetrate further inwards than the virial radius, deeper into the potential well and release more energy. For an NFW (Navarro et al. 1997) halo profile with typical cluster concentration (Bullock et al. 2001), gas penetrating to $0.1R_{\rm vir}$ will release ~ 3.5 times the energy it would at $R_{\rm vir}$ (Dekel & Birnboim 2008). The baryonic profile is a generalized NFW model Dekel & Birnboim (see eq. 4 in 2008) with a core ($\alpha = 0$) that is perhaps indicated by observations (Donahue et al. 2006) and hydrodynamic simulations (Faltenbacher et al. 2007; Kaufmann et al. 2008) [1]. Figure 1, left, shows a comparison between the global cooling rate (using Sutherland & Dopita 1993, and $Z = 0.3Z_{\odot}$) and the heating rate assuming accretion rate by Neistein et al. (2006); Birnboim et al. (2007), diffuse baryonic fraction $f_b = 0.05$ and clump fraction of $f_c = 0.05$. The Heating/Cooling ratio becomes positive for $M_{\rm vir} \geq 10^{13}M_{\odot}$ so the gas accreted as clumps to clusters is sufficient to counter the cooling. For clusters of $10^{15}M_{\odot}$ there is an overabundance of energy of two orders of magnitude, much larger than typical energy emission rates from AGNs.

[1] In later sections we will use a hydrodynamic simulation for the cluster formation and the need to assume a profile will become moot

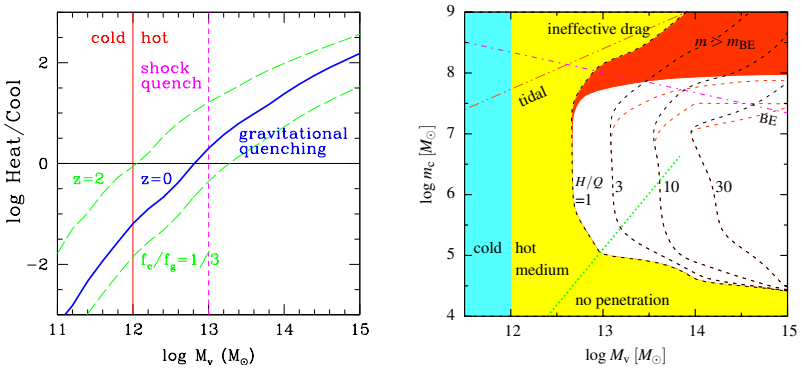

Figure 1. *Left:* Heating/Cooling rate as a function of virial mass for the fiducial case (blue, solid line): $f_b = 0.05$, $f_c = 0.05$, $Z = 0.3Z_\odot$ and $R_{final} = 0.1R_{\rm vir}$ at $z = 0$. Similar lines for $z = 2$ (upper,dashed green) and for $f_b = 0.075$, $f_c = 0.025$ (lower, dashed green) are also presented. Below $M_{\rm vir} = 10^{12}M_\odot$ the halo gas cannot be hot (Birnboim & Dekel 2003; Dekel & Birnboim 2006) and no hydrodynamic drag is possible. *Right:* allowed parameter space for clump heating mechanism on m_c/M_v space at $z = 0$, $Z = 0.3Z_\odot$ and $f_c = f_b = 0.05$: in white areas Heating/Cooling (H/Q) > 1. The black lines show H/Q of $3, 10, 30$. The yellow areas have H/Q¡1 and red areas are susceptible to Bonnor-Ebert instability. Both figures are originally from Dekel & Birnboim (2008) by the kind permission of John Wiley & Sons Ltd.

3. Physics of cold clumps

Drag forces. The clumps in focus here are cold (10^4K) gaseous clumps, in hydrostatic equilibrium with their surrounding hot gas. The hydrodynamic drag force is:

$$f_{drag} = -\frac{\pi}{2}C_d\rho_g V_r^2 r_c^2 \hat{V}_r, \qquad (1)$$

with ρ_g the ambient gas density, V_r the relative velocity between the clump and the ambient gas, $\hat{V}_r$ is the radius vector of that velocity, and r_c is the radius of the clump. C_d is the drag coefficient, and for gaseous spheres it is of order of 1 for subsonic velocities and supersonic velocities alike [2]. The drag force always act to decrease the kinetic energy of the clump. This energy is converted into thermal energy of the *hot gas* (see Murray & Lin (2004) and discussion in Dekel & Birnboim (2008)). The rate of heating is $\frac{dE}{dt} = f_d|V_r|$, and the trajectory of the clumps tends to become radial because the velocity in the radial direction is replenished by the gravitational force, but the tangential velocity decreases

[2]While the equation of drag is the same for the subsonic and supersonic case, the dissipation mechanism is different. For subsonic motions the sphere creates turbulence which dissipates to heat. For supersonic motions a bow shock travels in front of the sphere heating the ambient gas. In the transonic regime C_d can increase to a factor of a few, but then decrease back to $C_d \sim 1$ for supersonic and subsonic velocities

monotonically. From eq. 1 it is evident that the deceleration is more efficient for smaller clumps, larger velocities, and larger gas density.

Survivability of clumps. Kelvin Helmholtz (KH) instabilities cause the clump to disintegrate after it repels its own mass in ambient gas (Murray & Lin 2004). The clumps disintegrate into a few pieces (typically 2), each piece undergoing the same drag forces and KH instability. If the clumps are too small, conduction will cause the clump to expand and disintegrate. The conduction coefficient f_s (Spitzer 1962), depends strongly on the unknown magnetic properties of the gas and is assumed here to be $0.01 \leq f_s \leq 0.1$. A discussion on that is present in Maller & Bullock (2004). If, however, the clump is too massive, it will become gravitationally unstable and collapse under its own gravity and the external pressure. The Bonnor-Ebbert mass (Ebert 1955; Bonnor 1956) sets the maximal allowed clump mass.

Death of clumps. As clouds fragment and become more susceptible to conduction and small scale turbulence, heat from the surrounding hot gas will flow into the cold clump residue, heating it until it joins its surrounding halo. In this final stages, the clump "steals" energy from the hot gas, cooling it. The net effect, however, is heating because the clumps spends 3.5 times than it ultimately absorbs. This cooling has been taken into effect in the static and dynamic tests in the following sections. In cases where clumps exceed the Bonnor-Ebert mass (Jeans mass with external pressure confinement) the clump gas would turn into star without such "theft".

Local and global instabilities. The cooling rate of the baryons, in the Bremsstrahlung regime scales (for isobaric gas) scales as $\frac{de_{cool}}{dt} \sim \rho_g^2 T^{1/2} \sim \rho^{1.5}$. Field (1965) noted that heating must be scale with a power at least as large for the gas to be cooling-stable. However, the clump heating scales like ρ_g (eq. 1). This means that, assuming some parcel of gas that is initially in heating/cooling equilibrium, if gas is perturbed such that the cooling becomes slightly faster than the heating, the gas contracts, causing the discrepancy between heating and cooling to increase even further. If, on the other hand, heating is larger than the cooling, the gas will expand, causing the cooling to become even less efficient with respect to the heating. As we will show in Section 4.2., the later case actually occurs, and causes some of the shells to heat and expand more than their surrounding. This creates entropy inversions, which are regulated by convection. This local instability, as it turns out, does not effect the global stability of the halo: the location of the virial shock, the temperature, and the dynamics of the gas throughout the halo does not change as a result of this heating (see Section 4.2.).

Origin of clumps. In Section 4.1. we show that allowed masses for the gaseous clumps is between $10^5 - 10^8 M_\odot$. Mechanisms for formation of such clumps are still under investigation. The virial temperature that corresponds to mini-halos with baryonic mass $\leq 10^8 M_\odot$ is smaller than $10^4 K$ so even if dark matter mini-halos are formed, they cannot retain their gas after reionization. Cooling instability, especially in filaments or partly shocked gas at the edges of the clusters ($T \sim 10^5 - 10^6 K$) can potentially create such clumps. These clumps can also be produced within halos (Maller & Bullock 2004). No hydrodynamic simulation today has the resolution to investigate the formation of such clumps.

4. Numerical tests and simulations

4.1. Static Monte-Carlo simulations

The drag force equation and clump fragmentation have been incorporated into a Monte-Carlo simulation of a static NFW halo with a baryonic core (see Dekel & Birnboim 2008, for details). In these simulations the initial trajectories of 4000 clumps were drawn from reasonable distributions, and the heating rates were calculated as a function of radius, following fragmentation, evaporation, conduction, local Bonnor-Ebert masses, as well as dynamical friction. In some cases, a dark matter (DM) counterpart for the clumps was initially assumed. The DM subhalo generally gets ripped from the baryonic part during the first passage near the center, because the drag forces act on the baryons alone, and introduce forces between the DM and the baryons. Figure 1, right, describes results of the Monte-Carlo approach by mapping the allowed range in m_c/M_v parameter space. *For halos above* $10^{13}M_\odot$*, and clumps between* $10^5 - 10^8 M_\odot$*, the heating rate is larger than the cooling rate*, for the fiducial values described in the caption.

4.2. 1D hydrodynamic simulations

Figure 2. Results of a 1D Hydrodynamic simulation of a $3 \cdot 10^{14} M_\odot$ halo with $f_c + f_b = 0.1$ and $Z = 0.3 Z_\odot$. *Left:* Flow lines of Lagrangian shells (grey thin lines, with temperature colormap. Top panel - no clumps, second panel - $f_c = 0.01$ and $m_c = 10^7 M_\odot$, third panel - $f_c = 0.01, m_c = 10^7 M_\odot$ with mixing length model for convection ("clump+convection"), bottom panel - mass evolution of the central galaxy (red; solid - "no clumps", green; long-dashed - $f_c = 0.01$, blue; dashed - "clump+convection"). *Right:* Radial profiles at $z = 0$ of the "no clump" (red; solid) and "clump+convection" (blue; dashed) simulations. top - entropy, middle - temperature. Bottom - H/C for the "clump+convection" case.

The evolution of galaxy and cluster halos from initial perturbation has been studied with a 1D spherical Lagrangian hydrodynamic simulation with 1D dark matter shells that evolve separately through the baryonic shells, cooling and angular momentum (Birnboim & Dekel 2003; Dekel & Birnboim 2006; Birnboim et al. 2007). The effect of clump heating was added to the simulation as a sub-grid model of "clump shells" by assigning many clumps to shells similar to dark matter shells and allowing them to interact with the baryons via the drag equation and internal energy equation of the baryons. Each clump shell contains n clumps, and once the conditions for disintegration of clumps are met the clump mass of that shell is divided by 2 and n is multiplied by 2. Once clumps are killed (their mass drops below the conduction lower limit, $10^4 M_\odot$) the mass of the clump shell is added in situ to the baryonic shell overlapping the clump shell, and the new temperature is calculated by mixing the hot halo gas with the cold shell gas. Since the gas is cooling/heating unstable (see Section 3.), shells heat and expend in an unstable manner. To deal with this physical situation, gaseous shells are split into two when they become larger than their surrounding shells (AMR), and physical convection is modeled by mixing length theory (Spiegel 1963) was implemented.

Figure 2 shows results of three such simulations with similar initial profile that leads to a $3 \cdot 10^{14} M_{\odot}$ halo at $z = 0$. In the first, no clumps are added, the CD galaxy grows to $3 \cdot 10^{12} M_{\odot}$ and the star formation rates remains larger than $100 M_{\odot}$ yr^{-1} since $z = 1$. By assuming that 10% of the baryons are accreted as clumps the size of the CD galaxy is reduced to $1.5 \cdot 10^{12} M_{\odot}$, star formation rate reduced to virtually zero. The third simulation is similar to the second, except for mixing length model is used to smooth over the local instabilities. In all three simulations the virial mass and virial shock radius did not change indicating that the heating does not effect the global stability of the halo. The shape of the entropy profile and the central values are consistent with those of cooling flow profiles of Donahue et al. (2006). The hydrodynamic code and simulation results are described in detail in (Birnboim & Dekel 2009, in preparation)

5. Summary

We have shown that a sufficient amount of energy is released in the gravitational accretion to solve the overcooling problem of clusters (larger than $M_{\rm vir} \geq 10^{13} M_{\odot}$), if we assume that some part of the baryons penetrates to the inner parts rather that being stopped at the virial radius. The coupling between the incoming accreted mass and the ambient gas is achieved by assuming that the accreted baryons includes gaseous cold clump, that penetrate through the virial shock and heat the gas via hydrodynamic drag. A parameter space survey indicates that for halos larger than $10^{13} M_{\odot}$ and clump masses in the range $10^5 \leq m_c \leq 10^8 M_{\odot}$, clump heating can potentially solve the overcooling problem. The dynamic response of cluster halos to clump heating, cooling and mass deposition in the inner parts in then examined. For the set of values $M_{\rm vir} = 3 \cdot 10^{14} M_{\odot}$, $m_c = 10^7 M_{\odot}$, $f_b + f_c = 0.1$, $f_c = 0.01$, the resulting entropy and temperature profiles match typical observed cooling flow clusters reasonably well. The physical processes discussed here are already included in 3D hydrodynamic simulations but we note that to simulate the drag and the formation of such clumps each $10^7 M_{\odot}$ clump need to be well resolved, which is typically not the case for $10^{15} M_{\odot}$ clusters.

Acknowledgments. These proceedings summarize work carried out in collaboration with my PhD advisor and current collaborator, Avishai Dekel, whom I wish to thank.

References

Birnboim Y., Dekel A., 2003, MNRAS, 345, 349
Birnboim Y., Dekel A., Neistein E., 2007, MNRAS, 380, 339
Bonnor W. B., 1956, MNRAS, 116, 351
Bullock J. S., Kolatt T. S., Sigad Y., Somerville R. S., Kravtsov A. V., Klypin A. A., Primack J. R., Dekel A., 2001, MNRAS, 321, 559
Ciotti L., Ostriker J. P., 1997, ApJ, 487, L105+
Dekel A., Birnboim Y., 2006, MNRAS, 368, 2
Dekel A., Birnboim Y., 2008, MNRAS, 383, 119
Donahue M., Horner D. J., Cavagnolo K. W., Voit G. M., 2006, ApJ, 643, 730
Ebert R., 1955, Zeitschrift fur Astrophysik, 37, 217
Faltenbacher A., Hoffman Y., Gottlöber S., Yepes G., 2007, MNRAS, 376, 1327

Field G. B., 1965, ApJ, 142, 531
Kaufmann T., Bullock J. S., Maller A. H., Fang T., Wadsley J., 2008, ArXiv e-prints
Kim W.-T., Narayan R., 2003, ApJ, 596, 889
Maller A. H., Bullock J. S., 2004, MNRAS, 355, 694
Murray S. D., Lin D. N. C., 2004, ApJ, 615, 586
Narayan R., Medvedev M. V., 2001, ApJ, 562, L129
Navarro J. F., Frenk C. S., White S. D. M., 1997, ApJ, 490, 493
Neistein E., van den Bosch F. C., Dekel A., 2006, MNRAS, 372, 933
Press W. H., Schechter P., 1974, ApJ, 187, 425
Spiegel E. A., 1963, ApJ, 138, 216
Spitzer L., 1962, Physics of Fully Ionized Gases. Physics of Fully Ionized Gases, New York: Interscience (2nd edition), 1962
Sutherland R. S., Dopita M. A., 1993, ApJS, 88, 253

GALAXY EVOLUTION: EMERGING INSIGHTS AND FUTURE CHALLLENGES
ASP Conference Series, Vol.
@jourvol, © 2009
S. Jogee, I. Marinova, L. Hao, and G. A Blanc

Empirical Evidence for Quasar Feedback

Christy Tremonti

Max Planck Institut für Astronomie, Königstuhl 17, D-69117 Heidelberg, Germany

Aleksandar M. Diamond-Stanic

Steward Observatory, University of Arizona, 933 N Cherry Ave., Tucson AZ 85721, USA

John Moustakas

Department of Physics, New York University, 4 Washington Place, New York, NY 10003, USA

Abstract. In many modern theoretical models quasar feedback is invoked to drive gas and dust from galaxies and abruptly quench star formation. However, this idea has yet to be observationally confirmed. To gain insight into the role and relative importance of quasar feedback we are studying a sample of 35 massive post-starburst galaxies at $z \sim 0.6$. These objects are the likely remnants of major mergers, observed a few hundred million years after the peak of their star formation and quasar activity. In two-thirds of the sample we detect Mg II absorption lines that are blueshifted by 500–2400 km s^{-1} with respect to the host galaxy. These fossil galactic winds are significantly faster than winds observed in starburst galaxies. We estimate the mass and energy of the outflows and conclude that quasar feedback played a role in expelling the cool gas and quenching star formation.

1. Introduction

To gain leverage on the physical processes that govern galaxy evolution it is valuable to study galaxies at the extremes of parameter space. In particular, the formation of the most massive galaxies in the Universe poses numerous challenges to theoretical models of galaxy formation. It is generally accepted that massive, early-type galaxies form via mergers of gas-rich disk galaxies: the merger triggers a large burst of centrally concentrated star formation that consumes the gas reservoir, leading to a quiescent, passively evolving stellar population (Toomre & Toomre 1972; Mihos & Hernquist 1994). However, models that only include star formation feedback tend to produce galaxies that are too luminous and blue to match observations (Croton et al. 2006; Bower et al. 2006). Several modern theoretical models include quasar feedback as a way of rapidly quenching the starburst and producing redder, less luminous end products (e.g., Granato et al. 2004; Springel, Di Matteo, & Hernquist 2005; Hopkins et al. 2006). In these models a small fraction of the black hole accretion energy is coupled to

the surrounding gas, which drives out gas and dust in a powerful supergalactic wind.

Observationally, the role and relative importance of quasar feedback for the formation of massive, early-type galaxies remains an open question. In starburst galaxies, supernova-driven outflows with velocities of 50–500 km s^{-1} are commonly via the presence of gas absorption lines that are blueshifted relative to stellar features (e.g., Heckman et al. 2000). In principle AGN-driven winds might produce similar observational signatures with higher outflow velocities (Thacker, Scannapieco, & Couchman 2006). However the cool gas tracers commonly observed in starburst galaxies are typically ionized by the quasar (Wild et al. 2008). Moreover, the quasar outshines the host galaxy making it difficult to distinguish between absorption arising in parsec-scale nuclear clouds and kpc-scale galactic winds. To circumvent these issues we have elected to look for the remnants of AGN-driven galactic winds during the post-starburst phase, a few 100 Myr after the peak of the star formation and AGN activity (Tremonti, Moustakas, & Diamond-Stanic 2007).

2. Post-Starburst, Post-Quasar Galaxies

Post-starburst galaxies are characterized by strong stellar Balmer absorption from A-stars, but little nebular emission indicative of on-going star formation. Local post-starbursts (sometimes called "E+A" or "K+A" galaxies) typically have the kinematic and morphological signatures of pressure-supported spheroids (Norton et al. 2001), low surface brightness tidal tails indicative of a recent major merger (Yang et al. 2004, 2008) and the spectroscopic signatures of weak AGN activity (Yan et al. 2006; Yang et al. 2006). Post-starbursts are therefore presumed to be late-stage mergers that have passed through their quasar phase and are in transition to becoming early-type galaxies. As such they provide ideal testing grounds for AGN-feedback models.

We have obtained spectra of 35 post-starbursts at $z = 0.4$–0.8 at the 6.5-m MMT in order to search for evidence of galactic winds that may have played a role in shutting down star formation. We have selected galaxies at intermediate redshift because this may be an important epoch for the formation of early-type galaxies (e.g., Faber et al. 2007), and because the rest-frame near-UV is accessible in the optical. Coverage of the near-UV improves our ability to estimate the recent star formation history of our galaxies and it enables us to measure Mg II $\lambda\lambda 2796, 2803$ which is a sensitive probe of the ISM.

3. Quantifying Quenching: Clues from the Stellar Population

To gain insight into the recent star formation histories of our galaxies we compared their UV-optical spectra to the output of stellar population synthesis models (Bruzual & Charlot 2003). We adopted a star formation history designed to emulate a major merger between gas-rich disk galaxies and generated a large grid of synthetic spectra (λ = 2500–5000 Å). Free parameters of our model include the time since the peak star formation activity ($t_{\rm burst}$), the exponential decay time of the burst ($\tau_{\rm burst}$), the reddening, and the total mass of stars formed. Our modeling suggests that the galaxies are massive

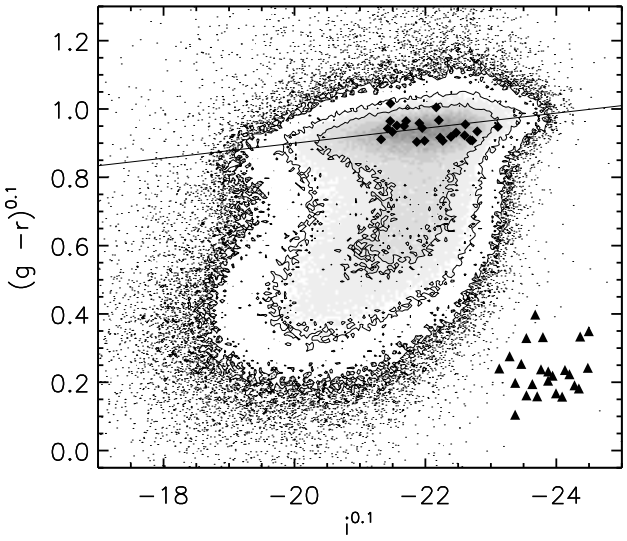

Figure 1. The expected evolution of our post-starburst galaxies on the color–magnitude diagram. The greyscale shows SDSS galaxies ($r_{\rm AB} < 17.77, z = 0.04$–$0.2$), with the mean color of the red-sequence denoted by a solid line. Triangles mark the position of our $z = 0.4$–0.8 post-starburst galaxies; diamonds show them evolved 2.5 Gyr forward in time. Our post-starburst have few counterparts in the local universe and are the progenitors of today's massive early-type galaxies.

($\log M_*/M_\odot \sim 10.5$–$11.5$) and minimally attenuated ($A_{\rm V} \sim 0.1$) and that they have very recently experienced a starburst ($t_{\rm burst} \sim 50$–350 Myr) that ended abruptly ($\tau_{\rm burst} \sim 25$ Myr). Figure 1 shows that these young, massive, dust-poor post-starbursts are more luminous and blue than the majority of galaxies in the local universe. Forward modeling of their stellar populations suggests that they will evolve onto the red-sequence in ~ 2.5 Gyr.

4. The Kinematics of Fossil Galactic Winds

Mg II $\lambda\lambda 2796, 2803$ is one of the strongest interstellar resonance absorption lines; however, it is also present in the atmospheres of A-stars and later spectral types. We use our best fit synthetic spectra to account for the stellar contribution to the lines. Figure 2 illustrates some examples. In roughly $^1/_3$ of galaxies the observed Mg II lines are predominantly stellar in origin. However, in the remainder (22/35) we measure significant interstellar absorption ($\rm EW_{2796} \sim 1$–5 Å). In many cases the ISM lines are so strong or blueshifted that the stellar contribution to the lines is insignificant. The depth of the Mg II absorption lines implies that the absorbing gas is in front of the bulk of the galaxies' stars (i.e., at kpc-scales).

We fit the ISM absorption lines following Rupke, Veilleux, & Sanders (2005a), using 1–3 velocity components. We record the velocity at line center

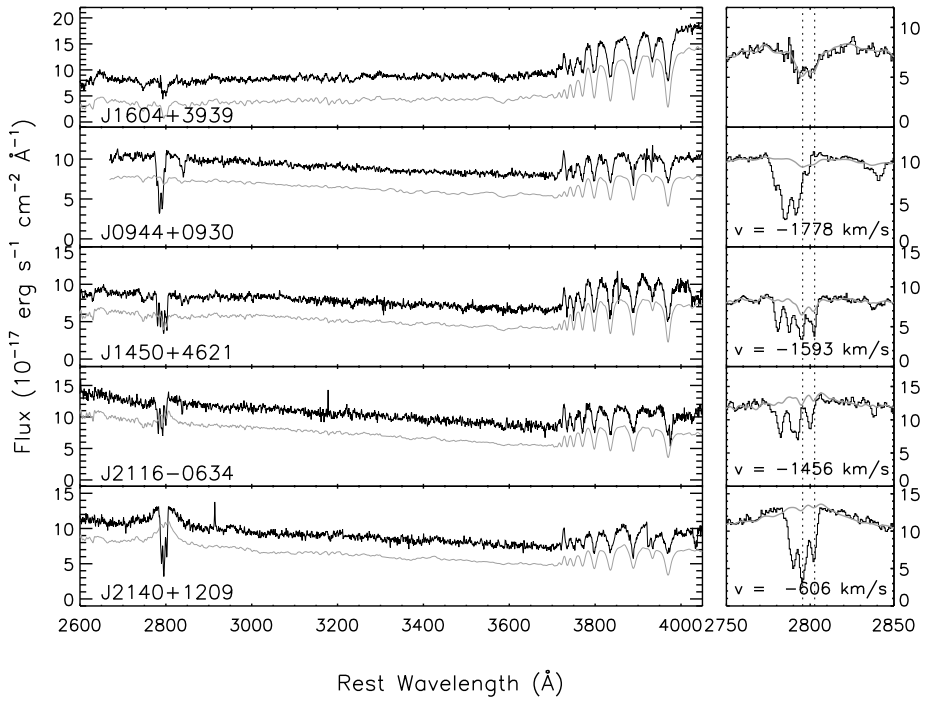

Figure 2. Example spectra (black) and continuum model fits (gray). In the lefthand panel, the continuum models are offset for clarity. The righthand panel highlights the region around the Mg II doublet. Dotted lines mark the rest wavelength of Mg II. The presence of blueshifted lines indicates an outflow. The velocity of the most blueshifted component is listed.

of each component and the maximum and EW-weighted average velocity of the components. The median values for the sample are $v_{\rm max} = -1230$ km s^{-1} and $v_{\rm avg} = -930$ km s^{-1}. In all cases the velocities are negative indicating that the absorption lines are blueshifted relative to the starlight. The large negative velocities and the high global covering factor implied by our $^2/_3$ detection frequency rule out tidal debris as the source of the absorbing gas. We hypothesize that the blueshifted lines originate in fossil galactic winds—winds that were launched near the peak of the starburst and AGN activity ~ 100 Myr ago.

In Figure 2 we plot absolute B-band magnitude versus ISM outflow velocity for our post-starburst galaxies and a variety of objects drawn from the literature. We include local starbursts (Schwartz & Martin 2004; Schwartz et al. 2006), Luminous and Ultra-Luminous Infrared Galaxies (LIRGs/ULIRGs; Rupke, Veilleux, & Sanders 2005b; Martin 2005), and $z \sim 3$ Lyman break galaxies (Pettini et al. 2001). For comparison, we also plot a sample of Low-ionization Broad Absorption Line quasars (LoBALs; Trump et al. 2006). In Figure 2 it is evident that more luminous starbursts drive faster outflows, but these rarely exceed 500 km s^{-1}. Notably, our post-starbursts have wind velocities

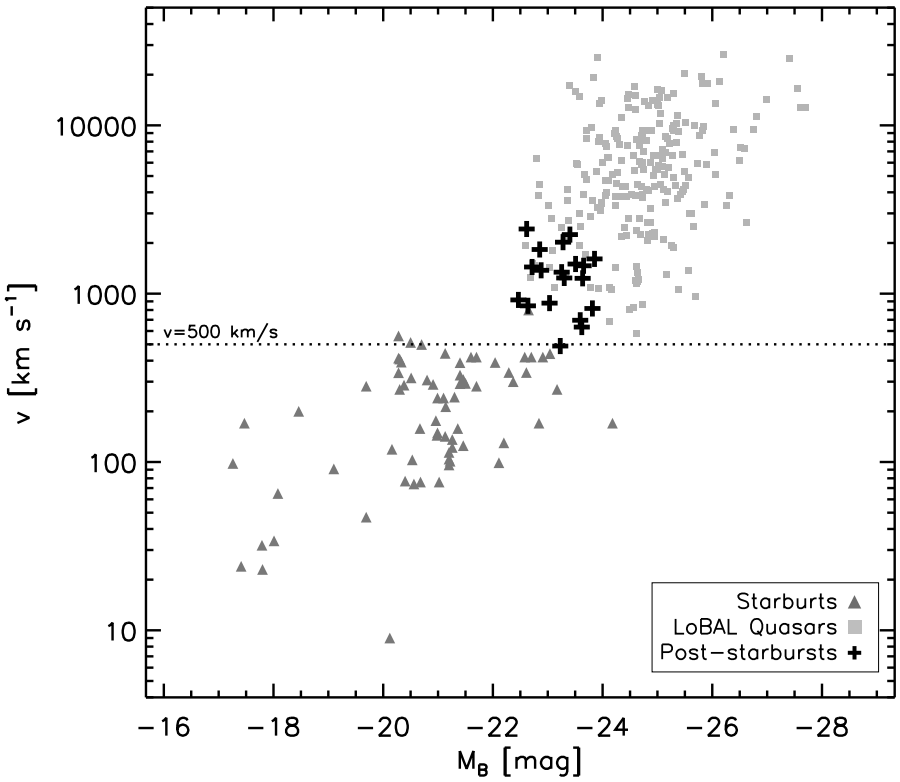

Figure 3. Outflow velocity versus absolute B-band magnitude. Our post-starburst galaxies (plus signs) have velocities higher than luminous starbursts (triangles) and at the lower end of the range of velocities observed in Low ionization Broad Absorption Line quasars (LoBALs; squares). This suggests that the post-starburst winds may have been driven by past quasar activity.

$\sim$ 2–5 times higher than than starbursts of comparable luminosity, suggesting that perhaps an additional power source contributed to driving the outflows.

LoBAL quasars, which are characterized by broad ($\sim$ 1000 km s^{-1}) Mg II absorption troughs, have mean outflow velocities of 500–30,000 km s^{-1} (Trump et al. 2006), overlapping at the low end with the velocities observed in our post-starbursts. LoBALs are prevalent in infrared-selected quasar samples which has led to speculation that they are young quasars in the process of removing their natal cocoons of gas and dust (Boroson & Meyers 1992; Farrah et al. 2007; Urrutia et al. 2009). However, it is presently unclear whether LoBAL outflows are a nuclear or galaxy-wide phenomena: detailed photoionization modeling of a handful objects has revealed outflowing gas at a wide range of scales ($\sim$ 0.1–10 kpc; de Kool et al. 2001, 2002; Korista et al. 2008). It is possible that the outflows observed in the LoBALs and post-starbursts represent the early and late phases of AGN-driven winds (the middle phase being invisible due to the ionization of Mg II by the quasar). Support for the notion that our post-starbursts are also post-quasars is provided by the spectra that exhibit weak

[O III] λ5007 lines, and in a few cases weak broad Mg II emission (lower panel of Fig. 2).

It is interesting to consider whether the outflows we observe could have been the direct cause of the abrupt drop in the star formation rate of our galaxies a few 100 Myr ago. This seems plausible if the winds entrained a large fraction of the cold ISM. We can crudely estimate the mass in the outflow using the Mg II column density that we derive from our line profile fits. (In the optically thin case the doublet ratio is 2:1; in our data the lines are moderately saturated.) We translate our Mg II columns into a total gas columns by correcting for the effects of ionization and depletion onto dust grains, and assuming a Mg/H ratio of 2.5 times the solar value. With these relatively crude corrections, we infer a median value of N(H)=2×10^{20} cm^{-2}.

The total mass in the outflow depends strongly on its geometry. Following Rupke et al. (2005b), we assume that the wind is a shell-like structure with a global covering factor equivalent to the detection frequency ($\sim 2/3$). To calculate the outer radius of the shell, $r_{\rm out}$, we adopt a simple picture where the wind is launched at the peak of the star formation and AGN activity and moves at constant velocity. Using the median values of the burst age ($t \simeq 100$ Myr) and outflow velocity ($v \simeq 1000$ km s^{-1}), we find $r_{\rm out} = vt = 100$ kpc. We consider two limiting cases: a thick shell with an inner radius $r_{\rm in} = 5$ kpc, and a thin shell with $r_{\rm in} = 99$ kpc. This yields masses of $M_{\rm wind} = 5 \times 10^9$ and 1.2×10^{11} M$_\odot$ for the thick and thin cases respectively, implying that between 5 and 50% of the galaxies' baryons are in the outflow. The energy needed to drive this outflow is 0.1–1.2 $\times 10^{60}$ ergs, an amount which is difficult to produce with supernovae and stellar winds even if the available mechanical energy couples to the ISM efficiently. The energy budget is more comfortably balanced by converting 0.05–1% of the rest mass of a 10^8 $M_\odot$ black hole into kinetic energy. For comparison, simulations typically adopt an efficiency factor of 0.5% (e.g., Springel et al. 2005).

5. The Case for Quasar Feedback

Our $z \sim 0.6$ post-starburst galaxies rank among the most luminous and massive galaxies in the universe ($M_{\rm B} = -22.5$ to -23.9 mag, $M_* = 0.2$–3×10^{11} $M_\odot$) and they offer a rare window on the formation of today's massive early-type galaxies. The detection of interstellar Mg II in $\sim 2/3$ of our galaxies enables us to probe the properties of the cold ISM. We find evidence for strong outflows in 22 systems, with velocities in the range $v_{\rm max} = -500$ to -2400 km s^{-1}. The median velocity is $v_{\rm max} = -1230$ km s^{-1}, which exceeds the 400–600 km s^{-1} velocities typical of luminous starburst galaxies (Heckman et al. 2000). We estimate that the outflows reach distances of $\sim$100 kpc and contain upwards of 10^9 $M_\odot$ of gas. Our estimates of the gas mass are uncertain due to corrections for dust depletion, ionization, metallicity, and geometry. However, our results are bolstered by recent observations of projected quasar pairs. Hennawi et al. (2006) detected optically thick H I absorption in 6 of 8 background quasars probing transverse distances of 20–150 kpc from foreground quasars. Prochaska & Hennawi (2009) obtained a deep Keck/HIRES spectrum of a sightline 108 kpc away from a $z \sim 2.4$ quasar and detected α-enhanced gas, consistent with the

outflow hypothesis. They infer $N_H = 4 \times 10^{20}$ cm, $M_{\rm wind} = 3 \times 10^{11} M_{\odot}$, and $E_{\rm wind} = 3 \times 10^{60}$ erg—numbers that agree remarkably with the values we infer for our post-starbursts. We conclude that quasars are likely to have played a role in driving powerful gas outflows and causing an abrupt truncation of star formation in massive galaxies.

Acknowledgments. C.A.T thanks the Alexander von Humboldt Foundation for their generous support.

References

Boroson, T. A., & Meyers, K. A. 1992, ApJ, 397, 442
Bower, R. G., Benson, A. J., Malbon, R., Helly, J. C., Frenk, C. S., Baugh, C. M., Cole, S., & Lacey, C. G. 2006, MNRAS, 370, 645
Bruzual, G., & Charlot, S. 2003, MNRAS, 344, 1000
Croton, D. J., et al. 2006, MNRAS, 365, 11
de Kool, M., Arav, N., Becker, R. H., Gregg, M. D., White, R. L., Laurent-Muehleisen, S. A., Price, T., & Korista, K. T. 2001, ApJ, 548, 609
de Kool, M., Becker, R. H., Gregg, M. D., White, R. L., & Arav, N. 2002, ApJ, 567, 58
Faber, S. M., et al. 2007, ApJ, 665, 265
Farrah, D., Lacy, M., Priddey, R., Borys, C., & Afonso, J. 2007, ApJ, 662, L59
Granato, G. L., De Zotti, G., Silva, L., Bressan, A., & Danese, L. 2004, ApJ, 600, 580
Heckman, T. M., Lehnert, M. D., Strickland, D. K., & Armus, L. 2000, ApJS, 129, 493
Hennawi, J. F., et al. 2006, ApJ, 651, 61
Hopkins, P. F., Hernquist, L., Cox, T. J., Di Matteo, T., Robertson, B., & Springel, V. 2006, ApJS, 163, 1
Korista, K. T., Bautista, M. A., Arav, N., Moe, M., Costantini, E., & Benn, C. 2008, ApJ, 688, 108
Martin, C. L. 2005, ApJ, 621, 227
Menci, N., Fontana, A., Giallongo, E., Grazian, A., & Salimbeni, S. 2006, ApJ, 647, 753
Mihos, J. C., & Hernquist, L. 1994, ApJ, 431, L9
Norton, S. A., Gebhardt, K., Zabludoff, A. I., & Zaritsky, D. 2001, ApJ, 557, 150
Pettini, M., Shapley, A. E., Steidel, C. C., Cuby, J.-G., Dickinson, M., Moorwood, A. F. M., Adelberger, K. L., & Giavalisco, M. 2001, ApJ, 554, 981
Prochaska, J. X., & Hennawi, J. F. 2009, ApJ, 690, 1558
Rupke, D. S., Veilleux, S., & Sanders, D. B. 2005a, ApJS, 160, 87
Rupke, D. S., Veilleux, S., & Sanders, D. B. 2005b, ApJS, 160, 115
Schwartz, C. M., & Martin, C. L. 2004, ApJ, 610, 201
Schwartz, C. M., Martin, C. L., Chandar, R., Leitherer, C., Heckman, T. M., & Oey, M. S. 2006, ApJ, 646, 858
Springel, V., Di Matteo, T., & Hernquist, L. 2005, ApJ, 620, L79
Thacker, R. J., Scannapieco, E., & Couchman, H. M. P. 2006, ApJ, 653, 86
Toomre, A., & Toomre, J. 1972, ApJ, 178, 623
Tremonti, C. A., Moustakas, J., & Diamond-Stanic, A. M. 2007, ApJ, 663, L77
Trump, J. R., et al. 2006, ApJS, 165, 188
Urrutia, T., Becker, R. H., White, R. L., Glikman, E., Lacy, M., Hodge, J., & Gregg, M. D. 2009, ApJ, 698, 1095
Wild, V., et al. 2008, MNRAS, 388, 227
Yan, R., Newman, J. A., Faber, S. M., Konidaris, N., Koo, D., & Davis, M. 2006, ApJ, 648, 281
Yang, Y., Zabludoff, A. I., Zaritsky, D., Lauer, T. R., & Mihos, J. C. 2004, ApJ, 607, 258
Yang, Y., Tremonti, C. A., Zabludoff, A. I., & Zaritsky, D. 2006, ApJ, 646, L33
Yang, Y., Zabludoff, A. I., Zaritsky, D., & Mihos, J. C. 2008, ApJ, 688, 945

GALAXY EVOLUTION: EMERGING INSIGHTS AND FUTURE CHALLLENGES
ASP Conference Series, Vol.
@jourvol, © 2009
S. Jogee, I. Marinova, L. Hao, and G. A Blanc

Broad Absorption Line Quasars and Galaxy Evolution

Beverley J. Wills

University of Texas Department of Astronomy C1400, 1 University Station, Austin, TX 78712 USA

Abstract. Luminous QSOs are signposts to galaxy evolution. Local supermassive black holes are the faded relics of quasars in their heyday at redshifts ~ 2. Relationships between the masses of these local supermassive black holes and their host galaxy bulges reveal an intimate link, fundamental to galaxy evolution: the newly evolving galaxy fuels the seed black hole through its accretion disk and by loss of angular momentum and energy in the form of outflowing winds. As the central engine approaches Eddington luminosities, winds drive away dusty gas, revealing a luminous QSO and halting star formation in the galaxy bulge. Relativistic winds are manifested in powerful radio jets in $\sim 10\%$ of quasars, and sub-relativistic winds are revealed by broad blueshifted absorption troughs in the "broad absorption line" (BAL) quasars. Historically, BALs avoid powerful radio quasars. Here we examine the BALs to investigate this inverse connection.

1. Introduction

Blueshifted absorption is apparently present in $\sim 60\%$ of Active Galactic Nuclei, from low-velocity outflows in the low-luminosity Seyfert nuclei, to the broadest, most blue-shifted outflows ($\sim c/4$) in luminous QSOs (Ganguly & Brotherton 2008). Knigge et al. (2008) show that the distribution of absorption strength (AI) is bimodal, with the highest AI corresponding to the classical BAL QSOs. They derive an intrinsic fraction of BAL QSOs of 17%. Whether or not a QSO shows BALs depends on orientation, ie, whether or not the absorbing outflow intercepts the line-of-sight. This much is clear from limits on resonance line radiation scattered by the absorbing clouds (Voit, Weymann, & Korista 1993); spectropolarimetry reveals partially obscured and unobscured scattering light paths in the same BAL QSO (Hines et al. 2001). Also supporting orientation is the similarity of the optical-UV emission line and continuum spectra of BAL and non-BAL QSOs (Weymann et al. 1991), although there are small, probably important differences (Ganguly et al. 2007). Orientation isn't the whole story because the fraction of classical BAL QSOs amongst all QSOs declines from 20% to $\lesssim 8\%$ with increasing radio luminosity (Shankar, Dai, & Sivakoff 2008, and references therein). There is quite strong evidence for a radio evolutionary link between BAL and non-BAL QSOs.

We noted in a qualitative way, possible differences among BAL features, illustrated in Figure 1. A classical smooth, deep, BAL trough, typical of radio-quiet QSOs, a less deep, broken trough that seems to be typical of radio-loud BAL QSOs, and relatively narrow structure seen in very radio-loud QSOs. The motivation for the present investigation is to search for differences in BAL

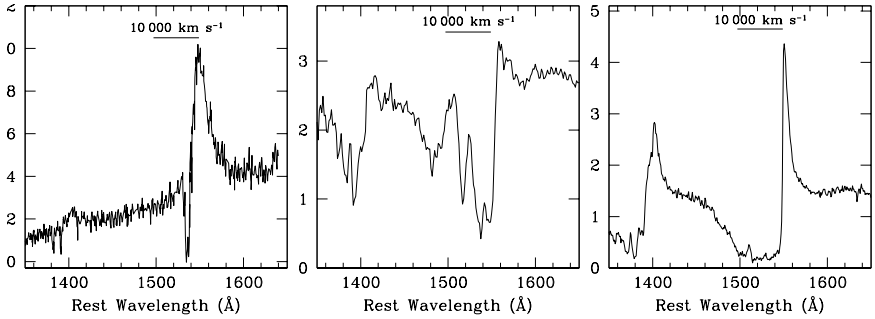

Figure 1. Left: Narrow Absorption Lines in the lobe-dominant RLQ 3C 270.1 (Anderson et al. 1987). Si IV emission is seen at $\sim$ 1397Å, with corresponding absorption. Middle: Narrow and broad absorption lines in the radio-loud BAL QSO, FIRST J101614.3+520916 (Gregg et al. 2000). Right: BALs in the classical, radio-quiet BAL QSO PHL 5200 (Korista et al. 1993). Note the horizontal bars representing a velocity scale.

characteristics as a function of other spectral properties, optical luminosity, and radio loudness (or radio luminosity).

2. Samples and Data

We use the C IVλ1549 region because it is readily accessible to ground-based observations, and is the cleanest region for defining a continuum against which to measure blueshifted absorption. We measured C IVλ1549 BAL troughs in 100 spectra available from Korista et al. (1993) (the LBQS sample), Ogle et al. (1999), Becker et al. (2000, 2001), Menou et al. (2001), and Brotherton et al. (1998): total rest-frame equivalent width EW, the difference in BAL EW about outflow velocities of 2000 km s^{-1} and 5000 km s^{-1} (e.g., $r2b$ = [(EW $>$ 2000 km s^{-1})$-$ (EW $<$ 2000 km s^{-1})]/EW), $v_{\rm max}$, $v_{\rm min}$, etc. We derived a consistent set of r magnitudes, corrected for extinction and k-corrected for continuum and emission lines (using the SDSS BAL QSO template). Thus we determined an absolute magnitude $M_{b{\rm r}}$ at b rest wavelength (H$_0$ = 70 km s^{-1} Mpc^{-1}). Rest-frame 5GHz luminosities were derived from flux densities in the NASA Extragalactic Database, or 21cm flux densities or upper limits, derived from FIRST maps. We also collected similar data for miniBAL absorption lines (Foltz et al. 1986; Baker et al. 2002). We calculated radio-loudness defined as the rest frame ratio of 5 GHz luminosity to that at B-band.

3. BALs and Radio Loudness

Figures 2–4 show the decline in BAL strength, $v_{\rm max}$, and the fraction of outflow with $v_{\rm max}$ $>$ 2000 km s^{-1}, with increasing radio-loudness (or radio luminosity). The radio-selected BAL QSOs lie intermediate between the classical optically-selected BAL QSOs and the most radio-loud QSOs, which have characteristics as shown in Fig. 1. We include absorption of small EW ($\lesssim$ few Å) and low $v_{\rm max}$ ($\lesssim$ few 100 km s^{-1}), but most of these are not related to BAL outflows (Knigge

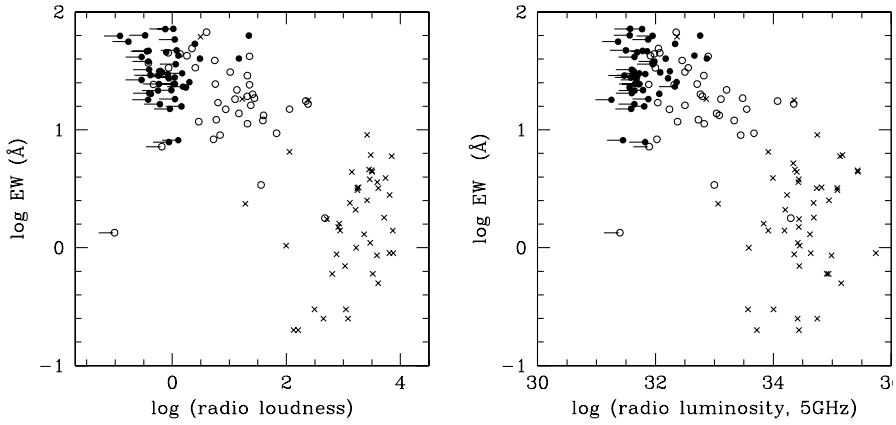

Figure 2. Total absorption EW vs. log (radio-loudness) (left) and log (radio luminosity) (right). Classical optically selected BAL quasars (•), radio-selected BAL quasars (○) and radio-loud non-classical BAL absorbers (×).

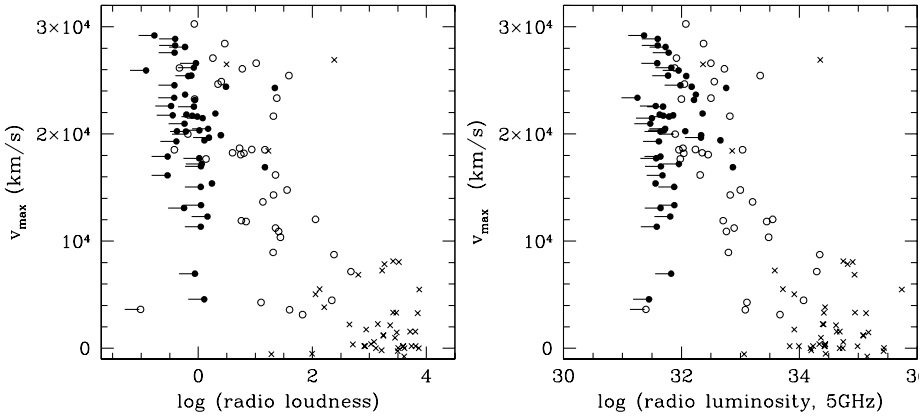

Figure 3. Maximum outflow speed $v_{\rm max}$ vs. log (radio-loudness) (left) and log (radio luminosity) (right). Symbols are as in Fig. 2.

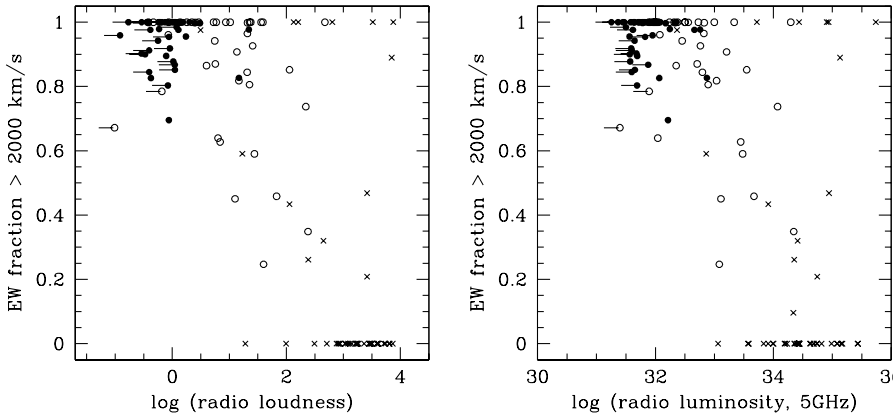

Figure 4. Fraction of EW for outflow speeds > 2000 km/s vs. log (radio-loudness) (left) and log (radio luminosity) (right). Symbols are as in Fig. 2.

et al. 2008). In Fig. 2 and 3 the significant trends are with the upper envelope of the distribution as small EW and $v_{\rm max}$ were not included in selection of classical optically-selected BAL QSOs (Weymann et al. 1991).

Shankar et al. (2008) do not find our significant trends of $v_{\rm max}$ with radio-loudness. Shankar et al. and some other studies investigate FIRST selected BAL QSOs, for which the sampling of the lowest (and highest) radio-loudness bins is quite sparse. Follow-up of these and other trends requires careful consideration of selection effects.

The clear decline of the fraction of BAL QSOs with increasing radioloudness, and the trends suggested in Figs. 2–4, point to a magnetohydrodynamic connection between powerful relativistic radio jets and sub-relativistic low-ionization outflows (disk winds). Unlike most radio-detected QSOs, most radio-detected BAL QSOs appear to have very small linear sizes $\lesssim 0.1$ pc indicating an early stage in radio source lifetime (Montenegro-Montes et al. 2009, and references therein). The most radio-loud BAL QSOs are those with clearest evidence for a symmetry axis. They are also suggested to have the highest black hole masses and among the lowest accretion ratios ($L/L_{\rm Edd}$) (Lacy et al. 2001; Boroson 2002). Therefore an evolutionary connection is suggested. I have not found a model that naturally predicts BALs should abhor powerful radio jets (Everett 2007).

Acknowledgments. We thank K. Korista, R. Becker, P. Ogle, and M. Brotherton for providing spectra. This research used the NASA/IPAC Extragalactic Database (NED, http://nedwww.ipac.caltech.edu/), and SDSS (http://www.sdss.org/).

References

Anderson, S. F., Weymann, R. J., Foltz, C. B., & Chaffee, F. H., Jr. 1987, AJ, 94, 278
Baker, J. C., Hunstead, R. W., Athreya, R. M., Barthel, P. D., de Silva, E., Lehnert, M. D., & Saunders, R. D. E. 2002, ApJ, 568, 592
Becker, R. H., White, R. L., Gregg, M. D., Brotherton, M. S., Laurent-Muehleisen, S. A., & Arav, N. 2000, ApJ, 538, 72
Becker, R. H., et al. 2001, ApJS, 135, 227
Boroson, T. A. 2002, ApJ, 565, 78
Brotherton, M. S., van Breugel, W., Smith, R. J., Boyle, B. J., Shanks, T., Croom, S. M., Miller, L., & Becker, R. H. 1998, ApJ, 505, L7
Everett, J. E. 2007, Ap&SS, 311, 269
Foltz, C. B., Weymann, R. J., Peterson, B. M., Sun, L., Malkan, M. A., & Chaffee, F. H., Jr. 1986, ApJ, 307, 504
Ganguly, R., & Brotherton, M. S. 2008, ApJ, 672, 102
Ganguly, R., Brotherton, M. S., Cales, S., Scoggins, B., Shang, Z., & Vestergaard, M. 2007, ApJ, 665, 990
Gregg, M. D., Becker, R. H., Brotherton, M. S., Laurent-Muehleisen, S. A., Lacy, M., & White, R. L. 2000, ApJ, 544, 142
Hines, D. C., Schmidt, G. D., Gordon, K. D., Smith, P. S., Wills, B. J., Allen, R. G., & Sitko, M. L. 2001, ApJ, 563, 512
Knigge, C., Scaringi, S., Goad, M. R., & Cottis, C. E. 2008, MNRAS, 386, 1426
Korista, K. T., Voit, G. M., Morris, S. L., & Weymann, R. J. 1993, ApJS, 88, 357
Lacy, M., Laurent-Muehleisen, S. A., Ridgway, S. E., Becker, R. H., & White, R. L. 2001, ApJ, 551, L17
Menou, K., et al. 2001, ApJ, 561, 645

Montenegro-Montes, F. M., Mack, K.-H., Benn, C. R., Carballo, R., González-Serrano, J. I., Holt, J., & Jiménez-Luján, F. 2009, Astronomische Nachrichten, 330, 157
Ogle, P. M., Cohen, M. H., Miller, J. S., Tran, H. D., Goodrich, R. W., & Martel, A. R. 1999, ApJS, 125, 1
Shankar, F., Dai, X., & Sivakoff, G. R. 2008, ApJ, 687, 859
Snellen, I., & Schilizzi, R. 2002, New Astronomy Review, 46, 61
Voit, G. M., Weymann, R. J., & Korista, K. T. 1993, ApJ, 413, 95
Weymann, R. J., Morris, S. L., Foltz, C. B., & Hewett, P. C. 1991, ApJ, 373, 23

GALAXY EVOLUTION: EMERGING INSIGHTS AND FUTURE CHALLLENGES
ASP Conference Series, Vol.
@jourvol, © 2009
S. Jogee, I. Marinova, L. Hao, and G. A Blanc

Identifying the Obscured Black-Hole Growth Phase of Distant Massive Galaxies

D. M. Alexander

Department of Physics, Durham University, Durham, DH1 3LE, UK

Abstract. It is well established that a dominant phase in the growth of massive galaxies occurred at high redshift and was heavily obscured by gas and dust. Many studies have explored the stellar growth of massive galaxies but few have combined these constraints with the growth of the supermassive black hole (SMBH; i.e., identified as AGN activity). In this brief contribution we highlight our work aimed at identifying AGNs in $z \approx 2$ luminous dust-obscured galaxies. Using both sensitive X-ray and infrared (IR)–submillimeter (submm) observations, we show that AGN activity is common in $z \approx 2$ dust-obscured systems. With a variety of techniques we have found that the majority of the AGN activity is heavily obscured, and construct diagnostics based on X-ray–IR data to identify some of the most heavily obscured AGNs in the Universe (i.e., AGNs obscured by Compton-thick material; $N_{\rm H} > 1.5 \times 10^{24}$ cm^{-2}). On the basis of these techniques we show that SMBH growth was typically heavily obscured ($N_{\rm H} \geq 10^{23}$ cm^{-2}) at $z \approx 2$, and find that the growth of the SMBH and spheroid was closely connected, even in the most rapidly evolving systems.

1. Introduction

There is no doubt that active galactic nuclei (AGN) are an important component in the formation and evolution of galaxies. The seminal discovery that massive galaxies in the local Universe harbor a super-massive black hole (SMBH) indicates that they must have hosted AGN activity over the past ≈ 13 Gyrs (e.g., Soltan 1982; Kormendy & Richstone 1995). Furthermore, the close relationship between the mass of the SMBH and the spheroid in local galaxies points towards a close connection between the growth of the SMBH and the host galaxy (e.g., Magorrian et al. 1998; Ferrarese & Merritt 2000). Finally, the most successful galaxy formation and large-scale structure models require AGN outflows to suppress star formation and reproduce the properties of massive galaxies in the local Universe (e.g., Croton et al. 2006; Bower et al. 2006).

Stellar population synthesis modelling of nearby galaxies and studies of the cosmic history of star formation indicate that the bulk of the stellar build up of massive galaxies must have occurred at high redshift ($z \approx 2$; i.e., when the Universe was $\approx 25\%$ the current age; e.g., Heavens et al. 2004; Hopkins et al. 2006). Under the assumption that the growth of the SMBH is concordant with that of the galaxy spheroid, the dominant growth phase of SMBH growth in massive galaxies must also have occurred at high redshift. Currently the most *efficient* identification of AGNs (and therefore SMBH growth) is made with deep X-ray surveys (e.g., Brandt & Hasinger 2005). For example, the deepest X-ray surveys (e.g., Alexander et al. 2003; Luo et al. 2008) are able to detect even

moderately luminous AGN activity at $z \approx 2$ ($L_{\rm X} \approx 10^{42}$–$10^{43}$ erg s^{-1}; i.e., > 10 times below the canonical threshold assumed for quasars). Furthermore, the high rest-frame energies probed by these surveys at $z \approx 2$ ($\approx$ 1.5–24 keV) means that the selection of AGNs is *almost* obscuration independent. This latter point is important since the dominant growth phase of massive galaxies appears to have been heavily obscured by dust and gas (e.g., Chapman et al. 2005; Le Floc'h et al. 2005).

In this brief contribution we hightlight some of our recent work aimed at identifying obscured AGN activity in distant rapidly evolving galaxies at $z \approx 2$; see §2 & §3. We discuss these results within the context of the SMBH–sperhoid growth phase of today's massive galaxies ($M_{\rm GAL} \approx 10^{11}\ M_{\odot}$); see §4.

2. Heavily Obscured Black-Hole Growth in the Most Luminous $z \approx 2$ Galaxies

Due to the negative K-correction for IR-luminous galaxies at $z > 1$, submm/mm surveys select the most bolometrically luminous systems in the Universe (e.g., Blain et al. 2002; $L_{\rm BOL} \approx 10^{13}\ L_{\odot}$). After intense multi-wavelength follow-up observations it is now clear that submm-emitting galaxies (SMGs; $f_{850\mu{\rm m}} > 4$ mJy) are gas-rich massive galaxies at $z \approx 2$ hosting energetic star-formation activity (e.g., Smail et al. 2002; Chapman et al. 2005); the stellar–dynamical and CO gas masses of these galaxies are typically $\approx 10^{11}\ M_{\odot}$ and $\approx 3 \times 10^{10}\ M_{\odot}$, respectively (e.g., Swinbank et al. 2004; Borys et al. 2005; Greve et al. 2005). The compactness and high inferred gas density of the CO emission from SMGs suggests that the CO dynamics trace the mass of the galaxy spheroid (e.g., Bouche et al. 2007). It is possible that every massive galaxy (> 1–$3\ L_{*}$) in the local Universe underwent at least one submm-bright phase at some time in the distant past (e.g., Swinbank et al. 2006). It is therefore interesting to ask the question: do these intense starbursts also host AGN activity?

Early comparisons between X-ray and submm surveys showed little overlap between the two populations. However, using the deepest X-ray observations available (the 2 Ms *Chandra* Deep Field-North survey; Alexander et al. 2003a), we found that a large fraction ($\approx$ 28–50%) of SMGs host X-ray weak AGN activity (Alexander et al. 2005a). With X-ray color-color diagnostics the amount of absorption towards the AGN in individual SMGs could be assessed. By stacking the X-ray data of AGNs with the same apparent amount of absorption, it was then possible to construct good-quality composite X-ray spectra, allowing the definitive features of X-ray absorption to be identified (photo-electric absorption cut off; possible Fe Kα emission); see Figure 1. These analyses indicate that the majority ($\approx$ 85%) of the AGNs in SMGs are heavily obscured ($N_{\rm H} \geq 10^{23}$ cm^{-2}) and some may be Compton thick ($N_{\rm H} > 1.5 \times 10^{24}$ cm^{-2}); see §3 for other constraints on Compton-thick AGNs. However, even correcting for the presence of absorption, the AGN activity in SMGs was typically found to be of moderate luminosity ($L_{\rm X} \approx 10^{44}$ erg s^{-1}). Given the huge bolometric luminosities of these systems, we suggested that, although AGN activity is often present, star formation is likely to dominate the energetics of SMGs. *Spitzer*-IRS observations have indeed shown that the mid-IR spectra of SMGs are dominated

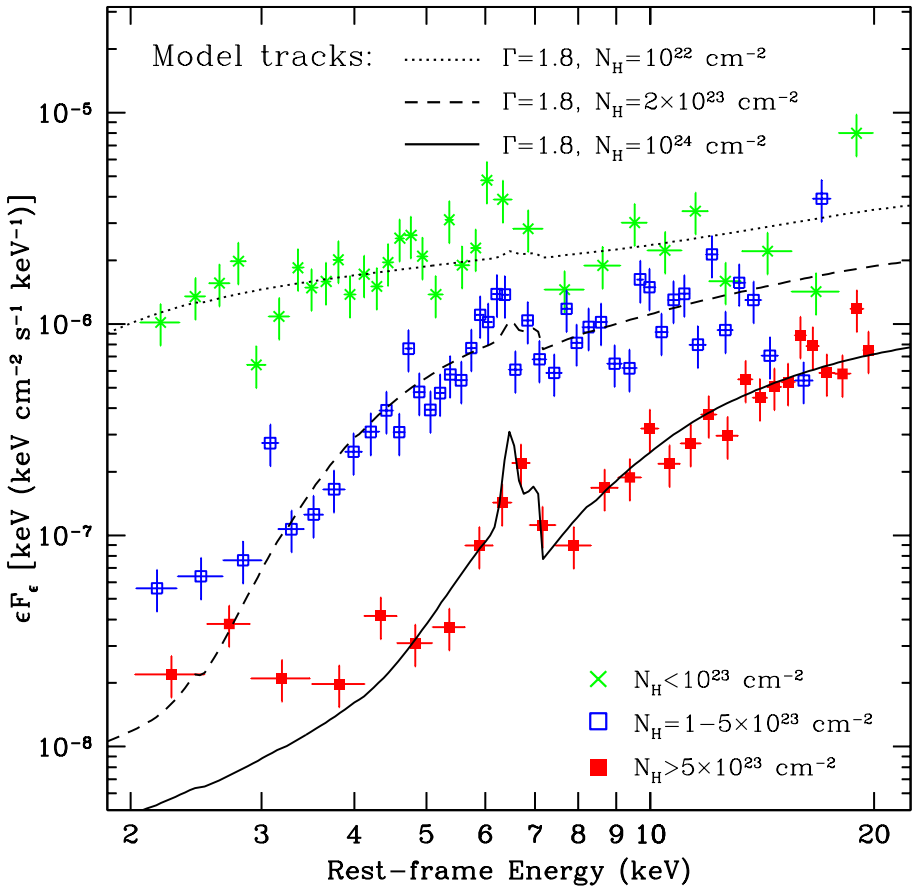

Figure 1. Composite rest-frame 2–20 keV spectra for the $z \approx 2$ SMGs hosting AGN activity in Alexander et al. (2005b). AGNs with comparable amounts of X-ray absorption have been stacked in rest-frame energy space; as indicated. The majority ($\approx 85\%$) of the AGNs are heavily obscured ($N_{\rm H} \geq 10^{23}$ cm^{-2}) and some may be Compton thick ($N_{\rm H} > 1.5 \times 10^{24}$ cm^{-2}). See Figure 7 of Alexander et al. (2005b) for more details.

by star-formation activity, but often have an underlying continuum component of AGN activity (e.g., Menendez-Delmestre et al. 2007; Pope et al. 2008).

3. Identification of a Large Population of Compton-thick Quasars at $z \approx 2$

The majority of the AGNs identified in the SMG population are obscured. However, even with a 2 Ms *Chandra* exposure, the most heavily obscured AGNs can be weak or undetected at X-ray energies, indicating that a large fraction of the growth of distant SMBHs could be missed. The most challenging sources to identify are Compton-thick AGNs with $N_{\rm H} > 1.5 \times 10^{24}$ cm^{-2}. In the local

Universe, Compton-thick AGNs comprise $\approx 50\%$ of the AGN population (e.g., Risaliti et al. 1999) and, given claims of a possible increase in AGN obscuration with redshift (e.g., La Franca et al. 2005), it is expected that at least $\approx 50\%$ of the distant AGN population will also be Compton thick. The most robust identification of Compton-thick AGNs is made with X-ray spectroscopy, where the presence of a high equivalent width Fe K emission line and a steeply rising reflection component at > 10 keV reveals that little or no X-ray emission is being seen directly (e.g., George & Fabian 1991). However, the extreme absorption towards a Compton-thick AGN renders the observed X-ray emission orders of magnitude fainter than the intrinsic emission (i.e., the emission corrected for absorption). For example, the nearby well-studied AGN NGC 1068 has an intrinsic X-ray luminosity comparable to AGNs identified in SMGs but, due to the presence of extreme absorption ($N_{\rm H} \approx 10^{25}$ cm^{-2}; i.e., heavily Compton thick), if placed at $z \approx 2$ it would have an estimated flux ≈ 10 times below the sensitivity limit of the 2 Ms CDF-N observations. This illustrates the considerable challenges in identifying distant Compton-thick AGNs.[1] Clearly, in order to be able to provide a complete census of AGN activity (and therefore the cosmic history of SMBH growth) it is necessary to be able to identify such heavily obscured AGNs without the need for high-quality X-ray spectroscopy; the latter will be challenging before the next generation of X-ray observatories, requiring $\gg 10$ Ms X-ray exposures.

Significant progress in the identification of X-ray undetected (potentially Compton thick) AGNs has been made using *Spitzer* observations of $z \approx 2$ massive galaxies (e.g., Daddi et al. 2007; Fiore et al. 2008). For example, selecting galaxies with excess IR emission over that expected from star-formation activity (on the basis of absorption-corrected UV emission), Daddi et al. (2007) revealed a large population of X-ray undetected IR-luminous galaxies with either extreme dust-obscured star formation or AGN activity. Using X-ray stacking analyses, Daddi et al. (2007) showed that, although individual galaxies were not detected in the X-ray band, the average stacked X-ray spectral slope is flat ($\Gamma \approx 0.9$). Such a flat X-ray spectral slope unambiguously indicates the presence of heavily obscured AGN activity in many systems, some of which may be obscured by Compton-thick material.

The work of Daddi et al. (2007) and Fiore et al. (2008) undoubtably provide important constraints on the space density of the most heavily obscured AGNs, and therefore of the most heavily obscured phases of SMBH growth. However, since these studies were based on X-ray stacking analyses there are significant uncertainties on (1) the fraction of obscured AGNs that are contributing to the stacked hard X-ray spectral slope (e.g., Donley et al. 2008), (2) the intrinsic luminosities of the AGNs, and (3) the fraction of the AGNs that are Compton thick, since both Compton-thin and Compton-thick AGNs can have flat X-ray spectral slopes. Using the latest 2 Ms *Chandra* observations of the CDF-S (Luo et al. 2008), we have been able to place constraints on issues (1) and (2) by detecting individual AGNs that were contributing to the stack in Daddi et al. (2007). This new analysis has shown that the fraction of obscured AGNs

[1]Indeed, only ≈ 50 Compton-thick AGNs have been robustly identified in the Universe, most at low redshift, a paltry $\approx 10^{-9}$ of the cosmic population (Comastri 2004)!

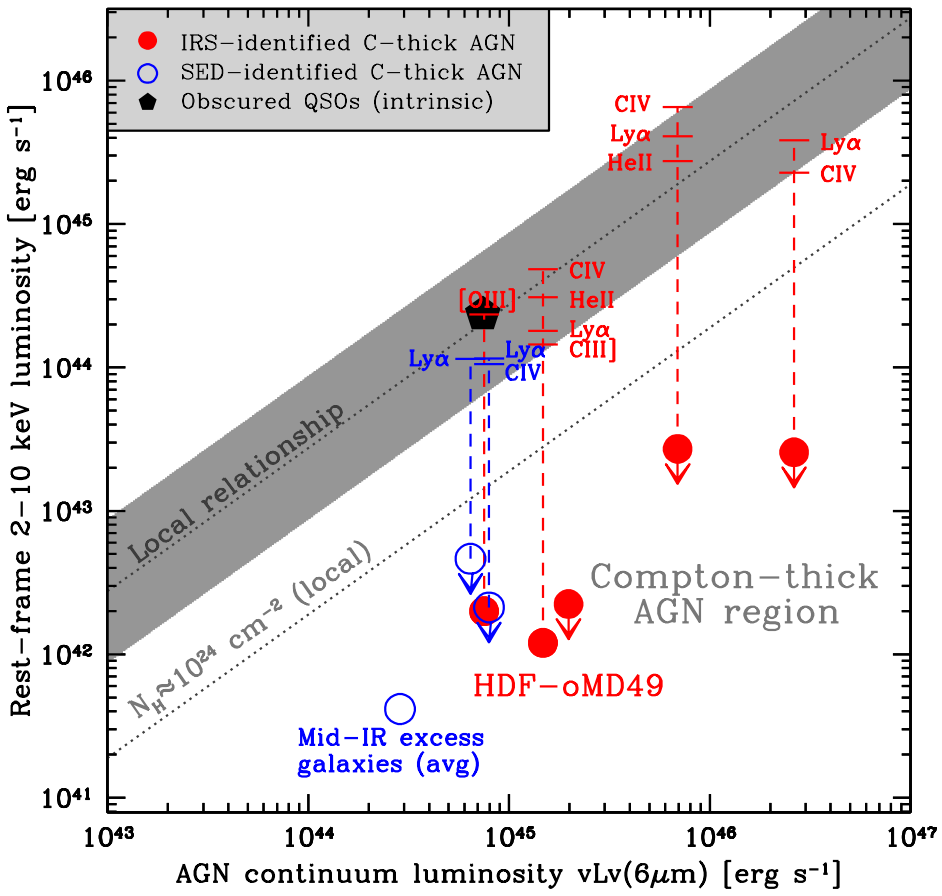

Figure 2. Diagnostic diagram for the identification of Compton-thick AGNs. X-ray luminosity (uncorrected for absorption) is plotted against the 6 μm AGN luminosity, obtained using either mid-IR spectroscopy or mid-IR spectral energy distributions. The intrinsic (absorption corrected) AGN luminosity is inferred from both the mid-IR AGN component and UV emission lines (as indicated). The plotted AGNs lie at $z \approx 2$ and have mid-IR and emission-line luminosities indicating AGN activity $\approx$ 2–3 orders of magnitude higher than indicated by the X-ray luminosity: these are the signatures of a Compton-thick AGN. See Figure 4 of Alexander et al. (2008b) for more details.

contributing to the X-ray stacking results is at least $\approx 25\%$, and that the AGNs have a broad range of luminosities from $\approx 10^{42} - 10^{44}$ erg s^{-1} (Alexander et al. 2009). However, without spectroscopic data, none of these studies are able to reliably determine how many of the AGNs are Compton thick (issue 3).

The robust identification of distant Compton-thick AGNs requires good quality spectra, in addition to continuum observations. In Alexander et al. (2008b) we made great strides in this direction by identifying luminous AGNs in seven X-ray weak/undetected $z \approx 2$ galaxies with AGN signatures from optical

and/or mid-IR (*Spitzer*-IRS) spectroscopy. The intrinsic X-ray luminosity of the AGNs in these galaxies could be estimated *both* from AGN-dominated optical emission lines and AGN-dominated mid-IR emission (distinguished from star formation processes using mid-IR spectroscopy), giving $L_{\rm X} \approx 10^{44}$–$10^{45}$ erg s^{-1}. However, by comparison, the X-ray constraints for these seven AGNs are ≈ 2 orders of magnitude lower than that predicted, indicating that the X-ray emission *must* be obscured by Compton-thick material; see Figure 2 and §3 in Alexander et al. (2008b). With these diagnostics it is therefore possible to identify distant Compton-thick AGNs in the absence of good-quality X-ray spectroscopy. Although limited in source statistics, the Alexander et al. (2008b) study was also able to place basic constraints on the space density of luminous Compton-thick AGNs ($L_{\rm X} > 10^{44}$ erg s^{-1}) at $z \approx 2$–2.5. The derived space density of (0.7–2.5)$\times10^{-5}$ Mpc^{-3} is consistent with that found for comparably luminous unobscured AGNs, indicating that Compton-thick SMBH growth was as ubiquitious as unobscured SMBH growth in the distant Universe. Since our method relied on the identification of optical emission lines, these constraints should be considered a lower limit on the Compton-thick AGN space density as there are likely to also be many Compton-thick AGNs with weak optical emission lines (e.g., NGC 6240 in the local Universe).

4. Joint Black-Hole–Galaxy Growth in $z \approx 2$ Galaxies

From a combination of X-ray, IR, and submm data with optical and mid-IR spectroscopy, we have been able to provide sensitive constraints on the ubiquity and properties of AGN activity in $z \approx 2$ dust-obscured galaxies. Can we use these constraints along with other multi-wavelength data to understand the relative SMBH–stellar growth in $z \approx 2$ galaxies? Interestingly we can.

The deep multi-wavelength of SMGs show that these galaxies at $z \approx 2$ host both heavily obscured AGN and star formation activity; see §2. Qualitatively, this joint SMBH–stellar growth found in SMGs is consistent with that expected given the SMBH–spheroid mass relationship in the local Universe. However, constraints on the masses of the SMBH and spheroid suggest that the SMBHs in SMGs may be smaller than that expected given the lcoal SMBH–spheroid mass constraints, indicating that the SMBH may be "catching up" with the growth of the SMBH (see Alexander et al. 2008a). The estimated growth rate of the SMBHs in SMGs do not appear to be sufficient to significantly overcome the growth rate of the spheroid, indicating that a more AGN-dominated growth phase may be required to place SMGs (and their progeny) on the locally defined SMBH–spheroid mass relationship (e.g., an optically bright quasar; Coppin et al. 2008). Although these constraints suggest that there is a "lag" in the SMBH growth in SMGs, given that SMGs are amongst the most rapidly evolving galaxies in the Universe, it is perhaps surprising that the relative SMBH–galaxy spheroid growth rate in these systems is even *approximately* in agreement with that expected from the SMBH–spheroid mass relationship. This may indicate that some kind of regulatory mechanism is at work to "control" the growth of these two components (i.e., energetic winds/outflows).

The constraints on the SMBH–galaxy growth in the $z \approx 2$ *Spitzer*-detected galaxies studied by Daddi et al. (2007) are weaker than those determined for

$z \approx 2$ SMGs, since they are typically less luminous (and therefore fainter at all wavelengths). However, based on the analyses of Daddi et al. (2007) and Murphy et al. (2009), there is clear evidence for both AGN activity and star formation in many of these systems. By decomposing the IR spectral energy distributions of the *Spitzer*-detected galaxies into AGN and star-formation components, Daddi et al. (2007) further estimate that the volume averaged SMBH–stellar growth in these systems is consistent with that expected given the local SMBH–spheroid mass relationship. By comparison to SMGs, the $z \approx 2$ *Spitzer*-detected galaxies are growing less rapidly and therefore are less likely to be able to deviate from the local SMBH–spheroid mass relationship. However, it is perhaps remarkable that the relative SMBH–stellar growth rates of both populations seem to be comparable.

Acknowledgments. I thank the Royal Society for generous support and my collaborators for allowing me to present this research.

References

Alexander, D. M., et al. 2003, AJ, 126, 539
Alexander, D. M., et al. 2005a, Nat, 434, 738
Alexander, D. M., et al. 2005b, ApJ, 632, 736
Alexander, D. M., et al. 2008a, AJ, 135, 1968
Alexander, D. M., et al. 2008b, ApJ, 687, 835
Alexander, D. M., et al. 2009, ApJ, submitted
Blain, A. W., et al. 2002, Phys. Rep., 369, 111
Borys, C., et al. 2005, ApJ, 635, 853
Bouché, N., et al. 2007, ApJ, 671, 303
Bower, R. G., et al. 2006, MNRAS, 370, 645
Brandt, W. N., & Hasinger, G. 2005, ARA&A, 43, 827
Chapman, S. C., Blain, A. W., Smail, I., & Ivison, R. J. 2005, ApJ, 622, 772
Comastri, A. 2004, Supermassive Black Holes in the Distant Universe, 308, 245
Coppin, K. E. K., et al. 2008, MNRAS, 389, 45
Croton, D. J., et al. 2006, MNRAS, 365, 11
Daddi, E., et al. 2007, ApJ, 670, 173
Donley, J. L., Rieke, G. H., Pérez-González, P. G., & Barro, G. 2008, ApJ, 687, 111
Ferrarese, L., & Merritt, D. 2000, ApJ, 539, L9
Fiore, F., et al. 2008, ApJ, 672, 94
George, I. M., & Fabian, A. C. 1991, MNRAS, 249, 352
Greve, T. R., et al. 2005, MNRAS, 359, 1165
Heavens, A., Panter, B., Jimenez, R., & Dunlop, J. 2004, Nat, 428, 625
Kormendy, J., & Richstone, D. 1995, ARA&A, 33, 581
La Franca, F., et al. 2005, ApJ, 635, 864
Le Floc'h, E., et al. 2005, ApJ, 632, 169
Luo, B., et al. 2008, ApJS, 179, 19
Magorrian, J., et al. 1998, AJ, 115, 2285
Menéndez-Delmestre, K., et al. 2007, ApJ, 655, L65
Murphy, E. J., et al. 2009, arXiv:0812.2927
Pope, A., et al. 2008, ApJ, 675, 1171
Risaliti, G., Maiolino, R., & Salvati, M. 1999, ApJ, 522, 157
Smail, I., Ivison, R. J., Blain, A. W., & Kneib, J.-P. 2002, MNRAS, 331, 495
Soltan, A. 1982, MNRAS, 200, 115
Swinbank, A. M., et al. 2004, ApJ, 617, 64
Swinbank, A. M., et al. 2006, MNRAS, 371, 465

GALAXY EVOLUTION: EMERGING INSIGHTS AND FUTURE CHALLLENGES
ASP Conference Series, Vol.
@jourvol, © 2009
S. Jogee, I. Marinova, L. Hao, and G. A Blanc

An Improved Black Hole Mass–Bulge Luminosity Relationship for AGNs

C. Martin Gaskell and John Kormendy

University of Texas at Austin, Department of Astronomy, Austin, TX 78712, USA

Abstract. Two effects have substantially increased the scatter in the AGN black hole mass–host galaxy bulge luminosity relationship derived from SDSS spectra. The first is that at a fixed black hole mass, $M_\bullet$, the SDSS spectrum depends strongly on redshift because an SDSS fiber sees a larger fraction of the total light of more distant galaxies. The second is that at a given redshift, the fraction of host-galaxy light in the fiber increases with decreasing galaxy luminosity. We illustrate the latter effect using the Kormendy et al. (2009) light profiles of Virgo ellipticals. With allowance for the two effects, we obtain a black hole mass—bulge luminosity ($M_\bullet$–$L_{\rm host}$) relationship for AGNs which has a scatter of only ±0.23 dex in mass. This is less than the scatter found for inactive galaxies, and is consistent with the measuring errors. We show that there is a corresponding tight linear relationship between the fraction of host galaxy light in AGN spectra, $L_{\rm host}/L_{\rm AGN}$, and the Eddington ratio, $L/L_{\rm Edd}$. This linearity implies that at a given $M_\bullet$, host luminosities of high-accretion-rate AGNs (NLS1s) and low-accretion-rate AGNs are similar. The $L_{\rm host}/L_{\rm AGN}$–$L/L_{\rm Edd}$ relationship provides a simple means of estimating the fraction of host galaxy light in AGN spectra. This means that the real amplitude of variability of low-accretion-rate AGNs is increased relative to NLS1s.

1. Introduction

It has long been recognized that the masses, $M_\bullet$, of supermassive black holes (SMBHs) are proportional to the stellar luminosities, $L_{\rm host}$, of the bulges of the galaxies in which they are located (see Kormendy & Richstone 1995 and Kormendy & Gebhardt 2001 for reviews). $M_\bullet$ can be most easily determined for AGNs. Dibai (1977) showed that $M_\bullet$ can be estimated for an AGN from the broad emission lines in a single-epoch spectrum, so long as the broad-line region (BLR) motions are gravitationally dominated. Reverberation mapping has verified that the BLR motions are dominate by gravity (Gaskell 1988), and has confirmed the accuracy of the Dibai method (see Bochkarev & Gaskell 2009). With the advent of the SDSS, the Dibai method has been used to estimate the masses of tens of thousands of black holes. Shen et al. (2008) give masses for 900 SDSS AGNs for which Vanden Berk et al. (2006) have spectroscopically estimated $L_{\rm AGN}/L_{\rm host}$, the ratio of AGN light to host galaxy light at 5100 Å in the rest frame. In this paper we use these data to study the dependence of $L_{\rm AGN}/L_{\rm host}$ on the accretion rate (which we will express by the Eddington ratio, $L/L_{\rm Edd}$), and to obtain an improved $M_\bullet$–$L_{\rm host}$ relationship.

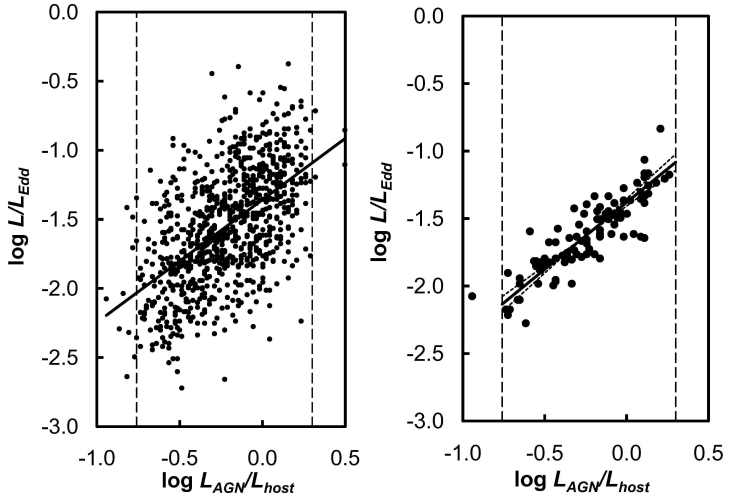

Figure 1. Eddington ratios, $L/L_{\rm Edd}$, as a function of $L_{\rm AGN}/L_{\rm host}$, the ratio of AGN flux to host galaxy flux at 5100 Å. The dashed vertical lines show the approximate upper and lower cutoffs of Shen et al. (2008). (a) (left panel) shows all low-redshift ($z < 0.45$) SDSS AGNs in the sample. The diagonal line is a linear regression on $\log L_{\rm AGN}/L_{\rm host}$. (b) (right panel) shows just 100 AGNs with $\log M_{\rm bh} = 7.7 \pm 0.2$, and $0.13 < z < 0.18$. The solid diagonal line is a censored OLS-bisector fit (Isobe et al. 1990), and the 68% confidence interval for the slope is shown by the two dotted lines.

2. Results

Fig. 1a shows $L_{\rm AGN}/L_{\rm Edd}$ as a function of $L_{\rm AGN}/L_{\rm host}$. Because of difficulties in measuring $L_{\rm AGN}/L_{\rm host}$ when the AGN is too bright or too faint compared with the galaxy, upper and lower cutoffs on the ratio have been imposed by Shen et al. (2008). Since $L_{\rm AGN}$ appears on both axes and since $M_\bullet \sim L_{\rm host}$, we expect a simple linear correlation between $L/L_{\rm Edd}$ and $L_{\rm AGN}/L_{\rm host}$. Fig. 1a does indeed show a correlation, but the scatter is very large. This scatter could be a consequence of measurement errors, or it could reflect intrinsic scatter in the $M_\bullet$–$L_{\rm host}$ relationship.

In Fig. 2a we show that if we take a narrow range of $M_\bullet$, then the luminosity deviation, $\Delta \log L_{\rm host}$, from the diagonal line in the left panel of Fig. 1 is a strong function of redshift. This has a simple explanation: at low redshift an SDSS fiber is only taking in a small part of the bulge of the host galaxy, so the luminosity of the bulge is underestimated for nearby galaxies. Fig. 2b uses the Kormendy et al. (2009) photometry of Virgo ellipticals to show that at a given redshift, the fraction of total bulge light in a an SDSS fiber decreases as the luminosity of the galaxy increases. The combination of the two effects will be discussed in detail elsewhere (Gaskell & Kormendy, in preparation), but the dramatic improvement in the $L/L_{\rm Edd}$–$L_{\rm AGN}/L_{\rm host}$ relationship can be illustrated simply by plotting AGNs in a narrow range of z and black hole mass. This is shown in Fig. 1b.

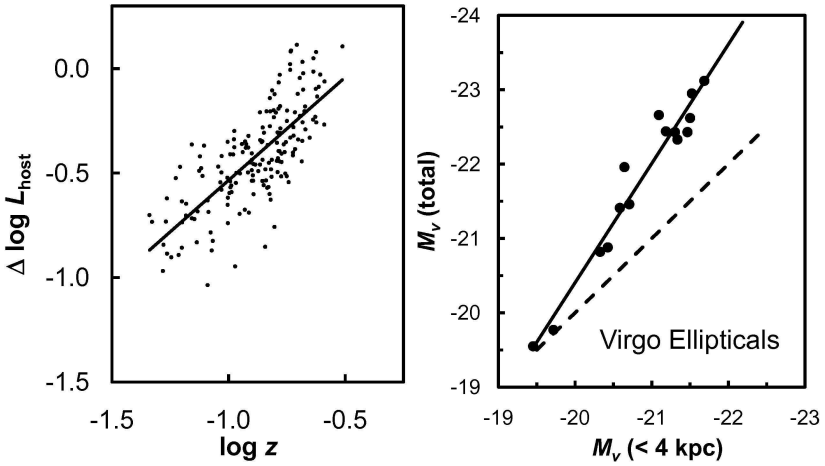

Figure 2. (a) estimated relative deficit, $\Delta \log L_{\rm host}$, of host galaxy light at λ5100 as a function of redshift for AGNs with $7.4 < \log M_\bullet < 7.6$. $\Delta \log L_{\rm host}$ is normalized to $\log z = -0.4$. The diagonal line is a linear regression on $\log z$. (b) The total absolute magnitudes of Virgo ellipticals (derived from Kormendy et al. 2009) as a function of the absolute magnitude measured within a fixed 4 kpc radius aperture. The solid line is a linear regression of the total magnitude on the 4 kpc magnitude. The dashed line shows what the relationship would be if all the light were within 4 kpc.

Fig. 3 shows the resulting $M_\bullet$–$L_{\rm host}$ relationship for AGNs over a narrow redshift range. $L_{\rm host}$ has been approximately corrected using the relationship for the Virgo ellipticals in Fig. 2b. The dispersion in mass in Fig. 3 is $\pm$0.23 dex which is better than the $\pm$0.30 dex dispersion Häring & Rix (2004) found for the $M_\bullet$–$L_{\rm host}$ relationship for non-active galaxies. Applying the luminosity correction from Fig. 2b also increases the slope of $M_\bullet$–$L_{\rm host}$ relationship for the SDSS AGNs. If we take an $M_\bullet$–$L_{\rm host}$ relationship of the form $M_\bullet \propto L_{\rm host}^{\alpha}$, then for the complete uncorrected Shen et al. (2008) sample (not shown), an OLS-bisector fit gives a slope of $\alpha = 0.69 \pm 0.02$, while a similar fit for the corrected subset of 100 AGNs in Fig. 3 gives $\alpha = 0.84 \pm 0.03$. If we take the luminosity-dependence of the mass/light ratio of bulges to be $M/L \propto L^{0.32\pm0.04}$ (Cappellari et al. 2006), then $M_{\rm bulge} \propto M_\bullet^{1.16\pm0.07}$.

3. Discussion

The small dispersion in the AGN $M_\bullet$–$L_{\rm host}$ relationship in Fig. 3 implies that the intrinsic relationship must be very tight (as tight as the $M_\bullet$–σ_* relationship), since much or all of the scatter can be accounted for by observational errors. The small dispersion also supports the reliability of AGN black hole masses determined via the Dibai method. As discussed in Bochkarev & Gaskell (2009), this implies that for the AGNs for which the method has been used, both the structure and intrinsic spectral energy distributions are very similar (Gaskell et al. 2004; Gaskell & Benker 2008). The slope in Fig. 1b (0.99 ± 0.11) shows that the hosts of high-accretion-rate AGNs do not systematically deviate from the $M_\bullet$–$L_{\rm host}$ relationship.

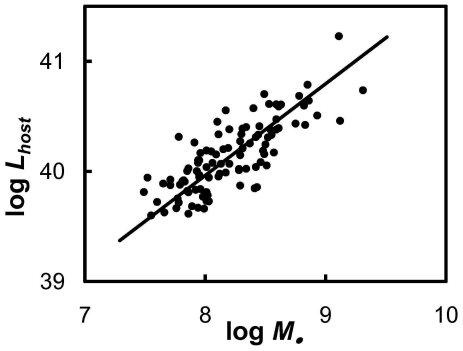

Figure 3. The $M_\bullet$–$L_{\rm host}$ relationship for 100 AGNs restricted to $0.13 < z < 0.34$ and with $L_{\rm host}$ corrected for the aperture effect. The diagonal line is the OLS-bisector fit, $M_\bullet \propto L_{\rm host}^{0.84}$.

Fig. 1b makes determination of host-galaxy contamination of AGN photometry and spectroscopy straight forward. One immediate result is to show that low $L/L_{\rm Edd}$ AGNs must have greater optical variability amplitudes on average than high $L/L_{\rm Edd}$ AGNs (NLS1s). Klimek, Gaskell, & Hedrick (2004) have already shown that even without corrections for host galaxy contamination, NLS1s seem to be less variable than non-NLS1s. Fig. 1b shows that this difference will be much greater when the higher galaxy contamination of non-NLS1s is allowed for.

Acknowledgments. This research has been supported through NSF grants AST 08-03883 (MG) and AST06-07490 (JK).

References

Bochkarev, N. G., & Gaskell, C. M. 2009, Ast. Lett., 35, 287
Cappellari, M., et al. 2006, MNRAS, 366, 1126
Dibai, É. A. 1977, Soviet Astron. Lett., 3, 1
Gaskell, C. M. 1988, ApJ, 325, 114
Gaskell, C. M. & Benker, A. J. 2008, ApJ, submitted [arXiv:0711.1013]
Gaskell, C. M., Goosmann, R. W., Antonucci, R. R. J., & Whysong, D. H. 2004, ApJ, 616, 147
Häring, N., & Rix, H.-W. 2004, ApJ, 604, L89
Isobe, T., Feigelson, E. D., Akritas, M. G., Babu, G. J., 1990, ApJ, 364, 104
Klimek, E. S., Gaskell, C. M., Hedrick, C. H. 2004, ApJ, 609, 69
Kormendy, J., Fisher, D. B., Cornell, M. E., & Bender, R. 2009, ApJS, 182, 216
Kormendy, J. & Gebhardt, K. 2001, in AIP Conf. Proc., 586 *20th Texas Symposium on Relativistic Astrophysics*, ed. J. C. Wheeler and H. Martel (New York: AIP), 363
Kormendy, J. & Richstone, D. 1995, ARA&A, 33, 581
Shen, J.-J., Vanden Berk, D. E., Schneider, D. P., & Hall, P. B. 2008, AJ, 135, 928
Vanden Berk, D. E. et al. 2006, AJ, 131, 84

GALAXY EVOLUTION: EMERGING INSIGHTS AND FUTURE CHALLLENGES
ASP Conference Series, Vol.
@jourvol, © 2009
S. Jogee, I. Marinova, L. Hao, and G. A Blanc

The Black Hole – Bulge Relationship for AGN at High Redshift

Gregory A. Shields & Sarah Salviander

Department of Astronomy, University of Texas, Austin, TX 78712, USA

Abstract. AGN afford an opportunity to study the evolution of the black hole – bulge relationship over cosmic time. The mass of the supermassive black hole can be estimated from the width of the broad emission lines in the spectrum or the AGN luminosity. The mass or velocity dispersion of the host galaxy's bulge may be estimated from the host galaxy luminosity, or from the widths of the narrow optical emission lines or the CO lines. All methods have uncertainties, and the results show substantial inconsistencies. There are indications that black holes at high redshift in optically luminous AGN reside in proportionally smaller host galaxies than today.

1. Introduction

The relationship between central, supermassive black holes and the bulges of host galaxies is a popular, if contentious, topic in extragalactic astrophysics. The proportionality of central black hole mass, $M_{\rm BH}$, and bulge luminosity in galaxies has been known for some time (Kormendy & Richstone 1995; Magorrian et al. 1998), but interest in the black hole – bulge relationship grew substantially after the discovery of a tight relationship between $M_{\rm BH}$ and the bulge velocity dispersion σ_* (Gebhardt et al. 2000; Ferrarese & Merritt 2000). This correlation may be a clue to some fundamental relationship between black hole growth and galaxy evolution. A number of theoretical scenarios for this relationship have been proposed, often involving feedback between the luminosity of the growing black hole and the gas reservoir in the galaxy (e.g. Ciotti & Ostriker 2007, and references therein). A key to the nature of this relationship is an understanding of the evolution of the black hole – bulge relationship over cosmic time. This is a difficult undertaking using quiescent galaxies at high redshift given the black hole's small sphere of influence. Alternatively, black hole masses may be estimated in active galactic nuclei (AGN) out to the highest observed redshifts ($z > 6$), using the broad emission lines in the spectrum or AGN luminosity. This affords an opportunity to study the black hole – bulge relationship at large look-back times, if a reliable measure of the host galaxy bulge can be obtained. Efforts to do this have mostly attempted either to infer σ_* from emission lines of gas orbiting in the bulge gravitational potential or to measure the host galaxy luminosity directly. Here we briefly review some results from these studies.

2. Black Holes and Bulges in AGN

We discuss in turn results from studies of the black hole – bulge relationship based on the optical and radio emission-line surrogacy for σ_* in AGN, direct measurement of σ_* from stellar lines in the AGN spectrum, and measurement of the host galaxy luminosity and mass.

2.1. Results from the Narrow Emission Lines

Nelson and Whittle (1996) found that the widths of the narrow AGN emission lines, in particular the strong [O III] $\lambda\lambda 5007, 4959$ doublet, are proportional to σ_*, albeit with much scatter. This can be expressed as $\sigma_{O3} \approx \sigma_*$, where σ_{O3} is the FWHM of [O III] divided by 2.35, appropriate for a Gaussian profile. This surrogacy is supported by agreement of σ_{O3} with M_{BH} from reverberation mapping in AGN (Nelson 2000) and with the luminosity of host galaxies of low redshift quasars (Bonning et al. 2005). Further support is drawn from the very narrow [O III] profiles of dwarf AGN such as Pox 52 (Barth et al. 2004).

Shields et al. (2003) used σ_{O3} to assess the redshift dependence of the black hole – bulge relationship in quasars up to redshift $z = 3.3$, using a combination of new and published spectral measurements. Black hole masses were derived in the now-standard manner from the broad emission line widths, specifically Hβ. This is made possible by evidence from reverberation mapping studies indicating that the radius of the broad emission line region (BLR) is predictable from the optical continuum luminosity (e.g. Kaspi et al. 2000, 2005). The black hole mass is then derived on the assumption that the line widths reflect orbital motion around the black hole. Shields et al. (2003) used the expression

$$M_{BH} = (10^{7.69}\ M_\odot) v_{3000}^2 L_{44}^{0.5}, \tag{1}$$

where $v_{3000} \equiv$ FWHM/3000 kms^{-1} and $L_{44} \equiv \nu L_\nu / (10^{44}$ erg s$^{-1})$ is the BLR continuum luminosity at 5100 Å. Details are uncertain, but the $L^{0.5}$ slope is supported by Bentz et al (2008). Given the black hole mass derived in this way, the issue is to compare it with the expected black hole mass based on the galaxy velocity dispersion and the present day black hole – σ_* relationship. This relationship is quantified by Tremaine et al. (2002) as

$$M_{BH} = (10^{8.13}\ M_\odot)(\sigma_*/200\text{ km s}^{-1})^{4.02}. \tag{2}$$

Using σ_{O3} in this expression to give M_{O3}, Shields et al. (2003) defined an offset $\Delta\log M = \log M_{BH} - \log M_{O3}$. They concluded that $\Delta\log$ M showed no evolution back to $z \approx 3$ to a tolerance of ~ 0.5.

A similar approach was used by Salviander et al. (2007) using quasars from the Sloan Digital Sky Survey (SDSS, http:// www.sdss.org). They used [O III] and Hβ for σ_* and M_{BH}, respectively, at $z < 0.8$, and [O II] and Mg II λ2800 for redshifts up to 1.2. After allowing for biases involving object selection and spectral noise, they found $\Delta\log M \approx 0.2$ at $z = 1$. The discussion of biases in Salviander et al. suggests that the error in $\Delta\log M$ may be as much as ± 0.2.

One of the biases discussed by Salviander et al. (2007) involves the preferential observability of brighter quasars (Malmquist bias) together with the slope of the quasar luminosity function and the intrinsic scatter in the black

hole – bulge relationship. Lauer et al. (2007) analyze this bias in detail as it relates to attempts to measure evolution in the black hole – bulge relationship using quasars. They conclude that the bias weakens or eliminates several claims of a positive $\Delta\log M$ at high redshift.

Bonning et al. (2005) collected six radio-loud quasars at $z \sim 2$ from the samples of Netzer et al. (2004) and Shemmer et al. (2004) and found a mean $\Delta\log M = -0.4$. Shields et al. (2006a) compared their measurements of $\sigma_{\rm O3}$ and 5100 Å continuum luminosity for the $z \approx 1.5 - 2$ VLT spectra of Sulentic et al. (2004) with $M_{\rm BH}$ calculated from the Sulentic et al. measurements of FWHM(Hβ) and found a mean $\Delta\log M$ of +0.31, or +0.48 for radio-quiet objects only. Taken together, these results indicate a degree of evolution at higher redshift consistent with the no-evolution claim of Shields et al. (2003).

2.2. CO Lines as Indicators of σ_*

Another possible indicator of the host galaxy bulge potential is the width of the radio CO emission lines. These are observed in a number of high redshift quasars, often gravitationally lensed systems (Solomon & Vanden Bout 2005). Shields et al. (2006b) used $\sigma_{\rm CO}$ as a surrogate for σ_* in quasars with redshifts up to 6.4, with $M_{\rm BH}$ derived from the width of the broad emission lines of Mg II or C IV $\lambda\lambda$1550 (the latter is controversial). After allowing for line-of-sight projection of the CO velocities, they find $\Delta\log M \approx 0.5$ for quasars at $z \approx 2$ increasing to $\Delta\log M \approx 1.5$ at $z = 4$ to 6. The large $\Delta\log M$ at high redshift results from very large black hole masses for these very luminous quasars, whereas the CO widths remain similar to those of the lower redshift objects. This raises the possibility of rapid black hole growth in the early universe without commensurate growth of the host galaxy. Uncertainties include the possibility that the CO widths are artificially low because of preferential face-on orientation of molecular gas disks in the observed quasars. Shields et al. (2006b) did not allow for the Malmquist bias mentioned above, and this suggests caution in concluding that the large $\Delta\log M$ is characteristic of galaxies at high redshift. Nevertheless, if the CO widths are reliable indicators, these results show that at least *some* black holes have undersized host galaxies at early times.

Ho (2007) has examined the use of CO line widths to gauge σ_* in high redshift AGN, following an alternative prescription for deriving σ_* from the width of CO than that of Shields et al. (2006b). Ho argued that the full width at near-zero intensity of the CO line is a better predictor of σ_* than the full width at half-maximum, and compared their σ_* with measurements for $M_{\rm BH}$ for a sample of quasars at redshifts up to $z \approx 6.4$. They found no significant deviation from the locally-observed black hole – bulge relationship for their low redshift ($z < 0.2$) sample. For their high redshift sample ($1.4 \leq z \leq 6.4$) they found deviation from the local relationship on the order of a factor of 4. This is substantially less than that of Shields et al., yet still indicative of a large degree of evolution in the black hole – bulge relationship for quasars at the highest redshifts.

2.3. Direct Measurements of σ_*

Direct measurement of σ_* in AGN is difficult given the brightness of the active nucleus, though for AGN of modest redshift and luminosity one may plausibly

separate the stellar light from that of the nucleus. Woo et al. (2006) and Treu et al. (2004, 2007) have measured σ_* in Seyfert galaxies at redshift $z \approx 0.4$ using high-S/N spectra from the Keck Telescope. They compared their measured σ_* to black hole masses calculated using the "photoionization method" described by Shields et al. (2003), and found substantial evolution in the black hole – σ_* relationship. Treu et al. (2007) determined $\Delta \log M \approx 0.5$. Observational biases were found to have a negligible effect on this result, while systematic errors in $M_{\rm BH}$ may account for a maximum of ~ 0.2 dex of the evolution. The degree of evolution found here suggests bulges increased in mass by 60% in the last 4 Gyr in the absence of substantial black hole growth. Treu et al. propose the consumption of disk stars during a major merger as a likely mechanism for bulge growth (see Croton 2006), a scenario supported by the large fraction of merging and interacting late-type spiral galaxies in their sample.

2.4. Host Galaxy Luminosity

Several studies have targeted the luminosity of the host galaxy in high redshift quasars to assess evolution of the black hole – bulge relationship. Peng et al. (2006a, 2006b) gathered data from literature and compared $M_{\rm BH}$ to the R-band host galaxy luminosity for a sample of quasars in the redshift range $1 < z < 4.5$, including quasars in lensed host galaxies in the latter study. They calculated the virial $M_{\rm BH}$ from the width of the quasar broad emission lines and continuum luminosity using published spectra or from the $M_{\rm BH}$ – quasar luminosity relationship. The luminosity of the host galaxy was estimated by converting and correcting published *HST* H- and J-band luminosities to R-band luminosity for the quasar host galaxies. They found that galaxies at $z \approx 2$ obeyed the local $M_{\rm BH}$ – spheroid luminosity relationship while quasars at $z \approx 1$ deviated from the local relationship in a way consistent with passive fading of the host spheroid. Passive fading of the $z \approx 2$ host galaxies alone is inconsistent with the current population of early type galaxies. Since the $M_{\rm BH}$ – spheroid luminosity relationship is an indicator of the more fundamental black hole mass – spheroid mass relationship, this result implies that the black hole mass – spheroid mass relationship for these galaxies has evolved by a factor of ~ 4 in the sense that at $z \geq 2$ black holes were proportionally more massive compared to the host spheroid. The host galaxies must grow by this factor—most likely through a combination of star formation and mergers—without substantially growing the black hole in order to catch up to the local relationship.

In addition to assessing the black hole mass – σ_* relationship, Treu et al. (2007) studied the black hole mass – bulge luminosity relationship in their sample of Seyfert galaxies at $z \approx 0.4$. These galaxies were compared to a sample of quiescent galaxies at $z = 0$, which were determined to be intrinsically similar to the Seyfert host galaxies by their placement on the fundamental plane. Treu et al. found 0.2 dex evolution in the black hole mass – bulge luminosity relationship, which cannot be explained solely by passive evolution. At minimum the host galaxy luminosity and mass must increase by 60% within 4 Gyr to arrive at the current black hole mass – bulge relationships. In the absence of black hole growth, Treu et al. posit that the bulge grows in luminosity and mass through the acquisition of new stars during mergers. Since the size of the bulge remains

relatively fixed, this also gives rise to an increasing σ_* required to bring the black hole – σ_* relationship into agreement with the locally observed relationship.

An alternative measure of the bulge potential is mass. Borys et al. (2005) examined the black hole mass – bulge mass relationship in a sample of submillimeter galaxies (SMGs) at redshift $z \sim 2$. SMGs are massive systems undergoing intense star formation and black hole activity, presumably as a result of major galaxy mergers, and may represent an earlier stage of galaxy growth than optical or radio selected AGN. Using previously published black hole masses from Alexander et al. (2005a, 2005b) Borys et al. conclude that SMGs at redshift $z \sim 2$ lie well below the local black hole mass – bulge mass relationship quantified by Marconi & Hunt (2003) in the sense that the black hole is proportionally small compared to the host bulge. The nuclei of these heavily-obscured SMGs precluded observation of the broad line region or measurement of the optical AGN flux, so lower limits for the black hole masses were determined from X-ray luminosities and assuming accretion at the Eddington limit. The bulge stellar masses were determined through NIR luminosities and an assumed theoretical mass-to-light ratio. Borys et al. found a resulting offset from the local relationship that could be as much as a factor of 50. Allowance for uncertainties in the black hole and stellar masses—assuming sub-Eddington accretion or starlight contamination by AGN emission—does not eliminate the trend. This result suggests a period of rapid black hole growth between a redshift of 2 and the present day.

Alexander et al. (2008) used a sample of SMGs with unobscured BLRs to study the black hole mass – bulge mass relationship. They calculated virial black hole masses using broad emission line widths following the method of Greene & Ho (2005), and compared these with stellar masses derived in the same manner as Borys et al. (2005) as well as CO dynamical masses. They also found that SMGs lie below the local black hole mass – bulge mass relationship, but not as drastically as suggested by Borys et al. With this weaker evolution—a factor of about 3 or more—and considering the large gas content of SMGs, black holes could plausibly grow to catch up to the local relationship provided accretion occurs near the Eddington limit.

3. Conclusions

The importance of understanding the black hole – bulge relationship has led to several studies using various techniques to assess its evolution over cosmic time. These approaches have uncertainties in the measurement techniques, and they are subject to substantial biases from selection effects. Definitive conclusions are not yet at hand. Most studies find either no significant evolution, or evolution in the sense of smaller bulges for a given black hole mass, especially at redshifts greater than unity. Some studies, however, find evolution in the sense of larger bulges for a given black hole mass.

Alexander et al. (2008) address the mixed results, noting that other groups have focused on evolved populations of optically-luminous AGN, whereas SMGs are AGN in an earlier stage of evolution. The contradictory results at lower redshifts may involve the nature of the galaxies involved: big spheroids finished evolving by $z \sim 1$, but smaller bulges are still evolving at $z \sim 0.4$

Acknowledgments. We thank Shardha Jogee, Bev Wills, and Todd Boroson for helpful discussions. G.A.S. gratefully acknowledges the support of the Jane and Roland Blumberg Centennial Professorship in Astronomy.

References

Alexander, D. M., Smail, I., Bauer, F. E., Chapman, S. C., Blain, A. W., Brandt, W. N., & Ivison, R. J. 2005a, Nat, 434, 738
Alexander, D. M., Bauer, F. E., Chapman, S. C., Smail, I., Blain, A. W., Brandt, W. N., & Ivison, R. J. 2005b, ApJ, 632, 736
Alexander, D. M., et al. 2008, AJ, 135, 1968
Barth, A. J., Ho, L. C., Rutledge, R. E., & Sargent, W. L. W. 2004, ApJ, 607, 90
Bentz, M. C., Peterson, B. M., Pogge, R. W., Vestergaard, M., & Onken, C. A. 2006, ApJ, 644, 133
Bonning, E. W., Shields, G. A., Salviander, S., & McLure, R. J. 2005, ApJ, 626, 89
Borys, C., Smail, I., Chapman, S. C., Blain, A. W., Alexander, D. M., & Ivison, R. J. 2005, ApJ, 635, 853
Ciotti, L., & Ostriker, J. P. 2007, ApJ, 665, 1038
Croton, D. J. 2006, MNRAS, 369, 1808
Ferrarese, L. & Merritt, D. 2000, ApJ, 539, L9
Gebhardt, K., et al. 2000, ApJ, 539, L13
Greene, J. E., & Ho, L. C. 2005, ApJ, 630, 122
Ho, L. C. 2007, ApJ, 669, 821
Kaspi, S., Smith, P. S., Netzer, H., Maoz, D., Jannuzi, B. T., & Giveon, U. 2000, ApJ, 533, 631
Kaspi, S., Maoz, D., Netzer, H., Peterson, B. M., Vestergaard, M., & Jannuzi, B. T. 2005, ApJ, 629, 61
Kormendy, J., & Richstone, D. 1995, ARA&A, 33, 581
Lauer, T. R., Tremaine, S., Richstone, D., & Faber, S. M. 2007, ApJ, 670, 249
Magorrian, J., et al. 1998, AJ, 115, 2285
Marconi, A., & Hunt, L. K. 2003, ApJ, 589, L21
Nelson, C. H. 2000, ApJ, 544, L91
Nelson, C. H., & Whittle, M. 1996, ApJ, 465, 96
Netzer, H., Shemmer, O., Maiolino, R., Oliva, E., Croom, S., Corbett, E., & di Fabrizio, L. 2004, ApJ, 614, 558
Peng, C. Y., Impey, C. D., Ho, L. C., Barton, E. J., & Rix, H.-W. 2006a, ApJ, 640, 114
Peng, C. Y., Impey, C. D., Rix, H.-W., Kochanek, C. S., Keeton, C. R., Falco, E. E., Lehár, J., & McLeod, B. A. 2006, ApJ, 649, 616
Salviander, S., Shields, G. A., Gebhardt, K., & Bonning, E. W. 2007, ApJ, 662, 131
Shemmer, O., Netzer, H., Maiolino, R., Oliva, E., Croom, S., Corbett, E., & di Fabrizio, L. 2004, ApJ, 614, 547
Shields, G. A., Gebhardt, K., Salviander, S., Wills, B. J., Xie, B., Brotherton, M. S., Yuan, J., & Dietrich, M. 2003, ApJ, 583, 124 (SO3)
Shields, G. A., Menezes, K. L., Massart, C. A., & Vanden Bout, P. 2006a, ApJ, 641, 683
Shields, G. A., Salviander, S., & Bonning, E. W. 2006b, New Astronomy Review, 50, 809
Solomon, P. M., & Vanden Bout, P. A. 2005, ARA&A, 43, 677
Sulentic, J. W., Stirpe, G. M., Marziani, P., Zamanov, R., Calvani, M., & Braito, V. 2004, A&A, 423, 121
Tremaine, S., et al. 2002, ApJ, 574, 740
Treu, T., Malkan, M. A., Blandford, R. D. 2004 ApJ, 615, L97
Treu, T., Woo, J.-H., Malkan, M. A., & Blandford, R. D. 2007, ApJ, 667, 117
Woo, J.-H., Treu, T., Malkan, M. A., & Blandford, R. D. 2006, ApJ, 645, 900

GALAXY EVOLUTION: EMERGING INSIGHTS AND FUTURE CHALLLENGES
ASP Conference Series, Vol.
@jourvol, © 2009
S. Jogee, I. Marinova, L. Hao, and G. A Blanc

Spectral Principal Component Analysis of SDSS Quasars: Beyond Eigenvector 1

Randi R. Ludwig and Beverley Wills

University of Texas at Austin, Department of Astronomy, 1 University Station, C1400 Austin, TX 78712, USA

Jenny E. Greene

Department of Astrophysical Sciences, Princeton University, Princeton, NJ 08544, USA; Hubble, Princeton-Carnegie Fellow

Edward L. Robinson

University of Texas at Austin, Department of Astronomy, 1 University Station, C1400 Austin, TX 78712, USA

Abstract. In 1992, Boroson & Green (hereafter BG92) discovered the so-called eigenvector 1; AGN exhibit an anti-correlation between [O III] λ5007 and optical Fe II emission, coupled with the width of broad-line Hβ, such that stronger [O III] corresponds to broader Hβ and weaker Fe II. They showed (see also Boroson 2002) that these relationships are related to black hole mass or Eddington accretion ratio, and thus to the central engine. Surprisingly, the physics at sub-parsec scales is correlated with narrow line emission arising up to hundreds of parsecs away. We revisit this fundamental relationship using the large numbers of quasar spectra provided by the Sloan Digital Sky Survey (SDSS). Our sample includes 9046 spectroscopically-identified QSOs from Data Release 5 (DR5) with a redshift range of $0.1 < z < 0.53$, on which we perform spectral principal component analysis (SPCA) using the code from Francis et al. (1992). We find a subset of objects with extremely large [O III] EW that behave independent of Hβ linewidth. These objects drive nonlinear correlations among the data, and mask the correlation of FWHM of Hβ for the rest of the data set. However, these objects comprise less than a few percent of the entire data set, and thus are rare enough that they did not drive the relationships seen in previous, smaller samples such as BG92. These strong [O III] objects do not seem to differ from the data set significantly in other spectral properties, such as luminosity, redshift, line shapes, and continuum slope. Additionally, we find that SPCA is not the best way to analyze large quasar samples, given that the spectra are nonlinearly distributed, while one of the assumptions in SPCA is that the spectra can be related linearly. A solution to this problem is cutting large samples into subsets, which then behave much more normally. Our subset that includes the bulk of the original data then recovers traditional QSO behavior, such as eigenvector 1.

1. Sample and Results

Our sample includes 9046 objects drawn from SDSS DR5 QSOs, with redshifts between $0.1 < z < 0.53$. We avoid low-luminosity AGN at low redshift ($z < 0.1$),

which have significant host galaxy emission, and cut objects with $z > 0.53$ to ensure coverage of the rest-frame optical region. We also cut objects with Hβ FWHM < 2000 km/s to exclude Type II AGN. Our sample was taken from Salviander et al. (2007), in which they fitted all the spectra with a power law continuum, Fe II pseudocontinuum, and used Gauss-Hermite polynomials to fit the [O III] doublet and the narrow and broad components of Hβ. We also omitted a few hundred objects which had failed fits for the Hβ, so that our entire remaining data can be used to analyze spectral properties.

We performed an SPCA on the entire data set that we refer to as ALL (see results in Figure 1). While ALL:PC1 exhibits some properties of the traditional eigenvector 1, such as an anti-correlation between [O III] and Fe II, it does not include the typical Hβ linewidth dependence. Also, because the principal components are supposed to be orthogonal, there should not be correlations between the component coefficients. However, on the right in Figure 1, we see a distinct nonlinear correlation between the coefficients. The quasar spectra simply include nonlinear relationships which are not appropriately treated by SPCA.

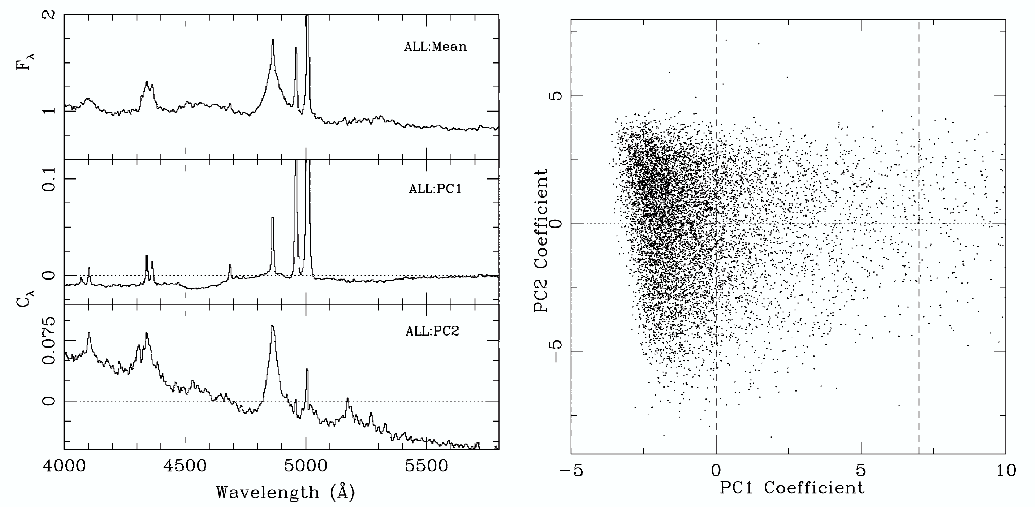

Figure 1. SPCA results for the entire data set. On the left we plot ALL:Mean, ALL:PC1, and ALL:PC2, and on the right we plot ALL:PC2 coefficients vs. ALL:PC1 coefficients. The horizontal lines denote zero. On the right, the vertical dashed lines represent our subset divisions for S1, S2, and S3, from left to right, respectively.

We divide our entire data set into three subsets, which then exhibit normal distributions when analyzed by independent SPCAs. The divisions were made using ALL:PC1, such that sample S1 is defined as ALL:PC1 < 0, which includes 6317 objects; S2 has $0 <$ ALL:PC1 < 7, which includes 2307 objects; and S3 has ALL:PC1 > 7, which includes only 422 objects.

2. How to Interpret SPCA Results

Performing SPCA on a sample yields a mean spectrum and principal component spectra that represent orthogonal sets of correlations in the data. The mean spectrum for any sample is computed as the normalized flux averaged over all objects in the sample, which is shown in the top left panel of Figure 1 for the entire data set. The principal components are not typical spectra, as in flux versus wavelength, but are representations of how wavelength regions correlate, represented by our C_λ. Wavelength regions that do correlate have the same sign of C_λ, while wavelength regions with the opposite sign are anti-correlated. Because the principal components are orthogonal, each PC is defined to be mathematically independent of correlations within other PCs. The dotted line denotes zero correlation, or $C_\lambda = 0$. In ALL:PC1, shown in the middle panel, there is a strong correlation among lines from the NLR, including [O III], the narrow line of Hβ, and He II, as well as a weak anti-correlation between the NLR and Fe II regions. ALL:PC2, shown in the bottom panel, includes the change in continuum slope across this region of the spectrum. This also correlates with the Balmer lines from the BLR.

However, as previously stated, the behavior of the entire data set is complex and not well described by linear analysis, so we were required to divide the data into subsets. The resulting principal components for each subset are shown in Figure 2. In S1, which includes $^2/_3$ of the original data set, we do recover the BG92 eigenvector 1, including the anti-correlation between Fe II and [O III] and the linewidth dependence of Hβ, as seen in S1:PC3.

3. Subset Analysis

S1 has $^2/_3$ of the objects from the entire data set, and has the most normal distribution of PC coefficients. This subset more closely recovers the traditional eigenvector 1 in S1:PC3, and is therefore the most robust subset for typical quasar behavior.

S3 is full of extreme objects, as revealed by their mean spectrum. They do have a similar amount of emission from the BLR, but they have extraordinarily strong NLR emission. The S3:PCs are completely dominated by behavior of the narrow lines, until S3:PC4, where the continuum slope and Balmer line relationship appears.

Seeking the physical cause of this exceedingly strong NLR emission, we use the spectral measurements from Salviander et al. (2007) and compare the distribution of properties between S3 and ALL. The luminosity and redshift distributions are highly similar, so there is not an obvious bias to explain this extreme behavior. The [O III] EW clearly is the physical parameter that defines S3, which is evident in S3:Mean. The [O III] FWHM distribution suggests S3 has slightly narrower lines, which is interesting. The color distribution for S3 is not redder, which we would expect if the BLR were somehow obscured. We find no conclusive signature of the physical cause for the strong NLR emission of the S3 objects, and conclude that their only trait that differs greatly from the rest of the data set is their extremely high [O III] EW.

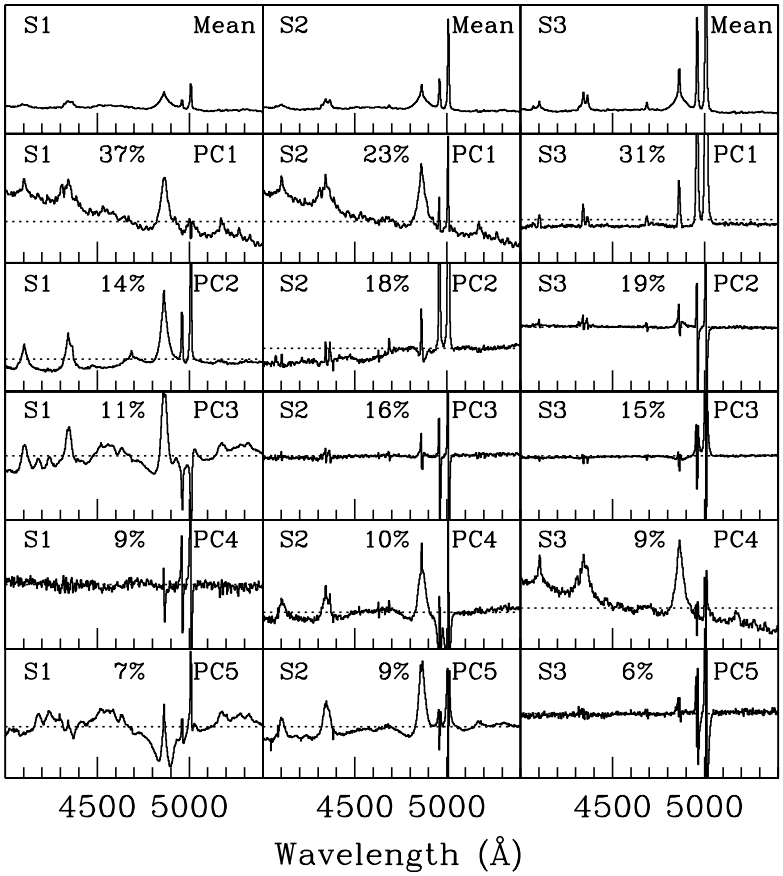

Figure 2. SPCA results for the three subsets, where the left column is S1 results, the middle column has S2 results, and the right column has S3 results. In the mean spectrum, notice the marked increase in NLR emission from S1 to S3. For the principal components, we show the percent variation accounted for by each component.

References

Boroson, T. A., & Green, R. F. 1992, ApJS, 80, 109; (BG92)
Boroson, T. A. 2002, ApJ, 565, 78
Francis, P. J., Hewett, P. C., Foltz, C. B., & Chaffee, F. H. 1992, ApJ, 398, 476
Salviander, S., Shields, G. A., Gebhardt, K., & Bonning, E. W. 2007, ApJ, 662, 131

GALAXY EVOLUTION: EMERGING INSIGHTS AND FUTURE CHALLLENGES
ASP Conference Series, Vol.
@jourvol, © 2009
S. Jogee, I. Marinova, L. Hao, and G. A Blanc

Bars in Starbursts and AGNs – A Quantitative Reexamination

Lei Hao,[1] Shardha Jogee,[1] Fabio Barazza,[2] Irina Marinova,[1] and Juntai Shen[1]

1. *Department of Astronomy, University of Texas, Austin, Texas 78712, USA.*

2. *Laboratoire d'Astrophysique, École Polytechnique Fédérale de Lausanne (EPFL), Observatoire de Sauverny CH-1290 Versoix, Switzerland*

Abstract. Galactic bars are the most important driver of the secular evolution in galaxies. They can efficiently drive gas into the central kiloparsec of galaxies, thus feed circumnuclear starbursts, and possibly help to fuel AGN. The connection between bars and AGN activities has been actively debated in the past two decades. Previous work used fairly small samples and reported conflicting results on the correlation between bars and AGN activites. Here we revisit the bar-AGN and bar-starburst connections using the analysis of bars in a large sample of about 2000 SDSS disk galaxies (Barazza et al. 2008). We found that AGN and star-forming galaxies have similar bar fractions, 47% and 50%, respectively. Both bar fractions are higher than that in inactive galaxies (29%). This study has important implications on the relationship between host galaxies and their central activities.

1. Introduction

Bars are fairly common in disk galalxies, about 2/3 of the disk galaxies are barred to some degree (Eskridge et al. 2000) and at least 1/4 of them host nested nuclear bars (Erwin & Sparke 2002). The non-axisymmetric bar can drive gas from the outer disk to the central part. This is supported by several observations that suggested barred galaxies have more concentrated gas in the central region of disk galaxies (e.g. Sakamoto et al. 1999; Sheth et al. 2004). Due to their efficiency in driving gas inflows in the disks, bars are strong candidates for the triggering of nuclear activities.

There is strong evidence for a connection between bars and nuclear starbursts. Barred galaxies show enhanced radio continuum and infrared emissions compared with unbarred ones (e.g. Hummel 1981; Hawarden et al. 1986), and starburst galaxies tend to be more barred compared with the non-starburst galaxies (e.g. Arsenault 1989; Huang et al. 1996; Ho et al. 1997). Bars can also set up resonances, such as the Inner Lindblad Resonance, which can prevent the gas from going further in. Therefore, material often builds up on a ring (a few hundred parsecs in radius) and the circum-nuclear starbursts can occur there.

The connection between bars and AGNs is less clear. Over the last two decades a large number of studies were carried out to identify if such a correlation

exists. Most of them compared the bar fraction of the AGN sample with that of a control sample of inactive galaxies. The results are controversial. For example, studies like Ho et al. (1997), Hunt & Malkan (1999), Mulchaey & Regan (1997), and Martini et al. (2003) found no excess of bars in Seyfert galaxies, while Knapen et al. (2000), Laine et al. (2002), and Laurikainen et al. (2004) reported a higher fraction of bars in Seyferts.

Previous studies are limited in several aspects. First, the sizes of the samples are often small, including only a few tens of AGNs and control galaxies. Second, the identifications of bars are not always consistent, some studies relied on the RC3 classifications. Third, the spectral classifications of galaxies as AGNs or inactive galaxies are significantly inconsistent. Most studies adopted the galaxy classifications in NASA/IPAC NED, which could be done by different people using different criteria. Our study tries to overcome these limitations by systematically investigating the bar fraction of AGNs and non-AGNs in a large number of galaxies from the Sloan Digital Sky Survey (SDSS).

2. The Sample and Their Spectral Classifications

Our sample is based on the one in Barazza et al. (2008). From the 3692 galaxies in the Sloan Digital Sky Survey (SDSS) with $18.5 < M_g < -22.0$ mag and redshift $0.01 < z < 0.03$, Barazza et al. (2008) selected 1961 disk galaxies via their blue colors. They applied ellipse fitting to find and characterize bars in these disk galaxies, and found 553 barred galaxies, 591 unbarred galaxies, and 648 highly-inclined galaxies ($i > 60^\circ$), from which the identification of bars are impossible. The remaining 169 disk galaxies either have failed or messy ellipse fittings, or the classifications were ambiguous. We ignore them from further analysis, and focus on the 1792 disk galaxies that have clear classifications of "inclined", "barred", or "unbarred".

All the 1792 disk galaxies have corresponding SDSS spectra, which are taken with a $3''$aperture, with a spectral resolution of 2200 covering a wavelength range from 3700 Åto 9000 Å. The spectral classification of these galaxies are done with various emission lines in the SDSS spectra. We process the spectra, measure the emission lines, and classify the galaxies following Hao et al. (2005). In particular, we measure the emission lines after removing the stellar absorption using a set of well-developed absoprtion-line templates. Galaxies with weak or no emission lines, defined specifically by having EW(Hα) < 3Å, are selected first. Such galaxies have little gas and is considered "inactive" in our study. The rest have strong enough emission lines indicating some activities in their nuclei. Galaxies with broad Hα emission lines (FWHM(Hα) > 1200 km/s) are automatically classified as AGNs, as broad emission lines are distinctive features of Seyfert 1 like AGNs. In our sample, there are 6 broad-line AGNs. For the remaining emission line galaxies, we classify them using the BPT diagram (Baldwin et al. 1981).

In Figure 1, we plot on the BPT diagram our sample of barred and unbarred galaxies in the left and right panel respectively. In the diagram, galaxies naturally distribute in two branches, indicating different excitation mechanisms. AGNs locate in the right branch, with stronger AGNs typically having higher [NII]/Hα and [OIII]/Hβ ratios. Galaxies with pure stellar excitation are located

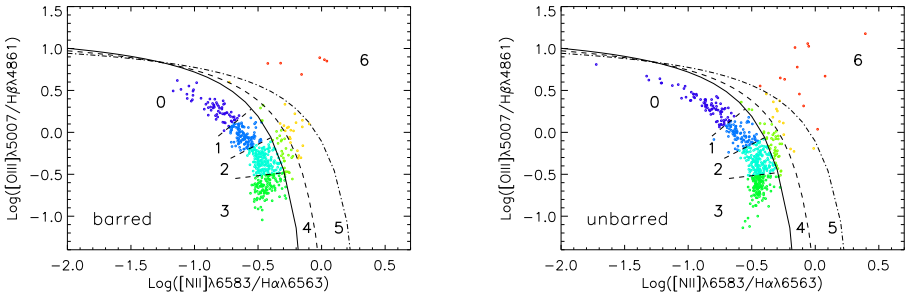

Figure 1. The BPT diagram for barred (left) and unbarred (right) galaxies in our sample. The solid line is taken from Kauffmann et al. (2003), and the dot-dashed line is taken from Kewley et al. (2001). We divide galaxies into 7 spectral classes by their locations on the diagram, marked with the numbers.

in the left branch, and those with lower metallicities have higher [OIII]/Hβ but lower [NII]/Hα ratios. The solid line, empirically defined by Kauffmann et al. (2003), separates the two branches. These authors classify galaxies below the line as star forming galaxies, and those above it as AGNs. The dot-dashed line is taken from Kewley et al. (2001), and demarcates the maximum position that can be obtained by pure photo-ionization models. Galaxies located above the line require an additional excitation mechanism, such as an AGN, or strong shocks. The general classification scheme using the two separation lines considers objects above Kewley's line as AGN dominated sources, between Kewley's and Kauffmann's line as composite AGN and starburst sources, and below the Kauffmann's line as star forming galaxies.

Since the locations of galaxies on the BPT diagram broadly reflect the properties of their nuclear activities, such as the dominance of the AGN component or the metallicity of the pure stellar-excited galaxies, we further devide galaxies into spectral classes of 0 to 6 based on their locations on the diagram (as shown in Figure 1). We would like to investigate whether the bar fraction changes with these nuclear properties. Galaxies with spectral classes of 0 to 3 are broadly considered as star-forming galaxies, and 4 to 6 as AGNs. We assign "inactive" galaxies, which have little emission lines as spectral class of -1.

3. Results

In Figure 1, we found no clear differences between the distributions of barred and unbarred galaxies on the BPT diagram. Another way to look at it is shown in the left panel of Figure 2, where we plot the bar fraction of galaxies with different spectral classifications (-1 to 6) defined by their locations on the BPT diagram (see Section 3). We found that inactive galaxies have the lowest bar fraction with only 29%. Galaxies with other spectral classes have similar bar fraction within the error bars. This is more obvious when we combine the spectral class of 0 to 3 as starbursts and 4 to 6 as AGNs. The bar fraction of "inactive" galaxies, starburst galaxies and AGNs are shown in the right panel of Figure 2.

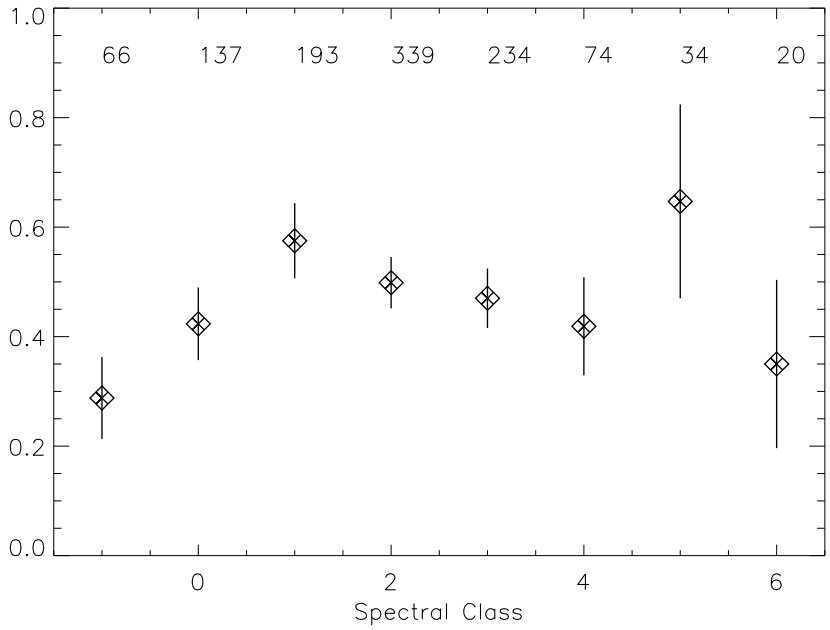

Figure 2. The bar fraction as a function of spectral classes defined in Figure 1 are shown in the left panel. Galaxies with spectral class of −1 are inactive galaxies. 0 to 3 can be considered star-forming galaxies, and 4 to 6 as AGNs. In the right panel, we show the bar fraction for galaxies of the three broad classifications.

We found that the bar fractions of AGNs and starburst galaxies are similar, at 50% and 47% respectively, both are about 60% higher than the bar fraction of the inactive galaxies.

Our result suggests that AGNs have an excess on the bar fraction if compared with the "inactive" galaxies, but show no excess if compared with the starburst galaxies. Therefore accurate and consistent spectroscopic classification of both the AGN sample and the control sample is important in evaluating the excess of bars in the AGN sample. Many previous studies have overlooked this issue. Among three studies (Ho et al. 1997; Hunt & Malkan 1999; Laurikainen et al. 2004) which we can clearly decide the dominant spectral classes of the comparing sample, our result agrees with two of them. The comparing sample in Ho et al. (1997) is mainly composed of star-forming galaxies and they found no excess of bar fraction in AGNs, which agrees with our result. Based on the classification in the NED, Laurikainen et al. (2004) divide galaxies into Seyferts, LINERs, starbursts, and inactive galaxies. They found a similar near-IR bar fraction for Seyfert galaxies, LINERS, and HII/starburst galaxies at 72%, compared to 55% in nonactive galaxies. The pattern also agrees with our result. The absolute values of the bar fraction in Laurikainen et al. (2004) are higher than ours. This could be due to two factors. First, typically the bar fraction in near-IR is known to be about 40% higher than the optical bar fraction since bars are more visible in the near-IR. Second, the number of barred galaxies could be

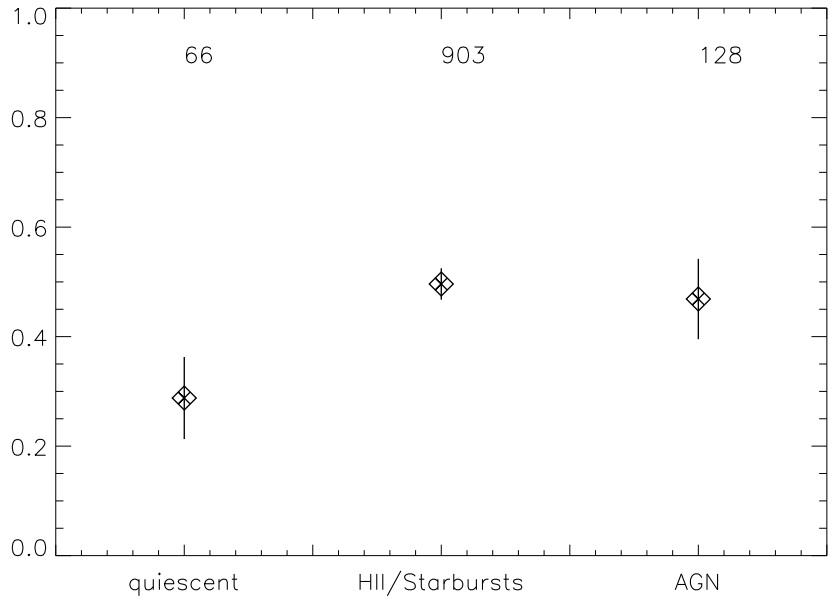

Figure 3. The bar fraction as a function of spectral classes defined in Figure 1 are shown in the left panel. Galaxies with spectral class of −1 are inactive galaxies. 0 to 3 can be considered star-forming galaxies, and 4 to 6 as AGNs. In the right panel, we show the bar fraction for galaxies of the three broad classifications.

underestimated by about 7% in Barazza et al. (2008), which regards galaxies exhibit twisted position angles, but otherwise bar-like features to be unbarred galaxies. These galaxies could be weakly barred galaxies. Our result however, disagrees with Hunt & Malkan (1999), who found that the Seyfert and LINERs in the Extended 12 μm Galaxy Sample (E12GS) have a bar fraction of 68% and 61%, similar to the inactive galaxies in the E12GS at 69%. Starforming galaxies in the sample have a higher bar fraction (85%) than both inactive galaxies and Seyferts.

From the ellipse fitting, Barazza et al. (2008) also obtained the ellipicity of bars. In figure 3, we show the bar ellipticity of barred galaxies in different spectral classes. The values of the bar ellipticity vary widely for every spectral class. We plot the mean of the bar ellipticity of each spectral class with big astrosoid and found it does not change with spectral classes. In particular, galaxies with stronger AGN component (from spectral class 4 to 6) do not show weaker bar strengths. Therefore, we found no indication of bar weakening by AGNs, this is consistent with the robustness of bars (Shen & Sellwood 2004).

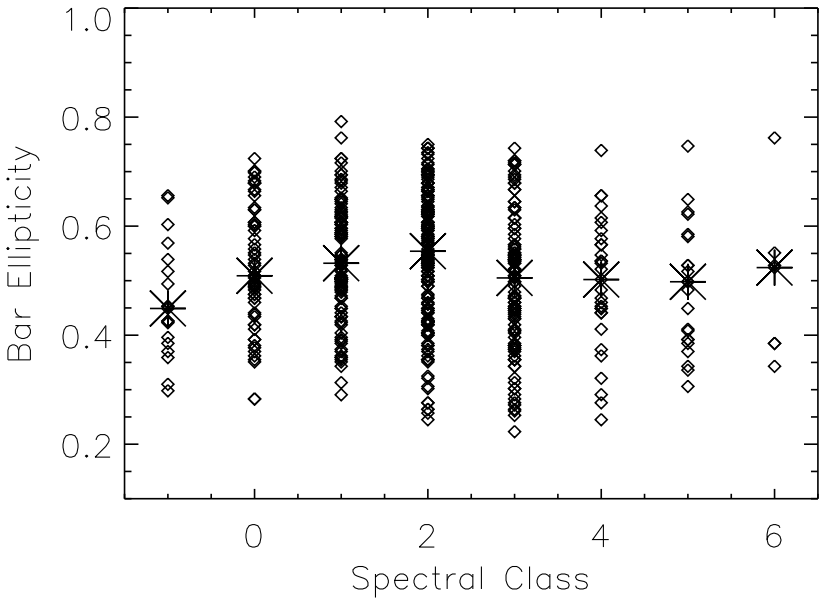

Figure 4. The bar ellipticity as a function of the spectral classes defined in Figure 1. The big asteroids are the mean ellipticity of galaxies in each spectral class.

4. Conclusions

With the bar information of ~ 2000 disk galaxies from the SDSS (Barazza et al. 2008), we study the bar fraction of AGNs, star-forming, and inactive galaxies from the sample. We find that the bar fraction of the AGNs is 47%, similar to the bar fraction of the star-forming galaxies (50%). Both are higher than the bar fraction of the inactive galaxies (29%). This suggests that accurate and consisitent spectral classification is important in evaluating whether there is an excess of bars in AGNs, and could be the reason for controversial results reported in previous studies on the issue.

References

Arsenault, R. 1989, A&A, 217, 66
Baldwin, J. A., Phillips, M. M., & Terlevich, R. 1981, PASP, 93, 5
Barazza, F. D., Jogee, S., & Marinova, I. 2008, ApJ, 675, 1194
Erwin, P., & Sparke, L. S. 2002, AJ, 124, 65
Eskridge, P. B., et al. 2000, AJ, 119, 536
Hao, L., et al. 2005, AJ, 129, 1783
Hawarden, T. G., Mountain, C. M., Leggett, S. K., & Puxley, P. J. 1986, MNRAS, 221, 41P
Ho, L. C., Filippenko, A. V., & Sargent, W. L. W. 1997, ApJ, 487, 591
Huang, J. H., Gu, Q. S., Su, H. J., Hawarden, T. G., Liao, X. H., & Wu, G. X. 1996, A&A, 313, 13

Hummel, E. 1981, A&A, 93, 93
Hunt, L. K., & Malkan, M. A. 1999, ApJ, 516, 660
Kauffmann, G., et al. 2003, MNRAS, 346, 1055
Kewley, L. J., Dopita, M. A., Sutherland, R. S., Heisler, C. A., & Trevena, J. 2001, ApJ, 556, 121
Knapen, J. H., Shlosman, I., & Peletier, R. F. 2000, ApJ, 529, 93
Laine, S., Shlosman, I., Knapen, J. H., & Peletier, R. F. 2002, ApJ, 567, 97
Laurikainen, E., Salo, H., & Buta, R. 2004, ApJ, 607, 103
Martini, P., Regan, M. W., Mulchaey, J. S., & Pogge, R. W. 2003, ApJ, 589, 774
Mulchaey, J. S., & Regan, M. W. 1997, ApJ, 482, L135
Sakamoto, K., Okumura, S. K., Ishizuki, S., & Scoville, N. Z. 1999, ApJ, 525, 691
Shen, J., & Sellwood, J. A. 2004, ApJ, 604, 614
Sheth, K., Blain, A. W., Kneib, J.-P., Frayer, D. T., van der Werf, P. P., & Knudsen, K. K. 2004, ApJ, 614, L5

GALAXY EVOLUTION: EMERGING INSIGHTS AND FUTURE CHALLLENGES
ASP Conference Series, Vol.
@jourvol, © 2009
S. Jogee, I. Marinova, L. Hao, and G. A Blanc

Stellar Feedback: A Multiphase Interstellar Medium and Galactic Outflows

Daniel Ceverino

Racah Institute of Physics, The Hebrew University, Jerusalem 91904, Israel

Abstract. I am presenting new results in our ongoing effort of improving the theory of galaxy formation in a ΛCDM Universe. I pay a special attention to the role of supernova explosions and stellar winds in the galaxy assembly. These processes happen at very small scales, they affect the interstellar medium (ISM) at galactic scales and regulate the formation of a whole galaxy. Previous attempts of mimicking these effects in simulations of galaxy formation use very simplified assumptions. I develop a much more realistic prescription for modeling the feedback, which minimizes any ad hoc sub-grid physics. I start with developing high resolution models of the ISM and formulate the conditions required for its realistic functionality: formation of multi-phase medium with hot chimneys, super-bubbles, cold molecular phase, and very slow consumption of gas. Once these effects are resolved in cosmological simulations, galaxy formation proceeds more realistically. For example, I do not have the overcooling problem. The angular momentum problem (resulting in a too massive bulge) is also reduced substantially: the rotation curves are nearly flat. The galaxy formation also becomes more violent. At high redshift, I routinely find substantial gas outflows from star-forming galaxies. I describe several scaling relations between outflow properties and galaxy properties: maximum velocity, mass and kinetic energy versus stellar mass and SFR. The simulations reproduce this picture only if the resolution is very high: better than 70 pc.

1. Introduction

The current cosmological paradigm, the ΛCDM Universe, has successfully explained the overall assembly of cosmic structures (Blumenthal et al. 1984; Davis et al. 1985; Spergel et al. 2007). In this picture ordinary matter ("baryons"), which emits and absorbs light, passively follows the evolution of the dark matter. This should be corrected, if I want to make a realistic theory of galaxy formation. This theory should include the physics of the baryons or gas. Galaxy formation is driven by a complex set of physical processes with very different spatial scales. Radiative cooling, star formation and supernova explosions happen at scales less than 1 pc, but they affect the formation of a whole galaxy. In addition, large-scale cosmological processes, such as gas accretion through cosmic filaments, and galaxy mergers, control the galaxy assembly (Dekel, Sari, & Ceverino 2009). As a result, a complex interplay between very different processes drives the formation of galaxies. Because of this complexity, cosmological dark-matter+gasdynamical simulations have become useful tools to study galaxy formation.

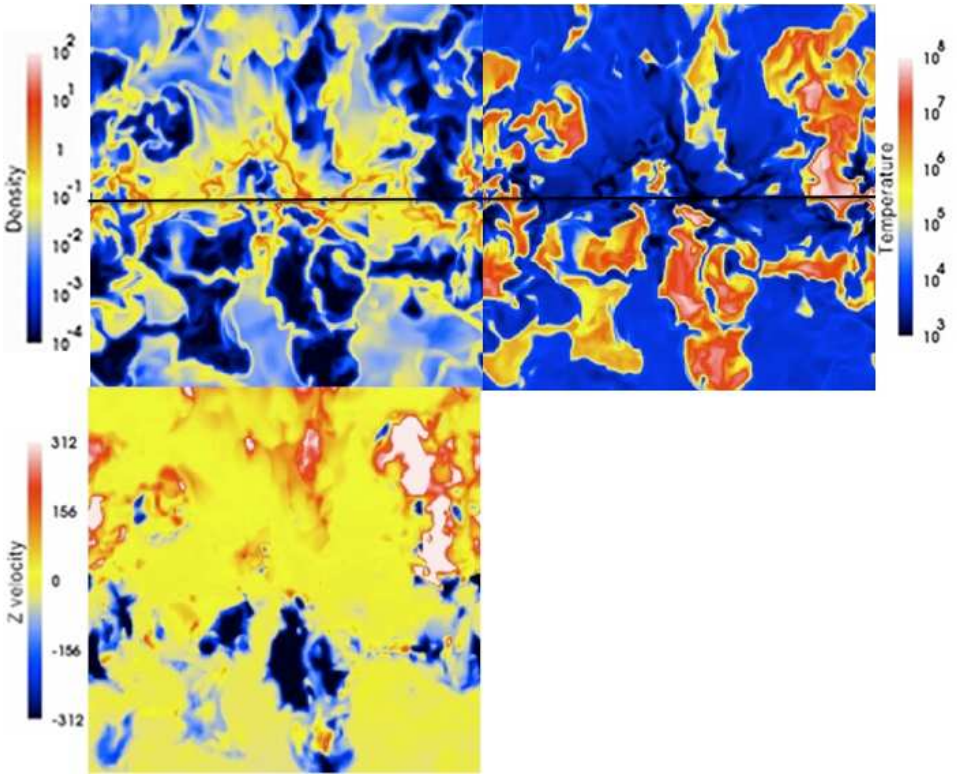

Figure 1. Snapshot of a model of a galactic disk after 113 Myr, showing the density in cm^{-3} (upper-left panel), temperature in Kelvin (upper-right panel), gas velocity in the z-direction (bottom panel). The views are perpendicular to the galactic middle-plane (horizontal black line). The three phases of the ISM are clearly visible: cold and dense clouds, warm and diffuse medium and hot bubbles with very low densities. Velocities exceeding 300 km s^{-1} can be seen in hot outflows at both sides of the galactic plane.

This proceeding summarizes the results from our simulations of galaxy formation. These numerical simulations were performed using the Eulerian gasdynamics + N-body Adaptive Refinement Tree code (Kravtsov et al. 1997; Kravtsov 1999, 2003). The physical processes of the gas include star formation, stellar feedback, metal enrichment, self-consistent advection of metals, cooling and heating rates from metallicity-dependent cooling and UV heating due to a cosmological ionizing background.

I have focus on the effect of supernova explosions and stellar winds in the formation of galaxies. Both mechanisms are referred globally as stellar feedback: the effect of stars in their surrounding interstellar medium. Our model assumes a constant injection of thermal energy over 40 Myr. This is equivalent to the injection of 2×10^{51} erg of energy from stellar winds and supernova explosions per each massive star with $M > 8$ $M_\odot$ during its lifetime. Note that this constant heating rate is the sum of the contributions from all massive stars in a single stellar population. See Ceverino & Klypin (2009) and Ceverino & Dekel (2009) for more details.

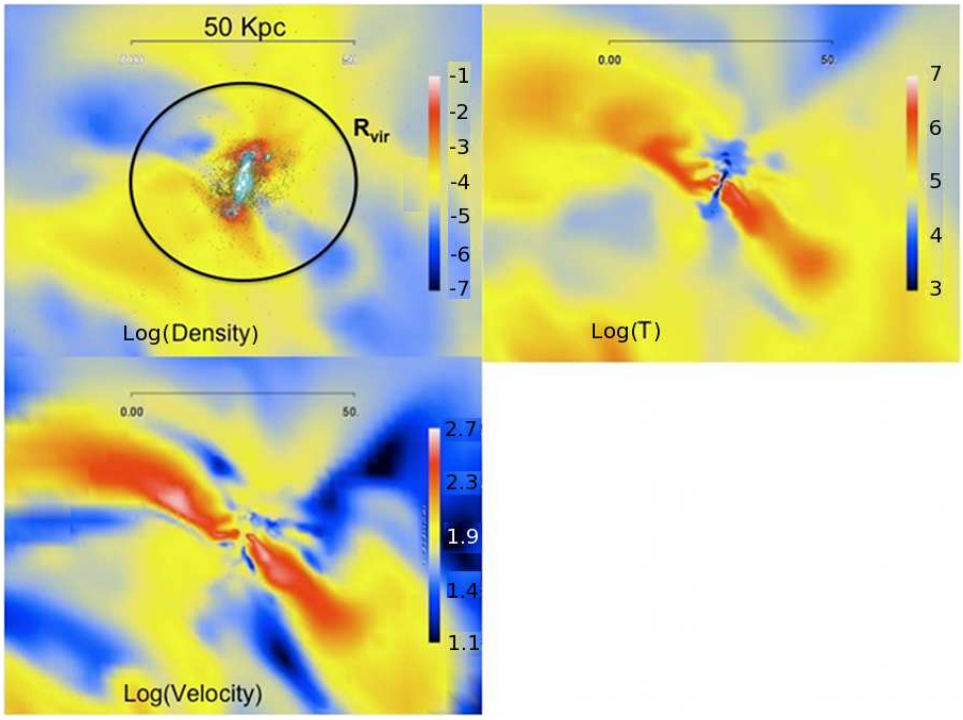

Figure 2. Slices of density (upper-left panel), temperature (uper-right panel) and velocity (bottom panel) of a dwarf starburst galaxy. It shows hot galactic outflows perpendicular to a cold (T$\sim 10^4$ K) galactic disk. The outflows show typical velocities of 200-500 km s^{-1}. The stellar component is superimposed in the upper-left panel.

I first study the effect of stellar feedback in the insterstellar medium (ISM), using simulations of a kpc-scale piece of the ISM with few parsecs resolution (Section 2). Then, I study the effect of stellar feedback in galaxy formation at high redshift using cosmological gasdynamical simulations (Section 3). Finally, Section 4 describes several scaling relations for the properties of galactic outflows.

2. Galactic Disk Model

Our first step in the understanding of the stellar feedback in galaxies is to estimate its effects on the ISM on small (galactic) scales. In order to do this, I run simulations of a $4 \times 4 \times 4$ kpc^3 piece of a galactic disk with a resolution of 14 pc.

Figure 1 shows representative slices perpendicular to the disk middle-plane. The medium is very inhomogeneous at different scales. Large bubbles of low density coexist with long filamentary structures of dense clouds. Overall, the medium covers more than 6 orders of magnitude in density and temperature. The cold phase (T$< 10^3$ K) forms dense and cold clouds near the galactic plane. The warm phase(10^3 K$<$T$< 10^4$ K) fills old cooled bubbles and low-density clouds. Finally, the hot phase (T$> 10^4$ K) is present in form of hot bubbles

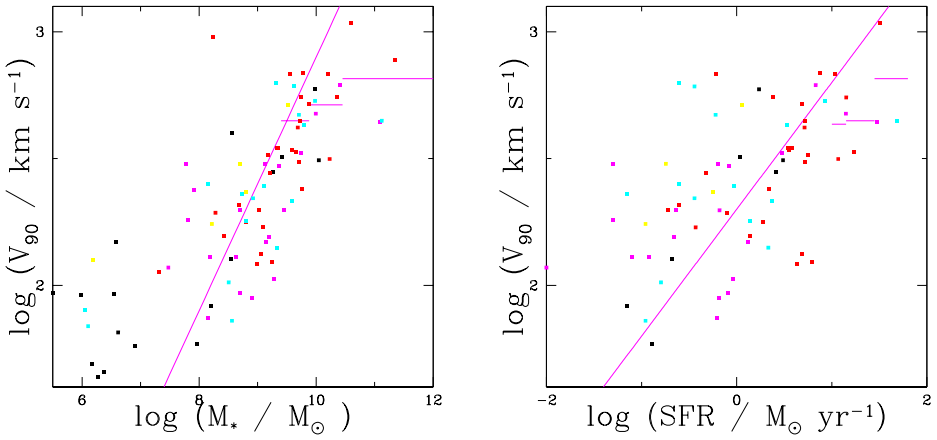

Figure 3. Correlations between the maximum outflow velocity, defined as the 90% percentile of the outflow (radial) velocity distribution (V90), and galaxy properties such as the stellar mass (left panel) and the star formation rate (right panel). Horizontal lines show outflows estimations from the DEEP2 survey (Weiner et al. 2008). The diagonal lines show the simple relations: V90 $\propto$ $M_{stars}^{1/2}$ and V90 $\propto$ $SFR^{1/2}$.

of few hundred pc wide and kpc-scale chimneys. The gas in these chimneys is flowing away from the plane with velocities exceeding $\pm$300 km s^{-1}. These bubbles even break the dense plane in hot spots surrounded by cold and dense shells. All this phenomenology associated with the hot phase is driven by stellar feedback. As a result, the effect of the stellar feedback is to sustain a three-phase ISM and to generate galactic-scale outflows.

3. Galactic outflows in a Dwarf Galaxy

Figure 2 shows a simulation of a dwarf galaxy at redshift z=2. Its virial mass is $M_{vir} = 2 \times 10^{10} M_\odot$. This corresponds to a maximum circular velocity of around 70 km s^{-1}. The model clearly shows a powerful galactic outflow perpendicular to the galactic disk. This wind contains hot and low-density gas that reaches velocities between 200-500 km s^{-1}. This outflow extends much beyond the virial radius.

Finally, figure 4 shows the correlations of stellar mass with outflow mass and kinetic energy. I found that a significant fraction of the baryons is lost for dwarf galaxies ($M_{stars} < 10^7$ $M_\odot$) as Dekel & Silk (1986) proposed. For massive galaxies ($M_{stars} > 10^{10}$ $M_\odot$), the mass in the outflow only is a small fraction of the total stellar mass. However, I found that the kinetic energy of the outflow scales linearly with stellar mass.

4. Scaling relations for galactic winds

I have compiled a sample of simulated galaxies with different baryonic masses between $10^6 M_\odot$ to 10^{11} $M_\odot$ between redshift 1.0-1.4 in order to study their

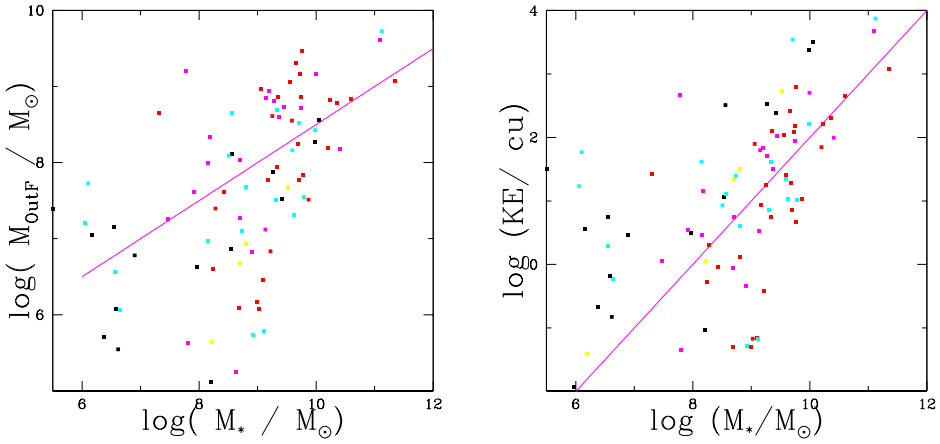

Figure 4. Correlations of the stellar mass with the outflow mass (left panel) and its kinetic energy (right panel). The lines shows simple relations: $M_{Outflow} \propto M_{stars}^{1/3}$ and $E_{kin} \propto M_{stars}$.

outflows properties and the link with their host galaxies. I have found several scaling relations between outflows properties and galaxy properties. First, I estimate the strength of the outflow as the 90% percentile of the outflow (radial) velocity distribution in the outflow of a given galaxy (V90). I define outflow material as the gas with positive radial velocity larger than the halo scape velocity.

Figure 3 shows the correlations of the maximum outflow velocity, measured as V90, with stellar mass and star formation rates. Each point is a single galaxy in the sample. Observational constrain from DEEP2 galaxies (Weiner et al. 2008) are shown as horizontal lines. I have shown that massive star-forming galaxies with typical baryonic masses of 10^{11} $M_\odot$ and star formation rates of $\sim$ 40 $M_\odot$/yr can drive powerful outflows with maximum velocities of several hundreds km s^{-1}.

Acknowledgments. Would like to thank Shardha Jogee for giving me the opportunity to attend this meeting.

References

Blumenthal, G. R., Faber, S. M., Primack, J. R., & Rees, M. J. 1984, Nat, 311, 517
Ceverino, D., & Klypin, A. 2009, ApJ, 695, 292
Ceverino, D., & Dekel, A. in preparation
Davis, M., Efstathiou, G., Frenk, C. S., & White, S. D. M. 1985, ApJ, 292, 371
Dekel, A., & Silk, J. 1986, ApJ, 303, 39
Dekel, A., Sari, R., & Ceverino, D. 2009, arXiv:0901.2458
Kravtsov, A. V., Klypin, A. A., & Khokhlov, A. M. 1997, ApJS, 111, 73
Kravtsov, A. V. 1999, Ph.D. Thesis,
Kravtsov A., 2003, *ApJ* (Letters) 590, 1
Spergel, D. N., et al. 2007, ApJS, 170, 377

GALAXY EVOLUTION: EMERGING INSIGHTS AND FUTURE CHALLLENGES
ASP Conference Series, Vol.
@jourvol, © 2009
S. Jogee, I. Marinova, L. Hao, and G. A Blanc

The Environmental Impact of Galaxy Evolution

Jesper Rasmussen

Carnegie Observatories, 813 Santa Barbara Street, Pasadena, CA 91101, USA (Chandra Fellow)

Trevor Ponman

School of Physics and Astronomy, University of Birmingham, Edgbaston, Birmingham B15 2TT, United Kingdom

Abstract. Galaxy evolution reveals itself not only through the evolving properties of galaxies themselves but also through its impact on the surrounding environment. The intergalactic medium in particular holds a fossil record of past galaxy activity, imprinted on its thermodynamic and chemical properties. This is most easily discerned in small galaxy groups, where the gravitational heating of this gas renders it observable by X-ray telescopes while still leaving its properties highly susceptible to the effects of galactic feedback. X-ray observations of the hot gas in groups can therefore provide a view of galactic feedback history that can complement dedicated studies of AGN and star formation activity at low and high redshift. Based on high-quality X-ray data of a sample of nearby groups, we present initial results of such a study and discuss some implications for the AGN and star formation history of the group members.

1. Galaxy Groups as Probes of Cosmic Feedback

In recent years, deep galaxy surveys such as GOODS (Giavalisco et al. 2004) have been providing a wealth of high-quality data on the properties of galaxies across a wide range of redshifts and masses. In combination with large-area surveys of the low-redshift Universe (e.g. the SDSS), this is enabling detailed studies of the history of stellar mass assembly, star formation activity, and nuclear activity across considerable look-back times, providing a much more detailed view of galaxy evolution than available just a decade ago.

However, a complete understanding of galaxy evolution and the processes driving it is unlikely to emerge from statistical considerations applied to large galaxy samples alone. One of several complimentary approaches is to consider the *impact* of galaxy activity on the surrounding environment. Groups of galaxies provide particularly useful laboratories for such studies, not only because they represent a very common galaxy environment in the nearby Universe, but also because they contain a hot intracluster medium (ICM) whose properties (thermal pressure, entropy, metallicity) are highly susceptible to non-gravitational processes such as those associated with galactic feedback from star formation and AGN activity. X-ray studies of this hot gas can therefore provide information on the integrated feedback activity of galaxies. Using a sample of 15 X-ray bright groups observed with *Chandra*, we are using measurements of

the metal distribution in groups to unravel some of the details of the history of star formation and nuclear activity in the group members.

2. Supernova Feedback and Star Formation History

From the *Chandra* data, we have measurements of the radial distribution of the abundance of iron and silicon in the intragroup gas for all 15 systems (details of the group sample and data reduction can be found in Rasmussen & Ponman 2007). For an assumed set of supernova (SN) yields (Iwamoto et al. 1999; Nomoto et al. 2006), the results for either element can be uniquely decomposed into contributions from SN Ia and SN II and the results then stacked to provide mean profiles for the entire sample. In Fig. 1 we show the resulting average contribution of SN Ia relative to that of SN II within the sample, plotted as a function of radius in units of r_{500}. The abundance pattern clearly implies a strong dominance of SN II enrichment at large radii, where most of the intragroup gas resides. Comparison to the ratio of SN Ia vs SN II measured in

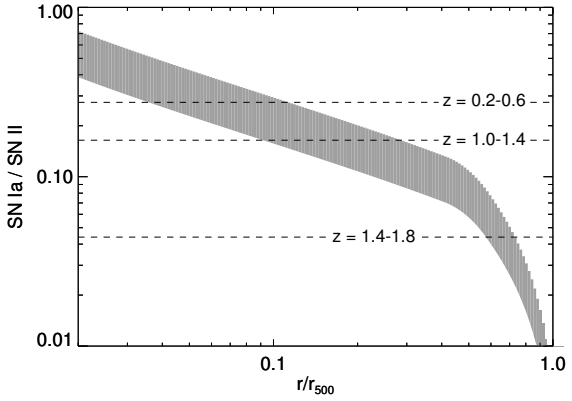

Figure 1. The mean number ratio of SN Ia vs. SN II in our groups as inferred from the ICM enrichment pattern, with the shaded region representing the typical relative uncertainty of 25%. For comparison, dashed lines show observed and predicted ratios in different redshift intervals from deep field data (Dahlen et al. 2004).

the GOODS survey (Dahlen et al. 2004) over a range of redshifts shows that our inferred SN ratios well outside the group cores, at $r \gtrsim 0.5r_{500}$, are inconsistent with observed values at low-to-intermediate redshifts ($z \lesssim 0.6$) but broadly agrees with predictions at $z \gtrsim 1.5$. The comparison data involve measured SN Ia rates out to $z \approx 1.8$, and SN II rates beyond $z \approx 1$ as predicted from evolutionary models of the cosmic star formation rate (see Fig. 2 in Dahlen et al. 2004). The immediate implication of Fig. 1 is that most enrichment, and hence SN and star formation activity in the groups, must have taken place reasonably close to the peak of the cosmic star formation rate at $z \sim 2 - 3$.

Further insight may be gained by considering the total metal mass in the groups generated by each of the two SN types, normalized by the aggregate K-band luminosity L_K of the group members. Using the adopted SN yields and

the SN rate per unit L_K (Mannucci et al. 2005) observed in local early-type galaxies (which dominate the optical output in our groups), these metal mass-to-light ratios can be translated into enrichment time-scales. The latter will be lower limits, however, because we do not account for metals locked in stars or metals ejected beyond r_{500} by galaxy winds, nor for the fact that L_K must have been smaller in the past due to the continued growth of stellar mass in group members and the addition of further members over time. Fig. 2 (left) shows the results for iron from SN Ia, revealing time-scales in excess of $\gtrsim 10$ Gyr in many cases and suggesting that SN Ia at current rates cannot have produced the required amount of Fe in several of the groups. This issue is even more

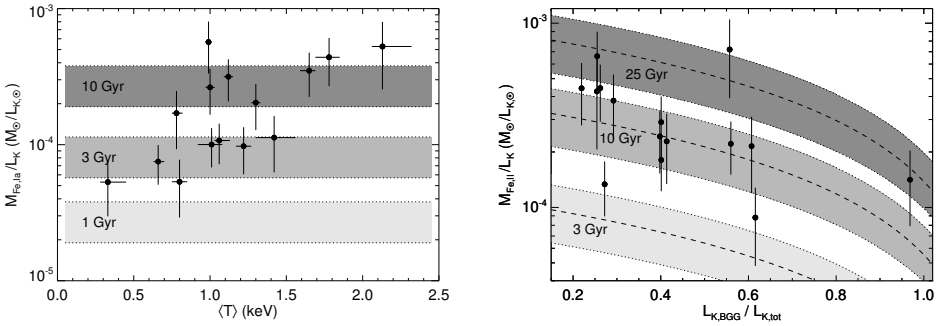

Figure 2. *Left:* K-band mass-to-light ratio of iron within r_{500} produced by SN Ia in the groups, as a function of mean X-ray temperature. Shaded regions show the corresponding time-scales for SN Ia in the group members to produce the observed metal mass, with uncertainties reflecting those of the SN Ia rates in local early-types. *Right:* The same for SN II, assuming SN rates in local spirals for all satellite galaxies, as a function of K-band luminosity ratio of the central galaxy to all group members.

acute for SN II, for which only upper limits to their rate in local early-types are available. Even if, for the sake of argument, assuming SN II rates in line with those of nearby late-type *spirals* for all galaxies except the central brightest group galaxy (BGG), the time-scales are still prohibitively large in most cases (Fig. 2 right). Hence, the inferred enrichment time-scales require much higher specific SN rates in the past in the group members, independently confirming the well-established need for a rise in the cosmic star formation rate density out to at least $z \sim 2-3$, as inferred from galaxy surveys. While similar results have been reported for massive galaxy clusters (e.g. Finoguenov, David, & Ponman 2000), this has not previously been tested at the far more common mass scale of galaxy groups.

3. Constraining SN and AGN Feedback

Assuming that energy and metals have been released proportionally from supernovae to the ICM, the SN ratios and metal masses implied by Figs. 1 and 2 allow us to estimate the total SN energy imparted to the hot gas for an assumed SN explosion energy of 10^{51} erg. The resulting values within r_{500}, shown in Fig. 3 (left), scatter around a mean of ~ 0.6 keV per ICM particle, with no clear trend

with group "mass" $\langle T \rangle$. Both the mean and scatter are in broad agreement with results of hydrodynamical simulations of groups involving momentum-driven galaxy winds to account for ICM enrichment (Davé, Oppenheimer, & Sivanandam 2008).

In principle, the inferred SN energies can also help constrain the impact of AGN feedback in the groups. As a first crude step, one could argue that the combined energy input from these feedback processes cannot substantially have exceeded the sum of the ICM thermal energy and its integrated energy losses without unbinding the hot gas (according to the virial theorem). Under this assumption, and evaluating the total radiative energy losses from the ICM on the basis of its current X-ray luminosity integrated over a 10 Gyr timescale, the resulting total allowed AGN heating energy in each group is shown in Fig. 3 (right). This would suggest that for a typical $T \sim 1$ keV system with

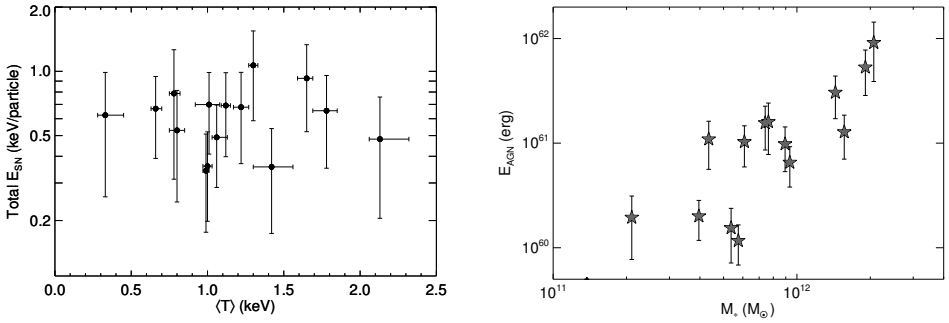

Figure 3. *Left:* SN energy per ICM particle associated with the observed ICM metal masses. *Right:* Total allowed AGN heating energy as a function of total stellar mass in each group.

a total stellar mass $M_* \sim 1 \times 10^{12}\ M_\odot$, the integrated AGN heating energy cannot substantially have exceeded $\sim 10^{49}$ erg per $M_\odot$ of stellar mass. To some extent, however, the above approach mainly probes the resilience of the *current* ICM to additional heating, and it also neglects any bulk kinetic energy imparted to the gas which may have modified its density distribution. Such a contribution could be substantial, especially in the poorest systems, but should more accurately reflect the maximum energy input that can have occurred in the groups. Hence, more robust constraints on AGN feedback would arise from assessing the amount of work done against gravity in establishing current gas mass fractions and distributions within r_{500} relative to those of massive clusters.

Assuming that the AGN heating energy in Fig. 3 has been released over a 10 Gyr timescale, the resulting time-averaged heating power in the groups is typically an order of magnitude larger than the current mechanical AGN luminosity of the BGG, as estimated from its observed 1.4-GHz radio power and the relation of Bîrzan et al. (2004). Significantly more powerful AGN activity in the past within these groups is thus allowed, but not necessarily required, by the above results, in qualitative agreement with the inferred rise in the AGN luminosity density out to $z \approx 2$ (e.g. Hopkins, Richards, & Hernquist 2007). Some further implications for AGN accretion and supermassive black hole growth can be obtained by estimating current central black hole masses

$M_{\rm BH}$ from the observed BGG bulge velocity dispersion (e.g. Gebhardt et al. 2000). The energies in Fig. 3 then provide rough upper limits to the efficiency $\eta \sim E_{\rm AGN}/(M_{\rm BH}c^2)$ with which mass accreted by a central black hole in the BGG's has been converted into heating energy in the groups. On average, this number is $\eta \approx 1-2\%$ for our sample, rising to $\eta \approx 5\%$ in the hottest groups. Although these numbers should clearly be regarded as tentative at present, it is interesting to note that they are consistent with estimates of the ratio between black hole accretion rate and AGN jet power in bright elliptical galaxies ($\approx 2\%$; Allen et al. 2006).

4. Summary

Our work demonstrates that the SN and AGN feedback history of galaxies can be probed by studying how such feedback processes have affected the hot gas surrounding galaxies in nearby galaxy groups. This provides a useful complementary approach to those based on large multi-wavelength galaxy surveys. Specifically, comparison of the observed amount of metals in the hot intragroup gas to the present-day optical properties of the group members indicate much higher supernova and star formation rates per stellar mass in the past. By further requiring that the observed metal masses be produced within a Hubble time, these findings could in principle be quantitatively checked against models predicting the redshift evolution of the specific star formation rate and stellar mass in galaxies of a given present-day mass.

Our observations also enable crude constraints on the integrated impact of AGN feedback from the group members, providing rough upper limits to the total AGN heating energy released per stellar mass, and to the efficiency with which central supermassive black holes have converted accreted mass into heating energy. With some modifications, our approach could eventually deliver robust constraints on models of galaxy formation and evolution which include the growth of central supermassive black holes and the associated AGN feedback.

Acknowledgments. JR acknowledges support provided by the National Aeronautics and Space Administration through Chandra Postdoctoral Fellowship Award Number PF7-80050.

References

Allen, S. W., Dunn, R. J. H., Fabian, A. C., Taylor, G. B., & Reynolds, C. S. 2006, MNRAS, 372, 21

Bîrzan, L., Rafferty, D. A., McNamara, B. R., Wise, M. W., & Nulsen, P. E. J. 2004, ApJ, 607, 800

Dahlen, T., et al. 2004, ApJ, 613, 189

Davé, R., Oppenheimer, B. D., & Sivanandam, S. 2008, MNRAS, 391, 110

Finoguenov, A., David, L. P., & Ponman, T. J. 2000, ApJ, 544, 188

Gebhardt, K., et al. 2000, ApJ, 539, L13

Giavalisco, M., et al. 2004, ApJ, 600, L93

Hopkins, P. F., Richards, G. T., & Hernquist, L. 2007, ApJ, 654, 731

Iwamoto, K., Brachwitz, F., Nomoto, K., Kishimoto, N., Umeda, H., Hix, W. R., & Thielemann, F.-K. 1999, ApJS, 125, 439

Mannucci, F., Della Valle, M., Panagia, N., Cappellaro, E., Cresci, G., Maiolino, R., Petrosian, A., & Turatto, M. 2005, A&A, 433, 807

Nomoto, K., Tominaga, N., Umeda, H., Kobayashi, C., & Maeda, K. 2006, Nuclear Physics A, 777, 424
Rasmussen, J., & Ponman, T. J. 2007, MNRAS, 380, 1554

Author Index

Željko I., 103

Agarwal, M., 46
Alexander, D. .M, 368
Ashby, M. L. N., 172

Böhm, A., 138, 249
Babul, A., 118
Bacon, D., 138, 249
Bacon, R., 131
Balcells, M., 79, 203
Balogh, M., 138, 249
Barazza, F., 389
Barazza, F. D., 138, 145, 249
Barden, M., 138, 249
Barentine, J. C., 150
Barro, G., 203
Bell, E. F., 138, 208, 249, 258
Birnboim, Y., 349
Blain, A., 308
Bouché, N., 60
Bromm, V., 323, 327
Brown, T. M., 110
Bullock, J. S., 240
Bureau, M., 168
Burkert, A., 3, 74
Buschkamp, P., 60

Caldwell, J. A. R., 138, 249
Cappellari, M., 131, 168, 180
Ceverino, D., 396
Combes, F., 31
Cox, T. J, 227
Cresci, G., 60

Daddi, E., 294
Davé, R., 333
Davies, R., 60, 131
de Zeeuw, P. T., 131, 180
Debattista, V., 154
Devereux, N., 172
Diamond-Stanic, A. M., 356
Dodge, C., 118
Dutton, A. A, 341

EDisCS collaboration, 145
Eisenhauer, F., 60
Elmegreen, B. G., 24
Emsellem, E., 131, 180

Förster Schreiber, N., 60
Falcón-Barroso, J., 131, 180
Fardal, M., 118
Flores, H., 319
Forestell, A., 176

GALEX Science Team, 123
Gallego, J., 203
García-Dabó, C. E., 203
Gaskell, C. M., 375
Gebhardt, K., 176
Genel, S., 60, 214
Genzel, R., 60
Gilbert, K., 118
Gonzalez, R. E., 315
Governato, F., 18
Graves, G. J., 96
Gray, M. E., 138, 249
Greene, J. E., 385
Greif, T. H., 323, 327
Guhathakurta, P., 118

Häußler, B., 138, 249
Hammer, F., 66, 319
Hao, L., 389
Heiderman, A., 138, 249
Heymans, C., 138, 249
Hicks, E., 60
Holley-Bockelmann, K., 254
Hopkins P. F., 220
Hriljac, P., 172

IMAGES collaboration, 66

Ippolito, J., 323

Jablonka, P., 145
Jahnke, K., 138, 249
Jogee, S., 74, 138, 194, 249, 389
Johnson, J. L., 323
Jurić, M., 103

Katz, N., 159
Kazantzidis, S., 240
Khochfar, S., 74, 187
Klessen, R., 323
Koda, J., 245
Kormendy, J., 74, 87, 150, 375
Krajnović, D., 131
Kravtsov, A., 271
Kuntschner, H., 131, 180

López-Sanjuan, C., 203
Lane, K., 138, 249
Lu, Y., 118
Ludwig, R. R., 385
Lutz, D., 60

Madau, P., 278
Marinova, I., 138, 249, 389
McDermid, R. M, 131
McDermid, R. M., 180
McIntosh, D. H., 138, 208, 249
Meisenheimer, K., 138, 249
Milosavljević M, 46
Milosavljević, M., 245
Moustakas, J., 356

Navarro, J. F., 10
Noeske, K. G., 286

OWLS team, 10

Pérez-González, P. G., 203
Padilla, N. D., 315
Peletier, R. F., 131
Peng, C. Y., 138, 249
Ponman, T., 401
Puech, M., 319
Purcell, C. W., 240

Rasmussen, J., 401
Reddy, N. A., 301
Rhee, G., 53
Rindler-Daller, T., 164
Robaina, A. R., 208
Robinson, E. L., 385
Rodrigues, M., 319
Rothberg, B., 264

Sánchez, S. F., 138, 249
Sales, L. V., 10
Salviander, S., 379
Sarzi, M., 131
Schiminovich, D., 123
Shapiro, K. L., 60
Shapiro, P.R., 245
Shen J., 154
Shen, J., 389
Shields, G. A., 379
Shlosman, I., 39
Sinha, M., 254
Skelton, R. E., 208, 258
Somerville, R., 138, 208, 249
Somerville, R. S., 258
Stacy, A., 327
STAGES collaboration, 208
Stewart, K. R., 235

Tacconi, L., 60
Taylor, A., 138, 249
Tremonti, C., 356

van de Ven, G., 131
van den Bosch, R. C. E, 131
van den Bosch, R. C. E., 180
van den Ven, G., 180
van Kampen, E., 138, 249
van den Bosch, F. C, 341

Weijmans, A., 180
Weinberg, M., 118, 159
Weinzirl, T., 74
Williams, M. J., 168
Willmer, C. N. A., 172
Willner, S. P., 172
Wills, B., 363, 385
Wisotzki, L., 138, 249
Wolf, C., 138, 249

Yoon, I., 159

Zamorano, J., 203
Zheng, X., 138, 249